VALORIZATION OF RESIDUES FROM AGRICULTURAL AND FOOD INDUSTRIES TOWARDS BIOFUELS AND BIOPRODUCTS USING BIOCHEMICAL AND THERMOCHEMICAL TECHNOLOGIES

A Dissertation

Presented to the Faculty of the Graduate School

of Cornell University

In Partial Fulfillment of the Requirements for the Degree of

Doctor of Philosophy

by

Borja Cantero-Tubilla

August 2017

VALORIZATION OF RESIDUES FROM AGRICULTURAL AND FOOD INDUSTRIES TOWARDS BIOFUELS AND BIOPRODUCTS USING BIOCHEMICAL AND THERMOCHEMICAL TECHNOLOGIES

Borja Cantero-Tubilla, Ph.D.

Cornell University 2017

The large volumes of organic waste streams produced daily as a part of our food and water supply systems create a global management challenge. Traditionally, these wastes are landfilled, composted, or used for the production of animal feed and fertilizers. However, the majority of this waste has a high potential for recovery of valuable bio-based products.

Hydrothermal processes are well suited for the valorization of wet organic waste. Hydrothermal liquefaction (HTL) is performed at temperatures ranging 250-350˚C and high pressures to exploit the special properties of hot liquid water. HTL yields a bio-crude oil, hydro-char, water-soluble compounds, and gas. These phases have the potential to be used as "building blocks" for the production of fuels and bio-products.

In this project, valorization of representative wastes: from food production (wine, apple cider, beer, and olive oil production), dairy industry (manure and whey), and wastewater treatment plant were screened at different temperatures, reaction times, and pH conditions. Carbon balances gave information about the influence of the raw material and reaction conditions in directing carbon to any of the four HTL products (i.e., char, oil, water and gas). In the HTL of cow manure, higher temperatures and longer residence

times favored the concentration of carbon from raw material into the oil phase (15%wt C at 250˚C and 5 min to 40%wt C at 300˚C and 60 min) at the expense of the char fraction. The energy quality of the bio-crude recovered resembled the bio-ethanol fuel, and it is far lower than the energy density found in commercial gasoline. This has to do with the oxygen content remaining in bio-crude oil that, lower than the feedstock, is much higher compared to commercial gasoline. Therefore, downstream upgrading processes are necessary to convert the obtained bio-crudes into drop-in fuels. Moreover, HTL products were characterized using novel FTIR techniques coupled with multivariate statistics, GCMS, and HPLC offering a deeper understanding on the mechanisms behind hydrothermal processing of waste.

BIOGRAPHICAL SKETCH

The author was born and raised in Madrid (Spain) where he studied at Nuestra Senora del Sagrado Corazon Elementary and Middle school, and Cristo Rey High school. He majored in Chemical Engineering at Complutense University of Madrid, where he graduated in 2009. He then moved to West Virginia University with a Fundacion Caja Madrid fellowship to study his M.S. in Chemical Engineering, researching the use of thermally treated agricultural waste to power direct carbon fuel cells. Upon receiving an Obra Social la Caixa fellowship, he started his Ph.D at Cornell University in 2013. His education in Science and Engineering was complemented in management at Loyola University of Chicago during 2008 summer. In addition, Borja acquired industrial experience in the chemical engineering and plastics fields, working as an intern in SABIC-ip during the 2009 summer, and consulting experience working for CIRAD in Thailand as consultant for the cassava starch industry for the Fall of 2015.

At Cornell University, Borja has worked as teacher assistant, events organizer, gym monitor, and served as president of the Engineering Graduate Students Association (2015), and Chemical Engineering class representative (2013-2014).

To my mother Ines Tubilla Cuadrado

To my grandfather Aurelio Tubilla Garcia

To my amazing friend Ghazal Shoorideh

ACKNOWLEDGMENTS

I would like to recognize some people and institutions that made my journey in this university an unique experience.

Thanks to Obra Social La Caixa fellowship for the funding support that made possible for me to come to Cornell. Thanks to the Chemical Engineering department, Cornell Engineering, and Biological and Environmental Engineering for giving me the resources to be able to complete my PhD.

Thanks to Prof. Tester for serving as chair of my committee, for his continuous support and his encouragement to always explore new possibilities.

Thanks to Prof. You, Prof. Scott, Prof. Wilson, and Prof. Walker for serving (or having served) in my committee.

Thanks to Prof. Archer for his help in making me a "proactive" person.

Everything started with Lola, Mari Carmen, Flor, Jesus, Paco, Isabel… all of them great teachers and mentors at Nuestra Senora del Sagrado Corazon, and Gloria, Alicia, Pilar, Jose, Ignacio, Laura… from Cristo Rey. They were all great mentors that taught me so many things, and got me interested in Science, Technology, and debate. The years I spent with them were the happiest of all. Great anecdotes and adventures.

I will always very grateful to Dr. Roy Posmanik for his patience in difficult moments and his help during my time at Cornell. He has been a great mentor from whom I have learned a lot. He pushed me to become a better scientist, engineer, and to "have fun" in my presentations.

Thank you very much to the great people I have been fortunate to work with: Celia Martinez, my "primo" Danilo Cantero, Deborah Sills, Monica Hoover, and Nathan Kruer-Zerhusen. Thank you for your passion, for sharing your knowledge with me, and for being absolutely awesome.

I am very grateful to have worked with the best engineers of the world: Glenn Swan, Doug Cavendish, and Karl Pendleton. You guys were amazing helping me with my numerous problems with my reactors, and I learned a lot from every single one of you. Kris Corda, Prof Bruce van Dover, and Thierry Tran made my experience at Cornell much better giving me a chance to work with them whenever I needed it the most. They were great mentors and a pleasure to work with.

Thanks to my family, specially my parents. My mother Ines Tubilla Cuadrado has been always there for me, worrying about her son. She knows I am a trouble-maker, but what you wanna do, it is what it is. Her infinite patience to hear all my bitching and complaining (that has been a lot) every single day is absolutely commendable. I love her and I should tell her this more often. I don't deserve the great mother I have.

As everything I do in my life, I want to thank and dedicate this dissertation to my grandfather Aurelio Tubilla Garcia. It doesn't matter how long ago he left, he is still with me and will always be. I know he would be very proud of his grandson getting a PhD, but not surprised. From now on, I will try to put in practice his last words for me: "*Disfruta de la vida, que es lo unico que te vas a llevar al otro mundo*" (Enjoy your life. It is the only thing that you can carry with you to the other side).

To end this chapter, I want to thank my friends at Cornell, Henry, Blaire, Arna, paella parties crew…. But specially thank my "sugar mommy" Ghazal. She is the best friend

I could have found at Cornell. We have had so much fun crashing to parties, meeting new people, exploring Thailand, and, in general, causing all sorts of trouble. She was my confident in hard moments always providing an unique sarcastic perspective to face problems. She had the ability to always cheer me up. I could fill this page with anecdotes, but I am afraid the library would rate this dissertation not suitable for graduate students to read… and they should.

Borja Cantero-Tubilla

Ithaca, NY, USA

July, 2017

TABLE OF CONTENTS

LIST OF FIGURES

CHAPTER I

Part I. FTIR methods development for the characterization of model cellulose and lignocellulosic biomass

CHAPTER III

CHAPTER VII

CHAPTER VIII

LIST OF TABLES

CHAPTER I

Part I. FTIR methods development for the characterization of model cellulose and lignocellulosic biomass

CHAPTER III

CHAPTER IV

Part II. Thermochemical valorization of model compounds and organic wet wastes from a variety of industries and characterization of the products: Influence of pH, temperature, and reaction time in product distribution and quality

CHAPTER V

CHAPTER VI

CHAPTER VII

CHAPTER VIII

CHAPTER I

INTRODUCTION AND MOTIVATION

1.1 Organic waste: An underused source of energy and platform chemicals

We live in a time where globalization has brought unprecedented levels of development never seen before in human history. The world is experiencing the most rapid expansion of the middle class (in income terms, population making between US$10 and US$50 per day) ever seen (Ferreira et al. 2013). In 2015, the global middle class count was above 3 billion people, with the majority of growth focused in Asia. Predictions indicate that for 2020 the majority of the global population will be classified as middle class. This will be the first time ever this occurs in the world's history (Kharas 2017). This development, together with the projected increase in world population of 30% by 2050 and the longer life expectation (United Nations Department of Economic and Social Affairs 2015) puts more stress in the water, food, and energy systems that ever before. This creates new challenges in terms of food security, water supply and quality, meeting growing energy demands, and intensive generation of waste streams. The increased environmental concerns associated with these challenges are driving communities to seek sustainable solutions (Zacharof 2016). Any proposed solutions should be comprehensive and feasible for the long term, involving both federal and state entities, and private corporations (industries and commercial facilities).

Waste today is considered a liability that can potentially hinder the scalability of industries (as the management of waste is becoming increasingly expensive and challenging). The Green Chemistry boom in the early 1990s was emphasizing waste remediation and prevention strategies. Today, the

focus is on the valorization of unavoidable wastes, beyond their current value obtained from traditional uses (combustion, fertilization, animal feed, etc.) (Tuck et al. 2012). Because of legislative, environmental, economic, and social pressures, it is projected that in the coming decades waste management strategies will focus on chemicals recovery, energy generation (drop-in transportation fuels), production of synthetic materials, and food (human and non-human). This focus is globally shared, with goals set by the United States Department of Agriculture (USDA) and the United States Department of Energy (USDOE) to obtain 20% of the transportation fuels and 25% of the chemical commodities from biomass by 2030. In addition, the European Union set a mandatory target of 10% for biofuel's share of energy consumption by 2020 (Zakzeski et al. 2010). The achievement of these ambitious goals, set in 2008, are being revised based on the actual economic and political landscape, leaning towards 7% biofuel's share for the European Union (Lane 2015).

Biomass is a resource widely available and distributed among different regions of the world, produced at high steady rates. In the US alone, between 650-770 million dry tons of biomass are available for energy production, with energy crops (400 million dry tons), agricultural residues (150-200 million dry tons), urban and mill wastes (43 million dry tons), manure (59 million dry tons), and forest biomass (20-50 million dry tons) as the main contributors (Oak Ridge National Laboratory 2011). Biomass contains, per se, high value chemicals and elements: carbon sources (carboxylic acids, carbohydrates), nitrogen sources (ammonia, proteins), phosphorous, minerals, metals, etc (Zacharof 2016). The exploitation of these resources can provide industries with additional income with major investments in infrastructure transformation. In addition, organic waste is suitable for valorization to produce hydro-carbon based liquid fuels and chemicals for an

expanding bio-based economy (Peterson et al. 2008, Tuck et al. 2012). Table 1.1 show the valorization value of biomass waste using different routes (Tuck et al. 2012).

Table 1.1. Approximate potential values of different routes of biomass waste valorization (Tuck et al. 2012).

	Potential value ($/t dry biomass)	**Potential Value (MM$) for U.S (based on 700 million ton dry biomass** (Oak Ridge National Laboratory 2011)**)**
Average bulk chemical	1,000	700,000
Transportation fuel	200-400	140,000-280,000
Cattle feed	70-200	49,000-170,000
Generating electricity	60-150	42,000-105,000
Landfill	-400	280,000

Traditional methods of waste disposal (landfilling, land spreading, or disposal in water streams) have proven environmentally hazardous, irresponsible, and increasingly expensive practices, and, therefore, they have been banned or restricted by law (Zacharof 2016). Combustion of waste and integration into combined heat and power cycles focus only in the biomass thermal potential, without considering the potential recovery of valuable chemicals. Alternative methods (anaerobic digestion, composting) are challenged by the increasing of waste generation in the last decades, and the products generated have problems associated with market demand, and bio stability. The high water content of these biomass resources limits the options for utilizing them in the medium and long term. For example, pyrolysis and combustion are not suitable technologies for the treatment of wet waste feedstocks as they require drying of the biomass prior to the thermal treatment. The drying process is thermally intensive as the high latent heat of water needs to be supplied, and the mass fraction water to evaporate is large (Peterson et al. 2008). However, the proposed biochemical and thermochemical valorization methods using hydrothermal conversion presented in this work are very well suited for the high water content biomass wastes. The

hydrothermal routes substantially reduce the volume of waste, and produces bio stable streams with minimal odor. In addition, upon process scaling-up, they have the potential to generate revenue for the company generating the waste.

The biochemical routes of valorization involve the use of enzymes (cellulases) or microorganisms to depolymerize lignocellulosic biomass into reduced 5 and 6 carbon sugars. These reduced sugars have been traditionally used as fermentation substrates for the production of bio-ethanol. However, they also have the potential to be precursors of other bioproducts including liquid alkanes, 5-hydroxymethyl-furfural, and furfural (Prado et al. 2017).

The goal of the research in biomass valorization is to envision organic wastes as a valuable commodity and a source for platform chemicals (Zacharof 2016, Tuck et al. 2012) and bio-energy by reclaiming the intrinsic value of waste by biochemical / thermochemical conversion processes (Tekin et al. 2014). The development of a sustainable, commercial-scale bio-based industry founded on the valorization of a variety of organic residues will reinvigorate the economy by creating new jobs and decreasing net greenhouse gas emissions, soil and water pollution on a life-cycle basis (NREL 2014).

1.2 Biochemical routes for organic waste valorization

Biochemical routes extract value from waste biomass by utilizing enzymatic and microbial processes (Tekin et al. 2014). A schematic of a traditional process for biochemical biomass valorization is presented in Figure 1.1. It has several major components, including: biomass pretreatment, cellulose hydrolysis (saccharification), sugars fermentation, and products recovery (distillation, solids recovery, steam and power generation) (Larson 2008).

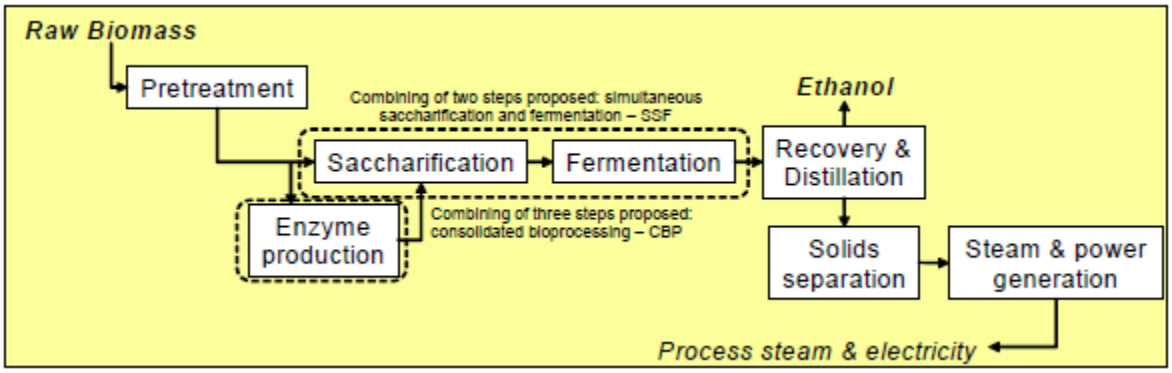

Figure 1.1. Biochemical route for lignocellulosic biomass conversion into second generation biofuels (Larson 2008)

The economic and technical difficulties to obtain concentrated sugars from lignocellulosic biomass remains a key challenge (Luterbacher et al. 2012, Liu et al. 2009, Luterbacher et al. 2013). The diverse physical and chemical structures of waste biomass pose many issues in developing efficient and economical hydrolysis processes for cellulose by cell-wall-degrading enzymes (CWDEs) (Arantes and Saddler 2010, Bansal et al. 2009). Success hinges on the development of technologies for low-cost production of monosaccharides by overcoming the recalcitrance of lignocellulosic plant cell walls. The cell wall microstructure of plants exist as cellulose microfibers packed into bundles and supported by a lignin and hemicellulose matrix. These structures (see Table 1.2) make the cell wall very useful for the plant as a structural and defensive element, therefore, making lignocellulosic biomass recalcitrant to enzymatic degradation (Luterbacher et al. 2013, Sills and Gossett 2012, Foston and Ragauskas 2012, Zhu et al. 2008). Thermochemical pretreatment of biomass can help overcome this recalcitrance, and is a critical step for the economic feasibility of biochemical conversion processes (Chundawat et al. 2007).

Table 1.2. Structural features that affect biomass recalcitrance and their effect in the efficiency of saccharification (Zhu et al. 2008). Positive effect means an increase in the structural feature increases saccharification efficiency. Negative effect means an increase in the structural feature decreases saccharification efficiency.

	Structural features	Effect in saccharification yield
	Surface area	Positive
	Crystallinity	Negative
	Degree of polymerization	No correlation
	Pore volume	Positive
Physical	Particle size	No correlation
	Lignin	Negative
	Hemicellulose	Negative
Chemical	Acetyl groups	Negative

Among the physical structural features that determines the rate and extend of enzymatic hydrolysis, surface area and cellulose crystallinity have been the most studied. Fan et al. (1981) studied the effect of different pretreatments, both physical and chemical, on the extent of hydrolysis using the cellulose model substrates Avicel and Solka Floc. They found an empirical expression that presents the yield of hydrolysis (sugar yield) as a function of surface area and crystallinity, and concluded that crystallinity is the major factor in determining the rate and extent of hydrolysis. However, in later work by Walker and Wilson (1991), it was argued that the role of surface area in this study was underestimated as the drying protocol used by the authors had collapsed the capillary structure of the biomass. It is broadly accepted that highly crystalline cellulose is less accessible to cellulases to form an enzyme-substrate complex than amorphous cellulose (Zhu et al. 2008). Our understanding of impact of physical features on the extent of hydrolysis was further expanded by Grethlein (1985). In this study several biomass resources were pretreated with dilute sulfuric acid before enzymatic hydrolysis. A batch solute exclusion measurement system, a form of size exclusion chromatography, was used to study the measure of pore size distributions for these biomass resources. Analysis of these distributions revealed that pretreatment of these biomass resources yielded a very large increase in pore volume accessible to

cellulases (average size of a cellulose is 51 Å). Grethlein concluded from his study that surface area and pore volume were the dominant factors determining the rate and extent of hydrolysis. Nevertheless, the debate of whether crystallinity or surface area is the dominant factor in determining the rate and extent of hydrolysis continues today (Arantes and Saddler 2010, Barakat et al. 2013), and it is part of the goals of this work to study whether celluloses acting alone or in cocktails alter the crystallinity of pretreated biomass during saccharification. Particle size is another physical feature that influences the rate and extent of enzymatic hydrolysis. Chang et al. (1997) have shown further reduction of particle size below 40-mesh (0.5mm) for switchgrass does not enhance the hydrolysis rate (Chang et al. 1997). This result was confirmed by Chundawat et al. (2007) using corn stover, and by Sinitsyn et al. (1991) using bagasse (Kim and Holtzapple 2006). Other authors contend that a 1mm particle size represents the threshold for improving enzymatic hydrolysis (Shill et al. 2011).

Higher cellulose degree of polymerization (DP) has been associated with lower accessibility to cellulose active sites. Cellulose bundles are rod-like chain molecules held together thanks to a network of inter- and intra-molecular hydrogen bonds. An increase in DP would result in a network of long fibers, considered stronger, and resistant to solvents and degrading agents compared with those of lower DP. Puri et al. (1984) were able to reduce the degree of polymerization of several biomasses (bagasse, wheat straw, *Eucalyptus regnants*, *Pinus radiata*, and cotton linters) by alkaline explosion, carbon dioxide explosion, and ozone pretreatment without altering the crystallinity of the material. That translated in an increase of enzymatic hydrolysis rate(Puri 1984). On the other hand, Sinitsyn et al. (1991) argued that DP does not noticeably influence the efficiency of hydrolysis, and explained Puri et al. (1984) observations as their pretreatment altered

the biomass further than just the degree of polymerization, and those changes were not characterized (Sinitsyn et al. 1991).

The chemical features that affect enzymatic hydrolysis of biomass are the composition of lignin, hemicellulose, and acetyl groups bound to hemicellulose (Singh et al. 2009). Lignin contributes to biomass recalcitrance because of its close association with cellulose microfibrils, limiting enzyme accessibility (Zhu et al. 2008, Kim et al. 2003, Selig et al. 2007). Lignin and its derivatives (phenols) are also toxic to microorganisms (Kim et al. 2003), and acts as a competitive adsorption site for cellulases (Chang et al. 1997, Zhu et al. 2008). Hemicellulose in lignocellulosic biomass also provides competitive bind sites for cellulases that limit enzymatic hydrolysis. Furthermore, the xylan backbones in native plant cells are extensively acetylated, affecting negatively the saccharification process by reducing the swelling capacity of biomass (Zhu et al. 2008).

Due to the aforementioned physical and chemical features responsible for biomass recalcitrance, the enzymatic hydrolysis of untreated biomass yields only 20% (or less) of the theoretical glucose yield (Liu et al. 2009). The enzymatic hydrolysis of mixed hardwood and switchgrass with a cellulase cocktail at 15FPU/g glucan during 72h, reported sugar yields below 10% in both cases (Luterbacher et al. 2012). The glucose yield reported by Samayan et al. (2010) for 24hr digestion of switchgrass was 12%. A little higher yield (15-20%) was reported by Sathitsuksanoh et al. (2011) in the 72 hr hydrolysis of switchgrass. Same hydrolysis time (but different enzymatic cocktail) yielded 20% sugar yield for untreated corn stover, with no significant effect of the cellulase loading (15, 30, and 60 FPU/g glucan) on the yield (Liu et al. 2009). This confirms the results observed by Kim et al. (2003) (2005) also for corn stover. Similar results were obtained by Li et al. (2011). Untreated cotton stalk yielded around 5% biomass digestibility upon 72 hr of enzymatic hydrolysis with 50FPU/g biomass enzymatic load (Haykir and Bahcegul 2013). Similar

result was reported for the hydrolysis of miscanthus at 48 hours with 20FPU/g cellulose (Shill et al. 2011). Rice straw conversion yield was reported between 5 and 20% for relative amount of enzyme of 10 and 100 %wt, respectively for 72 hr reaction (Nguyen et al. 2010). These low sugar yields for untreated biomass underscores the necessity of thermochemical pretreatment of biomass before enzymatic hydrolysis.

Although a costly step, post-harvesting processing and pretreatment are very important from an economic viewpoint. The main objective is to overcome the factors presented in Table 1.2 that contribute to biomass recalcitrance. It has an positive impact on product yields and concentration, the rate of hydrolysis and fermentation, and required enzyme loading (Kristensen et al. 2008). It entails three key processes as describe below: ("Replacing the Whole Barrel. To Reduce U.S. Dependence on Oil" 2013)

1. **Preconversion:** Biomass size reduction through chipping, grinding, and milling is an essential operation that modifies the feedstock in a physical and chemical fashion (Bitra et al. 2009). However, it is energy and capital cost intensive (Barakat et al. 2013). Size reduction increases the available surface area, reduces the degree of polymerization (Palmowski and Muller 2000), shears the biomass, and reduces mass transfer limitations during the hydrolysis process (Kratky and Jirout 2011). Ball milling of biomass is also known to decrease cellulose crystallinity (Zhu et al. 2008). Chundawat et al. (2007) argued that sorting lignocellulosic biomass during harvest based on its compositional and anatomical differences might be useful in separating more recalcitrant fractions (i.e., cobs, stalk) from lesser recalcitrant portions (i.e., leaves, husks). Montross et al. (2004) obtained a glucose yield of 91, 63, and 33% for untreated corn leafs, corn cobs, and corn stalks, respectively, compared with the about 20% glucose yield obtained from enzymatic

hydrolysis of untreated corn stover (no fractioned) (Liu et al. 2009, Kim and Lee 2005, Li et al. 2011) Besides feedstock fractionation, thermal and chemical pretreatment prepare feedstocks for an efficient saccharification.

2. **Formulation:** Treated or untreated biomass is blended in specific ratios, often with biological or chemical additives, to improve conversion efficiencies.
3. **Densification:** Temperature and pressure are used to produce a high quality, high density stable feedstock for efficient handling, storage, and transport.

Lignocellulosic biomass pretreatment technologies can be divided into thermal and chemical processes, and their combinations (hybrid processes).

Hydrothermal/thermal pretreatments: Feedstock is heated at temperatures between 120 and 220°C for 60-300 minutes and 1-2 minutes, respectively, to preferentially degrade hemicellulose and lignin, without affecting the structure of cellulose (cellulose degradation starts at 250°C) (Peterson et al. 2008, Hendriks and Zeeman 2009). The thermal pretreatment at 195°C for 6 min of presoaked wheat straw yields a reduction on xylan content from 24.5 to 5.2% based on dry matter (Kristensen et al. 2008). Solubilization and degradation of lignin to phenolic derivatives starts taking place at temperatures above 180°C. These phenolic groups present inhibitory effect on enzymatic hydrolysis and on microorganisms used for fermentation (Hendriks and Zeeman 2009). In addition, longer residence times degrade oligosaccharides and monosaccharides to furanic compounds that also have an inhibitory effect in enzyme activity (Luterbacher et al. 2012). Phenol derivatives from degradation of lignin and furan derivatives from degradation of carbohydrate need to be removed prior to saccharification (Chundawat et al. 2007). Among the thermal/hydrothermal pretreatment are:

1. **Steam pretreatment:** Steam at high temperatures (240-280°C) and pressures (1000psi) is applied to biomass at short residence time (few minutes). After the set time, the steam is released and the biomass is quickly cooled down (Hendriks and Zeeman 2009).
2. **Steam explosion:** Rapid decompression of wet biomass in the presence of saturated steam causes the water in the biomass to "explode" causing a mechanical disruption in the fiber structure (Hendriks and Zeeman 2009).
3. **Hot Liquid Water:** Researchers have demonstrated that pretreatment of corn stover with pressurized water at 190°C for 15 min can boost sugar yields up to 90% using enzyme load of 15FPU/ g glucan at 48 hr reaction (Mosier et al. 2005).

Chemical pretreatments: Refer to the use of chemicals to selectively dissolve lignin and hemicellulose without alteration of the cellulose fraction. Cellulose is more inert to the action of diluted acid used in pretreatment than hemicellulose and lignin. However, when concentrated acid is utilized (as companies like Virdia in Virginia that uses HCl at concentrations 1-40%) the pretreatment also constitutes the hydrolysis of biomass into sugars. In this case, the hydrolyzed sugars must undergo a detoxification/neutralization process before fermentation. Thus, dilute acids are preferred (sulfuric acid at concentration 0.22-0.98%) that utilizes mild temperatures (140-180°C), pressures (4-15 atm), and residence times ranging from 15 to 60 min (Balan et al. 2013). The main reaction that occurs is the hydrolysis of hemicellulose, especially xylan. Strong bases can be used to solubilize lignin by cleaving the lignin-hemicellulose linkages. Also, solvation and saphonication reactions cause biomass to swollen. Addition of concentrated alkalis as NaOH, KOH, or $Ca(OH)_2$ causes a "peeling" of end groups in biomass, what is an advantage for the later enzymatic hydrolysis. Alkali causes also some modifications on cellulose. It can change the cellulose structure to a form that is denser and thermodynamically more stable than the native

cellulose (process known as cellulose mercerization in the textile industry) (Sills and Gossett 2012) (Hendriks and Zeeman 2009). Sills et al. (2012) pretreated six substrates (two switchgrass cultivars harvested at different locations, big bluestem grass, a low impact high-diversity mixture of prairie biomasses, mixed hardwood, and corn stove) at three NaOH concentrations (5, 10, and 20 g NaOH per 100 g total solids). The sugar yield after enzymatic hydrolysis (15 FPU/g of glucan enzyme loading and 72 hours reaction) increased from around 10% of untreated substrates to around 65-75% for substrates treated with 20g NaOH per 100g total solids. Wet oxidation consists of the addition of an oxidizing compound, like hydrogen peroxide or peracetic acid, to the biomass suspended in water. This pretreatment is very lignin selective and proved very effective in boosting the yield of enzymatic hydrolysis. Pretreatment with 21% paracetic acid on hybrid poplar and sugar cane bagasses (120 hours reaction with enzyme *Spezyme/Novozym* 188 combination) increased hydrolysis yields from 6.8% (untreated) to a maximum of 98% (Teixeira et al. 1999).

Hybrid pretreatments: Thermal pretreatment in combination with acid pretreatment represents a hybrid approach to pretreatment. Lignocellulosic biomass is soaked with H_2SO_4 or SO_2 before steam pretreatment. The addition of the external acid catalyzes the hemicellulose solubilization , lowers optimal pretreatment temperature, and gives a better substrate for enzymatic hydrolysis (Hendriks and Zeeman 2009). Soderstrom et al. (2002) were able to obtained fermentable sugars yield of 80% from the enzymatic hydrolysis (96 hours) of softwood pretreated using the combination of SO_2 impregnation and steam. Thermal pretreatment in combination with alkaline pretreatment is another hybrid approach. A very common alkaline thermal pretreatment combines temperatures ranging 100-150°C with the addition of 0.1g $Ca(OH)_2$/g substrate. Ammonia-fiber explosion (AFEX) pretreatment is an approach currently being used by industry (Gollapalli et al. 2002). Ammonia is a weak alkali, and basic ammonia solutions (15%) selectively remove lignin.

Ammonia is used at high ratios of biomass (1-2g ammonia/g dry biomass) at 20atm and 100-120°C. Compared to acid pretreatment, the hemicellulose fraction is not significantly solubilized (Lau and Dale 2009). Chundawat et al. (2007) proved that AFEX pretreatment of a wide variety of particle sizes of corn stover improves sugar yields from 20% to about 80% at 72 hours reaction with Spezyme cellulases.

A hybrid process with high potential in terms of biomass transformations and cost efficiency is the one/two stages bi-phasic CO_2-H_2O pretreatment (studied by Professors Larry Walker and Jefferson Tester's research groups at Cornell University (Luterbacher et al. 2012). It brings together features of both chemical (with CO_2 acting as a mild acid catalyst) and thermal pretreatments. It is a novel pretreatment process that yields physico-chemical transformation of the lignocellulosic biomass macro and micro-structure. The physical evolution of biomass during this pretreatment has been studied using solid exclusion chromatography. Yang et al. (2014) (2015) observed the increase in pores size and surface area in mixed hardwoods and switchgrass pretreated using biphasic carbon dioxide and water at 200 bar and 210°C. Glucan to glucose yields above 80% were reported for the saccharification of mixed hardwoods and switchgrass pretreated using a two temperatures stage CO_2-H_2O (210°C, 1min followed by 160°C, 60min) (Luterbacher et al. 2012). The rationale behind using CO_2 as a weak acid for pretreatment is:

1. it is nontoxic (unlike ammonia),
2. it is nonflammable (unlike alcohols),
3. it does not cause degradation of sugars unlike steam explosion
4. it adds acidity to moist biomass that enhances pretreatment
5. it can be transported in solid (dry ice), liquid, and gas forms,
6. it is inexpensive,

7. it is readily available from the ethanol fermentation process, and
8. it presents a relatively easily achieved supercritical state

Enzymatic saccharification: The major goal of biomass pretreatment is to generate a substrate that is more amendable for enzymatic hydrolysis in order to achieve high sugar yields (concentrated solution of dissolved sugars, mainly monosaccharides). Cellulose is hydrolyzed by cellulases, which are modular proteins with at least two distinct modules: a catalytic domain and a carbohydrate-binding module attached via a flexible linker (Arantes and Saddler 2010, Kostylev and Wilson 2013). The efficient enzymatic hydrolysis of cellulose by cellulases requires a synergistic action of three groups of cellulases: endoglucanase, exoglucanase, and β-glucosidase. Endoglucanases randomly act internally on the amorphous regions of a cellulose polymer chain and generates oligosaccharides of different lengths for the exoglucanases action. They seem to have low or no processivity in the hydrolysis of the cellulose fiber, with the exception of some processive endoglucanases as Cel9A from *Thermobifida fusca* (Kostylev and Wilson 2013). Exoglucanases usually hydrolize cellulose in a sequential way starting from a side of cellulose chain, with cellobiose as major product (G2, two glucose molecules sugar). β-glucosidases have the role of hydrolyzing soluble sugars (oligosaccharides, G6-G2) into glucose. Most commercial glucanases are produced by *Trichoderma reseii*, and β-glucosidases from *Aspergillus niger* (Wu et al. 2010, Balan et al. 2013, Samayam and Schall 2010). Figure 1.2 shows the role for the different glucanases along with the degree of polymerization of cellulose and the relative speed of the different stages of enzymatic hydrolysis.

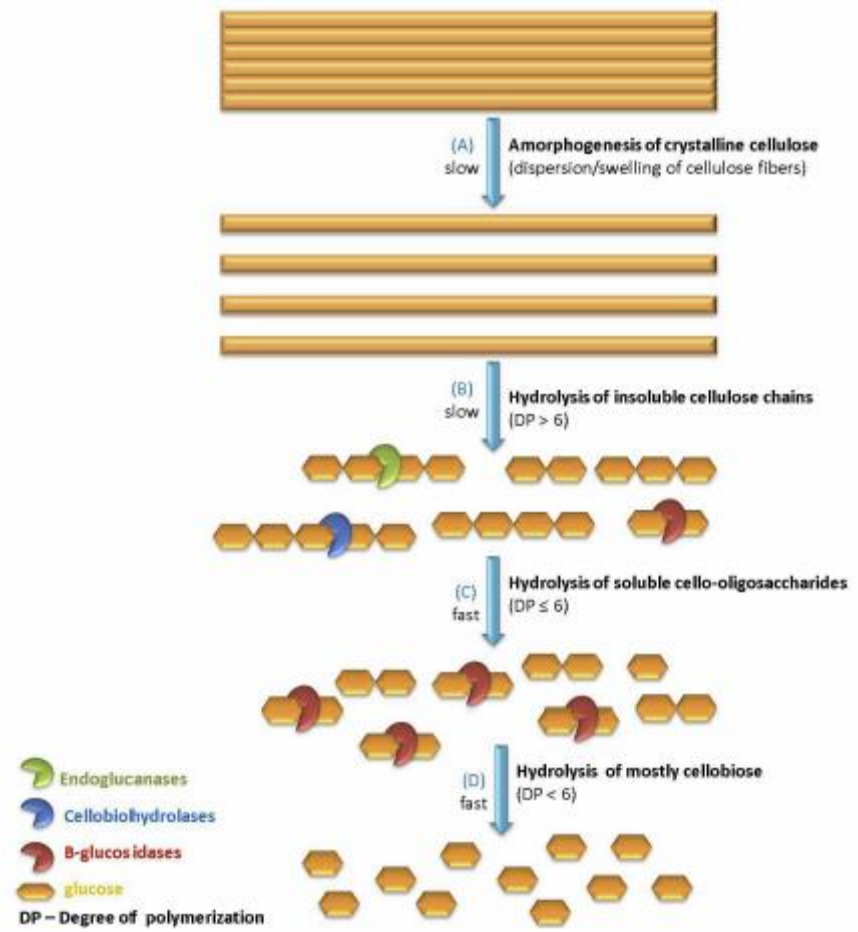

Figure 1.2. Enzymatic hydrolysis of cellulose (Arantes and Saddler 2010)

Kinetic modeling of enzymatic cellulose digestion is complicated by the insoluble and heterogeneous structure of the substrate, constantly changing over the course of the hydrolysis reaction (Kostylev and Wilson 2013). In order for cellulases to efficiently hydrolyze cellulosic substrates, they must first be able to access the polymeric chains, adsorb to them, and catalyze the depolymerization reaction. Many kinetic models for the enzymatic hydrolysis of cellulose have been developed and refined for over 30 years. The most common ones are based on a Michaelis-Menten model because this model is very successful in fitting experimental results. However, the Michaelis-Menten model is based on a number of assumptions (steady state reaction, and homogenous substrate) that are not physically realistic for the hydrolysis of cellulose (Kostylev

and Wilson 2013). In order to improve the use of Michaelis-Menten model for this process by capturing the time-dependent activity for the enzyme, Kostylev et al. (2013) proposed a two parameter model based on Michaelis-Menten, with reaction rate being time dependent. Empirical models have also be used to describe enzymatic hydrolysis. Some models relate the hydrolysis extent to the time and enzyme concentration using a power law, with coefficients and exponents dependent on cellulase source. Other models show the initial rate of hydrolysis of highly crystalline cellulose is proportional to the square root of time (Lee et al. 1980). There have been efforts to develop mechanistic models that seek to combine the kinetic of hydrolysis with the mass transfer/diffusion of the enzyme using mass balance equations for enzyme in solution, surface bound enzyme, and biomass density in the accessible fraction of the substrate (Luterbacher et al. 2013).

An actual subject of debate in enzymatic hydrolysis of biomass is the reason for the nonlinear kinetics observed in this cellulase-cellulose reaction system (sugar yield vs. hydrolysis time at a given enzyme concentration results in a hyperbolic curve that reach and asymptotic constant value of yield). This nonlinearity poses a challenge for the comparison of cellulases relative effectiveness on the rate and extent of reaction. From the industrial point of view, the goal is to obtain the highest yield with the lowest enzyme cost. The understanding of this nonlinear behavior may yield insights into ways to increase biomass saccharification efficiency using cellulases and other cell-wall degrading enzymes. There is still a debate about the reason of this behavior: enzyme inactivation, product inhibition, or substrate heterogeneity.

Sugars fermentation: After biomass is hydrolyzed into glucose (a 6 carbons sugar (C6) from the cellulose fraction) and xylose (a 5 carbons sugar (C5) from the hemicellulose fraction), they are fermented to different molecules using microorganism. Yeast, (*Saccharomyces cerevisiae*) which

is commonly used in the fermentation of C6 sugars obtained from sugar cane and corn, cannot ferment C5 sugars without extensive genetic engineering. Therefore, the fermentation process for lignocellulosic products requires two different microbial conversion processes or genetically-engineering microorganisms for the C6 and C5 sugars (*E. coli, Zynomonals mobilis, Pichia stipites, Thermoanaerobacterium saccharolyticum, and S. cerevisiae*). Mascoma Corporation is developing a process called consolidated bioprocessing (CBP) where lignocellulosic biomass is converted into ethanol in a single step combining enzyme production, hydrolysis, and fermentation (Hasunuma et al. 2013).

1.3 Thermochemical routes for organic waste valorization

Thermochemical conversion technologies degrade plant and waste biomass by thermal break down of complex molecules, with or without catalyst. It involves biomass deconstruction and upgrade of intermediates into a range of fuels and chemicals. It allows the efficient use of a broad range of feedstocks, ensuring supply across seasons, and potential energy security across regions. However, the variation of feedstock composition requires adjusting the parameters of the technology and causes modifications in the distribution and quality of products obtained. This variability in raw materials and operation conditions is not recommendable if the goal is to produce commodities with predictable properties in a consistent manner (NREL 2014). Therefore, to find a consistent and reliable feedstock composition, blending of wastes obtained from different sources and produced at different rates is an actual topic of research.

Thermochemical conversion of biomass and organic waste has been classified into three main groups: Combustion, pyrolysis, and hydrothermal technologies (Tekin et al. 2014, Elliott 2011).

1.3.1 Combustion

Biomass combustion is the oldest known source of heat and light known by humans. In fact, combustion is the simplest method for the generation of heat and electricity from biomass. The process of dried biomass combustion can be divided in three steps: devolatilization to char and volatiles (including depolymerization, and condensation reactions), combustion of the volatiles, and combustion of the char (Williams et al. 2001). The energy released upon combustion depends on the moisture and ash content, and elemental composition of the biomass. As combustion is an oxidative process of carbon, the more carbon a substrate has, the more energy content can be released by combustion. The biomass energy content can be characterized by the higher heating value. The heating values of the majority of biomasses range in between 10-20MJ/kg (Williams et al. 2001), with a decrease of about 0.2MJ/kg per 1% increase in ash content (Tekin et al. 2014). This technology is not suitable for wet substrates (moisture content above 30%), as the first step in the process requires drying the material, what consumes a great deal of energy considering the high latent heat of water (2.26MJ/kg). In addition, temperature of flame front decreases as moisture content increases, decreasing the heat generation (Liang et al. 2008). In fact, it has been reported that wet substrates with moisture content above 90% have a negative net energy production as the energy needed to evaporate water is higher than the calorific energy of the material (Tekin et al. 2014). Apart from this drawback, which makes combustion a non-efficient technology for valorization of wet organic wastes, combustion only exploits the energy potential of biomass into heat. It does not exploit the full added value of the chemistry and functionality of the biomass resource. Instead, the combustion of biomass generates greenhouse gases, and other harmful emissions (particulates, dioxins, etc.) which leads to tighter legislation for post-combustion

scrubbing of the gases (adsorption of harmful chemicals with catalysts) and disposal of the ash. This decreases the economical attractiveness of combustion technology (Verma et al. 2012).

1.3.2 Pyrolysis / Carbonization/ Torrefaction

Pyrolysis, carbonization, and torrefaction technologies can be defined as the thermal degradation of biomass at mild/high temperatures under inert atmosphere at atmospheric pressure (N_2, Ar) (Cantero-Tubilla et al. 2016). These technologies differ from combustion in that they are not oxidative processes. Their main differences are in the range of process temperatures and the product distribution yielded. Pyrolysis is done at temperatures between 350-650˚C, yielding a liquid fuel. Gas and solid fractions are considered by-products of the process. Torrefaction occurs at lower temperatures (200-350 ˚C) generating an energy-dense solid biofuel, and treating gases and liquids as by-products.

Pyrolysis can be classified into slow pyrolysis (carbonization), fast pyrolysis, and flash pyrolysis. Carbonization (slow pyrolysis) combine high temperatures with long residence times to produce a biochar. Fast pyrolysis requires heating rates above 10 to 200 ˚C/s and residence times below 2 seconds. Flash pyrolysis involves heating rates of 10^3-10^4 ˚C/s and residence times below 0.5 seconds (Kan, Strezov, and Evans 2016). These different reaction conditions influence the bio-oil yield. The fast pyrolysis results in bio-oil, gas, and char yields of 60–70 wt%, 13–25 wt%, and 12–15 wt% (dry weight), respectively. On the other hand, flash pyrolysis yields higher bio-oil (>75wt%) and less gas and char (12-13 wt%) (dry weight). Different types of reactors have been used in the pyrolysis of biomass including bubbling fluidized beds, circulating and transporting

fluidized beds, rotating cones, ablative pyrolysis, entrained flow reactors, vacuum pyrolysis, fixed beds, and microwave pyrolysis. (Bridgwater 2017).

The bio-oils obtained from biomass pyrolysis are not suited for direct use in diesel engines for long term, due to their high viscosity, poor volatility, high corrosiveness and tendency to generate coke as they are thermally unstable. Therefore, upgrading of bio-oils is a necessary step. Considerable research is underway focused on upgrading the oil through the identification of catalysts for hydrocracking and hydrodeoxygenation reactions (Adjaye and Bakhshi 1995, He and Wang 2013).

Pyrolysis of wet feedstock with high moisture content will generate a bio-oil with high water content. Therefore, drying the feedstock prior to pyrolysis (water content below 10% w.b) is required, what constitutes an energetic sink for the pyrolysis process (Wang et al. 2007).

1.3.3 Hydrothermal technologies

The high water content in organic wastes generated from different industries limits the variety of processing technologies suitable for the valorization of these wastes. As previously mentioned, combustion and pyrolysis require a prior drying of the substrate biomass to capture its full value. In the biochemical routes, the separation of water from the bio-ethanol requires distillation. This necessity for water removal can consume much of the energy contained in the biomass in the form of latent heat of evaporation. Therefore, new technologies, such as hydrothermal processing, that uses liquid water as a valorization reactant are receiving more attention by the chemical industry.

Hydrothermal technologies work under pressure to keep hot water in liquid state (always above saturation pressure of water at the temperature of interest, or above the critical pressure when

working in supercritical conditions). Pressurized hot liquid / supercritical water displays very interesting reaction properties as shown in Table 1.3. The decrease of viscosity and density with temperature increases the diffusion coefficient, leading to a decrease in mass transfer limitations and an increase in overall reaction rate (heterogeneous processes are processes in series where the limiting factor is the step with lower rate; usually mass transfer related processes). Viscosity decreases from 0.89 mPa s at room conditions to 0.11 mPa s at 250˚C and 5MPa (Tekin et al. 2014). On the other hand, the ionic product of water ($pKw = -\log_{10}([H_3O^-][OH^-])$) increases three order of magnitudes below the supercritical conditions of water (374˚C and 22MPa) (Abu Tayeh et al. 2016), presenting a maximum plateau around 250-300˚C. This increase in ionic product allows water to participate in acid-base reactions by acting as protons and hydroxyl ions source. The dielectric constant of water is high at ambient conditions. This is because the hydrogen bonding in the water structure, which avoids the miscibility of non-polar substances at ambient conditions. As the temperature increases, the dielectric constant of hot pressurized liquid water decreases, allowing water to behave as a non-polar solvent, and dissolving organic compounds. This, together with the favorable reaction kinetics of organic compounds above 250˚C, makes the hydrothermal medium very well suited for organic compounds valorization (Tekin et al. 2014, Peterson et al. 2008). Pressurized hot liquid water also presents higher thermal conductivity and heat capacity compared to room conditions. Thermal conductivity increases from 608 to 620 mW m^{-1} K^{-1} and heat capacity increases from 4.22 to 4.86 kJ kg^{-1} K^{-1} when water is heated up and pressurized from room conditions to 250˚C and 5MPa (Tekin et al. 2014).

Table 1.3. Evolution of properties of hot pressurized water as a function of temperature at constant pressure. This evolution of properties of pressurized liquid water makes it an attractive media for HTL (Peterson et al. 2008)

	Ambient water (0.1MPa)	Sub-critical water (30MPa)	Super-critical water (30MPa)
Temperature (˚C)	25	150-374	374-500
Density (g cm^{-3})	0.997	0.95-0.6	0.6-0.12
pK_w	14	11.4-11.5 (plateau at 11 at 275˚C)	11.5-17
Dielectric constant	78.5	48-12.5	12.5-2.5

The hydrothermal technologies yield four phases: a solid phase (hydro-char), gas, bio-oil, and aqueous phase. The separation of these phases can be controlled by tuning the solvatation properties of water. However, in real industrial practices the separation of bio-oils from aqueous phase requires organic solvents as dimethyl-chlorine and ethyl acetate (Posmanik et al. 2017, Tekin et al. 2014). If these solvents are not bio-based, but based on the oil industry, separation of phases will contribute negatively to the environmental effects evaluated in a life cycle assessment (Tuck et al. 2012).

Hydrothermal processes can yield a wide distribution and quality of products depending on the feedstock composition, reaction time, catalyst, water to biomass ration, and the temperature of the process (Tekin et al. 2014, Yin et al. 2010). For example, the amount of hydro-char recovered can be related to the amount of lignin in the feedstock (Déniel et al. 2016). Hydrothermal liquefaction technologies can be classified depending on the temperature and pressure of the process in: hydrothermal carbonization (HTC), aqueous phase reforming (APR), hydrothermal liquefaction (HTL), and hydrothermal gasification.

At temperatures between 150-250˚C and pressures around 2.5MPa, hydrothermal carbonization yields a hydro-char with properties similar to a low quality coal. These solids are mostly made of degradation products of hemicelluloses and lignin. Studies have shown that hemicelluloses and

lignin are rapidly hydrolyzed at temperatures above 180 and 200˚C respectively. On the other hand, cellulose requires at least 250˚C to start hydrolysis. At the HTC conditions, proteins and lipid fractions remain intact. Proteins start hydrolyzing at 250˚C, and aminoacids degrade rapidly above 300˚C. With respect to lipids, triglycerides hydrolyze above 280˚C (Déniel et al. 2016, Elliott et al. 2015, Peterson et al. 2008). The hydro-char generated is valuable as solid fuel and energy storage, as the heating value is higher compared to the feedstock, for soil amendment or fertilizer, as important nutrients, such as P and various N compounds are concentrated and can be recovered from this phase (Déniel et al. 2016).

In a very narrow window of temperatures between 215-265˚C and pressures around 10MPa, APR produces hydrogen used to hydrogenate biomass degradation products through heterogeneous catalytic reactions over precious metals (Déniel et al. 2016, Kruse 2009). This process is also known as subcritical hydrothermal gasification.

At higher temperatures and pressures (250-370˚C and 10-30MPa), hydrothermal liquefaction is the technology suited for the production of bio-oil. The composition of feedstock affects the bio-oil yield in grand extent. It has been reported that the yield of bio-oils is higher in feedstocks rich in lipids, followed by feedstocks rich in proteins. Lastly, carbohydrates rich feedstocks yield the lowest bio-oils (Vardon et al. 2011). The bio-oil obtained from HTL is a complex mixture of compounds (Elliott et al. 2015), that is determined by the composition of the feedstock (more protein can yield more nitrogenous compounds, undesired in the bio-oil composition). Compared to the biomass substrates, bio-oils present higher carbon and less heteroatoms content (especially oxygen, decreasing from 30-50% in the feedstocks to 10-20% in the bio-oil), and higher energy content (upgraded from 10 to 20MJ/kg in the feedstock to 30-36 or even 40 MJ/kg). More condensation reactions occur in HTL media than in fast pyrolysis, resulting in a bio-oil with less

oxygen content, higher carbon content (%wt), and therefore, higher heating content (35.7 vs. 22.6 MJ/kg) (Peterson et al. 2008, Elliott et al. 2015). Compared to the characteristic of bio-oils obtained from pyrolysis, hydrothermal liquefaction bio-oils are more viscous (15,000cps vs 59cps) and less dense than fast pyrolysis bio-oils. Nevertheless, similar to fast pyrolysis bio-oils, hydrothermal liquefaction bio-oils need to be upgraded through hydrodeoxygenation, or reduction over metals supported on ceramic catalysts, such as zeolites. However, it was reported that these upgrading processes are simpler in comparison to those needed for fast pyrolysis bio-oils (Peterson et al. 2008). Gas phase (rich in CO_2 from condensation and decarboxylation reactions), aqueous phase, and hydro-char produced by HTL are considered by-products of the process. Considerable research has been conducted in the last years towards understanding and characterizing these phases to reveal critical HTL reaction mechanisms. In addition, it is important to find niche markets for the generated by-products, in order to obtain the fully added value of the biomass resource. For example, Renmatix recovers pentose and hexose sugars from hemicellulose and cellulose respectively via two-step hydrolysis in high-temperature water (Tuck et al. 2012). Some research groups in California, Riverside are interested in water recovery from the HTL aqueous phase using membrane technology (Duan et al. 2016) .

Above the supercritical conditions of water, hydrothermal gasification takes place, resulting in the production of a synthetic fuel gas that contains H_2, CH_4, CO, CO_2, and light hydrocarbons in ratios depending on the temperature of the process. Therefore, three types of hydrothermal gasification can be distinguished: high temperature gasification to hydrogen (around 600˚C, carbon from biomass is mostly converted into CO_2) and lower temperature gasification to methane (around 400-500˚C, catalyst are generally needed for activity and selectivity). In these processes, no char

is produced (apart from the ash that the feedstock originally had, that could potentially act as a catalyst of the process depending on the inorganic composition).

The thermochemical technologies for biomass valorization reviewed in this section have several technical drawbacks including heating requirements, and a higher capital costs resulting from operation high pressures. In particular, higher capital costs for the hydrothermal gasification are a result of special alloys required for the process reactors and other parts of the system (Kruse 2009). To overcome the initial high capital costs, there is the option of short-term subsidization of the technology, or the financing of the equipment through a co-operative fashion. In this model, a group of industries or farms generating organic waste would come together to set up a thermochemical valorization facility. They would blend their wastes at a ration that maximize the production of bio-oil (or at the ration needed for the sometimes seasonally generation of waste), and share the potential benefits obtained from the generation of products. Apart from the economic benefit, these companies will be actively pursuing environmental responsible industrial practices that could attract environmentally committed investors.

Another disadvantage of hydrothermal processes is the large volume of water that needed to be heated to reaction temperatures. For example, the heat necessary to reach, 600˚C may exceed the energy content of the biomass at a water content higher than 80% (w.b) (Kruse 2009). However, this is still more advantageous than drying the substrates, as the specific heat of water is three order of magnitudes smaller than the latent heat of vaporization. This heat requirement drawback can be significantly mitigated by adopting comprehensive heat integration strategies, where the heat of output streams can be used to preheat input streams, to warm auxiliary utility lines, and to cool down systems by evaporative cooling. This means the necessity for the installation of efficient

heat exchangers. High-pressure heat exchangers have been proposed for these applications, as they are compact and relatively efficient.

1.4 Comparison between biochemical and thermochemical technologies for biomass valorization

As reported by Verma et al. (2012), thermochemical valorization technologies present advantages over biochemical processes. The fact that biochemical routes use microorganism and enzymes restrict the variety of feedstocks suitable for this technology compared to thermochemical processes. Even more, feedstocks need to be conditioned to make them suitable for the enzymatic action (pretreatment of the feedstock (Luterbacher et al. 2012), washing (Chundawat et al. 2007) etc.). These extra steps hinders the economic feasibility of the technology. Thermochemical processes are more productive than biochemical processes as they require, in general, less residence time. The reason for this is that biochemical processes present productivity issues associated to the biological mechanisms. For instance, the kinetics of hydrolysis of cellulose by cellulases presents a drop-off that limits the yield of digestion. In terms of the versatility of products obtained, the fact that enzymes and microorganism cannot easily degrade lignin (the structural part of biomass, accounting for around 10-25% of lignocellulosic biomass making it the second most abundant natural polymer after cellulose (Watkins et al. 2015)) narrows the distribution of products obtained compared to thermochemical technologies. This may change in the future, thanks to the advancement in genetically engineered microorganism and enzymes. In fact, recent reports have shown the non-selective adsorption of cellulases on lignin structures, what has a negative effect in hydrolysis yields (Converse et al. 1990). In addition, biochemical technologies generate secondary wastes that need to be processed. In terms of residence time for

the process, thermochemical processes present higher cellulose hydrolysis rate (few minutes or seconds vs. several hours) (Prado et al. 2017).

As mention in section 1.3, thermochemical technologies present also drawbacks in terms of heating requirements, and capital costs, being those larger than for biochemical technologies.

1.5 Chemicals recovered from organic waste and their economic value

The arrangement of carbon atoms in waste biomass has the potential to be easily deploy products of an equivalent or superior quality to the fossil-based products (Carole et al. 2004). This has to do with the high chemical complexity and functionality that waste biomass have, compared with the fossil based carbon sources (Sanders et al. 2007). In this section, the valuable products that can be obtained from biomass will be classified in four categories; products obtained from degradation of polysaccharides, lignin, triglycerides, and proteins.

1.5.1 Possible products obtained from polysaccharides

The traditional way of transforming sugars from biochemical valorization of lignocellulosic biomass has been through fermentation to ethanol, butanol, and lactic acid. Ethanol and butanol can be used as fuel additives (Ritter 2013). Lactic acid has an actual worldwide demand of 130,000-150,000 tons per year, and predicted to increase as it can be used as monomer for the production of poly-lactic acid (a renewable plastic) (Ghaffar et al. 2014, Lim et al. 2008).

Thermochemical technologies for biomass valorization go beyond the depolymerization of polysaccharides into reduced sugars, but degrade the sugars into other valuable products. Figure 1.3 shows the different reactions pathways for sugars under hydrothermal conditions. Retro-aldol, condensation, decarboxylation, and hydrogenation reactions can transform the sugars to platform

chemicals, and even to alkanes. Furfural and hydroxymethylfurfural (5-HMF) can be obtained in hydrothermal liquefaction process at acid pH through the catalytic dehydration of pentose and hexose sugars, respectively, as seen in Figure 1.3 (Yin et al. 2010). Unlike sugar-based fermentation products, which have been depleted of original functional groups, furfural and 5-HMF conserve most of the original chemical complexity of the feedstocks. Therefore, they are considered platform chemicals (building blocks for the synthesis of bio-based products with the potential to be converted to high-tonnage products) (Tuck et al. 2012) as presented in Figure 1.4 . Furfural, and 5-Hydromethylfurfural (5-HMF) can be used in the industry as solvents or precursors for pharmaceuticals, thermoresistant polymers, etc (Prado et al. 2017). The production of carboxylic acids in the HTL is also important, as succinic acid and levulinic acid are included with lactic acid, HMF and furfural in the "top 10" biobased products from biorefinery carbohydrates by the US Department of Energy (Bozell and Petersen 2010).

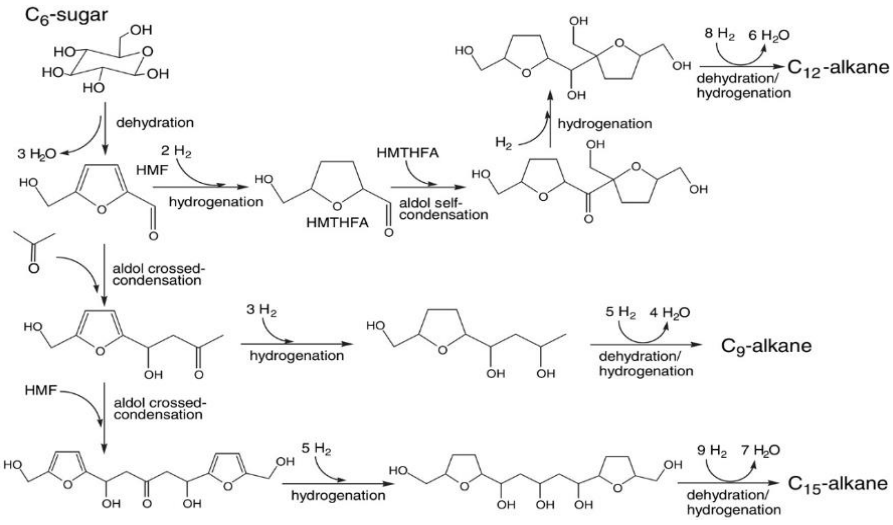

Figure 1.3. Glucose from enzymatic hydrolysis of biomass can be transformed into platform chemicals and liquid fuels (Huber et al. 2005)

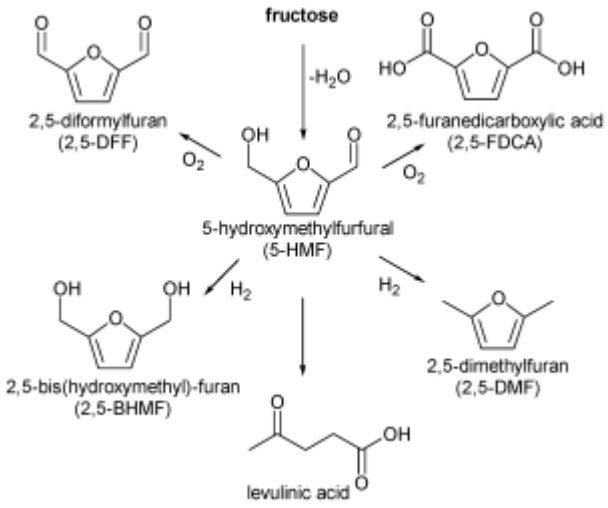

Figure 1.4. Different examples of reactions that can convert 5- HMF into valuable chemicals (Gallezot 2012)

Alkanes can also be produced in the HTL process through Fischer-Tropsch synthesis from CO and H_2 reaction. Hydrogen is produced from cattle manure when the conversion temperatures are higher than 260˚C, using N_2 as process gas. This synthesis gets promoted by the catalytic effect of the reactor walls (Fe and Ni) (Yin et al. 2010).

1.5.2 Possible products obtained from lignin

Lignin is the second most abundant bio-polymer (after cellulose), and the largest renewable feedstock that comprises aromatic structures. This is very important because key commercial chemicals are aromatic compounds (Tuck et al. 2012). Lignin is a three-dimensional amorphous cross-linked polymer of phenylpropanoid units (p-coumaryl, sinapyl, and coniferyl), linked by ether and C-C bonds as shown in Figure 1.5. It makes up 10-25% of lignocellulosic biomass, being able to reach even 30% for grasses. It provides structural resistance to plants, and protects the cellulose from animals and microorganisms.

Lignin currently is under-utilized in the processing of biomass feedstocks. In most biochemical valorization routes, lignin is removed in the pretreatment step, and used as an energy source for

the separation of fermentation products (burnt in the distillation boiler). Breaking lignin into useful chemicals is challenging. New catalysts are being discovered for this purpose (Tuck et al. 2012). The preferred route for lignin chemical exploitation is cleaving ether bonds that hold the structure of the macropolymer together, producing water-soluble phenolic derivatives that can be upgrade to bio-products (Zakzeski et al. 2010).

Possible lignin-derivated products are: activated carbon, binders (Yin et al. 2010), carbon fibers (Mainka et al. 2015), motor fuel, phenol derivatives (and antioxidants very appreciated in the pharmaceutical, cosmetic, and food industry), plastic materials (in combination with petrol derivatives to make the plastic more biodegradable), sorbents, etc (Lignimatch 2009).

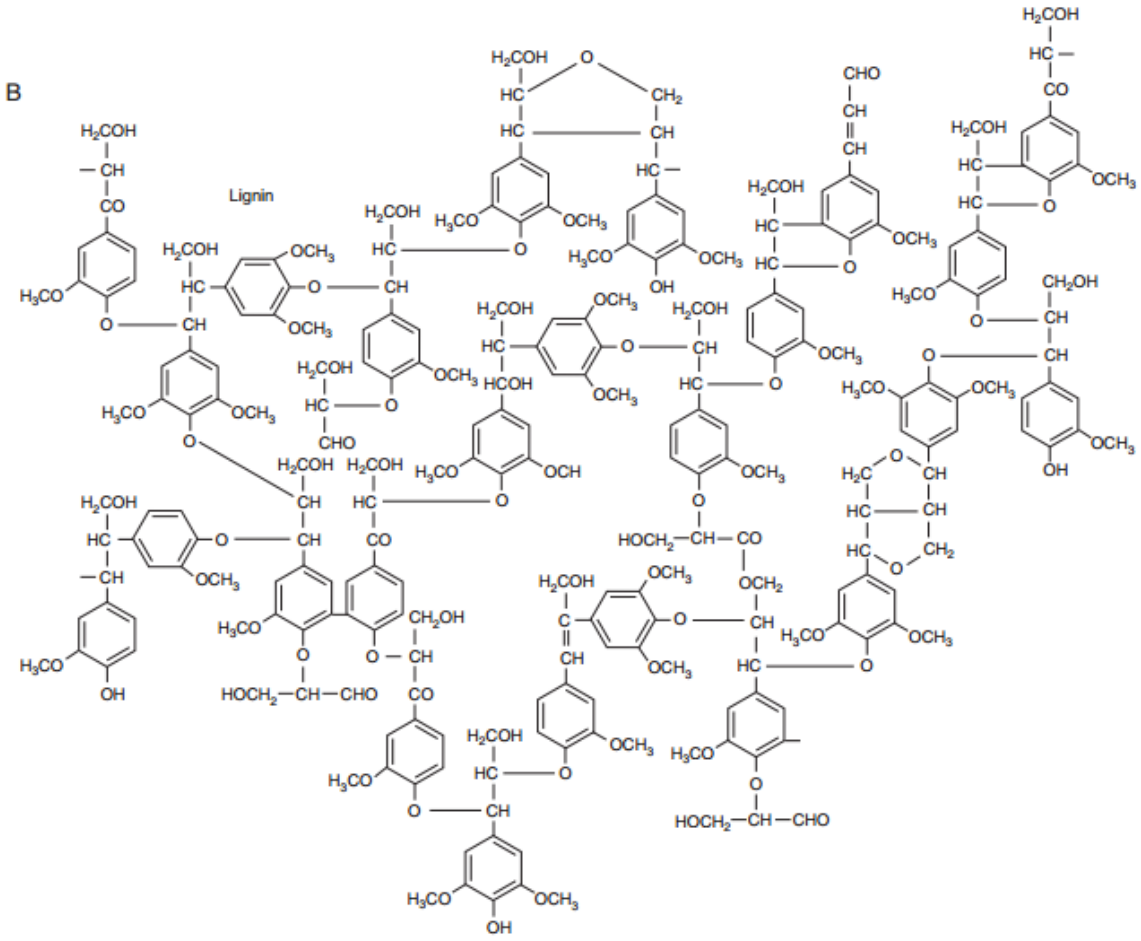

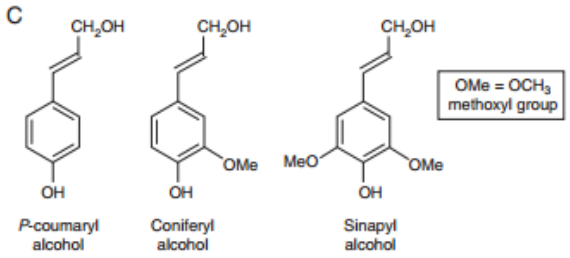

Figure 1.5. Lignin is a polymer with a complex structure. However, its high aromatic structure makes it very attractive for the chemical industry (Watkins et al. 2015)

1.5.3 Possible products obtained from proteins

The use of proteins from biomass valorization has been less explored than carbohydrates and lignin (Gallezot 2012). However, amino acids have a higher commercial value than other fractions of biomass (Peterson et al. 2008) as they are the only biomass components source of nitrogen. Two groups of amino acids can be distinguished: essential amino acids (cannot be synthesized by the body, so they have to be consumed from food), which are highly valuable in the food and pharmaceutical industry and non-essential amino acids that can be used as chemical feedstocks for fine and specialty chemicals in the cosmetic industry. All amino acids have a carboxylic acid and amine groups that can be reacted to produce highly functionalized chemicals, as derivatives of amines and diamines. In fact, amino acids' chemical composition and structure to important industrial chemicals, as ethylamine or acrylamide (Scott et al. 2007). Considering the future trends for valorization of feedstock rich in protein, it is expected that the availability of proteins will increase, and, therefore the price paid per ton of protein will decrease. There are estimations that 100 million tons of protein-rich waste could be produced every year if 10% of the global fuel demand were fulfilled by bioethanol and biodiesel (Kumar et al. 2015). Hence, it is expected that this generation of waste rich in protein will bring down protein price to $100-200 per ton. These expected low prices for protein will make the amino acids isolation and purification processes more economically attractive (Scott et al. 2007).

1.5.4 Possible products obtained from lipids

Fats and oils present in biomass are similar in chemical structure to traditional transportation fuels. They are non-polar, long aliphatic molecules typically containing carboxylic acid functionalities. However, in biomass, lipids are bound to a glycerol molecule forming triacylglycerides. Therefore, the first step for the production of free fatty acid that can be upgraded to bio-oils is the thermal split of triacylgycerides, that is reported to occur around 250˚C and 5MPa (Peterson et al. 2008). This is followed by the breakdown and reformation of free fatty acids to produce bio-crude oils (carboxylic acids, straight and branched aliphatic chains, esters, etc.). However, bio-crude also incorporate compounds from the degradation of proteins, carbohydrates, and lignin (aromatic compounds, phenol derivatives, nitrogenous ring structures etc.) what are not desired for a transportation fuel. In fact, the yield and quality of bio-crude is influenced by the ration of protein, lipids, and carbohydrate in feedstock. Higher lipid content feedstocks produce higher quality and yields bio-crudes. The bio-crude generated in thermochemical conversion processes of biomass are higher in oxygen and nitrogen content than desired for transportation fuels applications. The higher protein content in feedstock results in more nitrogen compounds in the bio-crude. On the other hand, the oxygen content in the bio-crude is lower than in the feedstock, what contributes to increase the energy content of bio-crude compared to feedstocks. The presence of heteroatoms in the bio-crude yields undesired qualities such as oil acidity, polymerization and coke formation, high viscosity, and high-boiling distribution. Furthermore, the high distribution of compounds in the biocrude (characterized in literature using Gas Chromatography-Mass Spectroscopy techniques) affects the combustion performance, storage stability, upgrading response, and ultimately, the economic value (Vardon et al. 2011). Therefore, bio-oil obtained from thermochemical conversion processes of biomass needs to be upgrade to decrease heteroatoms content, and narrow the distribution of compounds. This also represents an opportunity to extract

from the biocrude composition those molecules with low energy content interest, but high appreciation as platform chemicals (as furans).

1.6 Overview of feedstocks valorized in this work

Organic wastes from waste water management plants, dining halls, dairy, alcohol, and olive oil industry have been valorized in this project. These wastes were chosen because of their local availability, high water content, and the necessity for finding alternative routes for their management (that overcomes their potential environmental harm and, at the same time, can save money on disposal, or even generate valuable products and money inflow for the generating industry). It has been reported in literature that the wastes generated in the beverage, food, and agricultural industry are the best candidate for biorefinery feedstock, because of its size, reliable continue supply, and nutritive content (Zacharof 2016).

1.6.1 Manure

Cow manure refers to the mixture of feces and urine in a ratio of 3:1 (Gupta et al. 2016). It is a waste with high moisture content (13-15% solids) and is available in large quantities. Dairy cow produces between 45-50 kg of manure per day, the dairy industry in USA (with 9.35 million heads estimated for 2017) is responsible for the production of 175 million tons of manure per year (World Bank 2015, National Agricultural Statistics Service (NASS) 2017). Table 1.4 shows the average composition of different types of manure collected from 11 dairy farms in Central Valley (Ca) (University of California Cooperative Extension 2013). The high nutrient contents makes it a good fertilizer. However, the high organic content poses a challenge in terms of uncontrolled disposal.

Table 1.4. Median composition of different kind of manures (corral, pond solids, mechanical screen solids, and compost) collected form 11 dairy farms in Central Valley (Ca) (University of California Cooperative Extension 2013)

Property	Unit	Median	Minimun	Maximun
Volatile solids	%dry wt.	72	35	89
Total carbon	%dry wt.	35.6	18.1	43.9
Total N	%dry wt.	2.1	1.2	3.5
C:N	------	16.1	9.3	33.4
NH4-N	mg/kg dry wt.	1,346	13	6,282
NO3-N	mg/kg dry wt.	9	<1	312
Total P	%dry wt.	0.41	0.18	1.99
Total K	%dry wt.	0.57	0.15	4.37
pH	------	7.8	6.6	9.0
Conductivity	mS/cm	4.1	1.7	36

Traditional uses of manure include fertilizer, heat source for cooking, and construction material that provides good isolation (Gupta et al. 2016).

A proper manure management system is necessary to avoid adverse environmental effects, and to exploit the uses of manure as a source of energy and nutrients. Uncontrolled manure disposal (due to lack of managing systems or over-production) has negative effects in the soil, water, and air systems (Verma et al. 2012). Manure can degrade the soil quality by excessively increasing the concentration of potassium and phosphorous. In addition, potential run-off from soils can lead high nutrient loads in water streams or underneath aquifers, what can lead to eutrophication of the water sources. In addition, pathogens can be spread (Nasiru et al. 2013). Air quality can also be affected by the emission of odors, methane, and ammonia. Ammonia emissions also lead to excess of nitrogen in water reservoirs and soil acidification. Methane is one of the main greenhouse gases, that is partly responsible for climate change (Natural Resources Conservation Service 1995).

The semi-solid consistency of manure poses a handling challenge as it is too thick to pump, but too thin to spoon (Larimar et al. 2005). Depending on the application, manure can be mixed with

water to form a slurry that is pumped to an anaerobic digester for the production of methane, which can be converted into electricity. On the other hand, manure can be sun-dried to be used as bedding or to facilitate its transportation and land application. Lately, concerns have been raised on the fate of antibiotics given to cows and their subsequent appearance in the manure where it eventually is transported into the soil, or water through the manure runoff application (Reardon 2014).

Novel uses of manure are being currently investigated, in an effort to exploit its high fiber content: fabrication of paper, bio-polymers, and fabrics. The goal is to manage manure surplus from farms (manure management is a limiting factor to increase cattle heads in a farm) while producing an extra source of income for the farmer.

1.6.2 Waste activated sludge

Waste activated sludge, or simply known as sewage sludge or biosolids, are the solid or semi-solid organic material generated as a byproduct in a wastewater treatment plant (Department of Environmental Conservation 2015). Their disposal is one of the most expensive problems faced by wastewater plants (Egemen et al. 1999), mainly because of their high rate of production. In the state of New York, there are 642 publicly-owned treatment works (POWTs), 586 of which produce sewage sludge. They produce 1,000 dry tons of biosolids per day (Department of Environmental Conservation 2015).

The activated sludge from the primary settling in a waste water treatment plant is directed to a two stages digestion: in the first step (primary digestion) the raw sludge is heated to mild temperatures to accelerate biological conversion. In the secondary digestion, the mixture undergoes further digestion without mixing (to promote phases separation) or extra heating (Department of

Environmental Conservation 2015, Darmouth Engineering 2013). The settled sludge from both digestions tanks is thickened by dewatering using a variety of technologies (drying beds, belt filter press the most common, used by 26.2 and 22.4% of the POTWs in the state of New York, respectively). Centrifugation technology is only used in 26 POWTs (4% of POWTs), however, in terms of throughput, it dries almost a third of the state's waste sludge (Division of Materials Management Department of Environmental Conservation 2011) . The main goal is to reduce the volume of material to decrease transportation and disposal expenses. Nevertheless, dewatering is an energy intensive process, so, every effort oriented to minimize dewatering requirements will translate in substantial savings in utilities expenses for the POWT. An optional sludge stabilization phase reduces the level of pathogens, eliminates bad odors, and reduces the putrefaction potential. Figure 1.6 depicts a schematic of a sewage treatment process, and the treatment of activated sludge.

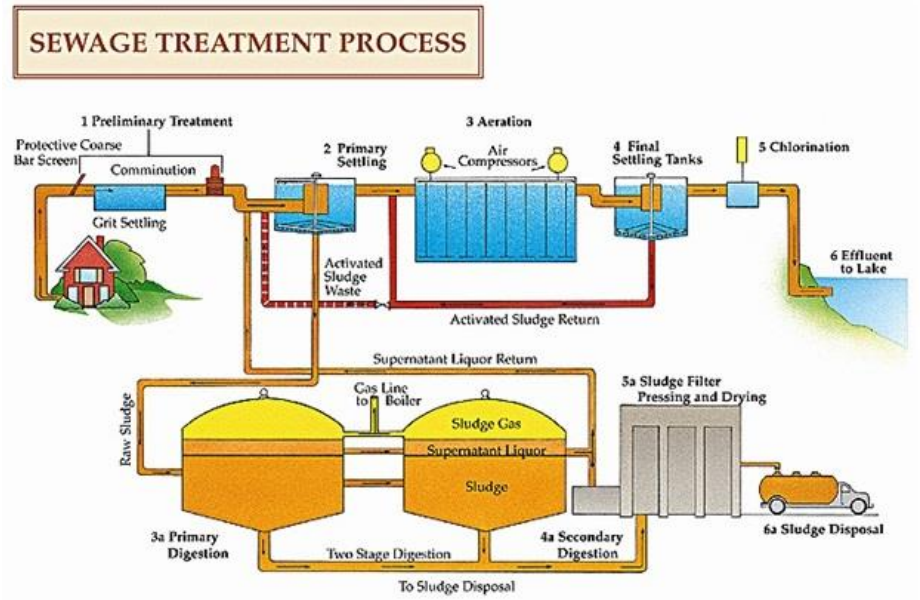

Figure 1.6. Schematic of a sewage treatment process (Department of Environmental Conservation 2015)

Table 1.5 shows the mean composition of the biosolids produced in New York POTWs. The high organic content and heavy metals poses a challenge in terms of biosolids disposal.

Table 1.5. Mean composition (dry weight basis) of biosolids from NY POWTs (Division of Materials Management Department of Environmental Conservation 2011)

Parameters	Unit	Median	Mean	Standard Deviation
pH	s.u.	7.30	7.50	1.25
Total Solids	%	21.40	19.11	10.41
Total Volatile Solids	%	61.20	60.96	11.43
Total Kjeldahl Nitrogen	%	4.90	4.51	2.05
Ammonia Nitrogen	%	0.90	1.06	0.87
Nitrate Nitrogen	%	0.10	0.10	0.00
Total Phosphorous	%	1.75	1.93	1.10
Potassium	%	0.10	0.2	0.16
Arsenic	mg/kg	5.60	8.91	8.56
Cadmium	mg/kg	3.60	4.46	4.33
Chromium	mg/kg	37.10	43.07	26.96
Copper	mg/kg	592.00	572.49	247.55
Mercury	mg/kg	1.10	1.39	1.04
Molybdenum	mg/kg	7.90	11.06	13.70
Nickel	mg/kg	19.50	24.63	20.24
Lead	mg/kg	59.40	90.29	93.02
Selenium	mg/kg	7.80	11.55	10.27
Zinc	mg/kg	832.00	888.56	540.62

In terms of management of this waste, landfilling is the most popular method, chosen by 321 POTWs (managing 52% dry weight basis of the total production of biosolids in the state of New York). Transportation of biosolids to landfills, together with the disposal fee makes landfilling an expensive option. The use of biosolids for direct land application (soil amendment), composting, chemical stabilization, and heat generation for drying, accounts for 30% dry weight of all the biosolids (117 POTWs use this option). Lastly, 13 % of the biosolids are incinerated (78 POTWs). Other options of disposal are used by 70 POTWs (12% of biosolids) (Division of Materials Management Department of Environmental Conservation 2011). Many municipalities are currently evaluating long-term management practices of these biosolids.

The main environmental challenge associated to landfilling or direct land application of this waste is the risk of the incorporation of adsorbed hydrophobic substances from the waste water streams, into the soil, rivers and streams, and aquifers (Miao et al. 2005). Recent studies have measured the levels of Triclosan in soils amended with biosolids from POTWs. Triclosan has a very toxic effect in some algae species, and inhibits an enzyme that blocks soil bacterial lipid synthesis (Ying and Kookana 2007). On the other hand, musks from shampoo, lotions, detergents, fabric softeners, and cleaning agents have been detected in soils amended with biosolids (Yang and Metcalfe 2006).

1.6.3 Food waste

According to the U.S. Department of Agriculture, food waste is defined as the product of reduction of edible food mass anywhere along the food chain. The term is usually used in a more broad sense to include non-edible (by humans) parts of foods, for instance banana peels, egg shells, bones (United States Department of Agriculture 2015). The USDA estimates 31% of the food supply was wasted at the retail and consumer level in 2010. This translates into a mass of 133 billion pounds with an associated value of $162 billion (United States Department of Agriculture 2015). The majority of this food waste is landfilled, accounting 21.4% of the municipal solid waste in 2011, when 258 million tons of municipal solid waste were generated according to the EPA. (United States Environmental Protection Agency 2014a). In Malaysia, the higher contribution of food waste into the municipal solid waste (45%) is attributed to the higher number of restaurants and a prevalent “eating out” culture (Godday and Pariatamby 2014). No differences were shown in the magnitude of food waste generation between developed and developing countries. However, there is a difference in the stage of the food chain when the majority of waste occur: in post-harvesting and processing stages in developing countries (40%), and in the retail and consumer levels in

developed countries (40%) (Girotto et al. 2015). In terms of trends that helps predict the evolution of food waste volume in the coming decades, the shift of the food industry towards the production of ready-to-eat food consumed in venues with limited methods for food stabilization predicts an increase in food waste (Zacharof 2016). In fact, the prohibition of donations of unsold or unused ready-to-eat food (liability issues) accentuates the problem (Tuck et al. 2012). The accurate quantification of national food waste is challenging because the traditional methods rely on interviews, inferential methods applied across the food system using factors obtained from sample populations, measurement of plate waste, and direct examination of garbage across different sample populations (Hall et al. 2009). In addition, food waste can be incorporated into the waste water system through food waste disposer built-in kitchen sinks. Life cycle assessments (LCA) have been applied to determine the effect (energy, cost, environmental) of different ways of managing food waste (Diggelman and Ham 2003) finding that the food water disposer / municipal wastewater system is the most beneficial in terms of land and energy use, and also in terms of reducing greenhouse emissions. However, it has a high impact in water usage and wastewater and waterborne wastes. In terms of the composition of the food waste in the USA, meats, poultry and fish accounts for 41% of net losses, followed by fruit and vegetables, and dairy at 17, and 14% respectively (Hickey and Ozbay 2014).

Because of its high organic content (80-90% volatiles/total solids) and moisture content ranging from 75-85%, food waste is a major source of odor emissions, vermin attraction, groundwater contamination, and toxic gas emissions (Kim et al. 2004). It has been reported that food waste generates 34% of all human-related methane emissions in the world through uncontrolled anaerobic fermentation in landfills. The emission of toxins affects the health of landfill workers and it has been associated to congenital malformation effects. It also provides a very good

environment for microbial growth, increasing the risk of pathogenic vector transfer (Hickey and Ozbay 2014).

Nowadays, the majority of food waste end up in landfills or in the waste water system. However, increasing efforts are been set up by local communities to compost food scraps in the household, and use this compost as a natural fertilizer. Some of the food waste is being processed and used as animal feed. A higher scale strategy uses food waste as substrate and co-substrate for anaerobic digestion and methane and hydrogen production (dark fermentation) thanks to its high carbohydrate content, the ease to hydrolyze, and the more restrictive regulation for landfilling disposal (United States Environmental Protection Agency 2014b). In Europe, 127 anaerobic digesters were processing the organic waste from municipal solid waste in 2006 (Levis et al. 2010).

1.6.4 Apple pomace

Apple pomace is a high moisture (70-75%) solid residue remaining after pressing the apples for juice. It is composed of crushed apple flesh-peels (95%), stalks (1%), and seeds (4-5%) (Ajila et al. 2012, Bhushan et al. 2008) and it is the main by-product of the apple juice and cider industries (Shalini and Gupta 2010). It is estimated that per ton of apples processed, 0.75 tons of juice and 0.25 tons of pomace are produced (Shalini and Gupta 2010). In 2013, the world production of apples was about 65 million metric tons, with China leading the rank with 32 million metric tons, far followed by USA, Turkey, and Poland with 3.2, 2.5, and 2.4 million metric tons, respectively. Figure 1.7 shows the evolution of world apple production between 2003 and 2013 (World Apple and Pear Association 2017).

The traditional land-spread or stream disposal of apple pomace is forbidden due to its high organic load (chemical oxygen demand between 250-300g/kg) (Shalini and Gupta 2010), and high moisture content (what is the perfect medium for pathogens proliferation). It is also a potential source of bad smells due to the rapid fermentation by natural flora (Bhushan et al. 2008).

The traditional uses of apple pomace include composting and fertilizer production, pectin extraction, power generation, and a component of cattle feed (although it has low digestable protein content and it is a seasonal resource (Hang et al. 1981, Wojdalski et al. 2016)). In addition, the rapid spoilage of the wet pomace, together with the difficulty of transportation (high moisture content makes it a bulky material), makes it only available for the feedstock located in surrounding communities (Bhushan et al. 2008).

The high content of nutritional valuable products in the pomace has triggered investigations to incorporate apple pomace in the human food chain in the last decades. Because of its high fiber content (36.8%), apple pomace is considered a valuable ingredient for the food industry. The incorporation of dry apple pomace in wheat flour (5,10, and 15%) has been investigated for the preparation of bakery products (Sudha et al. 2007). In addition, it enhances the physicochemical and nutritional value of meats by using it as filler in the production of sausages (Younis and Ahmad 2015). Its high polyphenol content has been proved to prevent cancer, cardiovascular diseases, and diabetes (Sudha et al. 2007, Younis and Ahmad 2015).

Because of its high sugar content (9-22% depending on the apples variety), fermentation of the pomace has been explored to produce ethanol, biogas, butanol, citric acid (Hang 1988), and enzymes (pectinases, β-glucosidases, β-fructofuranosidases, etc.) (Shalini and Gupta 2010).

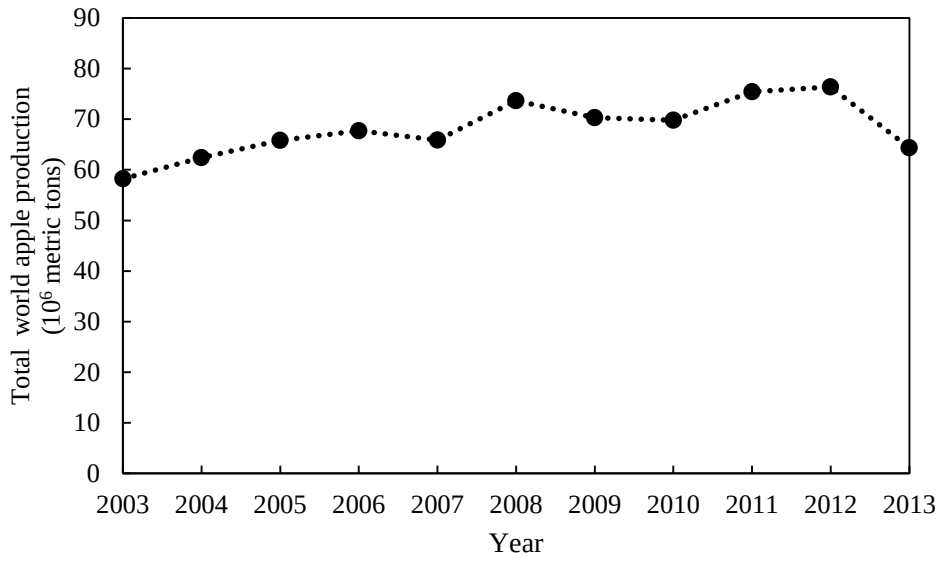

Figure 1.7. Total world apple production in million metric tons between 2003 and 2013 (World Apple and Pear Association 2017).

1.6.5 Red wine pomace

Grape wine is one of the most widely consumed alcoholic beverages in the world, with trends of growing demand. It is mainly produced in France, Italy, and Spain (accounting 16.4, 15.9, and 12.1% of the global production in 2014, respectively) (Zacharof 2016). However, the production of wine is increasing in other countries such as Australia and USA, where the wine culture is becoming more popular. Figure 1.8 shows the evolution of growth in the absolute and per-capita wine production in USA since 1965 (Wine Institute 2016). The process of wine making requires several steps (cultivation of grapes, harvest, press, fermentation, aging), and generates large amounts of organic and inorganic wastes. This waste can be divided in the agricultural residues from vines trimming and de-stemming, wastewater with suspended solids from the wine making process, and pomace from the skins, pulp, seeds, and stalks leftover when the grapes are pressed. On occasions, the stalks, skins and pulp, and seeds are separated because of their different

characteristics. Grape stalks are rich in lignin, nitrogen, and potassium, skins and pulp are rich in fiber and sugars, and seeds have high content of phenolic compounds and linoleic acid (Zacharof 2016). In this work, stalks, skins and pulp, and seeds were processed together.

It has been estimated that 1 ton of crushed grapes yields about 0.20 tons of pomace (Hogan et al. 2010, Baaka et al. 2015) . With and average crushing capacity of 100 tons of grapes per season (Zacharof 2016), the average winery has to handle 20 tons of pomace per year. In absolute terms, only Californian wineries produce more than 100,000 tons of grape pomace per year (Schrope 2012). These high volumes are problematic and hinder the expansion plans of wineries. Due to its high organic content, pomace cannot be directly disposed in the environment (Moncalvo et al. 2016). In addition, its accumulation can lead to vinegar fly infestation and it is a good medium for pathogens growth (Baaka et al. 2015).

Traditionally, grape pomace has been composted and use as fertilizer, or used as cattle food (Regional Distric of Okanagan-Similkameen 2010). However, the high content of phenolic derivatives and precursors of potential platform chemicals, makes the grape pomace a valuable biochemical resource for the pharmaceutical, chemical, material, cosmetic, food, and textile industries. In any case, these applications will produce much higher value than the $10 a ton currently paid for pomace as cattle feed (Schrope 2012).

Grape pomace can be incorporated into the food stream directly as flour, cooking oil, dried powder rich on fiber and antioxidants in cereal products, or indirectly as antioxidant phenolic extracts. It has been demonstrated that the high content of antioxidants and anti-hyperglycemic compounds in pomace can contribute to reduce risks of type-2 diabetes, cardiovascular diseases and cancer (Zhou and Raffoul 2012) . However, mycotoxines, biogenic amines, pesticides, and heavy metals have to be monitored to avoid their incorporation into the food chain (Moncalvo et al. 2016). The

textile industry has developed an interest in using grape pomace as a source for natural dyes for bleached wool fabrics (Baaka et al. 2015). In lignocellulosic biorefineries, the pomace can be hydrolyzed to a mixture of 6C, 5C sugars, oligosaccharides, and lignin phenols. This products can be further upgraded to ethanol, carboxylic acids, butanol, acetone and other valuable chemicals (Zacharof 2016).

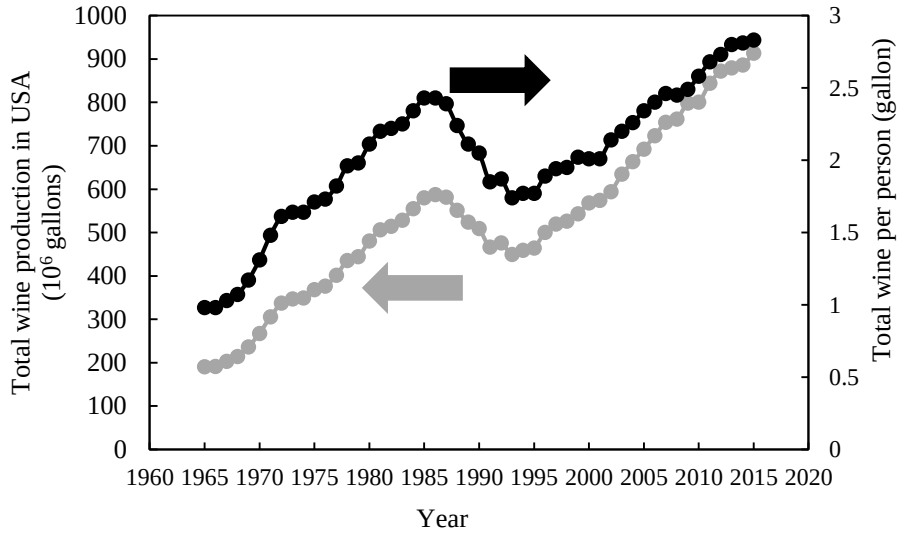

Figure 1.8. Evolution of the production of wine in U.S. and the wine consumption per capita (Wine Institute 2016). Plot in grey represents the total wine production in USA in 10^6 gallons. The black plot represents the total wine consumption per person.

1.6.6 Whiskey stillage

The stillage is the spent mash (fermented gains) remaining after the first distillation of alcohol. Its characteristics depend on the distilled substrate and process, but generally, it is a brown-ish, low pH, sweet smelling, high in protein and fiber liquor, with low or no sugar. In addition, it is high in dissolved and suspended organic material (Quinn and Marchant 1980).

Distilleries generate high volumes of stillage. A processing grain distillery generates, on average, a stillage volume ranging 10-13 or even 20 times the volume of ethanol produced (Sweeten et al. 2012), (Wilkie et al. 2000). It has a very high COD content, 100g/l, which makes it a serious environmental pollutant (the stillage generated by an ethanol plant with a production of 1,000m^3 per year (medium size) has the same pollution capacity as the sewage of a 500,000 habitants city) (Wilkie et al. 2000). In addition, the stillage fast deterioration in storage (spoils after a couple of days) makes the use of stillage a challenge. Traditionally, it was dumped unconverted in rivers or soil. This practice is forbidden for environmental concerns. Nowadays, the stillage is used for nutrient recovery (dehydration to produce dark grains and distiller's solubles), or as animal feed or fertilizer. Stillage can be also used as substrate for biogas production (Eriksson et al. 2016). Personal communication with Joe Myer from Myer Farm Distillery (that donated the whiskey stillage for this project, Figure 1.9), state the value of the hydrothermal liquefaction technology as an alternative for stillage management, having the potential to help the spirits industry as well as improve sustainability efforts. Brown-Forman, one of the largest American companies in the spirits business, owning brands such as Jack Daniel's and Woodford Reserve, are also interested in novel technologies for waste management to fulfill their commitment of zero-waste sent to landfills (O'Neill 2016).

Figure 1.9. Whiskey stillage donated by Myer Farm Distillers (Ovid, NY)

1.6.7 Whey

Whey is a by-product of fermented and coagulated dairy products (cheese, yogurt, paneer, chhana., etc.) (Samaddar and Kaviraj 2014, Goyal and Gandhi 2009). It is the yellowish-colored liquid that remains after the precipitation and removal of milk casein. Its pH is acid, with values ranging below 5 (acid whey, Greek yogurt whey) or 6-7 (sweet whey), depending on the method used for the precipitation of casein (Siso 1996). Whey is the most important waste effluent of the dairy industry together with manure. A kg of cheese produced generates 9 kg of whey (Siso 1996). This number decreased to 2-3 kg of whey per kg of Greek yogurt (Erickson 2017). In an industry producing 771,000 metric tons of Greek yogurt in 2015 (Erickson 2017), and 11.1 billion pounds in 2013 only in the U.S (International Dairy Food Association 2015), the volume of whey effluent generated constitutes a challenge.

Whey is a potential pollutant of terrestrial and aquatic environments, mainly because of its high organic matter content (BOD_5 ranging between 30,000 and 50,000 ppm, and COD ranging between 60,000 to 80,000ppm) (Siso 1996). Therefore, stream disposal is banned by increasingly strict laws regulating the quality of effluents. On the other hand, its use as fertilizer is being limited because of potential run-offs to aquifers. Acid whey disposal hit the news in 2011 when the owner of a hog farm in Ohio was convicted for spilling thousands of gallons of cheese whey into a nearby creek, resulting in the death of more than 36,000 fish (Smith 2015). Lactose, milk sugar, is the main compound responsible for the high BOD and COD. Therefore, the removal of lactose is required for the safe disposal of whey (COD drops to 10,000ppm after lactose removal) (Siso 1996). University of Wisconsin is leading efforts for the lactose removal using ultracentrifugation and nanofiltration technologies (Erickson 2017). In recent years, technology advancement has opened

new and effective ways to recover valuable whey constituents (shown in Table 1.6). Because of its high content of electrolytes and minerals, its use as a healthy recovery drink is being investigated (Goyal and Gandhi 2009). Recently, whey has been explored as an inoculum for fermentation, as it contains lactic acid bacteria (Samaddar and Kaviraj 2014). The biggest producer of Greek yogurt (Chobani) uses reverse osmosis technology to extract water from whey, which can be used for washing equipment and plant maintenance. This approach also reduces the volume of waste processed by municipal treatment facilities by 20%. Recently, whey has being investigated as a co-substrate for anaerobic digestion of manure to produce methane. The drawback of this technology is that whey's low pH is not suitable for the anaerobic microbial conversion (Smith 2015). General Mills Inc. filled a patent in 2013 for a method to neutralized acid yogurt whey to a pH of at least 6. This technology opens the door to use whey as food additive, sweetener, source of minerals for food (calcium, potassium), etc (Smith et al 2014).

Table 1.6. Composition of sweet and acid whey (Tsakali et al. 2010).

Contents	Sweet whey	Acid whey
Water (%)	93-94	94-95
Dry matter (%)	6-6.5	5-6
Lactose (%)	4.5-5	3.8-4.3
Lactic acid (%)	Traces	Up to 0.8
Total protein (%)	0.8-1.0	0.8-1.0
Whey protein (%)	0.6-0.65	0.6-0.65
Citric acid (%)	0.1	0.1
Minerals (%)	0.5-0.7	0.5-0.7
pH	6.2-6.4	4.6-5.0

1.6.8 Olive oil

The production of olive oil is one of the most important economic agro-food sectors in the Mediterranean regions, where the world production is concentrated as shown in Figure 1.10 (Robison and Silver 2016). It covers over 5 million hectares in the European Union member states. Spain, Italy, Greece, and Portugal are the main producers, with 2.4, 1.4, 1, and 0.5 million hectares cultivated, respectively (Gomez-Munoz et al. 2012). In terms of production, Spain leads the world production with 1,401.6 thousand tons for the 2015/2016 season, which represents half of the total European Union production for that season (International Olive Council 2016). In USA, the demand for olive oil has significantly increase over the last few years because of its health benefits. The production of local olive oil has increased to 14 thousand tons in the 2015/2016 season, with 13.3 thousand tons produced in California and marginal production in Texas and Georgia.

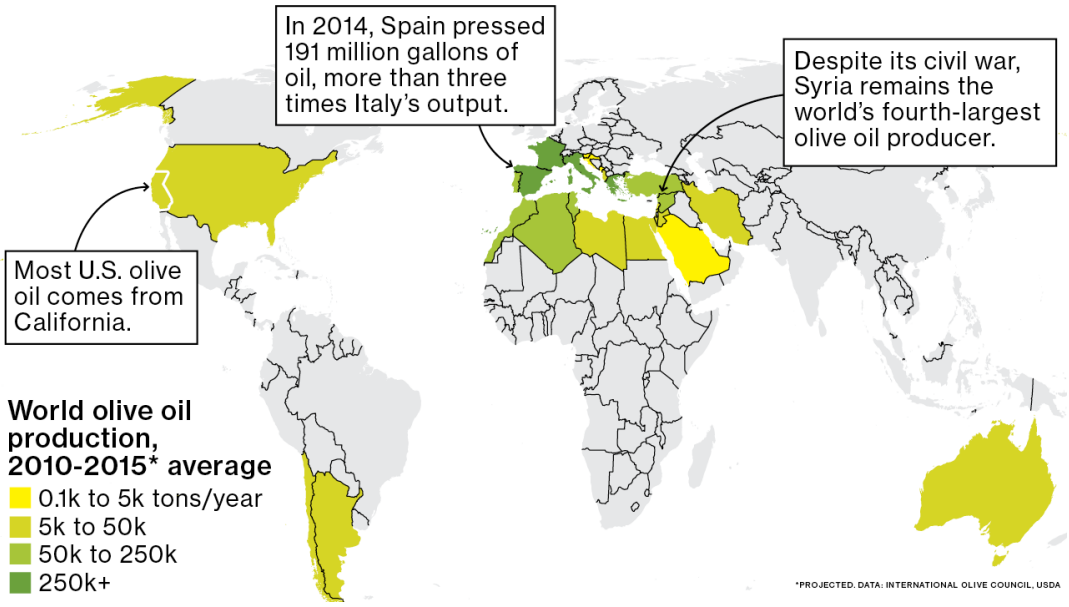

Figure 1.10. Main producers of olive oil are located areoun the Mediterranean sea (Robison and Silver 2016)

The olive oil industry generates large quantities of two byproducts: olive mill solid waste and olive oil waste water. The olive mill solid waste represents 80 %wt. of the olive used for olive oil

production. It is a semi-solid byproduct (30-70% water content depending on the olive oil extraction method (Azbar et al. 2004)) and is rich in carbohydrates (Abu Tayeh et al. 2016). It is composed of water, olive skin, pulp, and seeds and produced in the Mediterranean region between November and February at volumes ranging between 7 and 30 million m^3, depending on the season. Because of its low pH, phytotoxic and antimicrobial properties, relatively high salinity, organic load, and phenols and lipids content, this material can contaminate aquifers and produce undesirable smells (Serrano et al. 2017). Therefore, direct disposal of this waste to rivers or soil is forbidden in the majority producer countries (Gomez-Munoz et al. 2012).

The olive mill solids waste volume depends on the technology used for the extraction of olive oil. For the 2-phases process (press and centrifugation), the volume of solid waste is around four times the volume of the actual product. For the 3-phases process (polyphenols are washed out with water), the volume of solid waste is above three times the volume of olive oil. However, this process also produce considerable amount of waste water (vegetation water) that needs to be treated (Christoforou and Fokaides 2016). Hence, finding an application niche for the olive mill solid waste that adds to the company revenues by reducing disposal fees, is something that the olive oil industry is very interested in pursuing. To assess the use of this waste, I did a survey to olive oil co-ops and companies. In the San Sebastian Coop in El Romeral (Toledo, Spain), they dry the pomace in plastic pools in the field, and they use it as fuels for stoves. In Long Meadow Ranch (Napa Valley, California), they compost the pomace immediately after being produced and use it in their farm. Some studies have shown that the joint composting of olive oil pomace with cow manure and wheat straw decreases its phytotoxicity, making it a better soil conditioner and amendment agent (El-Darler et al. 2015). In California Olive Ranch, the majority of this waste is used as feedstock for the local cattle industry. However, the management of the olive mill waste

is a challenge that hinders the company plans for olive oil production increase in the short term. Another alternative is the recovery of phenolic compounds from the waste using ionic exchanger columns. These compounds have antioxidant properties, highly desired by food, pharmaceutical, and cosmetic companies. Anaerobic digestion is not an option for these substrates as they contain inhibitors of the microbial activity, unless it is washed to remove phenolic compounds and their derivatives (Chundawat et al. 2007).

1.7 Dissertation topics and structure

Chapter 2 of the dissertation provides the specific research objectives and the approach followed to achieve those objectives. This dissertation is divided into two parts: Part I: FTIR methods development for the characterization of model cellulose and lignocellulosic biomass (Chapters 3 and 4); Part II: Thermochemical valorization of model compounds and organic wet wastes from a variety of industries and characterization of the products: Influence of pH, temperature, and reaction time in product distribution and quality (Chapters 5 to 8). **Chapter 9** provides the overall conclusions and recommendations for future research of theses technologies derived from this work.

In part I methods development are described for the infrared characterization of crystallinity and key chemical bonds in both model cellulose (Bacterial Microcrystalline Cellulose, BMCC) and lignocellulosic biomass (hardwood and swtichgrass). Part I has two chapters: **Chapter 3** covers the characterization of model cellulose crystallinity upon enzymatic hydrolysis using individual and crude cellulases. It improved previously published methods to measure cellulose crystallinity using mid-infrared techniques. **Chapter 4** presents the characterization of lignocellulosic biomass upon thermochemical pretreatment with a special focus in the influence of particle size distribution and analysis of spectral signal processing techniques into the reproducibility and statistical consistency of measurements. This part provides the foundation for the FTIR work that was used in Part II of the dissertation to characterize the evolution of chemical bonding in the products (hydro-char and bio-oil) from hydrothermal liquefaction for waste valorization.

Part II of the dissertation covers the thermochemical valorization of model compounds and organic wet wastes from different industries, which have challenges for managing increasing amounts of

waste being produced. In **Chapter 5**, the hydrothermal liquefaction research in model compounds that conform organic wastes (carbohydrates, lipids, and proteins) will be expanded to study the kinetics over the course of reaction. **Chapter 6** studies how the adjustment of pH of selected feedstocks has an influence in the quality and the distribution of the phases generated in HTL process. **Chapter 7** studies the influence of the natural pH of the feedstocks and the temperature and reaction times on the hydrothermal valorization of organic wet wastes, focusing on the hydro-char. Lastly, **Chapter 8** expands Chapter 7, by integrating in the analysis the bio-oil phase and the aqueous phase generated in the reactions. It shows how the pH and conditions of reactions affect the product distribution and chemical composition.

1.8 References

Abu Tayeh, H, O Levy-Shalev, H Azaizeh, and C Dosoretz. 2016. “Subcritical Hydrothermal Pretreatment of Olive Mill Solid Waste for Biofuel Production.” *Bioresource Technology* 199: 164–72.

Adjaye, J, and N Bakhshi. 1995. “Production of Hydrocarbons by Catalytic Upgrading of a Fast Pyrolysis Bio-Oil. Part I: Conversion over Various Catalysts.” *Fuel Processing Technology* 45: 161–83.

Ajila, C, S Brar, M Verma, R Tyagi, S Godbout, and J Valero. 2012. “Bio-Processing of Agro-Byproducts to Animal Feed.” *Critical Reviews in Biotechnology* 32 (4).

Arantes, V, and JN Saddler. 2010. “Access to Cellulose Limits the Efficiency of Enzymatic Hydrolysis: The Role of Amorphogenesis.” *Biotechnology for Biofuels* 3 (4).

Azbar, N, A Bayram, A Filibeli, A Muezzinoglu, F Sengul, and A Ozer. 2004. “A Review of Waste Management Options in Olive Oil Production.” *Critical Reviews in Environmental Science and Technology* 34 (3): 209–47.

Baaka, N, M Ticha, W Haddar, S Hammami, and M Mhenni. 2015. “Extraction of Natural Dye from Waste Wine Industry: Optimization Survey Based on a Central Composite Design Method.” *Fibers and Polymers* 16 (1): 38–45.

Balan, V, D Chiaramonti, and S Kumar. 2013. “Review of US and EU Initiatives toward Development, Demonstration, and Commercialization of Lignocellulosic Biofuels.” *Biofuels, Bioproducts and Biorefining* 7 (6): 732–59.

Bansal, P, M Hall, M Realff, J Lee, and A Bommarius. 2009. “Modeling Cellulase Kinetics

on Lignocellulosic Substrates." *Biotechnology Advances* 27 (6): 833–48.

Barakat, A, H de Vries, and X Rouau. 2013. "Dry Fractionation Process as an Important Step in Current and Future Lignocellulose Biorefineries: A Review." *Bioresource Technology* 134 (0): 362–73.

Bhushan, S, K Kalia, M Sharma, B Singh, and P Ahuja. 2008. "Processing of Apple Pomace for Bioactive Molecules." *Critical Reviews in Biotechnology* 28 (4): 285–96.

Bitra, V, A Womac, C Igathinathane, P Miu, Y Yang, D Smith, N Chevanan, and S Sokhansanj. 2009. "Direct Measures of Mechanical Energy for Knife Mill Size Reduction of Switchgrass, Wheat Straw, and Corn Stover." *Bioresource Technology* 100 (24): 6578–85.

Bozell, J, and G Petersen. 2010. "Technology Development for the Production of Biobased Products from Biorefinery Carbohydrates—the US Department of Energy's 'Top 10' Revisited." *Green Chemistry* 12: 539–54.

Bridgwater, A. 2017. "Review of Fast Pyrolysis of Biomass and Product Upgrading." *Biomass and Bioenergy*, 1–27.

Cantero-Tubilla, B, K Sabolsky, E Sabolsky, and J Zondlo. 2016. "Investigation of Pretreated Switchgrass, Corn Stover, and Hardwood Fuels in Direct Carbon Fuel Cells." *Int J Electrochem Sci* 11 (1): 303–21.

Carole, T, J Pellegrino, and M Paster. 2004. "Opportunities in the Industrial Biobased Products Industry." *Applied Biochemistry and Biotechnology* 113–116: 871–85.

Chang, V, B Burr, and M Holtzapple. 1997. "Lime Pretreatment of Switchgrass." *Applied*

Biochemistry and Biotechnology 63–65 (1). Humana Press: 3–19.

Christoforou, E, and P Fokaides. 2016. "A Review of Olive Mill Solid Wastes to Energy Utilization Techniques." *Waste Management* 49: 346–63.

Chundawat, S, B Venkatesh, and B Dale. 2007. "Effect of Particle Size Based Separation of Milled Corn Stover on AFEX Pretreatment and Enzymatic Digestibility." *Biotechnology and Bioengineering* 96 (2): 219–31.

Converse, A, H Ooshima, and D Burns. 1990. "Kinetics of Enzymatic Hydrolysis of Lignocellulosic Materials Based on Surface Area of Cellulose Accessible to Enzyme and Enzyme Adsorption on Lignin and Cellulose." *Applied Biochemistry and Biotechnology* 24/25: 67–73.

Darmouth Engineering, Darmouth University. 2013. "Anaerobic Digestion of Wastewaster Sludge."

Déniel, M, G Haarlemmer, A Roubaud, E Weiss-Hortala, and J Fages. 2016. "Energy Valorisation of Food Processing Residues and Model Compounds by Hydrothermal Liquefaction." *Renewable and Sustainable Energy Reviews* 54: 1632–52.

Department of Environmental Conservation, NYS-DEC. 2015. "Recycling Biosolids from Wastewater Treatment Facilities."

Diggelman, C, and R Ham. 2003. "Household Food Waste to Wastewater or to Solid Waste? That Is the Question." *Waste Manage Res* 21: 501–14.

Division of Materials Management Department of Environmental Conservation, NYS-DEC. 2011. *Biosolids Management in New York State*.

Duan, W, A Ronen, J Leon, A Dudchenko, S Yao, J Delgado, A Yan, M Matsumoto, and D Jassby. 2016. “Treating Anaerobic Sequencing Batch Reactor Effluent with Electrically Conducting Ultrafiltration and Nanofiltration Membranes for Fouling Control.” *Journal of Membrane Science* 504: 104–12.

Egemen, E, J Corpering, R Padilla, N Brennan, and N Nirmalakhandan. 1999. “Evaluation of Ozonation and Cryptic Growth for Biosolids Management in Wastewater Treatment.” *Water Science and Technology* 39 (10–11): 155–58.

El-Darler, S, H Ahmed, M El Razik, and E Allam. 2015. “Detoxification of Olive-Mill Solid Waste and Its Probable Application as Organic Fertilizer.” *Journal of Fertilizers & Pesticides* 6 (2).

Elliott, D. 2011. “Thermochemical Processing of Biomass; Conversion into Fuels, Chemicals and Power.” In *Hydrothermal Processing*, 200–231. Chichester, UK.

Elliott, D, P Biller, A Ross, A Schmidt, and S Jones. 2015. “Hydrothermal Liquefaction of Biomass: Developments from Batch to Continuous Process.” *Bioresource Technology* 178: 147–56.

Erickson, B. 2017. “Acid Whey: Is the Waste Product an Untapped Goldmine?” *Chemical & Engineering News* 95 (6): 26–30.

Eriksson, O, D Jonsson, and K Hillman. 2016. “Life Cycle Assessment of Swedish Single Malt Whisky.” *Journal of Cleaner Production* 112 (January): 229–37.

Fan, L T, Y H Lee, and D R Beardmore. 1981. “The Influence of Major Structural Features of Cellulose on Rate of Enzymatic Hydrolysis.” *Biotechnology and Bioengineering* 23 (2): 419–24.

Ferreira, F, J Messina, J Rigoline, L Lopez-Calva, M Lugo, and R Vakis. 2013. “Economic Mobility and the Rise of the Latin American Middle Class. The World Bank.”

Foston, M, and Arthur J Ragauskas. 2012. “Biomass Characterization: Recent Progress in Understanding Biomass Recalcitrance.” *Industrial Biotechnology* 8 (4): 191–208.

Gallezot, P. 2012. “Conversion of Biomass to Selected Chemical Products.” *Chem.Soc.Rev* 41: 1538–58.

Ghaffar, T, M Irshad, Z Anwar, T Aqil, Z Zulifqar, A Tariq, M Kamran, N Ehsan, and S Mehmood. 2014. “Recent Trends in Lactic Acid Biotechnology: A Brief Review on Production to Purification.” *Journal of Radiation Research and Applied Sciences* 7 (2): 222–29.

Girotto, F, L Alibardi, and R Cossu. 2015. “Food Waste Generation and Industrial Uses: A Review.” *Waste Management* 45: 32–41.

Godday, O, and A Pariatamby. 2014. “Bio-Hydrogen Production from Food Waste through Anaerobic Fermentation.” *Sains Malaysiana* 43 (12): 1927–36.

Gollapalli, L, B Dale, and D Rivers. 2002. “Predicting Digestibility of Ammonia Fiber Explosion (AFEX)-Treated Rice Straw.” *Applied Biochemistry and Biotechnology* 98–100 (1–9): 23–35.

Gomez-Munoz, B, D Hatch, R Bol, and R Garcia-Ruiz. 2012. *Sustainable Development - Authoritative and Leading Edge Content for Environmental Management. Chapter 20: The Compost of Olive Mill Pomace: From a Waste to a Resource. Environmental Benefits of Its Application in Olive Oil Groves.* Environmental Sciences.

Goyal, N, and D Gandhi. 2009. “Comparative Analysis of Incian Paneer and Cheese Whey for Electrolyte Whey Drink.” *World Journal of Dairy & Food Sciences* 4 (1): 70–72.

Grethlein, H. 1985. “The Effect of Pore Size Distribution on the Rate of Enzymatic Hydrolysis of Cellulosic Substrates.” *Nat Biotech* 3 (2): 155–60.

Gupta, K, K Aneja, and D Rana. 2016. “Current Status of Cow Dung as a Bioresource for Sustainable Development.” *Bioresources and Bioprocessing* 3 (28).

Hall, K, J Guo, M Dore, and C Chow. 2009. “The Progressive Increase of Food Waste in America and Its Environmental Impact.” *PLOS ONE* 4 (11).

Hang, Y. 1988. Apple pomace as substrate for microbial production of citric acid. US4767705A, issued 1988.

Hang, Y, C Lee, E Woodams, and H Cooley. 1981. “Production of Alcohol Form Apple Pomace.” *Applied and Environmental Microbiology* 42 (6): 1128–29.

Hasunuma, T, F Okazaki, N Okai, K Hara, J Ishii, and A Kondo. 2013. “A Review of Enzymes and Microbes for Lignocellulosic Biorefinery and the Possibility of Their Application to Consolidated Bioprocessing Technology.” *Bioresource Technology* 135 (0): 513–22.

Haykir, N, and E Bahcegul. 2013. “Pretreatment of Cotton Stalk with Ionic Liquids Including 2-Hydroxy Ethyl Ammonium Formate to Enhance Biomass Digestibility.” *Industrial Crops and Products* 41 (0): 430–36.

He, Z, and X Wang. 2013. “Hydrodeoxygenation of Model Compounds and Catalytic Systems for Pyrolysis Bio-Oils Upgrading.” *Catalysis for Sustainable Energy*, 28–52.

Hendriks, A T W M, and G Zeeman. 2009. "Pretreatments to Enhance the Digestibility of Lignocellulosic Biomass." *Bioresource Technology* 100 (1): 10–18.

Hickey, M, and G Ozbay. 2014. "Food Waste in the United States: A Contributing Factor toward Environmental Instability." *Frontiers in Environmental Science* 2: 51.

Hogan, S, L Zhang, J Li, S Sun, C Canning, and K Zhou. 2010. "Antioxidant Rich Grape Pomace Extract Suppresses Postprandial Hyperglycemia in Diabetic Mice by Specifically Inhibiting Alpha-Glucosidase." *Nutrition & Metabilism* 7 (71): 1–9.

Huber, G, J Chheda, C Barrett, and Dumesic. J. 2005. "Production of Liquid Alkanes by Aqueous-Phase Processing of Biomass-Derived Carbohydrates." *Science* 308 (5727): 1446–50.

International Dairy Food Association, IDFA. 2015. "Cheese Production Reports."

International Olive Council, IOC. 2016. "World Olive Oil Figures."

Kan, T, V Strezov, and T Evans. 2016. "Lignocellulosic Biomass Pyrolysis: A Review of Product Properties and Effects of Pyrolysis Parameters." *Renewable and Sustainable Energy Reviews* 57: 1126–40.

Kharas, H. 2017. "The Unprecedent Expansion of the Global Middle Class. Un Update." *Global Economy & Development at Brookings*.

Kim, S, S Han, and H Shin. 2004. "Feasibility of Biohydrogen Production by Anaerobic Co-Digestion of Food Waste and Sewage Sludge." *International Journal of Hydrogen Energy* 29 (15): 1607–16.

Kim, S, and M Holtzapple. 2006. "Effect of Structural Features on Enzyme Digestibility of

Corn Stover." *Bioresource Technology* 97 (4): 583–91.

Kim, T, J Kim, C Sunwoo, and Y Lee. 2003. "Pretreatment of Corn Stover by Aqueous Ammonia." *Bioresource Technology* 90 (1): 39–47.

Kim, T, and Y Lee. 2005. "Pretreatment and Fractionation of Corn Stover by Ammonia Recycle Percolation Process." *Bioresource Technology* 96 (18): 2007–13.

Kostylev, M, and D Wilson. 2013. "Two-Parameter Kinetic Model Based on a Time-Dependent Activity Coefficient Accurately Describes Enzymatic Cellulose Digestion." *Biochemistry* 52 (33): 5656–64.

Kratky, L, and T Jirout. 2011. "Biomass Size Reduction Machines for Enhancing Biogas Production." *Chemical Engineering & Technology* 34 (3): 391–99.

Kristensen, J.B, L.B Thygesen, C Felby, H Jørgensen, and T Elder. 2008. "Cell-Wall Structural Changes in Wheat Straw Pretreated for Bioethanol Production." *Biotechnology for Biofuels* 1 (5).

Kruse, Andrea. 2009. "Hydrothermal Biomass Gasification." *The Journal of Supercritical Fluids* 47 (3): 391–99.

Kumar, M, Y Gao, W Shen, and L He. 2015. "Valorisation of Protein Waste: An Enzymatic Approach to Make Commodity Chemicals." *Frontiers in Chemical Science and Engineering* 9 (3): 295–307.

Lane, J. 2015. "EU Reshapes Its Biofuels Policy." *BiofuelsDigest*.

Larimar, J, W Powers, and A Sutton. 2005. *Manure Characteristics. Manure Management Systems Series*.

Larson, E. 2008. “Biofuels Production Technologies: Status, Prospects and Implications for Trade and Development.” United Nations Conference on Trade and Development.

Lau, M, and B Dale. 2009. “Cellulosic Ethanol Production from AFEX-Treated Corn Stover Using Saccharomyces Cerevisiae 424A(LNH-ST).” *Proceedings of the National Academy of Sciences of the United States of America* 106 (5): 1368–73.

Lee, Y, L Fan, and L Fan. 1980. “Kinetics of Hydrolysis of Insoluble Cellulose by Cellulase.” In *Advances in Biochemical Engineering, Volume 17*, 17:131–68.

Levis, J, M Barlaz, N Themelis, and P Ulloa. 2010. “Assessment of the State of Food Waste Treatment in the United States and Canada.” *Waste Management* 30 (8–9): 1486–94.

Li, C, G Cheng, V Balan, M Kent, M Ong, S Chundawat, L Sousa, et al. 2011. “Influence of Physico-Chemical Changes on Enzymatic Digestibility of Ionic Liquid and AFEX Pretreated Corn Stover.” *Bioresource Technology* 102 (13): 6928–36.

Liang, L, R Sun, J Fei, S Wu, X Liu, K Dai, and N Yao. 2008. “Experimental Study on Effects of Moisture Content on Combustion Characteristics of Simulated Municipal Solid Wastes in a Fixed Bed.” *Bioresource Technology* 99: 7238–46.

Lignimatch. 2009. “Future Use of Ligning in Value Added Products. A Roadmap for Possible Nordic/Baltic Innovation.”

Lim, L, R Auras, and M Rubino. 2008. “Processing Technologies for Poly(lactic Acid).” *Progress in Polymer Science* 33 (8): 820–52.

Liu, L, J Sun, M Li, S Wang, H Pei, and J Zhang. 2009. “Enhanced Enzymatic Hydrolysis and Structural Features of Corn Stover by FeCl3 Pretreatment.” *Bioresource*

Technology 100 (23): 5853–58.

Luterbacher, J, Q Chew, Y Li, Je Tester, and L Walker. 2012. "Producing Concentrated Solutions of Monosaccharides Using Biphasic CO2-H2O Mixtures." *Energy & Environmental Science* 5 (5). The Royal Society of Chemistry: 6990–7000.

Luterbacher, J, J Parlange, and L Walker. 2013. "A Pore-Hindered Diffusion and Reaction Model Can Help Explain the Importance of Pore Size Distribution in Enzymatic Hydrolysis of Biomass." *Biotechnology and Bioengineering* 110 (1): 127–36.

Luterbacher, J, J Tester, and L Walker. 2012. "Two-Temperature Stage Biphasic CO2–H2O Pretreatment of Lignocellulosic Biomass at High Solid Loadings." *Biotechnology and Bioengineering* 109 (6): 1499–1507.

Mainka, H, O Täger, E Körner, L Hilfert, S Busse, F Edelmann, and A Herrmann. 2015. "Lignin – an Alternative Precursor for Sustainable and Cost-Effective Automotive Carbon Fiber." *Journal of Materials Research and Technology* 4 (3): 283–96.

Miao, X, J Yang, and C Metcalfe. 2005. "Carbamazepine and Its Metabolites in Wastewater and in Biosolids in a Municipal Wastewater Treatment Plant." *Environmental Science Technology* 39: 7469–75.

Moncalvo, A, L Marinoni, R Dordoni, G Garrido, V Lavelli, and G Spigno. 2016. "Waste Grape Skins: Evaluation of Safety Aspects for the Production of Functional Powders and Extracts for the Food Sector." *Food Aditives & Contaminants: Part A* 33 (7): 1116–26.

Montross, M D, and C L Crofcheck. 2004. "Effect of Stover Fraction and Storage Method on Glucose Production during Enzymatic Hydrolysis." *Bioresource Technology* 92 (3):

269–74.

Mosier, N, Ri Hendrickson, N Ho, M Sedlak, and M Ladisch. 2005. "Optimization of pH Controlled Liquid Hot Water Pretreatment of Corn Stover." *Bioresource Technology* 96 (18): 1986–93.

Nasiru, A, N Ismail, and M Ibrahim. 2013. "Vermicomposting: Tool for Sustainable Ruminant Manure Management." *Journal of Waste Management*, 7.

National Agricultural Statistics Service (NASS), United States Department of Agriculture USDA. 2017. "Semi-Annual Cattle Report."

Natural Resources Conservation Service, USDA. 1995. "Animal Manure Management."

Nguyen, T, K Kim, S Han, H Cho, J Kim, S Park, J Park, and S Sim. 2010. "Pretreatment of Rice Straw with Ammonia and Ionic Liquid for Lignocellulose Conversion to Fermentable Sugars." *Bioresource Technology* 101 (19): 7432–38.

NREL. 2014. "Thermochemical Conversion: Using Heat and Catalysis to Make Biofuels and Bioproducts."

O'Neill, J. 2016. "Partners in Responsibility: Corporate Responsibility Report. Brown-Forman."

Oak Ridge National Laboratory, ORNL. 2011. "U.S. Billion-Ton Update: Biomass Supply for a Bioenergy and Bioproducts Industry. Oak Ridge National Laboratory. ORNL/TM-2011/224."

Palmowski, L M, and J A Muller. 2000. "Influence of the Size Reduction of Organic Waste on Their Anaerobic Digestion." *Water Science and Technology* 41 (3): 155–62.

Peterson, A, F Vogel, R Lachance, M Fröling, M Antal, Jr., and J Tester. 2008. "Thermochemical Biofuel Production in Hydrothermal Media: A Review of Sub- and Supercritical Water Technologies." *Energy & Environmental Science* 1 (1): 32.

Posmanik, R., D.A. Cantero, A. Malkani, D.L. Sills, and J.W. Tester. 2017. "Biomass Conversion to Bio-Oil Using Sub-Critical Water: Study of Model Compounds for Food Processing Waste." *The Journal of Supercritical Fluids* 119: 26–35.

Prado, J, R Vardanega, G Nogueira, T Forster-Carneiro, M Rostago, F Filho, and M Meireles. 2017. "Valorization of Residual Biomasses from the Agri-Food Industry by Subcritical Water Hydrolysis Assisted by CO2." *Energy & Fuels* 31 (3): 2838–46.

Puri, V. 1984. "Effect of Crystallinity and Degree of Polymerization of Cellulose on Enzymatic Saccharification." *Biotechnology and Bioengineering* 26 (10): 1219–22.

Quinn, J, and R Marchant. 1980. "The Treatment of Malt Whiskey Distillery Waste Using the Fungus Geotrichum Candidum." *Water Research* 14: 545–51.

Reardon, S. 2014. "Manure Fertilizer Increases Antibiotic Resistance." *Nature News*.

Regional Distric of Okanagan-Similkameen, RDOS. 2010. "Regional Organic Waste Management Strategy."

"Replacing the Whole Barrel. To Reduce U.S. Dependence on Oil." 2013. U.S. Department of Energy. Bioenergy Technologies Office.

Ritter, S. 2013. "Ethanol-To-Butanol Conversion A Biofuel Plus." *Chemical & Engineering News*.

Robison, P, and V Silver. 2016. "Is American Olive Oil about to Have Its Moment?"

Samaddar, Ayan, and Anilava Kaviraj. 2014. “Processing of Fish Offal Waste through Fermentation Utilizing Whey as Inoculum.” *International Journal of Recycling of Organic Waste in Agriculture* 3 (1).

Samayam, I, and C Schall. 2010. “Saccharification of Ionic Liquid Pretreated Biomass with Commercial Enzyme Mixtures.” *Bioresource Technology* 101 (10): 3561–66.

Sanders, J, E Scott, R Weusthuis, and H Mooibroek. 2007. “New TechnologiesBio-Refinery as the Bio-Inspired Process toBulk Chemicals.” *Macromolecules* 7: 105–17.

Sathitsuksanoh, N, Z Zhu, S Wi, and Z Percival. 2011. “Cellulose Solvent-Based Biomass Pretreatment Breaks Highly Ordered Hydrogen Bonds in Cellulose Fibers of Switchgrass.” *Biotechnology and Bioengineering* 108 (3): 521–29.

Schrope, M. 2012. “Winemaking Waste Could Become Biofuel Starter.” *Chemical & Engineering News*.

Scott, E, F Peter, and J Sanders. 2007. “Biomass in the Manufacture of Industrial Products—the Use of Proteins and Amino Acids.” *Applied Microbiology and Biotechnology* 75 (4): 751–62.

Selig, M, S Viamajala, S Decker, M Tucker, M Himmel, and T Vinzant. 2007. “Deposition of Lignin Droplets Produced During Dilute Acid Pretreatment of Maize Stems Retards Enzymatic Hydrolysis of Cellulose.” *Biotechnology Progress* 23 (6). American Chemical Society: 1333–39.

Serrano, A, F Fermoso, G Rodríguez-Gutierrez, J Fernandez-Bolaños, and R Borja. 2017. “Biomethanization of Olive Mill Solid Waste after Phenols Recovery through Low-Temperature Thermal Pre-Treatment.” *Waste Management* 61: 229–35.

Shalini, R, and D Gupta. 2010. “Utilization of Pomace from Apple Processing Industries: A Review.” *Journal Food Science & Technology* 47 (4): 365–71.

Shill, K, S Padmanabhan, Q Xin, J Prausnitz, D Clark, and H Blanch. 2011. “Ionic Liquid Pretreatment of Cellulosic Biomass: Enzymatic Hydrolysis and Ionic Liquid Recycle.” *Biotechnology and Bioengineering* 108 (3): 511–20.

Sills, D, and J Gossett. 2012. “Using FTIR to Predict Saccharification from Enzymatic Hydrolysis of Alkali-Pretreated Biomasses.” *Biotechnology and Bioengineering* 109 (2): 353–62.

Singh, S, B Simmons, and K Vogel. 2009. “Visualization of Biomass Solubilization and Cellulose Regeneration during Ionic Liquid Pretreatment of Switchgrass.” *Biotechnology and Bioengineering* 104 (1): 68–75.

Sinitsyn, A P, A V Gusakov, and E Yu Vlasenko. 1991. “Effect of Structural and Physico-Chemical Features of Cellulosic Substrates on the Efficiency of Enzymatic Hydrolysis.” *Applied Biochemistry and Biotechnology* 30 (1). Humana Press: 43–59.

Siso, M.I.González. 1996. “The Biotechnological Utilization of Cheese Whey: A Review.” *Bioresource Technology* 57 (1): 1–11.

Smith, E, W Wang, and V Ghosh. 2014. Yogurt whey and method. US2014038993 A1, issued 2014.

Smith, M. 2015. “There Is a Downside to All the Greek Yogurt You Are Eating. Vice News.”

Söderström, J, L Pilcher, M Galbe, and G Zacchi. 2002. “Two-Step Steam Pretreatment of Softwood with SO2 Impregnation for Ethanol Production.” In *Biotechnology for Fuels*

and Chemicals, 5–21.

Sudha, M, V Baskaran, and K Leelavathi. 2007. "Apple Pomace as a Source of Dietary Fiber and Polyphenols and Its Effect on the Rheological Characteristics and Cake Making." *Food Chemistry* 104: 686–92.

Sweeten, J, J Lawhon, G Schelling, T Gillespie, and C Coble. 2012. "Removal and Utilization of Ethanol Stillage Constituents." *Energy in Agriculture* 1: 331–45.

Teixeira, L C, J C Linden, and H A Schroeder. 1999. "Alkaline and Peracetic Acid Pretreatments of Biomass for Ethanol Production." In *Twentieth Symposium on Biotechnology for Fuels and Chemicals*, edited by BrianH Davison and Mark Finkelstein, 19–34. Humana Press.

Tekin, K, S Karagöz, and S Bektaş. 2014. "A Review of Hydrothermal Biomass Processing." *Renewable and Sustainable Energy Reviews* 40: 673–87.

Tsakali, E, K Petrotos, A Allessandro, and P Goulas. 2010. "A Review on Whey Composition and the Methods Used for Its Utilization for Food and Pharmaceutical Products." In *6th International Conference on Simulation and Modelling in the Food and Bio-Industry FOODSIM*.

Tuck, C, E Perez, I Horvath, R Sheldon, and M Poliakoff. 2012. "Valorization of Biomass: Deriving More Value from Waste." *Science* 337: 695–99.

United Nations Department of Economic and Social Affairs, UN. 2015. "World Population Projected to Reach 9.7 Billion by 2050."

United States Department of Agriculture, USDA. 2015. "U.S. Food Waste Challenge."

United States Environmental Protection Agency, EPA. 2014a. “Advancing Sustainable Materials Management: Facts and Figures.”

———. 2014b. “Food Waste to Energy: How Six Water Resource Recovery Facilities Are Boosting Biogas Production and the Bottom Line.”

University of California Cooperative Extension. 2013. “Dairy Manure Nutrient Content and Forms.” In *Manure Technical Guide Series. University of California Cooperative Extension*, 10.

Vardon, D, B Sharma, J Scott, G Yu, Z Wang, L Schideman, Y Zhang, and T Strathmann. 2011. “Chemical Properties of Biocrude Oil from the Hydrothermal Liquefaction of Spirulina Algae, Swine Manure, and Digested Anaerobic Sludge.” *Bioresource Technology* 102 (17): 8295–8303.

Verma, M, S Godbout, S Brar, O Solomatnikova, S Lemay, and J Larouche. 2012. “Biofuels Production from Biomass by Thermochemical Conversion Technologies.” *International Journal of Chemical Engineering* 2012: 18.

Walker, L P, and D B Wilson. 1991. “Enzymatic Hydrolysis of Cellulose: An Overview.” *Bioresource Technology* 36 (1): 3–14.

Wang, X, H Chen, K Luo, J Shao, and H Yang. 2007. “The Influence of Microwave Drying on Biomass Pyrolysis.” *Energy & Fuels* 22 (1).

Watkins, D, M Nuruddin, M Hosur, A Tcherbi-Narteh, and S Jeelani. 2015. “Extraction and Characterization of Lignin from Different Biomass Resources.” *Journal of Materials Research and Technology* 4 (1): 26–32.

Wilkie, A, K Riedesel, and J Owens. 2000. “Stillage Characterization and Anaerobic Treatment of Ethanol Stillage from Conventional and Cellulosic Feedstocks.” *Biomass and Bioenergy* 19 (2): 63–102.

Williams, A, M Pourkashanian, and J Jones. 2001. “Combustion of Pulverised Coal and Biomass.” *Progress in Energy and Combustion Science* 27: 587–610.

Wine Institute. 2016. “Wine Consumption in the U.S.”

Wojdalski, J, J Grochowicz, A Ekielski, K Radeka, S Stepniak, A Orlowski, I Flroczak, B Drozdz, T Zelazinski, and G Kosmala. 2016. “Production and Properties of Apple Pomace Pellets and Their Suitability for Energy Generation Purposes.” *Annual Set The Environment Protection* 18: 89–111.

World Apple and Pear Association, WAPA. 2017. “World Data Report.”

World Bank, WB. 2015. “Daily Manure Production per Animal.”

Wu. X, McLaren. J, Madl. R, and D Wang. 2010. “Biofuels from Lignocellulosic Biomass.” *Sustainable Biotechnology,* 19–41.

Yang, D, J Parlange, and L Walker. 2014. “Cellulases Significantly Alter the Nano-Scale Reaction Space for Pretreated Lignocellulosic Biomass.” *Industrial Biotechnology* 10 (6): 395–403.

———. 2015. “Revisiting Size-Exclusion Chromatography for Measuring Structural Changes in Raw and Pretreated Mixed Hardwoods and Switchgrass.” *Biotechnology and Bioengineering* 112 (3): 549–59.

Yang, J, and C Metcalfe. 2006. “Fate of Synthetic Musks in a Domestic Wastewater

Treatment Plant and in an Agricultural Field Amended with Biosolids." *Science of the Total Environment* 363: 149–65.

Yin, S, R Dolan, M Harris, and Z Tan. 2010. "Subcritical Hydrothermal Liquefaction of Cattle Manure to Bio-Oil: Effects of Conversion Parameters on Bio-Oil Yield and Characterization of Bio-Oil." *Bioresource Technology* 101 (10): 3657–64.

Ying, G, and R Kookana. 2007. "Triclosan in Wastewaters and Biosolids from Australian Wastewater Treatment Plants." *Environment International* 33: 199–205.

Younis, K, and S Ahmad. 2015. "Waste Utilization of Apple Pomace as a Source of Functional Ingredient in Buffalo Meat Sausage." *Cogent Food & Agriculture* 1 (1).

Zacharof, M. 2016. "Grape Winery Waste as Feedstock for Bioconversions: Applying the Biorefinery Concept." *Waste Biomass Valorization*, 1–15.

Zakzeski, J, P Bruijnincx, A Jongerius, and B Weckhuysen. 2010. "The Catalytic Valorization of Lignin for the Production of Renewable Chemicals." *Chem. Rev.* 110: 3552–99.

Zhou, K, and J Raffoul. 2012. "Potential Anticancer Properties of Grape Antioxidants." *Journal of Oncology* 2012: 8.

Zhu, L, J O'Dwyer, V Chang, C Granda, and M Holtzapple. 2008. "Structural Features Affecting Biomass Enzymatic Digestibility." *Bioresource Technology* 99 (9): 3817–28.

CHAPTER II
OBJECTIVES AND APPROACH

2.1 Dissertation Objectives

A key motivation of this work is to help industries whose potential for scalability is hindered by the management limitations and challenges of the waste they generate. In addition, if those wastes could be managed in a way that can create value (biofuels and platform chemicals), we would be able to shift a serious problem into a great opportunity. As a result, the main goal of this research is to provide improved understanding of several technology options for mitigating the environmental concerns related to industrial biomass treatment practices. Such improved understanding will inform methods to reinvigorate local bio-economies, and find sustainable alternatives for petroleum-derived products. Specifically, the objectives of this dissertation are

1. Methods development for the characterization of chemical structures and functionalities of products obtained from the thermochemical and biochemical conversion of a range of representative biomass feedstocks. This characterization is of capital importance to reveal obscure thermochemical reaction mechanisms on biomass, and to expand the variety of applications of the products obtained.
2. Investigate the effect of reaction conditions of hydrothermal processing of wet organic wastes. Of particular interest are the effects of reaction temperature and time, substrate composition and type, and pH on the product distribution (bio-oil, hydro-char, water-soluble molecules, and gas) as well as how reaction pathways and rates are influenced. This new

quantitative knowledge will provide a means for tuning reaction conditions to favor particular products, based on market demand.

2.2 Dissertation Approach

Part I. FTIR methods development for the characterization of model cellulose and lignocellulosic biomass

The first objective is addressed by applying infrared techniques in the characterization of a model substrate that accounts for part of the composition of lignocellulosic biomass. Existing literature methods using Fourier Transform Infrared are not satisfactory in terms of characterizing crystallinity of model cellulose upon enzymatic hydrolysis. Therefore, different experimental standardized methods will be used to prepare the substrate in such a way to provide reproducible spectra without any interference from internal standards or saccharification products in the hydrolizate. In addition, computational techniques will be developed to quantify and identify spectral peaks representing chemical bonds that are an accepted metric for crystallinity quantification. As a next step, real lignocellulosic biomass substrates will be considered, using a distribution of particle sizes to determine its effect in spectral signal intensity and reproducibility. Studies using two different sampling strategies in FTIR: Attenuated total reflectance (ATR) and high-throughput sampling (HTS-XT) will be used to evaluate their effectiveness. Computational techniques will be used to apply different processing strategies to spectral signals and determine the one that yields the lower spectral variance but maintaining the magnitude of the spectral features. The goodness of spectral signal processing techniques will be evaluated using the VM ratio. This index has been used in previous studies to determine the reduction of particle size effect

over spectral reproducibility upon signal processing in the near infrared region of the spectra for powdered medicines, sucrose, and hay. This is the first time, to the best of our knowledge, that this index will be used for biomass in the mid-infrared region of the spectra. In addition, the multivariate statistical method for spectra analysis Principal Component Analysis (PCA) was developed and validated. It proved to be a very useful technique to reduce the dimensionality of spectral data, and to extract information about the evolution of chemical structures and functionalities from complex spectra with many peaks from a great variety of functionalities and vibrational modes overlapping on each other (Convoluted spectra).

Part II: Thermochemical valorization of model compounds and organic wet wastes from a variety of industries and characterization of the products: Influence of pH, temperature, and reaction time in product distribution and quality

The techniques developed and tested in Part I will be utilized in Part II for the infrared characterization of chemical structure and functionality of products produced from hydrothermal liquefaction of wet organic wastes.

Given that the main objective of Part II of the dissertation is to characterize the reaction kinetics and pathways of biomass under hydrothermal liquefaction conditions, reactions of specific model compounds that constitute representative components of organic wastes (carbohydrates, lipids, and proteins) will be studied. Moving on to real biomass substrates, two substrates (manure and food waste) were selected to determine the effect of pH in carbon distribution toward the bio-oil, hydro-char, aqueous, and gas phase upon hydrothermal liquefaction at 300˚C and 60 minutes. The study was expanded by adding new substrates (olive oil pomace, apple pomace, red wine pomace,

activated waste sludge, whiskey stillage, and whey) and wider reaction conditions (reaction time 5 and 60minutes and temperatures 250 and 300˚C).

Our approach will be to run end-point experiments, where all the material from the reactor is discharged at a specific reaction time under a certain temperature. Although this approach will not provide detailed kinetic information, it will quantify mass balances for specific reaction temperatures, pressures and times. Gravimetric studies will be used to determine the mass yield towards bio-oils and hydro-char at the conditions studied. Using elemental analysis of bio-oils and hydro-char and the Total Organic Carbon for the aqueous phase, carbon balances can be independently determined. In addition, the phases were chemically characterized, and the results were related to the different pH of the substrate and reaction conditions. The techniques used will be FTIR (hydro-char), FTIR and GC-MS (bio-crude oil), and HPLC (aqueous phase). FTIR was coupled multivariate statistics to render more information about chemical bonding cleaved and formed during thermochemical processes.

Part I

FTIR methods development for the characterization of model cellulose and lignocellulosic biomass

CHAPTER III

MEASURING CELLULOSE CRYSTALLINITY AFTER ENZYMATIC DIGESTION USING FOURIER TRANSFORM INFRARED SPECTROSCOPY (FTIR)

This chapter was co-authored with Dr. Nathan Kruer-Zerhusen and Prof. David Wilson from the Department of Molecular Biology and Genetics at Cornell University. It was sent for publication to the journal Cellulose (2017) (Kruer-Zerhusen. N, Cantero-Tubilla. B, Wilson. D) and accepted for publication after reviews.

This chapter is dedicated to the memory of Professor David Wilson.

3.1 Introduction

Carbohydrates obtained from the breakdown of biomass can be utilized by various microorganisms to produce alcohols or combustible hydrocarbons for use as transportation fuels. The bottle-neck in the development of an efficient and economically feasible system to produce biomass fuels is the enzymatic hydrolysis of cellulose by cellulases (Kostylev and Wilson 2011). The digestion of insoluble cellulose is complicated by the multiple enzymatic steps required for cleavage and by the heterogeneity of the substrate, which changes during the reaction. A constant rate of hydrolysis is never achieved during cellulose digestion, and the rate begins to drop off rapidly after the initial digestion. A decrease in substrate reactivity with the extent of substrate digestion has been demonstrated, although the exact reasons for the increased recalcitrance are not easily determined (Kostylev and Wilson 2013).

Cellulose is a crystalline lattice of closely packed polysaccharide chains, non-covalently linked by an extensive hydrogen bonding network. Cellulases modify the cellulose substrate during digestion, and the impact of these structural changes on cellulase kinetics is not well understood

(Kostylev and Wilson 2013; Väljamäe et al. 2003; Xu & Ding 2007). Cellulose crystallinity, the degree of organization of the lattice, is correlated with more stable cellulose (Lionetto et al. 2012). Substrate recalcitrance is the combination of physical and chemical factors that contribute to reduced cellulase activity. Cellulose crystallinity is thought to play a major role in the activity of most cellulases. Although it is a commonly held hypothesis, the link between changes in crystallinity and cellulase digestion has not been conclusively established by existing work. Two hypotheses of the role of crystallinity in substrate recalcitrance have been investigated. Increasing cellulose crystallinity is an intuitive hypothesis; crystalline regions are more difficult to degrade, so as cellulases preferentially target the less ordered chains, the crystalline regions become more abundant and the reaction slows (Mansfield and Meder 2003; Park et al. 2010). Alternatively, increasing substrate heterogeneity has been described as the mechanistic basis of recalcitrance leading to decreasing cellulase activity. Accessible cellulose active sites decrease as substrate heterogeneity increases, leading to decreased surface area, collapsed pore structure, and surface obstacles that inhibit cellulase movement and activity (Zhang et al. 1999, Väljamäe et al. 1998). Directly testing these models requires measuring changes to cellulose structure, and the measurement of numerous non-covalent inter- and intra-molecular bonds presents a technical challenge.

The cellulase field has worked to understand the close relationship between cellulose recalcitrance and cellulase kinetics. Recalcitrance is most often observed indirectly as decreasing soluble sugar release during cellulase reactions (Kostylev and Wilson 2013). Cellulose crystallinity measurements are now more accessible using Fourier transform infrared spectroscopy (FTIR), X-ray diffraction (XRD), and nuclear magnetic resonance (NMR) (Park et al. 2010). Recent advances in atomic force microscopy (AFM) enable cellulose surfaces to be observed directly with low

resolution, or indirectly using single enzyme particles (Igarashi et al. 2009; Jeoh et al. 2013). Results from studies using multiple techniques have varied due to structural complexity and sample preparation, with some results correlating crystallinity and cellulase kinetics and other studies showing little or no effect.

FTIR is capable of rapid and noninvasive quantification of both covalent and non-covalent interactions within cellulose, enabling measurement of crystallinity of the material expressed as crystallinity indexes. FTIR is also applicable to more complex and industrially relevant cellulose applications, and may be used to investigate the effect of biomass type, pretreatment, and enzyme cocktail interactions on sugar release.

In early work using *Clostridium thermocellulm* cellulosomes, bacterial cellulose (BC) and *Valonia ventricosa* cellulose crystals, TEM showed significant physical changes to cellulose after hydrolysis but XRD and FTIR measurements showed the crystallinity of the residual cellulose unchanged (Boisset et al. 1999). Changes in crystallinity caused by *Cellulomonas fimi* endocellulases, exocellulases, and their synergistic mixtures were measured using both FTIR and solid state NMR (Mansfield and Meder 2003). The results showed that endocellulases increased the overall crystallinity, while exocellulases reduced it. The magnitude of changes was small but observed using both detection approaches. More recently, a report using High Throughput Screening FTIR (HTS-FTIR) has strongly suggested a correlation between cellulose crystallinity and cellulase digestion (Corgie et al. 2011). Using *Thermobifida fusca* cellulases (*Tf*Cel6B, *Tf*Cel5A, and *Tf*Cel9A), highly significant changes to cellulose crystallinity were observed which appeared to correlate with cellulase loading. This high-throughput FTIR approach has significant potential for use in exploring the relationship between crystallinity and cellulase digestion, however it may not be sufficiently discriminatory of the source of bonds within complex samples.

This chapter describes experiments using HTS-FTIR to measure cellulose crystallinity after digestion by *T. fusca* cellulases, in an attempt to correlate cellulase kinetic parameters to crystallinity changes. The goal was to validate and expand on the work of Corgie et al. (2011) using the same measurement approach, cellulose substrate, and cellulase loadings. Using a model cellulose substrate hydrolyzed using either individual cellulases, incomplete synergistic mixtures, or an intact cellulase secretome, this work builds upon several reports of a lack of correlation between cellulose crystallinity and extent of cellulose digestion (Boisset et al. 1999; Cao and Tan 2002; Chen et al. 2007; Corgie et al. 2011).

3.2 Materials and Methods

3.2.1 Substrates and enzymes

Cellulose substrates were prepared using methods described elsewhere (Kostylev and Wilson 2011), summarized in brief here. Bacterial cellulose (a gift from Monsanto, San Diego, CA) was resuspended overnight at 4 °C, then washed with Milli-Q water with four cycles of centrifugation and resuspension to eliminate soluble sugars. The final concentration of the substrate was determined by measuring dry weight in triplicate. Sodium azide was added to all substrates at a final concentration of 0.02% to prevent microbial contamination. The cellulases used, *Thermobifida fusca* Cel48A, Cel9A, Cel5A, lytic polysaccharide monooxygenase LPMO10B, and ER1 crude supernatant were prepared using previously described methods (Irwin et al. 2003; Kostylev and Wilson 2011; Li et al. 2010).

3.2.2 Hydrolysis assays assembly

Enzyme and substrate stocks (master mixes) were prepared separately at twofold concentration and combined in Eppendorf protein LoBind 96-well format microplates. Cellulose substrates, ranging in final concentration from 1.25-5.0 mg/ml were distributed by manually dispensing the substrate master mix using wide aperture pipette tips. An equal volume of enzyme master mix, final concentration of 10-1000 nM, was added using an Eppendorf EpMotion 5075Vac liquid handling robot, bringing each well to a final volume of 160 µl and a final buffer concentration of 50 mM sodium acetate (pH 5.5). Plates were sealed (AB-0745 seals, Fisher Scientific), then vortexed briefly on each corner to ensure substrate suspension at the start of incubation. Plates were incubated in a 48-plate tower incubator (StoreX STX40, Liconic US Inc, Woburn, MA) at 50 °C with constant horizontal shaking (150 rpm). Samples were removed at the appropriate times, increments of 2 to 24 hours, by a Zymark plate handling system (Twister II, PerkinElmer Inc., Waltham, MA). Reactions were immediately stopped by heating to 100 °C for 5 minutes within a PCR thermocycler heating block (PTC-100, MJResearch inc, Waltham, MA).

3.2.3 Extent of digestion quantification

Hydrolysis samples were centrifuged for 5 minutes at 4,000 rpm (RCF = 3313) to separate residual substrate, then 40 µl of supernatant was transferred to a new 96-wells microplate. For complete secondary hydrolysis of short oligosaccharides to glucose, 120 µl of excess Novo188 β-glucosidase (buffer exchanged with 50 mM NaOAc, pH 5.5, 10% glycerol, 0.22 CBU/ml) (Novozymes, Davis, CA) was added, maintaining the final buffer concentration of 50 mM sodium acetate (pH 5.5). A cellobiose standard curve was added to each plate to confirm complete hydrolysis, and plates were incubated for 16 hours as described above.

The extent of digestion was determined by quantifying released glucose using the bismuth-catalyzed p-hydroxybenzoic acid (PAHBAH) method of Lever (1977), modified for microscale analysis and validated using existing HPLC quantification methods (Kostylev et al. 2014). The PAHBAH reaction of 120 µl PAHBAH reagent added to 40 µl of hydrolysate was heated using a PCR thermocycler at 70 °C for 10 minutes, cooled to 4 °C for 5 minutes, and finally brought to room temperature as recommended by King et al. (2009). The reaction was transferred to flat bottom polystyrene plates (Costar 9017, Corning Inc., Corning, NY), and measured at 410 nm using a microplate spectrophotometer (Synergy 2, BioTek Instruments Inc., Winooski, VT). PAHBAH signal was blank removed and compared to the hydrolyzed G2 standard curve, quantified as units of anhydrous glucose (162 g mol^{-1}) (Olsen et al. 2014) shown in Figure 3.1. The extent of digestion was calculated relating the sugar released with the maximum sugar contained in the substrate using Eq 1:

$$\%\ \text{Digestion} = \frac{\mu\text{mol glucose released}}{\mu\text{mol glucose in BC}} * 100 \ ; \ \mu\text{mol glucose in BC} = \frac{\text{mg BC}}{0.162\ \text{mg}/1\ \mu\text{mol}}$$

Eq(1)

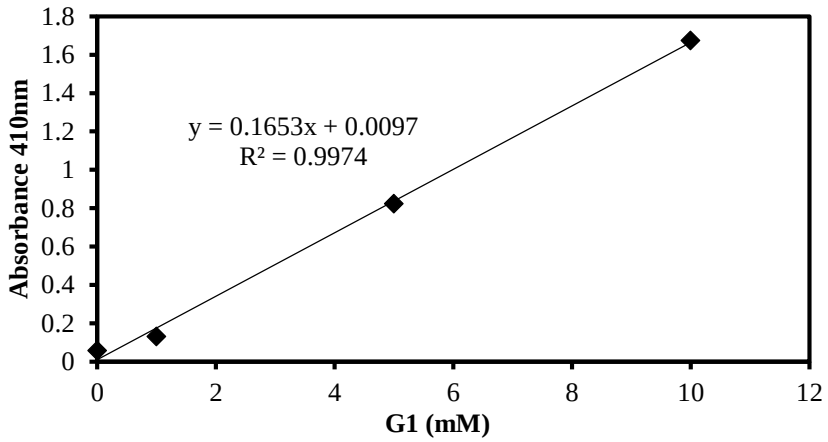

Figure 3.1. Standard curve to relate the signal developed by PAHBAH with the concentration of glucose.

3.2.4 Residual cellulose processing and plating for FTIR

The residual cellulose was washed and the concentration normalized prior to plating. These two steps, together with the lack of internal standard in FTIR measurements, constitute the main methods improvements compared to the experimental protocol used by Corgie et al. (2011). First, the cellulose within the assay hydrolysate was thoroughly resuspended, using narrow aperture pipette tips, and transferred to a 96-well filter plate (Pall 380 µl 0.45 µm filter plate, SUPOR membrane). For comparison of the effect or pipette tip aperture used for cellulose resuspension on the reproducibility of BC standard curve crystallinity measurements, either narrow or truncated tips were explored and shown in Figure 3.2. The liquid fraction was separated by vacuum filtration and stored for validation by HPLC. The residual cellulose was resuspended in Milli-Q water and washed three times on the filter to remove all soluble compounds. In order to normalize the residual cellulose concentrations for all the hydrolysis time samples, residual cellulose was thoroughly resuspended in an appropriate volume of Milli-Q water to account for the fraction of cellulose digested during hydrolysis. 50 µl of this suspension was transferred (either manually using a multichannel pipette or using the EpMotion liquid handling system) to clean and dried 96-well silicon FTIR-HTS plates (Bruker Optics, Germany). Each sample biological replicate was plated in triplicate on the FTIR plate. On each plate, a substrate standard curve of known concentrations was added in triplicate, and a well was left empty for background measurement. After samples were distributed onto the silicon plate, variance in surface tension caused occasional incomplete well coverage, which required manual spreading of the sample to evenly cover the well surface. This simple step decreases variance between replicates. Sample plates were placed in a freshly recharged desiccator for gradual drying at least 16 hours at room temperature. Drying was

completed by heating in a vacuum oven at 60 cm Hg vac. and 70 °C for at least 8 hours. The plates were allowed to return to 25 °C prior to measurement.

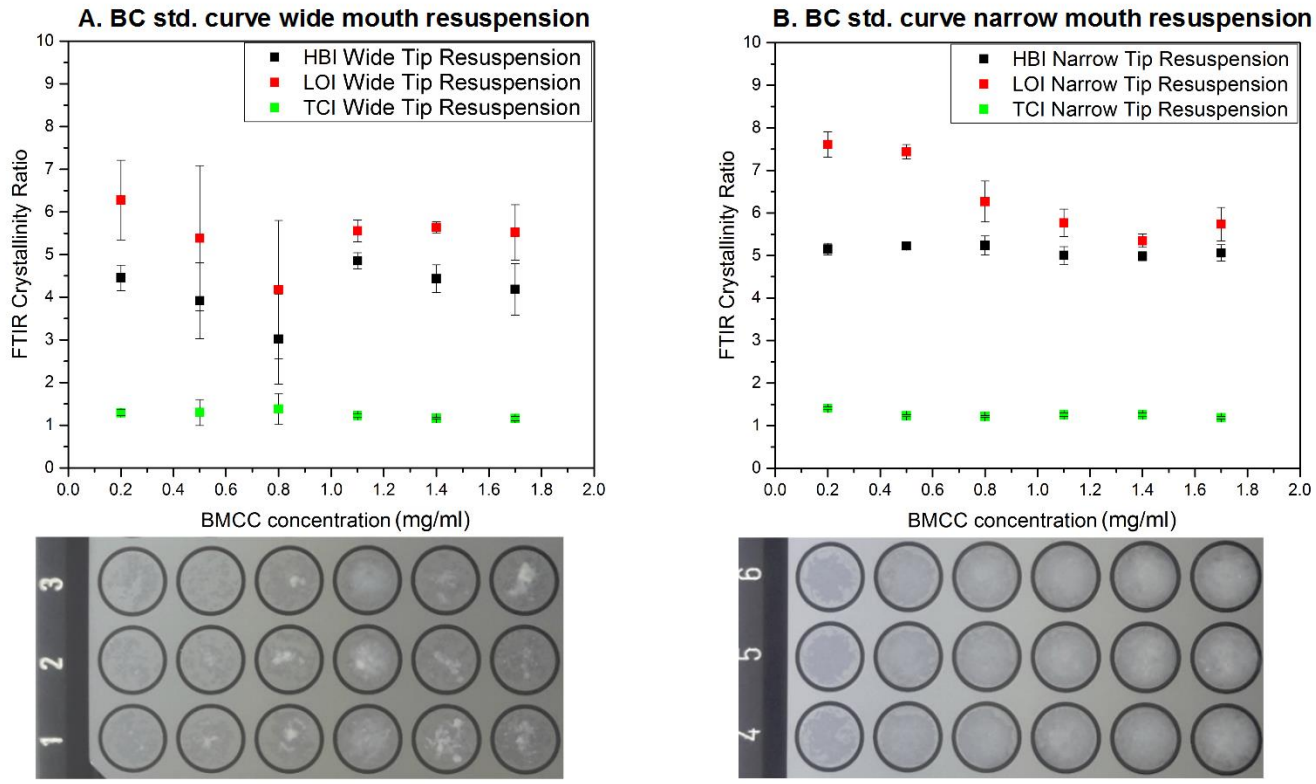

Figure 3.2. Effect of pipette tip aperture (used for BC resuspension and plating on the FTIR silicon plate) on BC crystallinity index values standard curve and variance. Error bars represent standard deviation of triplicate samples. A) Resuspension using wide-aperture tips. B) Resuspension using narrow-aperture tips. The pictures of the FTIR silicon plates are also shown. When resuspending and plating residual BC after digestion with narrow-aperture tips, a homogeneous thin film of material is achieved on the plate, leading to cleaner data (less variance). The reason for this is the shear stress imprinted on the fibers upon resuspension with the narrow-aperture tips. When using wide-mouth tip, chunks of materials are observed on the FTIR plate, leading to higher variance on the spectral data.

3.2.5 FTIR measurement and data processing

All FTIR spectra were collected in transmission mode and atmospheric compensated, between 7000 and 400 cm^{-1} wavenumbers, 2 cm^{-1} spectral resolution, and 32 scans per sample using a Bruker Vertex 70 FTIR spectrometer (Bruker Optics, Germany) equipped with a HTS-XT module.

Prior to detection, calibration of the equipment was performed according to manufacturer instructions. Two factor zero filling was applied during data collection.

Data processing was performed with the OPUS software package using a self-design macro script. The raw spectra were converted from transmittance to absorbance and cut to remove wavenumbers above 4000 cm^{-1}. Concave rubber band baseline correction was applied (10 iterations), and the resulting spectra were analyzed without normalization (as the concentration for the samples was experimentally normalized). The intensity values of second derivative peak heights for each sample (used for quantification based on the consistency of signal intensity after concentration normalization) were used to calculate the three standard crystallinity indexes described in literature. A crystallinity index (CI) is the ratio of a peak related to crystallinity to a peak not representing crystallinity within the same spectrum. Hydrogen bonding intensity (HBI) is the ratio between 3350 cm^{-1}/1337 cm^{-1}, lateral order index (LOI) is the ratio between 1427 cm^{-1}/895 cm^{-1}, and total crystallinity index (TCI) is the ratio between 1373 cm^{-1}/2900 cm^{-1}. The resulting values for each sample were imported into OriginPro 2015 (OriginLab, Northampton, MA) for visualization and graphing. The time course reaction kinetics were analyzed by applying the two-parameter power law fit to % digestion data according to Kostylev and Wilson (2011).

3.3 Results

3.3.1 Methods improvement

Cellulose samples with varying extents of digestion can only be compared meaningfully using the HTS-FTIR technique when many variables are carefully controlled. Changes to the HTS-FTIR sample preparation methods described by Corgie et al. (2011) were necessary in order to obtain

clean raw spectra and reliable measures of cellulose crystallinity. The sample preparation methods were improved to remove extraneous overlapping signals, provide accurate extent of digestion, and correct errors caused by varying cellulose concentration.

The FTIR spectrum of residual bacterial cellulose (processed following steps previously described) contains several characteristic regions serving as landmarks between 4000 cm^{-1} and 400 cm-1. They are presented in Figure 3.3A. These regions contain the peaks from individual chemical vibrational modes relevant for measuring crystallinity. A representative standard curve of BC spectra for a concentration range from 0.2 - 1.7 mg/ml in 0.3 mg/ml increments is shown in Figure 3.3B with values of the slope and chemical meaning of wavenumbers presented in Table 3.1. The spectra shown in Figure 3.3A closely match previously reported cellulose I FTIR spectra, indicating no alteration of cellulose structure during sample processing (Corgie et al. 2011). At the left of the cellulose FTIR spectrum is the hydrogen bonding region, which extends from 3800 cm^{-1} to 3000 cm^{-1} and contains signals from inter and intra-molecular interactions between hydrogen and oxygen. A key interaction is measured in the 3350 cm^{-1} peak, which results from the hydrogen bonding interaction between the 3OH-O5 adjacent to the β-glycosidic bond of the cellulose Iα structure (895cm^{-1}). Adjacent to this is the C-H bonding region, which is much narrower between 3000 cm^{-1} and 2800 cm^{-1}, and corresponds to the stretching of C-H moieties. In the middle of the Mid-IR wavenumber range, signals from other heteroatoms such as nitrogen as well as double bonds are absent from spectra of pure cellulose. The most complex region of cellulose FTIR spectra is the fingerprint region from 1430 cm^{-1} to approximately 850 cm^{-1}, which contains signals from the numerous sp^3 single bond vibrational modes. Finally, between 850 cm^{-1} and 400 cm^{-1} is the region containing multiple bands corresponding to heavy-atom bending and rotation (Mitchell 1990).

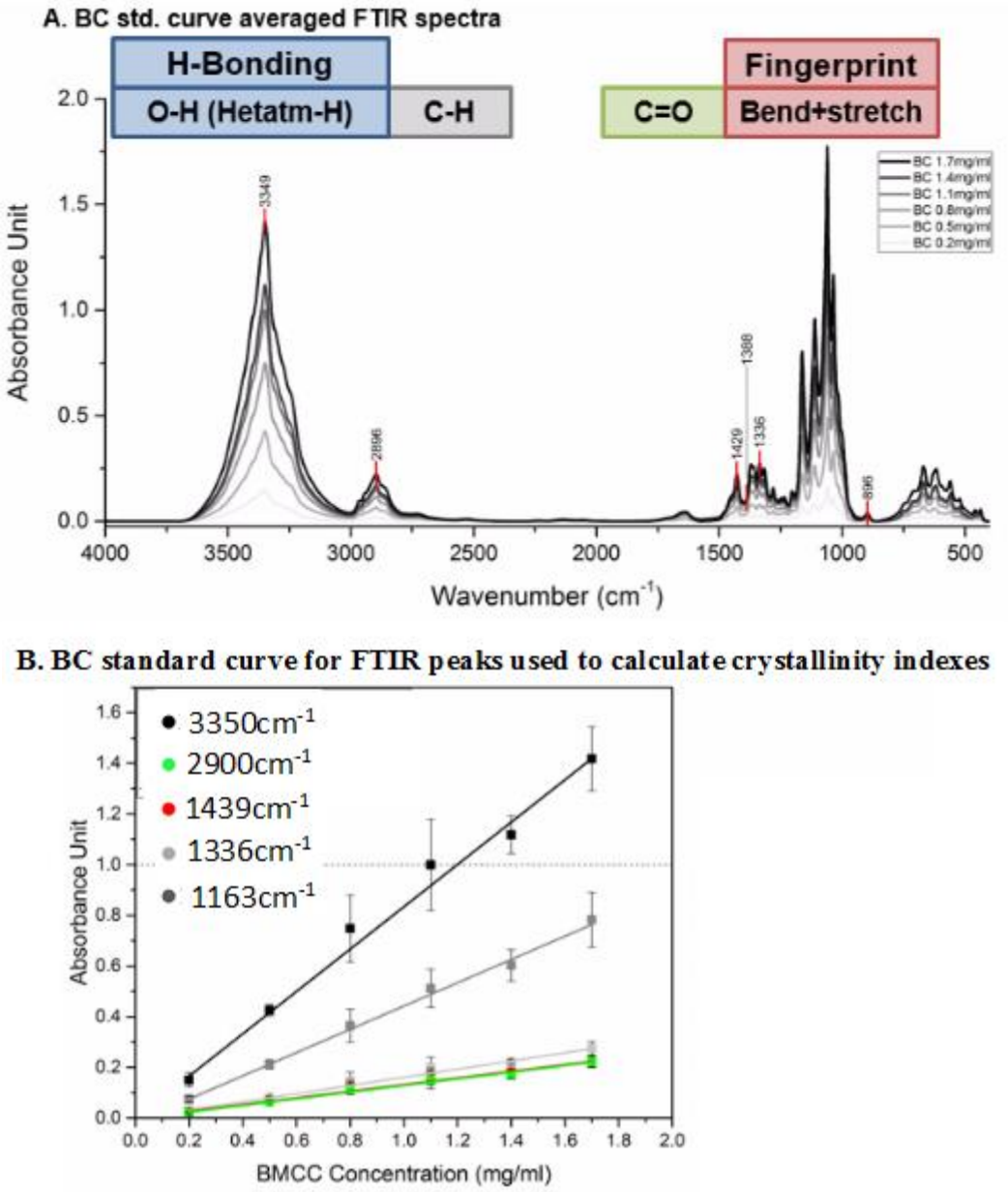

Figure 3.3. A) Bacterial cellulose FTIR spectra ranging from 0.2 to 1.7 mg/ml. B) Standard curve of peaks essential for crystallinity index calculation

Table 3.1. Values for the slope of the standard curves for bonds used for crystallinity index calculations

		f(A)=Mx	
Wavenumber (cm^{-1})	**Corresponding bond**	**M**	**R^2**
3350	O-H stretch	0.84	0.993
2900	C-H stretch	0.13	0.996
1439	C-H deformation (asymmetric)	0.13	0.998
1336	O-H in plane deformation	0.16	0.997
1163	COC asymmetric vibration	0.46	0.988

Crystallinity indexes calculated from ratios of individual peak heights, depend on the consistency of peak resolution, peak wavenumber, and peak shape over a large concentration range. Peak consistency is especially relevant as critical bonds may change in relative height after hydrolysis. Figure 3.3B demonstrates the cellulose detection range for FTIR-HTS. In this standard curve, the peak shapes of characteristic cellulose signal regions do not change with respect to concentration. The resulting values of individual peaks critical for determining cellulose crystallinity from this standard curve is shown Table 3.1. These peaks are consistent in wavenumber position, shape, and have a linear relationship with concentration. Not shown is the smaller 895 cm^{-1} peak used for calculation of the LOI crystallinity index.

The concentration of cellulose samples used is limited by the maximum signal intensity the FTIR detector can accurately measure. Based on the signal resulting from concentrations shown in Figure 3.3B, the working range for BC was determined to be under 1.25 mg/ml to remain below the manufacturer recommended signal limit of 1.0 AU for the maximum peak absorbance (Bruker). The samples presented in Figure 3.3 were processed using narrow aperture pipette tips, one of several method improvements to increase the crystallinity indexes data quality (as shown in Figure 3.2 where the crystallinity indexes for samples processed with narrow and wide aperture pipette tips at different cellulose concentrations are presented).

The concentration of the cellulose suspension plated in FTIR silicon plates determines the thickness of the cellulose film, and therefore the path length of light through the sample. The influence of cellulose concentration on crystallinity indexes was explored, and resulting data is shown in Figure 3.2B. While there is a high consistency for the TCI and HBI crystallinity indexes over the working concentration range of the transmission FTIR-HTS measurement approach, the effect of path length on LOI can be seen where LOI decreases with increasing BC concentration.

Due to this change in LOI, resuspension of residual cellulose to similar final concentrations (adjusting for % digestion after buffer exchange) was found to be an essential for meaningful data comparison.

After cessation of cellulose hydrolysis, samples contain several compounds at sufficient concentration to contribute to cellulose FTIR spectra: proteins (cellulases), cryoprotectants (glycerol), buffers (acetate), and hydrolysis products (free mono/oligosaccharides). These compounds share chemical bond compositions with cellulose, and thus produce peaks that overlap with those from cellulose vibrational modes. The polar compounds will interact non-covalently with cellulose when dried into the cellulose matrix, inflating certain signals such as the hydrogen bonding region centered at 3350 cm^{-1}. A buffer exchange and sample washing step was effective at removing soluble hydrolysate compounds to produce a clean spectrum of the residual cellulose. As shown in Figure 3.4A, three washing steps are sufficient to remove soluble sugars from the residual BC. Washing is validated in the resulting FTIR spectra, where characteristic bands from acetate (1660 cm^{-1} and 1560 cm^{-1}), sodium azide (2169 and 2050 cm^{-1}) or protein (1700-1500 cm^{-1}) are absent. Figure 3.4B shows the FTIR signal contribution to the BC signal of sodium acetate and sodium azide. These two have been reported in literature as internal standards for signal normalization (Fraser 1959) . This chapter was performed without internal standards.

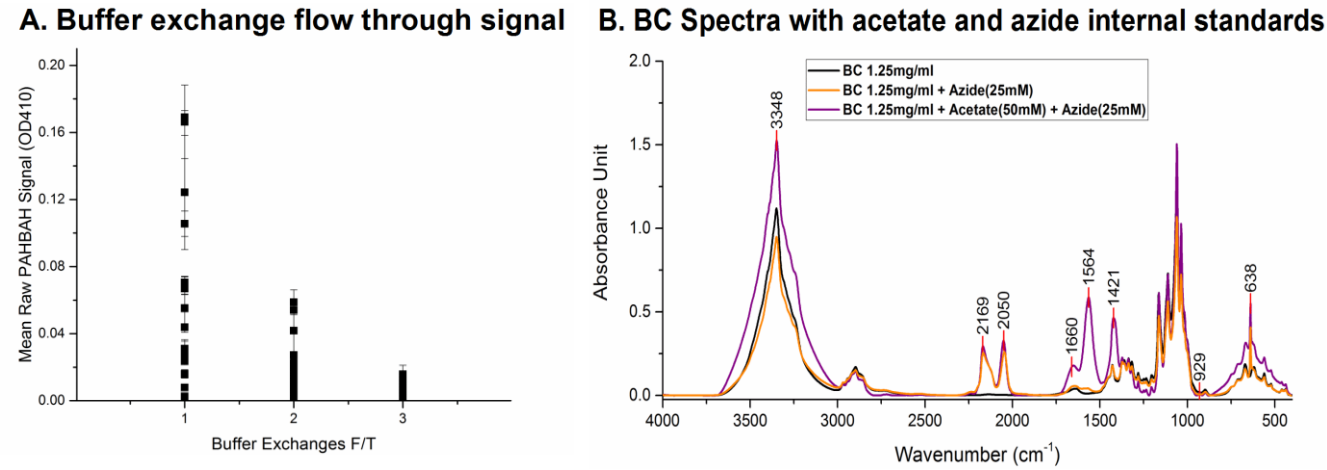

Figure 3.4. A) This figure shows the decrease of PAHBAH reducing end signals of solvent after sequential washes of the residual cellulose after digestion. Buffer exchange of hydrolysis assay samples using Milli-Q water, results in low oligosaccharide in the residual substrate, so less signal interference in FTIR spectra. B) FTIR signal contribution of internal standards used in literature. Acetate contributes signal at 3350, 1660, 1564, 1421 and 929 cm^{-1} most significantly. Azide contributes signal at 2169, 2050, and 638 cm^{-1}. In Corgie et al. (2011) sodium acetate used as internal standard was volatilized at drying oven conditions, resulting in its spread to neighboring wells and plates within the same space during the drying process. An alternative internal standard, sodium azide, was investigated and deemed to be feasible in cases where the pH is controlled to avoid volatilization of hydrazoic acid during the drying process. The azide signal is present in the 2200-2000 cm^{-1} wavenumber region and is sufficiently separated from BC signals to be a good candidate as internal standard for BC studies. In this work, no internal standard was used for signal normalization.

3.3.2 Evolution of crystallinity of model BC with digestion by individual *T. fusca* cellulases

Cellulases from the *T. fusca* model system were chosen based on their distinct mechanisms, extensive characterization, and prior investigation of their effect on cellulose crystallinity. Model cellulases were chosen to reproduce and expand on the significant results from Corgie et al. (2011), and to understand how their diverse mechanisms affect cellulose crystallinity. Initial hydrolysis assays were conducted prior to developing the method improvements described above, and resulting FTIR spectra are highly similar to those presented by Corgie et al. (2011). Cel9A cellulase was used for these methods comparison.

The most significant correlation between cellulase digestion and increasing crystallinity observed by Corgie et al. (2011) resulted from digestion by the processive endocellulase Cel9A. To

reevaluate the effect of Cel9A digestion on BC crystallinity, the conditions for the Cel9A time course hydrolysis assay were chosen to match the extent of digestion observed by Corgie et al. (2011), as seen in the color-filled diamonds in Figure 3.5. The enzymatic assay was performed on 1.25mg/ml BC by different Cel9A concentrations ranging from 0 to 1000nM. Table 3.2 shows the values of the fitting parameters of the data to a power law expression. The close agreement with prior extent of digestion results indicates that similar enzymes, substrates, and incubation conditions were employed in this work. In addition, a range of seven Cel9A concentrations from 10 to 1000 nM, and higher BC substrate concentrations (2.5, and 5 mg/ml) were tested and shown in Figure 3.6 (for 2.5mg/ml BC) and Figure 3.7 (for 5.0mg/ml BC). By comparing of the hydrolysis at different concentrations of substrate, the yield of digestion decreases as the BC concentration increases. For 5mg/ml BC, the yield of digestion did not reach 30% in 24 hours using the highest enzyme concentration, whereas, the digestion reached 50% and 75% for 2.5 and 1.25mg/ml BC, respectively. Lower digestion at higher substrate concentration meant an increase in residual substrate after reaction. When analyzed in FTIR, more substrate yielded higher spectral signal intensity, overcoming the upper threshold for the detector (1 absorbance unit) for assays at 5mg/ml BC.

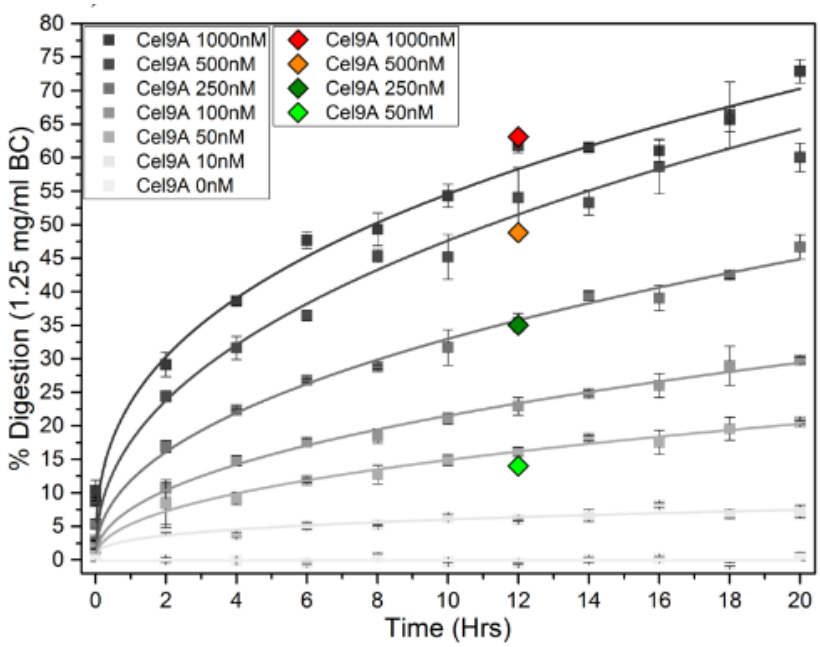

Figure 3.5. Yield of digestion for time course hydrolysis assay of BC (1.25mg/ml) using Cel9A. Data points shown in colored diamonds are those reported by Corgie et al. (2011), showing high agreement with the original assays from this work presented in grey scale. Every data point is the average of three replicate assays, and the errors bar are the standard deviation.

Table 3.2. Values of the two-parameter nonlinear fit of Cel9A time course digestion processed according to Kostylev and Wilson (2013) for 1.25mg/ml BC and different enzyme concentration.

	$f(t)=A\ t^b$		
Experiment	**A**	**B**	**R^2**
Cel9A 1000mM	23.5	0.36	0.96
Cel9A 500mM	17.6	0.43	0.95
Cel9A 250mM	11.8	0.44	0.98
Cel9A 100mM	7.6	0.45	0.98
Cel9A 50mM	5.3	0.44	0.97
Cel9A 10mM	2.9	0.31	0.77

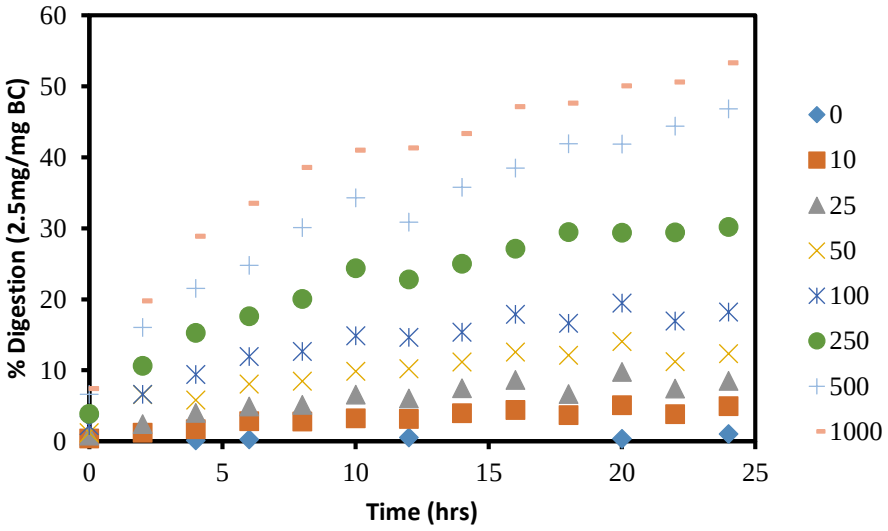

Figure 3.6. Yield of digestion for time course hydrolysis assay of BC (2.5mg/ml) using Cel9A at 8 different concentrations. Every data point is the average of three replicate assays and the errors bar are the standard deviation.

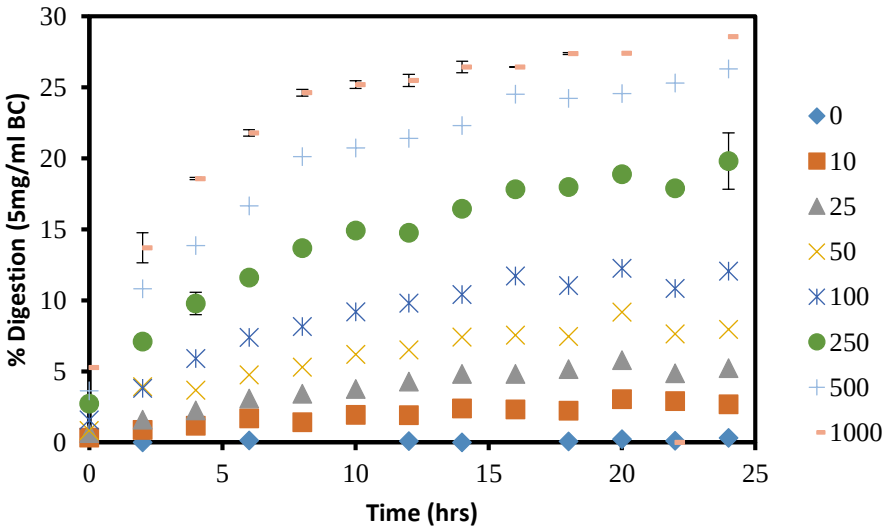

Figure 3.7. Yield of digestion for time course hydrolysis assay of BC (5.0mg/ml) using Cel9A at 8 different concentrations. Every data point is the average of three replicate assays, and the errors bar are the standard deviation.

The time course hydrolysis assay for Cel48A and its comparison with the results obtained from Corgie et al. (2011) are presented in Figure 3.8.

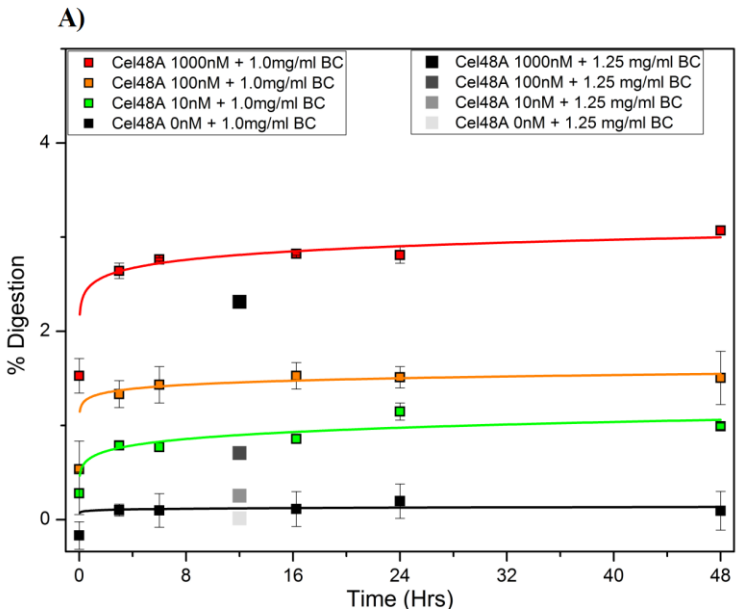

Figure 3.8. A) Yield of digestion for 48 hours hydrolysis using 1mg/ml BC and a range of Cel48A concentrations (0-1000 mM ten-fold variation). The grey scale data at 12 hours are the results from Corgie et al. (2011). The color assays are original from this chapter. Every data point is the average of three replicate assays, and the errors bar are the standard deviation.

Crystallinity index changes upon BC Cel9A digestion obtained in this chapter, and the comparison with the results from Corgie et al. (2011) are shown in Figure 3.9. Two representative data sets are shown, with similar results than observed for other concentration combinations that are omitted from the representation for clarity purposes. In addition, the lower digestion observed for 5mg/ml BC made the FTIR signal of the residue above the detector threshold, so the data for higher BC concentration was not further utilized. In all conditions, the crystallinity indexes of the residual substrate were not significantly different compared with the BC only negative control (represented as colored dots at 20 hours assay). Samples reported by Corgie et al. (2011) showed a strong correlation between digestion and crystallinity index ratio values (colored points). Figure 3.10 shows the crystallinity index HBI of BC hydrolysed with Cel48A and the comparison with the results obtained by Corgie et al. (2011) for 12 hours assays.

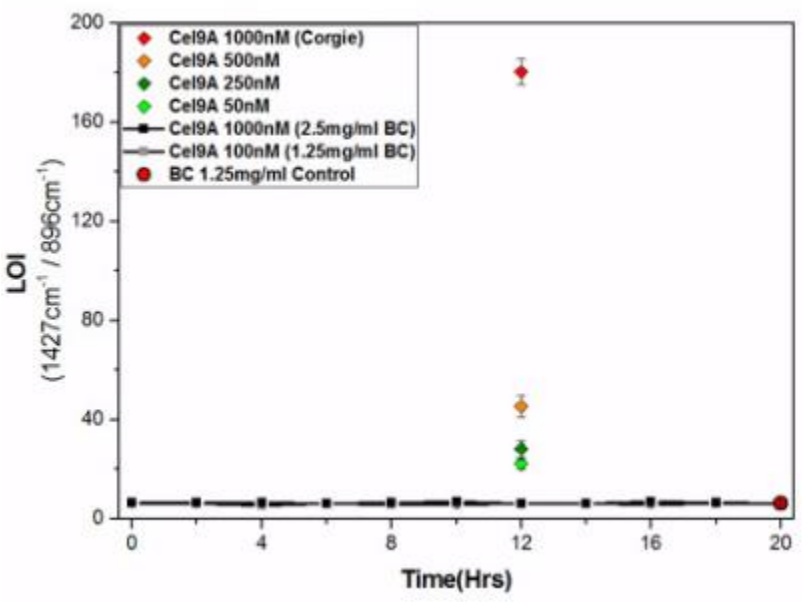
Cel9A 1000nM (Corgie)
Cel9A 500nM
Cel9A 250nM
Cel9A 50nM
Cel9A 1000nM (2.5mg/ml BC)
Cel9A 100nM (1.25mg/ml BC)
BC 1.25mg/ml Control
LOI
(1427cm-1 / 896cm-1)
Time(Hrs)

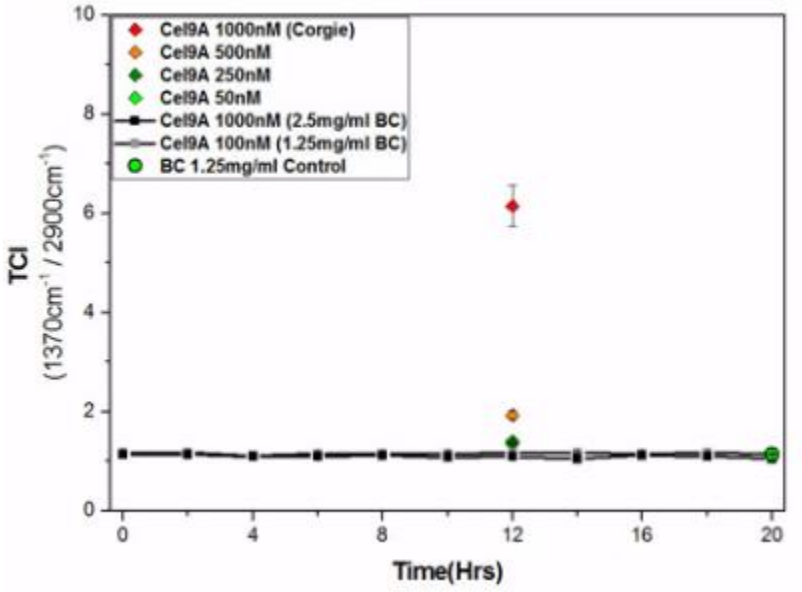
Cel9A 1000nM (Corgie)
Cel9A 500nM
Cel9A 250nM
Cel9A 50nM
Cel9A 1000nM (2.5mg/ml BC)
Cel9A 100nM (1.25mg/ml BC)
BC 1.25mg/ml Control
TCI
(1370cm-1 / 2900cm-1)
Time(Hrs)

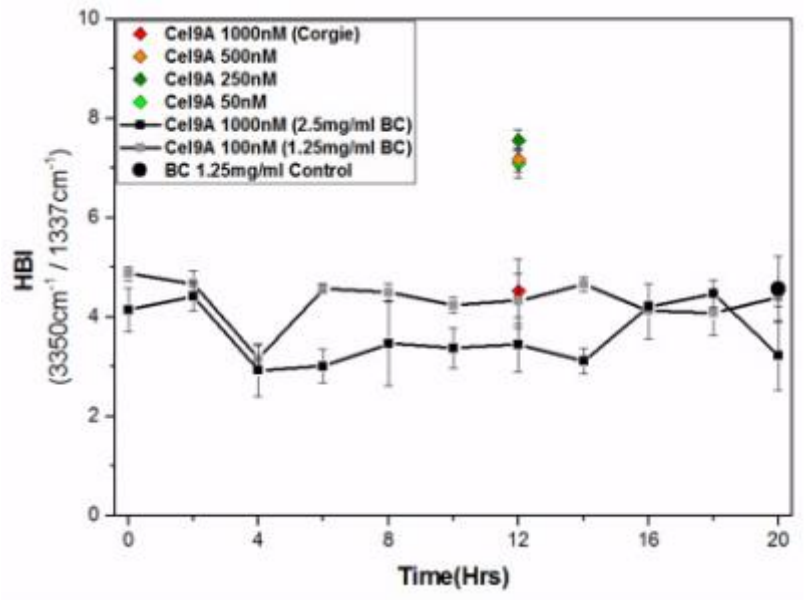

Figure 3.9. FTIR LOI, TCI, and HBI crystallinity index values of two concentrations of Cel9A and BC (black lines) plotted with respect to time for Cel9A hydrolysis. Values with colored diamond symbols are those reported by Corgie et al. (2011) using 1.25mg/ml BC. Values in large circles are those for BC only controls at 20 hours (no cellulase).

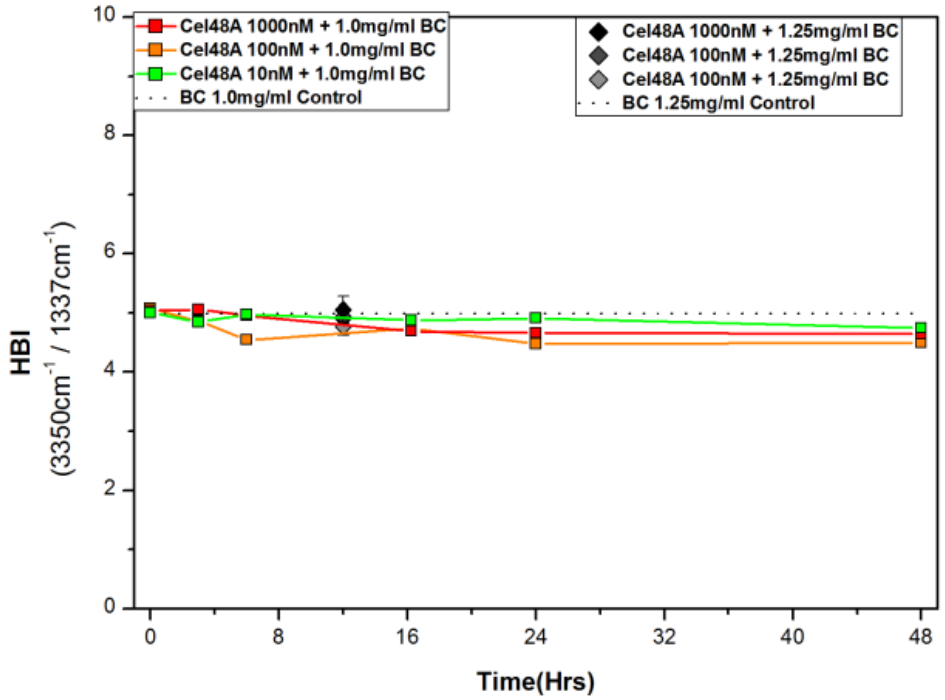

Figure 3.10. FTIR HBI crystallinity index values of three concentrations of Cel48A and BC concentration of 1.25mg/ml (colored lines) plotted with respect to time for Cel48A hydrolysis. Values with grey scale squares are those reported by Corgie et al. (2011) using 1.25mg/ml BC for 12 hours. Dotted line is the control for experiments without cellulase.

The cleavage activity of lytic polysaccharide monooxygenases (LPMOs) on bacterial cellulose structure was compared with hydrolytic cleavage by the classical endocellulase Cel5A. Two forms of the *T. fusca* type I LPMO TfLPMO10B were tested, full length wild type (WT) and the LPMO catalytic domain (CD) form. It was observed that digestion of BC by either Cel5A or AA10B resulted in no significant change to the three crystallinity indexes as compared to the substrate only negative control (Figure 3.11). Table 3.3 shows the kinetic parameter of the assay fitted to a power law expression.

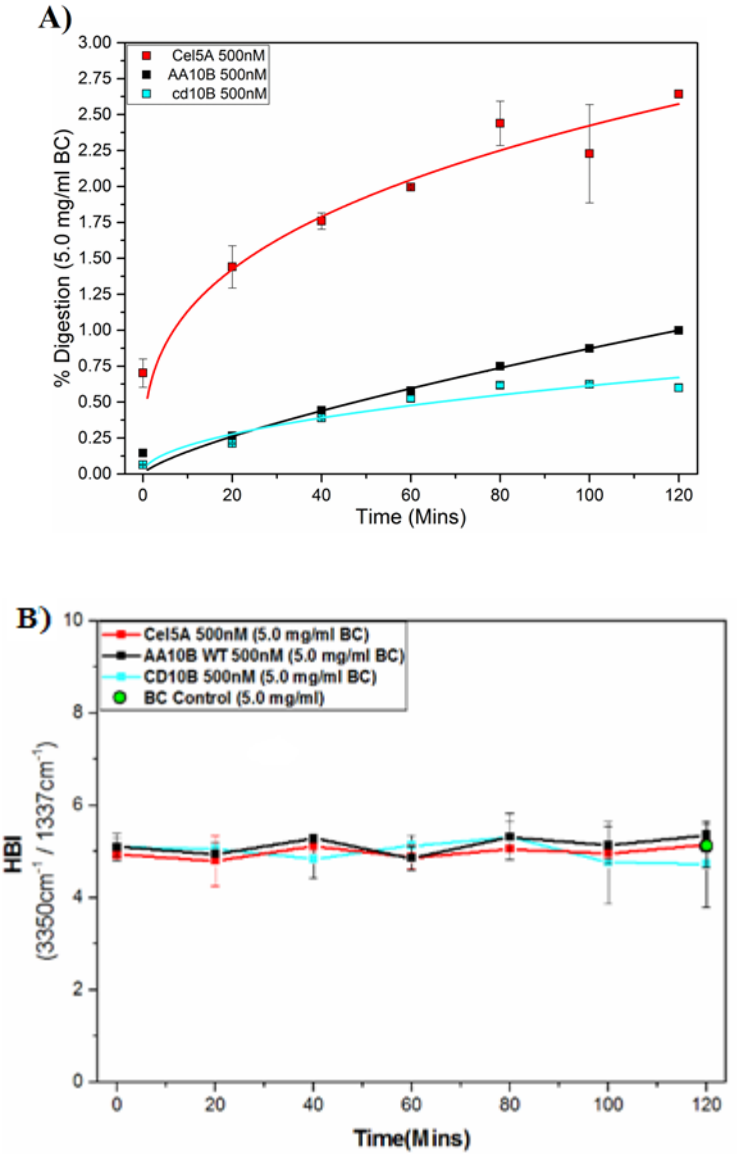

Figure 3.11. A) Yield of BC (5 mg/ml) hydrolysis assay by 0.5 uM TfCel5A (red), TfAA10B WT (black), and TfAA10B CD only (light blue). B) FTIR HBI crystallinity index values of BC after digestion with TfCel5A (red), TfAA10B WT (black), and TfAA10B CD only (light blue). Points represent the average of three values, with error bars corresponding to standard deviation. Green dot at the 2 hours digestion represent the value of crystallinity for the control assay (no cellulase).

Table 3.3. Kinetic parameters of the three enzymes showing differences in both A and b parameter.

	$f(t)=A\ t^b$		
Experiment	**A**	**b**	**R^2**
TfCel5A	0.53	0.33	0.92
TfAA10B WT	0.03	0.75	0.99
TfAA10B CD	0.06	0.52	0.89

3.3.3 Evolution of crystallinity of model BC with digestion by *T. fusca* ER1 cellulase mixture

To confirm that the lack of crystallinity index change after digestion was not caused by the low extent of hydrolysis (Cel48A), or the limitations of a monofunctional cellulase acting alone (Cel9A), *T. fusca* ER1 crude supernatant (a complete high activity cellulase system) was investigated over a wide range of % BC digestion. Cellulase mixtures, including all industrial fungal cocktails, interact synergistically to digest cellulose rapidly. *T. fusca* ER1 crude supernatant is a complex cocktail of many different enzymes, including numerous synergistic cellulases and auxiliary activity enzymes, that breaks down highly crystalline cellulose without experiencing the characteristic kinetic drop off of individual cellulases (Kostylev and Wilson 2013). Synergistic cooperation likely involves changes to cellulose structure that maximize the activity of the synergistic cellulases.

ER1 crude supernatant hydrolysis time course samples with a very high extent of digestion, (Figure 3.12) resulted in kinetic parameters shown in Table 3.4 agreeing with previously reported values (Kostylev and Wilson 2013).

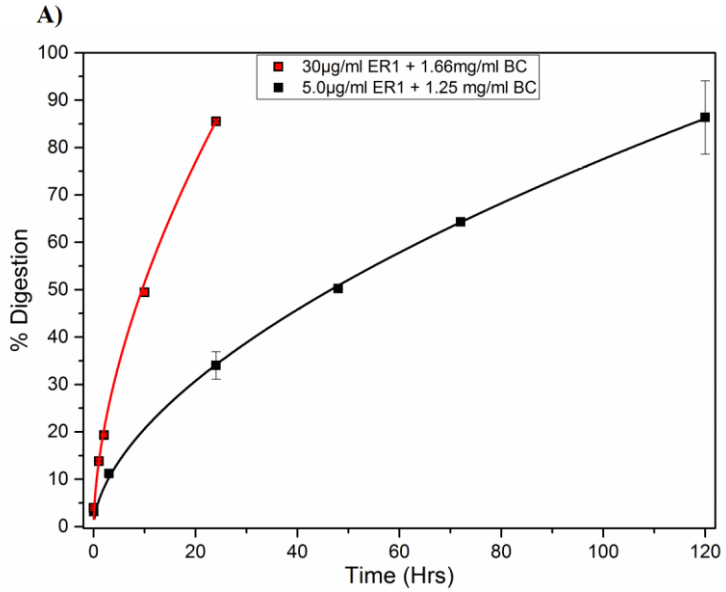

Figure 3.12. A) Digestion time course of ER1 crude supernatant on bacterial cellulose using Corgie et al. (2011) methods (Red color) and updated methods (Black color). Every data point is the average of three replicate assays, and the errors bar are the standard deviation.

Table 3.4. Values of the two-parameter nonlinear fit of ER1 time course digestion processed according to Kostylev and Wilson (2013).

	$f(t)=A\ t^b$		
Experiment	**A**	**b**	**R^2**
30µg/ml ER1	13.6	0.57	0.99
5.0µg/ml ER1	5.51	0.58	0.99

Quantification of crystallinity using the FTIR spectra of the residual BC after ER1 supernatant digestion either using previously reported methods or updated methods, are shown in Figure 3.13. Control without enzyme was also presented. FTIR spectra collected from residual BC using the updated methods described above show no changes to the LOI, HBI or TCI crystallinity indexes (Figure 3.13). Compared with results using previous methods, both the control and digested samples with updated methods show very consistent crystallinity index values over time.

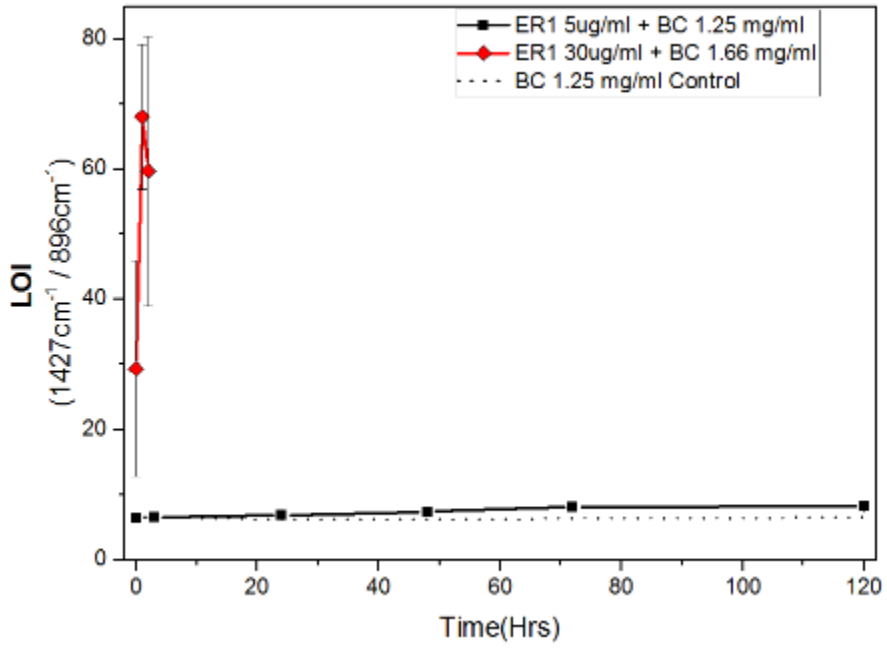
ER1 5ug/ml + BC 1.25 mg/ml
ER1 30ug/ml + BC 1.66 mg/ml
BC 1.25 mg/ml Control
LOI
(1427cm-1 / 896cm-1)
Time(Hrs)
0
20
40
60
80
100
120

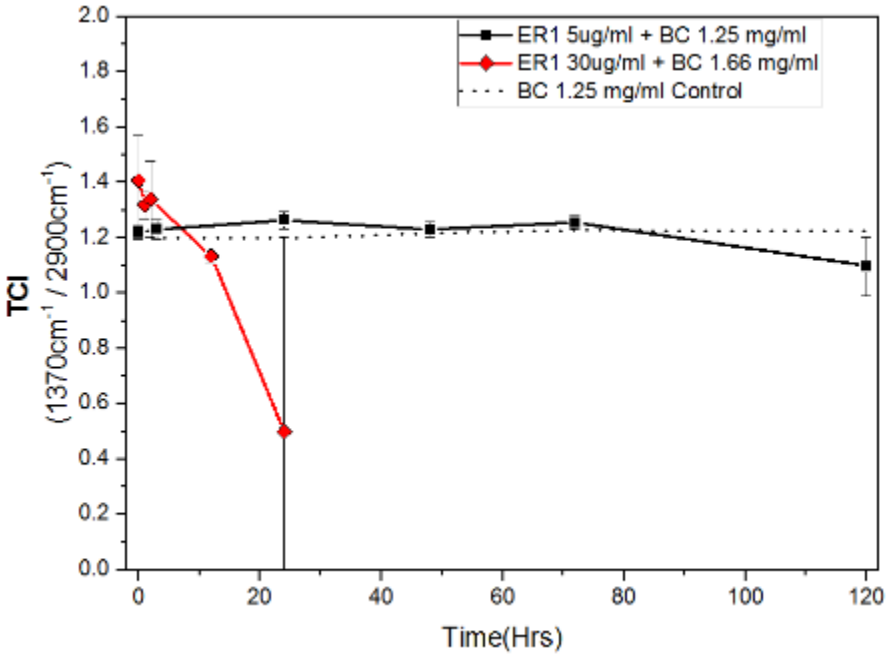
ER1 5ug/ml + BC 1.25 mg/ml
ER1 30ug/ml + BC 1.66 mg/ml
BC 1.25 mg/ml Control
TCI
(1370cm-1 / 2900cm-1)
Time(Hrs)
0.0
0.2
0.4
0.6
0.8
1.0
1.2
1.4
1.6
1.8
2.0
0
20
40
60
80
100
120

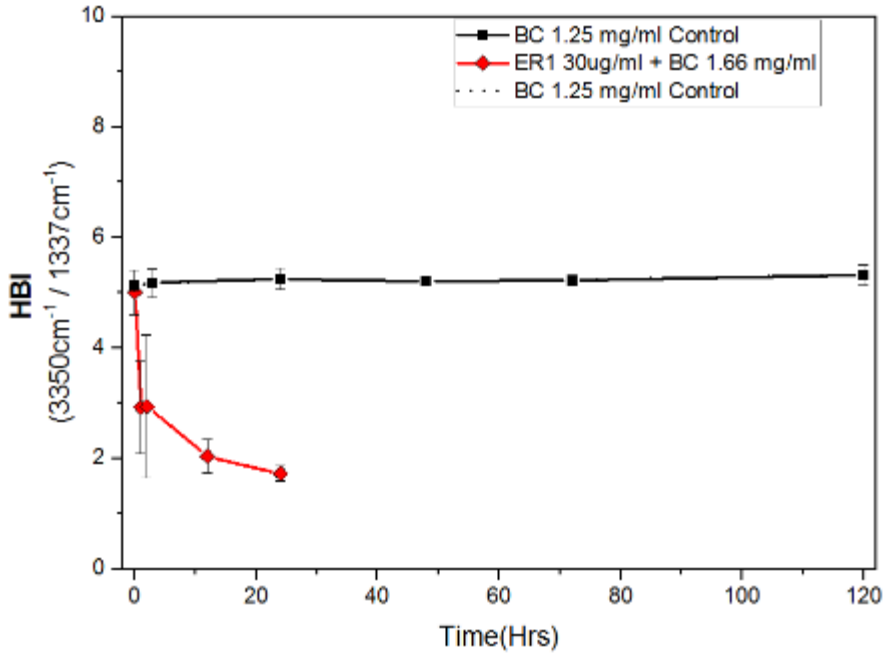

Figure 3.13. FTIR LOI, TCI, and HBI crystallinity index values of cellulose after digestion by ER1 crude supernatant. Samples prepared using previous methods are presented in red color. Results from updated methods are presented in black color. Control samples (without cellulose) are presented using black dotted lines

3.4 Discussion and integration of this chapter with the existing literature

During their cleavage of cellulose, cellulases reach a digestibility limit that indicates an accumulation of inhibitory substrate changes. However, the physical changes has not been definitively established. It can be hypothesized that cellulases remove more easily attacked regions to leave recalcitrant cellulose with increased crystallinity. The exocellulase Cel48A from *T. fusca* is effective in synergistic mixtures, but alone can only digest a small fraction of crystalline cellulose. In contrast, the processive endocellulase Cel9A is the most effective cellulase on crystalline cellulose. Cel9A reaches a higher extent of digestion than exocellulases, and therefore, it must change the substrate in a different way or overcome the recalcitrance that is produced. This difference in efficacy makes Cel9A a useful counterpoint to Cel48A to observe changes in crystallinity.

The results presented above indicate that cellulase digestion does not cause significant changes to cellulose crystallinity indexes when the samples are buffer exchanged, concentration normalized, gradually dried, and measured without normalization to an internal standard. However, large and reproducible changes to both the raw FTIR spectra and the resulting crystallinity indexes are observed when the previous processing methods are used. The most likely causes of these changes are the conversion of ordered cellulose to soluble mono- and oligosaccharide products, and the corresponding decreased path length of the dried cellulose sample.

Soluble products would be expected to significantly affect the resulting crystallinity indexes due to the changed structural interaction of these products with the bulk cellulose. The three crystallinity indexes depend on the relationship between peaks representing bond mobility or non-covalent interactions with those that are unaffected by lattice structure. Free oligosaccharides pack more randomly between the ordered microfibrils during drying, resulting in reduced non-covalent interactions while the signal from pyranose ring covalent bonds remained unchanged. The conversion of ordered cellulose to soluble products could produce the diminished spectra and changes to crystallinity indexes observed, despite the crystallinity of the residual cellulose remaining unchanged.

The action of individual cellulases are expected to reduce the samples path length, as the soluble oligosaccharide products are much smaller and contribute little to the packing of much larger cellulose microfibers. However, the signal reduction observed in previous reports with low extent of digestion is disproportionate to the amount of soluble products removed (Corgie et al. 2011). This may be explained as digestion induces more compact packing of the cellulose microfibers the less ordered and bulky surface chains were removed in these samples, resulting in a shorter path length without significant removal of mass. This change to packing may be entirely uncorrelated

with crystallinity if reorganization of surface chains results in the same degree of disorder on the individual microfiber scale (a likely scenario since highly disordered chains would have minimal inter-chain interactions).

Another possibility to explain significant crystallinity index changes for samples with high extent of digestion is the reduced coverage of the sample well by the residual cellulose. Cellulose samples that fail to cover the well surface would have more stray light, which does not pass through thick cellulose. Stray light causes the detector to receive more background light, leading to different effects on bands with different absorptivity (Chalmers 2002). In this work, this effect was avoided by concentration normalization and by manual spreading the sample to evenly cover the FTIR plate well surface.

This chapter focused on the evolution of crystallinity of BMCC digested by individual cellulases and an industrial crude. The rapid drop off of Cel48A (reducing end directed *T. fusca* exocellulase) activity on BC digestion suggested a rapid enrichment of substrate crystallinity. Though initial results using previous sample preparation for FTIR analysis supported this hypothesis, digestion samples processed with updated methods did not show the same trend. The processive endocellulase Cel9A provided test of the correlation between digestion and crystallinity for individual hydrolytic cellulases showing higher digestion yields. Cel9A is an important component of the *T. fusca* cellulase system, with high activity on both amorphous and crystalline cellulose regions. The Cel9A digestion mechanism is an initial endocellulolytic cleavage of a crystalline chain within the cellulose lattice, followed by processive cleavage. Cel9A produces the highest extent of digestion of any single *T. fusca* cellulase on crystalline cellulose, and showed the most significant change to all three crystallinity ratios in previous investigations. The increase of both LOI and TCI, with a decrease to HBI, indicated a significant increase in crystalline cellulose. This

was attributed to preferential digestion of exposed amorphous paracrystalline regions prior to engaging highly crystalline substrate. In the current work, Cel9A time course samples were prepared with an extent of digestion matching previously reported digestion values by Corgie et al. (2011), with values obtained using the PAHBAH method validated using HPLC quantification. When the residual cellulose was processed using updated methods, the crystallinity indexes did not change significantly during the course of digestion. This may be explained as Cel9A not exhibiting a preference towards cellulose regions of different crystallinity, or as the cellulose crystallinity equilibrating by some other mechanism. Cel9A plays a major role of the total ER1 crude activity on crystalline cellulose, so the next step was to see if the versatility in digestion strategies in ER1 cellulases modifies crystallinity over digestion. A rapid, high extend of digestion, approximately 85% within 24 hours, is achieved with a high loading of ER1 crude (red squares in Figure 3.12). When these residual cellulose samples were prepared for FTIR analysis using the previous methods, significant changes to crystallinity indexes were observed. A large increase to LOI and a rapid drop of both TCI and HBI suggested cellulose structure changes that would be advantageous for an efficient synergistic cellulase system. However, when ER1 crude supernatant hydrolysis time course samples at similar extent of digestion were processed with updated methods, no significant changes were observed in the crystallinity indexes, suggesting a lack of significant change to the residual BC structure over the course of digestion. This supports the hypothesis of simultaneous activity on each region of BC.

Lytic polysaccharide monooxygenases (LPMOs) are used as synergistic components of native or industrial enzyme mixtures at low concentration (often less than 2% of total products). Unlike their low extend of BC digestion (1% measured by soluble product), they produce a large synergistic effect (Cannella et al. 2012). It is commonly accepted they perform oxidative cleavage to degrade

crystalline polysaccharides, but the physical changes to the substrate that enable synergism with hydrolytic cellulases are not understood. The amorphogenesis model of LPMO activity was based upon a physical disruption of cellulose crystallinity resulting in a more digestible material (Arantes and Saddler 2010). However, using the same residual cellulose preparation methods for FTIR as with hydrolytic cellulases, no change to cellulose crystallinity was induced by LPMO attack. This observation does not support the amorphogenesis model of LPMO attack. In comparison, the classical endocellulase Cel5A is thought to predominately attack more amorphous and solvent exposed cellulose chains. In this chapter, no change to cellulose crystallinity was observed over the course of digestion.

3.5 Conclusions

The results presented in this chapter do not support the hypothesis that nonlinear cellulase kinetics on recalcitrant cellulose is due to increased cellulose crystallinity, as measured by the three most common FTIR crystallinity indexes. The substrate recalcitrance which inhibits cellulase activity appears to be a change to cellulose structure that does not involve crystallinity. These combined results suggest that during digestion, the removal of cellulose chains does not affect the substrate crystallinity. Chains from the more highly ordered crystalline microfiber core become surface chains as digestion proceeds. As they become exposed, these ordered chains may become more disordered through contact with solvent (swollen), resulting in continual equilibration of crystallinity to the starting value as digestion progresses. According to a surface erosion model, increasing cellulose recalcitrance is not caused by increasingly ordered chains, but through the accumulation of surface disorder with the same proportion of crystallinity as the starting material. The surface erosion model is the mechanistic explanation that is most in line with these results, and attributes increasing surface complexity as the basis of increasing cellulose recalcitrance. The results presented in this chapter successfully reproduced prior yield data using similar enzymes and equipment, but methodological changes produce data that do not support the cellulose crystallinity model of recalcitrance. Current results alter the interpretation of previously presented data, and provide a valuable direction for design of future recalcitrance investigation. The conclusions presented are in agreement with the current understanding of cellulose recalcitrance within plant biomass, where recalcitrance is correlated with increasing cellulose complexity rather than cellulose crystallinity (Hu et al. 2015). Moving toward the goal of biomass deconstruction for fuel and chemicals will require a more nuanced understanding of the subtle changes occurring to

the structure of cellulose, and how these changes influence cellulase activity within the context of real biomass substrates

3.6 References

Arantes, V, and JN Saddler. 2010. “Access to Cellulose Limits the Efficiency of Enzymatic Hydrolysis: The Role of Amorphogenesis.” *Biotechnology for Biofuels* 3 (4).

Boisset, C, H Chanzy, B Henrissat, R Lamed, Y Shoham, and EA Bayer. 1999. “Digestion of Crystalline Cellulose Substrates by the Clostridium Thermocellum Cellulosome: Structural and Morphological Aspects.” *Biochemical Journal* 340 (3): 829–35.

Cannella, D, CWC Hsieh, C Felby, and H Jogensen. 2012. “Production and Effect of Aldonic Acids during Enzymatic Hydrolysis of Lignocellulose at High Dry Matter Content.” *Biotechnology for Biofuels* 5 (26).

Cao, Yu, and Huimin Tan. 2002. “Effects of Cellulase on the Modification of Cellulose.” *Carbohydrate Research* 337 (14): 1291–96.

Chalmers, JM. 2002. “Mid-Infrared Spectroscopy: Anomalies, Artifacts and Common Errors.” *Handbook of Vibrational Spectroscopy*, 2327–47.

Chen, Y, AJ Stipanovix, WT Winter, DB Wilson, and YJ Kim. 2007. “Effect of Digestion by Pure Cellulases on Crystallinity and Average Chain Length for Bacterial and Microcrystalline Celluloses.” *Cellulose* 14: 283–93.

Corgie, S, H Smith, and L Walker. 2011. “Enzymatic Transformations of Cellulose Assessed by Quantitative High-Throughput Fourier Transform Infrared Spectroscopy (QHT-FTIR).” *Biotechnology and Bioengineering* 108 (7): 1509–20.

Fraser, R T M. 1959. “Sodium Azide as Internal Standard for Quantitative Infrared Analysis.” *Analytical Chemistry* 31 (9). American Chemical Society: 1602–3.

Hu, J, K Gourlay, V Arantes, JS Van Dyk, A Pribowo, and JN Saddler. 2015. “The Accessible Cellulose Surface Influences Cellulase Synergism during the Hydrolysis of Lignocellulosic Substrates.” *ChemSusChem* 8 (5): 901–7.

Igarashi, K, A Koivula, M Wada, S Kimura, M Penttila, and M Samejima. 2009. “High Speed Atomic Force Microscopy Visualizes Processive Movement of Trichoderma Reesei Cellobiohydrolase I on Crystalline Cellulose.” *The Journal of Biological Chemistry* 284 (52): 36186–90.

Irwin, D, TD Leathers, RV Greene, and DB Wilson. 2003. “Corn Fiber Hydrolysis by Thermobifida Fusca Extracellular Enzymes.” *Applied Microbiology and Biotechnology* 61 (4): 352–58.

Jeoh, T, M Santa-Maria, and P O’Dell. 2013. “Assessing Cellulose Microfibrillar Structure Changes due to Cellulase Action.” *Carbohydrate Polymers* 97 (2): 581–86.

King, BC, MK Donnelly, GC Bergstrom, LP Walker, and DM Gibson. 2009. “An Optimized Microplate Assay System for Quantitative Evaluation of Plant Cell Wall-Degrading Enzyme Activity of Fungal Culture Extracts.” *Biotechnology and Bioengineering* 102 (4): 1033–44.

Kostylev, M, M Alahuhta, M Chen, R Brunecky, ME Himmel, VV Lunin, J Brady, and DB Wilson. 2014. “Cel48A from Thermobifida Fusca: Structure and Site Directed Mutagenesis of Key Residues.” *Biotechnology and Bioengineering* 111 (4): 664–73.

Kostylev, M, and D Wilson. 2011. “Determination of the Catalytic Base in Family 48 Glycosyl Hydrolases.” *Applied and Environmental Microbiology* 77 (17): 6274–76.

———. 2013. “Two-Parameter Kinetic Model Based on a Time-Dependent Activity Coefficient Accurately Describes Enzymatic Cellulose Digestion.” *Biochemistry* 52 (33): 5656–64.

Lever, M. 1977. “Carbohydrate Determination with 4-Hydroxybenzoic Acid Hydrazide (PAHBAH): Effect of Bismuth on the Reaction.” *Analytical Biochemistry* 81 (1): 21–27.

Li, Y, DC Irwin, and DB Wilson. 2010. “Ncreased Crystalline Cellulose Activity via Combinations of Amino Acid Changes in the Family 9 Catalytic Domain and Family 3c Cellulose Binding Module of Thermobifida Fusca ce19a.” *Applied Environmental Microbiology* 76: 2582–88.

Lionetto, F, R Del Sole, D Cannoletta, G Vasapollo, and A Manffezzoli. 2012. “Monitoring Wood Degradation during Weathering by Cellulose Crystallinity.” *Materials* 5 (10): 1910–22.

Mansfield, S, and R Meder. 2003. “Cellulose Hydrolysis–the Role of Monocomponent Cellulases in Crystalline Cellulose Degradation.” *Cellulose* 10 (2): 159–69.

Mitchell, AJ. 1990. “Second-Derivative FT-IR Spectra of Native Celluloses.” *Carbohydrate Research* 197: 53–60.

Olsen, SN, K Borch, N Cruys-Bagger, and P Westh. 2014. “The Role of Product Inhibition as a Yield- Determining Factor in Enzymatic High-Solid Hydrolysis of Pretreated Corn Stover.” *Applied Biochemistry and Biotechnology* 174 (1): 146–55.

Park, S, JO Baker, ME Himmel, P Parilla, and DK Johnson. 2010. “Cellulose Crystallinity Index: Measurement Techniques and Their Impact on Interpreting Cellulase Performance.” *Biotechnology for Biofuels* 3 (10).

Väljamäe, P, K Kipper, G Pettersson, and G Johansson. 2003. “Synergistic Cellulose Hydrolysis Can Be Described in Terms of Fractal-like Kinetics.” *Biotechnology and Bioengineering* 84 (2): 254–57.

Väljamäe, P, V Slid, G Pettersson, and G Johansson. 1998. “The Initial Kinetics of Hydrolysis by

Cellobiohydrolases I and II Is Consistent with a Cellulose Surface-Erosion Model." *European Journal of Biochemistry* 253 (2): 469–75.

Xu, F, and H Ding. 2007. "A New Kinetic Model for Heterogeneous (or Spatially Confined) Enzymatic Catalysis: Contributions from the Fractal and Jamming (Overcrowding) Effects." *Applied Catalysis A: General* 317 (1): 70–81.

Zhang, S, DE Wolfgang, and D Wilson. 1999. "Substrate Heterogeneity Causes the Nonlinear Kinetics of Insoluble Cellulose Hydrolysis." *Biotechnology and Bioengineering* 66 (1): 35–41.

CHAPTER IV

METHODS DEVELOPMENT IN FTIR MEASUREMENTS AND SPECTRAL MANIPULATION FOR SWITCHGRASS AND HARDWOOD

4.1 Introduction

Fourier Transform Infrared (FTIR) has been used to investigate chemical changes occurring in lignocellulosic biomass upon pretreatment, and for the quantitative determination of biomass fractions (mainly lignin and hemicellulose). It enables faster and lower cost sampling compared with other approaches. By observing the evolution of infrared spectra of the hardwood *Populous deltoides* after aqueous/steam thermo-mechanical pretreatment at different severity factors (different temperatures and residence times), Bouchard et al. demonstrated the solubilization of hemicelluloses was correlated to the FTIR peaks 1736, 1370, and 1151cm^{-1}, which decreased with severity factor (Bouchard et al. 1990). Thermogravimetric analysis of pretreated biomass was used to confirm this result. However, when analyzing the evolution of lignin, the results given by FTIR and wet chemistry (ASTM D-1106-56) were in disagreement. ASTM assay measured a solubilization of lignin upon pretreatment. However, analysis of the FTIR peaks of 1604 and 1515cm^{-1} (characteristic of lignin) were unchanged. This is because FTIR does not measure absolute amount of chemical compounds (extensive property) but their concentration (intensive property). This feature of FTIR can (and has) result in erroneous conclusions in interpreting FTIR measurements obtain from lignocellulosic biomass pretreatment. It is for this reason that the majority of studies using FTIR to characterize chemical transformations were coupled with other characterization techniques. Chundawat et al. (2007) observed delignification of corn stover

pretreated by ammonia fiber explosion using the decrease of ester carbonyl peak at 1720 cm^{-1}. Scanning electron microscopy (SEM) and laser scanning confocal microscopy have been used to confirm the absence of lignin after ionic liquid pretreatment observed in FTIR spectra of switchgrass (Singh et al. 2009). In ammonia recycle percolation (ARP) pretreatment of corn stover, SEM and compositional analysis were in agreement with FTIR measurements of biomass delignification (Kim and Lee 2005). Biomass crystallinity is another feature that can be measured using FTIR. However, it requires a quantitative approach for meaningful analysis and interpretation of the FTIR spectra, and the necessity of careful sample preparation (Adapa et al. 2011), as demonstrated in Chapter III of this dissertation using cellulose.

Examples of quantitative uses of FTIR to measure the evolution of chemical bonding in biomass upon pretreatment are scarce in literature. The main reason for that is the challenges that different FTIR sampling techniques pose to spectra reproducibility, and therefore, to the development of accurate chemical bonds cleavage models. The most common cited sampling techniques for FTIR analysis of chemical composition of biomass are photoacustic (PAS) (Adapa et al. 2011), diffusive reflectance (DRIFT) (Bouchard et al. 1990), and potassium bromide pellet (KBr) (Guo et al. 2008). ATR (Attenuated total reflectance) has become popular in the last decade. It alleviates some of the complexity, level of cumbersome, and timely sample preparation that are common to the previously mentioned techniques and explain the poorly reproducible spectra (Chundawat et al. 2007). Using ATR a researcher can analyze 200 samples in one day (Allison 2011). For this reason, ATR is currently the leading sampling techniques for mid-infrared analysis of biomass (Chundawat et al. 2007). The ATR accessory has a trapezoid crystal (diamond, zinc selenide, germanium) mounted in a rugged plate. The powdered sample is pressed in direct contact to the flat surface of the crystal, allowing the IR beam to penetrate only a few microns into the sample.

As mentioned by Allison et al. (2011) it is important, for the sake of spectral reproducibility, to provide a powdered sample "sufficiently small and uniform". For the FTIR analysis of biomass, the influence of particle size is another factor that must be considered. It has been documented in the published literature that the spectra produced by a material relates both to the chemical composition and to the physical characteristics, specially particle size (Aucott et al. 1988). This can make spectral interpretation difficult, especially when analyzing pretreated biomass where the severity of pretreatment conditions decreases the particle size. However, to the best of our knowledge, there is no further information with respect to lignocellulosic biomass on how the particle size or the distribution of particle sizes within the sample affect the reproducibility of the FTIR spectra. One of the objectives of this work is to increase our understanding of how particle size and distribution of switchgrass and hardwood feedstocks affect the reproducibility of their FTIR spectra.

To overcome the individual sample preparation required for ATR sampling technique, FTIR offers the possibility of high throughput analysis of samples. The HTS-XT module (Bruker, Billerica MA) is an example of this type of sampling. The sample (liquid or solid suspension) is deposited on wells imprinted in microtiter plates of different materials (aluminum, silicon) depending of the mode of spectral measurement (reflectance and transmission respectively). The number of wells imprinted in the plates can vary from 96, 384 or even 1536 wells. In addition the wells can have different depths (flat for silicon plates and deep wells for aluminum plates) what is convenient for the analysis of liquid samples with different surface tensions (aqueous samples can be contained in flat wells, liquid samples with lower surface tension require the use of deep well plates). The plate with the samples is placed in the holding fixture of the HTS-XT module and the motorized stage moves it into the airtight optics of the module. Then, the individual positions (wells) are

measured successively by moving them into the focus of the IR beam. Moreover, plate stacking devices are available (Twister®) allowing for continuous 24 hour operation (GmbH 2007). Despite the obvious convenience of high throughput sampling technique to analyze biomass, there is not, to the best of our knowledge, any FTIR study on lignocellulosic biomass using HTS-XT. This may due to the challenge this technique poses in acquiring the spectra of solid particles. Unlike the ATR sampling technique, where the solid samples could be directly analyzed on the ATR crystal, HTS-XT module does not allow for solid samples to be directly deposited on the microtiter plate; solid particles can move from well to well on the plate introducing cross contamination inside the HTS-XT chamber. In addition, solid particles can be deposited on the optical devices inside the HTS-XT chamber, causing fatal errors in the measurements and/or the equipment. Thus, for HTS-XT measurements, the solid sample has to be prepared as a water suspension/solution to be transferred onto the plate. In addition, the homogeneity of the suspension is an important factor to make sure the aliquot transferred to the different wells within a plate is representative of the sample to analyze. This is especially true for non-water soluble particles such as biomass. In addition, because of the strong absorption of water in the mid-IR range, samples must be dried prior to analysis. This work will explore the use of HTS-XT to the FTIR analysis of switchgrass and hardwood.

Apart from the ongoing effort to improve the biomass FTIR spectral reproducibility through the development of novel sampling techniques, another way to decrease variance between spectra is the application of spectral processing techniques. There are multitude of signal processing techniques that can be used to decrease variance between replicate measurements. To the best of our knowledge, they have not been comprehensively compared for biomass analysis applications. Usually, researchers choose one processing technique, but the reasons for their choice remain

obscure. As an example, Sills and Gosset (2012) used vector normalization for their work using FTIR spectra to predict saccharification of alkali-pretreated biomasses. Vazquez et al. (2002) used FTIR spectroscopy to obtain mathematical models to estimate lignin and polysaccharide content in eucalyptus and pine acetosolv pulps oxygen prebleached. In their models, they used 13 characteristic bands for cellulose, hemicellulose, and lignin. Their processing technique consisted in using the spectral band that yield models that better fit experimental results as internal standard for normalization. Bouchard et al. (1990) used a characteristic cellulose peak at 1430 cm^{-1} (C-H deformation asymmetric (Pandey 1999), crystalline cellulose (Saprativ et al. 2013) as internal standard for normalization. The authors assumed that cellulose peak remained unaltered upon the aqueous/steam thermo-mechanical pretreatment of *Populus deltoids*. Although this approach can be valid for qualitative conclusions, it is not appropriate for quantitative applications as the authors reported the structural modifications on the crystalline fraction of cellulose. In addition, the complex spectra of lignocellulosic biomass made the peak represented by the 1430cm^{-1} the convoluted result of the aforementioned C-H bond in cellulose, and also the methoxyl –O-CH_3 group present in lignin (1470-1430cm^{-1}) (Yang et al. 2007). As delignification is reported, normalization with respect to the 1430cm^{-1} peak could obscure the changes undergoing the lignin fraction.

Some other authors have added internal standards to the samples to normalize their spectra. An internal standard is a compound different from the analyte of interest, added at known concentration, and with features that does not change during the processing of the sample. Different compounds have been used in FTIR analysis as internal standards:

- Sodium azide in the determination of sodium fluoroacetate in dried residues from soil dispersion (Fraser 1959).

- Sodium acetate in the analysis of bonds cleaved in Bacterial Microcrystalline Cellulose (BMCC) upon hydrolysis with different types of cellulases and mixtures (Corgié et al. 2011).
- Carbon black used for the development of models for determination of cellulose-hemicellulose-lignin composition in non-treated and steam exploded barley, canola, and wheat straw (Adapa et al. 2011).

In other cases, the spectra are not processed, or the technique used is not reported (Chundawat et al. 2007). Therefore, an objective of this work is to quantitatively assess the reduction of the spectral variance provided by a selection of spectral processing techniques (vector normalization, first derivative, second derivative, first derivative + vector normalization, and second derivative + vector normalization). The VM ratio was presented as an index to measure the reduction of the effect of particle size in spectral signal upon signal processing. This index has been previously used for powdered medicines, sucrose, and hay in the near infrared region of the spectra (Aucott et al. 1988, Ni et al. 2010). To our knowledge, this is the first time this index has been applied to biomass in the mid-infrared region of the spectra.

The FTIR spectra of lignocellulosic biomass is quite complex, especially in the finger print region. It is the result of the convoluted contribution of many functional groups from the different fractions of biomass. In addition, every functional group has different vibrational modes, featuring a collection of peaks. Therefore, a visual inspection of spectra is not efficient to extract information about chemical structure and functionalities. The use of multivariate techniques (chemometrics, Partial Least Squares, PLS, and Principal Component Analysis, PCA) has made IR spectrometry a powerful tool for quantitative determination of chemical bonds transformation (Corgié, Smith, and Walker 2011) and biomass composition changes during saccharification for a variety of

biomass feedstock (i.e. perennial grasses, hard and soft wood, and stover) (Sim et al. 2012, Chen et al. 2010). The use of Principal Component Analysis (PCA) is one method to find differences among spectra, and relate those differences to the chemical composition of the samples. In this work, this statistical technique will be presented and used to find chemical differences between swtichgrass and hardwood.

4.2 Materials and Methods

4.2.1 Biomass preparation

Hardwood and switchgrass used in this study were harvested in Fall 2012 from Cornell farms in Geneva (NY). The reported average particle size of 3/8". Using a conventional laboratory blender (MF 10 basic IKA WERKE) they were milled with MF 2, 0.5, and 0.25mm sieves at 5500rpm, and dried overnight at 105˚C. The samples ground at 0.5mm where separated in different particle sizes distribution using sieves of different mesh sizes. The fractions obtained are shown in Table 4.1.

Table 4.1. Separation of the particles ground at 0.5mm into different particle size fractions. *A.S.T.M E-11 Specification

	Sieve # *	
Fraction particle sizes (mm)	**Pass through**	**Collected**
0.5-0.25	35	30
0.25-0.125	60	120
0.125-0.075	120	200
<0.075	200	----

4.2.2 FTIR measurements

All spectra were collected with a Bruker Vertex 70 FTIR spectrometer (Bruker Optics, Billerica, Ma) in transmission mode and atmospheric compensated, between 7,000 and 400 cm^{-1}

wavenumbers, 2 cm^{-1} spectral resolution, and 32 scans per sample. As sampling module, the use of a single bounce attenuated total reflectance (ATR) sampling accessory (MIRacle) equipped with a ZnSe crystal (PIKE Technologies, Madison, WI) and the High Throughput HTS-XT (Burker Optics) were explored. Prior to spectra measurement, background scans were collected. For the ATR module, the sample was tightly pressed against the ATR crystal surface using the flat tip attached to the pressure clamp. A minimum of 8 replicates were collected for every particle size analyzed. The resulting transmission spectra was ATR corrected, cut between 4000 and 620 cm^{-1} (strong crystal IR absorption below 520 cm^{-1}) (MIRacle (TM) ATR for FTIR Spectrometers. Installation and user guide 2005) and baseline corrected using a concave rubber band method, provided with the OPUS software (Bruker Optics, Billerica, Ma). For the HTS-XT module, the samples at different particle sizes were suspended in DI water to a concentration of 10 mg/ml. A volume of 50 µl of these suspensions was transferred using wide aperture pipette tips to the wells of a silicon plate wafer, and dried in a vacuum oven at 50˚C. The solid particles were intimately bound to the Si plate, assuring a safe operation of the HTS module. Eight replicates were measured for every particle size as shown in Figure 4.1. The resulting spectra was converted from absorption to transmission, cut between 4000 and 400 cm^{-1} and baseline corrected as for the spectra collected using ATR.

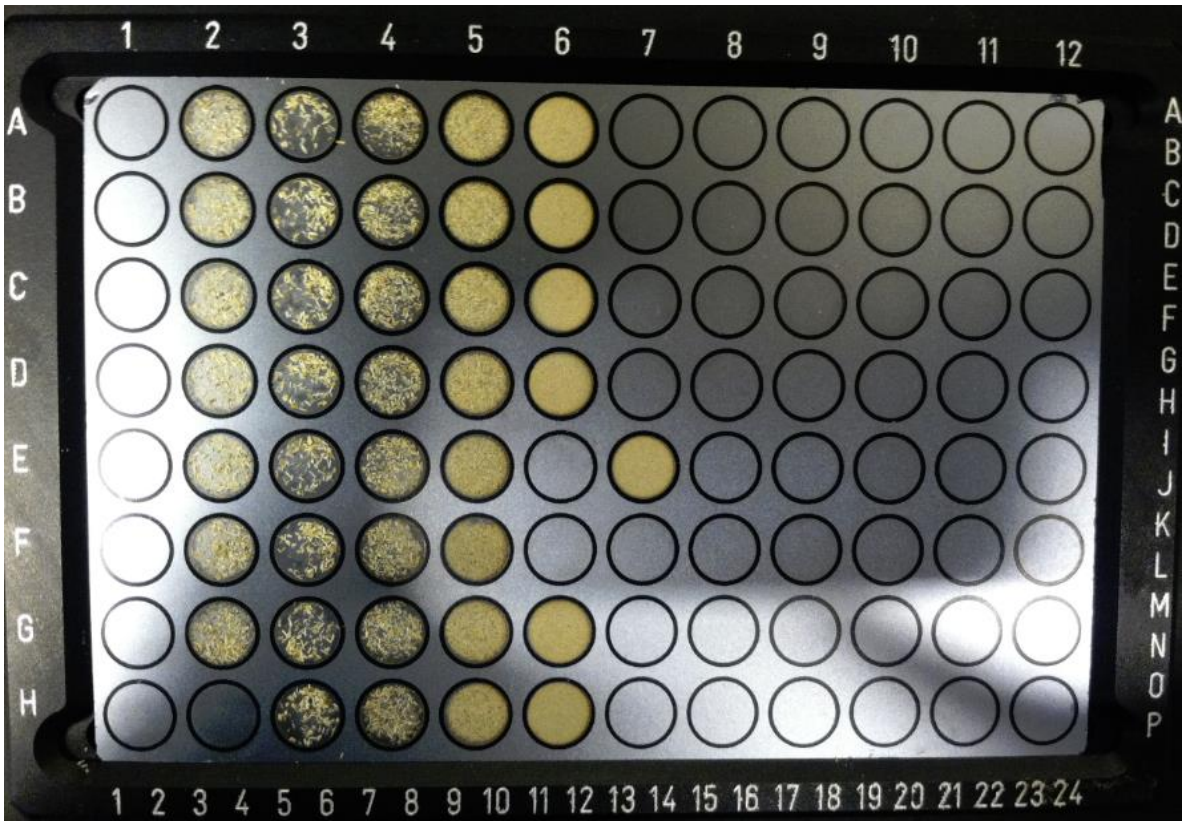

Figure 4.1. FTIR-HTSXT measuring Si plate with the different particle size fractions segregated from switchgrass generated ground at 0.5mm MF sieve (column 2). 0.25-0.5 mm fraction (column 3), 0.125-0.25mm (column 4), 0.125-0.075mm (column 5), and < 0.075mm (column 6 and position E7). Position A12 was used as background.

4.2.3 Statistical manipulation of spectra

For every particle size, the 8 spectral replicates were averaged. The coefficient of variance COV, calculated as ratio of the standard deviation to the average signal (%), was calculated to determine which biomass particle size renders highest COV. COV were only calculated for spectral regions with significant spectral intensities (fingerprint region between 1800-850 cm^{-1} (Pandey 1999), and 3600-2500 cm^{-1}).

To decrease COV, different spectral processing techniques offered by Bruker OPUS were evaluated. To compare the goodness of spectra transformation in reducing the signal variation, without reducing the magnitude of the spectral features, Aucott et al. (1988) developed the so-

called “VM” ratio, where “V” refers to the spectra variance, and “M” refers to the magnitudes of the spectral features. The parameter “V” in an overall measure of the variation of the signal attributable to particle size in this work. It is calculated as follows:

$$\boldsymbol{v_j = \sum_{i=1}^{m}(x_{ij} - \bar{x}_j)^2/(m-1)} \qquad \textbf{Equation 1}$$

$$\boldsymbol{V = (\sum_{j=1}^{n} \frac{v_j}{n})^{\frac{1}{2}}} \qquad \textbf{Equation 2}$$

where:

x_{ij} is the intensity of sample i at the wavenumber j

$\bar{x}_j$ is the mean intensity of all the samples for wavenumber j

m is the number of samples

n is the number of wavenumbers analyzed

The parameter “M” is a measure of the magnitude of the spectral features. It is calculated as follows:

$$\boldsymbol{M = \sum_{j=1}^{n-1}|\bar{x}_{j+1} - \bar{x}_j|/(n-1)} \qquad \textbf{Equation 3}$$

where:

$\bar{x}_{j+1}$ is the mean intensity of all the samples for wavenumber j+1

$\bar{x}_j$ is the mean intensity of all the samples for wavenumber j

$|\bar{x}_{j+1} - \bar{x}_j|$ determines de magnitudes of the spectral features. How the intensity changes from one wavenumber to the adjacent one

n is the number of wavenumbers analyzed

Smaller VM ratio yielded by a particular signal processing technique means an increase in the reproducibility of the spectra (less variance, V) without compromising the magnitudes of the spectral features, M.

4.2.4 Principal Component Analysis (PCA) for FTIR-ATR spectra

FTIR-ATR spectra for both switchgrass and hardwood for all the particle sizes obtained from the 0.5mm ground samples (5 replicates for 4 particle sizes totaling 20 spectra per biomass) were vector normalized. Principal Component Analyses (PCA) was used to identify chemical differences in structure and functionalities between both biomass and between particle sizes fractions within biomass. This was done to see if, as Chudawat et al. (2007) observed for corn stover, different particle sizes of switchgrass and hardwood feature different composition. PCA was performed by software package Rstudio (Rstudio, Boston, MA) on the spectral region ranging 2200–620 cm^{-1}. As PCA analysis is very sensitive to the presence of outliers, they were identified visually and using the threshold of 10 times the interquartile distance for intensities, and they were removed. The intensity values were mean-centered, and the z scores were calculated prior to PCA (Liu et al. 2012).

PCA renders two representations: 1) PCA bi-plot (score plot), and 2) loading plot. The PCA bi-plot represents the distribution of the samples over the directions of maximum variability of the data. The loading plot shows the contribution of individual wavenumbers into the linear combination that form the principal component (coefficients) (Reris and Brooks 2015). Those wavenumbers with higher loadings have more weight in the definition of a principal component. The spectral range between 2200 cm^{-1} and 1800 cm^{-1}, common to all the samples' spectra, was used as a control/threshold to determine which wavenumbers have the largest coefficients (in

absolute number), meaning the largest contribution in a principal component. The wavenumbers featuring loadings higher than the threshold region are accepted to be the most important ones in defining a principal component, and therefore responsible for the chemical modifications captured by the scattering of samples in the PCA bi-plot.

4.3 Results and discussion

4.3.1 Effect of particle size in spectral signal of switchgrass and hardwood using ATR

The FTIR spectra of ground switchgrass samples using the 2 mm, 0.5 mm, and 0.25 mm sieves were ATR collected, and the average of 8 replicates is presented in Figure 4.2a. Figure 4.2b represents the coefficient of variance calculated for the finger print region of the spectra, and for the region between 3500-2500 cm^{-1}. Switchgrass particles ground with the 2 mm sieve yields the lowest signal intensity in all the regions of the FTIR spectra. When the particle size decreases to 0.5 mm, signal intensity increases on average 1.1 to 1.4 fold for the spectra regions of interest. The decrease of particle size further than 0.5 mm has a mixed effect in the intensity of signal depending on the region of the spectra. For the region between 3500-2500 cm^{-1}, signal intensity is higher for 0.5 mm than for 0.25 mm switchgrass particles. However, in the finger print region of the spectra, this is reversed.

Hu et al. (2010) found an opposite trend analyzing the signal intensity of lactose particles ranging from 60 to 200 mesh in the near infrared region of the spectra. They found the decrease in particle size yields a lower signal intensity. However, they show agreement with this work in the different effect of particle size in signal intensity at different wavelength, what was observed at particles grounded at 0.5-0.25 mm in this work. The change in particle size does not modify the shape nor

the position of the spectral features. However, the peak at 2900 cm^{-1} seems to suffer some deformation at particle sizes of 0.25 mm suggesting this level of grinding can affect the aliphatic sp^3 carbon of biomass (wax content in the biomass) that the 2900 cm^{-1} peak represents (Nuopponen and Vourinen 2005).

The effect of particle size in the reproducibility of the spectra was measured calculating the coefficient of variance for 8 replicates for every particle size. Results are shown in Figure 4.2b. A decrease in particle size decreases the COV for the regions of interest (3500-2500 cm^{-1} and 1800-850 cm^{-1}) from around 15-20% for 2 mm particles to below 10% for 0.25mm particles, with the COV for 0.5 mm particles laying in the middle.

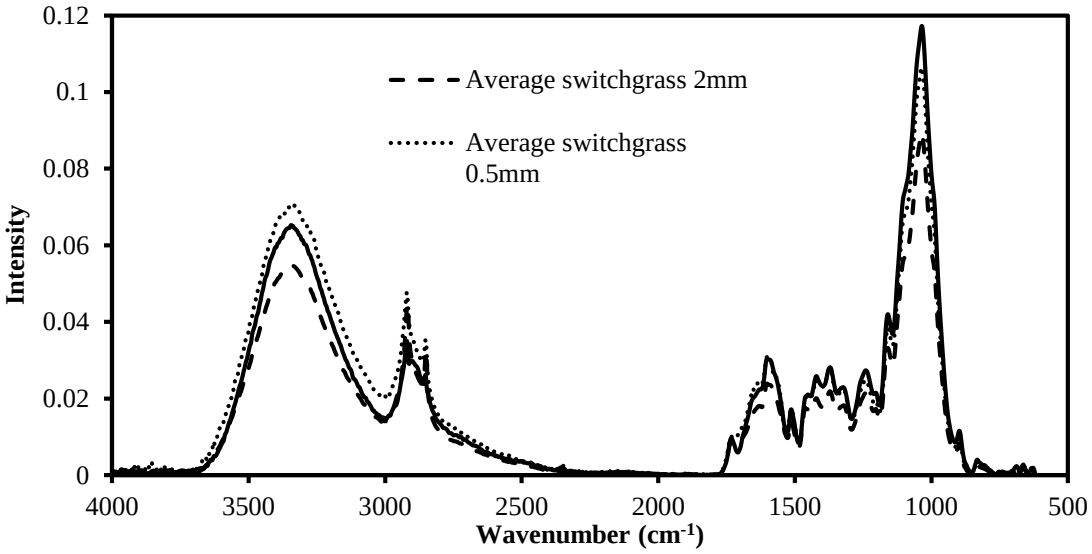

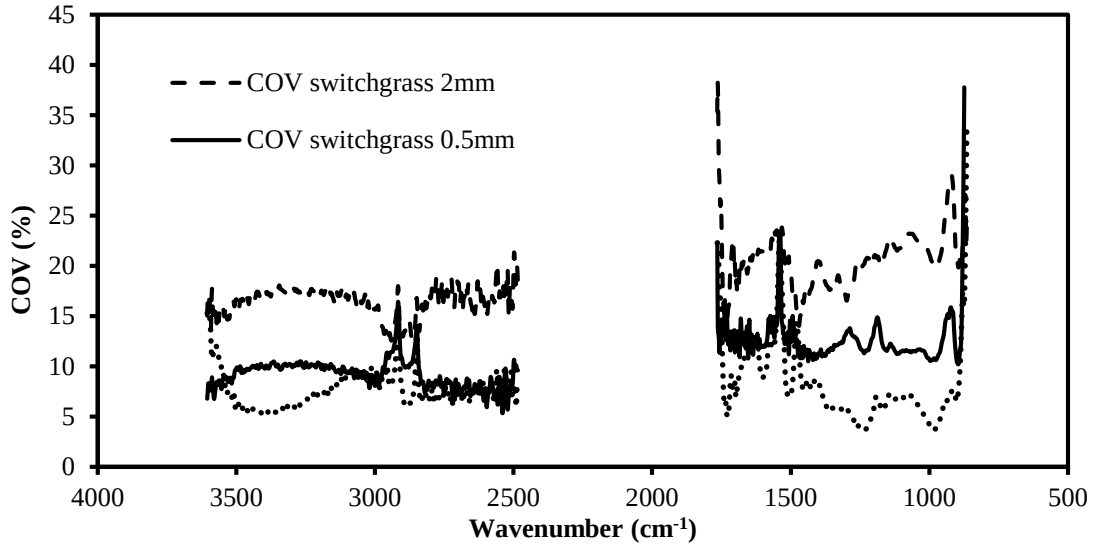

Figure 4.2. Effect of particle size on the a) signal intensity and the b) reproducibility of switchgrass ATR spectra.

Despite the increase of reproducibility and the increase of signal intensity yielded by the 0.25mm ground particles, the possibility of the grinding action affecting the structure of some fractions of the biomass led to the decision to adopt 0.5 mm ground particles as the optimal size for FTIR-ATR measurements. It features a signal intensity similar to the 0.25 mm particles, with only a little higher COV (above 10% for the regions of interest), but no apparent disturbance in the chemical structure of biomass.

At this stage, it is important to understand that the 0.5mm ground sample is conformed by a broad particle size distribution, containing particles ranging all the way from 0.5mm to just a few micrometers in size. As previously shown, the analysis of particles with different sizes in the ATR accessory yielded different signal intensities and, therefore, variance within the replicate spectra. To evaluate this effect, the switchgrass and hardwood particles ground at 0.5mm were fractioned at different particle sizes (0.5-0.25 mm, 0.25-0.125 mm, 0.125-0.075 mm, >0.075 mm) using sieves of different mesh sizes as described in the methods section in Table 4.1 . Five replicates of every fraction were analized using FTIR-ATR. The ATR signal was corrected, cut, and baseline

adjusted as explained in the methods section. The average signal for the 5 replicates are shown in Figure 4.3 a and b for switchgrass and hardwood, respectively. The average signal intensity increases with the decrease of particle size (increase of mesh sieve). The main objective of Figure 4.3 is to give a sense of the maximum variability that could be encountered when FTIR-ATR analyzing a 0.5 mm ground biomass sample (as high as 40% signal difference in the finger print region of the spectra).

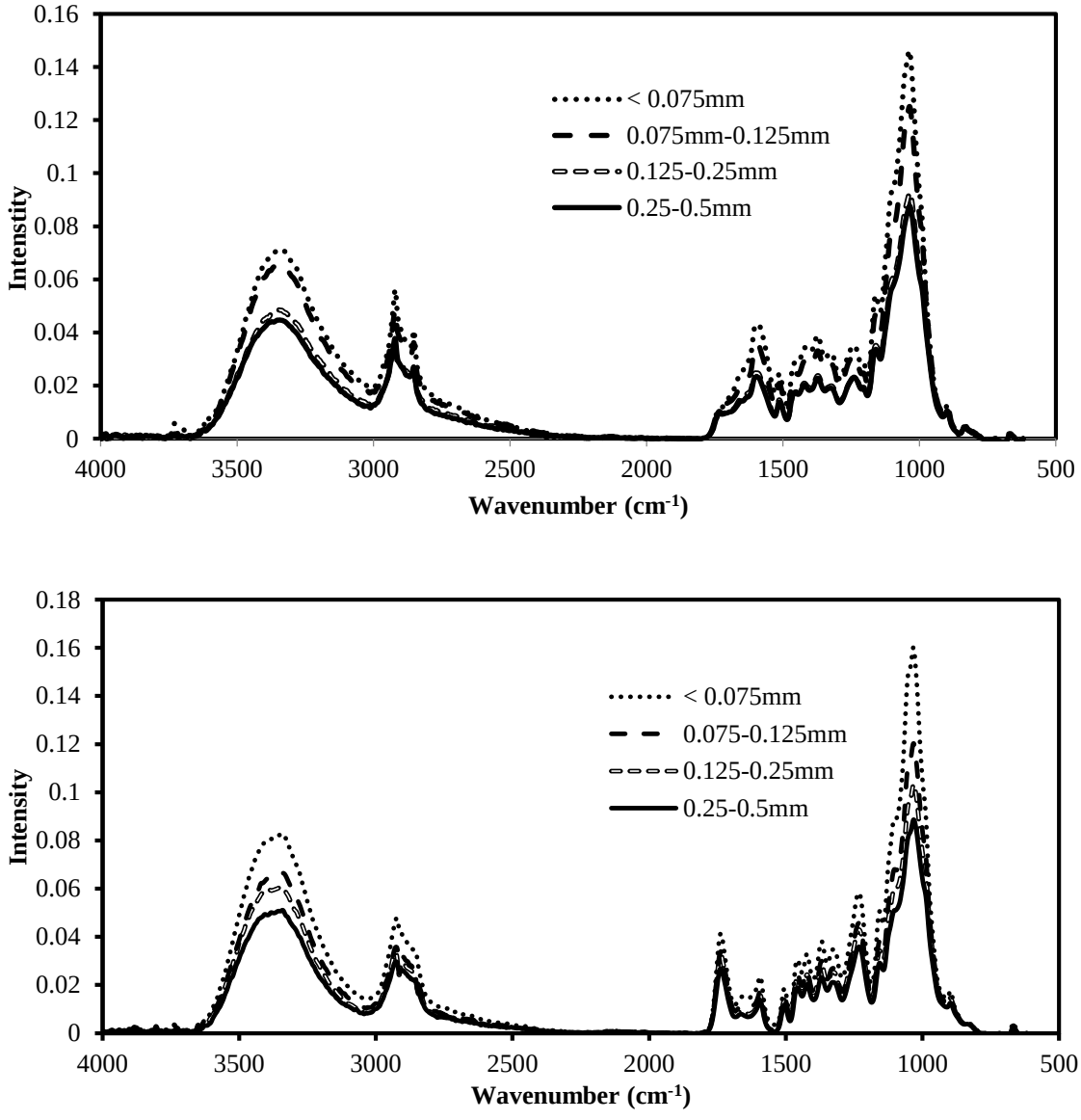

Figure 4.3. FTIR-ATR spectra of the particle size fractions obtained from 0.5mm ground a) swithgrass and b) hardwood

As discussed before, this variability has to be decreased in order to be able to quantify real chemical differences caused by the effect of pretreatment in biomass structure and functionality captured by FTIR-ATR. This can be accomplished by fractioning the sample and only analyzing very narrow particle size distribution fractions as Figure 4.3 showed. However, this option has the disadvantage of yielding a very limited compositional analysis of the biomass. The composition of various pre-milled corn stover particle size fractions were reported by Chundawat et al. (2007) and listed in Figure 4.4. Different fractions are derived from different parts of the biomass, so the composition slightly differs, mainly in terms of the hemicellulose and water-soluble components. Analyzing just a very narrow particle size window illustrates the challenge of analyzing an aliquot that is not fully representative of the bulk sample. The second option for variance decrease is the application of mathematical processing techniques to the spectral signal using FTIR OPUS software. Next sections will discuss the application of these techniques and how they are effective in reducing the effect of particle size in FTIR-ATR signal intensities.

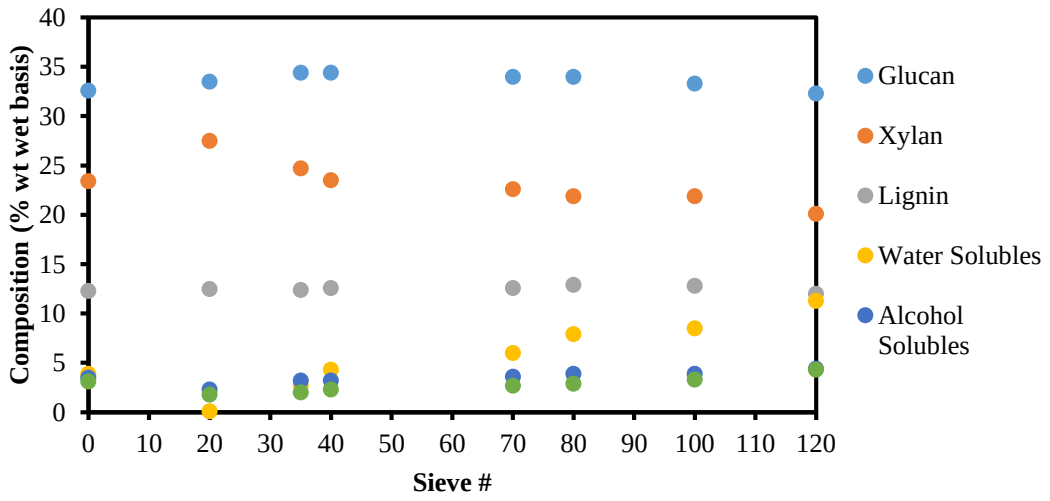

Figure 4.4. Different composition of various particle size fractions in corn stover. Sieve #0 are premilled particles. Sieve #20 particles larger than 850µm. Sieve #35 particles between 850-500 µm. Sieve #40 particles between 500-425 µm. Sieve #70 particles between 425-212 µm. Sieve #80 particles between 212 and 180 µm. Sieve #100 particles between 180 and 150 µm. Sieve #120 particles smaller than 150 µm. Galactan, arabinan, and mannan where not plotted as they only constitute up to 5% the composition of biomass (Chundawat et al. 2007).

4.3.2 Effect of particle size in spectral signal of switchgrass using HTS-XT

To analyze the effect of switchgrass particle size in the intensity and reproducibility of FTIR spectra collected using the HTS-XT module, 2 mm, 0.5 mm, and 0.25 mm ground particle size samples were used. They were suspended in DI water at a concentration of 10mg/ml and transferred to the wells of Si wafer for FTIR measurement. Figure 4.5a and b shows the average of 8 spectra collected at different particle sizes and their coefficient of variance, respectively. The signal intensity increases with the decrease of particle size as observed for ATR sampling technique. However, for HTS-XT this effect is more marked, with intensities increasing 4-5 fold between 2 and 0.25 mm particle size. In addition, the largest difference in intensity occurs between 0.5 and 0.25 mm size unlike occurring when the spectra was taken with ATR module. With respect to the effect of the particle size in the coefficient of variance of the spectral regions of interest, it decreases from 30-50% at 2 mm size to 10-20% at 0.25mm size (on average). This supposes an increase of the coefficient of variance compared to the measured using ATR technique (15-20% for 2mm particles and below 10% for 0.25 mm particles).

In terms of the magnitude of the spectral intensity, it is clear that HTS-XT yields higher intensity than ATR with independence of the particle size selected. This has to do with the higher surface area for analysis provided by the Si wafer well, compared to the ATR crystal. In addition, both sampling techniques are quite different in the way they collect spectra. Therefore, before selecting the sampling technique to measure the spectra of solid biomass, it is necessary to address if there are differences in terms of bond detection for both techniques. Ultimately, the spectral information will be used to establish a correspondence between the bands modification to the chemical bonds they represent. It is crucial to make sure that both techniques are sensitive enough to detect the same chemical bonds/show same peaks. To answer this concern, the finger print region (1750-900

cm^{-1}) will be considered as the peaks representing hydrogen bonds and sp3 carbon (wax) are clearly present in both sampling techniques (3400 and 2900 cm^{-1} bands respectively). The ratio between the signal obtained by HTS-XT and ATR for 0.5 mm ground switchgrass was used and represented in Figure 4.6. High value of this ratio for a specific wavenumber indicates the chemical bond featured by that wavenumber is detected by HTS-XT but not by ATR, while a low value of this intensity ratio will mean the opposite. It is clear that all the chemical bonds being featured in the fingerprint region are able to be detected by both sampling techniques. However, the sensitivity of each sampling technique for each bond is not the same as the intensity ratio does not show the same value over the wavenumber region of interest. This is important to take into account when comparing samples measured with two different FTIR sampling techniques.

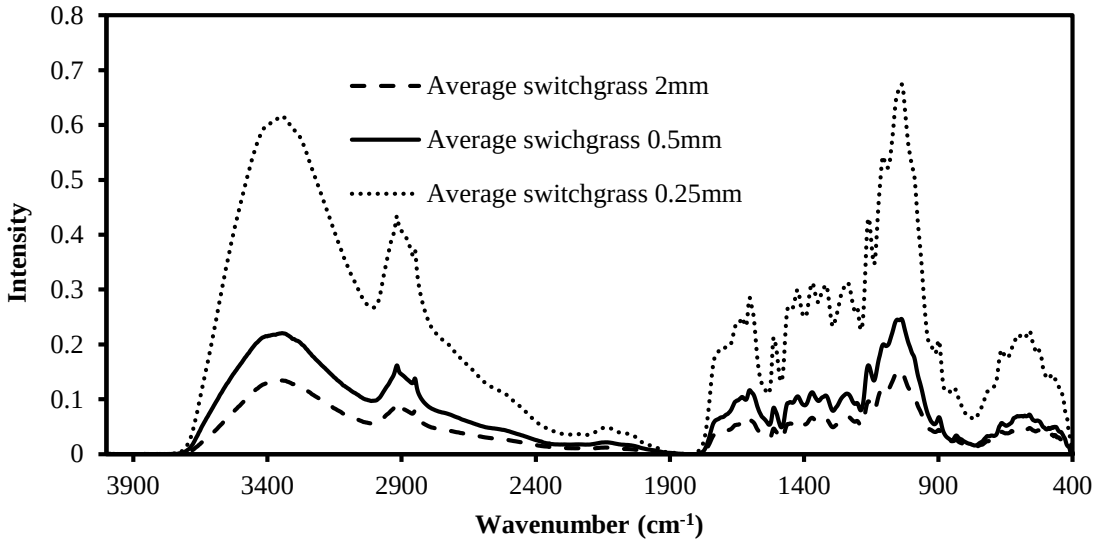

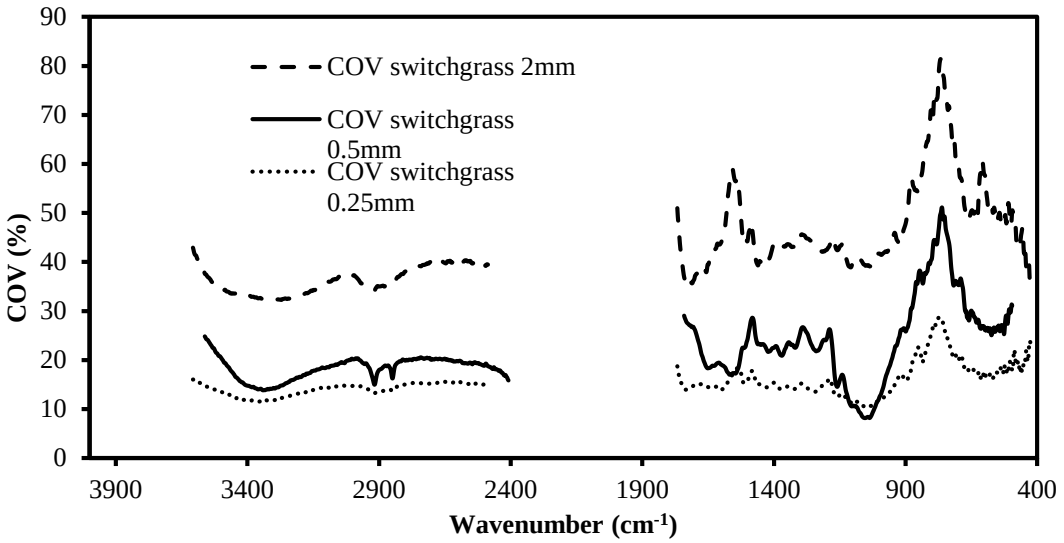

Figure 4.5. Effect of particle size on the a) signal intensity and the b) reproducibility of switchgrass HTS-XT spectra.

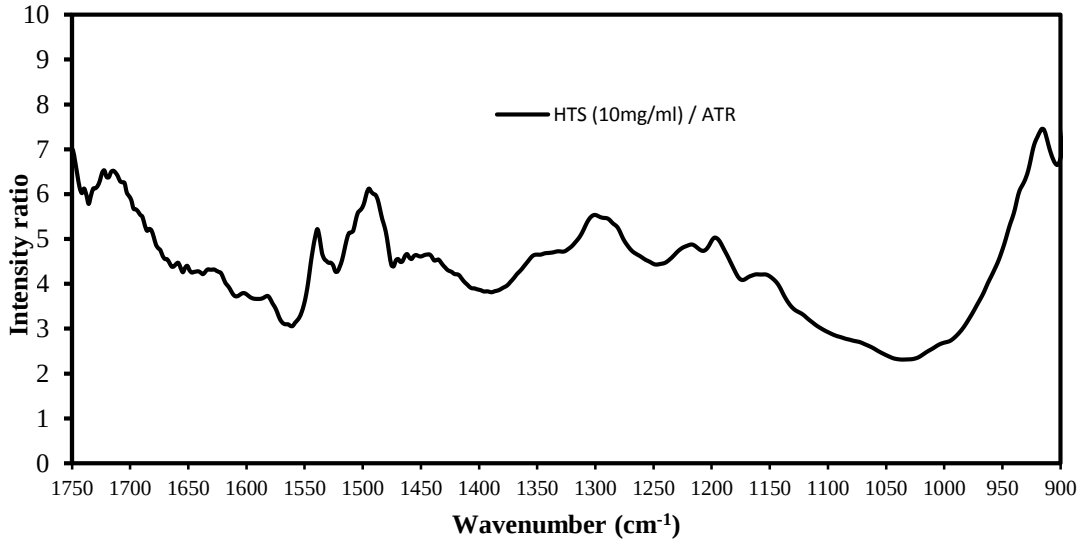

Figure 4.6. Ratio between the spectral signal for the fingerprint region for 0.5mm ground switchgrass acquired by FTIR-ATR and HTS-XT. Both sampling techniques are able detect bonding in the chemical region, but the sensitivity is different depending on the spectral region

As previously done for the ATR, 0.5 mm ground particle size was fractioned into different particle size distributions using the sieves described in Table 4.1. These particles were suspended in DI water at 10mg/ml and transferred to the Si plates for measurement. As shown in Figure 4.1, the smaller the particle size, more area of the well was covered by the biomass particles to analyze. That yielded to higher signal intensities as observed in Figure 4.7. This dependence of coverage

of the area of analysis wit particle size is not an issue for the ATR sampling technique because of the small surface of the crystal (1/8") and the application of pressure on the sample against the lens. Therefore, different intensities observed for the case of ATR are due to the influence of particle size alone and not coverage. However, for the case of HTS-XT, both, the particle size and sampling area covered (amount of biomass analyzed) affect the signal intensity. Hence, the differences in signal intensity observed in Figure 4.7 for the different particle sizes analyzed are much greater than for the case of ATR as sampling technique. ATR measured signal intensity increased 1.5 fold between the fraction at a particle size 0.5-0.25 mm and <0.075 mm. In the case of HTS-XT, this increase in intensity is 10 fold in average for the wavenumbers between 3500 and 2900 cm^{-1} and an average of 10-15 fold for the range between 1800 and 800 cm^{-1}.

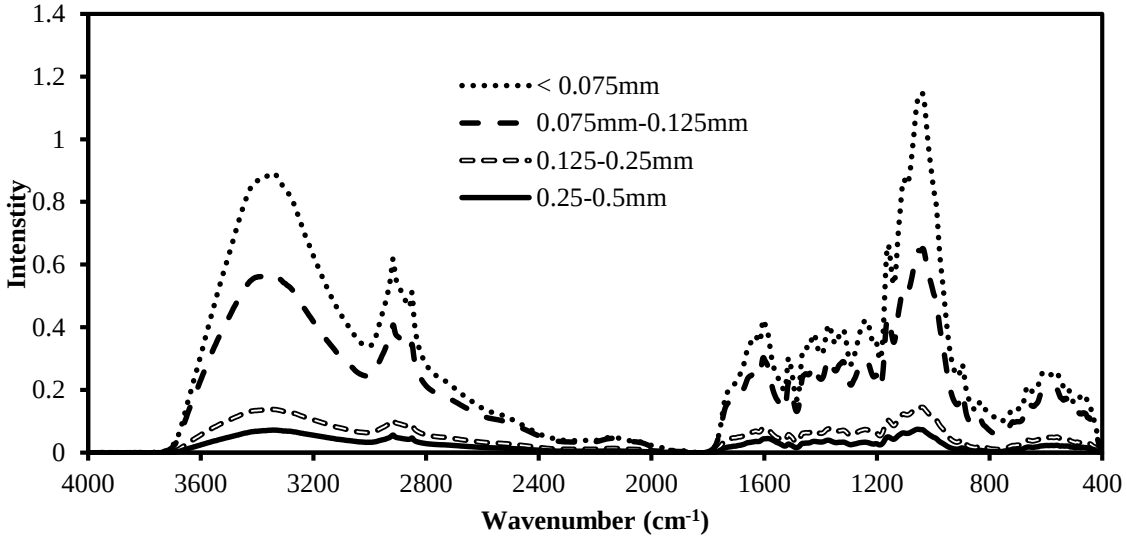

Figure 4.7. FTIR-HTSXT average spectra for the particle size fractions obtained sieving the 0.5mm ground switchgrass.

Figure 4.7 represents the maximum variability that replicates of switchgrass particles (generated using the 0.5 MF sieve) analyzed in HTS-XT can yield. Although this level of signal intensity distribution is unlikely to happen if the suspension is well homogenized before the transfer to the

sampling Si plate, techniques must be explored to avoid this situation that will hinder our ability to draw conclusions about signal (chemical bond) modifications at different pretreatment conditions.

4.3.3 Signal processing techniques to remove the effect of particle size on switchgrass and hardwood spectral signal using ATR

Five spectral processing techniques offered by OPUS FITR (vector normalization, first and second derivative, and derivatives combined with normalization) were explored as a way to decrease the signal variability caused by particle size for the different particle size fractions generated out of the MF 0.5mm ground sample (Table 4.1). Figure 4.8 represents the finger print region (1800-900 cm^{-1}) of the untransformed (a) and the processed spectra (b,c,d,e, and f) for 5 replicates for switchgrass. In Figure 4.8a, the difference in spectral intensity is an evidence of the influence of particle size in the signal intensity. The spectra with highest intensity correspond to samples with smaller particle size. The spectra with lowest intensity correspond to samples of larger particle size. The spectra transformed using the signal processing techniques mentioned above are plotted in Figure 4.8 b-f. In all of the cases, the spectra for all the replicates for the particle sizes measured are closer to each other. Therefore, these processing techniques are effective in removing the effect of particle size in spectral reproducibility. Figure 4.8 b, e, and f show that vector normalization is particularly good in reducing the signal variance. However, an index to quantitatively determine which processing technique is the most effective to decrease spectral variance without decreasing the magnitude of spectral features is necessary. For this purpose, the VM ratio explained in the methods section was used by several research groups to determine the reduction of effect of particle size in spectral signal for powdered medicines, sucrose, and hay in the near infrared region

of the spectra (Ni et al. 2010, Aucott et al.1988). To our knowledge, this is the first time this index has been applied to biomass in the mid-infrared region of the spectra.

The VM ratios for the different processing techniques calculated for switchgrass and hardwood using ATR are reported in Table 4.2.

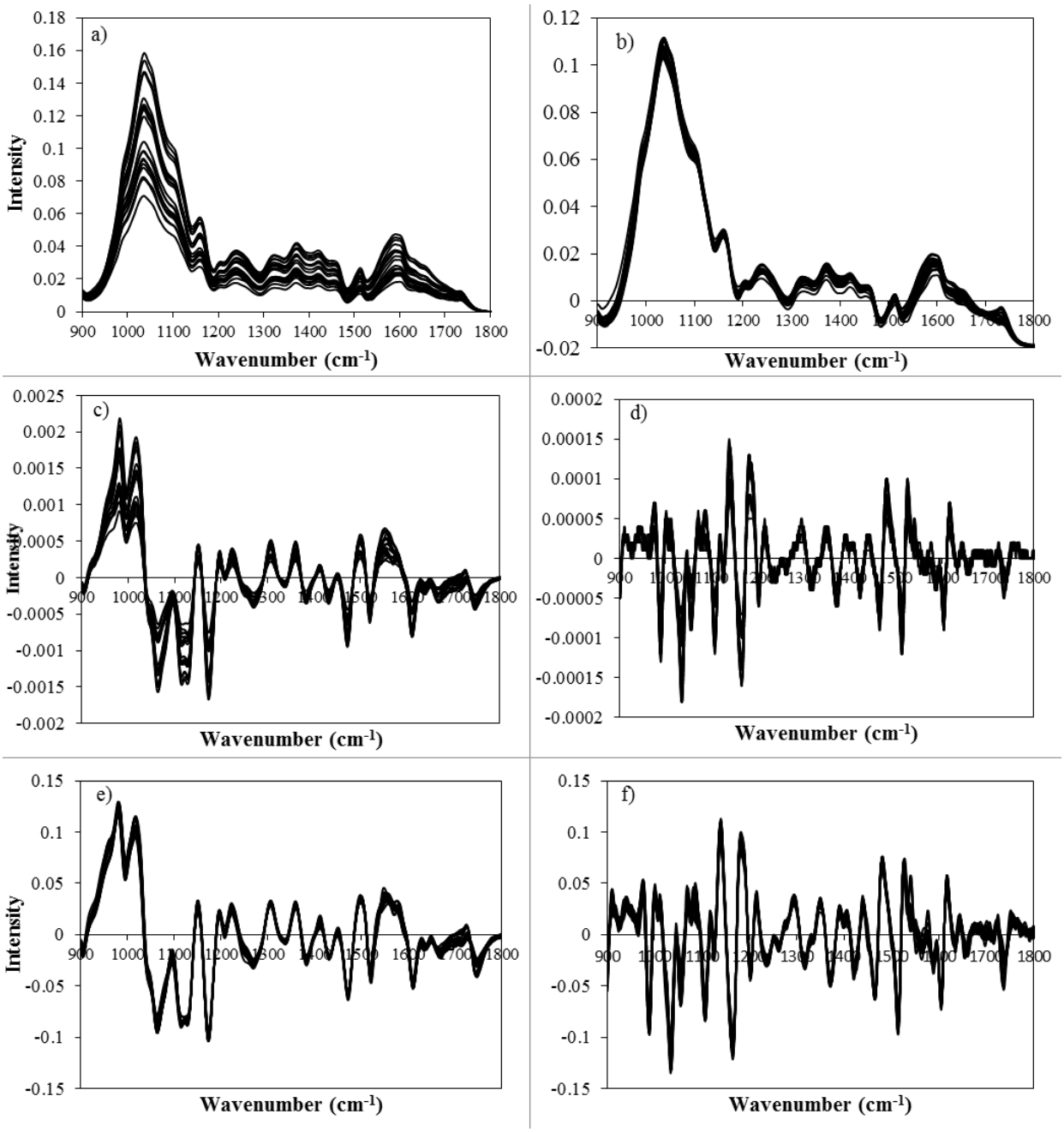

Figure 4.8. Unprocessed (a) and processed spectra of 5 replicates of switchgrass measured in FTIR-ATR at 4 different particle sizes fractioned from the 0.5mm ground sample. The transformations used in the spectra were: b) Vector normalization, c) First derivative, d) Second derivative, e) First derivative + Vector normalization, and f) Second derivative + Vector normalization.

Table 4.2. Values of VM ratio for the different OPUS software processing techniques performed in the spectra of hardwood and switchgrass measured in FTIR-ATR.

	Hardwood			***Switchgrass***		
Signal processing technique	**V**	**M**	**VM**	**V**	**M**	**VM**
Unprocessed	0.006107	0.000390	15.6	0.005996	0.000325	18.4
Vector normalization	0.001183	0.000415	2.8	0.001348	0.000363	3.7
First derivative	0.000093	0.000028	3.3	0.000079	0.000020	3.9
Second derivative	0.000012	0.000006	2.2	0.000011	0.000004	2.5
First derivative + Vector normalization	0.003157	0.001792	1.8	0.003379	0.001676	2.0
Second derivative + Vector normalization	0.008378	0.004079	2.1	0.008993	0.004060	2.2

All the considered signal processing techniques yielded a reduction in the VM ratio compared to the unprocessed spectra. Vector normalization of the spectral signal yields a 5-fold reduction in the mean variability of the signal caused by particle size differences without reducing the magnitude of spectral features (M). Taking either the first or second derivative of the signal decreases the mean variability, but it significantly decreases the magnitude of spectral features. The combination of derivation and vector normalization techniques yielded the minimum VM ratios without a significant reduction of variance. This observation can be explained by the increase in the magnitude of spectral features roughly defined as the difference in intensity between adjacent wavenumbers as seen in Equation 3. Among the processing techniques tested for FTIR-ATR, vector normalization was selected to be the most useful because of the significant decrease in VM ratio caused by a decrease in spectral variability, without altering the magnitude of the spectral features. This is true for both switchgrass and hardwood.

4.3.4 Signal processing techniques to remove the effect of particle size on switchgrass spectral signal using HTS-XT

Similar approach was followed for the spectral signal of switchgrass acquired using FTIR with the HTS-XT module for the particle sizes fractioned from the 0.5mm ground sample. In this case, the signal variability is due to particle size and coverage of the sampling well. Figure 4.9 shows the spectral signal unprocessed and processed using the aforementioned mathematical techniques. The unprocessed spectra in Figure 4.9a show large distribution of signal intensity, with higher intensity signals corresponding to smaller particle size and spectra at lower intensity corresponding to bigger particle size. The application of any processing technique largely decreases this signal distribution. Vector normalization proves to be a good processing technique bringing all the signals together, both applied to unprocessed spectra (b) or applied to the derived spectra (c and d for first and second derivative respectively).

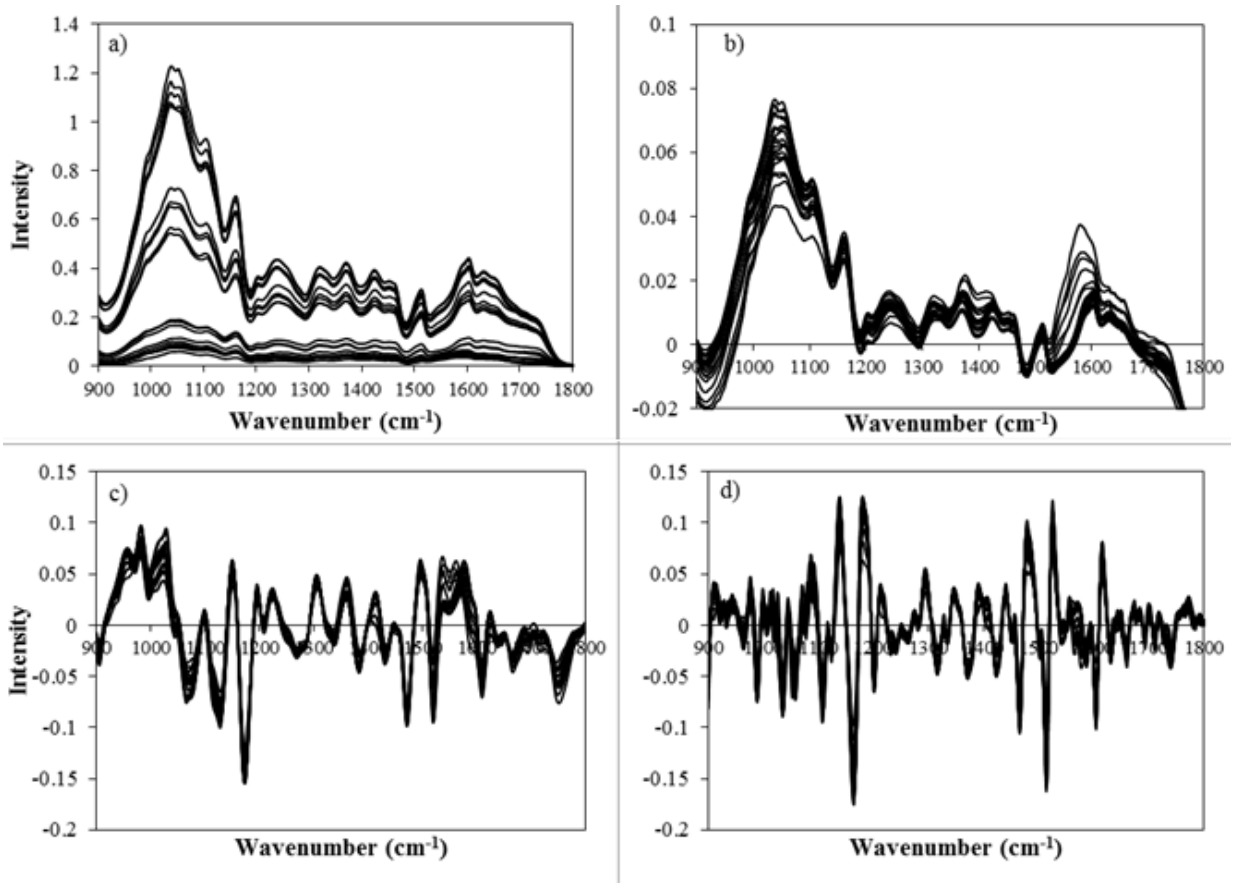

Figure 4.9. Unprocessed (a) and processed spectra of 5 replicates of untreated switchgrass measured in FTIR-HTSXT at 4 different particle sizes. The transformations used in the spectra were: b) Vector normalization, c) First derivative + Vector normalization, and d) Second derivative + Vector normalization.

As for ATR the quantitative evaluation of the efficiency of processing techniques in decreasing the influence of particle size while maintaining the magnitude of the spectral features was performed using the VM ratio. The application of Equations 1, 2, and 3 to all the sample replicates (unprocessed and processed with the 5 processing techniques) yielded the results shown in Table 4.3. The unprocessed spectra presents a high VM ratio (almost 5-fold increase compared to the VM ratio for unprocessed spectra using ATR as sampling technique). This is a major drawback for FTIR of solid biomass using HTS-XT. Normalization contributes in decreasing the variance of the signal but it does have a penalty in terms or reduction of magnitude of spectral features, unlike in ATR where M was unchanged. If preceded by derivative treatment of the spectra (first or second

derivative) vector normalization decreases variance while increases magnitude of spectral features yielding the lowest values of VM ratio, very similar to the ones obtained for ATR. First and second derivation of the spectra are not good preprocessing techniques as they decrease spectral features by more than 10-fold (first derivative) and 100-fold (second derivative).

Table 4.3. Values of VM ratio for the different OPUS software preprocessing techniques performed in the spectra of untreated switchgrass measured in FTIR-HTSXT.

	Switchgrass		
Signal processing technique	**V**	**M**	**VM**
Unprocessed	0.14811	0.00171	86.5
Vector normalization	0.00304	0.00035	8.7
First derivative	0.00116	0.00011	10.7
Second derivative	0.00012	0.00002	5.4
First derivative + Vector normalization	0.00503	0.00193	2.6
Second derivative + Vector normalization	0.00832	0.00409	2.0

Among the processing techniques tested for FTIR-ATR, second derivative combined with vector normalization was selected to be the most useful because of the significant decrease in VM ratio caused by a 20-fold decrease in spectral variability, increasing the magnitude of the spectral features.

4.3.5 FTIR-ATR of hardwood and switchgrass coupled with PCA

Principal components analysis for the vector normalized FTIR-ATR spectra of both hardwood and switchgrass was performed for the 2200-620 cm^{-1} spectral region. All the particle sizes obtained from the fractionation from 0.5mm ground sample were used for the analysis (20 samples per biomass). The first two principal components accounted for more the 98% of the spectral variation, with the first PC (PC1) and the second PC (PC2) accounting for 86.3 and 11.8%, respectively. Figure 4.10a shows the bi-plot representing PC2 vs. PC1. Two clusters of data are clearly form

along PC1: switchgrass at positive values of PC1, and hardwood at negative values of PC1. To determine the wavenumbers that have higher weights in the definition of PC1, the loading plot (Figure 4.10b) shows the wavenumbers with higher loads (above the threshold defined in the 2200-1800 cm^{-1} region of the spectra). The spectral regions that differ the most between switchgrass and hardwood are around 1740, 1260-1220, and 1150-950 cm^{-1}, what agrees with the observations of Pandey et al. (Pandey 1999). The signal at 1740 cm^{-1} is attributed to the carbonyl groups in the branched chains of hemicellulose (Bouchard et al. 1990), confirming a previous observation that hardwood has higher holocellulose (cellulose and hemicellulose) content than softwood and grasses (Pandey 1999). The signal around 1260-1220 cm^{-1} corresponds to the ether bonds between guaiacyl rings of lignin. This confirms differences previously observed between the chemical nature of hardwood and softwood lignin and serves as a validation of the PCA technique to use FTIR spectra to disclose chemical differences between different biomass. Softwood and grass lignin is mainly composed of guaiacyl units, with small amounts of coumaryl, and traces of syringyl units. On the other hand, hardwood lignin is composed of guaiacyl and syringyl units (Pandey 1999, Hu et al. 2010). More evidences of the different nature of lignin are found in the 1150-950 cm^{-1} region, that includes signal corresponding to the CH vibrations of guaiacyl and syringyl units, and the C-O vibrations of primary and secondary alcohols (Pandey 1999).

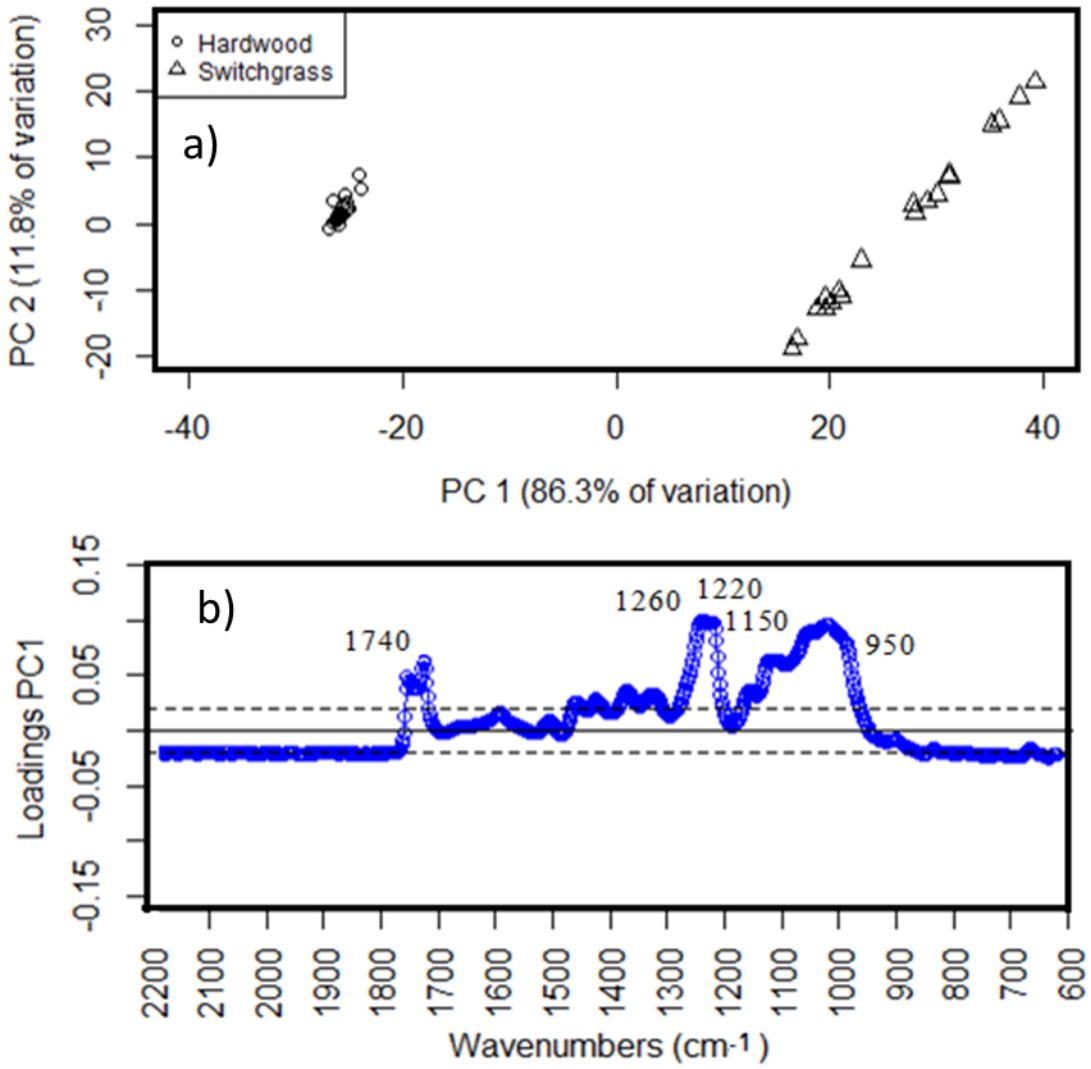

Figure 4.10. PCA analysis of the FTIR-ATR of hardwood and switchgrass. a) Biplot showing two well defined clusters corresponding to both biomasses, b) Loadings plot representing wavenumbers that carry higher weight in the definition of PC1.

Chundawat et al. (2007) pointed out different particle sizes for corn stover feature slightly different chemical compositions. PCA for the FTIR-ATR of the different particle sizes obtained from 0.5mm ground samples for switchgrass and hardwood was performed. Figure 4.11a shows the biplot for the different particle sizes for hardwood. Samples are scatter along PC1 depending on the particle size. For larger particle sizes, no clusters can be differentiated along PC1. When moving to smaller particle sizes, the chemical structure gets more different between fractions, as clusters can be formed along PC1 (the criteria for cluster definition is the k-means Euclidean distance). For these samples PC1 only explains about half of the total data variation (50.6%). To reveal the wavenumbers (and chemical bonding) responsible for this scattering along PC1, the loading plot was generated and presented in Figure 4.11b. No discrete functionality constitute the main difference between particle sizes, but the wide range of wavenumbers between 1500 and 1000 cm^{-1} with loadings larger than the threshold between 2200-1800 cm^{-1} indicate that the source of difference between particle sizes is more compositional based, agreeing with Chundawat et al. (2007). Very similar behavior can be observed for switchgrass (Figure 4.12) with the exception that for these samples the threshold loadings for the loading plot is too high. Therefore, no useful information can be obtained about what wavenumbers (chemical bonding) carry more weight in the scatter of samples along PC1 observed in the biplot.

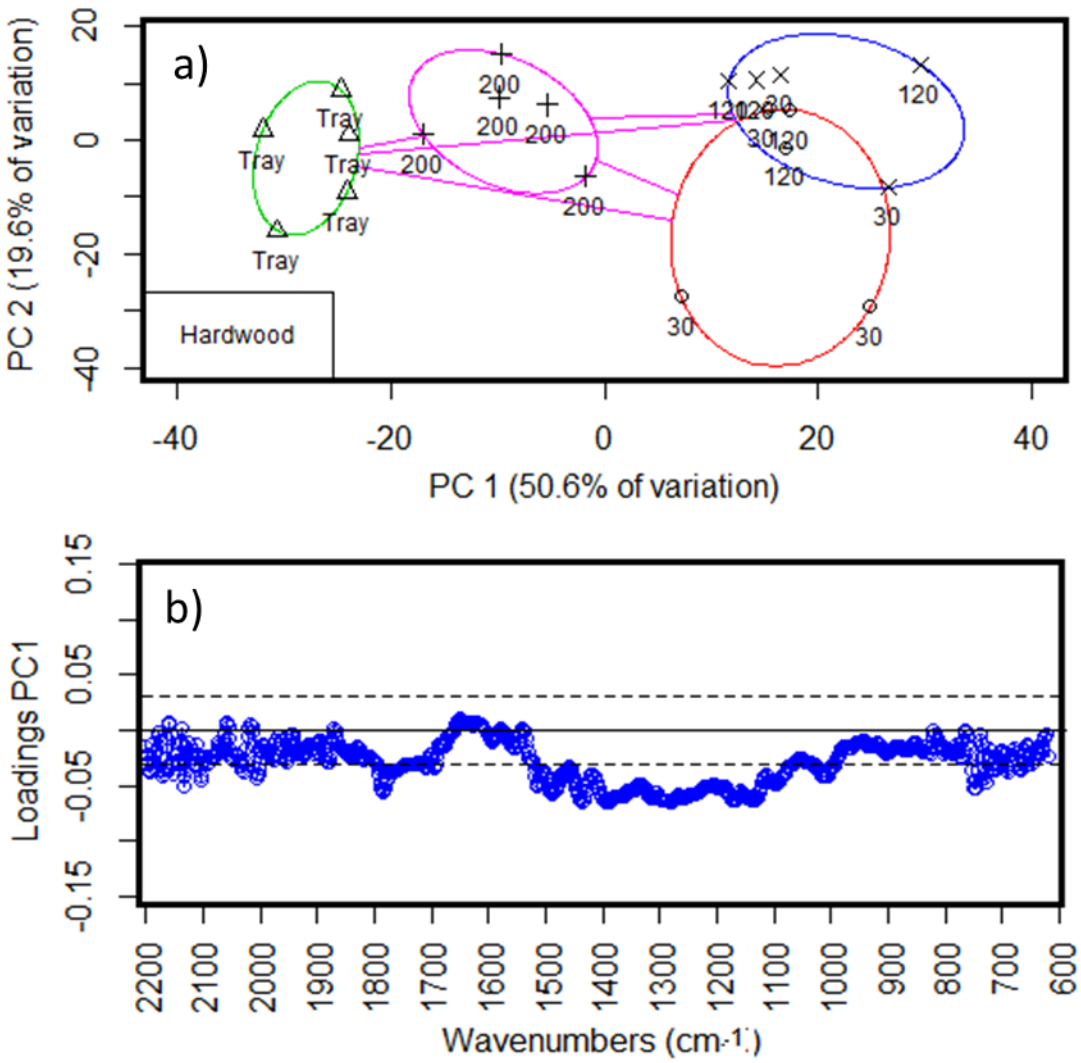

Figure 4.11. PCA analysis of the FTIR-ATR of hardwood at different particle sizes obteined from the 0.5mm ground sample. a) Biplot representing PC2 vs. PC1. The clusters that contain and group particles at different particle sizes were defined statistically using the k-means Euclidean distance criteria (A. Singh, Yadav, and Rana 2013). The numbers correspond to the sieve # where the particles where collected (Table 4.1). Tray correspond to the particles collected after passing the 200 mesh sieve. b) Loadings plot used to identify the wavenumbers that have higher weight in the definition of PC1.

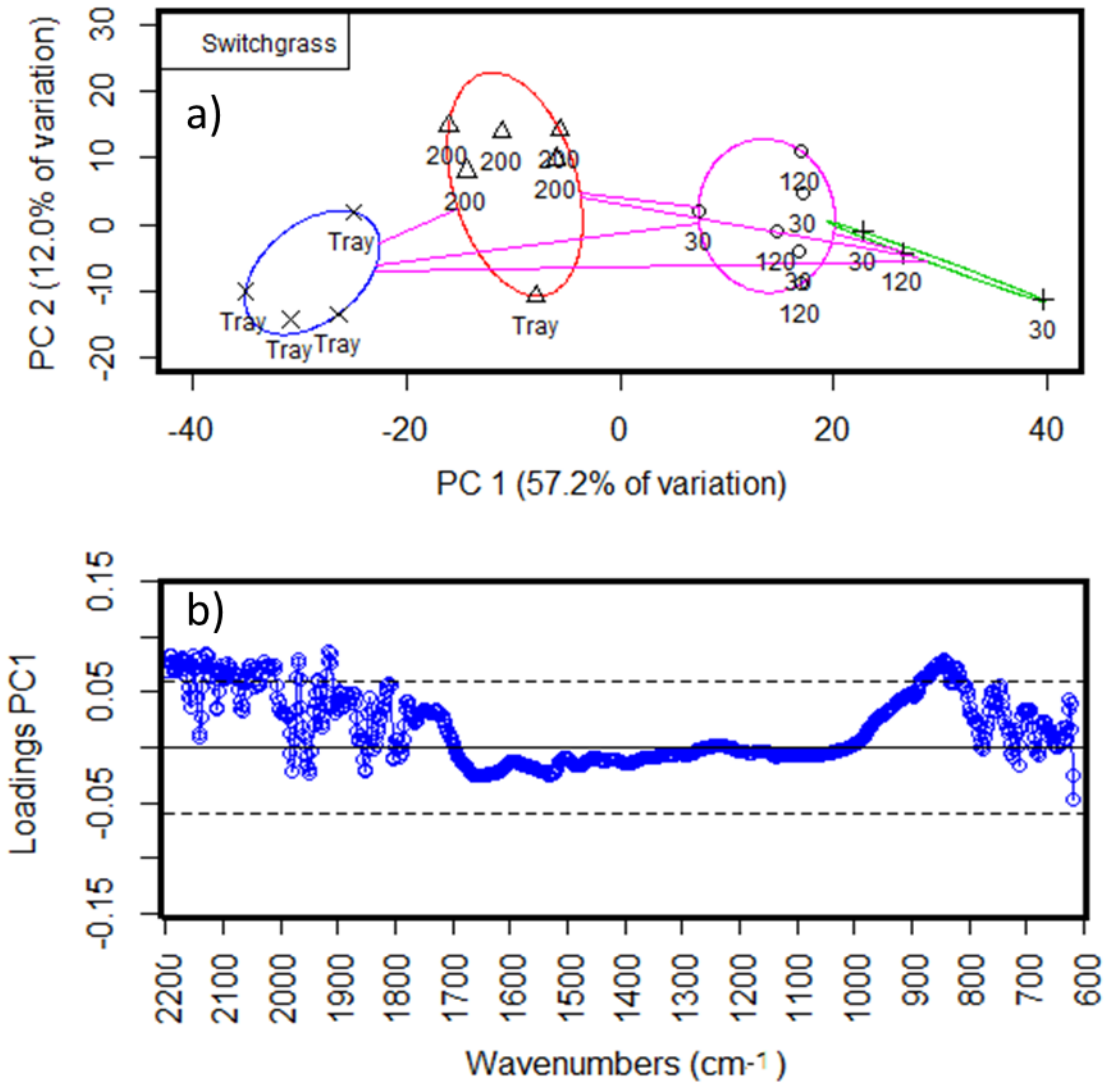

Figure 4.12. PCA analysis of the FTIR-ATR of switchgrass at different particle sizes obteined from the 0.5mm ground sample. a) Biplot representing PC2 vs. PC1. The clusters that contain and group particles at different particle sizes were defined statistically using the k-means Euclidean distance criteria (Singh et al. 2013). The numbers correspond to the sieve # where the particles where collected (Table 4.1). Tray correspond to the particles collected after passing the 200 mesh sieve. b) Loadings plot used to identify the wavenumbers that have higher weight in the definition of PC1.

4.4 Conclusions

Particle size strongly influences spectral signal intensity for dried switchgrass and hardwood obtained from ATR and HTS-XT sampling methods. Larger particle sizes yield lower signal intensities and lower spectra reproducibility. Particle size ground using 0.5 mm sieve was selected as the one that yields lower coefficient of variance without spectral modifications based on grinding intensity. On the other hand, 0.5mm ground particles are composed of a distribution of sizes that can yield reproducibility challenges that can be solved by applying computational signal processing techniques. Signal processing techniques are required to decrease spectral variability of samples at different particle size, while maintaining spectral feature magnitude to be considered acceptable. Vector normalization, and signal derivation combined with vector normalization were found to be the most effective processing techniques that achieve the above-mentioned requirements for spectra obtained using ATR and HTS-XT respectively. Principal Components Analysis (PCA) was effective in predicting the functionality differences between different fractions of switchgrass and hardwood, mainly concentrated in the composition of lignin and the amount of hemicellulose. These conclusions were shared by other studies using traditional and well-established wet chemical analysis (acid digestion of biomass) to elucidate the composition of biomass. This agreement serves as a validation of the FTIR combined with PCA technique to reveal biomass differences. It will be used as the main analytical technique in chapter VII of this dissertation to determine the functionalities, and chemical differences among hydrochar obtained from the thermochemical processes of a variety of waste feedstocks from food and agricultural industries.

The comprehensive analysis of a wider variety of biomass samples using FTIR would benefit the scope and accuracy of the methods developed in this chapter regarding sample treatment and

preparation for FTIR. A next valuable future step would be to relate FTIR spectral features from pretreated biomass under several temperatures, pressures, and reaction times with compositional information obtained from wet chemistry analysis. These relations could potentially be fitted into a model using least square regression methods or other multivariate statistical techniques to predict pretreated biomass composition based on spectral features.

4.5 References

Adapa, T, L Schoenau, G Canam, and T Dumonceaux. 2011. "Quantitative Analysis of Lignocellulosic Components of Non-Treated and Steam Exploded Barley, Canola, Oat and Wheat Straw Using Fourier Transform Infrared Spectroscopy." *Journal of Agricultural Science and Technology B* 1 (12): 177–88.

Allison, G. 2011. "Chapter 4: Application of Fourier Transform Mid-Infrared Spectroscopy (FTIR) for Research into Biomass Feed-Stocks." In *Fourier Transforms - New Analytical Approaches and FTIR Strategies.*, 71–88. Intech.

Aucott, L, P Garthwaite, and S Buckland. 1988. "Transformations to Reduce the Effect of Particle Size in near-Infrared Spectra." *Analyst* 113 (12): 1849–54.

Bouchard, J, T Nguyen, E Chornet, and R Overend. 1990. "Analytical Methodology for Biomass Pretreatment — Part 1: Solid Residues." *Biomass* 23 (4): 243–61.

Chen, H, C Ferrari, M Angiuli, J Yao, C Raspi, and E Bramanti. 2010. "Qualitative and Quantitative Analysis of Wood Samples by Fourier Transform Infrared Spectroscopy and Multivariate Analysis." *Carbohydrate Polymers* 82 (3): 772–78.

Chundawat, S, B Venkatesh, and B Dale. 2007. "Effect of Particle Size Based Separation of Milled Corn Stover on AFEX Pretreatment and Enzymatic Digestibility." *Biotechnology and Bioengineering* 96 (2): 219–31.

Corgié, S, H Smith, and L Walker. 2011. "Enzymatic Transformations of Cellulose Assessed by Quantitative High-Throughput Fourier Transform Infrared Spectroscopy (QHT-FTIR)." *Biotechnology and Bioengineering* 108 (7): 1509–20.

Fraser, R T M. 1959. “Sodium Azide as Internal Standard for Quantitative Infrared Analysis.” *Analytical Chemistry* 31 (9). American Chemical Society: 1602–3.

GmbH, Bruker Optik, ed. 2007. “HTS-XT User Manual.” *Bruker Optik GmbH*. Billerica MA.

Guo, G, W Chen, W Chen, L Men, and W Hwang. 2008. “Characterization of Dilute Acid Pretreatment of Silvergrass for Ethanol Production.” *Bioresource Technology* 99 (14): 6046–53.

Hu, Z, R Sykes, M Davis, E Brummer, and A Ragauskas. 2010. “Chemical Profiles of Switchgrass.” *Bioresource Technology* 101: 3253–57.

Kim, T, and Y Lee. 2005. “Pretreatment and Fractionation of Corn Stover by Ammonia Recycle Percolation Process.” *Bioresource Technology* 96 (18): 2007–13.

Liu, S, R Fu, L Zhou, and S Chen. 2012. “Application of Consensus Scoring and Principal Component Analysis for Virtual Screening against β-Secretase (BACE-1).” *PLOS ONE* 7 (6): 1–13.

MIRacle (TM) ATR for FTIR Spectrometers. Installation and user guide. 2005. *PIKE Technologies, Inc.*, issued 2005.

Ni, Z, C Hu, and C Feng. 2010. “Analyzing the Methods to Remove Artifacts Encountered in the Development of a NIR Quantitative Model for Powder Medicines.” *Journal of Analytical & Bioanalytical Techniques* 1 (3).

Nuopponen, M, and T Vourinen. 2005. “Thermal Modifications in Softwood Studied by FT-IR and UV Resonance Raman Spectroscopies.” *Journal of Wood Chemistry and Technology* 24 (1): 13–26.

Pandey, K. 1999. “A Study of Chemical Structure of Soft and Hardwood and Wood Polymers by FTIR Spectroscopy.” *Journal of Applied Polymer Science* 71 (12): 1969–75.

Reris, R, and J Brooks. 2015. “Principal Component Analysis and Optimization: A Tutorial.” *14th INFORMS Computing Society Conference*, 212–25.

Saprativ, P, A Ghosh, D Debasish, M Jawed, and A Goyal. 2013. “Scale up and Efficient Bioethanol Production Involving Recombinant Cellulase (Glycoside Hydrolase Family 5) from Clostridium Thermocellum.” *Sustainable Chemical Processes* 1 (19).

Sills, D, and J Gossett. 2012. “Using FTIR to Predict Saccharification from Enzymatic Hydrolysis of Alkali-Pretreated Biomasses.” *Biotechnology and Bioengineering* 109 (2): 353–62.

Sim, S, M Mohamed, N Lu, M Sarman, and S Samsudin. 2012. “Computer-Assisted Analysis of Fourier Transform Infrared (FTIR) Spectra for Characterization of Various Treated and Untreated Agriculture Biomass.” *BioResources* 7 (4): 5367–80.

Singh, A, A Yadav, and A Rana. 2013. “K-Means with Three Different Distance Metrics.” *International Journal of Computer Applications* 67 (10): 13–17.

Singh, S, B Simmons, and K Vogel. 2009. “Visualization of Biomass Solubilization and Cellulose Regeneration during Ionic Liquid Pretreatment of Switchgrass.” *Biotechnology and Bioengineering* 104 (1): 68–75.

Vazquez, G, S Freire, G Antorrena, and J Gonzalez. 2002. “Characterization of Eucalyptus Globulus and Pinus Pinaster Acetosolv Pulps Prebleached with O_2 by FTIR and DRIFT Spectroscopy.” *Holz Als Roh- Und Werkstoff* . 60 (1): 25–30.

Yang, H, R Yan, H Chen, D Lee, and C Zheng. 2007. “Characteristics of Hemicellulose, Cellulose

and Lignin Pyrolysis.” *Fuel* 86 (12–13): 1781–88.

Part II

Thermochemical valorization of model compounds and organic wet wastes from a variety of industries and characterization of the products: Influence of pH, temperature, and reaction time in product distribution and quality

CHAPTER V

KINETICS OF THE HYDROTHERMAL LIQUEFACTION REACTION FOR ORGANIC WASTE MODEL COMPOUNDS AND THEIR DEGRADATION PRODUCTS

5.1 Introduction

Model compounds were used as the first approach to study the hydrothermal liquefaction (HTL) process, before moving to real substrates. This is in line with the rationale used in this dissertation for the study of the biochemical conversion of biomass.

The investigation of the HTL process for model compounds is not new in literature. In our group at Cornell, Posmanik et al. (2017) performed reactions at several temperatures (250, 300, and 350˚C) and residence times (20 and 60 minutes) using potato starch as a model for carbohydrates, bovine serum albumin (BSA) as a model for protein, and linoleic acid as a model for lipids. Teri et al. (2014) used cornstarch and cellulose as model compounds for carbohydrates, soy protein and albumin as model compounds for proteins, and castor oil and sunflower oil as lipids. They performed reactions at two temperatures (300 and 350˚C) and over a larger range of reaction times (10, 20, 30, 45, 60, and 90 minutes).

The Posmanik (2017) and Teri (2014) studies were “end-point experiments”, in the sense that after a specific reaction time, the reaction was quenched and all the products were collected. In this chapter, the approach is different, as different aliquots of the HTL media will be collected at discrete times and temperatures until the volume of HTL media is depleted. This protocol renders samples that are suitable for the analysis of intensive properties like pH and concentration of

species, more than for extensive properties (recovery of mass of solids, bio-crude, etc.). In addition, this chapter presents the use of HPLC for the characterization of HTL media, to distinguish it from earlier studies.

The goal of the research discussed in this chapter was to elucidate the kinetics of model feedstocks representing carbohydrates and their degradation products (cellulose, glucose, levulinic acid), lipids (linoleic acids), and proteins (bovine serum albumin) to better understand the hydrothermal liquefaction reactions and products obtained. The features of the reactor used for the collection of HTL samples at different temperature and/or time conditions, the analytical techniques used, and preliminary results about the HTL media pH, and the chemical species obtained will be discussed in some detail. This data will be used as a platform for the development of kinetic models for HTL reactions to be carried out in our group in the future.

5.2 Experimental set-up

The reactor used to study the kinetic of hydrothermal liquefaction of model compounds was a 316 stainless steel, 1000 mL bolted closure reactor from Autoclave Engineers (Erie, PA), with a maximum allowable working pressure of 5,500 psi (380 bar) at 650 F (345˚C). The reactor was mounted on an open light-duty floor stand, with a lifting mechanisms using to move the vessel. A refrigerated magnetically controlled shaft and impeller was incorporated to stir the contents of the reactor. In addition, the reactor was equipped with a porous metal diffuser to maximize the input gas distribution, a thermo-case where a thermocouple was inserted to measure the temperature inside the reactor, and a cooling coil connected to the building water used to quench the reaction after the desired reaction time. Figure 5.1 shows the fittings inside the reactor. An extra port in the

reactor was used to incorporate a pressure gauge (Duro United Instruments, Northvale, NJ) and a pressure transducer (Model 280E Setra Systems, Boxborough, MA). An electrical heating jacket equipped with a thermocouple was used to heat up the reactor. A data acquisition and reactor control system, Sentinel Series (Autoclave Engineers®, Eire, PA), was used to control the heating of the reactor and the mixing speed, and to monitor the pressure and temperature inside the reactor as well as the temperature of the heating jacket. The reactor was connected to a gas tank through a high-pressure pump (Thar Process, Pittsburgh, PA). To complete the reactor set-up, venting valves and a back-pressure regulator, BPR (Tescom, Elk River, MN) were used to decompress the reactor. The BPR and the venting valves were covered with heating tape (Omega Engineering, Stamford, CO) to prevent freezing of the lines during decompression.

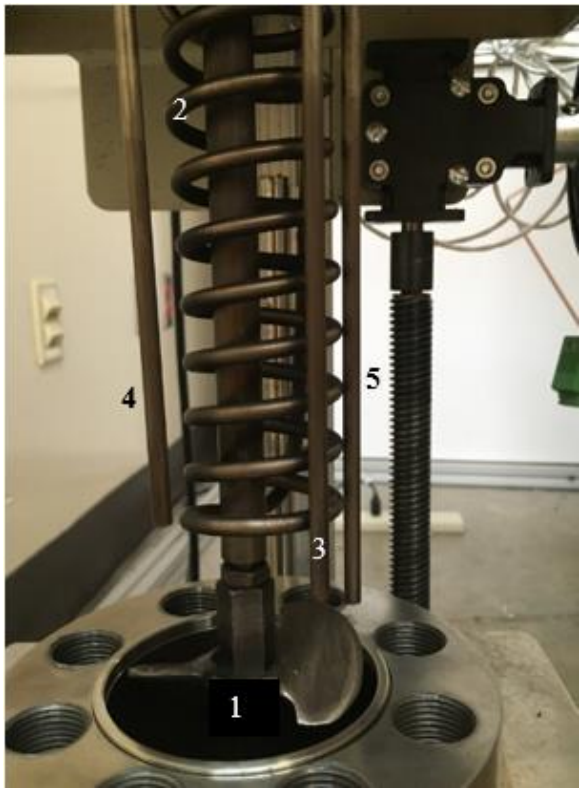

Figure 5.1. Fitting inside the reactor: 1) Stirrer with propeller, 2) heat exchanger coil for reaction quenching, 3) thermo-well for thermo-par, 4) gas inlet, 5) sampling line.

The set-up described above was designed for purely batch operations, where the substrate was introduced in the reactor, the reactor was sealed, pressurized and heated up. After the reaction, the reactor was cooled down to room temperature, decompressed, and opened to collect the reaction products. This design was not functional for kinetic experiments, where it was necessary to collect aliquots of reaction content at the desired times and temperature conditions. In addition, changes needed to be done in the reactor design to improve the safety for reaction operation. The proposed modifications in the reactor design to adapt it to continuous sampling under safe conditions were the product of multiple trial and error experiments. The modifications are listed below and showed in Figure 5.2:

- In terms of improving safety of operation, the stems of the decompression valves were enlarged and passed through the polycarbonate panels that constituted a physical barrier between the reactor and the operator. With this modification, all the reactor operation occurred behind protective panels. Two decompression valves were used to have spare in case of line clogging.
- A second digital manometer was placed in the reactor inlet line. Taking pressure lectures at two different points of the system decreased the chance of wrong measure of pressure caused by clogged lines.
- A line for pumping liquid at high pressure though the lines of the reactor was added to the reactor input. This was necessary to flush the system with acetone and water after every reaction to avoid cross-contamination between experiments.
- An extra output line was added to one of the ports in the reactor for sample collection. The sample collection line reached the bottom of the reactor to collect as much volume as possible (decreasing liquid dead volume). This line was equipped with two 3 meters copper

coil heat exchangers submerged in an ice bath to cool and quench the sample before decompression (Figure 5.2). A ball-valve was used to decompress and collect the sample. The used of a needle valve was attempted (their graphite yarn seat is more resistant to high temperatures). However, its use was discharged as the small amount of solids produced in the process were sufficient to clog the needle valve.

- In terms of operation, the reactor was always pressurized using both the inlet and the sampling line. When the reactor was pressurized using only the inlet line, the material inside the reactor was pushed to the sampling line resulting in clogging it.

Figure 5.2. Pictures of the reactor used for studying the kinetic of HTL of model compounds. 1) Enlarged stem of exhaust valves for safe operation. 2) Heat exchangers to quench sample before depressurization (with ball valve, 3) and collection (4). 5) Pressure transducer in input line. 6) Pressure transducer directly connected to a port of the reactor.

A schematic of the reactor system is shown in Figure 5.3. The blue line represents the building water used to cool down the magnet of the stirrer and to quench the reaction. During experiments, water is continuously flows through the stirrer magnet to keep it cool. However, when the reaction is terminated, the ball valve in the blue line is opened for water to be directed through the coil heat exchanger inside the reactor to quench the reaction. The manifold in the line acts as a water reservoir to have sufficient water flow to feed both cooling requirements. The purple line represents the reactor input line. Process gas or liquid can be fed into the reactor by operating the three-way valve. Either of those streams can be pressurized using the high-pressure pump. By operating one of the three needle valves placed downstream from the pump, the system can be purged, (top valve in the purple line in the diagram), and the gas or the liquid can be fed into the reactor using the input line (middle and bottom valves in the purple line in the diagram). The bottom valve in the diagram is placed in a line that is shared between the input and the output lines of the reactor. The combination of the middle and bottom valve in purple line were operated to pressurize the system as mentioned above. The green line represents the reactor output line. It is equipped with two heat exchangers submerged in iced water, used to quench the sample before being depressurized. Depressurization and sample collection is performed operating the ball valve in this green line. The red lines represent the safety lines, used to depressurized the system after the reaction, or in case of emergency (rupture disc). These needle valves were operated from outside of the reactor area, behind a polycarbonate panel, as above mentioned.

The temperature measurement and control was performed by the temperature transducer (TT in the diagram), inserted in the reactor inside a thermo-well. The pressure measurement and control was performed by a pressure transducer located in the input line (PT in the diagram), and second transducer combined with an analogic manometer connected directly to a port of the reactor.

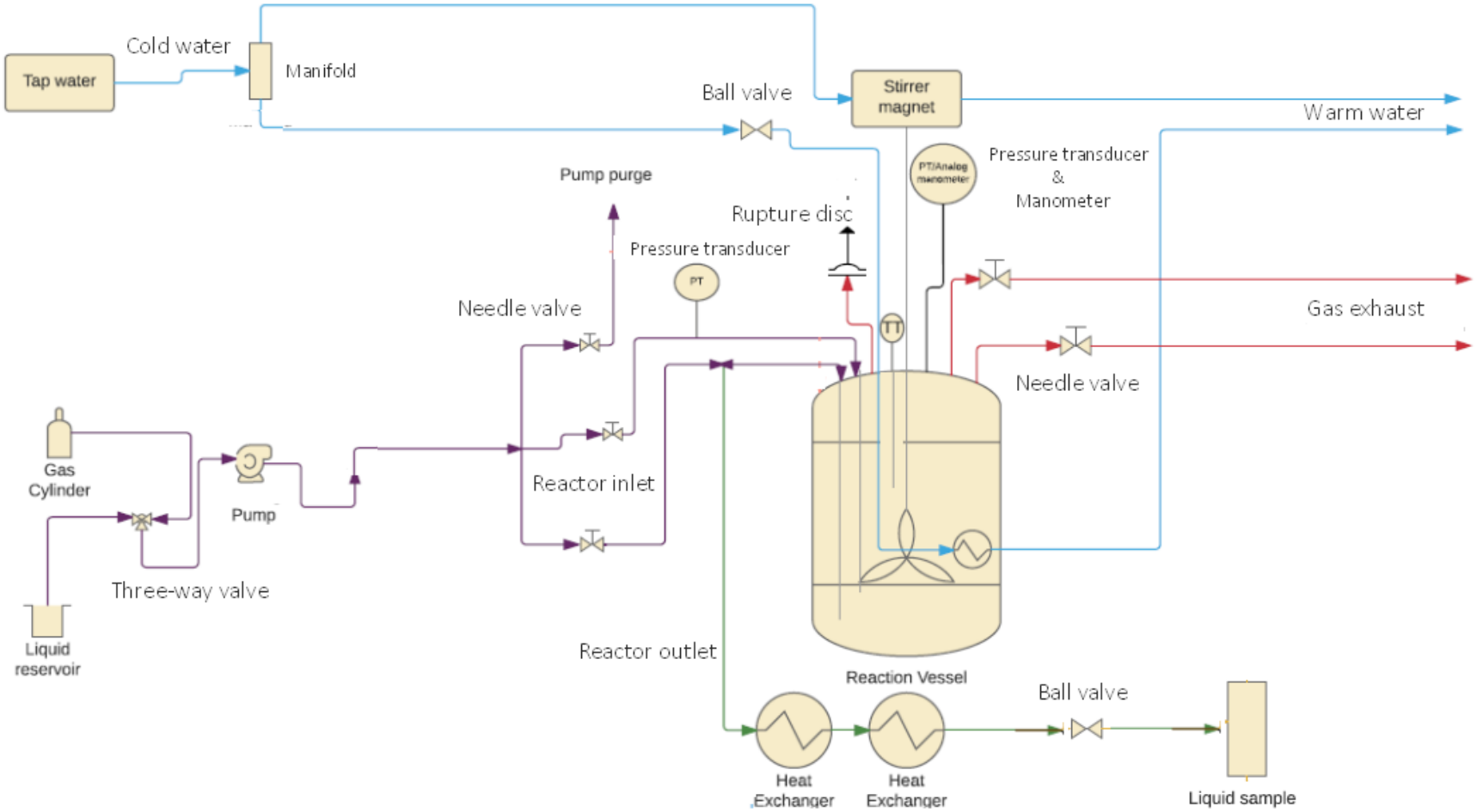

Figure 5.3. Scheme of the reactor used to study the kinetic of the HTL process of model compounds

5.3 Experimental protocol

The model substrates used in this chapter were a representation of carbohydrates (glucose and cellulose (Fibrous cellulose powder CF11 Whatman)), carbohydrates degradation products under HTL conditions (levulinic acid), lipids (linoleic acid), and proteins (Bovine serum albumin, BSA). These model substrates are a representation of the building blocks of biomass and organic waste. Their individual study under HTL will provide information to better understand the process applied to industrial organic feedstocks (Posmanik et al. 2017). The concentrations used in these experiments were 50 g/l (5%) for glucose, cellulose, levulinic acid, and BSA, and 20g/l (2%) for linoleic acid. The solutions were prepared using deionized water. The use of diluted solutions respond to two main reasons: to accurately mimic the behavior for HTL of real substrates (typical concentrations for HTL are below 2% (Yin et al. 2010)), and to avoid the formation of high volume of solids from the HTL of these compounds, that results in clogging sampling line.

A reaction volume of 700 ml for all the experiments was prepared and fed to the reactor. After bolting the vessel and tight seal the system, the oxygen in the head-space was purged by flowing N_2 gas (purple line in Figure 5.3) until a pressure of 100-200 psig (7-14 bar) was reached, before the reactor was decompressed (red line in Figure 5.3). This protocol was repeated 3 times, and can be observed at the beginning of the representation of pressure profiles presented below. Once purged, the reactor was pre-pressurized with 200 psig of N_2. At this point, the reactor was heated up to the desired temperature. The temperature profiles are presented in Figure 5.4 (a-e). The reaction was considered to start (t=0) when the temperature of the reactor reached 80˚C. The black dots represent the conditions where samples were collected from the reactor. After finishing reaction (no more sample to be collected), the heating was stopped and the reactor was quenched

by flowing water through the reactor coil (blue line in Figure 5.3). Figure 5.5 (a-e) shows the pressure profiles of the reactions, together with the saturation pressure of water for every temperature condition according to steam tables (grey line). Working above the saturation pressure of water assures water is in liquid conditions through the entire experiment (HTL conditions). The consecutives pressurization-depressurization steps with N_2 gas to purge the oxygen from the reactor's head-space can be observed at initial times on the pressure profiles shown in Figure 5.5 (a-e). The changes in system pressure during reaction (red line) match perfectly the changes on vapor pressure of water (grey line), that is an only function of temperature. This indicates, the change in pressure during the reaction respond to changes in heating input from the electrical jacket to keep the temperature set-point, and not from leakage of gaseous contents from the reactor. The pressure and temperature profiles demonstrated that the conditions of the reactions were not altered by the sample collection. The conditions for the sample collection for each experiment are summarized in Table 5.1.

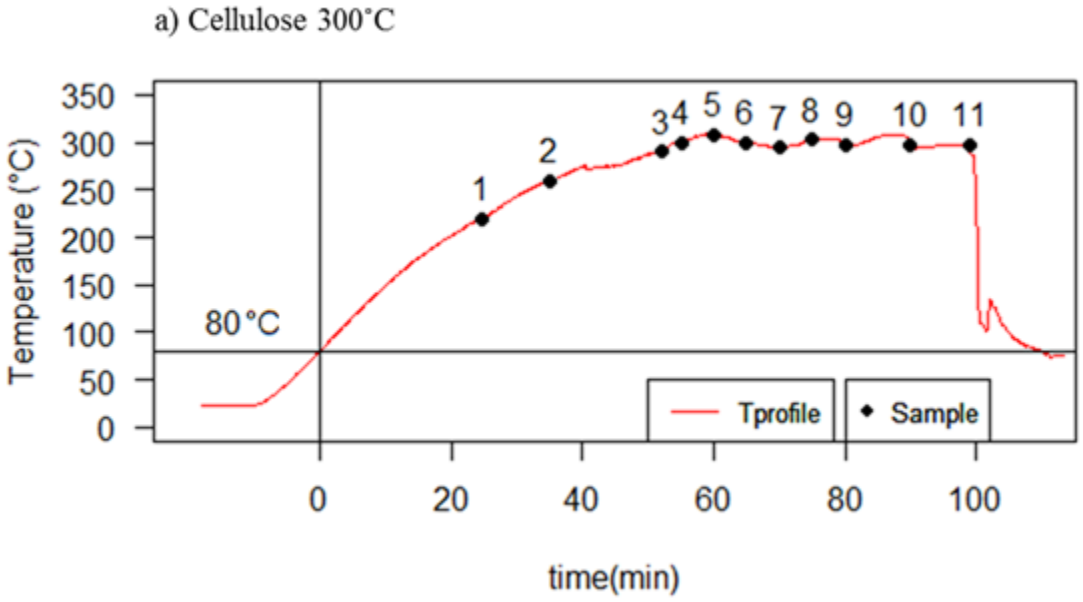

b) Glucose 300˚C

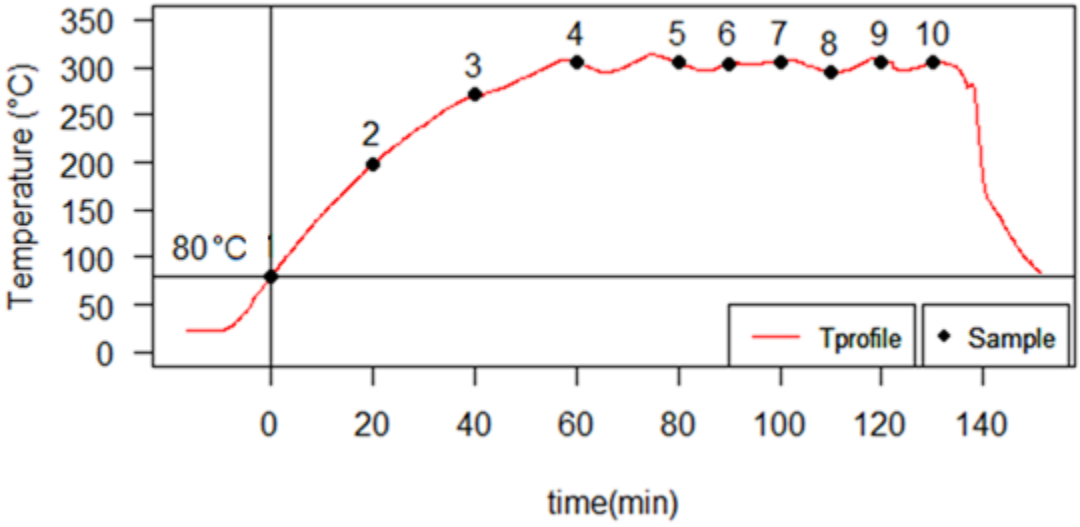

c) Glucose 275˚C

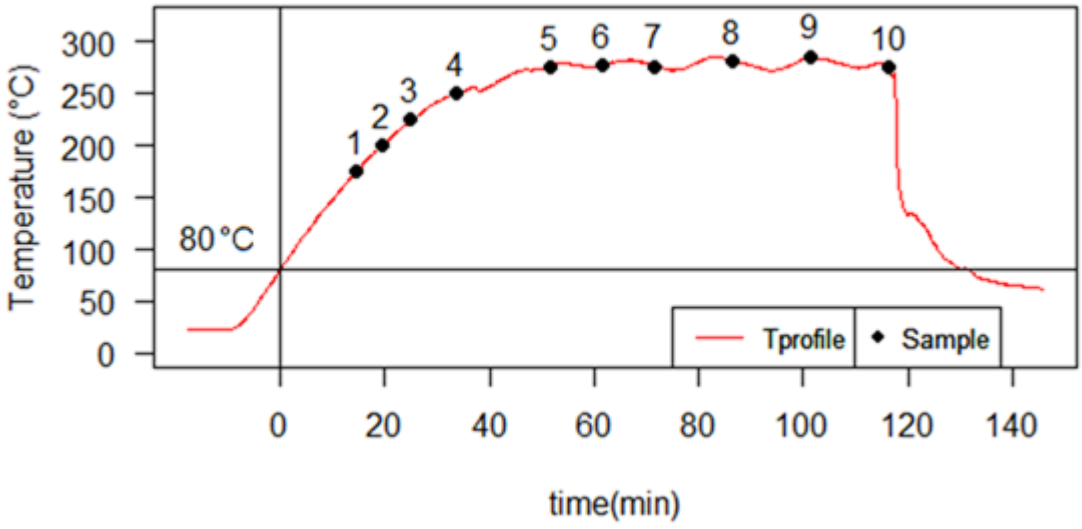

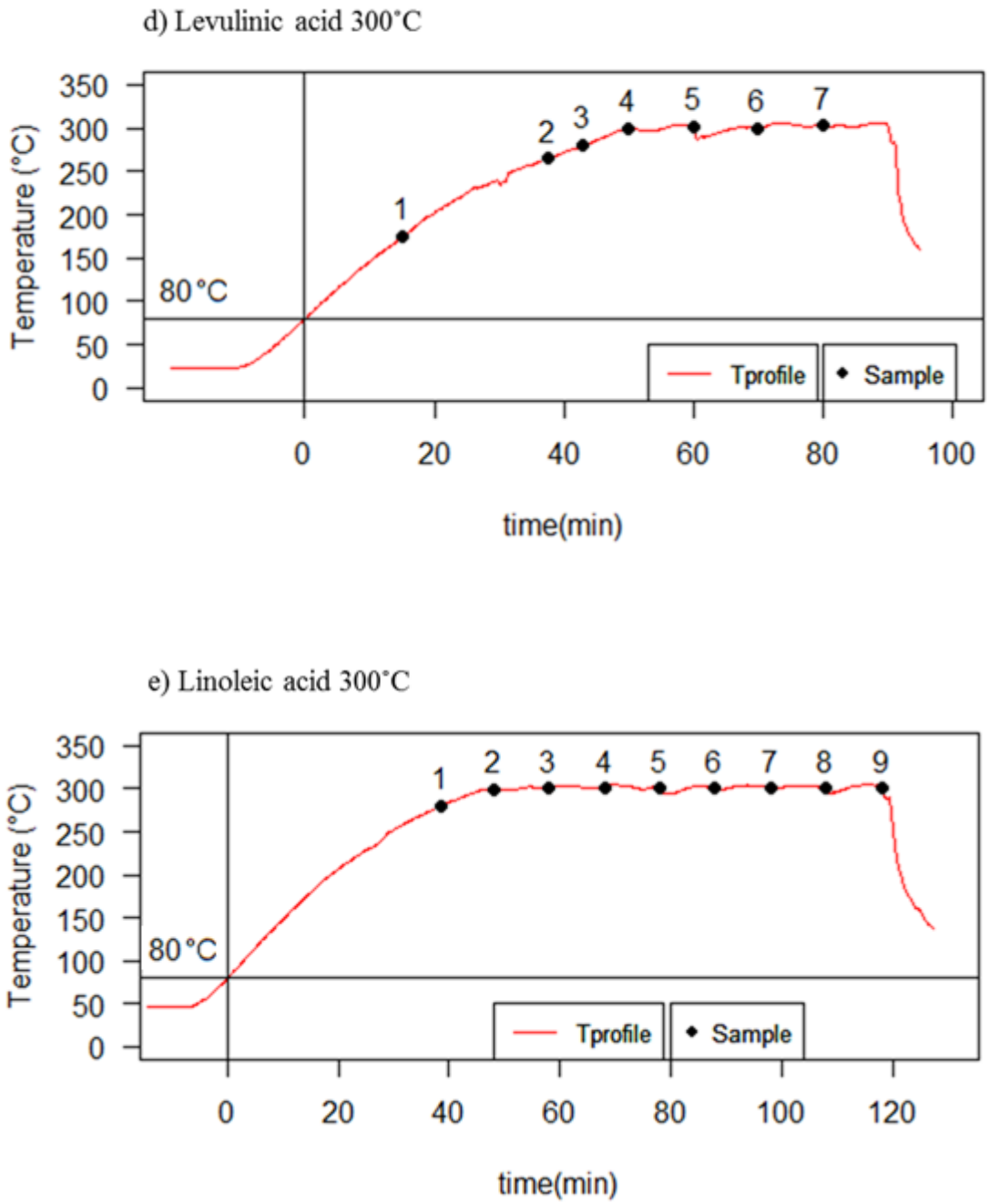

Figure 5.4. Temperature profiles for kinetics experiments for model compounds: a) Cellulose 300˚C. b) Glucose 300˚C. c) Glucose 275˚C. d) Levulinic acid 300˚C. e) Linoleic acid 300˚C. The black dots represent sample collection conditions.

a) Cellulose 300˚C

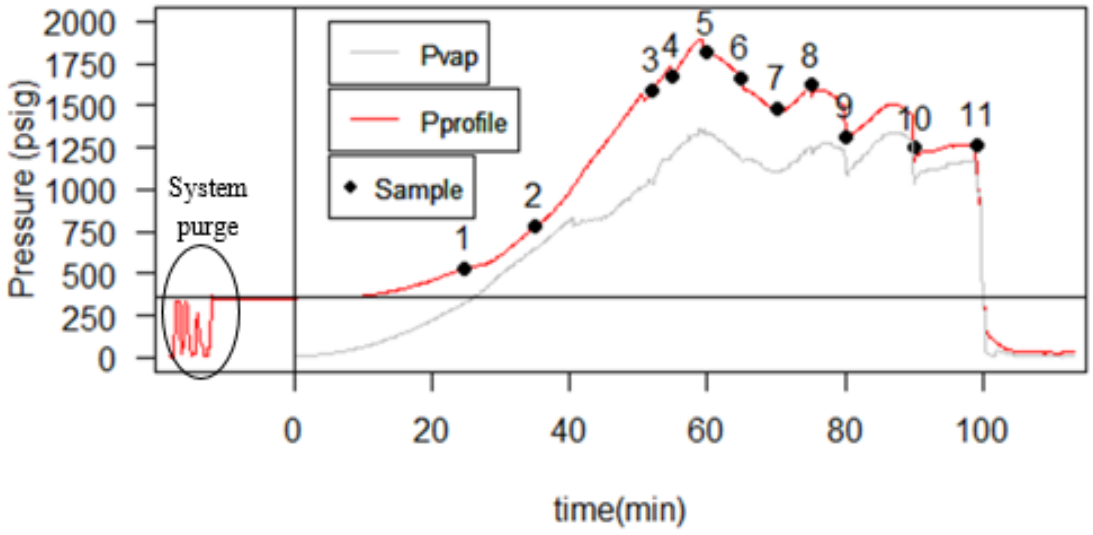

b) Glucose 300˚C

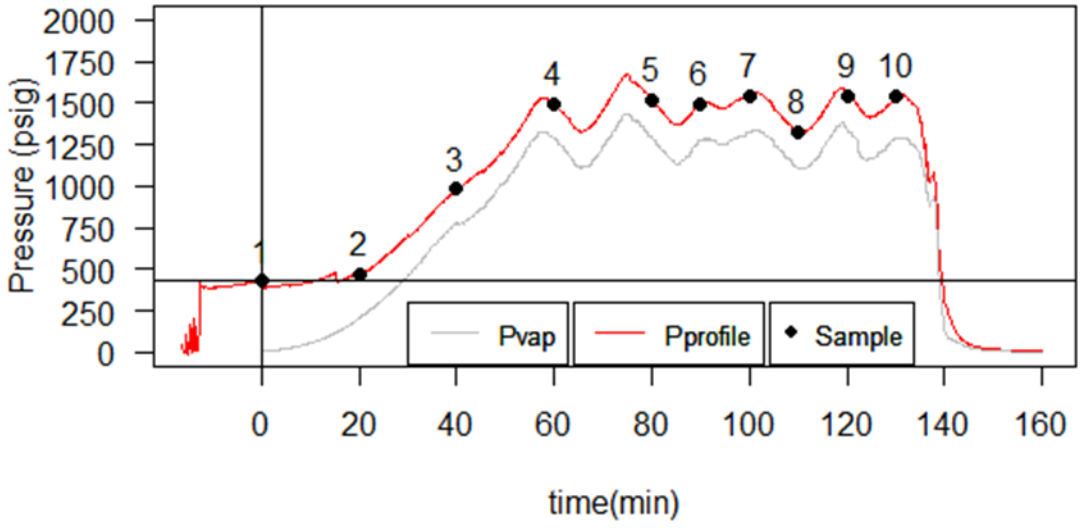

c) Glucose 275˚C

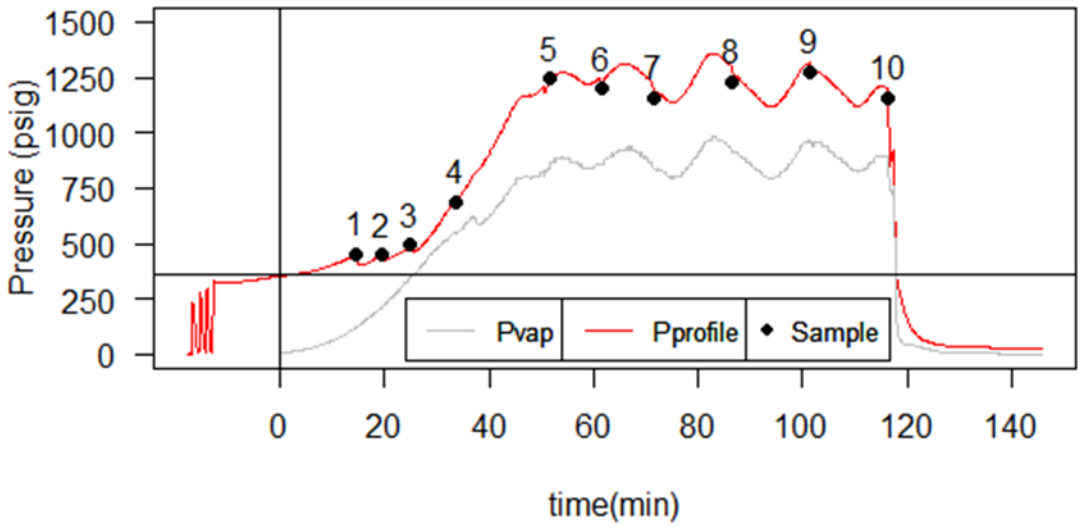

d) Levulinic acid 300˚C

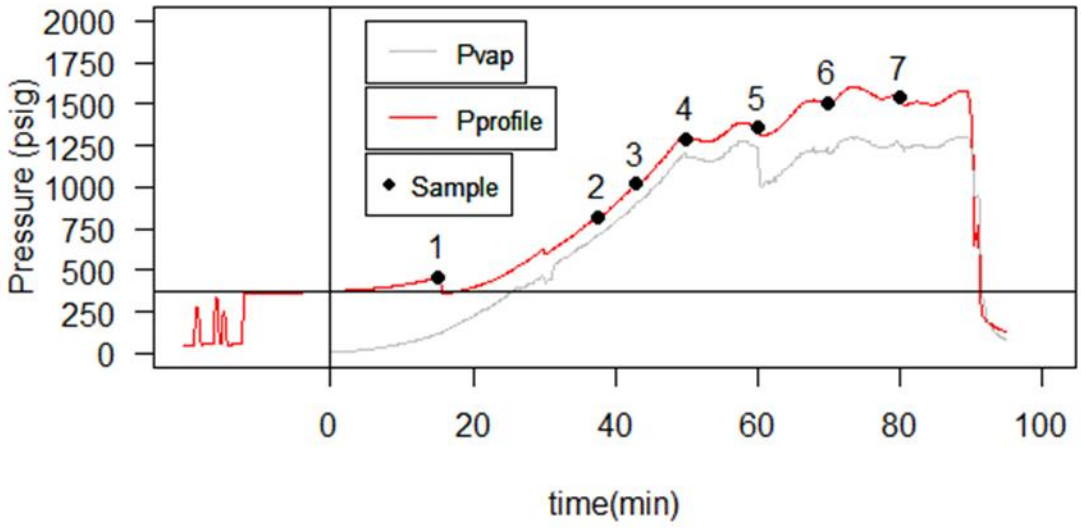

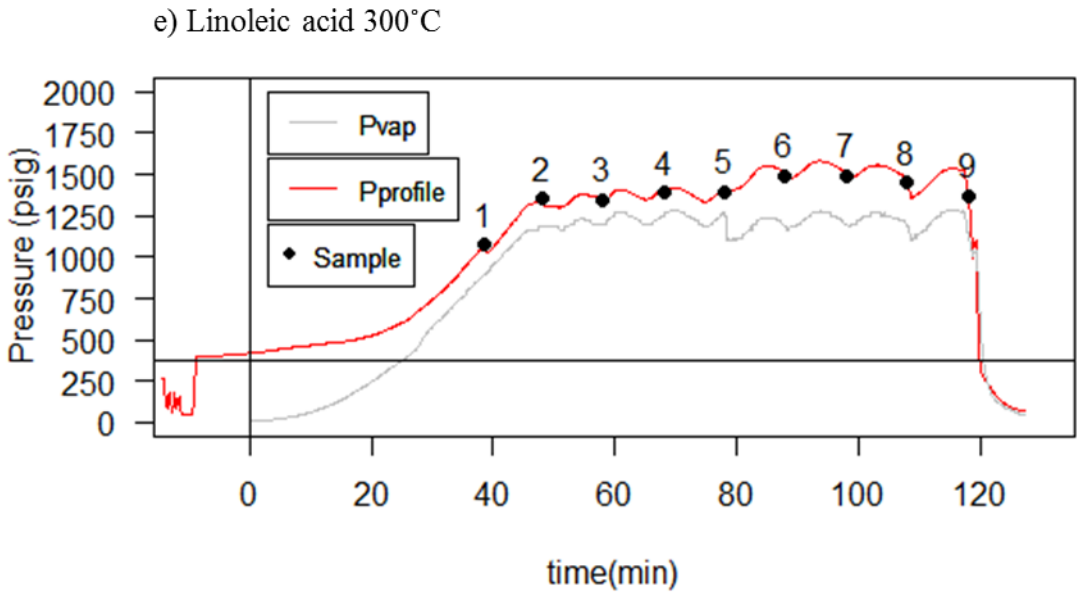

Figure 5.5. Pressure profiles for kinetics experiments for model compounds: a) Cellulose 300˚C. b) Glucose 300˚C. c) Glucose 275˚C. d) Levulinic acid 300˚C. e) Linoleic acid 300˚C. The black dots represent sample collection conditions.

Table 5.1. Correspondence of black dots presented in temperature and pressure profiles with sampling conditions for every experiment. Only one run was done for each set of conditions. Reproducibility was checked and determined at ±5% with three runs for cellulose at 300˚C.

	Cellulose 300˚C			Glucose 300˚C		
Sampling #	time (min)	T (˚C)	P (psig)	time (min)	T (˚C)	P (psig)
1	24.7	220	533	0	80	428
2	35	260	784	20	198	469
3	52	290	1589	40	271	981
4	55	300	1678	60	305	1497
5	60	308	1812	80	305	1521
6	65	299	1667	90	304	1494
7	70	294	1482	100	305	1546
8	75	303	1620	110	294	1323
9	80	298	1314	120	305	1541
10	90	297	1250	130	305	1543
11	100	298	1266			

	Glucose 275˚C			Levulinic acid 300˚C		
Sampling #	time (min)	T (˚C)	P (psig)	time (min)	T (˚C)	P (psig)
1	14.67	175	451	15.2	175	457
2	19.5	200	449	37.5	265	821
3	25	225	492	42.8	280	1017
4	33.5	250	690	50	300	1288
5	51.5	275	1242	60	302	1357
6	61.5	277	1198	70	300	1505
7	71.5	276	1159	80	303	1538
8	86.5	281	1232			
9	101.5	285	1275			
10	116.5	275	1156			

	Linoleic acid 300˚C			BSA 300˚C		
Sampling #	time (min)	T (˚C)	P (psig)	time (min)	T (˚C)	P (psig)
1	38.5	280	1076	30	250	975
2	48	299	1352	38	280	1080
3	58	304	1343	48	300	1385
4	68	302	1391	53	300	1401
5	78	300	1396	58	300	1415
6	88	301	1489	68	300	1397
7	98	300	1492			
8	108	299	1448			

The sample collection was designed to avoid cross-contamination among samples. At the desired sampling time (Table 5.1), the ball valve in the reactor output line (green line in Figure 5.3) was opened. Around 25 ml of sample were quenched by flowing through the heat exchangers, submerged in iced water, and depressurized before being collected. This first sample was discharged and the protocol was repeated to collect the first sample (25ml) that will be analyzed. This procedure was repeated as many times as samples collected, with the precaution of discharging around 25ml of reactor volume prior to every sample collected for analysis. We did this because after sample collection, the piping in the output line of the reactor remained filled with this sample. By purging the sampling line with 25 ml of sample, that we discharged, we made

sure that the sample collected was representative for the desired sampling conditions, without cross-contamination from previous sample. After all the sample volume was collected, the reactor was cooled down and depressurized. A dead-volume of 100ml remained in reactor after the experiment, as the sampling line could not reach the bottom of the reactor (where the impeller is).

5.4 Analytical techniques

After collection, the samples were quenched in an ice bath. After that, they were vacuum filtrated using pre-weighted filter papers (Whatman No. 1) to separate the solids. Solids were dried at 105˚C and weighted. The liquid phase was pH measured at ambient conditions (using an Accumet AB150 probe ,Fisher Scientific, Hampton, NH). To prepare samples for HPLC analysis, they were filtrated using syringe filters, and vortexed. The HPLC used (Shimadzu, Columbia, MD) has a refractive index detector. Samples were eluted at 0.6mL/min through an HPX-87H Bio-Rad Aminex column (BioRad, Hercules, CA) operating at to 65˚C. 5mM sulfuric acid solution in nanopure water was used the mobile phase. Runs were 60 minutes in this study. This column was selected for this chapter because of its capability to analyze carbohydrates in solution with carboxylic acids, volatile fatty acids, short-chain fatty acid, alcohols, ketones, and natural metabolites (Bio-Rad 2017). Standards of sugars, carboxylic acids, and carbonyl compounds were used for peak identification and quantification. Table 5.2 shows the standards with the retention times and the factor (slope of calibration curve) that relates signal intensity with concentration used for the standard. The validity of this calibration has 100mM as upper limit.

Table 5.2. Standards used in HPLC. Retention times and the factors relating signal intensity with concentration obtained after running the standard at known concentrations are shown.

	RT (min)	Slope
Cellotetrose	6.39-6.406	192524
Cellotriose	6.691-6.699	160127
Cellobiose	7.38-7.384	101813
Glucose	9.146-9.53	51374.23
Fructose	9.853-9.869	50899.92
Malonic acid	9.749-7.796	21118.81
Succinic acid	11.427-11.438	24591.83
Lactic acid	12.736-12.744	16493.12
Glycoaldehyde	12.722-12.736	28138.68
Formic acid	13.798-13.801	4295.244
Acetic acid	15.032-15.043	7909.359
Levunilic acid	15.326-15.38	24067
Butyric acid	21.05-21.073	18586.65
Acetone	21.818-21.83	7251.524
HMF	28.113-28.183	43826.91
Furfural	41.577-41.826	33092

5.5 Results and discussion

As a carbohydrate model compound, cellulose can be used to model the HTL of manure (Mau et al. 2016). The HTL of cellulose produced about 7 grams of solids (20 wt% yield referred to mass of cellulose fed at the beginning of the experiment). It is important to notice that the use of extensive properties in this study (i.e., mass of solid recovery) has to be considered with precaution as the mass of solids obtained in every sample are representative of the conditions where the sample was collected, but not necessarily representing other conditions. Cellulose starts degrading at temperatures above 250˚C, in agreement with previous studies (Peterson et al. 2008), followed by a decrease in solid formation after 75 minutes (sample 8 for cellulose in Table 5.1).

This chapter's study focused on the study of intensive properties of the HTL system (pH, and molecules concentration, properties that do not depend on the volume of sample collected). Figure

5.6 shows the pH evolution in the HTL media for the different samples collected. The initial pH of the cellulose suspension at room temperature was 5.5. pH for the samples collected was measured after reaction is terminated at ambient conditions. The HTL produced an acidification of the reaction media, as the pH decreases as the temperature increases. Once the temperature of the reaction reached at 300˚C, pH stabilized at 2.5. These results indicate that cellulose degrades into carboxylic acid under HTL conditions, with a stronger effect of temperature than reaction time. HPLC of the reaction media was performed (Figure 5.7) to confirm this observation, and to determine the nature and concentration of monosaccharides and carboxylic acids obtained in the process. The initial solution of cellulose was HPLC analyzed to make sure no soluble sugars were present (Figure 5.7 Room temperature). At temperature below 220˚C, no degradation of cellulose is observed. However, when the temperature increased to 250˚C, cellulose starts to degrade to short chain oligomer sugars (cellotriose, cellotetrose, cellobiose) and glucose. Glucose itself starts isomerizing to fructose and degrading towards HMF. At 290˚C, the short sugars are hydrolyzed to glucose, increasing its concentration, and more degradation products of glucose appear in the system: carboxylic acids as formic acid and succinic acid, and furfural. The formation of carboxylic acid explain the acidification of the HTL media observed. When the reaction reaches 300˚C, monosaccharides are almost totally degraded towards carboxylic acids, furfural, and HMF. At longer times at 300˚C, the carboxylic acids degrade to other products, same as HMF. Furfural is the only product obtained from the degradation of glucose (through isomerization to fructose), that remains in the HTL media at longer reaction times under 300˚C. The evolution of concentration for the compounds, based on HPLC data and calibration curves presented in Table 5.2 are shown in Figure 5.8. The appearance or more peaks without identification (no standards for those peaks) shows the dynamism of HTL process in the evolution of degradation products

towards other new species. A kinetic approach to fit the concentration data of molecules identified by HPLC and shown in Figure 5.8 to a kinetic model that could be used for explanation and prediction of HTL routes and molecules production, is undergoing based on the experimental information here presented.

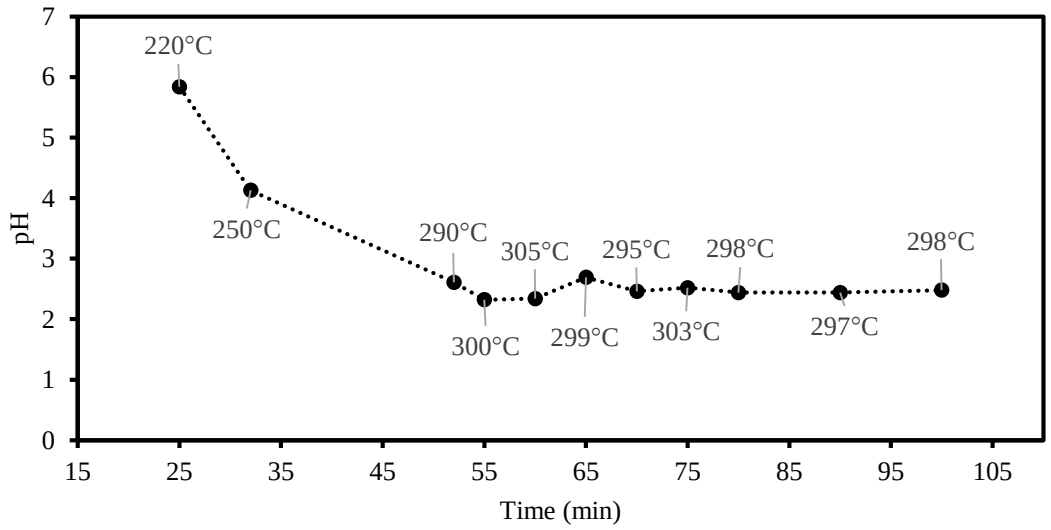

Figure 5.6. pH of the HTL media measured at ambient conditions for cellulose after reaction at different temperature and/or time conditions

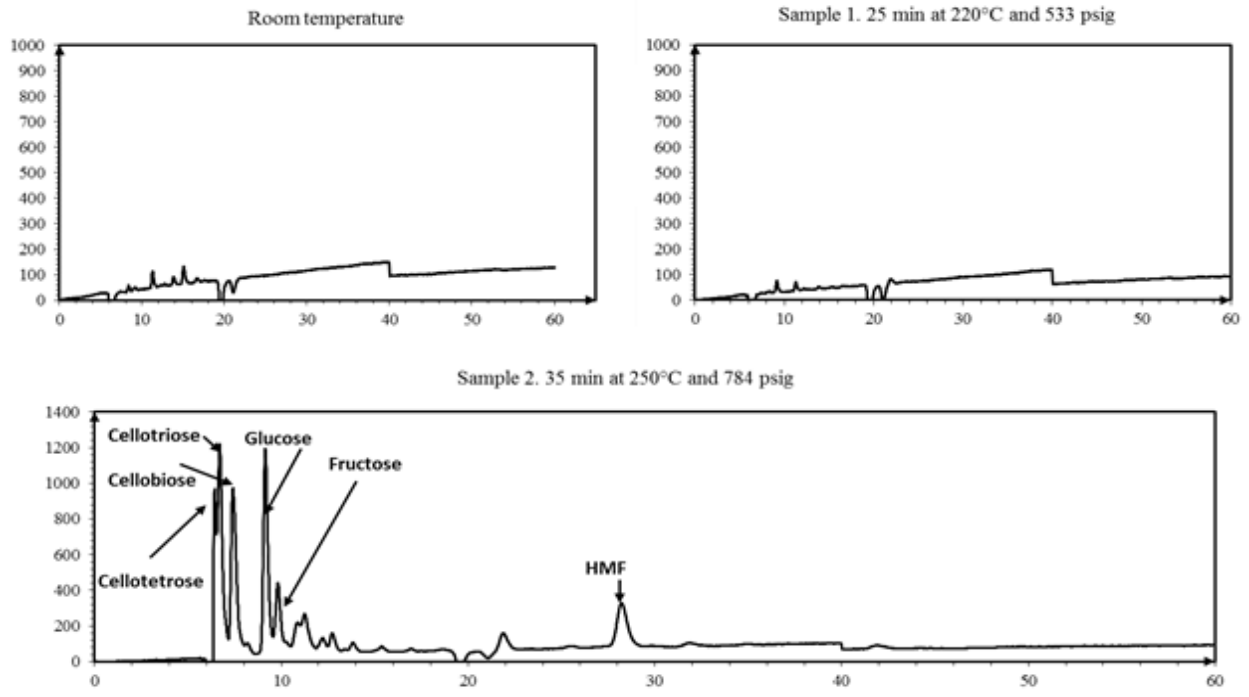

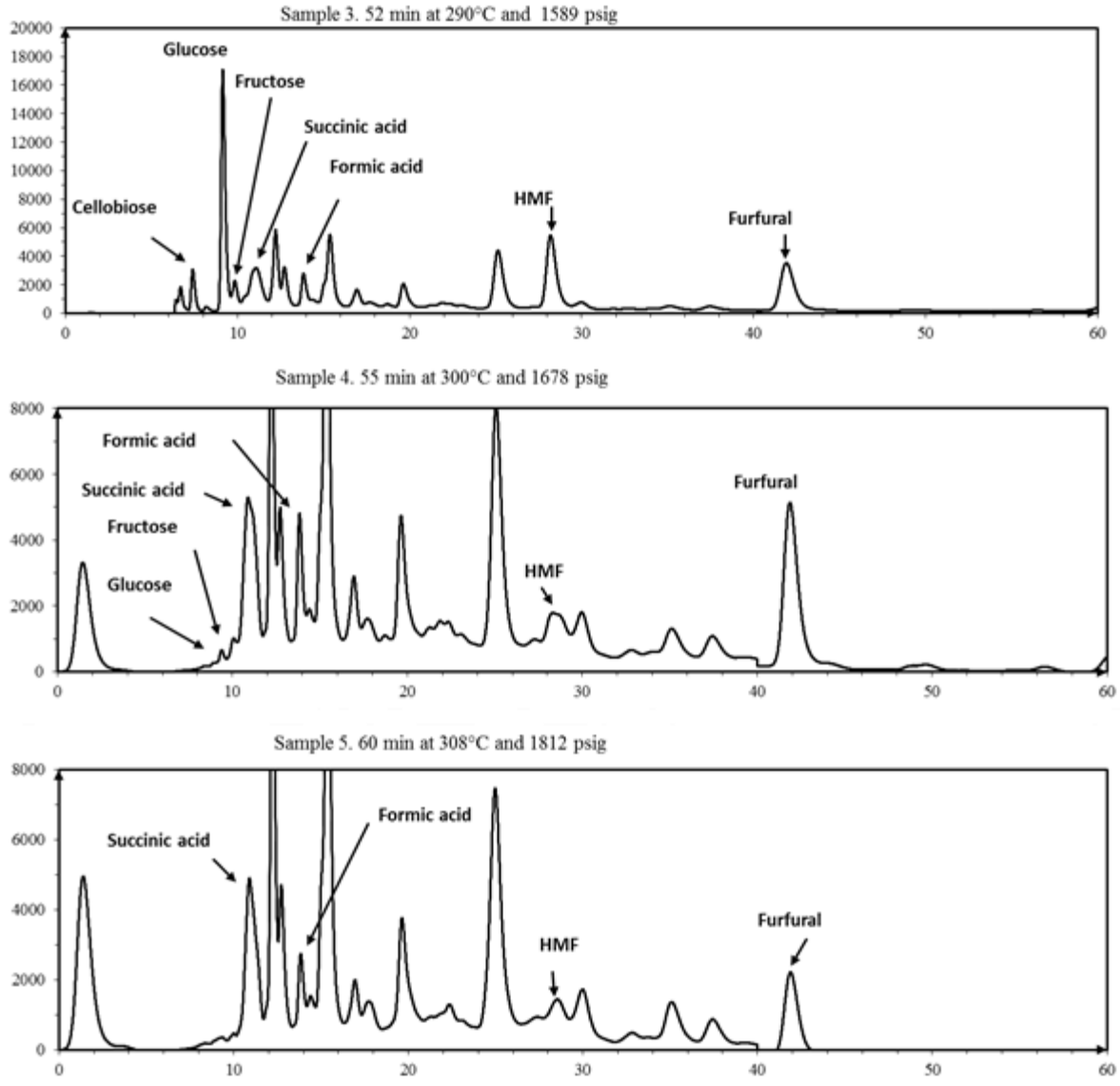
Sample 3. 52 min at 290°C and 1589 psig
Glucose
Fructose
Succinic acid
Formic acid
Cellobiose
HMF
Furfural
Sample 4. 55 min at 300°C and 1678 psig
Formic acid
Succinic acid
Fructose
Glucose
HMF
Furfural
Sample 5. 60 min at 308°C and 1812 psig
Succinic acid
Formic acid
HMF
Furfural

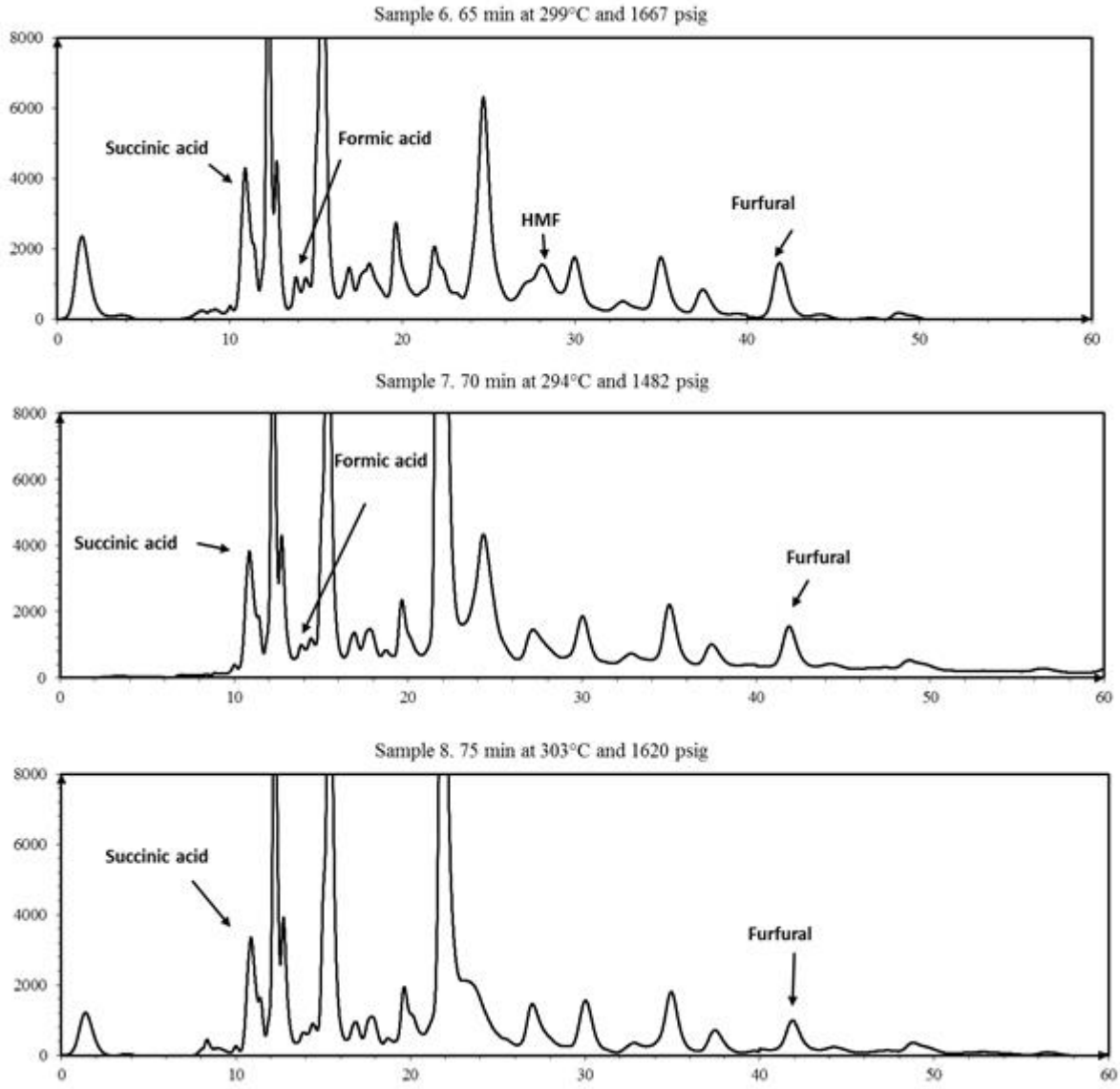
Sample 6. 65 min at 299°C and 1667 psig
Succinic acid
Formic acid
HMF
Furfural
Sample 7. 70 min at 294°C and 1482 psig
Succinic acid
Formic acid
Furfural
Sample 8. 75 min at 303°C and 1620 psig
Succinic acid
Furfural

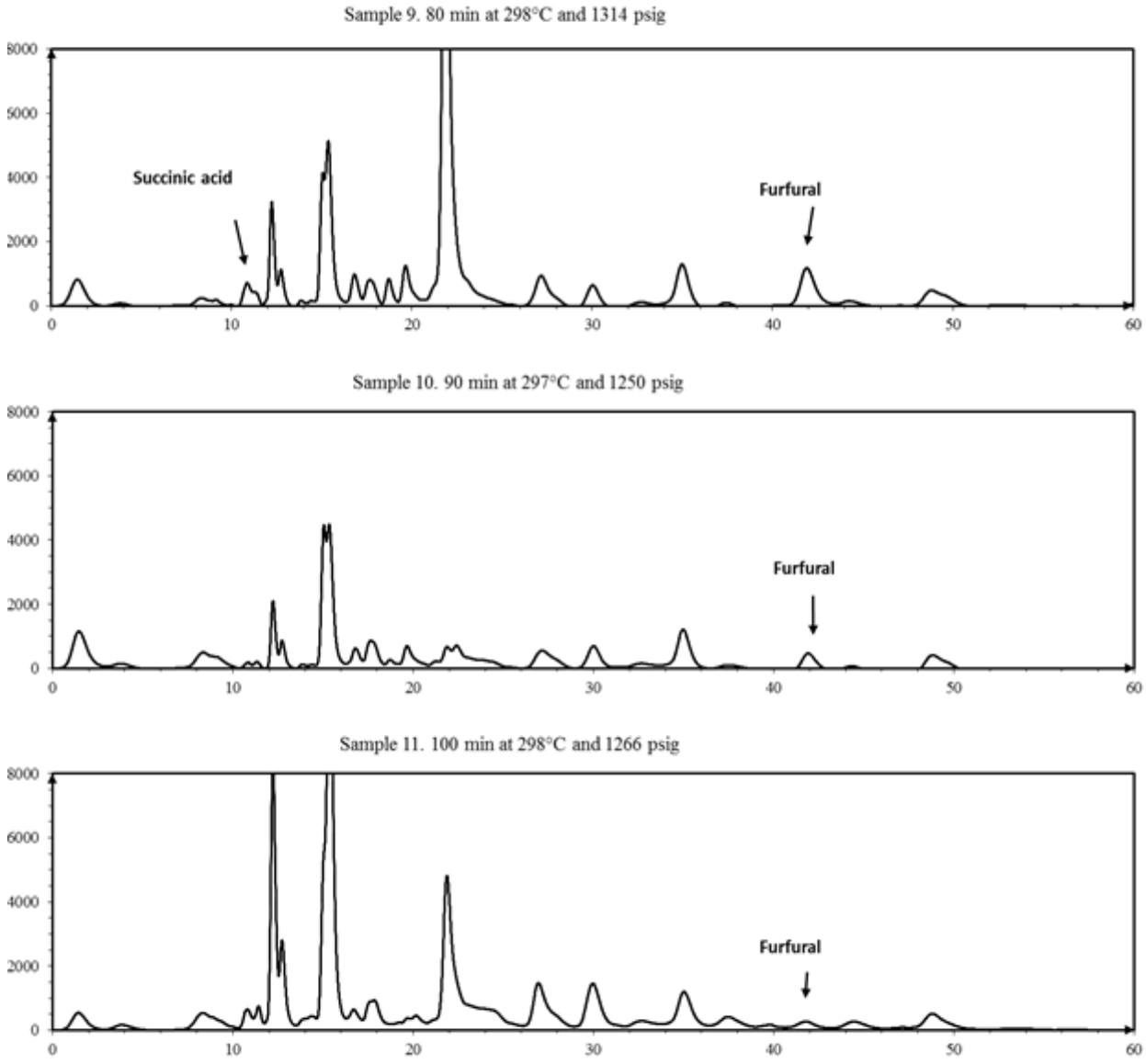

Figure 5.7. HPLC chromatograms of HTL reaction media for cellulose after reaction at different temperatures and/or times. The x-axes represents the retention time. The y-axes represent HPLC signal, that can be related to molecule concentration using the factors presented in Table 5.2 from calibration curves. Some peaks were impossible to identify based on the standards used in this project

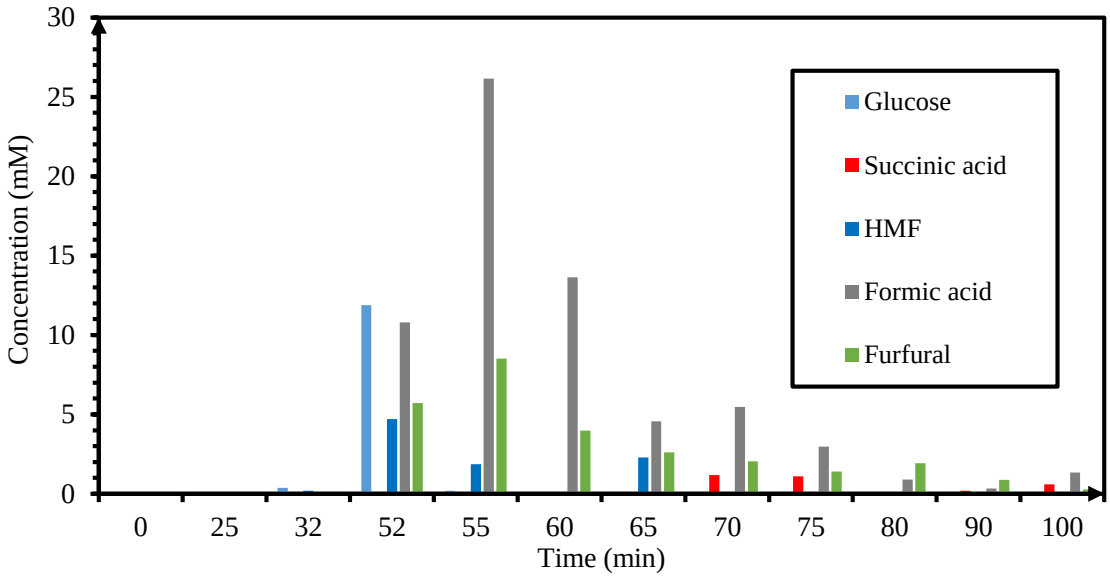

Figure 5.8. Concentration of main components of HTL media of cellulose model compound reacted at 300˚C.

The presence of furfural in the HTL reaction media can be confirmed by the characteristic brown-ish color of the samples observed in Figure 5.9. The most intense color is shown in sample 4, that is the sample with higher furfural concentration as shown as the highest area under the furfural peak in HPLC. The fading of color at longer reaction times can be correlated to the decrease in furfural concentration (decrease of area under the peak in HPLC chromatograms).

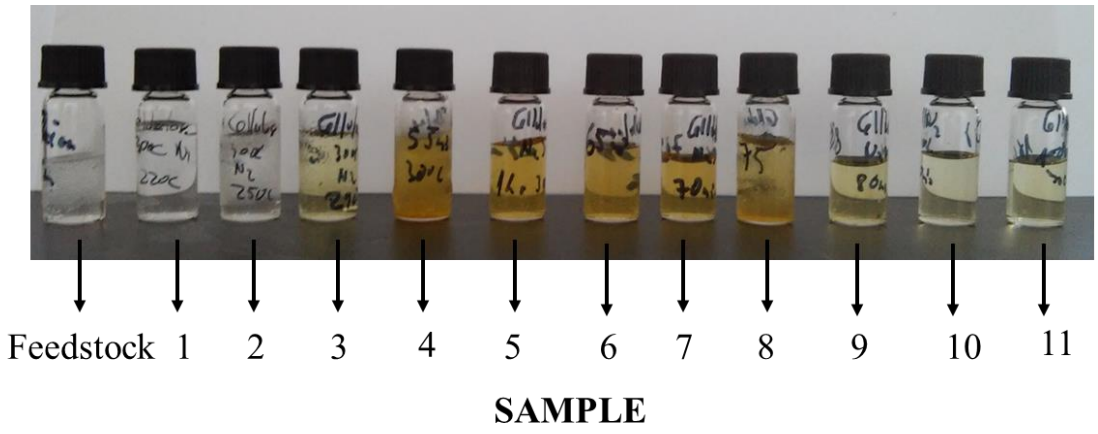

Figure 5.9. Color of HTL media for cellulose after reaction at different temperatures and/or time conditions. The conditions for every sample can be found in Table 5.1.

Following the protocols and techniques here used for cellulose, the HTL for the other model compounds was performed, collecting samples at different reaction times and temperatures to study the kinetic of the process, and the samples were analyzed for pH and HPLC. The mass yield of solids obtained from HTL of glucose at 300˚C totaled 15 wt% referred to mass of glucose fed to the reactor. The peak of solid formation occurred at shorter reaction times at 300˚C.

Figure 5.10 shows the evolution of pH under HTL process. As observed for cellulose, HTL produces an acidification of the media, reaching the same pH value around 2.5. This observation makes sense, considering the first step in the degradation of cellulose is the hydrolysis to glucose, and from there, reactions should be common to the reactions using glucose as model compound. Figure 5.11 shows the HPLC chromatograms of HTL of glucose and concentrations are presented in Figure 5.12. Glucose starts degrading at some point between 200 and 270˚C and totally disappears from the system after 1 hour reaction. The main degradation products detected at 270˚C were succinic acid, formic acid, HMF, and furfural. Fructose appears as an isomerization product of glucose at small concentrations, to rapidly disappear from the system. HMF is formed below 270˚C, and it degrades as the temperature increases to totally disappear from the system at short reaction times at 300˚C. On the other hand, furfural is always presented in the system at small concentrations, what can be confirmed by the color of the samples shown in Figure 5.13. Succinic and formic acid are formed early in the HTL process, below 270˚C. As observed for cellulose, succinic acid is more stable than formic acid under HTL conditions, remaining longer in the system before totally disappearing after 2 hours of reaction.

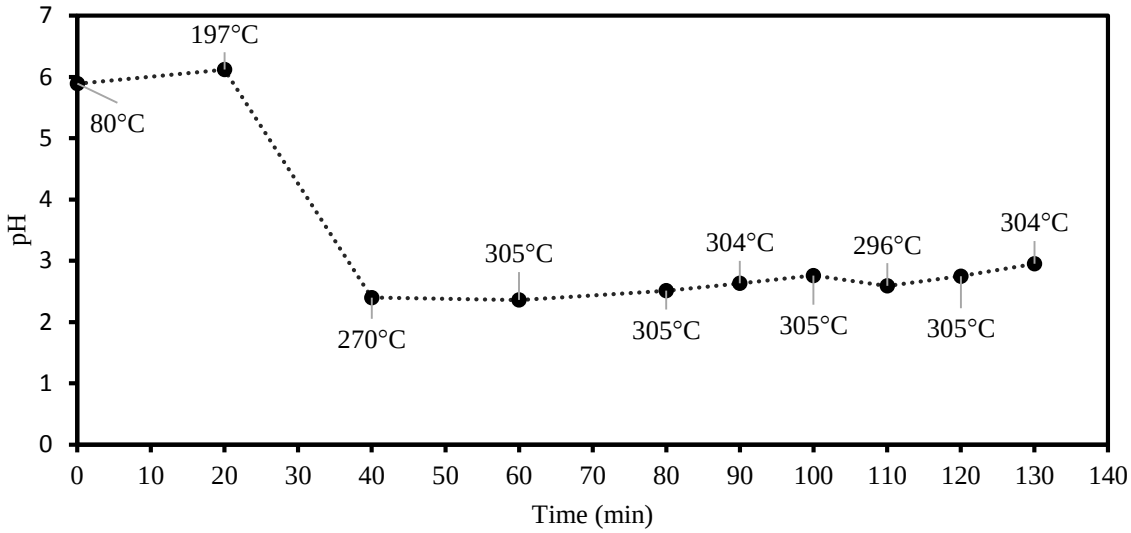

Figure 5.10. pH of the HTL media measured at ambient conditions for glucose after reaction at different temperature and/or time conditions

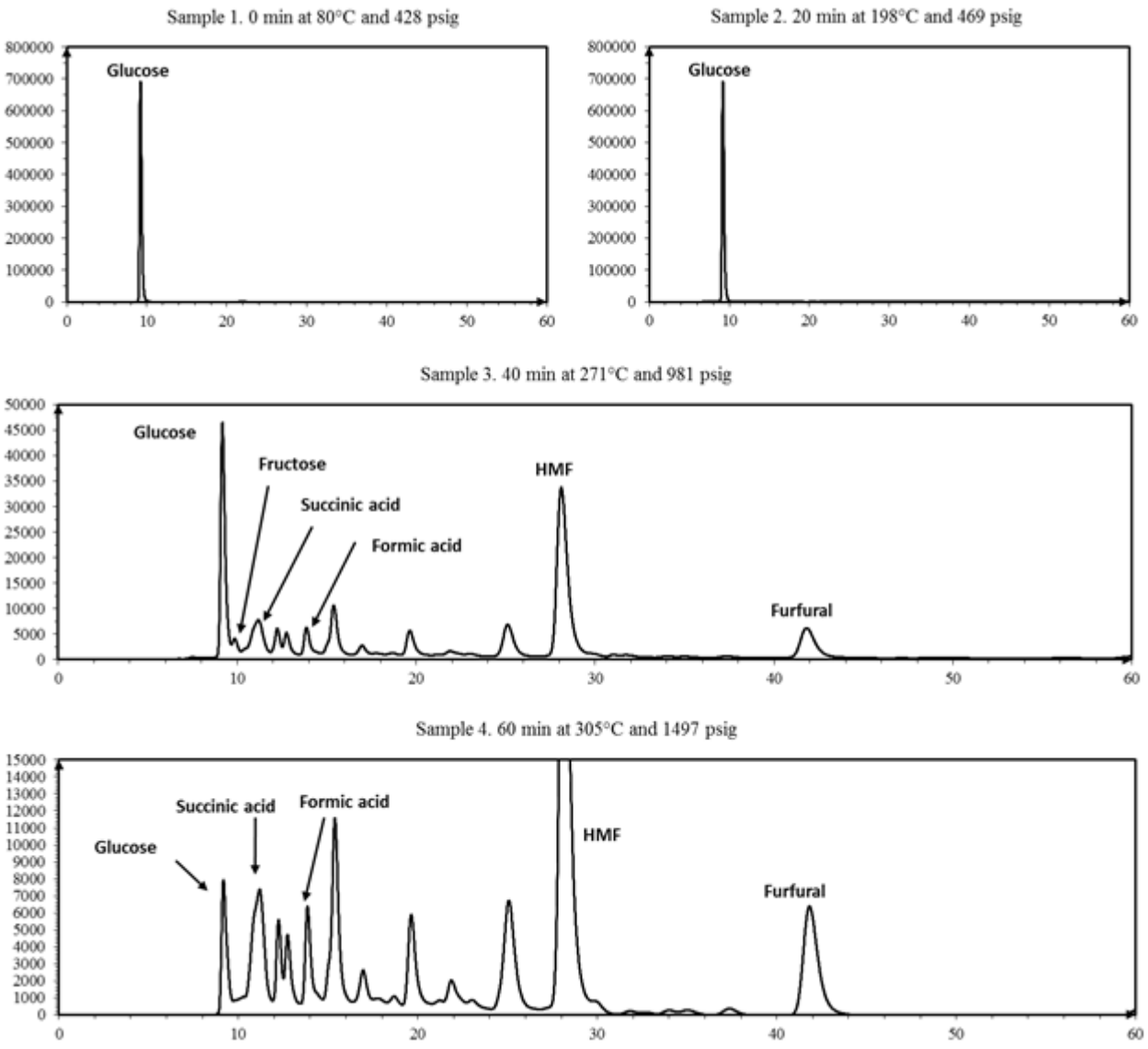
Sample 1. 0 min at 80°C and 428 psig
Glucose
Sample 2. 20 min at 198°C and 469 psig
Glucose
Sample 3. 40 min at 271°C and 981 psig
Glucose
Fructose
Succinic acid
Formic acid
HMF
Furfural
Sample 4. 60 min at 305°C and 1497 psig
Glucose
Succinic acid
Formic acid
HMF
Furfural

Sample 5. 80 min at 304°C and 1521 psig

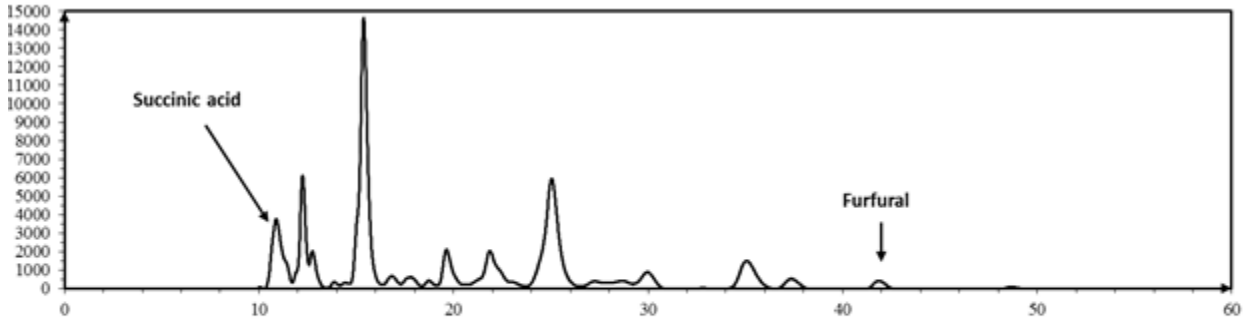

Sample 6. 90 min at 304°C and 1494 psig

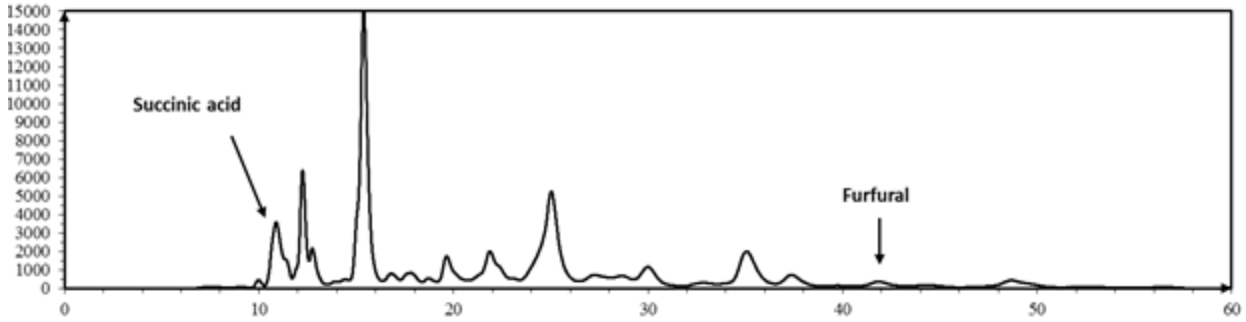

Sample 7. 100 min at 305°C and 1546 psig

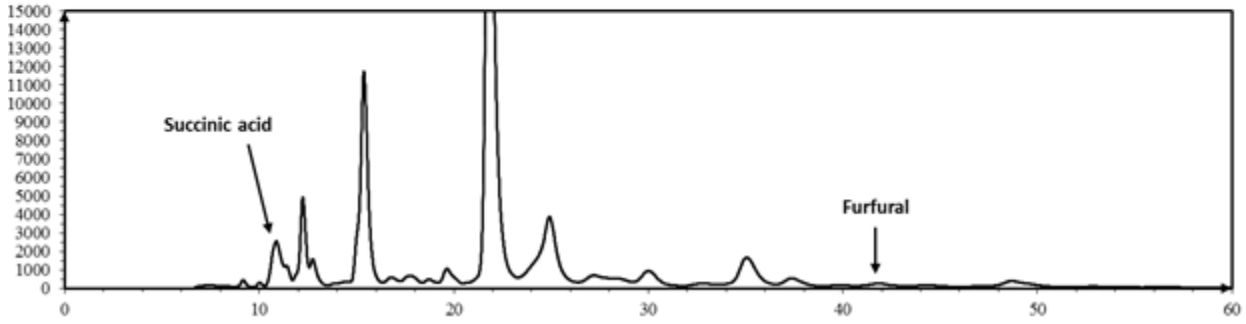

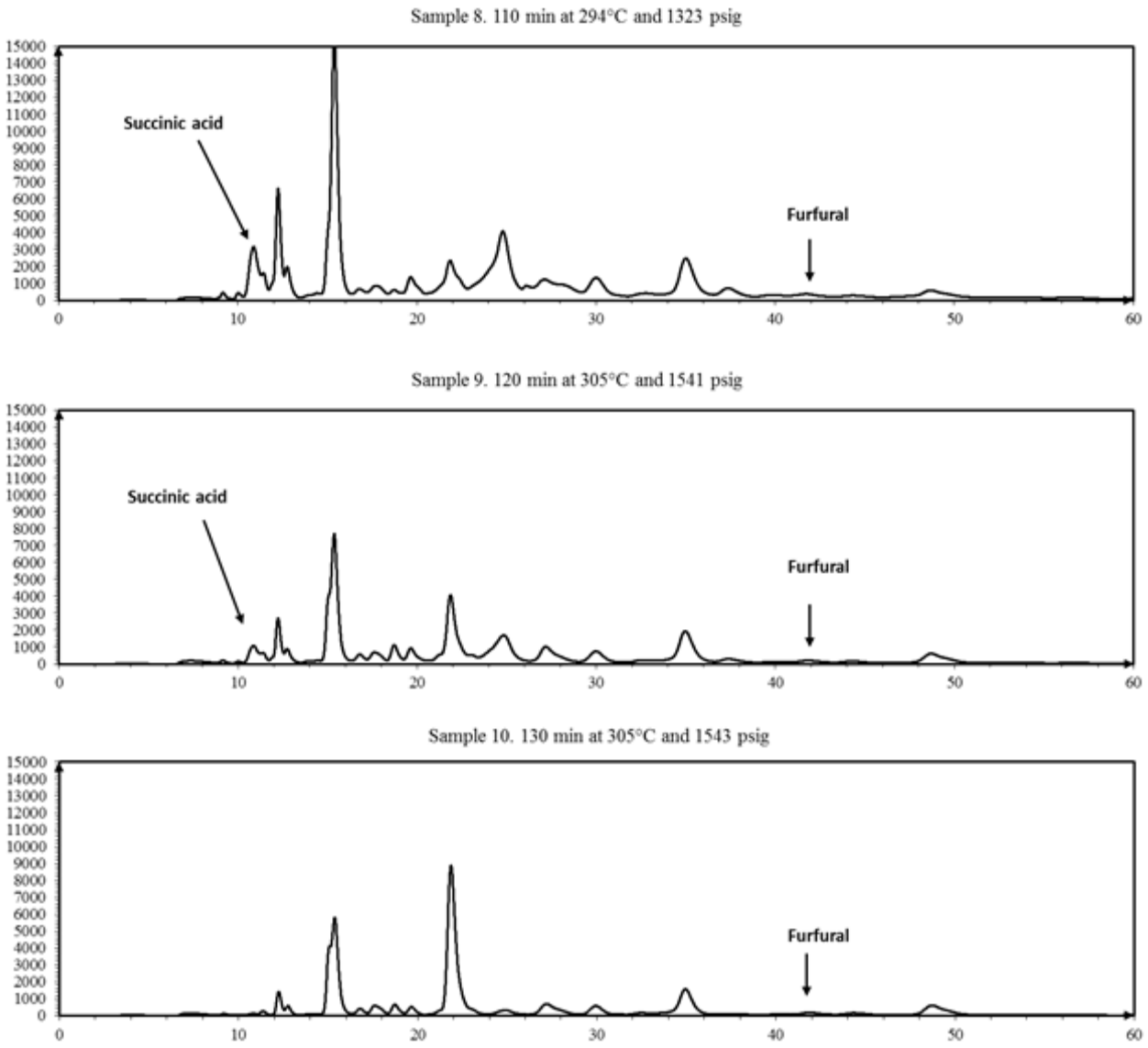

Figure 5.11. HPLC chromatograms of HTL reaction media for glucose after reaction at different temperatures and/or times. The x-axes represents the retention time. The y-axes represent HPLC signal, that can be related to molecule concentration using the factors presented in Table 5.2 from calibration curves. Some peaks were impossible to identify based on the standards used in this project

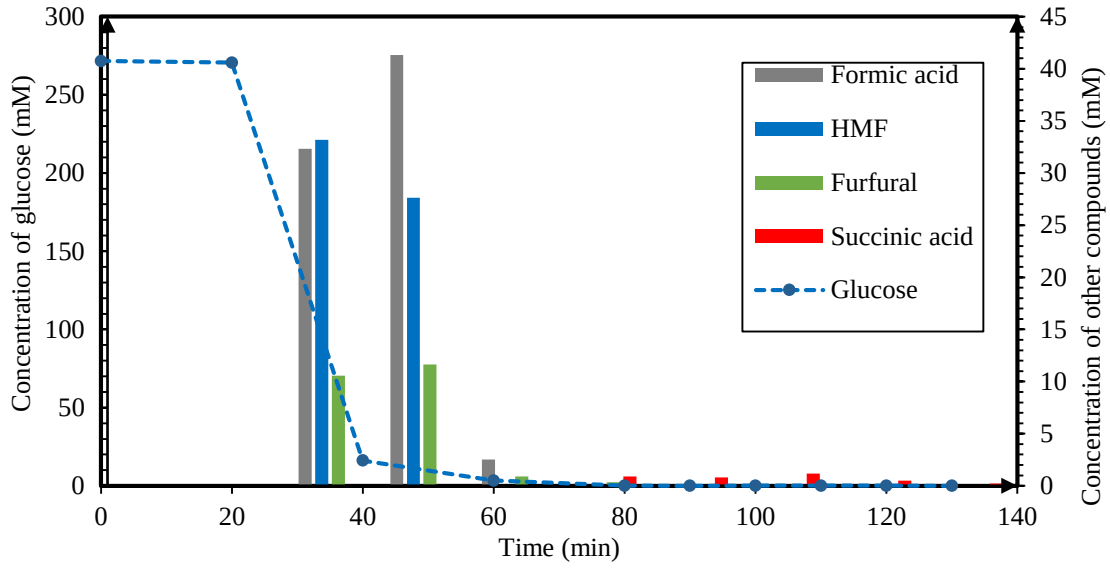

Figure 5.12. Evolution of the concentration of compounds found in the glucose HTL media at 300˚C.

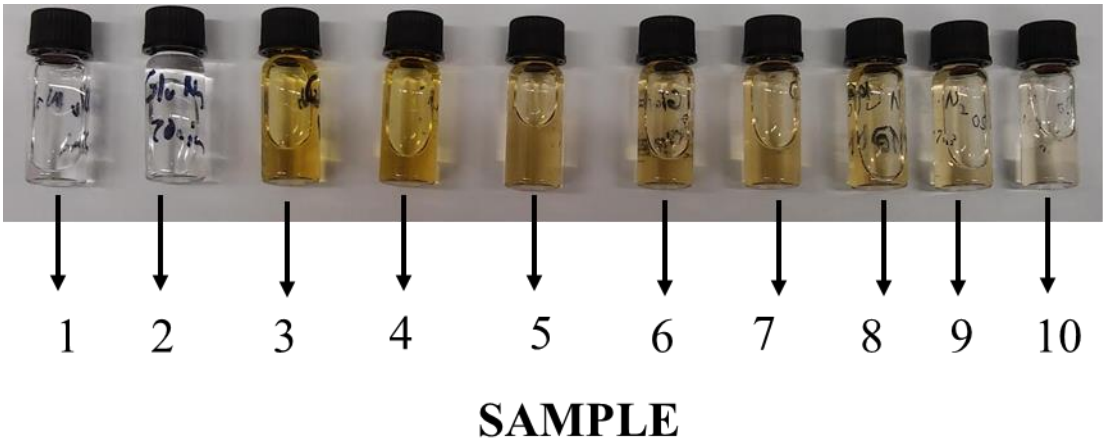

Figure 5.13. Color of HTL media for glucose after reaction at different temperatures and/or time conditions. The conditions for every sample can be found in Table 5.1.

The way the sample collection was designed in the HTL experiment with glucose at 300˚C did not capture the initial stages of glucose degradation. It was shown to occur somewhere between 200 and 270˚C by Figure 5.11. Therefore, the next experiment was designed to collect extra samples in this temperature interval, at 225 and 250˚C, to understand how the glucose starts degrading under HTL conditions. After collecting all the solids (including the solids from samples used to

flush the system between samples collection), the yield to solids was calculated in 12 wt%, referred to glucose initially fed in the reactor.

Figure 5.14 shows the pH evolution of the HTL media, with the same media acidification and final pH value (around 2.5) observed for 300˚C, in Figure 5.10. Figure 5.15 and Figure 5.16 shows respectively the HPLC chromatogram and the concentrations of the samples collected at different conditions, to study the evolution of species obtained from glucose at the reaction at 275˚C. At 225˚C, the first signs of glucose degradation appeared. The glucose concentration decreased around 20%, and new peaks were resolved in the HPLC chromatogram. One of the first degradation reactions is the glucose isomerization to fructose, what is not stable under HTL conditions and steadily degrades to finally disappear from the system at short reaction times. The formation of small concentrations of succinic acid, formic acid, furfural, and HMF occurs under 225˚C. At 250˚C, the concentration of these degradation products increased at the expense of glucose and fructose. Between 250 and 275˚C, the concentration of glucose dropped significantly, fructose disappeared from the system, and the concentration of carboxylic acids and furfural remained constant. On the other hand, HMF concentration decreased. New chromatogram peaks corresponding to unidentified compounds showed up. This indicates the complexity of the composition generated by HTL of glucose, and the difficulty to identify compounds based on the use of HPLC standards. The experiment at 270˚C provided the opportunity to investigate how HTL at lower temperature differed from 300˚C. Glucose, succinic, and formic were never totally depleted from the system in the time range here studied, what constituted a difference from the process at 300˚C. This indicated the degradation kinetics of these compounds is slower at 275 than it is at 300˚C. HMF stills disappears from the system, but at longer reaction time than at 300˚C. Furfural remains in the system in the full time of reaction, but the concentration decreases.

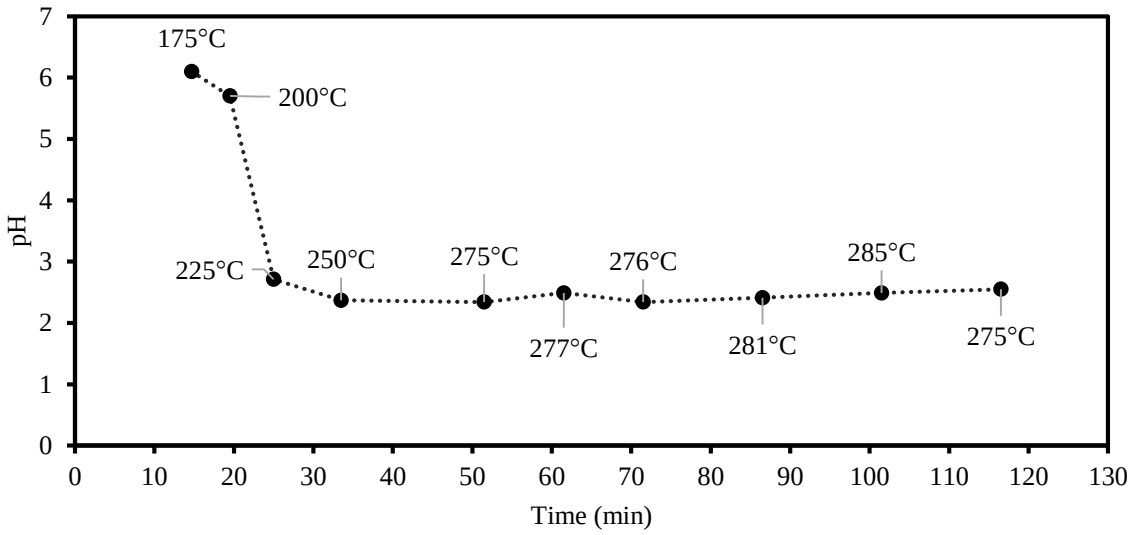

Figure 5.14. pH of the HTL media measured at ambient conditions for glucose after reaction at different temperature and/or time conditions

Sample 1. 14.67 min at 175°C and 451 psig

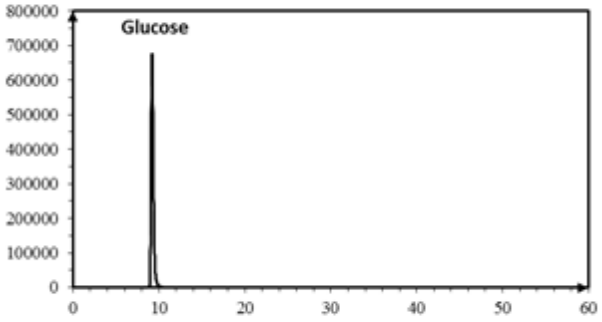

Sample 2. 19.5 min at 200°C and 449 psig

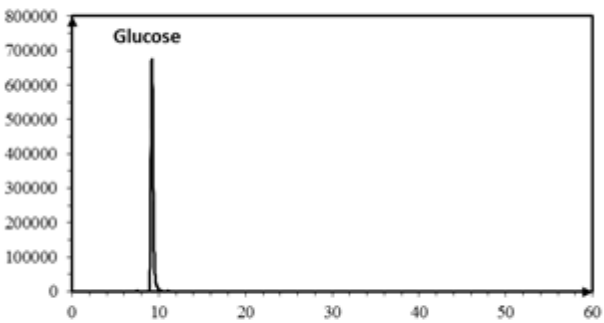

Sample 3. 25 min at 225°C and 492 psig

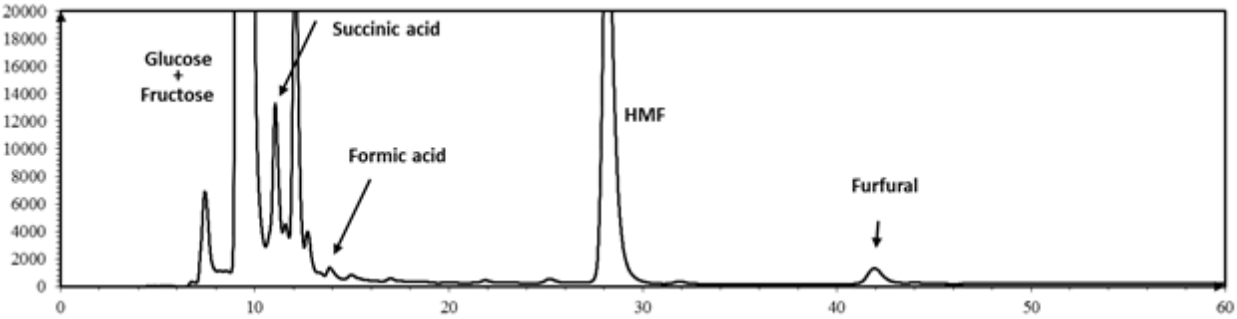

Sample 4. 33.5 min at 250°C and 690 psig

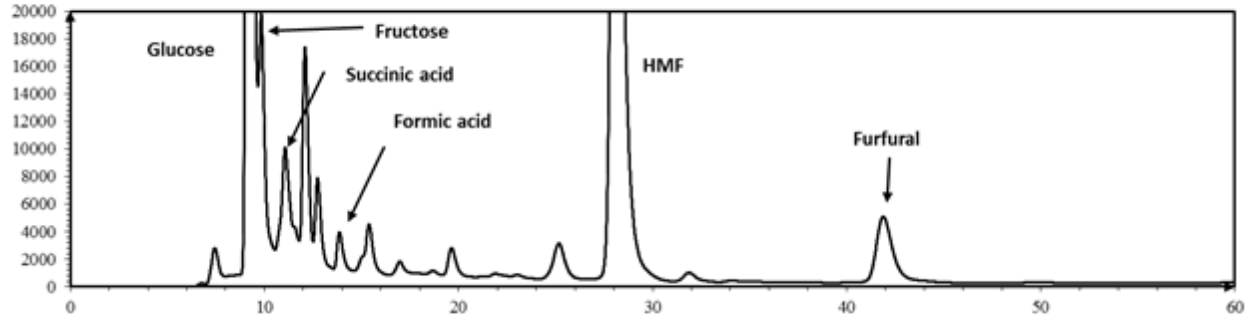

Sample 5. 51.5 min at 275°C and 1242 psig

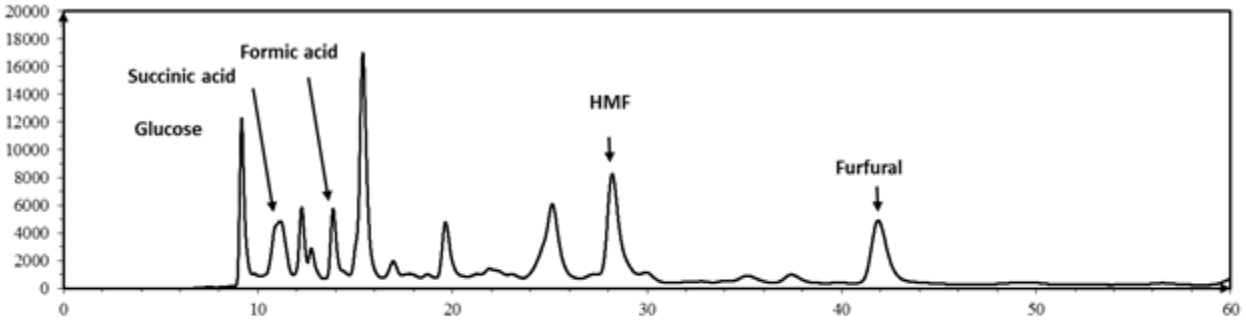

Sample 6. 61.5 min at 277°C and 1198 psig

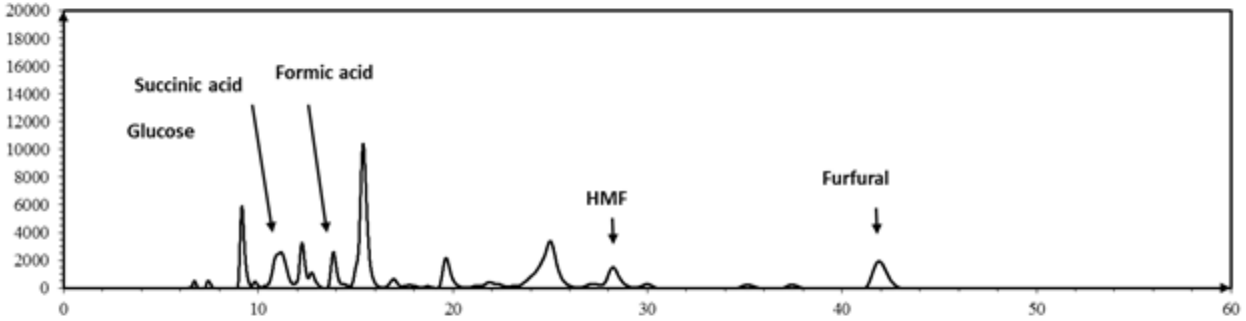

Sample 7. 71.5 min at 276°C and 1159 psig

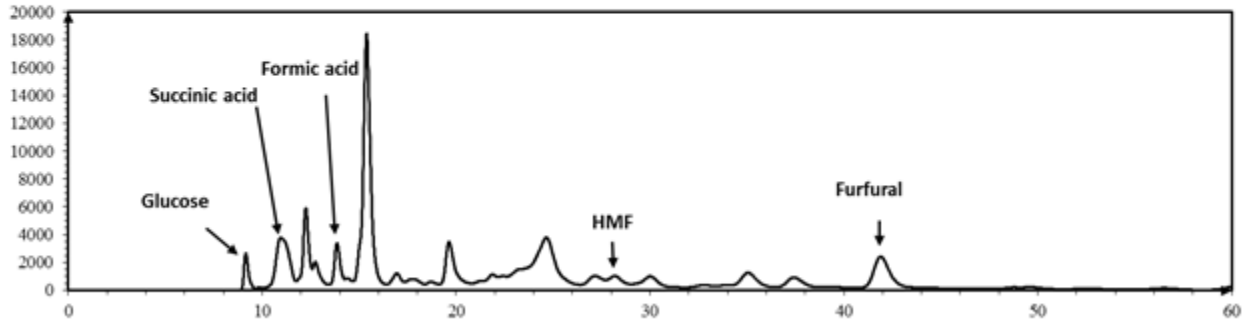

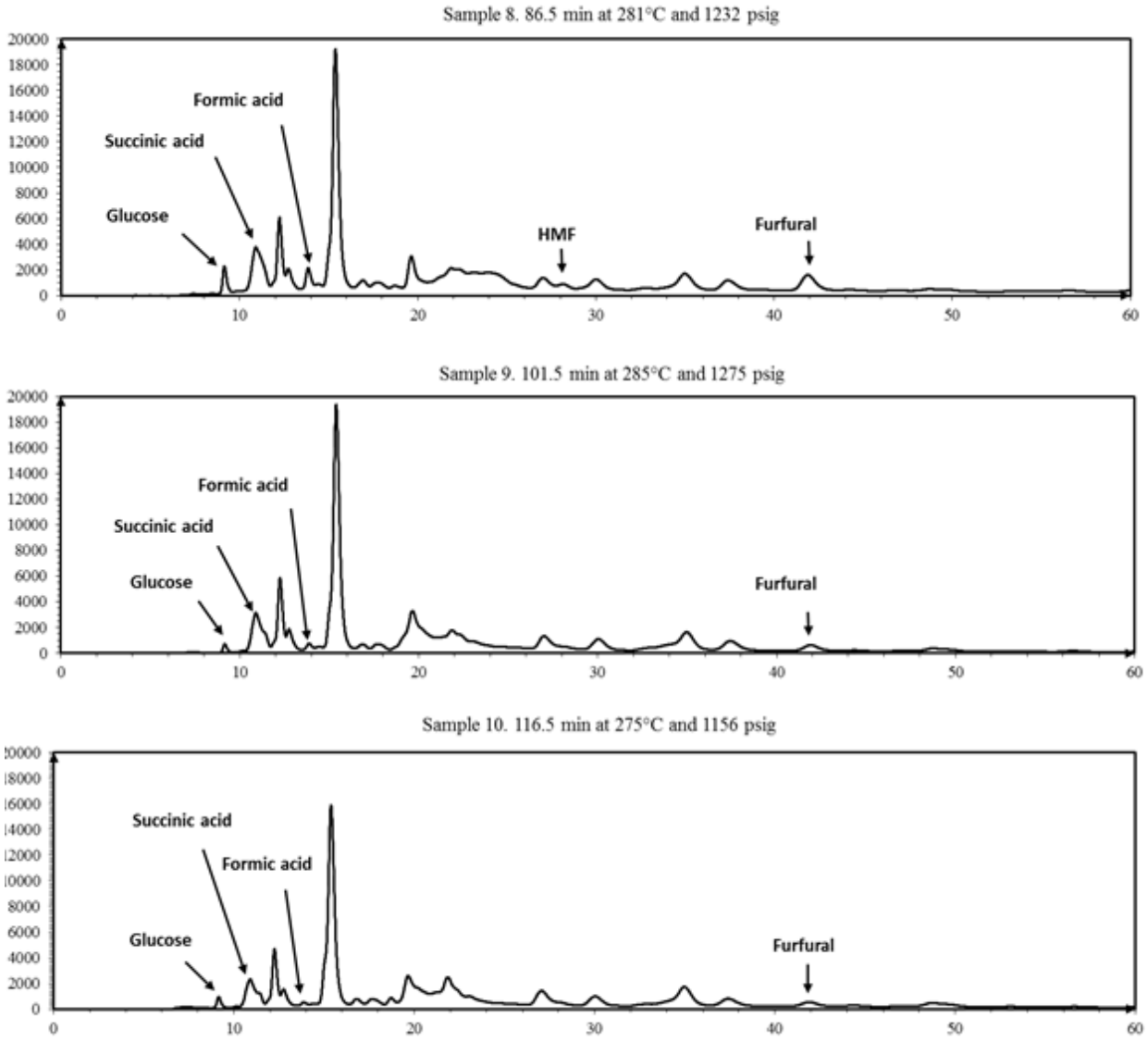

Figure 5.15. HPLC chromatograms of HTL reaction media for glucose after reaction at different temperatures and/or times. The x-axes represents the retention time. The y-axes represent HPLC signal, that can be related to molecule concentration using the factors presented in Table 5.2 from calibration curves. Some peaks were impossible to identify based on the standards used in this project

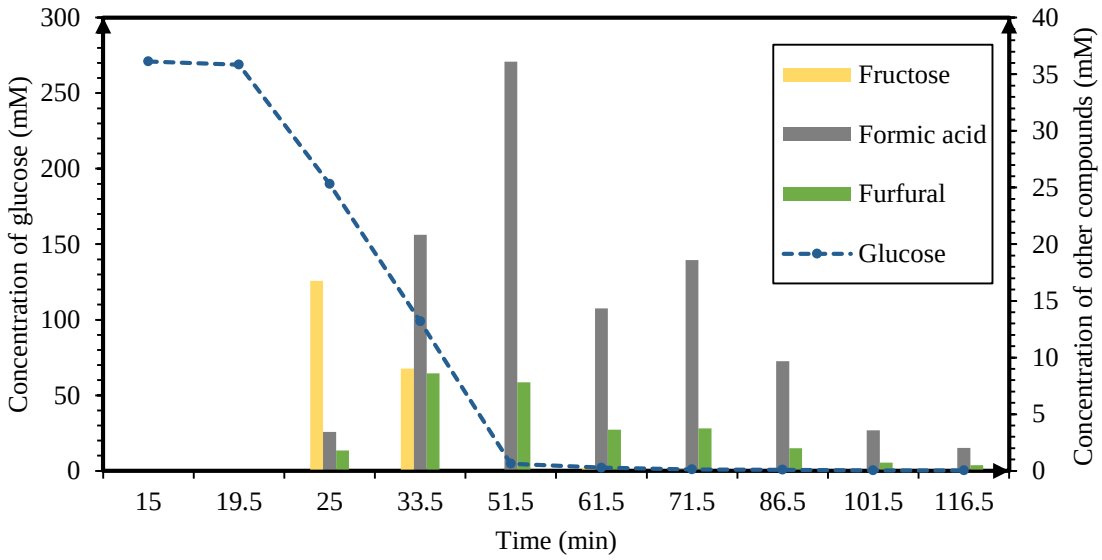

Figure 5.16. Evolution of the concentration of compounds found in the glucose HTL media at 300˚C.

As observed in Figure 5.7, Figure 5.11, and Figure 5.15, the complexity of HTL lays on the dynamism of the system. Original molecules presented in the feedstock degraded towards degradation products, which, at the same time present reaction paths towards other molecules (Peterson et al. 2008). Therefore, apart from HTL kinetic studies with model compounds, it would be interesting to reproduce these studies with products obtained from HTL of model compounds and see their evolution. This study would provide valuable information about the best conditions to recover those products from biomass. Following this logic, it was of interest to study the fate of levulinic acid, as an important degradation product from the HTL of carbohydrates. Levulinic acid has the potential to be used as precursor to a large number of products for the pharmaceutical, food, cosmetics, agrochemical, plastic, and biofuel industries. Derivatization and functionalization can open a lot of possibilities to increase the value and the uses of this acid (Bozell et al. 2000, Lane 2016, Van-der-Hoeven 2015). However, in the HTL reaction experiments of glucose and cellulose it was not possible to unequivocally identify levulinic acid, as its retention time is very similar to the retention time of acetic acid that is

another product of carbohydrate degradation under HTL conditions (15.35 vs. 15.04 minutes respectively as observed in Table 5.2). More work in peak deconvolution is undergoing may be able to identify and calculate the concentration of these two carboxylic acids.

After levulinic acid samples filtration, no solids were formed at any time or temperature under HTL conditions.

Figure 5.17 shows the pH of the HTL media. Starting with a pH of 2.2, HTL process did not change the pH of the levulinic acid solution. The HPLC chromatograms shown in Figure 5.18 for the first and last sample collected from the reactor confirms the stability of levulinic acid under HTL conditions. It does not degrade to any other molecule, as confirmed by the non-extra peaks shown in HPLC, and the constant concentration of levulinic acid throughout the HTL process. Figure 5.19 shows the invariant color of the levulinic acid solutions obtained from the reactor at the conditions shown in Table 5.1. This constituted a main difference compared to the behavior of cellulose and glucose, which samples presented color provided by furfural formation.

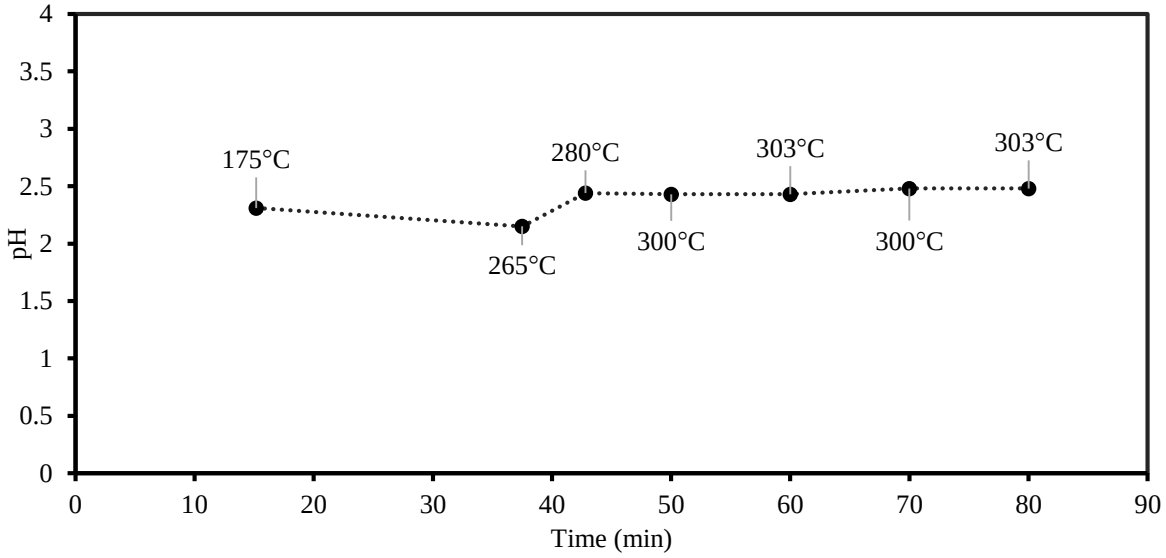

Figure 5.17. pH of the HTL media measured at ambient conditions for levulinic acid after reaction at different temperature and/or time conditions. Initial pH was 2.2

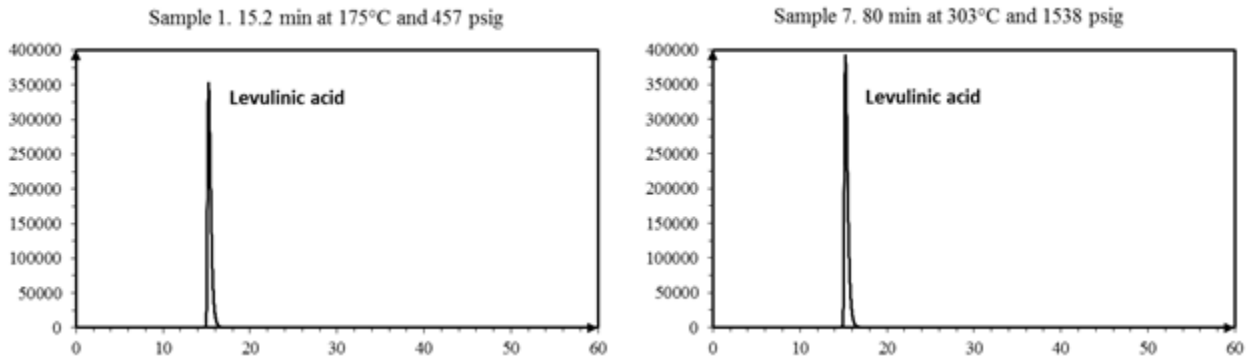

Figure 5.18. HPLC chromatograms of HTL reaction media for levulinic after reaction at different temperatures and/or times. The x-axes represents the retention time. The y-axes represent HPLC signal, that can be related to molecule concentration using the factors presented in Table 5.2 from calibration curves.

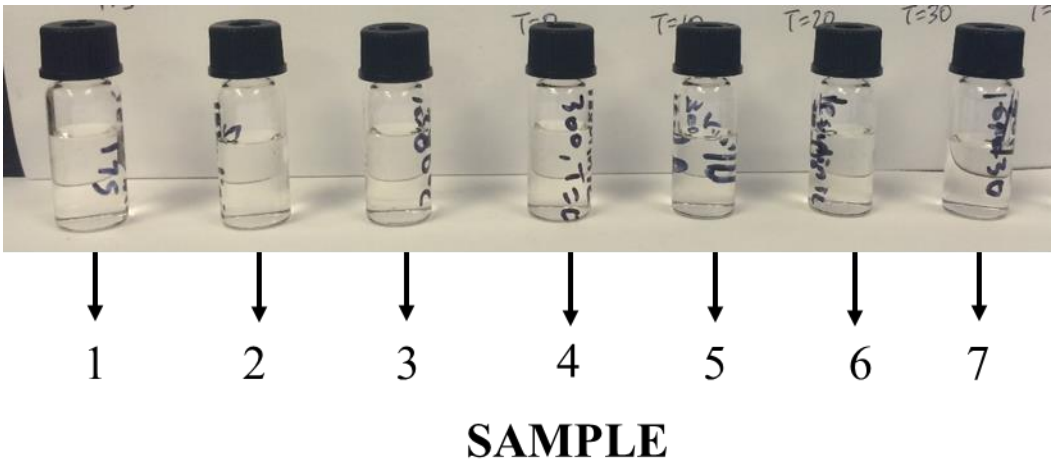

Figure 5.19. Color of HTL media for levulinic acid after reaction at different temperatures and/or time conditions. The conditions for every sample can be found in Table 5.1.

Linoleic acid was used as a model compound for the lipid fraction of biomass. After samples filtration, no solids were formed on the HTL of linoleic acid under the conditions studied.

Figure 5.20 shows the pH for the linoleic acid HTL media. Considering the pH of the initial solution was 5.0, HTL produces an acidification of the media towards a constant value of 4.0.

Figure 5.21 shows the HPLC of the HTL media for the shorter and longer reaction time samples. As a difference with other model compounds, the HTL media from linoleic acid was solvent extracted with dicloromethane, and ethyl acetate. This measure was adopted to separate the aqueous phase form any bio-crude formed in the HTL process, as a way to protect the HPLC column from damage / clogging from bio-crude oil. However, the HPLC chromatogram showed two peaks with independence of the reaction conditions. We suspects (and we confirmed) these two peaks correspond to the solvents used for extraction, that were incorporated in the aqueous phase in enough concentration to mask the detection of any product from the HTL of linoleic acid.

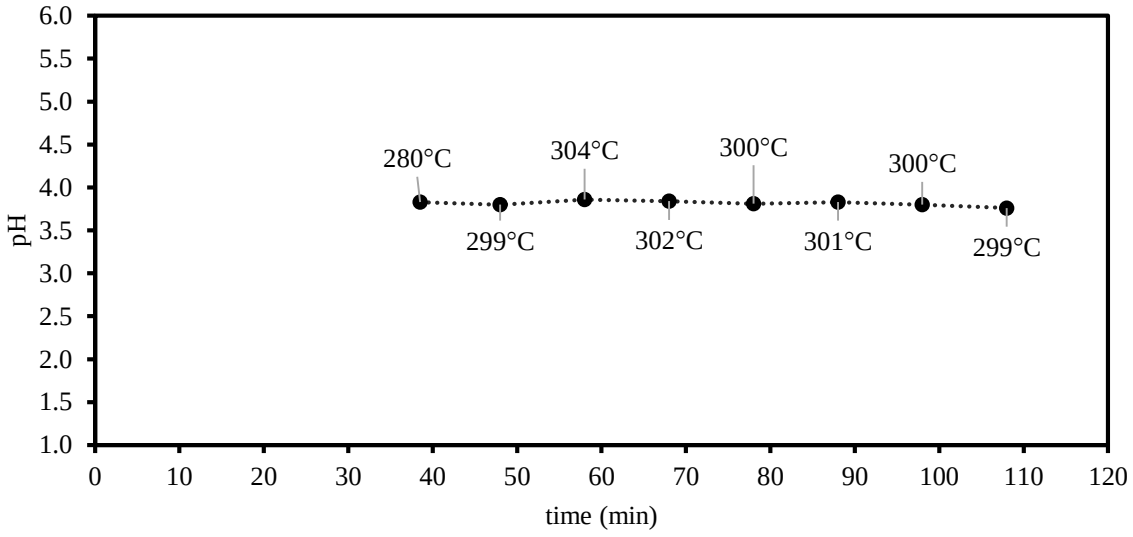

Figure 5.20. pH of the HTL media measured at ambient conditions for linoleic acid after reaction at different temperature and/or time conditions.

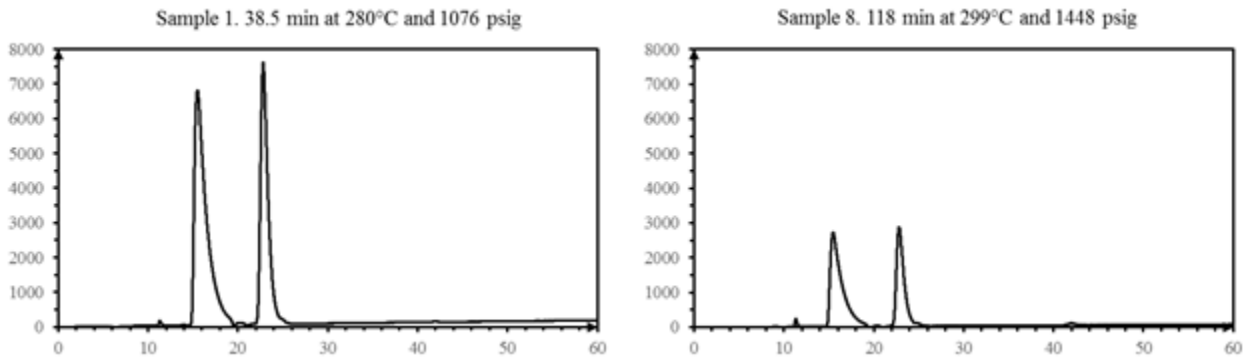

Figure 5.21. HPLC chromatograms of HTL reaction media for linoleic after reaction at different temperatures and/or times. The x-axes represents the retention time. The y-axes represent HPLC signal, that can be related to molecule concentration using the factors presented in Table 5.2 from calibration curves.

The model compound used for proteins was Bovine Serum Albumin (BSA). This protein is typically used as model compound due to its well-known structure (Posmanik et al. 2017). After filtration of the reaction media, no solids were collected for any of the samples. Figure 5.22 shows the HPLC chromatograms of BSA HTL media. The chromatograms are more complex in terms of numbers of peaks than observed for glucose and cellulose, especially at retention times higher than 25 minutes. Because of the amide bonds characteristic of proteins, the presence of nitrogen compounds was expected in the aqueous phase. However, the lack of nitrogen-based standards limited our capabilities for the identification of these nitrogen compounds derived from the amide bonds. Short-chain carboxylic acid were detected (formic acid, succinic acid, and acetic acid). Succinic and acetic acid were found more stable than formic acid under HTL conditions. Figure 5.23 shows the HTL samples after collection. They all share a constant white cloudiness likely produced from protein denaturing at the high pressure and temperature conditions of HTL.

Sample 1. 30 min at 250°C and 975 psig

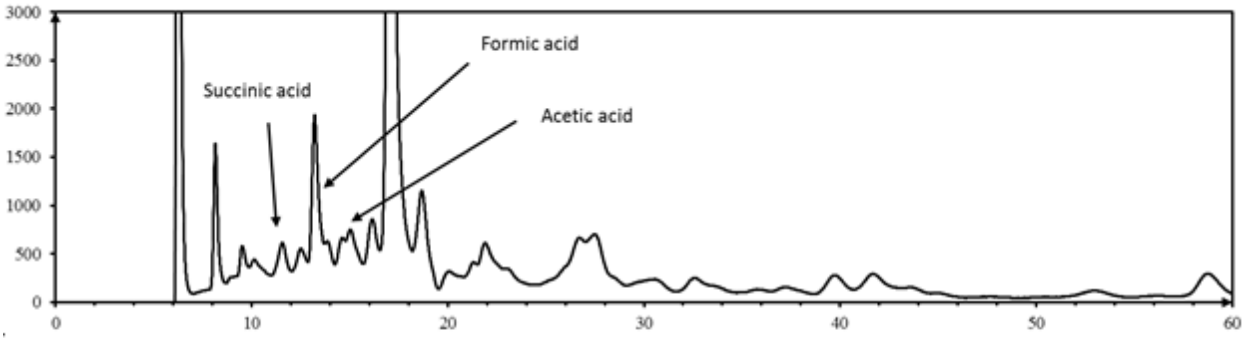

Sample 2. 38 min at 280°C and 1080 psig

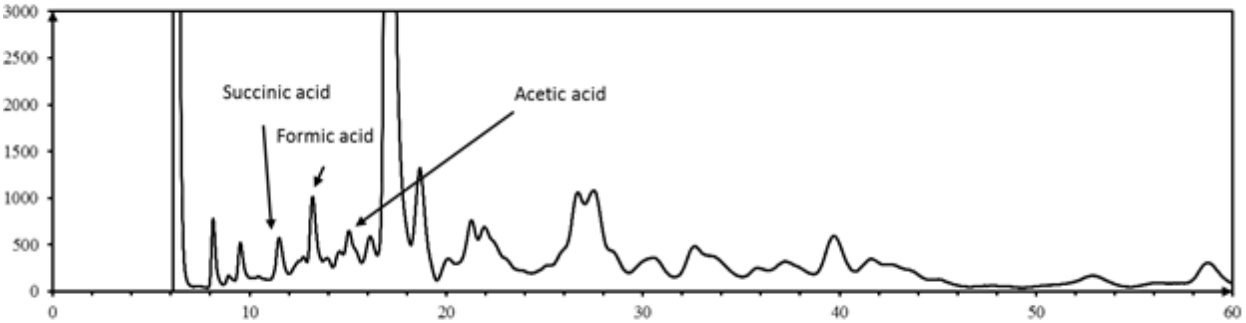

Sample 3. 48 min at 300°C and 1385 psig

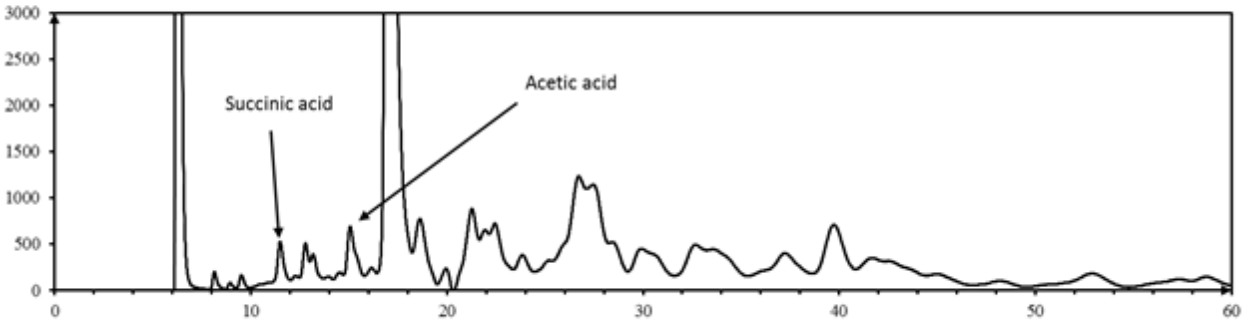

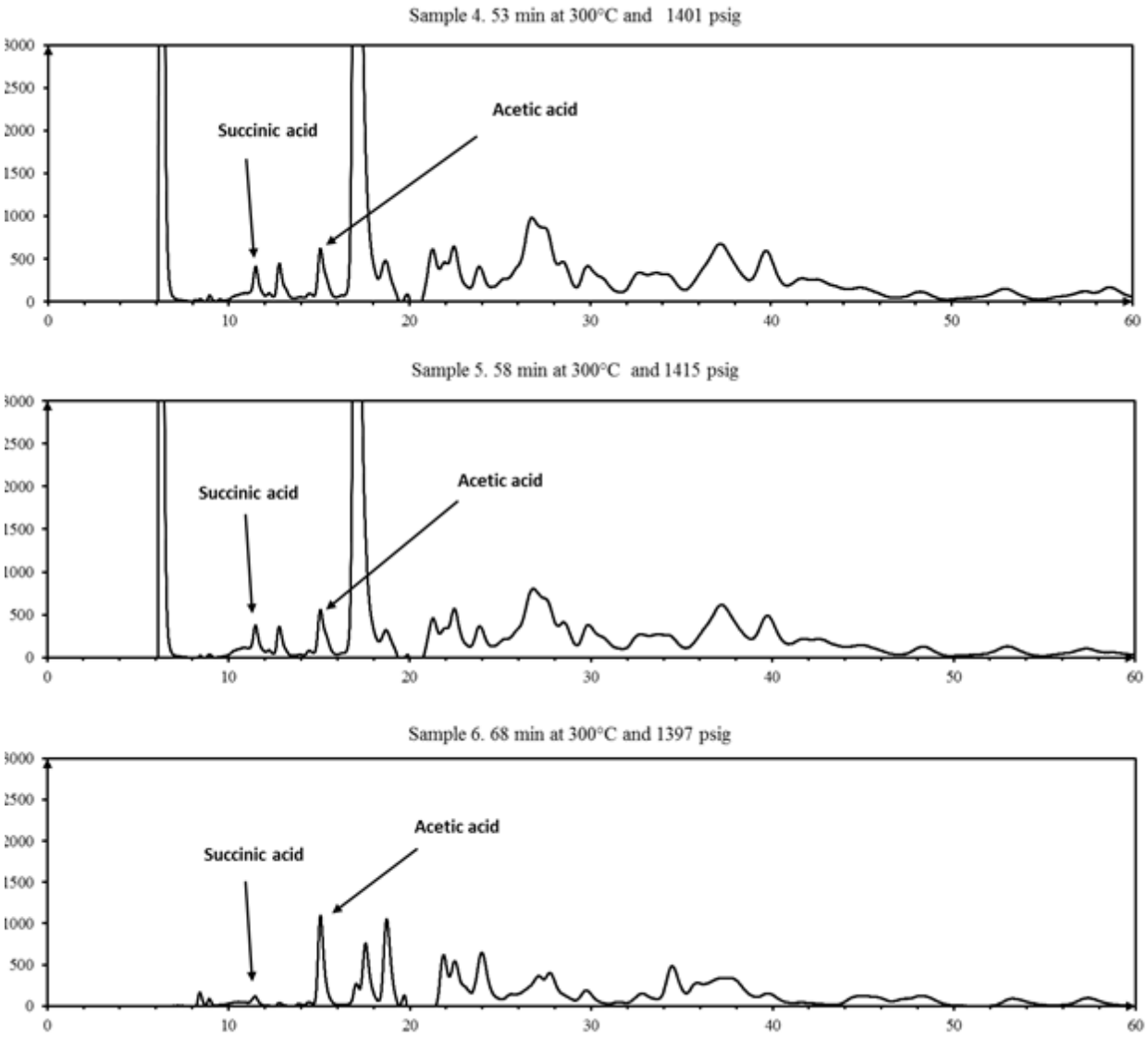

Figure 5.22. HPLC chromatograms of HTL reaction media for BSA after reaction at different temperatures and/or times. The x-axes represents the retention time. The y-axes represent HPLC signal, that can be related to molecule concentration using the factors presented in Table 5.2 from calibration curves. Some peaks were impossible to identify based on the standards used in this project

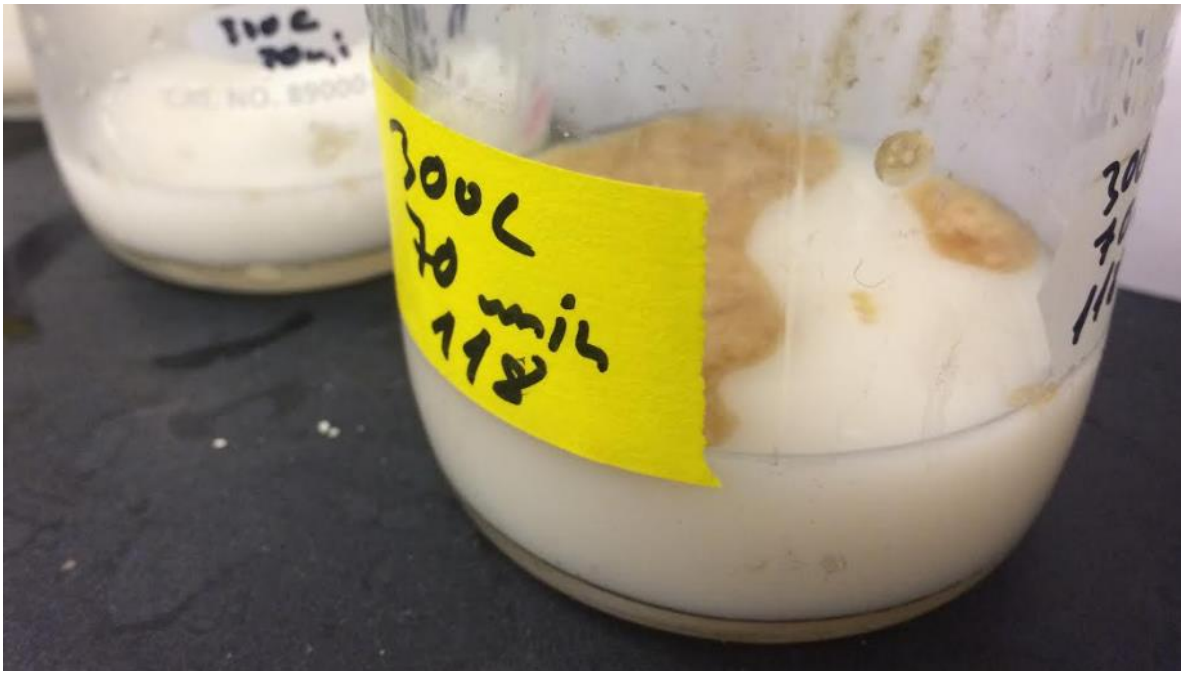

Figure 5.23. HTL reaction media for BSA after reaction at 58 (background) and 68 minutes at 300˚C. Samples 5 (background), and 6 from Table 5.1.

5.6 Conclusions and recommendations

This study investigated the kinetics of model organic waste compounds and degradation products under hydrothermal liquefaction conditions. The work represents an ongoing effort in our group focused on developing kinetic models that capture and reproduce reaction paths and the intermediate products formed in these reactions. This chapter presented a detailed description of the HTL experimental set-up and experimental protocols, followed by a description of the analytical techniques used to analyze samples collected at different conditions of temperature and/or time. HTL process proved a very dynamic set of reactions, with model components found in organic feedstocks degrading to complex mixtures of degradation products. In addition, these degradation products evolve under HTL conditions to form new chemical species, an opportunity to generate a variety of products for potential applications as platform chemicals. These could

include succinic acid and levulinic acid, as well as many others. On the other hand, the complexity of reactions occurring at HTL conditions poses a challenge in terms of quantitative understanding of reaction selectivity, separation, and purification.

The key findings of this chapter are that only glucose and cellulose as carbohydrates model compounds produce solids under HTL conditions. Protein (BSA) and lipid (linoleic acid) model compounds did not produce any solids. Therefore, when performing HTL of organic substrates, we know the origin of the solids produced, and how to tackle the composition of the feedstock in order to decrease the production of the hydro-char. The HTL media gets acidified upon degradation of carbohydrates, with no change in pH observed for linoleic acid as model compound for lipids. This work also provided preliminary insight of the type of products and their concentration obtained from HTL of model compounds. The main products identified in this project were furfural, HMF and carboxylic acids. An important finding was the stability of levulinic acid (a chemical with potential future importance as platform chemical obtained from renewable resources) is stable under the HTL conditions here studied. This observation was confirmed by the constant concentration of levulinic acid through the reaction conditions, and the constant pH value displayed.

A key recommendation is to find ways to overcome the limitations of the analytical techniques used to identify and determine the concentration of degradation products from HTL of model compounds. The main two limitations were the impossibility to correspond many peaks observed in HPLC chromatograms to chemical compounds, and the lack of peak resolution. To overcome the first limitation, we recommend using more standards, especially nitrogen derived standards to be able to identify more compounds in the HPLC chromatogram of model protein. On the other hand, resolving peaks was challenging for certain products with very similar retention times for

the HPX-87H Bio-Rad Aminex column used in HPLC (e.g., lactic acid and glycoaldehyde, levulinic acid and acetic acid as presented in Table 5.2). The detection of sugars and sugar degradation products could be better resolved using a HPX-87H Bio-Rad Aminex column for HPLC, and/or gas chromatography.

While the HTL reaction studies of the model compounds have proven useful for in identifying important trends, the analysis of the results of these studies are preliminary. Ongoing efforts are taking place in our group to develop kinetic models that can help to characterize and predict the complex pathways occurring in HTL processes.

5.7 References

Bio-Rad. 2017. “Description Aminex HPX-87H and HPX-87P Column for HPLC.”

Bozell, J, L Moens, D Elliot, Y Wang, G Neuenscwander, S Fitzpatrick, R Bilski, and J Jarnefeld. 2000. “Production of Levulinic Acid and Use as a Platform Chemical for Derived Products.” *Resources, Conservation and Recycling* 28: 227–39.

Lane, J. 2016. “BiofuelsDigest. Levulinic Acid as a New Platform for Green Chemistry: The Digest’s Multi-Slide Guide to GF Biochemicals.”

Mau, V, J Quance, R Posmanik, and A Gross. 2016. “Phases’ Characteristics of Poultry Litter Hydrothermal Carbonization under a Range of Process Parameters.” *Bioresource Technology* 219: 632–42.

Peterson, A, F Vogel, R Lachance, M Fröling, M Antal, Jr., and J Tester. 2008. “Thermochemical Biofuel Production in Hydrothermal Media: A Review of Sub- and Supercritical Water Technologies.” *Energy & Environmental Science* 1 (1): 32.

Posmanik, R., D.A. Cantero, A. Malkani, D.L. Sills, and J.W. Tester. 2017. “Biomass Conversion to Bio-Oil Using Sub-Critical Water: Study of Model Compounds for Food Processing Waste.” *The Journal of Supercritical Fluids* 119: 26–35.

Teri, G, L Luo, and P Savage. 2014. “Hydrothermal Treatment of Protein, Polysaccharide, and Lipids Alone and in Mixtures.” *Energy & Fuels* 28 (12): 7501–9.

Van-der-Hoeven, D. 2015. “Bio Based Press. Levulinic Acid, the next Green Chemical Building Block.”

Yin, S, R Dolan, M Harris, and Z Tan. 2010. “Subcritical Hydrothermal Liquefaction of Cattle Manure to Bio-Oil: Effects of Conversion Parameters on Bio-Oil Yield and Characterization of Bio-Oil.” *Bioresource Technology* 101 (10): 3657–64.

CHAPTER VI

ACID AND ALKALI CATALYZED HYDROTHERMAL LIQUEFACTION OF DAIRY MANURE AND FOOD WASTE

This chapter was co-authored with Dr. Roy Posmanik, Celia Martinez, Dr. Danilo Cantero, Dr. Deborah Sills, and Professors Maria Jose Cocero and Jefferson Tester. It was adapted from the document that was sent for publication to the journal Green Chemistry (2017).

6.1 Introduction

As global population grows, the consumption of food, water, and energy will also increase and subsequently intensify agricultural production. Sustainable management of animal manure and food waste is a major challenge worldwide. In the U.S., for example, dairy and food industries generate approximately 19 and 36 million tons of waste per year, respectively (NRDC 2012, USDA 2000). The majority of residues, rich in organic carbon and valuable nutrients, are currently disposed in landfills. Recycling these waste streams, however, may lower the use of energy-intensive resources and reduce "end-of pipe" pollution such as greenhouse gases, and soil and water pollutants (UNEP 2010). Waste to energy strategies for manure and food waste are primarily based on biological processes, which convert organic wastes into biogas via anaerobic digestion. Incomplete digestibility of the waste by anaerobic microorganisms limits biogas conversion yields to 40–50% and generates large volumes of a secondary liquid effluent, containing an aqueous mixture of carbohydrates, proteins, lipids, minerals and nutrients (Déniel et al. 2016, Pham et al. 2014). These resources should be further processed to reduce their environmental impact, and maximize their economic value (Monlau et al. 2015). Hydrothermal conversion of biomass using sub- and supercritical water represents a promising solution for waste streams with high water contents.

Hydrothermal liquefaction (HTL) of organic wastes is based on fast hydrolysis reactions, followed by dehydration and decarboxylation of sugars, lipids, proteins, and their degradation products, using subcritical water (Peterson et al. 2008). The HTL process generates four products: bio-crude oil, hydro-char, an aqueous phase, and an exhausted gas stream. The relative amounts of the four products depends on reaction conditions (e.g., time, temperature, working gas, pressure, pH, biomass-to-water ratio), as well as the presence of catalysts (Yin et al. 2010, Toor et al. 2011). The main product, in terms of economic value, resulting from HTL of biomass is bio-crude oil that can be used as a precursor for biofuels (Toor et al. 2011). Therefore, bio-crude is traditionally the phase whose optimization in yield and quality is more extensively researched in literature. HTL can reduce the oxygen content of biomass to approximately 10% by dehydration and decarboxylation reactions (Posmanik et al. 2017). Furthermore, process conditions (reaction time, temperature, pressure) during HTL may be manipulated to adapt to different feed compositions that maximize bio-crude oil yields and minimize its oxygen content. The optimum processing temperature is expected to be between 250 and 350°C, and HTL reactions are usually completed within 20–60 minutes (Posmanik et al. 2017, Theegala and Midgett 2012). As a consequence of the biomass hydrolysis, an aqueous-soluble carbon phase is also produced and should be utilized.

HTL benefits from changes in the physico-chemical behavior of water as reaction conditions approach the critical point (374°C and 22.1MPa) (Peterson et al. 2008). When increasing the temperature up to ~300°C, at pressures above the vapor pressure of water at this temperature (liquid state), water becomes less polar, as its dielectric constant drops, and its ionic product (K_w) increases up to three orders of magnitude (Déniel et al. 2016). The drop in the dielectric constant leads to higher solubility of organic compounds. The higher K_w favors ionic reactions and therefore increases activities of both acid and base catalyzed reactions (Peterson et al. 2008). In fact, water

at around 300°C, i.e., subcritical water, presents the highest value for the ionic product, thus creating a medium with high concentrations of H^+ and OH^-, which favors acid/base catalyzed reactions. In addition, biomass reaction pathways under hydrothermal conditions are affected by the media pH (Yin and Tan 2012). For example, under acidic conditions, glucose is converted primarily to 5-hydroxymethylfurfural (HMF), whereas under alkaline conditions glucose degradation shifts to produce short-chain carboxylic acids. Since HMF is an important building block for the production of dimethylfuran (DMF) as well as other biofuel precursors (Rosatella et al. 2011), its production in subcritical water may positively affect the HTL process and increase biomass conversion into bio-crude oil (Jin and Enomoto 2011).

The majority of the current literature, focused on model compounds, illustrates the important role of pH in the formation of HTL bio-crude oil. However, complex biomasses such as manure and food waste may complicate the process due to cross-interactions between carbohydrates, proteins, and lipids as well as with their degradation products (Posmanik et al. 2017). Low carbon oil yields in HTL systems usually result in high fractions of organic carbon in the aqueous product (Posmanik et al. 2017). Consequently, the objective of the current study was to elucidate the role of acidity and alkalinity of the hydrothermal media on bio-crude oil production from manure and food waste.

6.2 Materials and methods

6.2.1 Materials

The feedstocks used for this study were digested cattle manure and food waste. Digested cattle manure was received from an anaerobic digester located on a dairy farm (Sunnyside farm, Scipio Center, NY). Carbohydrate rich food waste was sorted from Cornell University dining halls (Ithaca, NY) and its composition was characterized in the lab (fruits 15.4 wt. %, vegetables, 47.1 wt. %, grains/breads 37.5 wt. %). Manure and food waste had average solids contents of 8 and 10 wt. %, respectively. Milli-Q water was used as reaction medium for all experiments. Phosphoric acid (H_3PO_4) and sodium hydroxide (NaOH) were selected as acid and base additive, respectively, to manipulate the HTL media pH. For HTL bio-crude and aqueous phase separation (liquid-liquid), dichloromethane (DCM), ethyl acetate (EA), and acetone were used as solvents. For HPLC analysis, the following standards were used: glucose, fructose, arabinose, xylose, succinic acid, glycolaldehyde, lactic acid, formic acid, acetic acid, and HMF. All chemicals (≥99% purity) were purchased from Sigma Aldrich.

6.2.2 Methods

6.2.2.1 Experimental procedure

The HTL batch reactor used in this study was described in detail in a previous study (Posmanik et al. 2017) and it is shown in Figure 6.1. Briefly, a 500 mL stainless steel vessel (Model 4575 Parr Instruments Co.) was loaded with 200 mL of feedstock solution. The initial solids concentrations loaded to the reactor for all experiments were 4 wt. % for manure and 5 wt. % for food waste.

Once the biomass was loaded, the reactor was closed and the oxygen in the head-space was purged with nitrogen (N_2) and pre-pressurized up to a pressure of 2.5 MPa. For the experiments adding the acid and alkaline additives, a high-pressure pump (Varian, PrepStar, SD1 system, Agilent Technologies) was used to inject them in the reactor. 15 mL of 5M H_3PO_4 and 25 mL of 1M NaOH were added for acidic and alkaline runs, respectively. The contents of the reactor were stirred (100 rpm) during the reaction using a magnetic agitator. Then, the temperature was set to 300°C and the reaction time for all runs was set to 60 minutes. The reaction time started when temperature inside the reactor reached 80°C and ended when the product was collected. The reaction temperature profile is shown in Figure 6.2. The first step was the heating ramp from 80 to 300°C, which took approximately 20 minutes. Then, the reactor temperature was maintained at 300°C for additional 40 minutes. Finally, sample collection lasted additional 3–5 minutes. The experiments were run in triplicate.

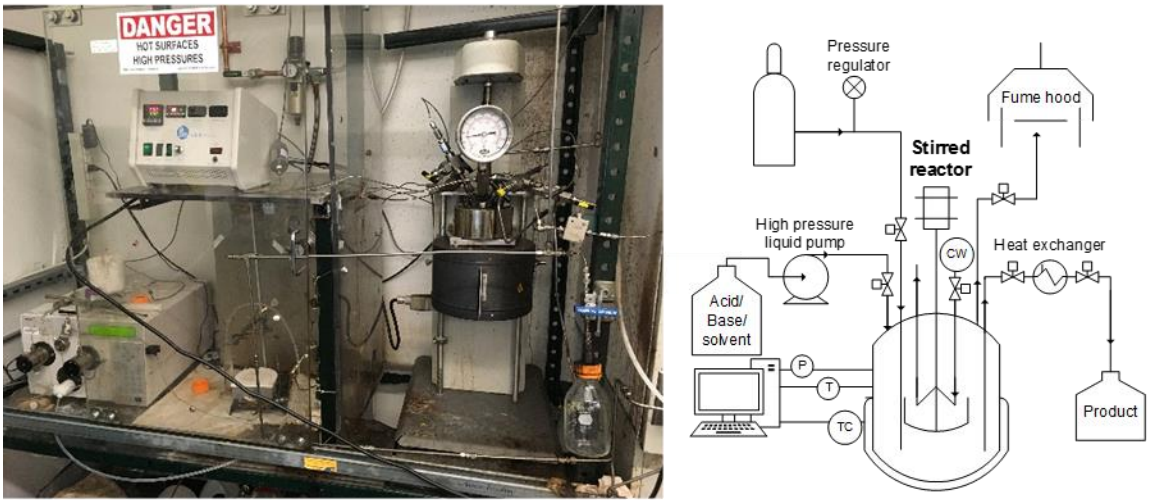

Figure 6.1. Experimental setup for the hydrothermal liquefaction experiments. P, pressure reading; T, temperature reading; TC, temperature control; CW, cooling water.

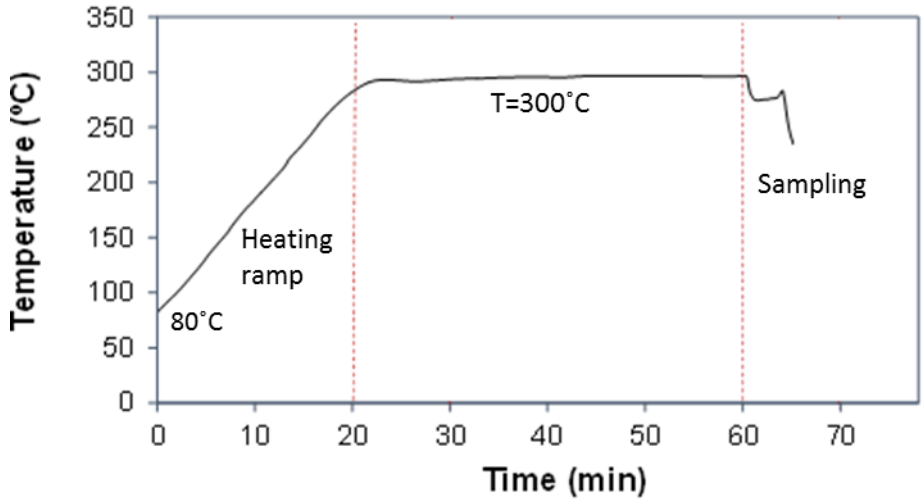

Figure 6.2. Temperature profile of a representative HTL experiment.

6.2.2.2 Sample collection and phase separation

After reaction was completed, the reactor content was collected through a heat exchanger connected to the reactor's outlet to rapidly quench the liquid effluent. This fraction was called the product sample. To recover remaining product, the reactor was washed with 100 mL acetone, followed by 100 mL deionized water. As a result of the washing procedure, a wash sample was collected for further separation. After collecting all samples, the heater was turned off and the cooling loop at the reactor was opened. After completely cooling of the reactor, the remaining solids inside the reactor were collected and added to the wash sample.

Phase separation was conducted following the procedure reported previously (Posmanik et al. 2017) and is described in Figure 6.3**.** First, collected samples were vacuum filtered to separate all solids. Solids were washed with acetone to recover the adsorbed oil, what is named as oil 1 in Figure 6.3. The remaining solids were dried overnight at 105ºC and the dried fraction was labelled as hydro-char. Then, the oil and aqueous phase presented in the liquid sample were separated using solvents of different polarities, in order to quantify and analyze them. Sample aliquots of 20 mL

were mixed in a separating funnel with 20 mL DCM and 20 mL deionized water. The bottom phase containing the heavy oil was collected and labelled as oil 2. Then, to recover the light oil phase, 20 mL of EA were added to the funnel. The bottom phase was removed and labelled as aqueous phase and the top phase was collected and named as oil 3. The same procedure was followed for the wash sample separation, obtaining oil 4 and oil 5 samples for DCM and EA fractions, respectively. Each of the oil fractions were dried, and the mass determined by weight difference with pre-weighted empty vials. These oils were kept for further analyses.

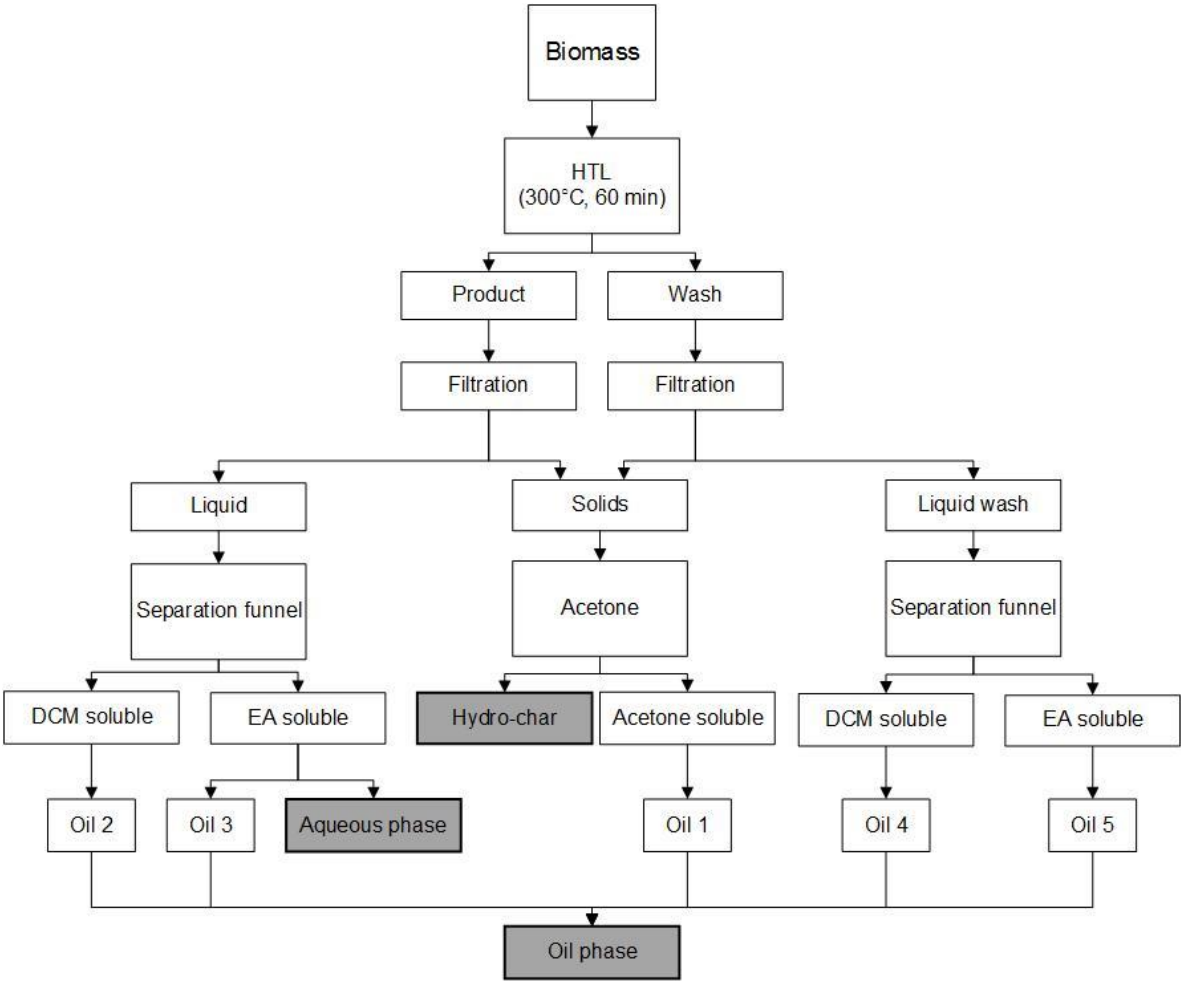

Figure 6.3. Product recovery and phase separation procedure used to collect bio-crude oil, aqueous product, and hydro-char samples.

6.2.2.3 Analysis

The C, H, and N content (wt.%) of dried feedstocks, hydro-char, and bio-crude oil were measured using a CE440 elemental analyzer (Exeter Analytical, North Chelmsford, MA). The ash content of feedstocks and hydro-char was determined following 4 hours at 550°C (ASTM 2003). The oxygen content was not provided directly from elemental analysis, but calculated as the difference between the wt. % of residual (difference to 100% of the sum percentage of C, H, and N) and the wt. % of ash (Yin et al. 2010). We assumed the sulfur concentration was negligible (Vardon et al. 2011). Based on the elemental composition, the higher heating value of each feedstock and bio-crude oil products was calculated using the Dulong's formula (Akalin et al. 2012) (Eq. 1).

$$HHV = 0.338 \times C + 1.428\ (H - \frac{O}{8}) \qquad (1)$$

Where HHV is the higher heating value (MJ/kg), and C, H, and O are the wt. % of carbon, hydrogen, and oxygen in the dried sample, respectively.

The carbon in the aqueous product was analyzed by total organic carbon analysis (TOC) using a TOC-Vcph analyzer (Shimadzu Corporation, Kyoto, Japan). Consequently, the carbon distribution among all three HTL phases (oil, aqueous, and hydro-char) was calculated. Carbon recovery was defined as the total amount of carbon in each phase relative to the carbon in the feedstock and was calculated with Eq. (2).

$$CR_i = \frac{M_i \times C_i}{M_{feed} \times C_{feed}} \qquad (2)$$

where *CR* is carbon recovery (wt. %); '*i*' is the phase (oil, aqueous or hydro-char); 'M_i' is the mass (g) of product '*i*'; 'C_i' is the carbon concentration (wt. %) in product '*i*'; 'M_{feed}' is the mass (g) of feedstock; and 'C_{feed}' is the carbon concentration (wt. %) of the feedstock.

The composition of the HTL aqueous samples were characterized using high performance liquid chromatography (HPLC) to determine monosaccharides and carboxylic acids content. A Shimadzu HPLC equipped with an Aminex HPX-87H column and UV and refractive index detectors was used. The mobile phase used was 5mM sulfuric acid with a flow of 0.6 mL/min, and the column was held at 65ºC. The volume of sample injected was 20 µL and the run time was 40 minutes. A change index (CI), was calculated for each compound detected in HPLC and identified with the standards used, to evaluate the effect of acid or base additives on the aqueous product composition (monosaccharides and carboxylic acids) (Eq. 3). The CI compares the compositions of the aqueous products that were generated with and without acid or base. A positive or negative CI_i means that the aqueous phase from the acid/base modified reaction had a higher or lower amount of product (*i*) compared to the aqueous phase from the non-modified reaction, respectively. A CI_i value equal to zero indicates that the acid/base had no effect on the production of the specific compound.

$$CI_i = \frac{C_{i,\,modified} - C_{i,\,non-modified}}{C_{i,\,non-modified}} \qquad (3)$$

Where '*CI*' is change index; '*i*' is the specific product; '$C_{i,\,modified}$' is concentration of '*i*' in the product from an acid or base modified HTL reaction; and '$C_{i,\,non\text{-}modified}$' is concentration of product '*i*' following a HTL reaction without additive.

The bio-crude oil chemical composition was analyzed using gas chromatography couple with mass spectroscopy (GC-MS). The system consisted on an Agilent 7890A gas chromatograph with an Agilent 19091S-433 column (30 m x 250 µm x 0.25 µm) using Helium was carrier gas and Agilent 5975C VL MSD mass selective detector (Agilent Inc, Palo Alto, CA). Bio-crude oil samples were dissolved in DCM, injected with a split ratio 10:1 into an injection port at 310°C. The temperature program consisted of a 4 min at 50°C, followed by a heating ramp to 110°C at 2°C/ min, hold at

110°C for 3 min, and heating up to 300°C at 2°C/ min with a final hold at 300°C for additional 3 min. A mass spectral library was used to identify the separated compounds.

The hydro-char fraction was analyzed using Fourier transform infrared spectroscopy (FTIR). This analysis was used to determine the specific chemical functionalities presented in hydro-char obtained from each feedstock at each reaction conditions. FTIR spectra were collected between 7000 and 400 cm^{-1} wavenumbers using a Bruker Vertex 70 FTIR spectrometer (Bruker Optics, Ettlingen, Germany) in transmission mode using an attenuated total reflectance (ATR) sampling accessory (MIRacle) equipped with a ZnSe crystal (PIKE Technologies, Madison, WI). Prior to FTIR measurement dried hydro-char samples were grounded with a mortar and pestle. Triplicates of every sample were collected to assure reproducibility of the results. Spectra were transformed to absorption mode, ATR corrected, cut above 4000 cm^{-1} and below 620 cm^{-1} (to avoid spectral regions with high absorption from ATR crystal), baseline corrected, and vector normalized using the OPUS software package. For a comprehensive comparison of functional groups among hydro-char generated under different HTL conditions, the FTIR spectra were analyzed using principal component analysis (PCA). The PCA was performed in a region of the spectra that includes the fingerprint region (1800–620 cm^{-1}) (Sills and Gossett 2012), using software package Rstudio (RStudio, Inc., Boston, MA). Additional details about the FTIR–PCA analysis are described elsewhere (Cantero-Tubilla et al. n.d.).

6.3 Results and discussion

6.3.1 Conversion yields

Acid and alkaline additives affected the carbon yields of the oil, aqueous, and solid fractions produced by HTL (Figure 6.4). The effect of acid and base additives on the HTL reaction was more significant for manure (Figure 6.4a) than for food waste (Figure 6.4b). For manure, the bio-crude oil yield with the addition of acid was 52±3 wt. % (carbon basis), 46% higher than the yield without acid. However, when using the alkaline additive, the bio-crude oil carbon yield from manure was 42±2 wt. %, only 19% higher than the yield without the additive. Other studies studying the conversion of cattle manure in sub-critical water, suggested similar bio-crude oil yields at 260–340°C (Yin et al. 2010, Xiu et al. 2010). For temperatures below 250°C, hydro-char was reported as the main product from the hydrothermal conversion of manure (Mau et al. 2016). In this study, the use of acid/base additives decreased the production of hydro-char from manure at 300°C (Figure 6.4a). Hydro-char yields from manure were 18±2 and 20±1 wt. % (carbon basis) under acidic and alkali conditions, respectively. This translates into a decrease in carbon content on hydro-char of 32% and 18% compared to the yields without additives, respectively. The aqueous product carbon yield from manure was 19±3 wt. % when the hydrothermal conversion was under acidic conditions, and thus similar to the yields with no acid additive (Figure 6.4a). On the other hand, the addition of base, increased the aqueous product carbon yield to 29±5 wt. %. This aqueous product has opportunities for added value uses, as it can be used for different applications such as direct fertilization (Mau et al. 2016) or further gasification via anaerobic digestion or catalytic hydrothermal gasification (Elliott et al. 2015).

Distribution of carbon among the different fractions obtained from HTL of food waste showed a different trend compared to manure. The carbon yield towards bio-crude oil was 37±5 wt. % with the addition of acid, very similar to the yields without acid additive (Figure 6.4b). The use of the base additive resulted in slightly lower bio-crude oil carbon yield (33±3 wt. %). Hydro-char carbon yield from food waste with no acid/base addition was 11±2 wt. %, considerably lower than carbon yields towards hydro-char found in HTL of manure. Interestingly, the addition of acid to food waste increased the hydro-char carbon yield to 17±1 wt. % while the addition of base decreases the yield to 3±1 wt. %. The aqueous phase was the dominant product for food waste, with carbon yields of 36±5 wt. %, 34±2 wt. % and 41±3 wt. % for the HTL with acid additive, base additive and no additive, respectively (Figure 6.4b).

The large differences in carbon yields towards HTL phases between food waste and manure are mainly based on the chemical compositions and structures of these feedstocks. Food waste usually contains a large variety of compounds, such as fibers, sugars, proteins, and lipids (Déniel et al. 2016). The food waste that was used in this study is carbohydrate rich containing mostly fruit and vegetables waste, as well as breads and grains. Therefore, fruit and vegetable sourced fibers (i.e., cellulose, hemicellulose, and lignin) were a dominant component in this feedstock. Unlike manure, food waste is naturally an acidic feedstock, thus the reaction media without additive presented a pH of 4.0 ± 0.1 (measured after reaction at ambient conditions), due to the sugar degradation to short carboxylic acids (Posmanik et al. 2017). This explains the small differences in bio-crude oil yields with or without the addition of acid to the media (Figure 6.4b). Manure, on the other hand, is an alkaline feedstock, and therefore, the reaction media without additive presented a high pH of 9.1 ± 0.3 (measured after reaction at ambient conditions). Hence, he addition of acid had a notable effect on bio-crude oil yield (Figure 6.4a). Figure 6.4 also shows that for all treatments, except for

alkaline food waste, 81–92% of the carbon in the feedstock was recovered in the bio-crude oil, aqueous, and hydro-char phases, suggesting that the amount of gasified material in the studied system was lower than 20% in the worst case.

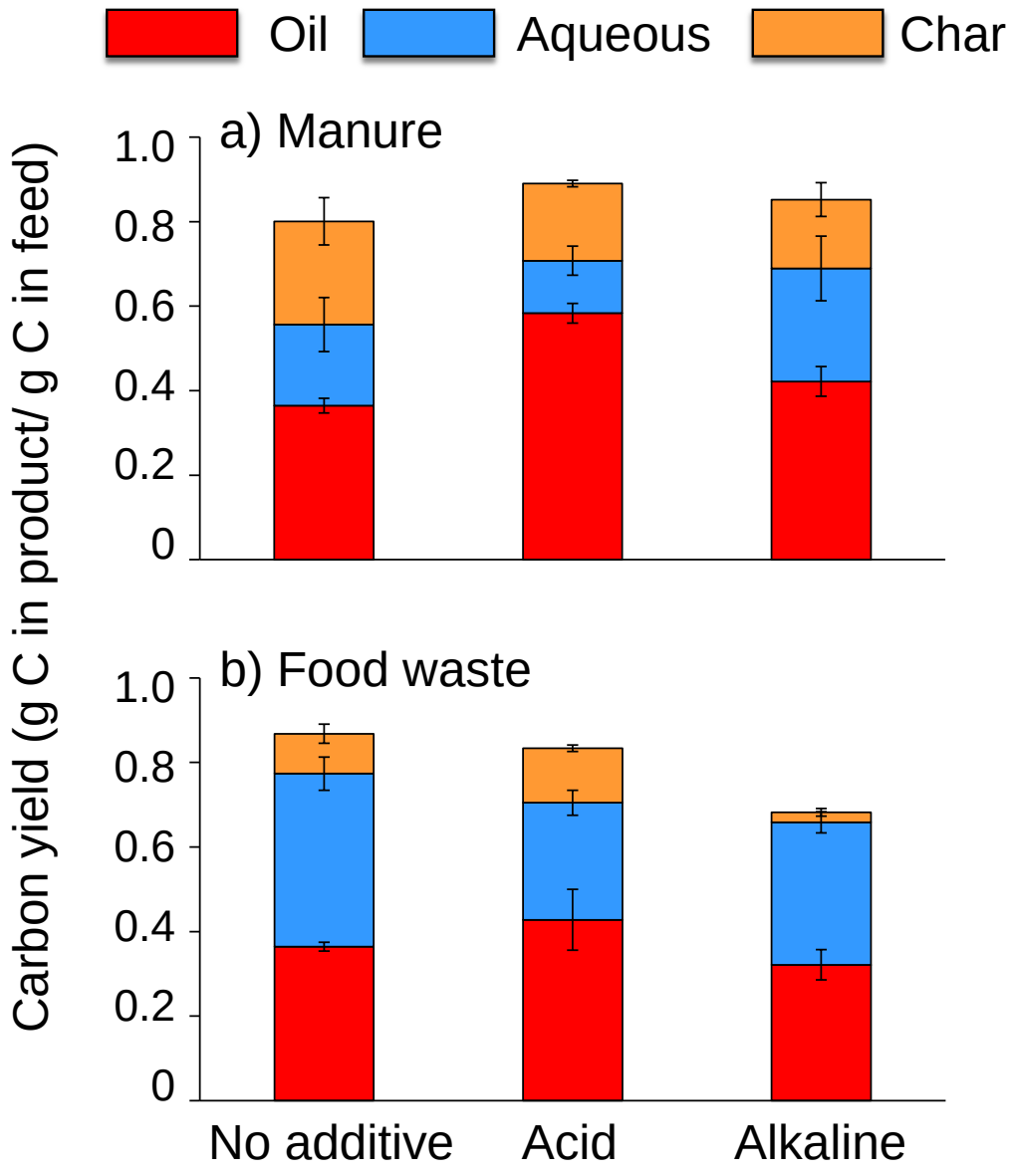

Figure 6.4. Distribution of the carbon (g in product/ g in feedstock) among the main three products (oil, aqueous and char) from the hydrothermal liquefaction of manure (a) and food waste (b) at the three different HTL conditions (no additive, acid, and alkaline).

6.3.2 Bio-crude oil composition

As primary product of HTL, bio-crude oil is richer in carbon and hydrogen than the initial feedstocks, while the oxygen content decreased. Dairy manure, a feedstock with 36 wt. % carbon and 24 wt. % oxygen (Table 6.1), was valorized via HTL, by producing a bio-crude oil with double carbon content and oxygen content lower by more than 40%. This change in elemental composition had a positive effect in the energy density of the bio-crude, as the HHV of the bio-crude oil was 140% higher than for the raw feedstock. Food waste had a higher carbon and oxygen content than manure. Interestingly, the elemental characteristics of bio-crude oil obtained from food waste were comparable to manure (Table 6.1). In other words, the elemental composition of the produced bio-crude oil demonstrates that HTL valorizes food waste to a lesser extent than for manure. In terms of energy density, HTL generate a bio-crude oil product with HHV of 32–36 MJ/kg from both feedstocks. These values are similar to HHVs of bio-crude oil obtained from HTL of woody biomass (Toor et al. 2011), algae (Gerber Van Doren et al. 2017) and anaerobic sludge (Vardon et al. 2011).

The removal of oxygen in HTL is a main goal of the valorization process. It occurs by decarboxylation, which removes oxygen in the form of carbon dioxide and by dehydration, which removes oxygen in the form of water (Peterson et al. 2008). The relative importance of these mechanisms in the HTL process can be demonstrated by the atomic oxygen to carbon ratio (O/C, associated with decarboxylation reactions) and the atomic hydrogen to carbon ratio (H/C, associated with dehydration reactions). For both manure and food waste, the atomic oxygen to carbon ratio was reduced from 0.6 to 0.1–0.2 after HTL (Table 6.1). The hydrogen content was increased from 3.9 wt. % in manure and 7.0 wt. % in food waste to 8.0 and 8.9 wt. % in the bio-crude oil from manure and food waste respectively.

The H/C ratio for manure feedstock does not get modified by HTL towards bio-crude. On the other hand, food waste bio-crude oil presents a slightly lower H/C ration than the feedstock. These values of atomic ratios suggested that the main mechanism for oxygen removal in HTL towards bio-crude oil for manure was decarboxylation, while both decarboxylation and dehydration contributed to the removal of oxygen from food waste. The fact that the O/C decreased with less reductions in the H/C is an advantage from the point of view of the oil quality and its downstream upgrading to drop-in fuel.

The addition of acid or base to the hydrothermal media may play a role on the relative importance of both decarboxylation and dehydration reactions, that can be accelerated or suppressed (Peterson et al. 2008). For manure, decarboxylation was enhanced by either acid or base addition, as the bio-crude oil had a lower O/C than the ratio in bio-crude oil produced from non-modified HTL, with no change in H/C ratio. On the other hand, food waste behaved differently, with lower O/C for the base-modified bio-crude oil (compared to the acid-modified). In addition, dehydration reactions for food waste were probably suppressed by the alkaline additive, as H/C ratio is higher than for acid additive and non-additive reactions. Higher H/C ratio suggests lower removal in the form of H_2O. Another important feature of the composition of bio-crude oil is its nitrogen content. HTL process concentrates nitrogen in the bio-crude oil phase for all the conditions studied. However, thanks to the higher rate of carbon concentration, the atomic N/C ratio was reduced to below 0.04, similar to values reported by others (Chen et al. 2014). Interestingly, for both feedstocks, alkaline conditions resulted in lower nitrogen content in the bio-crude oil (Table 6.1). A possible explanation of this pattern may be a volatilization of NH_3. However, the exhaust gas composition was beyond the scope of this study.

Table 6.1. Elemental composition of the feedstocks and bio-crude oil. Carbon, nitrogen, hydrogen, and oxygen contents are given as percentage on a dry weight basis, H/C and O/C are the atomic ratios of elements and higher heating values (HHV) are given as MJ/kg. All values represent mean values of three replicate experiments ± standard errors.

	Manure				**Food waste**			
	Feedstock	***No additive***	***Acid***	***Alkaline***	***Feedstock***	***No additive***	***Acid***	***Alkaline***
C	35.6±0.2	73.0±2.1	73.9±1.4	75.9±2.8	47.9±0.5	73.3±1.7	70.6±0.4	74.1±2.0
H	3.9±0.1	8.0±0.6	8.7±1.1	7.6±0.3	7.0±0.2	8.9±0.6	8.1±0.8	9.2±0.2
N	2.4±0.0	3.3±0.8	3.8±1.5	2.6±1.5	2.7±0.1	4.2±1.1	3.4±1.2	2.8±0.8
O*	24.2±0.1	15.8±2.3	13.6±1.3	14.0±1.4	36.6±0.5	13.4±1.5	17.8±0.6	13.9±1.3
H/C	1.4	1.3±0.1	1.4±0.2	1.2±0.1	1.7	1.4±0.1	1.4±0.1	1.5±0.0
O/C	0.6	0.2±0.0	0.1±0.0	0.1±0.0	0.6	0.1±0.0	0.2±0.0	0.1±0.0
HHV	13.3±0.5	33.4±0.5	34.8±1.8	34.0±1.1	19.7±1.0	34.8±1.3	32.5±0.7	35.4±1.0

*Oxygen content was calculated by difference (including the ash content).

GC-MS can provide additional insight on the distribution of low boiling point products contained in the bio-crude oil (Table 6.2). For each bio-crude oil sample, approximately 80% of the chromatogram peak area was identified with the help of a MS library, and products were categorized into several groups, such as cyclic hydrocarbons, phenol derivatives, furans, fatty acids and straight amide derivatives. For the bio-crude oil produced from HTL of manure without additives, the majority of the GC-MS peak area (~60%) was related to compounds that were categorized as cyclic hydrocarbons while the rest were categorized as N heterocyclic compounds, phenols and alkenes. In general, under HTL conditions fatty acids may decarboxylate into hydrocarbons and carbon dioxide. However, this reaction may be suppressed under different pH. The addition of acid to the HTL media shifted the bio-crude oil composition towards straight fatty acids (68%) and amides (6%) (Table 6.2). The base addition had less effect on the oil composition (compared to the non-modified HTL), presenting both cyclic and straight compounds. Food waste,

showed a different pattern than manure. Bio-crude oil from HTL without additives contained a wider distribution of compounds, categorized as straight fatty acids (26%), cyclic hydrocarbons (20%) and N heterocyclic compounds (18%) (Table 6.2). The addition of acid to food waste shifted the bio-crude oil composition to furan compounds (as dehydration products from HMF). On the other hand, the addition of base to food waste favored the production of phenols as well as straight fatty acids at the expense of cyclic hydrocarbons.

Table 6.2. Bio-crude oil composition from hydrothermal liquefaction of manure and food waste with and without the addition of acid or base. All components were characterized by GC–MS and categorized into several groups. Values represent % of total relative peak area.

	Manure			Food waste		
Group	*No additive*	*Acid*	*Alkaline*	*No additive*	*Acid*	*Alkaline*
Alkenes	3.4	N.D	4.6	2.6	N.D	N.D
N heterocyclic compounds	6.5	2.8	4.6	18.1	N.D	4.2
Cyclic hydrocarbons	59.4	6.3	20.8	19.9	10.3	2.8
Phenols	3.7	4.3	4.7	9.9	8.3	11.4
Furans	N.D	N.D	N.D	1.9	45.6	0.0
Long fatty acids	N.D	67.5	38.0	26.4	15.0	64.8
Straight amides	N.D	5.8	N.D	1.0	N.D	1.0
Total:	*73.1*	*86.7*	*72.7*	*79.8*	*79.3*	*84.2*

N.D, not detected

6.3.3 HTL aqueous product composition

The effect of acid and base additives on hydrothermal conversion of manure and food waste can be further elucidated by the composition of the aqueous phase (Table 6.3). For manure, the

dominant forms of dissolved organic carbon were lactic and acetic acids. The recovery of lactic acid ($C_3O_3H_5$) from manure with no additive was 26±4 mg C per g of C in the feedstock. The addition of acid decreased this value by 85%, while the addition of base increases increased this value by 88% as demonstrated by the CI values for lactic acid (Figure 6.5a). A similar trend was observed for acetic acid ($C_2O_2H_4$). The hydrothermal reaction without acid/base resulted in an acetic acid recovery of 38±4 mg C per g of C in manure feed (Table 6.3) with a negative CI value of 44% for acid and a positive CI value of 176% for alkali (Figure 6.5a). Small concentrations of succinic acid ($C_4H_6O_4$) and formic acid (CH_2O_2) were also found in the aqueous product from hydrothermal conversion of manure (Table 6.3). Succinic acid had a negative CI value of 36% when acid was added and a positive CI value of 72% following a base-modified reaction (Figure 6.5a). Interestingly, formic acid had negative CI values of 31 and 23% for acid and base additives, respectively (Figure 6.5a). The production of short chain organic acids (C1–4) in HTL was also reported for cellulose (Yin and Tan 2012, Yin et al. 2011) as well as rice straw (Chen et al. 2016) and algal feedstocks (Tommaso et al. 2015). Moreover, the studies with cellulose, focusing on the influence of alkalinity on hydrothermal reaction pathways, confirm our observations regarding the higher production of short chain organic acids due to alkali conditions (Yin and Tan 2012, Yin et al. 2011). This observation is important from the point of view of bio-crude oil production and may explain the lower oil yields from manure obtained with alkali additive (Figure 6.4). 5-HMF ($C_6H_6O_3$), a degradation products of C6 sugars (i.e., glucose and fructose) (Rosatella et al. 2011), showed an opposite trend to lactic and acetic acids with a positive CI value for acid and a negative value for the base (Figure 6.5a). In other words, the acidic conditions induced the production of HMF by 85%, while the alkali conditions suppressed it by 62% (Figure 6.5a). This phenomenon was reported by other researchers looking at hydrothermal conversion of cellulose (Yin et al. 2011,

Yin and Tan 2012). Moreover, these studies suggest that acidic conditions may enhance HMF polymerization to solids, while alkaline conditions are more likely to cause short chain acids and aldehydes in bio-crude oil to decompose to gases. The positive CI value of HMF for the acidic (Figure 6.5) condition together with the higher oil yields (Figure 6.4) suggest that adding acid to HTL media me enhance the production of bio-crude oil from manure towards the production of HMF.

The recovery of monosaccharides (i.e., glucose, fructose, xylose, and arabinose) from manure was very small, less than 5 mg C per g of C in manure feedstock. This observation was not modified by the addition of acid/base to the reaction media (Table 6.3). The recovery of monosaccharides for the acid-modified reaction decreased more than 2-fold (< 2 mg C per g C in manure) compared to base-modified and non-modified reactions (~4.3–4.4. mg C per g C in manure).

For the HTL of carbohydrate rich food waste, lactic acid was the main product in aqueous phase, with recovery values significantly higher than for manure — in the range of 70–120 mg C per g of C in the feedstock (Table 6.3). The addition of acid suppressed the formation of lactic acid by 26% while alkali conditions increased its formation by 34% (Figure 6.5b). Lactic acid is a valuable co-product as a precursor for bio-based chemicals, such as ethyl lactate and poly-l-lactic acid — biodegradable and environmental friendly solvents and plastics (He et al. 2008). Lactic acid was found to be stable at hydrothermal conditions below 240°C, while above this point it is gradually degraded (Yoshida et al. 1999). Since our experiments were performed at 300°C, some of the lactic acid was probably degraded, yet, future work aimed to selectively recover lactic acid from food waste at alkaline sub-critical water should be considered. Acetic and succinic acids were also generated from food waste. Both products had negative CI values of 49% for the acid-modified reaction and positive values of 26 and 13%, respectively, for the base-modified reaction (Fig. 5b).

Acetic acid was reported as a stable intermediate product in hydrothermal processing of almost all food wastes (Jin et al. 2001, Calvo and Vallejo 2002). Acetic acid is also an important resuable organic chemical. One of the industrial uses of acetic acid is to produce calcium magnesium acetate — a noncorrosive road deicer for cold areas (He et al. 2008). HMF formation from food waste was in general lower than for manure (Table 6.3), yet, the same trends were observed with a positive (45%) CI value for acid and a negative (57%) value for the alkaline additive (Figure 6.5b). Dehydration reactions that were probably enhanced by the addition of the acid, as discussed in previous section, were probably leading towards the production of HMF (He et al. 2008), as demonstrated by its higher CI value.

Compared to manure, the recovery of monosaccharides from food waste after hydrothermal conversion was remarkably higher— 55±3 mg C per g of C in food waste feedstock with no additive (Table 6.3). The addition of acid to the hydrothermal media decreased the recovery of monosaccharides to a value of 18±0.8 mg C per g of C in food waste feed (Table 6.3) with a negative CI value of 67% (Figure 6.5 b). On the other hand, the small CI value for the alkaline condition suggests no effect on the recovery of monosaccharides from food waste (Figure 6.5b), similar to manure (Figure 6.5 a).

In addition to the discussed short-chain organic acids, monosaccharides, and HMF, the aqueous product from HTL at the studied conditions may contain other soluble compounds such as levulinic acid (Yin and Tan 2012), amino acids and their derivatives, as well as nitrogen heterocyclic compounds (Tommaso et al. 2015, Posmanik et al. 2017). Glutamic acid, for example, is one of the main amino acids in soybean protein. It was reported to degraded under hydrothermal conditions to pyroglutamic acid (Yoshida et al. 1999). Moreover, our research group reported that

hydrothermal conversion of protein-rich biomass at 300°C may recover pyroglutamic acid at the range of 35–60 mg/g biomass (Posmanik et al. 2017).

The composition of the HTL aqueous phase show opportunities for further valorization using catalytic hydrothermal gasification (Elliott et al. 2013, Elliott et al. 2015) as well as anaerobic digestion (Tommaso et al. 2015, Posmanik et al. 2017, Chen et al. 2016). In addition, internal heat and power recovery from this phase can be designed as part of a process integration strategy to reduce external energy demands and to lower environmental and operating costs (Gerber Van Doren et al. 2017). High concentrations of nitrogen and phosphorous of the HTL aqueous product may suggest another direction for valorization, e.g., using it for direct fertilization (Mau et al. 2016). Furthermore, catalytic hydrothermal gasification may allow the recovery of those nutrients as salts by precipitation and filtration (Elliott et al. 2015).

Table 6.3. Profile of products obtained in the aqueous phase from hydrothermal liquefaction of manure and food waste at the conditions studied. Values are mg carbon in product per g of carbon in feed and represent mean values of three replicate experiments ± standard error.

		Manure (mg C in product / g C in feedstock)			**Food waste (mg C in product / g C in feedstock)**		
Compound	***Structure***	***No Additive***	***Acid***	***Alkaline***	***No Additive***	***Acid***	***Alkaline***
Glucose	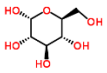	1.1±0.1	N.D	1.7±0.2	2.5±0.4	N.D	2.4±0.9
Fructose		1.2±0.3	1.0±0.6	0.9±0.0	32.1±1.9	4.2±0.4	25.1±5.4
Xylose		N.D	N.D	N.D	1.4±0.3	N.D	1.2±0.1
Arabinose		2.1±0.5	1.3±0.8	1.7±0.1	18.8±0.6	14.1±0.4	8.7±0.2
Succinic acid		3.2±1.0	2.1±1.0	4.4±0.7	12.1±.4	6.1±.6	13.3±0.7

Lactic acid		25.9±3.5	5.9±2.6	49.1±0.7	93.1±2.6	69.2±0.5	123.3±7.2
Formic acid		7.7±1.2	5.3±0.2	5.3±1.7	36.9±1.5	11.7±0.2	37.2±2.1
Acetic acid		38.3±3.7	34.7±1.0	105.1±5.8	39.2±2.0	20.2±0.7	44.9±13.1
HMF	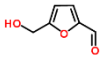	2.9±0.3	5.4±0.7	1.2±1.0	1.3±0.2	1.9±0.1	0.7±0.4

N.D, not detected; HMF, 5-hydroxymethylfurfural.

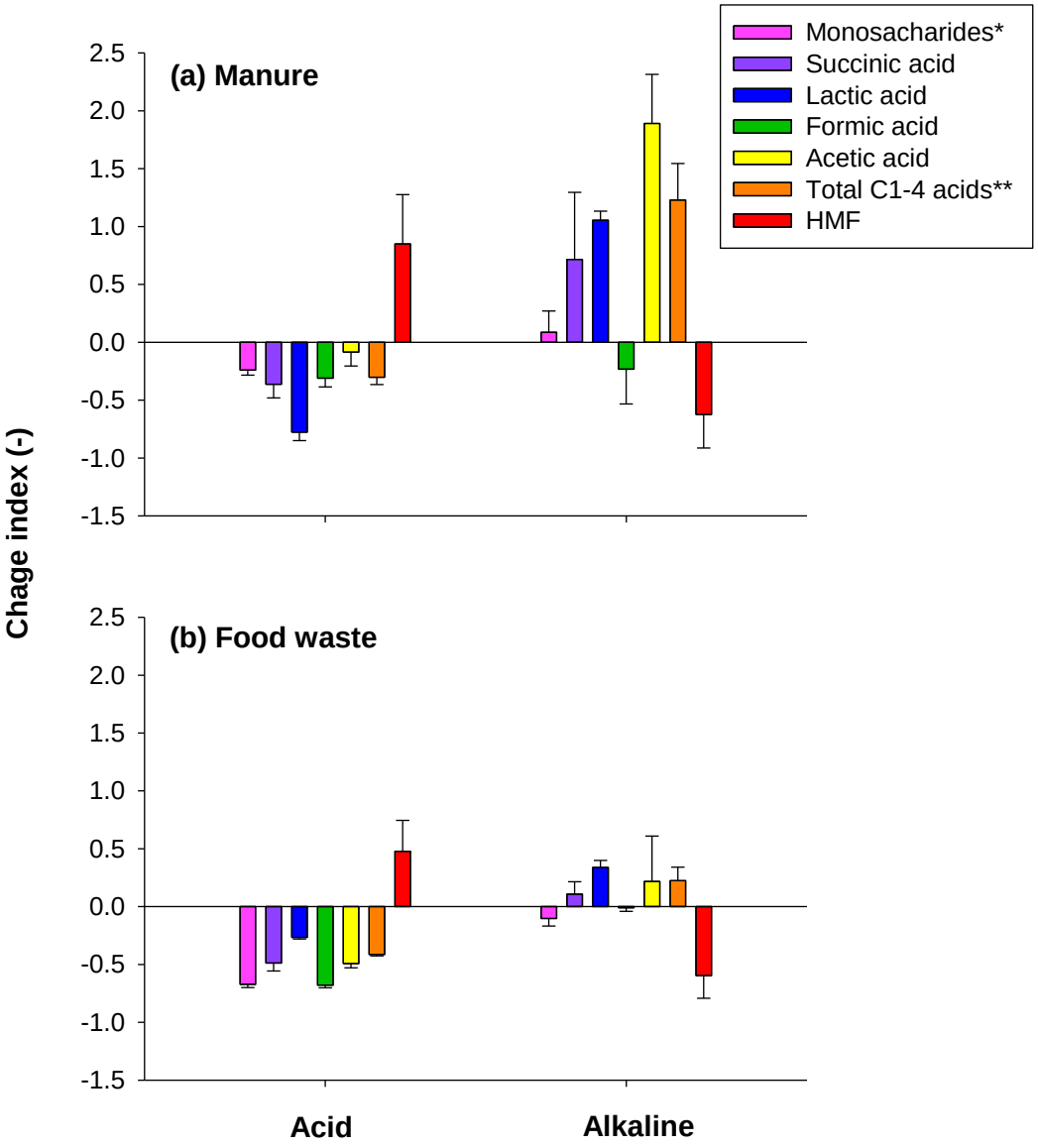

Figure 6.5. Change indexes (CI) of aqueous products following hydrothermal conversion of (a) manure; and (b) food waste under acid and alkaline additives (indexes were calculated based on the comparison to the reactions with no additive). Bars represent mean values of three replicate experiments ± standard deviation of the data. *Monosaccharides represent the sum of glucose, fructose, xylose and arabinose; **Total C1–4 acids represent the sum of formic, acetic, lactic and succinic acids.

6.3.4 Hydro-char characterization

The addition of acid or base to the reaction media affects the chemical nature of the hydro-char produced from both feedstocks as demonstrated by the FTIR spectra (Figure 6.6a and Figure 6.7a). Figure 6.6b–c and Figure 6.7b–c show the PCA bi-plots and loading plots for manure and food waste, respectively. For all hydro-char products, the FTIR spectra suggest a complete disappearance of hydrogen bonds (3700–3000 cm^{-1}) (Abidi et al. 2014) . This observation is consistent with the depletion of oxygen in the hydro-char composition measured by elemental analysis (data not shown).

Hydro-char generated from dairy manure under acid conditions (Figure 6.6a), showed a significantly different FTIR spectra than under alkaline conditions and with no additive, with a complete disappearance of the 1400 and 870 cm^{-1} bands that represent the carboxylate group stretching (Magalhaes et al. 2012) and the glyosidic linkage for cellulose and hemicellulose (Xu et al. 2013), respectively. Furthermore, the PCA bi-plot showed three distinct clusters for hydro-char generated from dairy manure (Figure 6.6b). Two big groups can be differentiated along PC1 axis (representing 71.5% of data variation): alkaline and non-additive at negative values of PC1, and acid additive at positive values of PC1. This scattering suggests that hydro-char generated from dairy manure via HTL with no additive or with alkaline additive may share similar functional group properties, yet different from those in hydro-char generated under acid additive. The loading plot for manure hydro-char (Figure 6.6c) demonstrates that the major contribution for the samples

clustering along PC1 results from differences in FTIR spectra at 1637, 1258, 1028, 970 and 868 cm^{-1}. Interestingly, other researchers reported that the bands at 1028 and 970 cm^{-1} refer to mineral phosphate residues in bio-chars (Liu, He, and Uchimiya 2015). Since phosphoric acid was used as acid additive in our experiments, this evidence is a further validation for the FTIR-PCA approach. Variation among hydro-char obtained at different conditions from dairy manure were related mostly to changes of chemical bonds in the lignin fraction as shown in Table 6.4.

For hydro-char generated from carbohydrate rich food waste, there were decreases in infrared absorbance at 2920 and 2850 cm^{-1}, which represent the asymmetrical and symmetrical C-H stretching vibrations for aliphatic groups (sp^3 carbon) (Abidi et al. 2014) what can be observed specially for HTL with acid additive. This phenomenon was also observed in bio-char produced from 500°C pyrolysis of biomass (Strezov 2012). In addition, hydro-char generated under alkali additive showed a significantly different FTIR spectra compared to the hydro-char generated with acid additive and no additive. This was mostly due to bands at 1030–1015 cm^{-1}, which represent C-O stretching in primary alcohols. The PCA bi-plot shows only two clusters for hydro-char generated from carbohydrate rich food waste along PC1, that alone explains 91.2% of the data variation (Figure 6.7b). The hydro-char generated under HTL without additive and with acid additive overlap in the PCA bi-plot at negative values of PC1. On the other hand, hydro-char form HTL with alkaline additive appear at positive values of PC1. The loading plot (Figure 6.7c) demonstrates that FTIR spectra wavenumbers at 1150, 1105, 976, 905 and 638 cm^{-1} are responsible for the scattering shown in bi-plot. These wavenumbers represent modifications in cellulose, hemicellulose, and pectin (Table 6.4).

Since carbohydrate rich food waste is acidic, both the reactions with no additive and with acid additive occur in a low pH media (2.0–4.1), suggesting similar conditions and therefore similar

FTIR spectra. Dairy manure, on the other hand, is a high pH feedstock, thus both non-modified and base-modified reactions occur in a higher pH (8.8–10), generating hydro-char products with similar FTIR spectra. In summary, the FTIR-PCA analysis demonstrates that the pH conditions in HTL of dairy manure and carbohydrate rich food waste, generate hydro-char products with different chemical structures. The different chemical structures result primarily from reaction phenomena associated with decomposition of fibers in the raw biomass- lignin in manure and pectin in food waste. (Table 6.4). This information is important for understanding the HTL reaction mechanisms and chemical pathways for manure and food waste. Moreover, improved characterization of the hydro-char could potentially expand the range of applications and utilization opportunities of this product, currently considered as a by-product of the HTL process. There are several opportunities for hydro-char utilization such as its use for soil amendment, production of nanostructured materials, production of adsorbent materials, wastewater purification, energy production, carbon sequestration and reduction of greenhouse gas emissions (Mau et al. 2016, Libra et al. 2011, Qambrani et al. 2017).

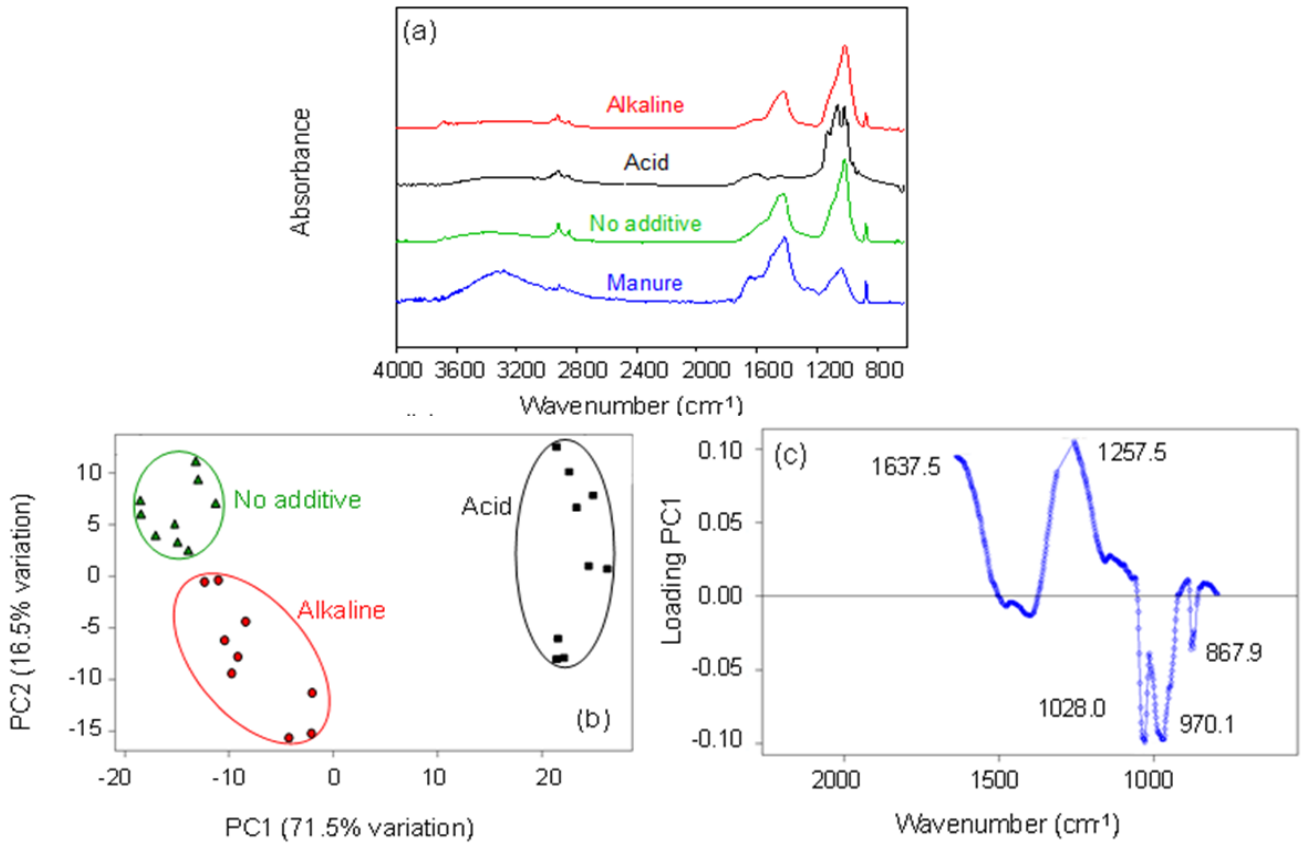

Figure 6.6. FTIR spectral signature of hydro-char generated from manure under modified (acid or alkaline) and non-modified hydrothermal liquefaction. (a) FTIR spectra of manure and its hydro-char products; (b) PCA bi-plot with cluster sample grouping and scattering along PC1 axis; and (c) PCA loadings plot representing the specific wavenumber that contribute to the scattering shown in bio-plot.

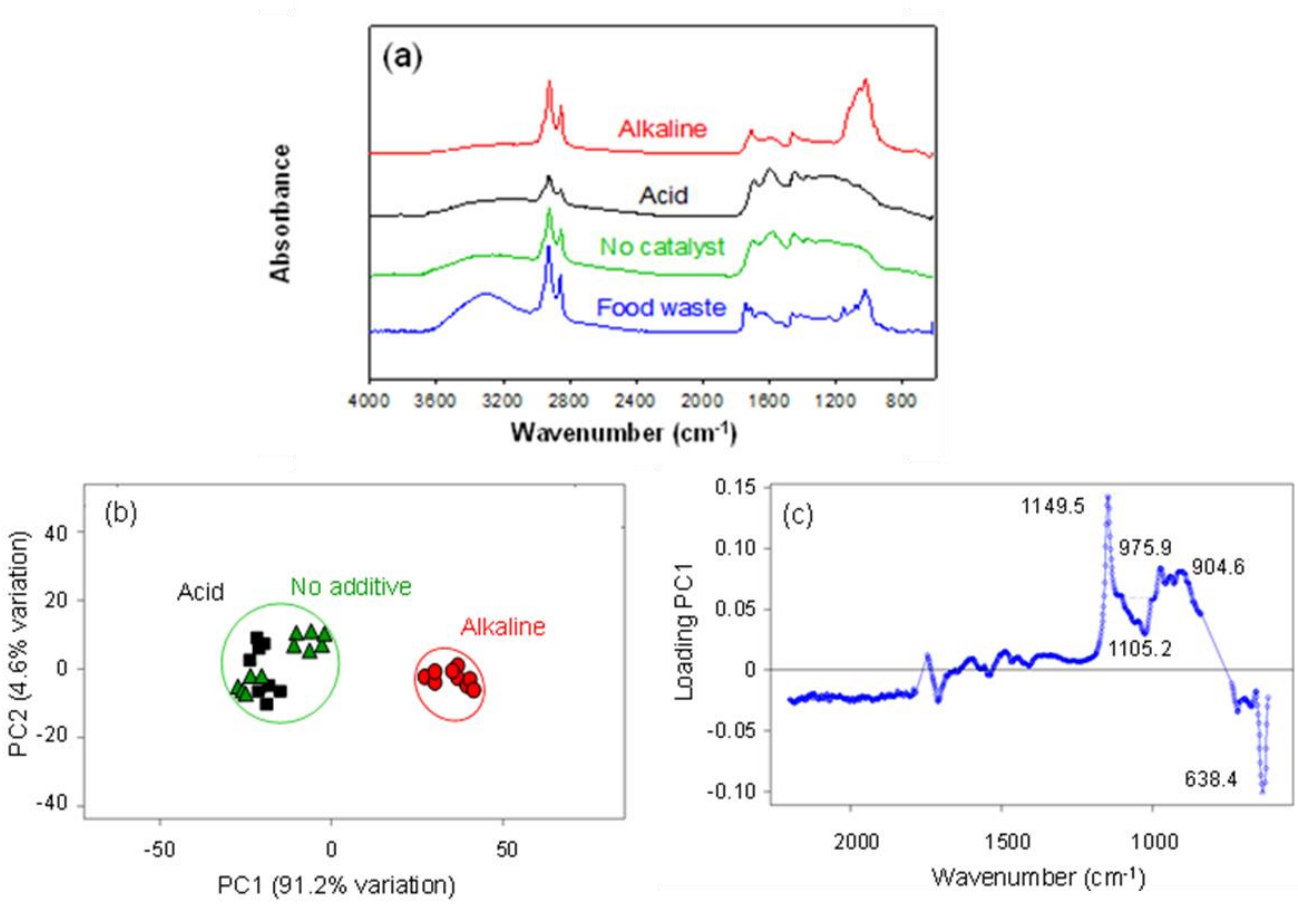

Figure 6.7. FTIR spectral signature of hydro-char generated from manure under modified (acid or alkaline) and non-modified hydrothermal liquefaction. (a) FTIR spectra of food waste and its hydro-char products; (b) PCA bi-plot with cluster sample grouping and scattering along PC1 axis; and (c) PCA loadings plot representing the specific wavenumber that contribute to the scattering shown in bio-plot.

Table 6.4. Assignment of specific FTIR wavenumbers typically found in biomass with the functional group and biomass fraction they represent, according to literature.

Wavenumber (cm^{-1})	Functional group	Composition	References
Manure:			
1637	C=O stretching	Carbonyl (lignin)	(Nuopponen and Vourinen 2005, Qambrani et al. 2017)
1258	C-O stretching	Guaiacyl (lignin)	(Poletto and Zattera 2013, Kline et al. 2010)
1028, 970	Mineral phosphate residues		(Liu et al. 2015)
868	Aromatic C-H deformation	Guaiacylpropane (lignin)	(Qambrani et al. 2017, Poletto and Zattera 2013)
Food waste:			
1150	Symmetric C-O stretching	Hemicellulose, pectin	(Qambrani et al. 2017, Baum et al. 2017)
1105	Ring deformation	Pectin	(Baum et al. 2017, Fellah et al. 2009)
976	Aromatic C-H bonds	Cellulose, pectin	(Reza et al. 2015, Baum et al. 2017, Fellah et al. 2009)
905	Ring deformation	Cellulose	(Xu et al. 2013, Nuopponen and Vourinen 2005)
638	Aromatic C-O deformation	Cellulose	(Corgié et al. 2011)

6.4 Conclusions

This chapter explored the role of acid and base additives on hydrothermal conversion of manure and food waste – two significant organic waste streams. Our data demonstrates the stronger effect of the acid addition to the HTL media on the processing of manure compared to food waste. Higher bio-crude oil yields were observed for manure that was hydrothermally treated with the addition of acid. The chemical compositions of HTL products (i.e., oil, aqueous, and solid) varied among feedstocks and additives. The increased bio-crude oil yield were due to different chemical pathways that enhanced production of oil precursors such as HMF. On the other hand, enhanced production of short-chain fatty acids and monosaccharides may explain the low oil yields as observed in reactions under alkaline conditions. The oil composition suggests a strong effect of the acid additive on dehydration processes that remove oxygen from biomass during hydrothermal conversion. Finally, it was observed that the produced hydro-char, from acid- and base-modified HTL reactions of manure and food waste were chemically different based on the FTIR-PCA analysis. The FTIR-PCA showed that this variation among clusters of hydro-char products was related to lignocellulose decomposition pathways. Beyond better clarifying the chemical pathways, our results may suggest further valorization opportunities of HTL co-products. While bio-crude oil can be upgraded to drop-in fuels, using existing refinery technology, the utilization of both aqueous co-product and hydro-char may provide additional resource recovery opportunities. Future research is therefore needed to explore all utilization alternatives, including bio-based chemical, agricultural applications, adsorption materials, water recovery and more. Understanding the effect of acid and base additives on the chemical pathways as well as the properties of all HTL co-products is essential for choosing among utilization alternatives.

6.5 References

Abidi, N, L Cabrales, and C Haigler. 2014. "Changes in the Cell Wall and Cellulose Content of Developing Cotton Fibers Investigated by FTIR Spectroscopy." *Carbohydrate Polymers* 100: 9–16.

Akalin, M, K Tekin, and S Karagoz. 2012. "Hydrothermal Liquefaction of Cornelian Cherry Stones for Bio-Oil Production." *Bioresource Technology* 110: 682–87.

ASTM, Annual book of ASTM standards Volumen 11.05. 2003. "ASTM E1755-01 Standard Method for the Determination of Ash in Biomass."

Baum, A, M Dominiak, S Vidal-Melgosa, G William, K Sondergaard, P Hansen, A Meyer, and J Mikkelsen. 2017. "Prediction of Pectin Yield and Quality by FTIR and Carbohydrate Microarray Analysis." *Food and Bioprocess Technology* 10 (1): 143–54.

Calvo, L, and D Vallejo. 2002. "Formation of Organic Acids during the Hydrolysis and Oxidation of Several Wastes in Sub- and Supercritical Water." *Industrial & Engineering Chemistry Research* 41 (25): 6503–9.

Cantero-Tubilla, B, D Cantero, C Martinez, J Tester, L Walker, and R Posmanik. n.d. "Characterization of the Solid Products from Hydrothermal Liquefaction of Waste Feedstocks from Food and Agricultural Industries." *Jornal of Supercritical Fluids*.

Chen, H, J Wan, K Chen, G Luo, J Fan, J Clark, and S Zhang. 2016. "Biogas Production from Hydrothermal Liquefaction Wastewater (HTLWW): Focusing on the Microbial Communities as Revealed by High-Throughput Sequencing of Full-Length 16S rRNA Genes." *Water Research* 106: 98–107.

Chen, W, Y Zhang, J Zhang, L Schideman, G Yu, P Zhang, and M Minarick. 2014. "Co-

Liquefaction of Swine Manure and Mixed-Culture Algal Biomass from a Wastewater Treatment System to Produce Bio-Crude Oil." *Applied Energy* 128: 209–16.

Corgié, S, H Smith, and L Walker. 2011. "Enzymatic Transformations of Cellulose Assessed by Quantitative High-Throughput Fourier Transform Infrared Spectroscopy (QHT-FTIR)." *Biotechnology and Bioengineering* 108 (7): 1509–20.

Déniel, M, G Haarlemmer, A Roubaud, E Weiss-Hortala, and J Fages. 2016. "Energy Valorisation of Food Processing Residues and Model Compounds by Hydrothermal Liquefaction." *Renewable and Sustainable Energy Reviews* 54: 1632–52.

Elliott, D, P Biller, A Ross, A Schmidt, and S Jones. 2015. "Hydrothermal Liquefaction of Biomass: Developments from Batch to Continuous Process." *Bioresource Technology* 178: 147–56.

Elliott, D, T Hart, A Schmidt, G Neuenschwander, L Rotness, M Olarte, A Zacher, K Albrecht, R Hallen, and J Holladay. 2013. "Process Development for Hydrothermal Liquefaction of Algae Feedstocks in a Continuous-Flow Reactor." *Algal Research* 2 (4): 445–54.

Fellah, A, P Anjukandi, M Waterland, and M Williams. 2009. "Determining the Degree of Methylesterification of Pectin by ATR/FT-IR: Methodology Optimisation and Comparison with Theoretical Calculations." *Carbohydrate Polymers* 78: 847–53.

Gerber Van Doren, L, R Posmanik, F Bicalho, J Tester, and D Sills. 2017. "Prospects for Energy Recovery during Hydrothermal and Biological Processing of Waste Biomass." *Bioresource Technology* 225: 67–74.

He, W, G Li, L Kong, H Wang, J Huang, and Ji Xu. 2008. "Application of Hydrothermal Reaction in Resource Recovery of Organic Wastes." *Resources, Conservation and Recycling* 52 (5):

691–99.

Jin, F, and H Enomoto. 2011. “Rapid and Highly Selective Conversion of Biomass into Value-Added Products in Hydrothermal Conditions: Chemistry of Acid/base-Catalysed and Oxidation Reactions.” *Energy Environ. Sci.* 4 (2): 382–97.

Jin, F, A Kishita, T Moriya, and H Enomoto. 2001. “Kinetics of Oxidation of Food Wastes with H2O2 in Supercritical Water.” *The Journal of Supercritical Fluids* 19 (3): 251–62.

Kline, L, D Hayes, A Womac, and N Labbe. 2010. “Simplified Determination of Lignin Content in Hard and Soft Woods via UV-Spectrophotometric Analysis of Biomass Disolved in Ionic Liquids.” *BioResources* 5 (3): 1366–83.

Libra, J, K Ro, C Kammann, A Funke, N Berge, Y Neubauer, M Titirici, et al. 2011. “Hydrothermal Carbonization of Biomass Residuals: A Comparative Review of the Chemistry, Processes and Applications of Wet and Dry Pyrolysis.” *Biofuels* 2 (1): 71–106.

Liu, Y, Z He, and M Uchimiya. 2015. “Comparison of Biochar Formation from Various Agricultural By-Products Using FTIR Spectroscopy.” *Modern Applied Science* 9 (4): 246.

Magalhaes, A, M Almeida, M Bezerra, N Ricardo, and J Feitosa. 2012. “Application of FTIR in the Determination of Acrylate Content in Poly(sodium Acrylateco-Acrylamide) Superabsorbent Hydrogels.” *Quim. Nova* 35 (7): 1464–67.

Mau, V, J Quance, R Posmanik, and A Gross. 2016. “Phases’ Characteristics of Poultry Litter Hydrothermal Carbonization under a Range of Process Parameters.” *Bioresource Technology* 219: 632–42.

Monlau, F, C Sambusiti, E Ficara, A Aboulkas, A Barakat, and H Carrere. 2015. “New Opportunities for Agricultural Digestate Valorization: Current Situation and Perspectives.”

Energy Environ. Sci. 8 (9): 2600–2621.

NRDC. 2012. "Wasted: How America Is Losing Up to 40 Percent of Its Food from Farm to Fork to Landfill."

Nuopponen, M, and T Vourinen. 2005. "Thermal Modifications in Softwood Studied by FT-IR and UV Resonance Raman Spectroscopies." *Journal of Wood Chemistry and Technology* 24 (1): 13–26.

Peterson, A, F Vogel, R Lachance, M Fröling, M Antal, Jr., and J Tester. 2008. "Thermochemical Biofuel Production in Hydrothermal Media: A Review of Sub- and Supercritical Water Technologies." *Energy & Environmental Science* 1: 32–65.

Pham, T, R Kaushik, G Parshetti, R Mahmood, and R Balasubramanian. 2014. "Food-Waste-to-Energy Conversion Technologies: Current Status and Future Directions." *Waste Management* 38 (December): 399–408.

Poletto, M, and A.J Zattera. 2013. "Materials Produced from Plant Biomass. Part III: Degradation Kinetics and Hydrogen Bonding in Lignin." *Materials Research* 16 (5): 1065–70.

Posmanik, R, D Cantero, A Malkani, D. Sills, and J Tester. 2017. "Biomass Conversion to Bio-Oil Using Sub-Critical Water: Study of Model Compounds for Food Processing Waste." *Jornal of Supercritical Fluids* 119: 26–35.

Posmanik, R, R Labatut, A Kim, J Usack, J Tester, and L Angenent. 2017. "Coupling Hydrothermal Liquefaction and Anaerobic Digestion for Energy Valorization from Model Biomass Feedstocks." *Bioresource Technology* 233: 134–43.

Qambrani, N, M Rahman, S Won, S Shim, and C Ra. 2017. "Biochar Properties and Eco-Friendly Applications for Climate Change Mitigation, Waste Management, and Wastewater

Treatment: A Review." *Renewable and Sustainable Energy Reviews* 79: 255–73.

Reza, M, R Emerson, M H Uddin, G Gresham, and C Coronella. 2015. "Ash Reduction of Corn Stover by Mild Hydrothermal Preprocessing." *Biomass Conversion and Biorefinery* 5 (1): 21–31.

Rosatella, A, S Simeonov, R Frade, and C Afonso. 2011. "5-Hydroxymethylfurfural (HMF) as a Building Block Platform: Biological Properties, Synthesis and Synthetic Applications." *Green Chemistry* 13 (4): 754–93.

Sills, D, and J Gossett. 2012. "Using FTIR Spectroscopy to Model Alkaline Pretreatment and Enzymatic Saccharification of Six Lignocellulosic Biomasses." *Biotechnology and Bioengineering* 109 (4): 894–903.

Strezov, V. 2012. "System Approach to Biomass Pyrolysis: Product Characterisation." In *The Third International Conference on Bioenvironment, Biodiversity, and Renewable Energies*.

Theegala, C, and J Midgett. 2012. "Hydrothermal Liquefaction of Separated Dairy Manure for Production of Bio-Oils with Simultaneous Waste Treatment." *Bioresource Technology* 107 (March): 456–63.

Tommaso, G, W Chen, P Li, L Schideman, and Y Zhang. 2015. "Chemical Characterization and Anaerobic Biodegradability of Hydrothermal Liquefaction Aqueous Products from Mixed-Culture Wastewater Algae." *Bioresource Technology* 178: 139–46.

Toor, S, L Rosendahl, and A Rudolf. 2011. "Hydrothermal Liquefaction of Biomass: A Review of Subcritical Water Technologies." *Energy* 36 (5): 2328–42.

UNEP. 2010. "International Panel for Sustainable Resource Management, Working Group on the Environmental Impacts of Products and Materials." Paris, France.

USDA. 2000. “Manure Nutrients Relative to the Capacity of Cropland and Pastureland to Assimilate Nutrients: Spatial and Temporal Trends for the United States.”

Vardon, D, B Sharma, J Scott, G Yu, Z Wang, L Schideman, Y Zhang, and T Strathmann. 2011. “Chemical Properties of Biocrude Oil from the Hydrothermal Liquefaction of Spirulina Algae, Swine Manure, and Digested Anaerobic Sludge.” *Bioresource Technology* 102 (17): 8295–8303.

Xiu, S, A Shahbazi, V Shirley, and D Cheng. 2010. “Hydrothermal Pyrolysis of Swine Manure to Bio-Oil: Effects of Operating Parameters on Products Yield and Characterization of Bio-Oil.” *Journal of Analytical and Applied Pyrolysis* 88 (1): 73–79.

Xu, F, J Yu, T Tesso, F Dowell, and D Wang. 2013. “Qualitative and Quantitative Analysis of Lignocellulosic Biomass Using Infrared Techniques: A Mini-Review.” *Applied Energy* 104: 801–9.

Yin, S, R Dolan, M Harris, and Z Tan. 2010. “Subcritical Hydrothermal Liquefaction of Cattle Manure to Bio-Oil: Effects of Conversion Parameters on Bio-Oil Yield and Characterization of Bio-Oil.” *Bioresource Technology* 101 (10): 3657–64.

Yin, S, A Mehrotra, and Z Tan. 2011. “Alkaline Hydrothermal Conversion of Cellulose to Bio-Oil: Influence of Alkalinity on Reaction Pathway Change.” *Bioresource Technology* 102 (11): 6605–10.

Yin, S, and Z Tan. 2012. “Hydrothermal Liquefaction of Cellulose to Bio-Oil under Acidic, Neutral and Alkaline Conditions.” *Applied Energy* 92: 234–39.

Yoshida, H, M Terashima, and Y Takahashi. 1999. “Production of Organic Acids and Amino Acids from Fish Meat by Sub-Critical Water Hydrolysis.” *Biotechnology Progress* 15 (6):

1090–94.

CHAPTER VII

CHARACTERIZATION OF THE SOLID PRODUCTS FROM HYDROTHERMAL LIQUEFACTION OF WASTE FEEDSTOCKS FROM FOOD AND AGRICULTURAL INDUSTRIES

This chapter was written in collaboration with Dr, Roy Posmanik, Dr. Danilo Cantero, Celia Martinez, Prof. Larry Walker, and Prof. Jefferson Tester. It was published in the Journal of Supercritical Fluids on July 2017.

7.1 Introduction

The large volumes of organic waste streams produced daily as a part of food and water supply systems create a global challenge. In the U.S., the organic fraction of municipal solid waste accounts for more than 150 million tons per year (United States Environmental Protection Agency 2014). Moreover, every year, the U.S. food and dairy industries generate approximately 36 and 19 million tons of organic waste, respectively (Gunders 2012, United States Department of Agriculture 2000). Traditionally, organic waste streams have been landfilled, composted, incinerated or used for the production of animal feed and fertilizers (Qian et al. 2017, Ekpo et al. 2016), and typically seen as an economic burden to the industry generating them, hindering the scalability of processes (Yin et al. 2010). However, since these wastes are rich in carbohydrates, proteins, lipids, nutrients, and minerals (Ekpo et al. 2016), they present a high potential for the recovery of valuable bio-based products that are receiving increase attention. This valorization and global sustainability concerns have created opportunities for the development of advance technologies for producing valuable bio-based products (Tuck et al. 2012). A common feature and challenge to valorizing these waste streams is their high water content. This represents an

economic hinder for conventional thermochemical technologies (i.e., dry gasification or pyrolysis) where water has to be removed by vaporization prior to the chemical process.

Given the high latent heat of water vaporization, energy requirements for drying are substantial for high water content wastes, alternative treatment methods are often proposed. Hydrothermal technologies provide opportunities for a more energy efficient valorization of wet biomass (Vardon et al. 2011, Nazem and Tavakoli 2017). By carrying out reactions under high pressure, water remains in liquid state, offering unique properties that are highly advantageous for chemical conversion (Tekin et al. 2014, Peterson et al. 2008). High pressure liquid water increases its reactivity for reforming organic compounds by increasing its ionic product and decreasing its dielectric constant. In addition, high pressure liquid water decreases interphase mass transfer resistances (reduction of viscosity and density) as it approaches the critical point (374 °C and 22.1 MPa). Furthermore, organic compounds in the raw material gain capacity to react when temperature increases to 250 °C (Tekin et al. 2014, Elliott et al. 2015). All of these advantages make hydrothermal processing of wastes, a promising valorization technology from both an engineering and economical perspectives.

Hydrothermal processes can be classified depending on the processing temperature and pressure, yielding different product distribution (Tekin et al. 2014, Déniel et al. 2016). At subcritical conditions (i.e., 250–374 °C and 2.5–22 MPa), the hydrothermal liquefaction (HTL) process primarily produces a bio-crude oil with low oxygen content and higher heating value than the raw material (Vardon et al. 2011, Biller et al. 2015). In addition, a gas phase, aqueous phase, and solids (hydro-char) are also produced as co-products of the HTL process. To enhance the economic feasibility of the HTL process, it is important to characterize all these co-products, in order to find a market niche for them. The hydro-char can be used in generating electricity and process heat, as

well as the recovery of inherent nutrients (Ekpo et al. 2016) for soil amendment/bio-remediation (Jien and Wang 2013). These solids are usually characterized by analyzing their moisture content, elemental composition, ash, surface area, volatile mater, and metal retention capabilities (Liu et al. 2015).

Fourier Transform Infrared (FTIR) coupled with Attenuated Total Reflectance (ATR) is a low-cost, rapid, non-destructive, and easy technique to investigate the chemical changes on functional groups and structures of hydro-char upon hydrothermal processing at different operating conditions. FTIR has been previously used as a substitute for "wet protocols" to determine the composition of energy crops (Allison et al. 2009), the effect of biomass pre-treatments (Abu Tayeh et al. 2016, Kline et al. 2010, Sim et al. 2012, Chundawat et al. 2007) and pyrolysis (Liu et al. 2015). However, the FTIR spectra of biomass are commonly composed of a mixture of many overlapping peaks, making it difficult to assign as a particular vibrational mode. Chemometrics have been applied in the last 30 years to extract relevant information from FTIR data. The use of multivariate statistical data analysis such as Principal Component Analysis (PCA) is one method to find differences among spectra, and relate those differences to the chemical composition of the samples (Kline et al. 2010).

The majority of HTL research has focused on documenting the process conditions that maximize bio-oil yields. Little to no attention has been placed on HTL co-products such as the aqueous phase and the hydro-char (Vardon et al. 2011). Hydro-char is often overlooked as a by-product. However, its chemical characterization is important for determining HTL reaction mechanisms and chemical pathways at different temperatures and reaction times. The goal of this study is to expand on existing work performed in HTL, using representative waste feedstocks from a variety of industries: dairy industry (manure and yogurt whey) municipal wastewater treatment, food

industry (dining halls, apple cider, wine, whiskey and olive oil). Specifically, this chapter emphasized characterization and quantification of mass yields, along with chemical compositions of the hydro-char by-products using FTIR coupled with PCA. To the best of our knowledge, this is the first study entirely focused on hydro-char produced by HTL processing of a diverse set of waste streams. Improved characterization of these hydro-char could potentially expand their range of applications and opportunities beyond soil remediation or the production of a solid fuel.

7.2 Materials and methods

7.2.1 Feedstocks characterization

The feedstocks used in this study come from a variety of industries. Manure digestate was taken from a privately owned dairy waste anaerobic digester (Sunnyside farm, Scipio Center, NY). Waste activated sludge was collected from the municipal anaerobic digester of a wastewater treatment facility (Ithaca, NY). Carbohydrate rich food waste (15.4 wt% fruits, 47.1 wt% vegetables, and 37.5 wt% grains/breads) was sorted from Cornell University dining halls (Ithaca, NY). Apple pomace (residue remaining after apple pressing to obtain the juice) was collected from Cornell Orchards (Ithaca, NY). Niagara red wine pomace was given by Swanbay Cellars (Alexandria Bay, NY). Whiskey stillage (residue after first distillation of the mash) was taken from Myer Farm Distillers (Ovid, NY). Yogurt whey was given by FAGE USA Dairy Industry Inc. (Johnstown, NY). Olive oil pomace was given by California Olive Ranch (Chico, CA). All feedstocks were first grounded and homogenized in a blender without the addition of water. Their pH was measured using an Accumet AB150 probe (Fisher Scientific, Hampton, NH). They were characterized for wt% dry solids (overnight at 105 °C) and ash content (4 hours at 550 °C) (ASTM

2003). The elemental composition (C, H, N; wt%) was determined using a CE-440 elemental analyzer (Exeter Analytica, North Chelmsford, MA) yielding less than 0.5wt% difference among triplicates. The oxygen content was calculated as the difference between the wt% of residual (difference to 100% of the sum of C, H, and N wt%) and wt% ash in the feedstocks (Yin et al. 2010). Based on the elemental composition, the higher heating value of each feedstock was calculated using the modified Dulong's formula (Posmanik et al. 2017) as given in Eq. 1.

$$HHV = 0.338 \times C + 1.428\ (H - \frac{O}{8}) \qquad \text{Eq. (1)}$$

Where HHV is the higher heating value (MJ/kg), and *C, H,* and *O* are the mass percentages of carbon, hydrogen, and oxygen in the solids, respectively.

7.2.2 Experimental set-up

The HTL batch reactor used in this study consisted in a 500 mL, stainless steel vessel (Model 4575 Parr Instruments Co., Moline, IL) with a maximum operation pressure of 34.5 MPa. The vessel was heated with an electric heating jacket monitored with a reactor controller (Model 4848 Parr Instruments Co., Moline, IL) and stirred at 100 rpm, with a magnetically attached shaft. The pressure was monitored using a pressure gauge (Duro United Instruments, Northvale, NJ) and recorded using a pressure transducer (Model 280E Setra Systems, Boxborough, MA). It is equipped with a sampling inlet for liquid and gas as well as effluent outlet connected to the reactor with a custom-made heat exchanger to quench the reaction liquid products. The reactor inlet was connected to a high pressure pump (Varian, PrepStar, SD1 system, Agilent Technologies, Santa Clara, CA) and a N_2 tank. A picture and a scheme of the experimental set-up is available in Figure 7.1. Prior to each experiment, 200 mL of the feedstock prepared at 4 wt% dry solids using

deionized water, was load in the reactor (8 g of dry solids). This concentration was selected as it has been previously reported that water mass ration plays an important role in bio-crude oil production. Yin et al (2010) showed that the increase of manure to water ratio affects negatively the yield of bio-crude oil formation. The remaining 300 mL head-space was purged with N_2, and the reactor was pressurized with N_2 at 2.5 MPa prior to heating to a specific target temperature. After the desired reaction time, a sample fraction was collected by cooling down through the heat exchanger (depicted in Figure 7.1**)** and depressurizing. The reactor vessel was also quenched by flowing tap water through a cooling coil located inside the reactor (CW in Figure 7.1). To wash the reactor and associated tubing, 100 mL of acetone was pumped into the reactor and then purged through the heat exchanger (referred as wash fraction). Once the reactor reached room temperature, it was depressurized, opened, and all the remaining solids were collected. All the lines were flushed with deionized water to remove acetone residues.

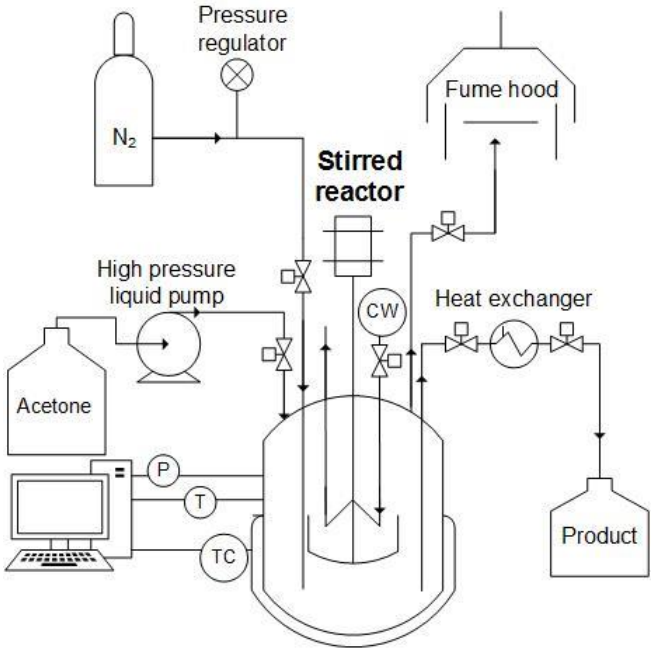

Figure 7.1. Scheme of the experimental set-up. P, pressure reading; T, temperature reading; TC, temperature control on electric heating jacket; CW, cooling water.

7.2.3 Experimental conditions

Temperature and reaction time were the reactor operating parameters studied in this chapter. These, along with biomass/water ratio, are the parameters that most influence the quality and the yield of HTL products (Yin et al. 2010). Experiments were performed at 250 and 300 °C and corresponding pressures of 5.5 and 11 MPa, respectively, to maintain water in liquid phase. This temperature range was chosen for this chapter as water presents maximum ionic product, (therefore acid-base catalytic reaction get kinetically more favorable), energy-dense bio-crude oil is the main phase produced, avoiding repolymerization to char (Déniel et al. 2016), and the working pressures were moderate, safe for the experimental setting used. For each of these thermal conditions, two reaction times were chosen, 5 and 60 minutes to study the dynamic process of bio-crude oil / hydrochar transformation. These times referred to the duration that the reactor was maintained at the desired temperature (i.e., not including the average 15 °C/min heating ramp). Every experiment was done in triplicate. The temperature and pressure profiles for the four conditions studied are shown in Figures AI-1 and AI-2 (Appendix I).

A severity factor for each experiment was calculated (*log R_0*) using Eq. 2 (Posmanik et al. 2017) to assess the combine effect of temperature and time (Posmanik et al. 2017, Y. Kim et al. 2014, Rogalinski et al. 2008) .

$$logR_0 = log\left[\sum_{i=1}^{n} t_i \times exp\left(\frac{T_i - T_b}{w}\right)\right] \qquad \text{Eq. (2)}$$

where *t* is the reaction time (min), T_i is reaction temperature (°C), T_b is the reference temperature (100 °C), *w* is a fitter parameter based on the activation energy of hemicellulose hydrolysis (14.75), and *n* is the number of measurements. Table 7.1 shows the value of severity factor corresponding to the conditions studied.

Table 7.1. Temperatures, reaction times, and the calculated severity factors (calculated based on Eq. 2) used in this study.

Temperature (°C)	Time (min)	Severity factor ($\log R_0$)
250	5	5.54
250	60	6.23
300	5	7.21
300	60	7.78

7.2.4 Sample preparation and characterization

Following each experiment the pH was measured and shown in Table AI-1 (Appendix I). The solid, aqueous, and bio-crude phases were separated as described elsewhere (Posmanik et al. 2017). Focusing on the hydro-char recovery, the solid obtained from the reactor was gravimetrically filtrated using pre-weighted filter paper (Whatman No.1). The hydro-char solids were washed with acetone to remove the bio-crude oil adsorbed on them. Same protocol was applied to separate the solids from the washing effluent and the residues from reactor clean-up. All hydro-char samples were dried overnight at 105°C and the mass yields were calculated as the ratio of the total hydro-char mass obtained in the reaction to dry feedstock mass initially fed in the reactor. The elemental composition, ash content, HHV, and FTIR analysis were performed for the sample fraction as describe in section 2.1 and 2.5 for FTIR (i.e., the solids from washes were included only for mass yield calculations).

7.2.5 FTIR-ATR analysis

FTIR spectroscopy analysis was used to determine the specific organic chemical groups in feedstocks and hydro-char obtained at each reaction conditions. All spectra were collected with a Bruker Vertex 70 FTIR spectrometer (Bruker Optics, Billerica, Ma) in transmission mode and atmospheric compensated, between 7000 and 400 cm^{-1} wavenumbers, 2 cm^{-1} spectral resolution, and 32 scans per sample using a single bounce attenuated total reflectance (ATR) sampling accessory (MIRacle) equipped with a ZnSe crystal (PIKE Technologies, Madison, WI). Prior to spectra measurement, background scans were collected. Dried samples were grounded with a mortar and pestle. FTIR were obtained by tightly pressing the sample against the crystal surface. A minimum of three measurements, using a different sample for each measurement, were collected to assure reproducibility of the results. Spectral analyses were performed with the OPUS (Bruker Optics, Billerica, Ma) software package. The raw spectra were converted from transmittance to absorbance by applying the ATR correction. The resulting spectra was cut to remove wavenumbers above 4000 cm^{-1} and below 620 cm^{-1}, to eliminate saturated regions of the spectra due to the ATR crystal. Concave rubber band baseline correction was applied (10 iterations), and the resulting spectra was vector normalized (Déniel et al. 2016, Liu et al. 2015).

7.2.6 Principal component analysis (PCA) of FTIR spectra

Normalized FTIR spectra for all hydro-chars were prepared for Principal Component Analyses (PCA), using software package RStudio (RStudio, Inc., Boston, MA). First, wavenumbers above 2200 cm^{-1} were removed, to focus the PCA only on the fingerprint region of the biomass (1800–620 cm^{-1}). The range between 2200 cm^{-1} and 1800 cm^{-1} is common to all FTIR spectra, and was

used as a control/threshold for interpretation of PCA results. Outliers (spectra with intensities 10 times apart the interquartile distance for any wavenumber) were eliminated. The resulting intensity values were mean-centered, and the z scores were calculated (correlation matrixes were used for PCA) (S. Liu et al. 2012). PCA renders two representations that provide useful information: 1) PCA bi-plot (score plot); and 2) loading plot. The PCA bi-plot depicts about how the samples distribute over the directions of maximum variability of the data. The loading plot shows the contribution of individual wavenumbers into the linear combination that form the principal component (coefficients) (Reris and Brooks 2015). PCA bi-plot was used to determine if the operating conditions (temperature and time) had an effect in modifying the chemical structure of hydro-char from the specific feedstock. If samples representing different levels of the variable studied form two well-defined clusters, then the studied variable has a real effect in the chemistry of hydro-char. On the other hand, if no separate clusters can be identified, the variable studied was assumed to not have an effect in hydro-char chemical structure. Clusters were defined using the k-means Euclidean distance as criteria (Singh et al. 2013). To identify the nature of these chemical modifications, the principal component that scatters the clusters, was decomposed into its constituent wavenumbers, and the value of the coefficients are shown as the loading plot. To determine which wavenumbers have the largest coefficients (in absolute number), meaning the largest contribution in the principal component that scatter the data, a threshold value was determined between 2200–1800 cm^{-1}. The wavenumbers with coefficients at larger absolute value that those for the threshold region were chosen to be the most important ones in defining the principal component, and therefore responsible for the chemical modifications captured in the PCA bi-plot.

7.3 Results and Discussion

7.3.1 Feedstock composition

Characterization of all feedstocks including pH, dry solids content, ash content, elemental composition, and the corresponding HHVs for the raw feedstocks are summarized in Table 7.2. All feedstocks had high water content (above 65%). Feedstocks can be classified in two groups based on their ash content. “Low processed wastes” — food waste, pomaces and stillage — present lower ash content (<10 wt%) and “high processed wastes” — manure, waste activated sludge and yogurt whey — with ash content between 30–55 wt%. Higher ash content was mainly at the expense of carbon content as determined by elemental analysis (Table 7.2) and therefore, had a negative effect on the HHV, ranging between 6 to 12 MJ/kg, for high processed wastes and between 18 to 23 MJ/kg, for low processed wastes.

Table 7.2. Characterization of all feedstocks. Percentage of dry solids in the feedstocks and percentages (on a dry weight basis) of ash, carbon, nitrogen, hydrogen, and oxygen. Higher heating values (HHV) are given as MJ/kg. Values represent the mean of three replicates ± standard deviation.

	pH	**Dry solids**	**Ash**	**C**	**N**	**H**	**O**	**HHV**
Manure	7.6	8.1±0.1	33.8±0.3	35.6±0.2	2.4±0.0	3.9±0.1	24.2±0.1	13.3±0.5
Waste activated sludge	7.5	1.1±0.0	38.8±0.5	30.9±0.3	3.9±0.2	4.2±0.2	22.2±0.4	12.5±0.6
Food waste	3.7	8.9±0.2	5.6±0.0	47.9±0.5	2.7±0.1	7.0±0.2	36.6±0.5	19.7±1.0
Apple pomace	4.0	28.6±0.6	1.7±0.6	48.1±0.5	1.1±0.0	6.6±0.2	42.6±0.3	18.0±0.9
Red wine pomace	4.1	34.5±0.8	9.6±0.3	50.5±0.4	2.7±0.2	5.7±0.2	31.6±0.7	19.6±0.9
Whiskey stillage	3.8	16.6±0.1	3.7±0.2	46.9±0.1	4.1±0.2	6.5±0.0	38.8±0.1	18.3±0.7
Yogurt whey	3.9	6.2±0.1	54.1±0.4	19.8±0.1	0.7±0.0	2.6±0.1	22.7±0.0	6.3±0.2
Olive oil pomace	5.1	32.2±0.2	3.9±0.7	56.1±0.3	2.5±0.0	7.1±0.1	31.5±0.2	23.2±1.1

7.3.2 FTIR spectral signature of raw feedstock

The FTIR spectra of all feedstocks are presented in a waterfall configuration to visualize differences in the chemical structure (Figure 7.2). The broad band at 3350 cm^{-1} presents in all spectra, but it especially significant for feedstocks related to alcoholic beverages (apple pomace, red wine pomace and whiskey stillage). This band, represents the O-H stretching vibrations of hydrogen bonded hydroxyl groups (Liu et al. 2015). Differences among apple pomace, red wine pomace and whiskey stillage, in terms of the nature of the hydrogen bonding can also be observed. While in apple pomace the maximum of the broad band was located around 3340 cm^{-1}, in the case of red wine pomace and whiskey stillage, this maximum was shifted to slightly lower wavenumbers (Figure 7.2). This shift suggests differences in the nature of hydrogen bonded hydroxyl groups (intra- vs. inter molecular hydrogen bonding at 3340 and 3290 cm^{-1}, respectively) (Abidi et al. 2014). Food waste, apple pomace, yogurt whey, and olive oil pomace have a marked aliphstic character as shown by the 2920 and 2850 cm^{-1} bands (Figure 7.2). These bands represent the asymmetric and symmetric C-H stretching vibrations for aliphatic groups (sp^3 carbon). In the case of yogurt whey, this aliphatic character is combined with an aromatic structure, as shown by the 1600 cm^{-1} band, corresponds to the aromatic skeletal C=C vibration, and the 1130–1030 cm^{-1} band, corresponds to C-H aromatic deformation (Galletti et al. 2015). Red wine pomace also shows aromatic character, but the aliphatic character is almost inexistent. Another common feature to food waste, apple pomace, and yogurt whey that distinguishes these feedstocks from the others, is the band at 1740–1750 cm^{-1}, represents carbonyl groups (Mossoba 1998, Shi and Yang 2012). Moving on to the fingerprint region of the spectra (1800–620 cm^{-1}), the lack of peak definition, but rather wide bands common to all spectra make difficult to state further chemical differences

among feedstocks by visual inspection of the spectra. However, it can be observed that manure spectra has two unique features, different from the other feedstocks: the well-defined peak at 875 cm^{-1} represents glycosidic linkages in hemicellulose (Xu et al. 2013), and the wide band at 1410 cm^{-1}, suspected to be convolution of many individual peaks (Figure 7.2). The assignments of the characteristic vibrations in the FTIR spectra of biomass are given in appendix I.

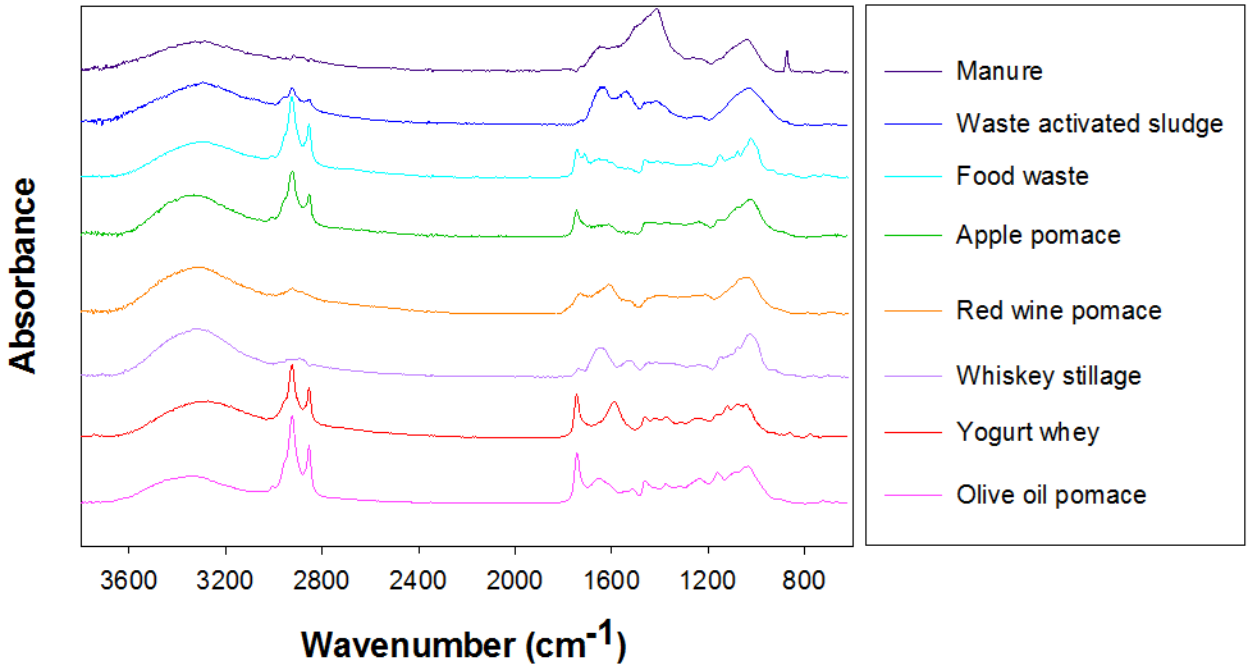

Figure 7.2. FTIR spectra for all studied feedstocks.

PCA for the FTIR spectra of all feedstocks was performed in the fingerprint region (1800–620 cm^{-1}). It was used to identify samples that possess similar chemical structures. The first three principle components (PCs) accounted for 83.4% of the spectral variation, with the first PC (PC1), the second PC (PC2), and the third PC (PC3) explaining 35.3%, 26.9%, and 21.2% of the spectral variation, respectively. Because of the similar importance of PC2 and PC3 in the spectral variation explanation, bi-plots for both PC2 vs. PC1, and PC3 vs. PC1 were represented and shown in Figure 7.3. The analyses shows that food waste, apple pomace, and whiskey stillage share the positive

PC1 and negative PC3 quadrant in the PC1 vs. PC3 bi-plot. In addition, these three feedstocks can be clustered together, indicating that they shared common chemical structures. Interestingly, these three feedstocks present the highest oxygen content (Table 7.2). This information is valuable to make future decisions about combining wastes from these different industries for further valorization.

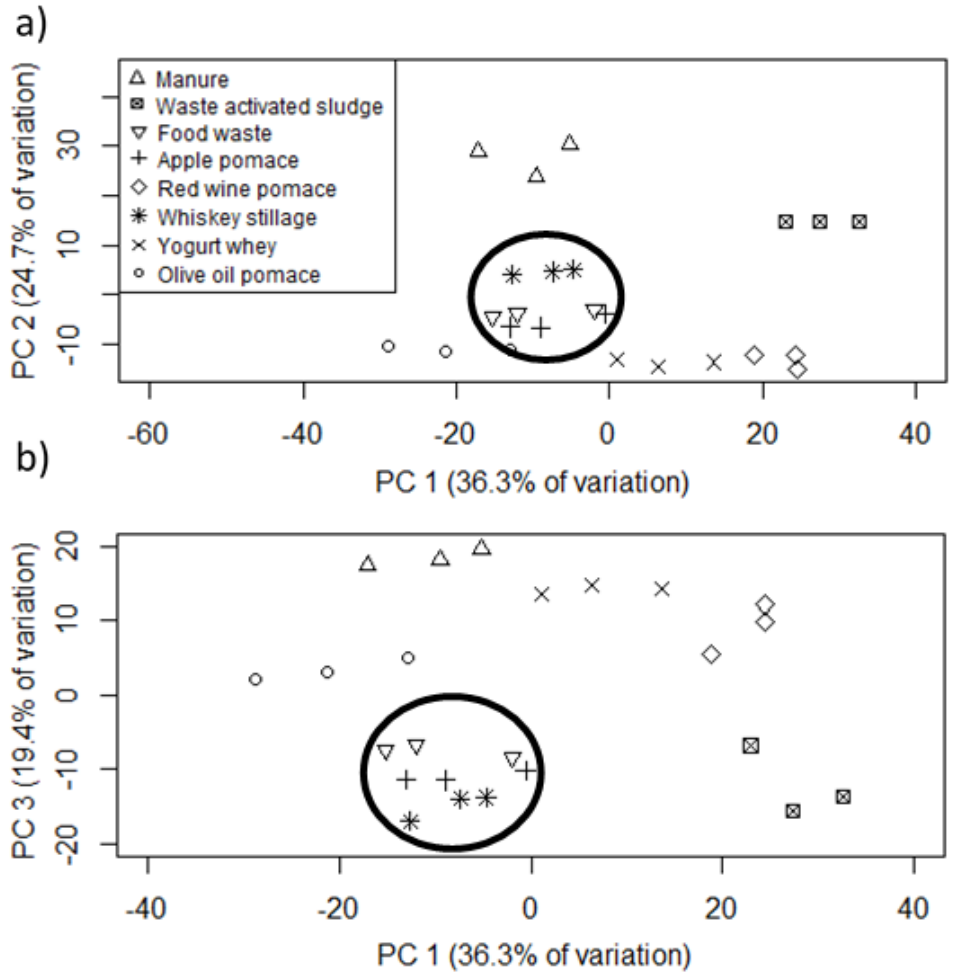

Figure 7.3. Comparison between different feedstocks using a principal component analysis (PCA) bi-plot ordination according to their FTIR-ATR spectral signature. Values on x and y axis represent the percentage of the total variation explained by a) principal components 1 (PC1) and 2 (PC2); and b) principal components 1 (PC1) and 3 (PC3)

7.3.3 Hydro-char production mass yield

The effect of reaction severity on the hydro-char mass yields is summarized in Figure 7.4 The results show that the hydro-char yield depends on the reaction temperature and reaction time for all the feedstocks studied. The one exception was yogurt whey, where the yield remains constant, around 4 wt% In general, when temperature increases from 250 to 300°C, hydro-char yields decreases. This decrease was more pronounced for the short reaction time of 5 min than for 60 min. For example, for the 5 min HTL reaction of manure and olive oil pomace, increasing the temperature from 250 to 300°C decreased the hydro-char yields by 15% and 19%, respectively. One the other hand, for the 60 min reaction, the same change in temperature decreased hydro-char yields only by 7% and 10%, respectively. In addition, the effect of reaction time on the hydro-char yield was found to be depended on the temperature and feedstock. For example, for all feedstocks other than yogurt whey, increasing the reaction time from 5 to 60 min at 250°C decreased the hydro-char yields. On the other hand, the same increase of reaction time at 300°C had either no effect or a slight positive effect on the yields of hydro-char (with the exception of waste activated sludge, where the yield decreases). This result suggest a balance between the hydrolysis of biomass, and the decomposition of bio-oils generating either char, tar or gas (Yin et al. 2010).

Similar trends for the effect of temperature and reaction time on hydro-char yields have been previously observed on the HTL of agricultural residues and cattle manure (Yin et al. 2010) An increase in HTL temperature favored biomass hydrolysis and the production of oligomers and monomers through condensation, dehydration, and decarboxylation reactions. At a temperature of 250°C or higher, cellulose, hemicellulose, and lignin degrade, being gradually transformed into bio-oil. At longer reaction times, free radical reactions (self-condensation) enhance the re-polymerization of monomers and the bio-oil decomposition, resulting in the formation of char (Yin

et al. 2010, Li et al. 2013). The use of phenol and other heterogeneous catalyst as co-reagent may decrease hydro-char yields by enhancing fragmentation reactions, stabilization of phenolic monomers, and avoiding re-polymerization (Déniel et al. 2016, Li et al. 2013). In addition, the use of CO as process gas may stabilize active intermediates in the decomposition of biomass and prevent the formation of hydro-char (Yin et al. 2010). Among feedstocks studied here, manure and waste activated sludge yielded the highest hydro-char ranging from 30 to 45 wt% and 17 to 42 wt%, respectively. In addition to their remarkably higher ash content (Table 7.2), the pH of the HTL media probably played a key role in this phenomenon. The pH of the HTL feedstock was not adjusted for this study and, therefore, was affected by the natural pH of each feedstock. The pH for the HTL media after reaction for both manure and waste activated sludge was alkaline, ranging from 8 to 8.5 and very constant with severity factors. On the other hand, the pH of the HTL media for all other feedstocks was acidic (3.5–5), resulting in remarkably lower hydro-char yields (Figure 7.4). The pH values of the HTL media after reaction are presented in Table AI-1 (appendix I). The role of pH in hydro-char mass yields was stronger than the ash content of the raw feedstocks, as demonstrated by a linear regression model (Table AI-2 in appendix I).

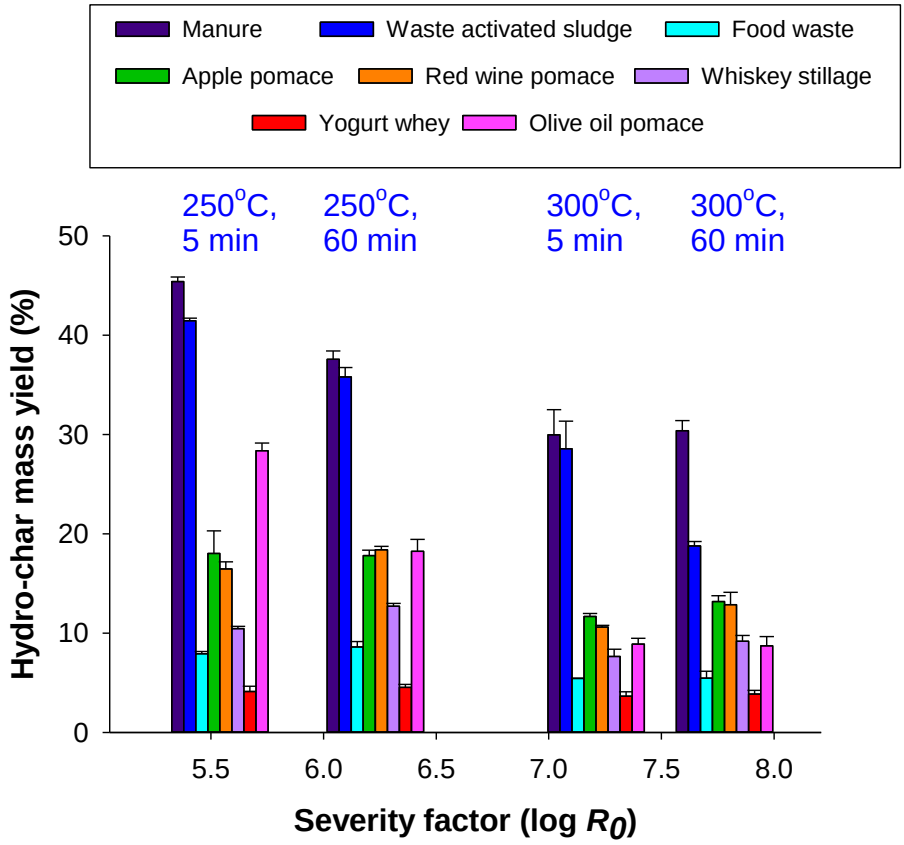

Figure 7.4. Hydro-char mass yields as a function of severity factor for studied feedstocks. Corresponding temperatures and time are documented at the top of the figure. Error bars represent the standard deviation of triplicate experiments.

7.3.4 Elemental composition and higher heating value

Elemental composition for all generated hydro-char is given in Table AI-3 (appendix I), and Table 7.3 using apple pomace as example. The results show that regardless the feedstock or the severity factor, the obtained hydro-char contained less oxygen than its raw feedstock. However, in terms of carbon content, the hydro-char generated from manure and waste activated sludge contained less carbon compared to raw feedstocks, while hydro-char generated from the other feedstocks are richer in their carbon content. This behavior can be explained by the difference in pH of the HTL media among feedstocks as discussed in section 3.3. According to Yin et al. (2010) different pH render different routes for hydro-char formation from decomposition of bio-oil. At lower pH, 5-

(hydroxymethyl) furfural (HMF), one of the main decomposition by-product of glucose, is transformed to bio-crude oil and hydro-char. On the other hand, bio-oil generated under alkaline conditions mainly contains phenol derivatives, rather than HMF. These phenols self-condense to produce hydro-char. Therefore, different degradation routes at different pH may generate hydro-char with different chemical characteristics, which can be validated by differences in carbon content. A way to use elemental information to characterize the aromaticity, cyclation, and unsaturation of carbon of the feedstocks and hydro-char is the C/H atomic ratio given in Table 3 for apple pomace and Table AI-3 (appendix I) for the rest of substrates. It is accepted that an increase in this ratio means an increase in aromaticity of the solid (Chiaberge et al. 2009). Among all feedstocks, manure and red wine pomace present the higher C/H ratio (0.75 vs. ~0.6 for the other feedstocks). This result was expected for red wine pomace considering the high load of phenol derivatives that it contains (Zacharof 2016, Sanchez-Guerrero et al. 2008). However, this ratio is considerably high for manure based on its composition (mainly cellulose) (Yin et al. 2010). In addition, the C/H ratio increased with severity factor for all hydro-char. The average increase in C/H ratio for all feedstocks ranged between 20–100%, with manure and waste activated sludge at the low end (20 and 33% increase, respectively), and whey, apple pomace, and food waste showing increase of C/H near 100%. Whiskey stillage and olive oil pomace shared a 77% increase, and red wine presented a 55% increase.

The increase in carbon content, together with the decrease in oxygen content in hydro-char upgrade this co-product to a more energy-rich material, as determined by its HHV (Figure 7.5, Table AI-4, appendix I). As observed in Figure 7.5, an increase in the severity factor positively affected the HHV of the hydro-char, with the exception of manure and waste activated sludge. Furthermore, manure and waste activated sludge yielded a hydro-char with lower energy content that the initial

biomass (-33% on average for the case of waste activated sludge). The feedstocks that produce hydro-char with higher HHV (ranging 23–32 MJ/kg) were food waste, apple pomace, red wine pomace, whiskey stillage, and olive oil pomace. These numbers are in the same order as medium/high rank coals (27 MJ/kg) (Li et al. 2013) and the bio-char obtained from pyrolysis of agricultural residues (27–30 MJ/kg) (Mohammed et al. 2015). The highest energy upgrade for the hydro-char was found for food waste, with 72, 83, 85, and 98% increment in HHV as severity factor increases. Since hydro-char is a co-product of the HTL process (aimed to produce mainly bio-crude oil), this phenomenon should be further investigated in order to maximize the total energy recovery from waste feedstocks. While lower HHV in hydro-char may suggest a better energy recovery in the oil phase, producing a valuable by-product is an advantage from the versatility perspective of HTL technology.

Table 7.3. Elemental analysis and ash content of apple pomace hydro-char generated at each reaction condition. Values are percentage on a dry weight basis and represent mean of three replicate experiments ± standard deviation.

Temperature (˚C)	**Time (min)**	**C**	**N**	**H**	**Ash**	**O**	**Atomic C/H**
Apple pomace		48.1±0.5	1.1±0.0	6.6±0.2	1.7±0.6	42.6±0.3	0.61±0.04
250	5	63.2±1.5	1.0±0.0	6.2±0.2	0.8±0.3	28.8±1.6	0.84±0.01
250	60	69.8±0.3	1.4±0.0	5.0±0.2	0.8±0.2	22.9±0.3	1.16±0.03
300	5	73.0±0.3	1.6±0.1	4.3±0.1	1.0±0.2	20.1±0.1	1.42±0.04
300	60	74.4±0.1	1.6±0.03	4.3±0.1	1.2±0.3	18.5±0.3	1.45±0.02

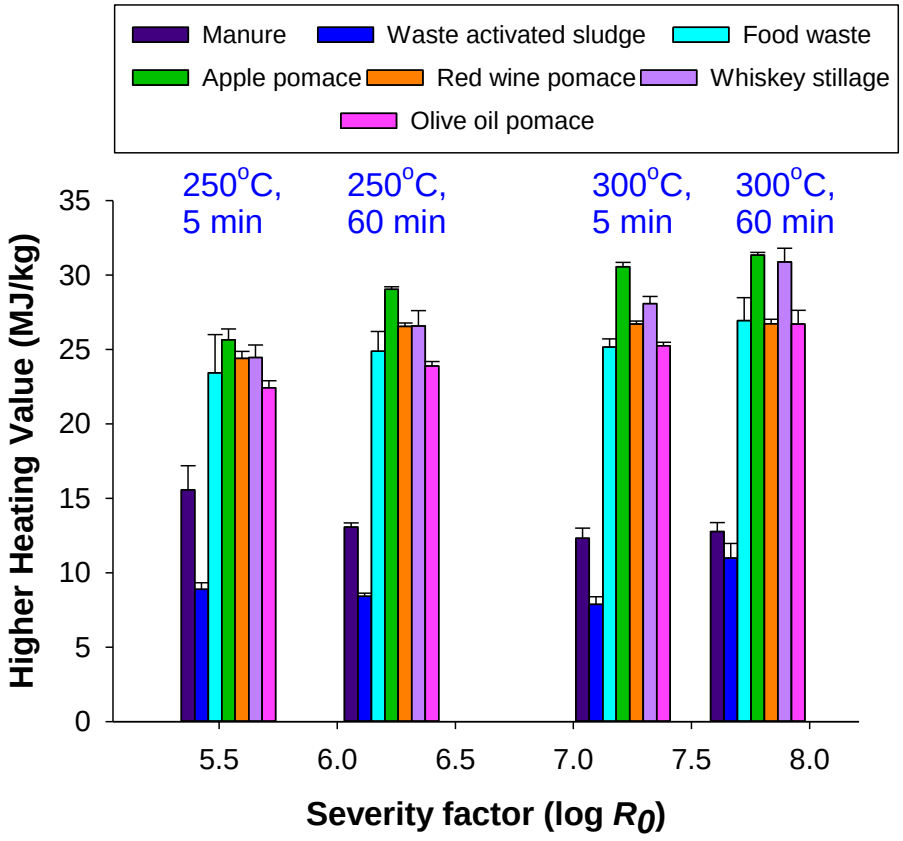

Figure 7.5. Hydro-char higher heating value as a function of severity factor for studied feedstocks. HHVs for yogurt whey hydro-chars were not given due to difficulties to determine the ash content. Corresponding temperatures and time are documented at the top of the figure. Error bars represent the standard deviation of triplicate experiments.

7.3.5 De-hydration vs. de-carboxylation reactions as ways for oxygen removal

One of the main goals of the hydrothermal liquefaction process is the removal of oxygen and other heteroatoms (mainly N from proteins, and sulfur) from the biomass to obtain a high energy dense hydrochar and bio-crude oil (Peterson et al. 2008). As shown in Dulong's equation presented in Equation 1, oxygen has a negative effect in the energy content of a material. Furthermore, the elimination of oxygen will make the percentage of carbon and hydrogen to increase in the bio-crude and hydrochar (Table 7.3), what is favorable for the energy density of the material. The

removal of oxygen from biomass occurs via condensation reactions, mainly dehydration and decarboxylation reactions (Midgett 2008). To elucidate which reaction plays a more important role in the oxygen depletion of biomass, the van Krevelen diagrams are widely used. It represents the atomic H/C ratio vs. atomic O/C ratio. Higher values of the y-axis represent reactions involving hydrogenation of the material, while lower values of the y-axis represent dehydrogenation. On the other hand, higher values of the x-axis represent oxidation processes, and lower values reduction processes. In terms of condensation reactions, lower values of atomic O/C ratio with a slight increase on atomic H/C ratio indicates decarboxylation reactions are the main path for biomass oxygen depletion (as carbon dioxide molecules). However, a decrease of both atomic H/C ratio and O/C ratio (with 2-fold higher decrease rate in H/C ratio, of in other words, the slope of van Krevelen diagram is 2), indicates de-hydration reactions (condensation reaction where oxygen is lost as water molecules) are dominant. In addition, the van Krevelen diagrams were used to compare the hydrochar obtained from the HTL of biomass with different types of coal: Lignite, sub-bituminous, bituminous, and anthracite (Kim et al. 2015).

Figure 7.6 shows the van Krevelen diagram for apple pomace and the hydrochar obtained after HTL at the severity factors studied as an example. Figures AI-3 to AI-8 in appendix I show the van Krevelen diagrams for the other feedstocks used in this chapter, with the exception of yogurt whey. In all of the cases, because of the diagonal direction of the atomic H/C vs. O/C ration representation at increasing severity factors, dehydration reactions appear to be the main mechanism for oxygen removal. Comparing the feedstock with the higher severity factor (7.78), the O/C ratio decreased from 0.66 to 0.18 (0.48 units), while the H/C ratio decreased from 1.64 to 0.69 (0.95 units). This indicates a rate of decrease of H/C ratio almost 2-fold higher than the decrease of O/C. This proved some decarboxylation reactions are marginal compared to de-

hydration. The fact that carbon is maintained within the hydrochar, and not lost as CO_2 in the gas phase, makes the biomass valorization under these conditions a promising process. In terms of comparing the hydrochar produced from the HTL of apple pomace with different forms of coals, the van Krevelen diagram show that the closest resemblance is with sub-bituminous coal. This type of coal accounted for 47% of the coal produced in the U.S in 2015, and it is paid at 14.63$ per short ton because of its high abundance and low heating value (U.S Energy Information Administration 2016).

For the rest of the substrates studied, Table 7.4 shows the slope of the van Krevelen diagram. Dehydration is the main oxygen depletion mechanism for food waste, and red wine pomace. For HTL of manure, activated sewage sludge, and whiskey stillage, the slopes of the van-Krevelen diagram were 0.92, 0.96, and 1.49, respectively. This reveals decarboxylation plays an important role in the HTL of these substrates. In terms of comparison with coals, red wine pomace, food waste, whiskey mash, and olive oil hydrochar generated at high severity factors resemble sub-bituminous coal. On the other hand, manure and activated sewage sludge hydrochar cannot be related to any form of coal using the van Krevelen diagram.

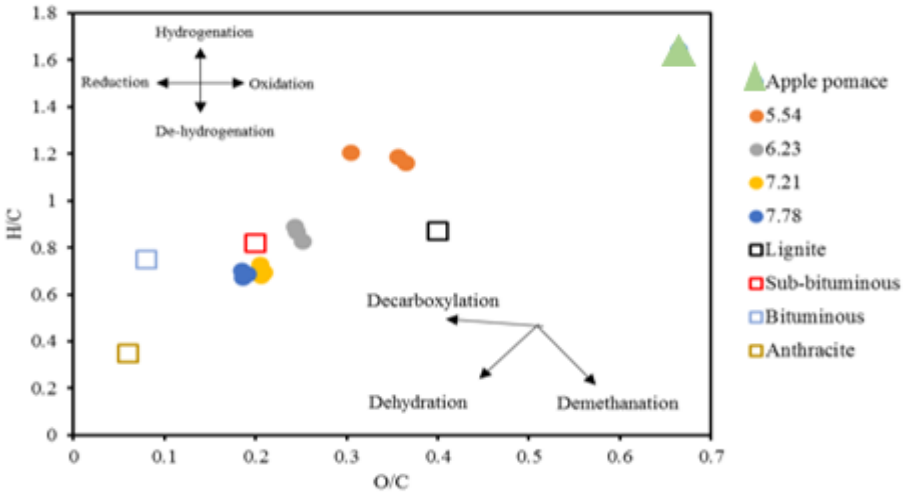

Figure 7.6. Van Krevelen diagram for apple pomace, and comparison with forms of coal

Table 7.4. Slope of van Krevelen diagrams for all the substrates studied (but whey). The slope was calculated using the data point representing the feedstock and the average data point representing the hydrochar generated at higher severity factor (7.78).

Substrate	Slope van Krevelen
Manure	0.92
Activated sewage sludge	0.96
Food waste	2.24
Apple waste	2.00
Red wine pomace	2.28
Whiskey stillage	1.49
Olive oil pomace	3.09

7.3.6 FTIR-ATR spectral signature of hydro-char

The FTIR spectra of the feedstocks and the hydro-char generated at four severity factors studied are presented in a waterfall configuration, and provided in the appendix I (Figures. AI-9 to AI-16). FTIR-ATR spectra changes for the hydro-char revealed significant changes in chemical composition of the biomass, which became more marked with the severity factor. First, the FTIR spectra of all the hydro-char showed a rapid disappearance of intra and inter molecular hydrogen bonds hydrogen bonds (3336 and 3286 cm^{-1} respectively), even at low severity factors. This is consistent with the decrease of H and O percentages in the hydro-char compared to the feedstocks (Table 7.2**,** Table 7.3, and Table AI-3 in appendix I). A common feature for food waste, apple pomace, and yogurt whey is a decrease in the 2920 and 2850 cm^{-1} bands that represents the asymmetric and symmetric C-H stretching vibrations for aliphatic groups (sp^3 carbon). This disappearance of the hydrogen bonds and the aliphatic C-H groups has been observed as well in bio-char produced from 500 °C pyrolysis of sugar cane, wattle, and hemp tree (Strezov 2012) . In addition, the appearance of the band at 1620–1680 cm^{-1} at low severity factor (corresponding to 250 °C) indicated the unsaturation of carbon to produce alkenyl C=C double bonds. The increase

in severity factor (corresponding to 300 °C) increased the aromatic character of the hydro-char as the band at 1600 cm^{-1}, that corresponds to the aromatic skeletal C=C vibration, and the band 1130–1030 cm^{-1}, that correspond to in plane C-H aromatic deformation, gain in intensity. This observation agrees with the increase in the atomic C/H ratio (Table 7.3 and Table AI-3 in appendix I). Food waste, apple pomace and yogurt whey, presented a common removal of the aldehyde and ketone carbonyl groups at low severity factors (1740 cm^{-1} band). It is interesting to note that for the majority of the feedstocks studied, the spectra of the hydro-char generated at severity factors of 5.54 and 6.23 are very similar, and different to those generated at 7.21 and 7.78 indicating temperature is the factor that affects chemical structure of hydro-char, more than reaction time.

7.3.7 Principal component analysis (PCA) to distinguish among FTIR spectra of hydro-char generated from all feedstocks

PCA for the FTIR spectra of all generated hydro-char was performed in the fingerprint region (1800–620 cm^{-1}). Figure 7.7 a shows the PCA bi-plot for all hydro-char generated from every feedstock (shape labelled) for all temperatures and reaction times (colored) studied. Three distinct clusters of data are observed. On the quadrant along negative scores for PC1 and PC2, are the spectra for the hydro-char from waste activated sludge, on the quadrant along negative scores for PC1 and positive scores for PC2 the hydro-char from manure, and the rest of the hydro-char at positive values of PC1 forming a big indivisible cluster. This clustering suggests that hydro-char from food waste, apple pomace, red wine pomace, whiskey stillage, yogurt whey, and olive oil pomace may share similar functional group properties, different from those in hydro-char from manure and waste activated sludge. In terms of application, the hydro-char from those feedstocks could potentially be combined and have common uses.

When comparing Figure 7.3 with Figure 7.7 a, feedstocks (food waste, apple pomace, red wine pomace, whiskey stillage, and yogurt whey) with different initial chemical structures converged on to a common chemical structure upon HTL processing, but diverged from manure and waste activated sludge. This convergence of hydro-char structures in the PCA bi-plot upon thermal treatment has also being reported in the pyrolysis of agricultural by-products (Liu et al. 2015). Hydro-char scattering along PC1 responded to the differences in the above explained pH dependent bio-oil degradation pathway to hydro-char. This analysis demonstrates that the hydro-char generated at HTL of manure and waste activated sludge (alkaline pH) has significant chemical differences than hydro-char from the other waste feedstocks (acid pH).

The loading plot in Figure 7.7 b indicates the key chemical differences that are responsible for clustering the samples along PC1 (that account for 66.8% of the spectral variance). In other words, wavenumbers with higher loading values (positive or negative) contribute the most to the clustering separation in the PCA bi-plot along PC1 (Figure 7.7 a). The bands responsible for separating the hydro-char generated from food waste, apple pomace, red wine pomace, whiskey stillage and yogurt whey from the hydro-char generated from manure and waste activated sludge along PC1 are 1734, 1495–1390, 1128, 927, and 871 cm^{-1} (Figure 7.7 b). The correspondence of these bands to a chemical structure can be found in Table AI-5 (appendix I). These bands denote very high differences in the cellulose (carbonyl groups and glycosidic linkages) and lignin fraction (broad band between 1495 and 1390 cm^{-1}) of the two big clusters along PC1. This observation agrees with the pH depended pathways for the hydro-char formation via 5-HMF (degradation product of cellulose and hemicellulose) or phenol derivatives (degradation product of lignin) in HTL bio-crude oil. This broad band potentially includes a lot of information about lignin chemical bonds as shown in Table A5. To extract more specific information about these differences in the

lignin fraction of the two clusters, the deconvolution of the band was attempted via the 2nd derivative processing of the spectral signal followed by vector normalization (data not shown). Examples in literature have shown this spectral signal processing technique is useful for bands deconvolution (Painter et al. 1983, Poletto and Zattera 2013). However, the 2nd derivative approach does not allow to identify the specific bonds responsible for clustering as observed in the PCA bi-plot. Therefore, we decided to use only vector normalization as discussed in Figure 7.7 a.

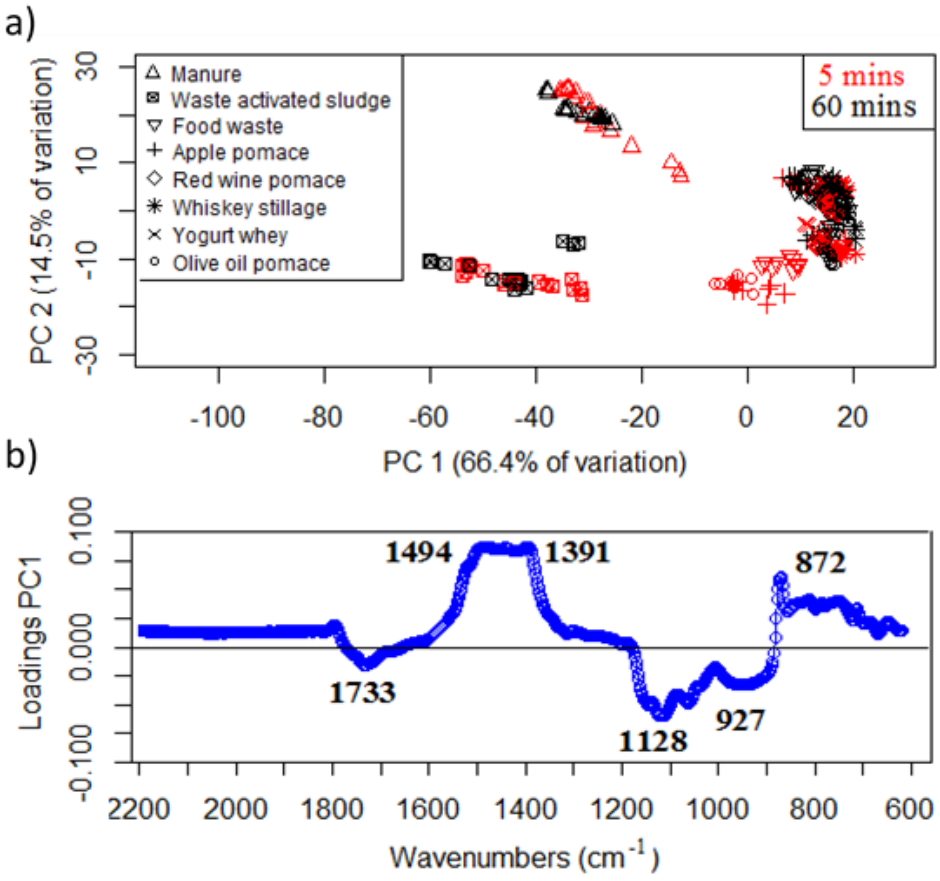

Figure 7.7. PCA for FTIR spectra of hydro-char generated from all feedstocks at all experimental conditions studied: (a) bi-plot for all FTIR spectra showing the effect of the feedstock; and (b) loading plot of PC1 vs. FTIR wavenumber showing the specific wavenumbers that contributed to the clustering

7.3.8 Principal component analysis (PCA) to distinguish among FTIR spectra of hydro-char generated at different HTL conditions

The FTIR-PCA approach allowed for a comprehensive comparison of functional groups, with spectral band evolution upon HTL conditions, and interpretation based on previous studies. With these premises, the FTIR spectra for all hydro-char generated by HTL from the different feedstocks at all thermal conditions were analyzed using PCA. Figure 7.8 showed the PCA bi-plot and loading plot for apple pomace hydro-char at 60 minutes reaction time as an example. Figures AI-17 to AI-31 in appendix I showed the bi-plots and loading plots for all other feedstocks. In the bi-plot, PCA data for each feedstock was subjected to cluster analyses to explore the effect of HTL conditions (i.e., temperature and reaction time) on chemical structure of the generated hydro-char. When different clusters were defined, a loading plot was established to explore the specific wavenumbers contributing to the cluster definition. Table 7.5 summarizes the effect of reaction temperature (i.e., 250°C and 300°C) on the chemical structure of hydro-char generated at chosen reaction times. Waste activated sludge was the only feedstock where PCA bi-plot did not provided clusters of data sharing processing conditions along any principal component. For all the hydro-char at both long and short reaction times, temperature had an effect on chemical composition (with the exception of red wine pomace at long reaction time). The PCA bi-plot for hydro-char always exhibited two clusters scattered along PC1, with negative values corresponding to low temperature and positive values corresponding to high temperature. The loading plots were analyzed to determine the wavenumbers (chemical bonds) modified with the effect of temperature.

For manure, PCA bi-plots show the influence of temperature at long and short reaction times. Loading plots reflected the numerous functional groups that were transformed by temperature at both reaction times (Table 7.5). Most of functional groups were associated with a chemical bond in the biomass (Table AI-5 in appendix I). Common to both long and short reaction times were the

transformation of alcohol groups (C-O phenolic groups at 1292 cm^{-1} and aliphatic primary alcohols at 1028 cm^{-1}) and the cleavage of glycosidic bond in the cellulose and hemicellulose fraction (870–875 cm^{-1}). For food waste, PCA suggested an increase in aromatic structures (positive band at 1506 cm^{-1} and negative band at 1160 cm^{-1}), a decrease in carbonyl groups and an increase of alcohol functional groups. Hydro-char from apple pomace showed a very clear decrease in ester groups as confirmed by the sharp negative band at 1726 cm^{-1}. For yogurt whey, the increase of HTL temperature at long reaction time, increased the aromatic content of hydro-char. Bands with positive loadings at 1500 and 1600 cm^{-1} combined with a positive score PC1 (63% data variance) for high temperature, and higher C/H values, confirmed this observation (Kline et al. 2010). HTL temperature, for 5 minutes reaction time, has an effect in the chemical structures associated with the 1155 and 1124 cm^{-1} bands (related to the skeletal structure of hemicellulose and cellulose, and the C-H deformation of aromatics) for red wine pomace, whiskey stillage, yogurt whey, and olive oil pomace.

Lastly, the effect of reaction time on the chemical structure of the hydro-char generated at both reaction temperatures was considered. Only hydro-char from whiskey stillage and olive oil pomace had their chemical structure modified by reaction time at 300 °C according to the bi-plot (data not shown). For whiskey stillage, the nature of these modifications was not possible to determine, using the loading plot. However, the loading plot for olive oil suggests that the main chemical modifications occurred in the chemical bonds corresponding to the oxygenated functional groups (1766, 1691, 1600 and 1406 cm^{-1}), and aliphatic C-H bonds (1353 and 977 cm^{-1}) as shown in Table AI-5 (appendix I). Coupling this information with the oxygen depletion shown in the elemental composition of the hydro-char with reaction time, de-oxygenation reactions from these functional groups in the hydro-char structure may occur.

Table 7.5. Effect of reaction temperature on the chemical structure of hydro-char generated from all feedstocks at long and short reaction times. The existence of the temperature effect was determined by spectra data clustering along the first principal component (PC1) in the PCA bi-plot, based on reaction temperature. Wavenumbers with higher weight in the definition of PC1 were determined based on the loading plot of this principal component, as presented in details in Figures. AI-17 to AI-31 in appendix I.

Feedstock	**Time (min)**	**Temperature affected**	**Loading plot wavenumbers (cm^{-1})**
Manure	60	Yes	1681, 1596, 1548, 1500, 1394, 1290, 1170, 1128, 1093, 1060, 1028, 872
	5	Yes	1693, 1583, 1371, 1292, 1188, 1139, 1085, 1028, 983, 870
Waste activated sludge	60	No	----------
	5	No	----------
Food waste	60	Yes	1780, 1627, 1506, 1386, 1159, 1078, 990
	5	Yes	1145, 711
Apple pomace	60	Yes	1726, 1162, 1130, 972, 660
	5	Yes	N/A
Red wine pomace	60	No	----------
	5	Yes	1803, 1716, 1652, 1159, 1124, 1083, 977, 860-734
Whiskey stillage	60	Yes	N/A
	5	Yes	1793, 1691, 1155, 1122
Yogurt whey	60	Yes	1600, 1500
	5	Yes	1577, 1481-1359, 1159-925

Olive oil pomace	60	Yes	N/A
	5	Yes	1780, 1128, 910, 723

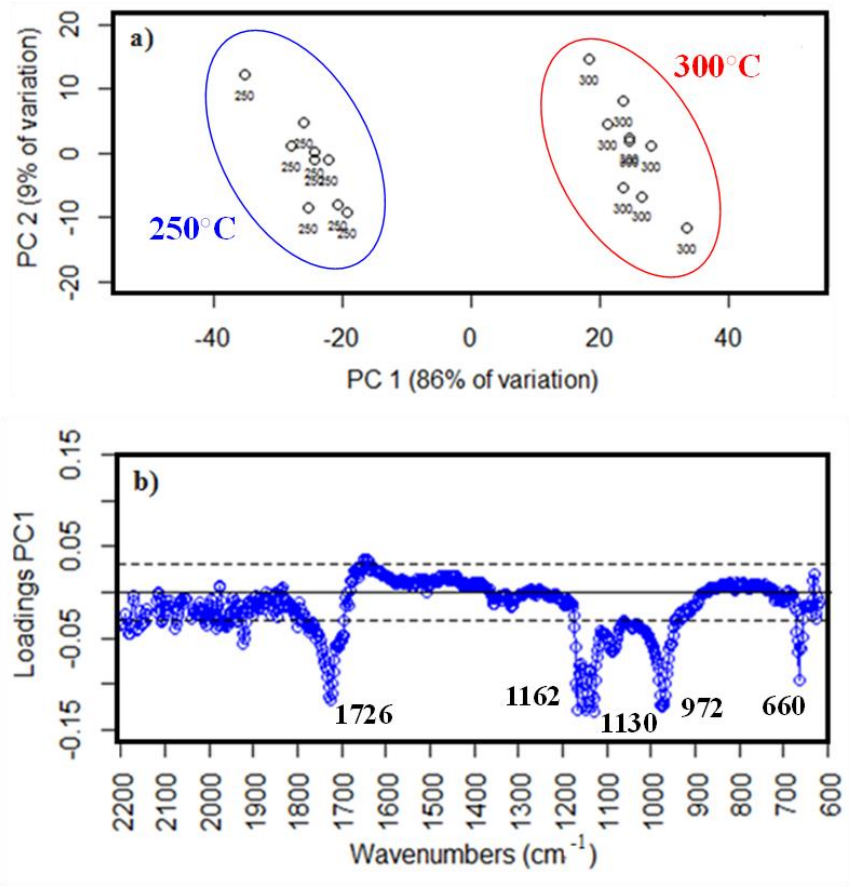

Figure 7.8. PCA for FTIR spectra of hydro-char generated from apple pomace: (a) bi-plot for all FTIR spectra of hydro-char generated at 60 minutes showing the effect of the temperature; and (b) loading plot of PC1 vs. FTIR wavenumbers showing the specific wavenumbers that contributed to the scattering provided in Table 7.5**.**

7.4 Conclusions

In this chapter, we characterized hydro-char generated as a by-product of HTL of waste biomasses, such as dairy manure, waste activated sludge, and food processing wastes. Temperature, reaction

times, and pH affected the chemical pathways of hydro-char formation, as well as its mass yields, and heating values. HTL of feedstocks with acidic pH resulted in lower yields of hydro-char compared to alkaline feedstocks. FTIR-ATR coupled with PCA revealed the effects of pH and reaction conditions on the chemical structure and functional groups present in hydro-char. This technique demonstrates that hydro-char obtained from alkaline feedstocks (e.g., manure and waste activated sludge) are chemically different from the hydro-char obtained from acidic feedstocks (i.e., food processing waste). This variation is mostly due to different decompositions phenomena of cellulose and lignin.

7.5 References

Abidi, N, L Cabrales, and C Haigler. 2014. “Changes in the Cell Wall and Cellulose Content of Developing Cotton Fibers Investigated by FTIR Spectroscopy.” *Carbohydrate Polymers* 100: 9–16.

Abu Tayeh, H, O Levy-Shalev, H Azaizeh, and C Dosoretz. 2016. “Subcritical Hydrothermal Pretreatment of Olive Mill Solid Waste for Biofuel Production.” *Bioresource Technology* 199: 164–72.

Allison, G, C Morris, E Hodgson, J Jones, M Kubacki, T Barraclough, N Yates, I Shield, A Bridgwater, and I Donnison. 2009. “Measurement of Key Compositional Parameters in Two Species of Energy Grass by Fourier Transform Infrared Spectroscopy.” *Bioresource Technology* 100 (24): 6428–33.

ASTM, Annual book of ASTM standards Volumen 11.05. 2003. “ASTM E1755-01 Standard Method for the Determination of Ash in Biomass.”

Biller, P, B Sharma, B Kunwar, and A Ross. 2015. “Hydroprocessing of Bio-Crude from Continuous Hydrothermal Liquefaction of Microalgae.” *Fuel* 159: 197–205.

Chiaberge, S, G Guglielmetti, L Montanari, M Salvalaggio, L Santolini, S Spera, and P Cesti. 2009. “Investigation of Asphaltene Chemical Structural Modification Induced by Thermal Treatments.” *Energy & Fuels* 23: 4486–95.

Chundawat, S, B Venkatesh, and B Dale. 2007. “Effect of Particle Size Based Separation of Milled Corn Stover on AFEX Pretreatment and Enzymatic Digestibility.” *Biotechnology and Bioengineering* 96 (2): 219–31.

Déniel, M, G Haarlemmer, A Roubaud, E Weiss-Hortala, and J Fages. 2016. "Energy Valorisation of Food Processing Residues and Model Compounds by Hydrothermal Liquefaction." *Renewable and Sustainable Energy Reviews* 54: 1632–52.

Ekpo, U, A Ross, M Camargo-Valero, and L Fletcher. 2016. "Influence of pH on Hydrothermal Treatment of Swine Manure: Impact on Extraction of Nitrogen and Phosphorus in Process Water." *Bioresource Technology* 214: 637–44.

Elliott, D, P Biller, A Ross, A Schmidt, and S Jones. 2015. "Hydrothermal Liquefaction of Biomass: Developments from Batch to Continuous Process." *Bioresource Technology* 178: 147–56.

Galletti, A, A D'Alessio, D Licursi, C Antonetti, G Valentini, A Galia, and N Nassi. 2015. "Midinfrared FT-IR as a Tool for Monitoring Herbaceous Biomass Composition and Its Conversion to Furfural." *Journal of Spectroscopy* 2015: 12.

Gunders, D. 2012. "Wasted: How America Is Losing Up to 40 Percent of Its Food from Farm to Fork to Landfill. Natural Resources Defense Council."

Jien, S, and C Wang. 2013. "Effects of Biochar on Soil Properties and Erosion Potential in a Highly Weathered Soil." *CATENA* 110: 225–33.

Kim, D, K Yoshikawa, and K Park. 2015. "Characteristics of Biochar Obtained by Hydrothermal Carbonization of Cellulose for Renewable Energy." *Energies* 8: 14040–48.

Kim, Y, T Kreke, N Mosier, and M Ladisch. 2014. "Severity Factor Coefficients for Subcritical Liquid Hot Water Pretreatment of Hardwood Chips." *Biotechnology and Bioengineering* 111 (2): 254–63.

Kline, L, D Hayes, A Womac, and N Labbe. 2010. "Simplified Determination of Lignin Content

in Hard and Soft Woods via UV-Spectrophotometric Analysis of Biomass Disolved in Ionic Liquids." *BioResources* 5 (3): 1366–83.

Li, C, Z Yang, D Zhou, L Zhang, S Zhang, and J Chen. 2013. "Hydrothermal Liquefaction of Desert Shrub Salix Psammophila to High Value-Added Chemicals and Hydrochar with Recycled Processing Water." *BioResources* 8 (2): 2981–97.

Liu, S, R Fu, L Zhou, and S Chen. 2012. "Application of Consensus Scoring and Principal Component Analysis for Virtual Screening against β-Secretase (BACE-1)." *PLOS ONE* 7 (6): 1–13.

Liu, Y, Z He, and M Uchimiya. 2015. "Comparison of Biochar Formation from Various Agricultural by-Products Using FTIR Spectroscopy." *Modern Applied Science* 9 (4): 246–53.

Midgett, J. 2008. "Assessing a Hydrothermal Liquefaction Process Using Biomass Feedstocks." *LSU Master's Theses* 241.

Mohammed, I, Y Abakr, F Kazi, S Yusuf, I Alshareef, and S Chin. 2015. "Pyrolysis of Napier Grass in a FIxed Bed Reactor: Effects of Operating Conditions on Product Yields and Characteristics." *BioResources* 10 (4): 6457–78.

Mossoba, M. 1998. *Spectral Methods in Food Analysis: Instrumentation and Applications*. Edited by CRC Press.

Nazem, M, and O Tavakoli. 2017. "Bio-Oil Production from Refinery Oily Sludge Using Hydrothermal Liquefaction Technology." *The Journal of Supercritical Fluids*.

Painter, P, M Starsinic, E Squires, and A Davis. 1983. "Concerning the 1600 Cm-1 Region in the IR Spectrum of Coal." *Fuel* 62.

Peterson, A, F Vogel, R Lachance, M Fröling, M Antal, Jr., and J Tester. 2008. "Thermochemical

Biofuel Production in Hydrothermal Media: A Review of Sub- and Supercritical Water Technologies." *Energy & Environmental Science* 1 (1): 32.

Poletto, M, and A.J Zattera. 2013. "Materials Produced from Plant Biomass: Part III: Degradation Kinetics and Hydrogen Bonding in Lignin." *Materials Research* 16 (5): 1065–70.

Posmanik, R., D.A. Cantero, A. Malkani, D.L. Sills, and J.W. Tester. 2017. "Biomass Conversion to Bio-Oil Using Sub-Critical Water: Study of Model Compounds for Food Processing Waste." *The Journal of Supercritical Fluids* 119: 26–35.

Qian, L, S Wang, and P Savage. 2017. "Hydrothermal Liquefaction of Sewage Sludge under Isothermal and Fast Conditions." *Bioresource Technology*.

Reris, R, and J Brooks. 2015. "Principal Component Analysis and Optimization: A Tutorial." *14th INFORMS Computing Society Conference*, 212–25.

Rogalinski, T, T Ingram, and G Brunner. 2008. "Hydrolysis of Lignocellulosic Biomass in Water under Elevated Temperatures and Pressures." *The Journal of Supercritical Fluids* 47 (1): 54–63.

Sanchez Guerrero, M, J Sineiro Torres, and M Nunez. 2008. "Extraction of Polyphenols from White Distilled Grape Pomace: Optimization and Modelling." *Bioresource Technology* 99: 1311–18.

Shi, J, and Q Yang. 2012. "The Structural Changes of the Bagasses Hemicellulose during the Cooking Proces Involving Active Oxygen and Solid Alkali." *Carbohydrate Research* 359 (0): 65–69.

Sim, S.F, M Mohamed, N.A Lu, M.S Sarman, and S.N Samsudin. 2012. "Computer-Assisted Analysis of Fourier Transform Infrared (FTIR) Spectra for Characterization of Various

Treated and Untreated Agriculture Biomass." *BioResources* 7 (4): 5367–80.

Singh, A, A Yadav, and A Rana. 2013. "K-Means with Three Different Distance Metrics." *International Journal of Computer Applications* 67 (10): 13–17.

Strezov, V. 2012. "System Approach to Biomass Pyrolysis: Product Characterisation." In *The Third International Conference on Bioenvironment, Biodiversity, and Renewable Energies*.

Tekin, K, S Karagöz, and S Bektaş. 2014. "A Review of Hydrothermal Biomass Processing." *Renewable and Sustainable Energy Reviews* 40: 673–87.

Tuck, C, E Perez, I Horvath, R Sheldon, and M Poliakoff. 2012. "Valorization of Biomass: Deriving More Value from Waste." *Science* 337: 695–99.

U.S Energy Information Administration, eia. 2016. "Coal Explained. Coal Prices and Outlook."

United States Department of Agriculture, USDA. 2000. "Manure Nutrients Relative to the Capacity of Cropland and Pastureland to Assimilate Nutrients: Spatial and Temporal Trends for the United States."

United States Environmental Protection Agency, EPA. 2014. "Advancing Sustainable Materials Management: Facts and Figures."

Vardon, D, B Sharma, J Scott, G Yu, Z Wang, L Schideman, Y Zhang, and T Strathmann. 2011. "Chemical Properties of Biocrude Oil from the Hydrothermal Liquefaction of Spirulina Algae, Swine Manure, and Digested Anaerobic Sludge." *Bioresource Technology* 102 (17): 8295–8303.

Xu, F, J Yu, T Tesso, F Dowell, and D Wang. 2013. "Qualitative and Quantitative Analysis of Lignocellulosic Biomass Using Infrared Techniques: A Mini-Review." *Applied Energy* 104: 801–9.

Yin, S, R Dolan, M Harris, and Z Tan. 2010. “Subcritical Hydrothermal Liquefaction of Cattle Manure to Bio-Oil: Effects of Conversion Parameters on Bio-Oil Yield and Characterization of Bio-Oil.” *Bioresource Technology* 101 (10): 3657–64.

Zacharof, M. 2016. “Grape Winery Waste as Feedstock for Bioconversions: Applying the Biorefinery Concept.” *Waste Biomass Valorization*, 1–15.

CHAPTER VIII

A COMPREHENSIVE STUDY ON THE EFFECT OF HYDROTHERMAL LIQUEFACTION (HTL) REACTION CONDITIONS AND FEEDSTOCKS CHARACTERISTICS ON THE MASS AND ENERGY DISTRIBUTION TOWARDS HTL PHASES, AND PHYSICO-CHEMICAL CHARACTERIZATION OF BIO-CRUDE OIL

8.1 Introduction

We live in a time where globalization has brought unprecedented levels of development never seen before in human history, where people have more access to resources (water, food, and energy) than ever before. This development, together with the increase in population creates new challenges in terms of food security, water supply, energy demand, and intensive generation of waste streams (Mortensen et al. 2011). Research in sustainability is aiming for a technology that can offer a comprehensive solution for these present and future world challenges.

Waste biomass is a widely distributed resource produced at high steady rates. The Green Chemistry boom in the early 1990s emphasized waste remediation and prevention strategies. However, organic waste generated from dairy and food industries, and municipal water treatment plants contains high value chemicals and elements: carbon sources (carboxylic acids, carbohydrates), nitrogen sources (ammonia, proteins), lipids, phosphorous, minerals, metals, etc. (Zacharof 2016, Tekin 2015). Therefore, the projection for the next decades is that waste management strategies will focus on chemicals recovery, energy generation (drop-in transportation fuels), production of synthetic materials, and food (human and non-human) (Pedras et al. 2017, Tuck et al. 2012).

Organic waste from dairy and food industries has high water content. Therefore, conventional technologies for waste management present environmental and energy efficiency challenges. Landfilling this waste, or use it as soil remediation or fertilizer has the risk associated to run-offs to water bodies and their eutrophication (Verma et al. 2012). Combustion and pyrolysis technologies require prior drying of the substrate (Déniel et al. 2016), with the enthalpy penalization associated with the latent heat of vaporization of water. Hydrothermal liquefaction (HTL) is a promising technology to enhance chemical transformation of organic waste into liquid fuels and platform chemicals such as 5-HMF, lactic acid, succinic acid, levulinic acid, etc, included in the "top 10" biobased products from biorefinery carbohydrates by the US Department of Energy (Bozell and Petersen 2010). HTL uses the special characteristics of hot pressurized liquid water at subcritical conditions as reaction medium. At temperatures above 250˚C and below critical temperature, liquid water can act as an acid-base catalyst (as the ionic product increases 3 orders of magnitude under these conditions), can dissolve organic molecules (decrease of dielectric constant), and decrease mass transfer limitations in heterogenous chemical reactions (decrease of density and viscosity) (Peterson et al. 2008). Four phases are produced in the HTL process of organic wastes: hydro-char, bio-crude oil, aqueous phase, and gas (Tekin et al. 2014). Research has traditionally focused on the influence of reaction features (temperature, reaction time, pH, pressure, process gas, water to biomass ratio, catalyst) on the yield and nature of bio-crude oil (Yin et al. 2010, Tekin 2015). HTL has been used in a wide range of model and real substrates: carbohydrates, lignin, proteins, fatty acids (Posmanik et al. 2017), swine manure, cattle manure, algae, digested anaerobic sludge (Yin et al. 2010, Vardon et al. 2011), olive seeds (Tekin 2015), cornelian cherry stones (Akalin et al. 2012), waste water from paper industry (Sugano et al. 2008), fish meat (Yoshida et al. 1999), woody biomass (Tekin et al. 2012), and agricultural residues (Toor

et al. 2011). The research in this chapter studied the HTL process on feedstocks that, to the best of our knowledge, have not been valorized using this technology.

Bio-crude oil is a complex mixture of molecules (aliphatic and cyclic compounds, aromatic and phenolic derivatives, esters, nitrogen ring structures, carboxylic acids, etc.) obtained from the decarboxylation, reforming, dehydration, deamination, solvolysis, and depolymerization of carbohydrates, lignin, proteins, and lipids constituent of the biomass (Akhtar and Amin 2011) (Toor et al. 2011, Elliott et al. 2015). This high compositional complexity is a burden for its use as drop-in fuel. Compared to commercial gasoline and diesel, bio-crude oil presents higher heteroatoms content, higher acidity, and higher viscosity (10-10,000-fold) (Ramirez et al. 2015 Xiu et al. 2010). In addition, it is highly corrosive and can polymerize under engine operation conditions, affecting the combustion performance (Vardon et al. 2011). Therefore, research has focused in the upgrade of these bio-crude oils to decrease heteroatoms content through hydrodeoxygenation, catalytic cracking on noble metals supported in ceramic catalyst, such as zeolites, and esterification (Mortensen et al. 2011, Choudhary and Philips 2011, Ramirez et al. 2015).

Feedstocks obtained from the dairy industry (manure and whey), food industry (food waste, apple pomace, wine pomace, olive oil pomace, and whiskey stillage) and from municipal water treatment plants were used in this chapter. These substrates were chosen for their high moisture content, increasing production volumes (what poses a management challenge to the generating industry), local availability, potential for environmentally harm if miss-handled, and high potential for valorization towards bio-crude oils and platform chemicals. The primary focus of the research in this chapter is to examine and compare the influence of HTL temperature, reaction time, and substrates characteristics (pH, ash content) in the feedstock carbon pathway towards the different

phases obtained in HTL, their elemental composition, energy recovery, and higher heating value. A second objective of this chapter is to assess the quality of the different phases obtained from the HTL of the wide variety of feedstocks. Gas Chromatography Mass Spectroscopy (GC-MS) and thermo-gravimetric analysis (TGA) were performed to determine the distribution of low-boiling molecules obtained in bio-crude oils. Fourier Transform Infrared (FTIR) was used for the analysis of the functionalities in bio-crude oils. The analysis of the aqueous phase was completed using High Performance Liquid Chromatography (HPLC).

The information on production yields and quality of the different phases obtained from hydrothermal liquefaction of individual feedstocks have the potential to be used as a starting point to design organic waste blends. These blends will generate a more consistent feedstock with the potential to yield a consistent product distribution and quality, helping to overcome the variability associated with the high seasonal generation of some of the organic wastes.

8.2 Materials and methods

8.2.1 Feedstocks sources and characterization

Feedstocks used in the research of this chapter are representative of the organic waste generated by the dairy and food industries, and municipal water treatment plants. Dairy manure digestate was provided by the anaerobic digester of Sunnyside dairy farm (Scipio Center, NY). Waste activated sludge was collected from the municipal anaerobic digester of a wastewater treatment facility (Ithaca, NY). Carbohydrate rich food waste (15.4 wt% fruits, 47.1 wt%. vegetables, and 37.5 wt% grains/breads) was sorted from Cornell University dining halls (Ithaca, NY). Apple pomace (residue remaining after apple pressing to obtain the juice) was collected from Cornell

Orchards (Ithaca, NY). Niagara red wine pomace was provided by Swanbay Cellars (Alexandria Bay, NY). Whiskey stillage (residue after first distillation of the mash) was taken from Myer Farm Distillers (Ovid, NY). Yogurt whey was donated by FAGE USA Dairy Industry Inc. (Johnstown, NY). Olive oil pomace was provided by California Olive Ranch (Chico, CA).

Upon reception, all feedstocks were prepared for characterization by grinding and homogenizing in a blender. Their pH was measured using an Accumet AB150 probe (Fisher Scientific, Hampton, NH). The solid content (wt% dry solids in feedstock) was determined gravimetrically after overnight drying of a representative feedstock aliquot at 105°C. Ash content, inorganic fraction of the feedstock, was measured gravimetrically as a wt% of dry solids after 4 hours calcination at 550°C (ASTM 2003). To complete the feedstock characterization, the elemental composition (C, H, N; wt% of dry solids) was determined using a CE-440 elemental analyzer (Exeter Analytica, North Chelmsford, MA). The oxygen content was estimated by subtraction of the inorganic content and the combined C, H, and N (wt% of dry solids) to 100% (Yin et al. 2010). Other heteroatoms (as sulfur) were neglected due to their low presence in these feedstocks (Teri et al. 2014). All measurements to characterize the feedstocks were performed in triplicate.

Based on the elemental composition, the higher heating value of each feedstock was calculated using the modified Dulong's formula (Tekin et al. 2014) as given in Eq. 1.

$$HHV = 0.338 \times C + 1.428\ (H - \frac{O}{8}) \qquad \textit{Eq. (1)}$$

where HHV is the higher heating value (MJ/kg), and *C*, *H*, and *O* are the mass percentages of carbon, hydrogen, and oxygen in the solids, respectively.

All the information regarding the characterization of feedstocks has been already presented in Chapter VII (Cantero-Tubilla et al. 2017).

8.2.2 Hydrothermal liquefaction

Feedstocks were adjusted in their solid content to 4 wt% dry solids using deionized water (18.2 mΩ - cm) prior to be loaded in the reactor. Approximately 200ml of feedstock solution was loaded in the 500 ml stainless steel reactor (Model 4575 Parr Instruments Co., Moline, IL). The reactor was sealed, and the head-space was purged with N_2, before pressurizing the system to 25MPa (25 bar). A built-in control system (Model 4848 Parr Instruments Co., Moline, IL) controlled the power input to the electric heating jacket used to reach and regulate reaction temperature (250 and 300˚C). The pressure was monitored using a pressure gauge (Duro United Instruments, Northvale, NJ) and logged-in using a pressure transducer (Model 280E Setra Systems, Boxborough, MA).

After the desired reaction time (5 and 60 minutes), the content of the reactor was collected by depressurizing the system, and directing the sample through a heat exchanger designed in the outlet line of the reactor. This fraction is to be referred as "sample fraction". To maximize the collection of bio-crude oils, 100 ml of acetone were pumped inside the reactor using a high-pressure pump (Varian, PrepStar, SD1 system, Agilent Technologies, Santa Clara, CA). This second fraction ("wash fraction") was collected same way as for the sample fraction. At this point, the reactor was quenched by flowing water through the cooling coil located inside the reactor. After reaching room temperature, the reactor was depressurized, opened and the remaining content was collected. To avoid cross-contamination between experiments, the lines were washed with deionized water after the experiment was completed.

8.2.3 Experimental conditions

Temperature and reaction time were the reactor operating parameters studied in this chapter. These, together with biomass/water ratio, are the parameters with most influence in the quality and the yield of HTL products (Nazem and Tavakoli 2017). Experiments were performed at 250 and 300°C and pressures of 5.5 and 11MPa, respectively (above the vapor pressure of water at those temperatures, 4 and 8.7MPa, respectively) to maintain water in liquid phase. For each of these thermal conditions, two reaction times were chosen, 5 and 60 minutes. These reaction times referred to the duration that the reactor was maintained at the desired temperature (i.e., not including the average 15°C/min heating ramp). The slow heating ramp might increase the amount of hydro-char produced in the process (Toor et al. 2011). However, the heating ramp is difficult to avoid in laboratory-scale batch systems as pumping biomass at high pressure leads to lines clogging using HPLC pumps. As a matter of fact, biomass pumping has been reported as one of the main challenges for the research of HTL in laboratory scale (Cantero et al. 2015). On the other hand, the volume of the reactor used in this research together with the thickness of the reactor walls, made the heating rate slower than the values reported in literature with smaller reactors (Luterbacher et al. 2010) (volumes of several ml heated in sand-baths vs 500ml reactor heated with electrical heating jacket used in this chapter). Every experiment was done in triplicate. The temperature and pressure profiles for the four conditions studied in this chapter are shown in chapter VII using the experiments with apple pomace as example.

A severity factor for each experiment was calculated (*log R_0*) using Eq. 2 to assess the combine effect of temperature and time (Posmanik et al. 2017, Kim et al. 2014, Rogalinski et al. 2008).

$$logR_0 = log\left[\sum_{i=1}^{n} t_i \times exp\left(\frac{T_i - T_b}{w}\right)\right] \qquad \textit{Eq. (2)}$$

where *t* is the reaction time (min), T_i is reaction temperature (°C), T_b is the reference temperature (100 °C), *w* is a fitter parameter based on the activation energy of hemicellulose hydrolysis (14.75), and *n* is the number of measurements [23]. Table 7.1 in Chapter VII shows the value of severity factor corresponding to the conditions studied.

8.2.4 HTL phase separation

Each sample collected from the reactor consist on a mixture of solids (hydro-char), aqueous products, and bio-crude oil. These phases were separated using filtration and solvent extraction techniques, based on the different polarity of molecules. The gases from the reactor head-space were not collected.

The different samples collected from the reactor (sample fraction, wash fraction, and reactor discharge) were individually vacuum filtrated using pre-weighted filter papers (Whatman No.1) to separate the hydro-char from the liquid phase. The liquid phase from the sample fraction was collected and the volume and pH were measured. An aliquot of 20 ml was transferred to a separatory funnel to separate the bio-crude oil from the aqueous phase. Moderately polar solvent dimethyl chloride (DCM, Sigma Aldrich) and deionized water were added to the funnel at equal volume. Literature reports that chlorinated solvents, specially DCM, provides the highest yields in bio-crude recovery (Qian et al. 2017). After vigorous shaken, the bottom phase (heavy oil, DCM-soluble fraction (Teri et al. 2014)) was collected in a pre-weighted Erlenmeyer beaker. At this point, ethyl acetate (EA, Sigma Aldrich) was added to the funnel (20ml), and the decanter was shaken. Ethyl acetate has lower polarity than DCM (Reichardt 1994). After phase segregation, the bottom phase in the funnel is considered the aqueous phase. It was collected and heated at 80˚C

for 2 hours to eliminate traces of DCM and EA (DCM presents some solubility in water (Donghai and Savage 2014)) and the volume was measured as preparation for further characterization. As pointed out by Barreiro et al (Barreiro et al. 2015), the contact of DCM with water-soluble compounds could have extracted them to the bio-crude oil fraction, reducing the yield of organic compounds in the aqueous phase. In addition, these water-soluble molecules diminish the quality and energy content of the bio-crude oil, by decreasing its C and H content and increasing O and N content (Donghai and Savage 2014). The remaining content of the funnel (light oil, AE-soluble fraction (Teri et al. 2014)) was combined with the DCM-soluble fraction, both containing low polar molecules produced in the HTL process, and conforming the bio-crude oil phase. Bio-crude oil was recovered by evaporation of the organic solvents, and the mass of bio-crude oil was gravimetrically measured. This step might cause the evaporation of volatile low molecular weight organic molecules, reducing the carbon balance closure (Barreiro et al. 2015). This bio-crude oil from the "sample fraction" was used for physico-chemical characterization.

The hydro-char recovered after filtration of the different samples obtained from the reactor were washed with acetone to remove adsorbed bio-crude oils (Jazrawi et al. 2013). These effluents were pooled with the wash fraction obtained from washing the reactor with acetone (as described in the previous section). The hydro-char were then dried at 105˚C, and their mass was gravimetrically determined. This hydro-char obtained from the sample fraction was used for physico-chemical characterization as discussed in chapter VII

The volume of the liquid phase obtained after filtration of the wash fraction, combined with the effluents of hydro-char washing, was measured, and a 20ml aliquot underwent the same procedure to separate the bio-crude oil from the aqueous phase described before. The aqueous phase was

discharged, and the bio-crude oil obtained with this fraction was gravimetrically measured and not further characterized.

8.2.5 Bio-crude oil characterization

The mass of bio-crude oil obtained from both the sample fraction and wash fraction was gravimetrically measured. Elemental analysis (C, H, N; wt% of dry bio-crude) of the bio-crude oil was obtained only from the sample fraction, and used as the standard oil composition for all the collected fractions. We considered this phase to better represent the characteristics of the bio-crude oil formed in the HTL process, as, unlike the bio-crude oil from wash fractions, it was not being in contact with acetone at the conditions of the reaction. It is not clear if this interaction modified the characteristics of the bio-crude oil in the wash fraction. The elemental analysis was conducted using a CE-440 elemental analyzer (Exeter Analytica, North Chelmsford, MA). Oxygen content was determined by mass difference (Barreiro et al. 2015). Other heteroatoms (as sulfur) were neglected as they represent less than 1wt% of the bio-crude elemental composition (Luo et al. 2016, Toor et al. 2011, Ramirez et al. 2015, Biller and Ross 2011).

The carbon yield (wt%) of the bio-crude oil was calculated referring the mass of carbon obtained in the bio-crude oil (g) to the mass of carbon in the feedstock (g). Higher heating value (HHV, MJ/kg) was estimated using the modified Dulong's formula presented in Eq.1. The energy content in the bio-crude oil (kJ) was calculated using the HHV and the mass of bio-crude oil obtained. Referring the energy content in the bio-crude to the energy content in feedstock, the energy recovery in bio-crude oil (%) was calculated (Qian et al. 2017).

The physico-chemical characterization of the bio-crude oil obtained from the sample fraction was performed using Fourier Transform Infrared (FTIR) to study the functional group composition, thermogravimetric analysis (TGA) and Gas Chromatography (GC) coupled with Mass Spectrometry (MS) to separate and determine low-boiling point compounds present in the bio-crude oil.

FTIR spectra was collected using a Bruker Vertex 70 FTIR spectrometer (Bruker Optics, Billerica, Ma) in transmission mode and atmospheric compensated, between 7000 and 400 cm^{-1} wavenumbers, 2 cm^{-1} spectral resolution, and 32 scans per sample using a single bounce attenuated total reflectance (ATR) sampling accessory (MIRacle, PIKE Technologies, Madison, WI). Prior to spectra measurement, background scans were collected. A drop of bio-crude oil dissolved in DCM was evaporated on the ZnSe crystal and the resulting sample thin film was pressed against the crystal for spectral measurement. The resulting spectra was cut to remove wavenumbers above 4000 cm^{-1} and below 620 cm^{-1}, baseline corrected, vector normalized using OPUS (Bruker Optics, Billerica, Ma) software package.

For GC-MS analysis, the bio-crude oil was dissolved in DCM as this solvent has been widely use for the GC-MS of bio-oil (Villadsen et al. 2012) (Donghai and Savage 2014). Agilent 7890A gas chromatograph with an Agilent 19091S-433 column (30 m x 250 µm x 0.25 µm) and Agilent 5975C VL MSD mass selective detector (Agilent Inc, Palo Alto, CA) was used. The sample was injected with a split ratio 10:1 and the injection port temperature was at 310 °C. The temperature program consisted of a 4 min soak at 50 °C, followed by ramps to 110 °C at 2 °C / min , hold of 3 min, and to 300 °C at 2 °C / min , and a final hold of 3 min. Helium served as the carrier gas. A mass spectral library was used to identify separated compounds.

8.2.6 Hydro-char characterization

The mass of hydro-char from the different fractions obtained from the HTL process was gravimetrically determined. The elemental composition (C, H, N, O, ash wt% dry solids), and the Higher Heating Value, was determined as described elsewhere (Cantero-Tubilla et al. 2017). The energy content of the hydro-char (kJ) and energy of the feedstock recovered in the hydro-char (%) was calculated as explained above.

The physico-chemical characterization of the hydro-char was performed using FTIR coupled with multivariate statistics methods (Principal Components Analysis, PCA) (Cantero-Tubilla et al. 2017).

8.2.7 Aqueous phase characterization

Bio-crude oil was extracted from the liquid effluents of HTL using medium polar solvents (DCM and EA) leaving behind the so called aqueous phase, a phase with higher polarity compounds (sugars, short carboxylic acids, aldehydes, ketones, etc.) dissolved in water. This phase was characterized in terms of the Total Organic Carbon (TOC) using a Shimadzu Corporation TOC (Kyoto, Japan) with 680˚C combustion chamber, and equipped with a non-dispersive infrared (NDIR) gas analyzer. Aliquots were diluted 100-fold, and 100 pm C from sucrose solution was used as standard.

To characterize the composition of the aqueous phase, an aliquot was vortexed and filtrated using syringe filters (0.2µm Nylon membrane, VWR) before analysis in High performance liquid chromatography ,HPLC (Shimadzu,Columbia, MD) using a refractive index detector. Samples

were eluted at 0.6 mL/min through an HPX-87H Bio-Rad Aminex column (BioRad, Hercules, CA), heated to 65˚C, using 5mM sulfuric acid solution in nanopure water as the mobile phase. Standards of sugars, carboxylic acids, and carbonyl compounds were used for peak identification and quantification.

8.3 Results and discussion

8.3.1 Bulk characterization of HTL phases

8.3.1.1 Carbon yields

Hydrothermal liquefaction of biomass produces 4 phases: hydrochar, bio-crude oil, aqueous phase, and gas phase. The relative distribution of those phases is dependent of reaction parameters (temperature, pressure, headspace gas, reaction time, biomass/water ratio, agitation) and substrate characteristics (pH, composition) (Yin et al. 2010) . The versatility of the HTL process lays on the capability of modifying the distribution of phases by changing the reaction parameters. Therefore, it is one of this chapter's interest to study how reaction temperature and time affect this products distribution. The challenge to compare HTL phase distribution is to find a metric that is applicable to all the phases using the same calculation basis. Mass yield was found not be an appropriate metric. Literature reports mass yield for hydro-char referred to the dry mass of feedstock, whereas, the mass yield for bio-crude oils is reported referred to dry-ash-free substrate (d.a.f, referred to volatiles). This way of referring mass yields for these phases makes sense as bio-crude oils do not contain ash from feedstock. The different calculation basis makes inconsistent the comparison between bio-crude mass yields to hydro-char mass yields, though, this comparison has been

previously performed in literature (Eboibi et al. 2014). In addition, the mass yield of aqueous phase was difficult to calculate. Therefore, the metric used in this chapter to calculate the yield of the HTL process toward different phases was the elemental carbon yield (wt%). In the methods section we explained how we calculated the mass of the different phases and their C content (wt%). The carbon yield was calculated referring the mass of carbon in the different phases to the mass of carbon initially fed in the reactor. The C yield for the gas phase was not measured and it is the difference to 100% from the other phases' C yield.

Figure 8.1 shows the carbon yield for the HTL of manure at the 4 severity factors studied, as an example. Manure is the substrate with maximum carbon recovery in the bio-crude oil (40.8%) as well as in the hydro-char, bio-crude, and aqueous phase combined (91.5%). The increase of severity factor had a clear effect on the C distribution among the phases. At the lowest severity factor, carbon is mainly found in the hydro-char (46%) with small amounts being part of the aqueous phase and bio-crude (21.6 and 15.4, respectively). This observation agrees with previous studies reporting hydro-char as the main product for hydrothermal liquefaction of manure (Mau et al. 2016). The increase of severity factor enriched bio-crude with carbon, at the expense of hydro-char, whose carbon content decreased to 25.9% at the highest severity factor. Comparing the effect of temperature for 5 minute reaction time (severity factor 5.54 vs. 7.21) an increase in temperature striped carbon away from the hydro-char and this carbon got almost equally distributed towards the bio-crude and the aqueous phase. However, at long reaction times (comparing severity factor 6.23 vs. 7.78), the carbon striped from hydro-char was preferentially directed towards bio-crude. Comparing the effect of reaction time for 250˚C, carbon got depleted from the hydro-char and transferred mainly to bio-crude as reaction time increases. However, for 300˚C, the effect or reaction time is different, with a slight increase on hydro-char C yield at longer reaction time. This

suggested repolymerization of HTL compounds towards solids phase. Bio-crude oil got richer in carbon at the expense of aqueous phase. This indicates that longer reaction times at 300˚C has an effect in stripping away functionalities that provides polarity to molecules (hydroxyl, carbonyl groups, etc.), so more molecules can be extracted with low-polar solvents (DCM and EA). Figure 8.1 provides comprehensive information for manure, about the reaction conditions needed to favor the production of a specific phase versus the others.

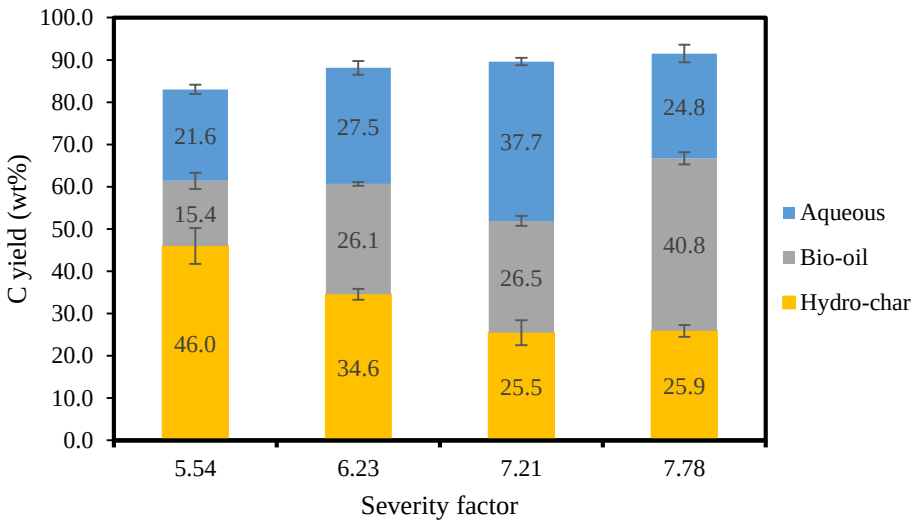

Figure 8.1. Carbon yields towards the different phases obtained from HTL of manure at all the severity factors studied. The values presented are the average of three experiments and the error bars represent the standard deviation.

The carbon yield distribution for the HTL of the other substrates is presented in Figures AII-1 to 6 in appendix II. Balances for whey were not presented, as the carbon content in the aqueous phase was somehow over-measured. Interestingly, for the other substrates the formation of gas seems to be more prominent than for manure, as less carbon is detected in the combination of bio-crude, hydro-char, and aqueous phase. C content in gas phase can get as large as 35 wt% C as observed for the red wine pomace feedstock. Experimental failure to recover carbon in hydro-char, bio-crude oil, or aqueous phase is an unlikely explanation for this result, as the C yield error measured for the triplicate experiments are small in every case. An increase in reaction time at low

temperature decreased carbon content in hydro-char for activated sewage sludge and olive oil. This carbon got mainly incorporated into the gas phase for long reaction time. On the other hand, food waste, apple pomace, red wine pomace, and whiskey stillage experienced a concentration of carbon in hydro-char at the expense of bio-crude (food waste and whiskey stillage) and aqueous phase (apple pomace and red wine pomace). For high temperature, an increase in reaction time did not significantly change the carbon content in hydro-char or aqueous phase for any of the substrates studied. This effect of reaction time on C content in bio-crude depends on the feedstock: it increased for manure, activated waste sludge, and whiskey stillage and decreased for the rest of the substrates.

The carbon yields presented in this section showed the high dynamism of HTL processes, and the opportunities that it offers in terms of favoring the production of different phases based on reaction conditions, and substrate characteristics.

8.3.1.2 Bio-crude oil yields

Focusing on the production of bio-crude oil as the main product of the HTL process, a common metric used is the mass yield referred to dry-ash-free feedstock. Figure 8.2 shows the bio-crude mass yield for HTL using manure feedstock as an example. The highest severity factor yielded the highest mass yield for bio-crude oil at 31.1 wt%. This result agrees with reported mass yield for bio-crudes obtained from manure under similar conditions (30.2% for swine manure (Vardon et al. 2011)). The mass yields for the bio-crudes obtained from the rest of the substrates are presented in Figures AII-7 to 13 in appendix II. All bio-crude mass yields range between 15-25%, with olive oil pomace showing the maximum yield between 25-35% for every severity factor. This result can be explained by the fact that substrates rich in lipids present higher conversion efficiency towards

bio-crude oils (Biller and Ross 2011). As previously observed for carbon yield (wt%) in the bio-crude, an increase in severity factor does not always lead to a higher conversion efficiency. Increase of reaction time at constant temperature seems to have a negative effect in the bio-crude mass yield when the feedstock is acidic (food waste, pomaces, and stillage). However, when the feedstock presents a basic pH (manure and activated sewage sludge), the increase of reaction time produces an increase in bio-crude mass yield. This confirms the important role played by pH in the quality and yield of products obtained in HTL process. A similar effect on the hydro-char mass yield based on feedstock pH was presented in chapter VII of this dissertation. On the other hand, the effect of temperature at constant reaction time is negligible in the mass yield of bio-crude, only playing an important role for manure feedstock.

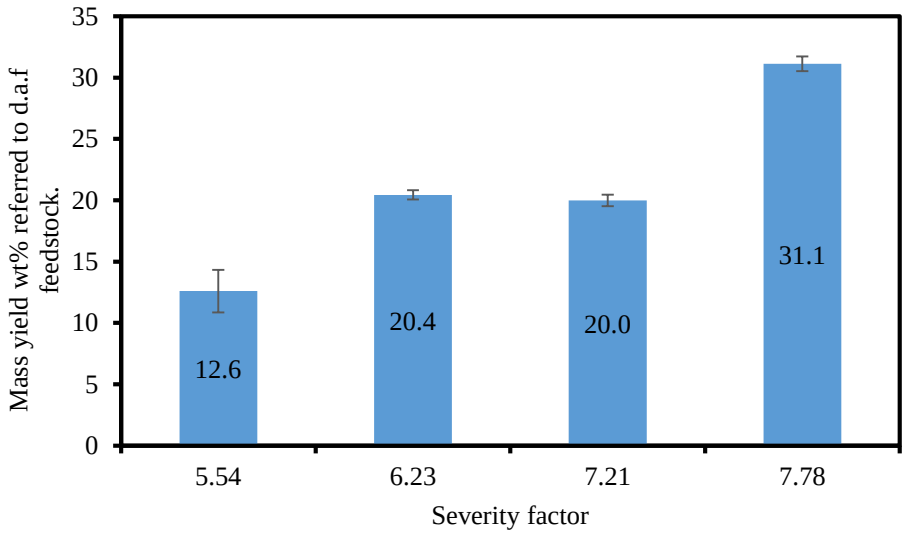

Figure 8.2. Mass yield of bio-crude oil (wt%, referred to volatiles) obtained from HTL of manure for all the severity factors studied. The values presented are the average for three experiments and the error bars represent the standard deviation.

8.3.1.3 Higher heating value and elemental composition of bio-crude oils

One of the main goals of the HTL process is the obtain a bio-crude oil that presents higher energy density than the initial feedstock, by removal of oxygen (Elliott et al. 2015). A metric used to measure the energy density of a material, based on its elemental composition, is the Higher Heating Value (HHV, MJ/kg). An increase of HHV represents an increase in the energy density of the material. The HHV of the hydro-char obtained from HTL of the studied feedstocks is addressed in chapter VII of this dissertation. The HHV of the aqueous phase could not be calculated, because of the lack of technical capabilities to provide information of the full elemental composition of this phase, apart from C content obtained from TOC. The high dilution of this phase, together with the small volumes employed in the elemental analyzer, made it impossible to go above the instrument mass sample threshold for analysis.

Figure 8.3 represents the HHV of the feedstocks studied at the lowest HTL severity factor (5.54), what corresponds to the mildest reaction conditions at 250˚C and 5 minute reaction time. In addition, these HHV values are compared with the HHV of the raw feedstocks, commercial fuels (bio-diesel, bio-ethanol, and gasoline), and bio-crudes obtained from other thermal valorization technologies for biomass (pyrolysis bio-oil before upgrading). The values of HHV obtained at higher severity factors are presented in Table AII-1 and Figures AII- 15-17. For a given feedstock, comparing between HHV values of bio-crude oils obtained at different severity factors, we observed very similar values. This indicates that the severity factor does not affect the energy quality of the bio-crude oil obtained from HTL process. This has to do with the fact that reaction conditions do not affect the elemental composition of bio-crude oil significantly. This observation was confirmed when presenting the elemental composition of bio-crudes.

Comparing the HHV values for the bio-crude oils from different feedstocks, Figure 8.3 and Figures AII-14-16 show that food waste, whiskey stillage, olive oil pomace, and activated sewage sludge bio-crudes present the highest energy density (38.8, 35.2, 33.2, and 31.2 MJ/kg at 5.54 severity factor, respectively). In terms of energy density valorization, compared to the raw feedstock, yogurt whey bio-crude is 4-fold more energy dense that the initial feedstock.

It is one of the research interests to frame the bio-crude oils produced in the HTL processes within the landscape of commercial fuels and bio-crudes obtained from other biomass valorization technologies. Figure 8.3 shows the HHV of gasoline (46.52 MJ/kg), bio-diesel (40.15 MJ/kg), bio-ethanol (29.84 MJ/kg), and pyrolysis bio-oil before upgrading (16-19 MJ/kg) (Yin et al. 2010). The bio-crude oils produced by HTL present much higher energy density than the ones produced by pyrolysis, what constitutes an advantage in favor of the HTL technology for biomass valorization towards bio-crude. HTL bio-crude oils are similar in terms of HHV values to bio-ethanol. Food waste produces the most energy dense bio-crude oil, comparable to bio-diesel fuel. The bio-crude oils obtained in this project are still far in their energy content from commercial gasoline. This can be explained by the different composition between those fuels as presented in the coming section. Upgrading the bio-crude oils from HTL could make their energy density closer to values of commercial gasoline.

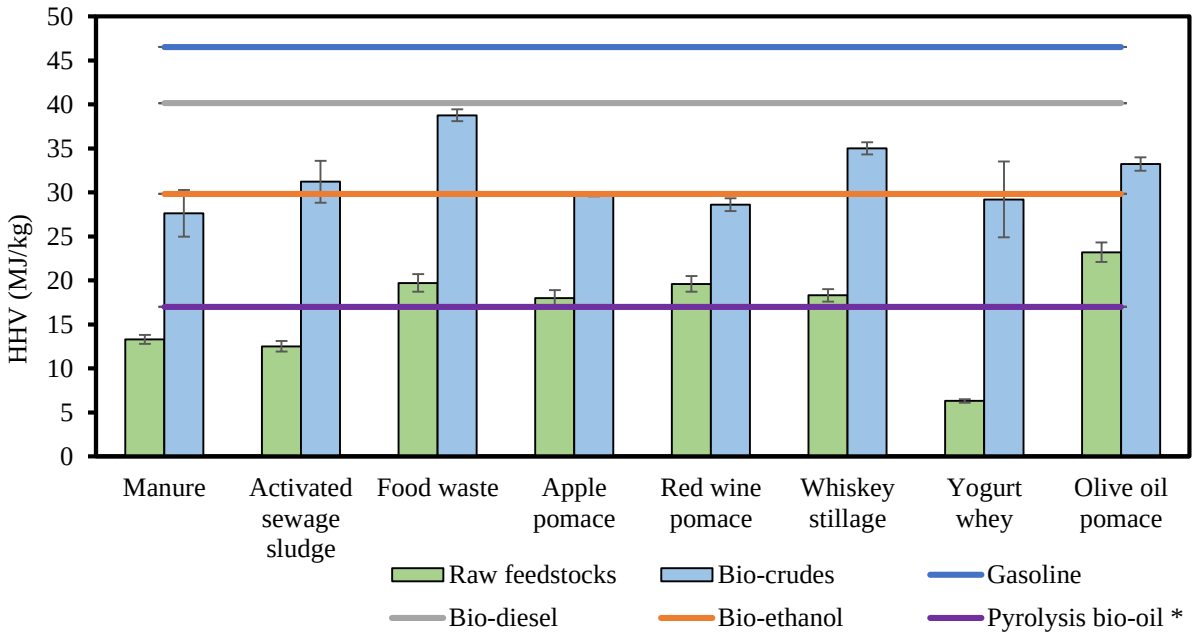

Figure 8.3. HHV (MJ/kg) for the bio-crude oils obtained from feedstocks HTL at severity factor 5.54 (250˚C and 5 minutes). The values are the average of three experiments, with error bars representing standard deviation. Also presenting the HHV of raw feedstocks, gasoline, bio-diesel, bio-ethanol and pyrolysis bio-oils from agricultural resifues* (before upgrading) for comparison purposes (Yin et al. 2010) (horizontal lines).

The calculation of HHV is based on elemental composition (Eq. 1). Therefore, to explain the differences in HHV values between HTL bio-crude oils obtained in this work, and the HHV of commercial fuels, the insight of elemental composition is presented. As mentioned for the study of HHV, reaction conditions do not have an influence in the elemental composition of the bio-crude oil obtained from HTL of the feedstocks studied in this work. Therefore, only the elemental compositions for bio-crudes obtained at low severity factor were presented.

Figure 8.4, Figure 8.5, Figure 8.6, and Figure 8.7 represent the C, H, N, and O content (wt%) of bio-crudes for 5.54 severity factor (250˚C and 5 minutes reaction time), respectively. The elemental composition of the raw feedstock is also presented for comparison purposes. The elemental compositions of bio-oils obtained at other severity factors were shown in Figures AII-18 to 29 in appendix II, as well as in Table AII-2.

Figure 8.4 and Figure 8.5 showed the concentration of carbon and hydrogen in the bio-crude oil, respectively. The carbon content of the bio-crudes laid between 60-70 wt%, more concentrated than in the feedstocks (30-50 wt%). Bio-crudes present a carbon content that is in between the values found for pyrolysis bio-oils and bio-diesel. However, C content is 10-20% lower than for gasoline, what contributes to the smaller HHV of bio-crudes compared to gasoline. Hydrogen content increased from 2-6 wt% in the raw feedstocks, to 6-11 wt%, in the bio-crude oils. These values were slightly above than for bio-oils obtained from pyrolysis.

Nitrogen has traditionally being considered as a non-desired element to be present in a fuel composition, as it contributes to higher fuel viscosity, and nitrogen oxide emissions upon combustion (Eboibi et al. 2014). However, nitrogen-enriched gasoline have been lately presented in the market, claiming that nitrogen is a good additive to fight carbon deposits in engines (McCoy 2009). The nitrogen present in the bio-crude oils from HTL comes from the protein fraction of biomass. HTL of alkaline pH feedstocks (manure and activated sewage sludge) enriched bio-crude oils with nitrogen. On the other hand, for acidic feedstocks the nitrogen content in bio-crude decreases (food waste, whiskey stillage, and olive oil pomace), or remains almost constant (apple pomace and red wine pomace), compared to raw feedstocks. The nitrogen content of bio-diesel, bio-ethanol, pyrolysis bio-oils and gasoline is very close to 0 wt%, justifying the necessity of bio-crude oil upgrading to decrease nitrogen content.

With respect to the oxygen content, one of the goals of the HTL process is to leach oxygen out of the biomass, contributing to produce a higher energy density bio-crude. Figure 8.7 showed the decrease in oxygen content of the bio-crude with respect to the raw feedstock, for all feedstocks. However, it was found that oxygen depletion under HTL highly depends on the type of substrate. Manure and activated sewage sludge only show a slight de-oxygenation towards bio-crude. On the

other hand, HTL is very efficient for biomass oxygen removal for food waste, apple pomace, red wine pomace, whiskey stillage, and olive oil pomace. Without detailed information about the composition of the feedstocks (in terms of lipids, carbohydrates, and protein content), these results suggest that acid pH of the feedstock positively contributes to the removal of oxygen from biomass under HTL. However, the oxygen content remains between 10-25 wt% of the bio-crude elemental composition. These values need to be brought down through upgrading processes previously discussed, in order to convert these bio-crudes into gasoline and drop-in fuels in general (presenting almost 0 wt% oxygen).

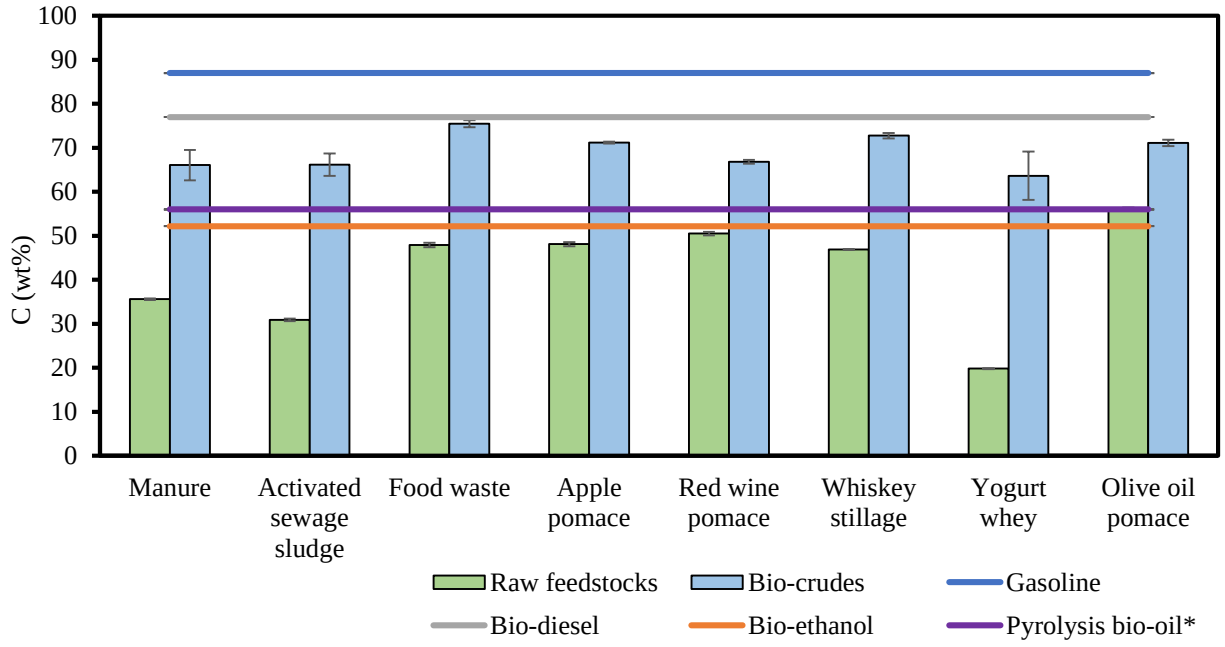

Figure 8.4. C content (wt%) for the bio-crude oils obtained from feedstocks HTL at severity factor 5.54 (250˚C and 5 minutes). The values are the average of three experiments, with error bars representing standard deviation. Also presenting the C content of raw feedstocks, gasoline, bio-diesel, bio-ethanol and pyrolysis bio-oils from agricultural residues* (before upgrading) for comparison purposes (Yin et al. 2010) (horizontal lines).

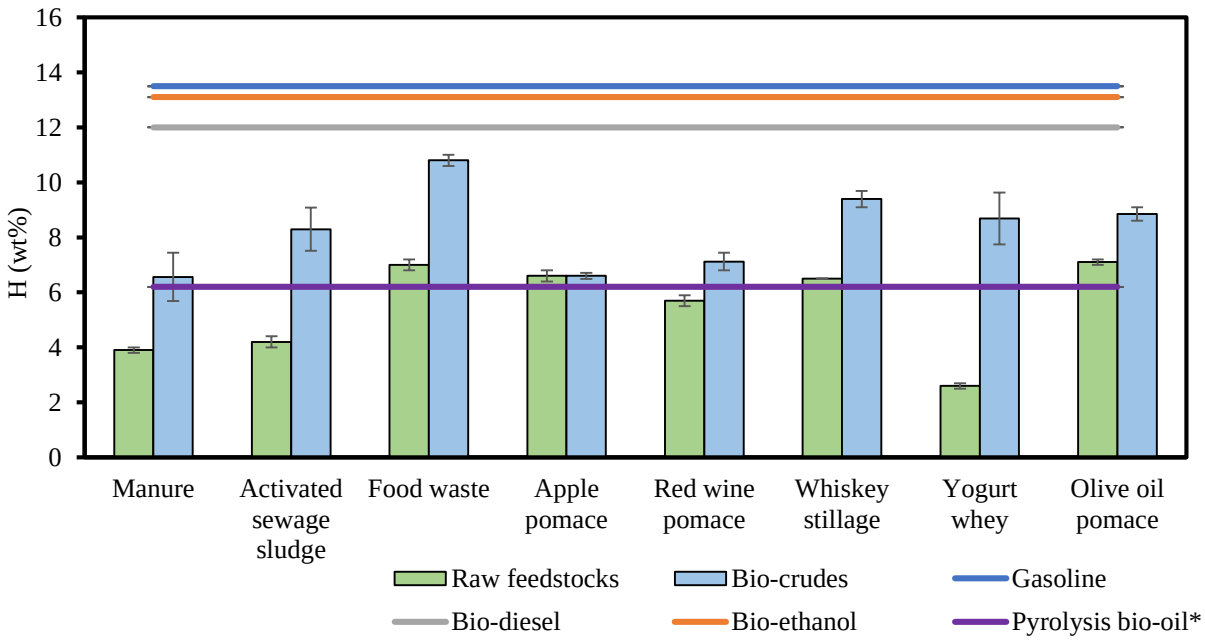

Figure 8.5. H content (wt%) for the bio-crude oils obtained from feedstocks HTL at severity factor 5.54 (250˚C and 5 minutes). The values are the average of three experiments, with error bars representing standard deviation. Also presenting the H content of raw feedstocks, gasoline, bio-diesel, bio-ethanol and pyrolysis bio-oils from agricultural residues* (before upgrading) for comparison purposes (Yin et al. 2010) (horizontal lines).

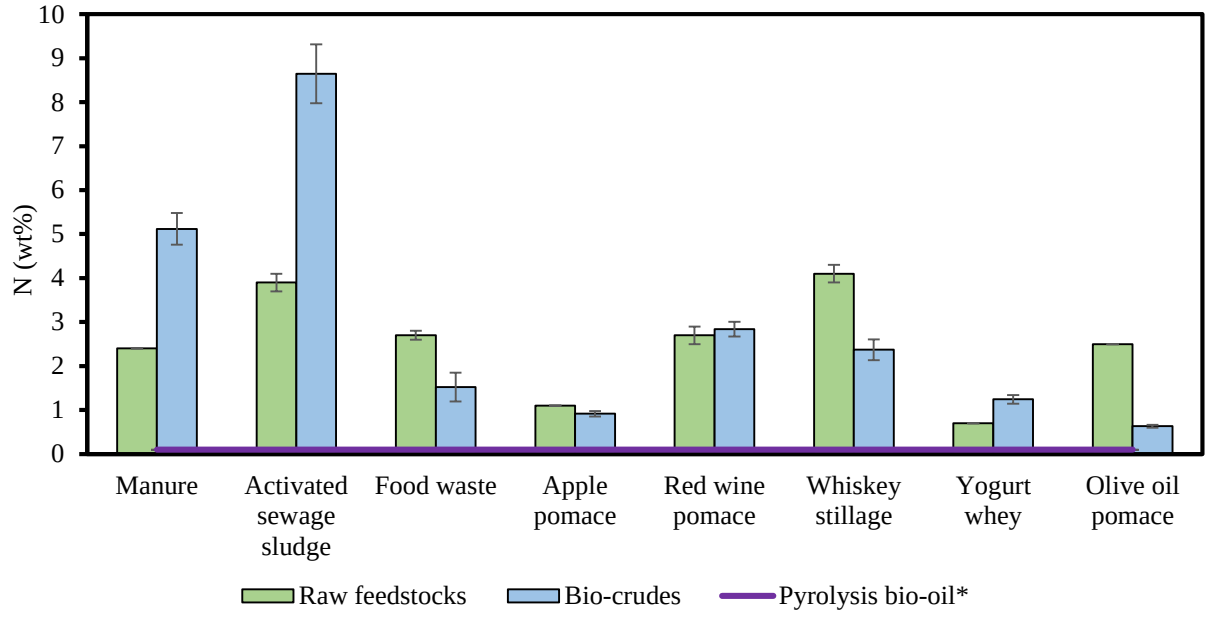

Figure 8.6. N content (wt%) for the bio-crude oils obtained from feedstocks HTL at severity factor 5.54 (250˚C and 5 minutes). The values are the average of three experiments, with error bars representing standard deviation. Also presenting the O content of raw feedstocks, gasoline, bio-diesel, bio-ethanol and pyrolysis bio-oils from agricultural residues* (before upgrading) for comparison purposes (Yin et al. 2010) (horizontal lines). Gasoline, bio-diesel, and bio-ethanol contains 0 wt% N.

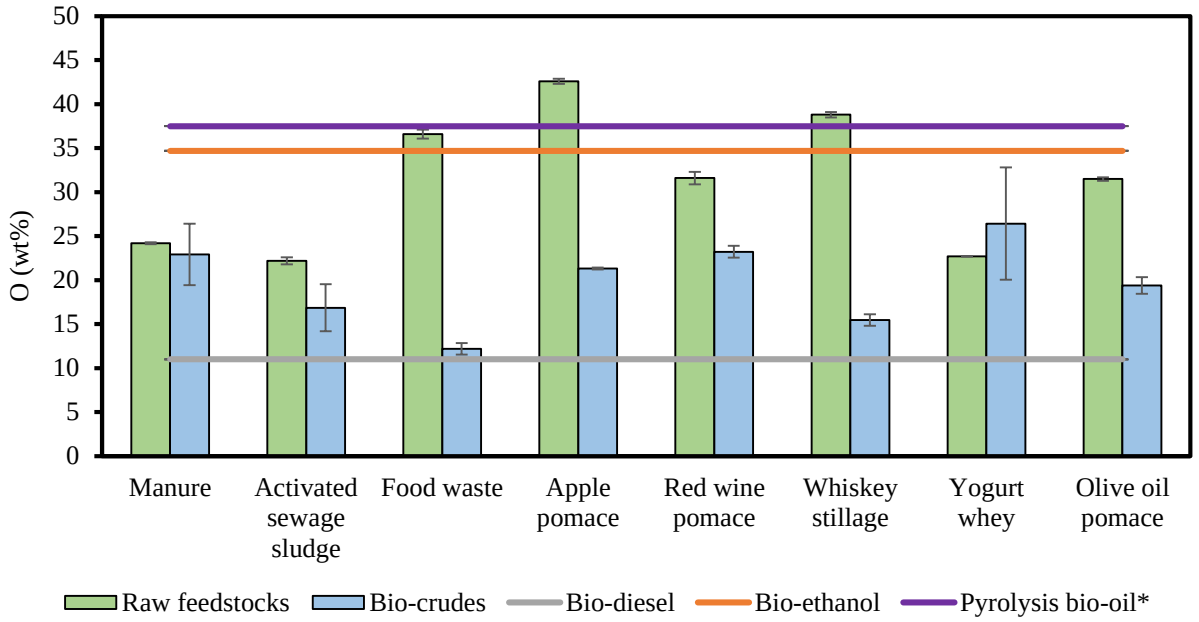

Figure 8.7. O content (wt%) for the bio-crude oils obtained from feedstocks HTL at severity factor 5.54 (250˚C and 5 minutes). The values are the average of three experiments, with error bars representing standard deviation. Also presenting the N content of raw feedstocks, gasoline, bio-diesel, bio-ethanol and pyrolysis bio-oils from agricultural residues* (before upgrading) for comparison purposes (Yin et al. 2010) (horizontal lines). Gasoline and bio-diesel contain 0 wt% O.

As introduced in chapter VII, the van Krevelen diagram provides information about mechanisms of de-oxygenation, by presenting the atomic ratios H/C vs. O/C. The representation of the van Krevelen diagrams for all the severity factor studied for each substrate reveals that the relative importance of de-hydration and de-carboxylation reactions, as the main mechanisms for substrate de-oxygenation, is highly dependent on the substrate and not so much on the reaction conditions. As shown in Figure 8.8a, apple pomace showed a combination of both condensation mechanisms, with a preference for de-hydration, as the slope of the van Krevelen diagram has a value of 1.2 (2 is the slope value for only de-hydration condensation mechanisms). On the other hand, the other substrates present a preference for de-carboxylation as condensation mechanism, as shown for manure as an example in Figure 8.8b.

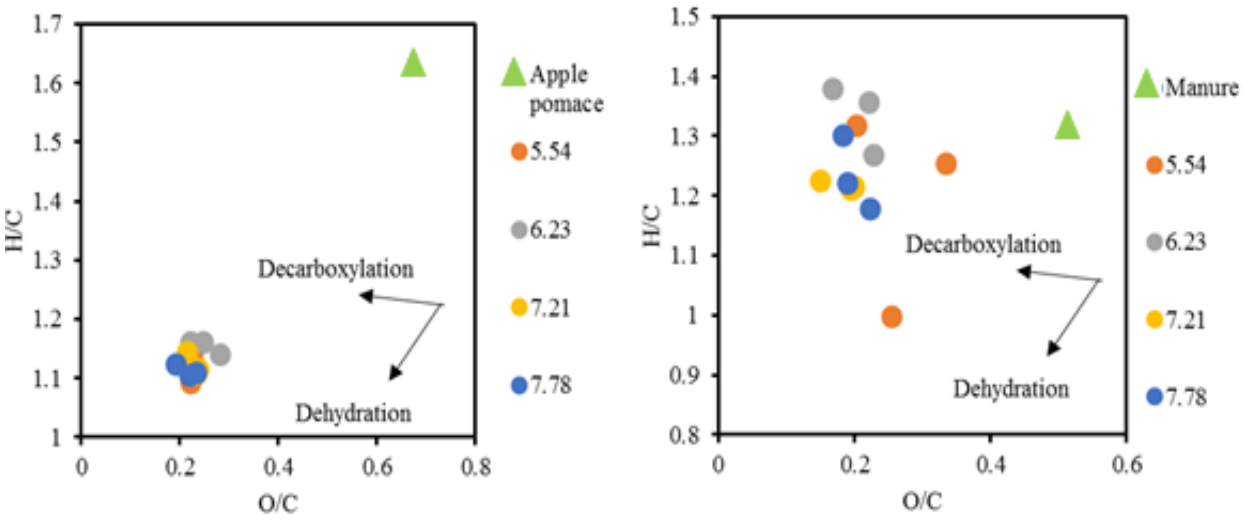

Figure 8.8. Van Krevelen diagram from bio-crudes obtained from apple pomace and manure. It shows the relative importance of de-hydration and de-carboxylation as condensation reactions to deplete oxygen from biomass.

As showed in chapter VII for the hydro-char, van Krevelen diagrams are also useful to compare the HTL phase with counterpart fuels, in terms of elemental composition. Bio-crude oils were compared to bio-ethanol, bio-diesel, pyrolysis bio-oils from agricultural residues, and gasoline. Red wine pomace and manure feedstocks laid in the van Krevelen diagram close to pyrolysis bio-oils, suggesting some similarities in elemental ratios. The bio-crude oils obtained from HTL of activated sewage sludge and food waste presented elemental compositional ratios close to bio-diesel.

8.3.1.4 Energy recovery

The higher heating value (HHV) is an intensive property that provides information about the energy quality of the material, as it has been presented in the previous section for bio-crude oil, and in chapter VII for hydro-char. However, it is necessary to combine this metric with the extension of material production (mass yield), to obtain an extensive property (energy recovery), that provides insight about the distribution of the energy content in the feedstock into the different

phases obtained in HTL process. Different approaches have been proposed to perform energy balances in HTL processes (Biller and Ross 2011). They differ in their level of accuracy and detailed analysis in considering processing energy (heating requirements) used in the liquefaction reaction (Eboibi et al. 2014). In this chapter, the energy content in the feedstock, as well as in the HTL hydro-char and bio-crude oil phases, was calculated by multiplying the HHV of the phase to the mass obtained for each phase. Table 8.1 shows energy content in the mass of the different feedstocks fed in the reactor (kJ). Manure and activated sewage sludge presented the lowest energy content, followed by food waste, apple and red wine pomace, whiskey stillage, and olive oil pomace is the substrate with higher energy content. The distribution of this energy into the different HTL phases at the 4 severity factors studied in this chapter were presented in a Sankey diagram configuration (where the width of flow lines is proportional to the energy percentage). Figure 8.9 presents the results for manure as an example, and Figures AII-30 to 35 in appendix II presents the rest of the substrates. Figure 8.9 showed that severity factor affect the distribution of energy towards the different phases. For the case of manure, lower severity factors concentrated the energy of manure feedstock in the hydro-char phase. When the severity factor increased (reactions at 300˚C), bio-crude oil is the phase containing the majority of the energy of the feedstock.

Table 8.1. Energy content of the initial feedstock fed into the reactor. This energy was distributed towards the different phases forming the HTL media upon reaction at different severity factors. Values are the averages of three experiments and errors represent the standard deviation.

Manure	Activated sewage sludge	Food waste	Apple pomace	Red wine pomace	Whiskey stillage	Olive oil pomace
91.2 ± 0.4 kJ	28.9 ± 0.2 kJ	110.0 ± 0.7 kJ	152.7 ± 2.1 kJ	158.3 ± 0.8 kJ	170.8 ± 0.5 kJ	190.3 ± 2.3 kJ

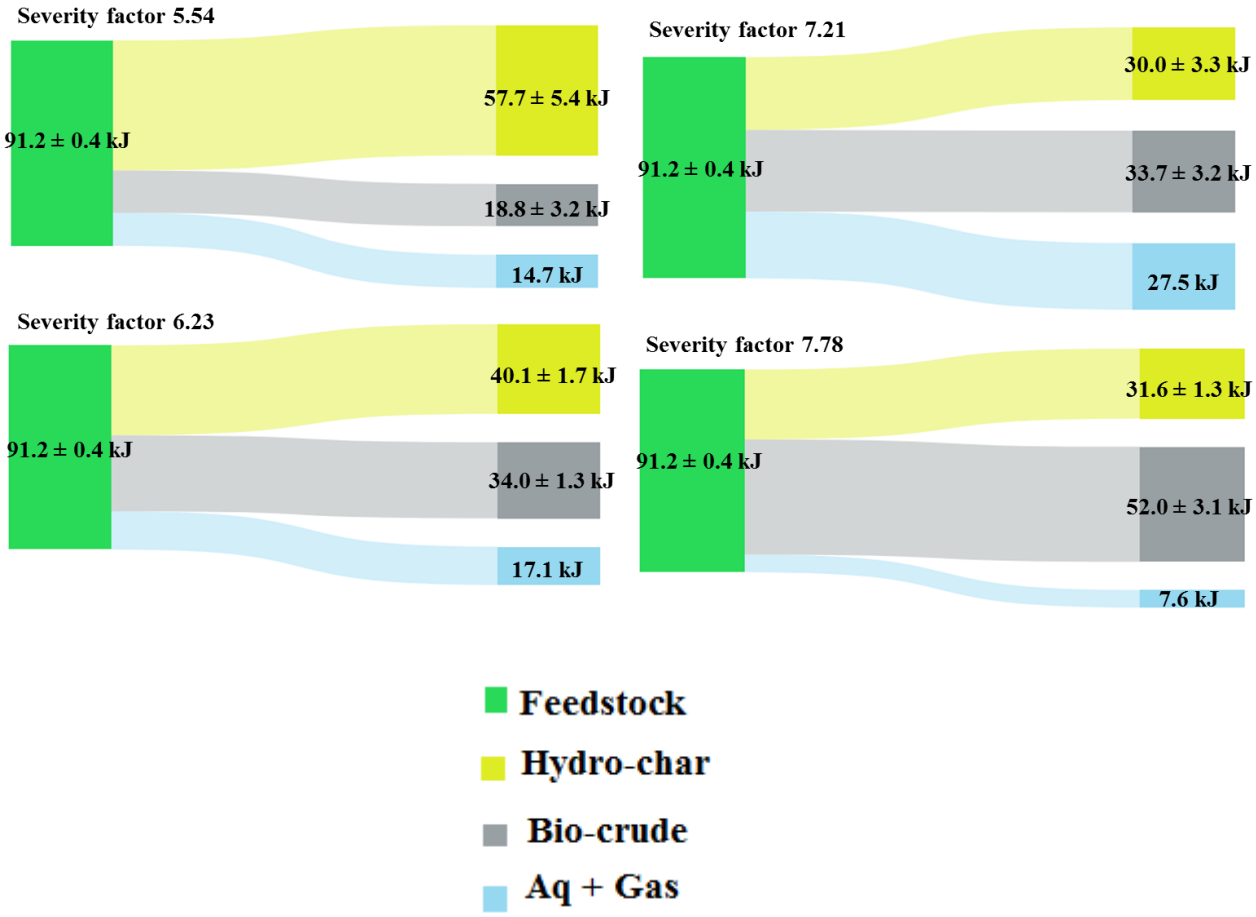

Figure 8.9. Sankey diagram to represent the distribution of the energy contained in manure fed in the reactor towards the different phases upon HTL reaction at different conditions. Values for hydro-char and bio-crude oil are the average of three experiments, and the error represent the standard deviation. The energy content of Aq + gas phase was determined by difference to the energy content of the feedstock

Referring the energy content of the HTL phases to the energy content of the feedstock, energy recovery (%) was calculated using equation 3. It was proved to be an useful metric to compare between energy distribution towards HTL phases between feedstocks.

$$Energy\ recovery_i\ (\%) = \frac{Mass_i * HHV_i}{Mass_{Feedstock} * HHV_{Feedstock}} \qquad Eq.\ (3)$$

where, i refers to the phase of interest (bio-crude oil or hydro-char), mass $_{feedstock}$ (g) is the amount of feedstock fed in the reactor, mass$_i$ represents the amount of phase i obtained in HTL process, and HHV is the higher heating value (kJ/g) of the feedstock or the phase i obtained in HTL. The energy recovery of aqueous phase and gas phase was not measured, and it was calculated combined, as the difference to 100%.

The energy recovery is shown for manure in Figure 8.10 and for the other feedstocks in Figures AII-36 to 41 in appendix II. To summarize the findings from energy recovery, Table 8.2 showed the HTL phase with the highest energy concentration from the HTL process of all feedstocks studied at all the severity factors. The aqueous and gas phase from activated sewage sludge, apple pomace, and red wine pomace presented the highest energy concentration for all severity factors studied. This show the potential that these phases have for further valorization, what proves the versatility of HTL technology. On the other hand, HTL of food waste concentrated the energy of the feedstock into the bio-crude oil phase. Manure, whiskey stillage, and olive oil pomace presented an evolution in energy concentration from hydro-char to bio-crude oil (manure), and from bio-crude oil to aqueous and gas phase (whiskey stillage and olive oil pomace) as the severity factor increases. Manure is the only feedstock with hydro-char as the most energy concentrated HTL phase, what occurs for reactions at 250˚C.

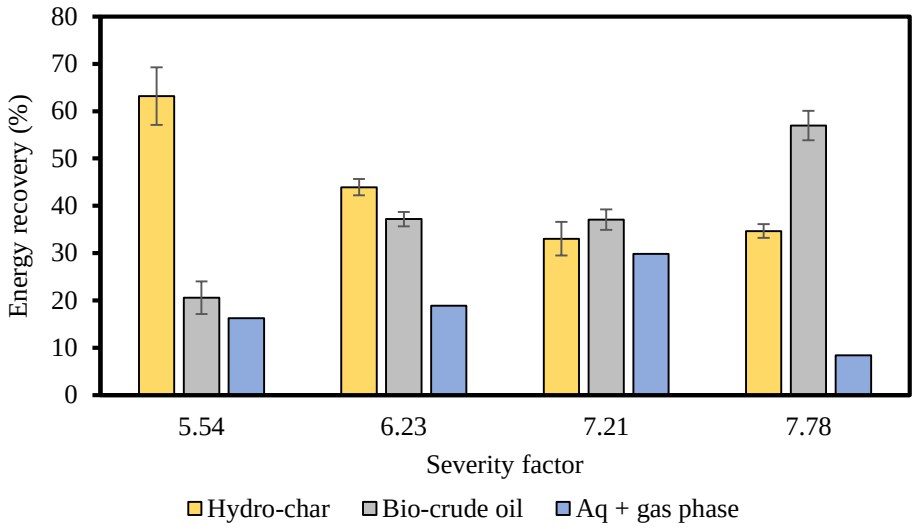

Figure 8.10. Energy recovery (%) from feedstock within the phases obtained from HTL process for manure. The values presented are average of three experiments, and the error bars represent the standard deviation. Aq + gas phases energy recovery were calculated combined by difference to 100%

Table 8.2. Phase with the highest energy concentration obtained from HTL process of the different feedstocks and severity factors. Values represent averages of three experiments. Aq + gas phase energy content and energy recovery were calculated combined by difference to the energy content of feedstock and 100%, respectively.

Severity factor	Manure	Activated sewage sludge	Food waste
	Hydro-char (63.2%)	Aq + gas (44.6%)	Bio-crude oil (69.8%)
5.54	57.7 kJ	12.9 kJ	76.7 kJ
	Hydro-char (43.9%)	Aq + gas (44.3%)	Bio-crude oil (51.4%)
6.23	40.1 kJ	12.8 kJ	57.0 kJ
	Bio-crude oil (37.0%)	Aq + gas (60.5%)	Bio-crude oil (67.1%)
7.21	33.7 kJ	17.5 kJ	74.1 kJ
	Bio-crude oil (57.0%)	Aq + gas (50.6%)	Bio-crude oil (60.0%)
7.78	\52.0 kJ	14.6 kJ	64.8 kJ

Severity factor	Apple pomace	Red wine pomace	Whiskey stillage	Olive oil pomace
	Aq + gas (40.1%)	Aq + gas (56.7%)	Bio-crude oil (45.4%)	Bio-crude oil (45.6%)
5.54	62.5 kJ	90.0 kJ	77.5 kJ	86.7 kJ
	Aq + gas (38.6%)	Aq + gas (51.2%)	Aq + gas (52.3%)	Bio-crude oil (41.4%)
6.23	59.0 kJ	81.1 kJ	89.2 kJ	79.2 kJ
	Aq + gas (40.1%)	Aq + gas (55.3%)	Aq + gas (58.6%)	Aq + gas (47.0%)
7.21	62.0 kJ	87.5 kJ	100.4 kJ	89.8 kJ
	Aq + gas (41.8%)	Aq + gas (54.3%)	Aq + gas (47.9%)	Aq + gas (54.3%)
7.78	64.3 kJ	85.5 kJ	81.9 kJ	103.3 kJ

As previously mentioned in this chapter, bio-crude oil is traditionally considered the most desired phase in HTL processes, while hydro-char, aqueous phase, and gas phase are viewed as by-

products of the reaction. Therefore, values for the bio-crude energy recovery, rather than for the other phases, from a variety of feedstocks (mainly algal systems) and conditions can be found in literature. Table 8.3 collected the values of energy recovery and energy content in bio-crude oil found in this chapter, to compare with other studies.

Table 8.3. Energy recovery (%) and energy content (kJ) of bio-crude oil obtained in HTL of studied feedstocks at all severity factors. Values represent the average of three experiments.

Severity factor	Manure	Activated sewage sludge	Food waste
5.54	(20.6%) 33.7 kJ	(25.8%) 7.4 kJ	(69.8%) 76.7 kJ
6.23	(37.2%) 34.0 kJ	(31.6%) 9.1 kJ	(51.4%) 57.0 kJ
7.21	(37.0%) 33.7 kJ	(21.6%) 6.2 kJ	(67.1%) 74.1 kJ
7.78	(57.0%) 52.0 kJ	(32.6%) 9.5 kJ	(60.0%) 64.8 kJ

Severity factor	Apple pomace	Red wine pomace	Whiskey stillage	Olive oil pomace
5.54	(33.5%) 51.2 kJ	(22.7%) 35.8 kJ	(45.4%) 77.5 kJ	(45.6%) 86.7 kJ
6.23	(32.8%) 49.9 kJ	(23.8%) 37.7 kJ	(29.1%) 49.9 kJ	(41.4%) 79.2 kJ
7.21	(39.2%) 60.3 kJ	(30.2%) 47.8 kJ	(29.6%) 50.4 kJ	(43.3%) 82.2 kJ
7.78	(35.2%) 53.6 kJ	(28.2%) 44.8 kJ	(36.5%) 62.4 kJ	(35.6%) 67.8 kJ

The bio-crude oil obtained from the HTL process of food waste, olive oil pomace, and manure (at the highest severity factors) presented the highest energy recoveries between 70-40%. These values are comparable to the energy recovery in bio-crude oils obtained from HTL of *Chlorella vulgaris*, *Spirulina*, and *Nannochloropsis occulta* (65-50%), at 350˚C for 1 hour (severity factor of 8.5 as calculated with equation 2), (Biller and Ross 2011), from lignocellulosic biomass obtained in a continuous flow reactor (64%) (Elliott et al. 2015), and higher than values from aquatic plants treated at 350˚C for 15 minutes (35%) (Lu et al. 2013). However, the values obtained from olive oil pomace are almost half than for sunflower oil (86.7%), indicating that the higher amount of lipids remaining in the pomace would drive HTL process into bio-crude oil. The energy recoveries from bio-crude oil obtained in this work are higher than the values obtained

from model compounds: glucose (9.1%), starch (13.5%), albumin (29%), soya protein (30.5%), and aminoacids asparagine (13.4%) and glutamine (10.7%) (Biller and Ross 2011).

Reaction conditions, together with feedstock composition, influence the distribution of energy from the initial substrate into the different HTL phases. Understanding these effects is of capital importance to optimize the versatility of the HTL process to obtain a distribution of phases at the desired energy quality. In addition, the energy contents and recoveries presented in this chapter could constitute the base for future gate-to-gate Life Cycle Analysis (LCA) evaluating the energy flows in HTL, and how to optimize blending of feedstocks to obtain desired products.

8.3.2 Physico-chemical characterization of bio-crude oils

8.3.2.1 FTIR of bio-crude oils

FTIR provided information about the distribution of functionalities in the bio-crude oils. However, the collection of FTIR spectra from bio-crude oils was challenging. The low surface tension of the DCM solvent used to dissolve the bio-crude made it impossible to use the high-throughput sampling module under transmittance mode. The 50µl drop of DCM with bio-crude placed in every well of the Si sampling plate could not be contained in within the sampling well boundaries. Instead, it spread to adjacent wells, making it impossible to get reproducible measurements above the FTIR detector threshold. Considering the amount of samples to analyze, the idea of using the high-throughput sampling module was further explored. An aluminum sampling plate, where the sample can be contained in deep wells without transferring among adjacent wells, was used as shown in Figure 8.11. This sampling technique works in reflection mode using liquid nitrogen to cool down the MCT detector. This approach failed in getting spectra in the working intensity range

of the detector. To obtain reproducible spectra, the sampling wells have to be totally covered in bio-crude oil after drying the DCM solution. To achieve complete coverage, the well was filled several times with 50µl of DCM solution and the solvent was evaporated. The yielded spectra, however, were above 1 unit of absorbance, considered the detector threshold. Decreasing the amount of sample added to the well resulted in highly variability between replicates. Due to these difficulties associated to the use of HTS-XT high-throughput module of the FTIR, bio-crude oil samples were FTIR analyzed using the ATR sampling module, where every sample needs to be prepared individually (Vardon et al. 2011).

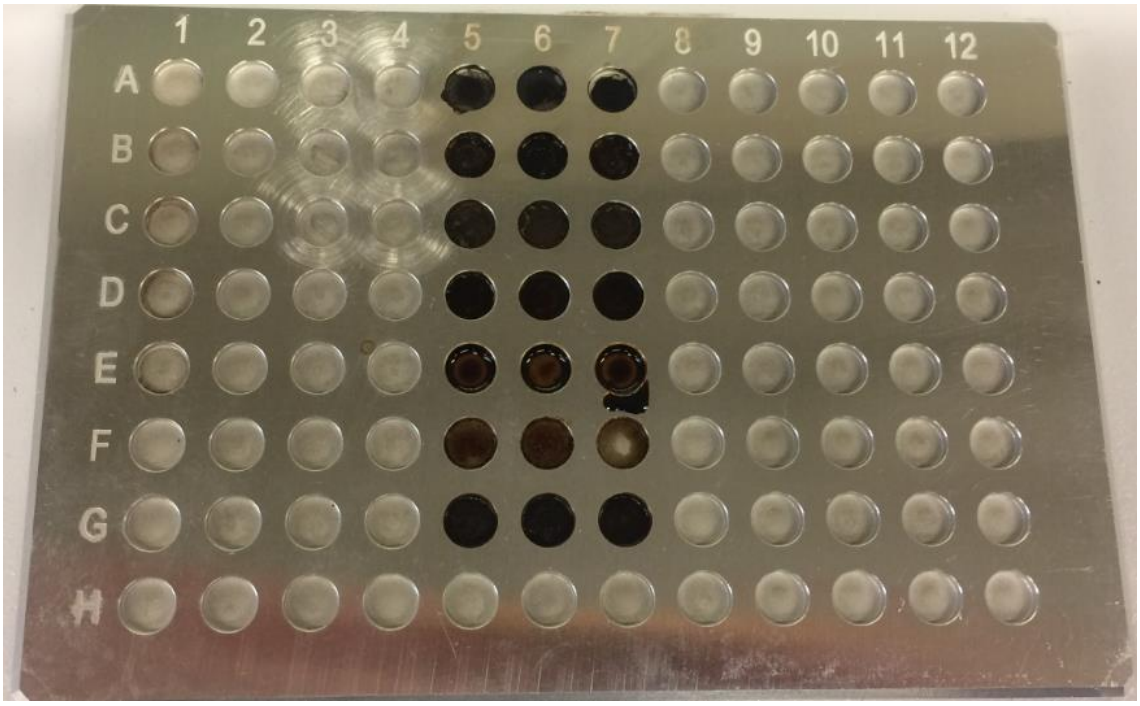

Figure 8.11. Aluminum plate with deep wells was a sampling technique explored for FTIR analysis of bio-crude oils obtained from HTL

The FTIR of bio-crude oils obtained from manure and red wine pomace are presented in Figure 8.12 as example. The spectra for the bio-crude oil for the other substrates is presented in Figures AII-42 to 46 in appendix II. Comparing the FTIR spectra of bio-crude oils to the spectra of the feedstock (Figure 7.2 in chapter VII), the spectral bands distributions are completely different,

confirming the evolution of the material under hydrothermal liquefaction conditions. Moreover, the complexity of the spectra in the 1730-1150 cm^{-1} region showed functionalities related to heteroatoms, as expected from the analysis of the elemental composition. This is consistent to previous studies performing FTIR of bio-crudes from swine manure (Vardon et al. 2011). In addition, the lack of spectral signal around the 3350 cm^{-1}, representing hydroxyl groups (and hydrogen bonding associated with them) informs about the non-polarity of the molecules conforming the bio-crude oil.

Reaction conditions had a different effect on the chemical structure of bio-crude oil obtained from different feedstocks as revealed by FTIR. For bio-crudes obtained from manure, temperature has a great influence in their chemical structure as the spectra of bio-oils at low temperature (severity factors 5.54 and 6.23), significantly differed from bio-oils obtained at high temperature (severity factors 7.21 and 7.78). Temperature increased the aliphatic character of the bio-oils as observed by the higher intensity of 1920 and 2850 cm^{-1} bands (that represent the aliphatic C-H stretch) and the appearance of the 1355 cm^{-1} band that represents C-H bends (Lobo and Bonilla 2003). The new spectral features at 1710 and 1220 cm^{-1} for high temperature HTL were associated to carboxylic groups (Syngellakis 2014) , and to the carbohydrate and lignin fraction of biomass (Bekiaris et al. 2015), respectively. Reaction time presented much lower influence than temperature in the chemical functionalities of manure bio-crude.

On the other hand, reaction temperature presented much lower effect in the chemical features of bio-crudes obtained from other substrates (food waste and fruit pomaces). Unlike reported by Vardon et al (2011) and Xiu et al (2010) for swine manure bio-crude oils, and Barreiro et al (2015) for macro-algae bio-crudes, vibrations at 2920 and 2850 cm^{-1} (representing C-H stretch in aliphatic structures) are not prominent in the bio-crude oils obtained in this research. Carbonyl groups are

represented by the 1740 cm^{-1} band, and were clearly observed for all the feedstocks. This observation agrees with the presence of oxygen remaining in the bio-crude oil as determined by elemental composition analysis. However, the intensity of this band appears to slightly decrease as the severity factor of the HTL process increases, what agrees with the oxygen depletion trend in bio-crude previously observed. This effect is clearly observed in red wine pomace bio-crude oils obtained at increasing severity factors. In addition, the functionalities previously described for manure at 1350 and 1220 cm^{-1} are shared (in variable magnitudes) among the bio-crude oils obtained from all feedstocks at all severity factors.

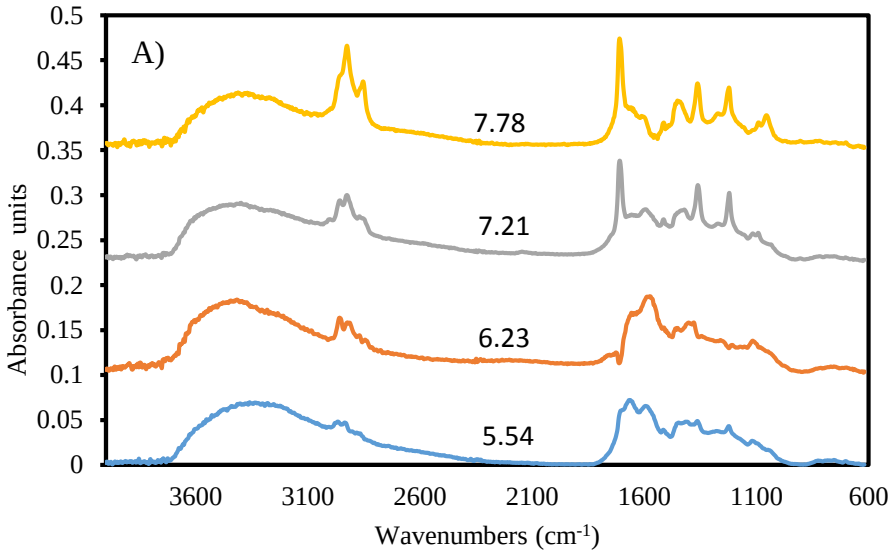

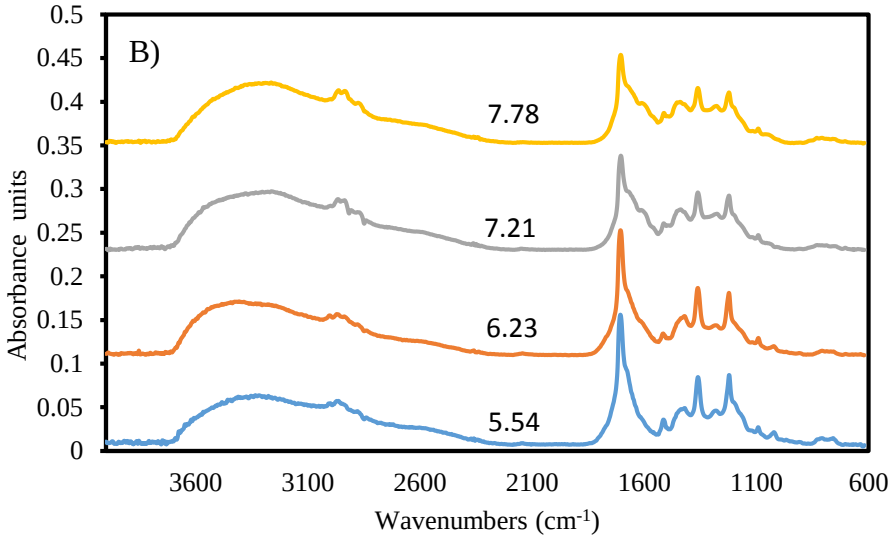

Figure 8.12. FTIR spectra for the bio-crude oils obtained from A) manure and B) red wine pomace for all the severity factors studied. Every spectra is the average of 3 experiments and 32 scans per experiment.

Comparing the bio-crude oil spectra obtained in this work with conventional petroleum crudes and heavy asphaltic crudes, they show differences. Petroleum crudes present stronger peaks associated with aliphatic fractions at 2920 and 2850 cm^{-1}. In addition, they present weaker peaks associated with functionalities composed of heteroatoms (oxygen, nitrogen, sulfur), as the content of these elements in commercial gasoline, and crudes is much lower than presented for the bio-crudes obtained in this work (Figure 8.6 and Figure 8.7).

8.3.2.2. GC-MS bio-crude oils

Gas chromatography coupled with mass spectrometry (GC-MS) was utilized to detect low-boiling point compounds of the bio-crude oils generated from HTL of the feedstocks at all the severity factors studied. Gas chromatography sorts the molecules based on their polarity, and the mass spectroscopy identify the molecules that leave the GC column at different retention times by ionizing and breaking them in small fragments that are detected. A software library bring the

molecule fragments together and identify the molecule with a certain level of confidence. The use of GC-MS in this project has a double objective: to compare between the compounds that form the different bio-crude oils and analyze the effect of reaction time, temperature, and feedstock features in the quality of the bio-oils (Vardon et al. 2011), and to compare the bio-crude oils obtained to commercial drop-in fuels gasoline and diesel (Yin et al. 2010).

In chapter VI, GC-MS was used to identify the compounds from bio-crude oil obtained from HTL of manure and food waste at different pH. The relative amount of the different compounds was reported as the area under the peak referred to total area under all the peaks (%). However, investigation is undergoing with the collaboration of Bucknell University Civil an Environmental Engineering department (Prof. Deborah Sills) to be more quantitative and yield values of concentration rather than relative abundance (%). The approach to achieve this goal is the use of an internal standard of known concentration, so areas can be converted to concentrations by comparison with this internal standard. However, the selection of the internal standard is not trivial. It must show up at a retention time such it does not overlap and mask peaks representing compounds of interest in the sample to analyze. On the other hand, the chosen concentration is important to don't overwhelm the scale of the chromatogram, so peaks from compounds of interest can be observed.

Following these two guidelines, pentadecanoic acid methyl ester was tried, and rejected as its retention time (51 minutes) is at the range of the expected compounds from bio-oils, based on previous studies. Phenol has a retention time of 11 minutes, what makes it a perfect candidate for internal standard. However, the determination of the phenol ideal concentration is being challenging, as too high concentration, mask GC-MS peaks, but at low concentration it does not show up on the chromatogram. To add to the difficulty, the concentration of the samples to analyze

is not uniform, therefore, the concentration of phenol used as internal standard should be tailor to each individual sample.

We expect to develop a consistent GC-MS method to throw light to the low-boiling point composition of the bio-oils obtained in this chapter.

8.3.3 Characterization of the composition of the aqueous phase

HPLC was used to determine the composition of the aqueous phase obtained from HTL. As mentioned in the methods section, aqueous phase was separated from the bio-crude oil phase in the HTL media obtained after the reaction. This phase separation was performed by liquid-liquid extraction. To avoid the presence of traces of the separation solvents in aqueous phase, it was heated up to eliminate those solvents. The volumes of the aqueous phase were measured, and concentrations of molecules obtained were normalized to 20ml, that is the volume aliquot analyzed from HTL sample. Figure 8.13 shows the composition profile of the aqueous phase obtained from whiskey stillage at all the conditions studied. Small amounts of reduced sugars (glucose and fructose) are formed under HTL conditions. At low temperature HTL, a wide distribution of carboxylic acids are formed, with concentrations non-dependent on reaction time. However, at high temperature HTL, formic and acetic acids are the ones formed at higher concentrations. This resembles the observation for the aqueous phase for food waste obtained in chapter VI. However, for food waste, the amount of fructose obtained was significantly higher than for whiskey stillage, what may have to do with the differences in the composition between both feedstocks. In addition, the concentration of these two acids increased with reaction time. Similarities in the prominent production of carboxylic acid during HTL are found also for apple pomace feedstock and food

waste (Figure AII-47 and AII-48 in appendix II). For these feedstocks, the concentration of carboxylic acids is much lower than for the case of whiskey stillage, (acetic acid concentration of 20mM for apple pomace vs. 120 mM found at 250˚C for whiskey stillage). For apple pomace, succinic acid appears as one of the acids with highest presence in the aqueous phase together with acetic and formic acid. At 300˚C, lactic acid also shows up in the system at concentration of 10mM (independent of reaction time), that is in the same order than concentrations observed for succinic and formic acid at these conditions. Acetic acid is the carboxylic acid produced at higher concentrations at this temperature, above 20 mM, independent of reaction time. For food waste, formic acid is the most abundant carboxylic acid, at 50 mM concentration, for 250˚C reactions. Glycoaldehyde showed up at a concentration of 25 mM, increasing with reaction time. At high temperature, concentration of formic acid increased to 60 mM, and it was affected positively by reaction time. On the other hand, glycoaldehyde shows a decrease in concentration with reaction time at this condition, from 25mM at short reaction time to 10 mM at long reaction time, showing that at high temperature, retro-aldol condensation reactions from glucose got suppressed at longer reaction times (Cantero et al. 2015).

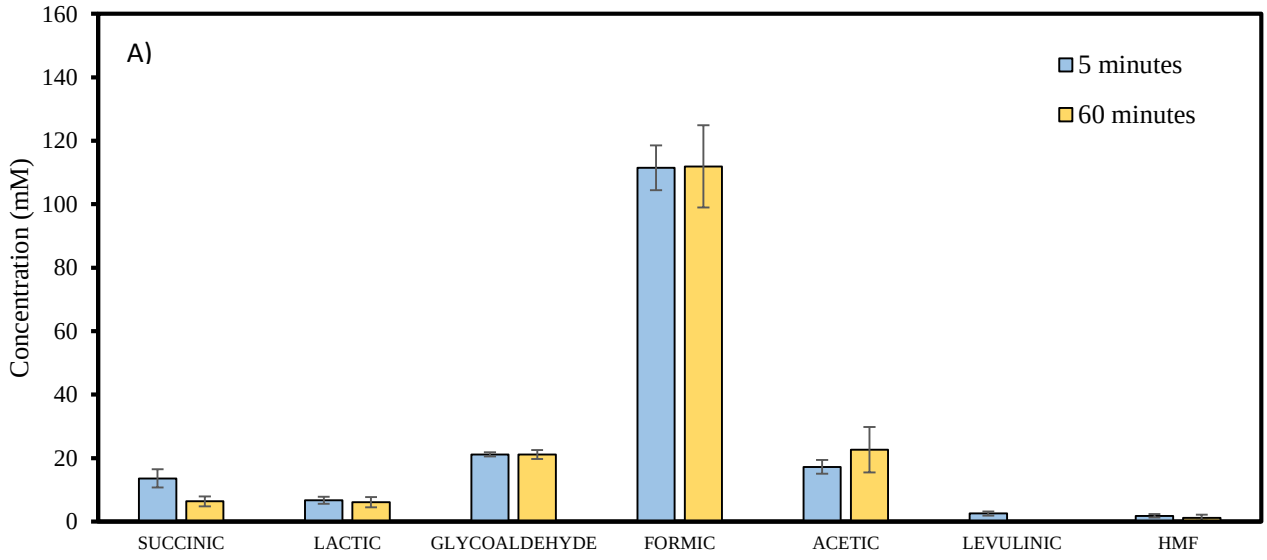

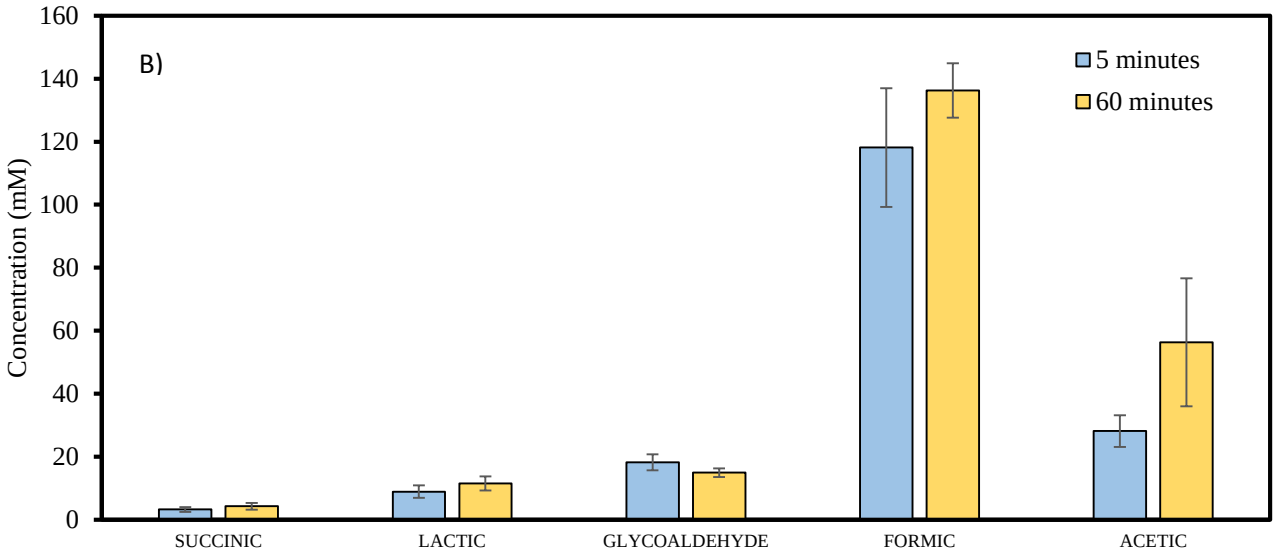

Figure 8.13 HPLC for aqueous phase of whiskey stillage at A) 250 and B) 300˚C. The values presented are the average for three experiments, and the error bars represent the standard deviation.

Preliminary analysis of the HPLC chromatograms for the rest of the substrates studied in this chapter shows different short chain carboxylic acid formation depending on the feedstock.

8.4 Conclusions

This chapter has presented a comprehensive study on how the elemental composition and pH of the feedstocks, together with reaction conditions can benefit the production of some HTL phases, at the expense of others, and their influence in the quality of the phases obtained. One of the main findings of this study is that severity factor influences the mass of bio-crude oil produced, but does not have an effect in the elemental composition of the bio-oils obtained. The repercussion of this observation is wide. As the energy density is a sole function of elemental composition, it does not change with severity factor. On the other hand, carbon yield, and energy recovery from feedstock in the bio-crude oil are affected by severity factor, as these properties are extensive properties, therefore, affected by the mass of bio-crude oil obtained. In terms of the energy quality of the bio-

crude oils obtained in this research, it resembled the energy density of bio-ethanol, but still far lower than the values for commercial gasoline, due to their higher heteroatoms content.

The role of the pH of the feedstock affects the extension of oxygen reduction in the bio-crude oil. Feedstocks with acid pH decreased the oxygen content in the bio-crude at higher extent that substrates with alkaline pH. In addition, nitrogen gets concentrated in the bio-crude for alkaline pH feedstocks, while the nitrogen content in bio-crude obtained from acid feedstocks is lower than for the initial substrate.

The physico-chemical characterization of phases was also an interest of the research in this chapter. For the bio-crude oils, FTIR and GC-MS were performed, and a method for quantitative analysis using an internal standard is being developed. For the aqueous phase, HPLC revealed the formation of short chain carboxylic acids at HTL conditions, mainly acetic, formic, succinic, and lactic acid. The characterization of this phase, considered a by-product of the HTL process, is important to show valorization potential.

Some recommendations are inspired from the research of this chapter. We recommend to further characterize feedstocks in terms of carbohydrates, protein, and lipid composition using Dairy One assays to further elucidate the effect of the composition of the feedstock in the yield and quality of the bio-crude oil obtained in HTL processes. Furthermore, the study of the potential effect of the feedstock ash composition in HTL processes was out of the scope of this study. The compositional analysis of the ash obtained after feedstock calcination using Inductively Coupled Plasma-Mass Spectroscopy (ICP-MS) could be of interest for future studies. In addition, this information could provide guidance in the selection of catalysts to optimize the yield and/or quality of a specific phase, taking advantage of the versatility of the HTL process demonstrated in this chapter.

8.5 References

Akalin, M, K Tekin, and S Karagoz. 2012. "Hydrothermal Liquefaction of Cornelian Cherry Stones for Bio-Oil Production." *Bioresource Technology* 110: 682–87.

Akhtar, J, and N Amin. 2011. "A Review on Process Conditions for Optimum Bio-Oil Yield in Hydrothermal Liquefaction of Biomass." *Renewable and Sustainable Energy Reviews* 15: 1615–24.

ASTM, Annual book of ASTM standards Volumen 11.05. 2003. "ASTM E1755-01 Standard Method for the Determination of Ash in Biomass."

Barreiro, D, B Gomez, U Hornung, A Kruse, and W Prins. 2015. "Hydrothermal Liquefaction of Microalgae in a Continuous StirredTank Reactor." *Energy & Fuels* 29: 6422–32.

Bekiaris, G, J Lindedam, C Peltre, S Decker, G Turner, J Magid, and S Bruun. 2015. "Rapid Estimation of Sugar Release from Winter Wheat Straw during Bioethanol Production Using FTIR-Photoacoustic Spectroscopy." *Biotechnology for Biofuels* 8 (85): 1–12.

Biller, P., and A.B. Ross. 2011. "Potential Yields and Properties of Oil from the Hydrothermal Liquefaction of Microalgae with Different Biochemical Content." *Bioresource Technology* 102 (1): 215–25.

Bozell, J, and G Petersen. 2010. "Technology Development for the Production of Biobased Products from Biorefinery Carbohydrates—the US Department of Energy's 'Top 10' Revisited." *Green Chemistry* 12: 539–54.

Cantero-Tubilla, B, D Cantero, C Martinez, J Tester, L Walker, and R Posmanik. 2017. "Characterization of the Solid Products Form Hydrothermal Liquefaction of Waste

Feedstocks from Food and Agricultural Industries." *Journal of Supercritical Fluids*.

Cantero, D.A, C.M Martinez, M.D Bermejo, and M.J Cocero. 2015. "Simultaneous and Selective Recovery of Cellulose and Hemicellulose Fractions from Wheat Bran by Supercritical Water Hydrolysis." *Green Chemistry* 17 (1): 610–18.

Choudhary, T, and C Philips. 2011. "Renewable Fuels via Catalytic Hydrodeoxygenation." *Applied Catalysis A: General* 397: 1–12.

Déniel, M, G Haarlemmer, A Roubaud, E Weiss-Hortala, and J Fages. 2016. "Energy Valorisation of Food Processing Residues and Model Compounds by Hydrothermal Liquefaction." *Renewable and Sustainable Energy Reviews* 54: 1632–52.

Donghai, X, and P Savage. 2014. "Characterization of Biocrudes Recovered with and without Solvent after Hydrothermal Liquefaction of Algae." *Algal Research* 6: 1–7.

Eboibi, B, D Lewis, P Ashman, and S Chinnasamy. 2014. "Effect of Operating Conditions on Yield and Quality of Biocrude during Hydrothermal Liquefaction of Halophytic Microalga Tetraselmis Sp." *Bioresource Technology* 170: 20–29.

Elliott, D, P Biller, A Ross, A Schmidt, and S Jones. 2015. "Hydrothermal Liquefaction of Biomass: Developments from Batch to Continuous Process." *Bioresource Technology* 178: 147–56.

Jazrawi, C, P Biller, A Ross, A Montoya, T Maschmeyer, and B Haynes. 2013. "Pilot Plant Testing of Continuous Hydrothermal Liquefaction of Microalgae." *Algal Research* 2 (3): 268–77.

Kim, Y, T Kreke, N Mosier, and M Ladisch. 2014. "Severity Factor Coefficients for Subcritical Liquid Hot Water Pretreatment of Hardwood Chips." *Biotechnology and Bioengineering* 111

(2): 254–63.

Lobo, H, and J Bonilla. 2003. *Handbook of Plastic Analysis*. CRC Press.

Lu, W, Y Guo, B Zhang, and C Wang. 2013. "Comprehensive Analysis on Elements, Energy Recovery, and Oil Compositions of Biomass Deoxy-Liquefaction." *Energy & Fuels* 27 (4): 2157–66.

Luo, L, J Sheehan, L Dai, and P Savage. 2016. "Products and Kinetics for Isothermal Hydrothermal Liquefaction of Soy Protein Concentrate." *ACS Sustainable Chemistry & Engineering* 4: 2275–2733.

Luterbacher, J, J Tester, and L Walker. 2010. "High-Solids Biphasic CO2–H2O Pretreatment ofLignocellulosic Biomass." *Biotechnology and Bioengineering* 107 (3): 451–60.

Mau, V, J Quance, R Posmanik, and A Gross. 2016. "Phases' Characteristics of Poultry Litter Hydrothermal Carbonization under a Range of Process Parameters." *Bioresource Technology* 219: 632–42.

McCoy, M. 2009. "The Gasoline Wars." *Chemical & Engineering News* 87 (14): 20–21.

Mortensen, P, J Grunwaldt, P Jensen, K Knudsen, and A Jensen. 2011. "A Review of Catalytic Upgrading of Bio-Oil to Engine Fuels." *Applied Catalysis A: General* 407: 1–19.

Nazem, M, and O Tavakoli. 2017. "Bio-Oil Production from Refinery Oily Sludge Using Hydrothermal Liquefaction Technology." *The Journal of Supercritical Fluids*, March.

Pedras, B, M Salema-Oom, I Sa-Nogueira, P Simo, A Paiva, and S Barreiros. 2017. "Valorization of White Wine Grape Pomace through Application of Subcritical Water: Analysis of Extraction, Hydrolysis, and Biological Activity of the Extracts Obtained." *Journal of*

Supercritical Fluids 128: 138–44.

Peterson, A, F Vogel, R Lachance, M Fröling, M Antal, Jr., and J Tester. 2008. "Thermochemical Biofuel Production in Hydrothermal Media: A Review of Sub- and Supercritical Water Technologies." *Energy & Environmental Science* 1 (1): 32.

Posmanik, R., D.A. Cantero, A. Malkani, D.L. Sills, and J.W. Tester. 2017. "Biomass Conversion to Bio-Oil Using Sub-Critical Water: Study of Model Compounds for Food Processing Waste." *The Journal of Supercritical Fluids* 119: 26–35.

Qian, L, S Wang, and P Savage. 2017. "Hydrothermal Liquefaction of Sewage Sludge under Isothermal and Fast Conditions." *Bioresource Technology*.

Ramirez, J, R Brown, and T Rainey. 2015. "A Review of Hydrothermal Liquefaction Bio-Crude Properties and Prospects for Upgrading to Transportation Fuels." *Energies* 8: 6765–94.

Reichardt, C. 1994. "Solvatochromic Dyes as Solvent Polarity Indicators." *Chem. Rev.* 94: 2319–58.

Rogalinski, T, T Ingram, and G Brunner. 2008. "Hydrolysis of Lignocellulosic Biomass in Water under Elevated Temperatures and Pressures." *The Journal of Supercritical Fluids* 47 (1): 54–63.

Sugano, M, H Takagi, K Hirano, and K Mashimo. 2008. "Hydrothermal Liquefaction of Plantation Biomass with Two Kinds of Wastewater from Paper Industry." *Journal of Materials Science* 43 (7): 2476–86.

Syngellakis, S. 2014. *Biomass to Biofuels*. Wessex, UK: WIT Press.

Tekin, K. 2015. "Hydrothermal Conversion of Russian Olive Seeds into Crude Bio-Oil Using a

CaO Catalyst Derived from Waste Mussel Shells." *Energy & Fuels* 29: 4382–92.

Tekin, K, S Karagöz, and S Bektaş. 2014. "A Review of Hydrothermal Biomass Processing." *Renewable and Sustainable Energy Reviews* 40: 673–87.

Tekin, K, S Karazog, and S Bektas. 2012. "Hydrothermal Liquefaction of Beech Wood Using a Natural Calcium Borate Mineral." *Journal of Supercritical Fluids* 72: 134–39.

Teri, G, L Luo, and P Savage. 2014. "Hydrothermal Treatment of Protein, Polysaccharide, and Lipids Alone and in Mixtures." *Energy & Fuels* 28 (12): 7501–9.

Toor, S, L Rosendahl, and A Rudolf. 2011. "Hydrothermal Liquefaction of Biomass: A Review of Subcritical Water Technologies." *Energy* 36 (5): 2328–42.

Tuck, C, E Perez, I Horvath, R Sheldon, and M Poliakoff. 2012. "Valorization of Biomass: Deriving More Value from Waste." *Science* 337: 695–99.

Vardon, D, B Sharma, J Scott, G Yu, Z Wang, L Schideman, Y Zhang, and T Strathmann. 2011. "Chemical Properties of Biocrude Oil from the Hydrothermal Liquefaction of Spirulina Algae, Swine Manure, and Digested Anaerobic Sludge." *Bioresource Technology* 102 (17): 8295–8303.

Verma, M, S Godbout, S Brar, O Solomatnikova, S Lemay, and J Larouche. 2012. "Biofuels Production from Biomass by Thermochemical Conversion Technologies." *International Journal of Chemical Engineering* 2012: 18.

Villadsen, S, L Dithmer, R Forsberg, J Becker, A Rudolf, S Iversen, B Iversen, and M Glasius. 2012. "Development and Application of Chemical Analysis Methods for Investigation of Bio-Oils and Aqueous Phase from Hydrothermal Liquefaction of Biomass." *Energy & Fuels* 26:

6988–98.

Xiu, S, A Shahbazi, V Shirley, and D Cheng. 2010. “Hydrothermal Pyrolysis of Swine Manure to Bio-Oil: Effects of Operating Parameters on Products Yield and Characterization of Bio-Oil.” *Journal of Analytical and Applied Pyrolysis* 88 (1): 73–79.

Yin, S, R Dolan, M Harris, and Z Tan. 2010. “Subcritical Hydrothermal Liquefaction of Cattle Manure to Bio-Oil: Effects of Conversion Parameters on Bio-Oil Yield and Characterization of Bio-Oil.” *Bioresource Technology* 101 (10): 3657–64.

Yoshida, H, M Terashima, and Y Takahashi. 1999. “Production of Organic Acids and Amino Acids from Fish Meat by Sub-Critical Water Hydrolysis.” *Biotechnology Progress* 15 (6): 1090–94.

Zacharof, M. 2016. “Grape Winery Waste as Feedstock for Bioconversions: Applying the Biorefinery Concept.” *Waste Biomass Valorization*, 1–15.

CHAPTER IX

CONCLUSIONS AND RECOMMENDATIONS

9.1 Conclusions

The research presented in this dissertation has increased fundamental knowledge in the bio-chemical and thermo-chemical conversion and valorization of biomass. A variety of organic waste have been reacted under several reaction conditions using hydrothermal liquefaction technology. This organic waste are feedstocks representative of agricultural, dairy, and food industries, some of them (olive oil pomace, apple pomace, whiskey stillage) were studied for the first time using this thermochemical conversion processes. Analytical methods have been developed to characterize products of the hydrothermal liquefaction process (hydro-char, bio-crude oil, and aqueous phase), giving an unique insight on their chemistry and properties. Results of these investigation were published in the Journal of Supercritical Fluids, and the Journal Cellulose. In addition, a new manuscript was submitted to the Journal Green Chemistry.

In every chapter of this dissertation the most relevant conclusions of the research performed in the chapter have been already reflected. The purpose of this chapter is to summarize these conclusions.

9.1.1 Biochemical conversion of biomass. FTIR methods development

Studying the evolution of crystallinity of model cellulose over enzymatic hydrolysis of free cellulases, it is important to explain the kinetic drop-off observed after initial hydrolysis yield. The reason for this drop-off is still unclear, with different studies attributing it to different features of

the enzymatic hydrolysis process. It has been proposed that enzyme inactivation by the reduced sugars produced in the process is the reason for this plateau on digestion. On the other hand, modifications of the substrate during the hydrolysis process (amorphogenesis) is an alternative explanation. Preferential digestion of easier access areas of the substrate, leaving the crystalline fractions, more difficult to digest, behind has been also proposed. The research performed in this dissertation built-up from previous infrared methods to characterize the residual substrate after hydrolysis. The main conclusions of this chapter are summarized for endocellulases, exocellulases, and crude enzymes

- Extent of cellulose digestion does not cause any significant change to the cellulose crystallinity
- Enzyme loading does not change cellulose crystallinity over the course of digestion
- Cellulase inhibition appears to have a structural cause that does not involve crystallinity (i.e. modification of surface area or porosity distribution of cellulose over digestion)

The development of reliable infrared methods (FTIR) to characterize pretreated biomass and phases obtained from hydrothermal liquefaction of biomass was another interest of this dissertation. The effect of particle size and particle size distribution over the signal intensity and variability of FTIR spectra of switchgrass and hardwood was discussed. Two sampling techniques were used; attenuated total reflectance (ATR) and high-throughput sampling (HTS-XT). In addition, different statistical techniques to reduce signal variability were attempted and evaluated. The main conclusions from this work are summarized as follows

- Particles obtained from a 0.5mm sieve are the ideal size to yield good spectral intensity without compromising spectral features due to particle size reduction process

- Vector normalization of the spectral signal renders the lowest signal variability among replicates analyzed at different particle sizes. By doing so, this technique maintains the magnitude of spectral features

9.1.2 Hydrothermal processing of model wastes

For the study of the thermo-chemical conversion of biomass by hydrothermal liquefaction (HTL), the first step was to understand the kinetics of model compounds (carbohydrates, protein, and lipids) under typical values of HTL temperatures and reaction times (300˚C and 60 minutes). In addition, degradation products of carbohydrates were investigated. The evolution of the composition of the hydrothermal liquefaction media over a range of times and temperatures was measured using HPLC. Collaboration is underway to fit the evolution of concentration of species over HTL process into a kinetic model that could explain and predict the formation of molecules of interest. The main conclusions of this study are.

- HTL is a dynamic and versatile process that produce a wide range of molecules at different concentrations depending on reaction conditions.
- Cellulose and glucose degrade to furans and hydroxymethyl-furfural derivatives at short reaction times (5-15 minutes). Carboxylic acids are the most abundant products at long reaction times (20-60 minutes)
- Levulinic acid (a product cataloged by the U.S department of energy as one of the top 12 bio-cased molecules) is formed as result of sugars degradation. Once formed, it presents stability with reaction time at HTL conditions studied in this project.

Effect of pH and reaction conditions on yields and chemical characteristics of the phases obtained from hydrothermal liquefaction of a variety of feedstocks was assessed. The main conclusions sorted by phases are:

Hydro-char

- pH modification of the feedstock has a clear effect in the yield and quality of hydro-char obtained from dairy manure and carbohydrate-rich food waste at HTL of 300˚C and 60 minutes. Reaction with addition of alkaly decreased hydro-char yield for food feedstocks, while acid media showed a yield decrease for dairy manure and an increase for carbohydrate-rich food waste.
- HTL depletes oxygen from feedstock towards hydro-char for all feedstocks. De-hydration is the preferential route for oxygen removal for naturally acidic feedstocks (carbohydrate-rich food waste, fruit pomace, whiskey stillage and yogurt whey). Decarboxylation is the preferred mechanisms for naturally alkaline feedstocks (dairy manure and activated waste sludge)
- Hydro-char obtained from naturally alkaline and acidic feedstocks differ in their energy density (per unit mass) and chemical functionalities as assessed using infrared techniques coupled with principal component analysis
- The insight into the chemistry of hydro-char obtained from different sources at different HTL conditions will contribute to finding niches of application for this product, that can contribute to the economics of the HTL process

Bio-crude oil

- Modification of the pH of the feedstock does not change the bio-crude oil yield from carbohydrate-rich food waste. However, for dairy manure, the addition of acid boosted yield about 60%
- The pH of the feedstock also affects the composition of bio-crude obtained. For dairy manure, acid addition shifts composition from cyclic-hydrocarbon based HTL to long chain fatty acid as main compound, an effect also observed for alkaline addition (at low extension). Bio-crude from food waste is more compositionally diverse. Acid addition produces furanic compounds, while alkaline addition shifts the composition to phenols and fatty acids
- Reaction conditions affect the bio-crude oil yields obtained from the variety of feedstocks studied
- Reaction conditions did not have an effect in the composition of the bio-crude oil obtained, and therefore, in the energy density of the product
- The energy density (per unit mass) of the bio-crude oil obtained in this project resembled that for bio-ethanol. Carbohydrate-rich food waste showed the highest potential for valorization as the bio-crude oil obtained presented energy density comparable to bio-diesel

Aqueous phase

- Modification of the pH of the feedstocks affects the composition of the aqueous phase obtained for dairy manure and carbohydrate-rich food waste. Acid addition increased the

formation of HMF and furan related products in the aqueous phase. On the other hand, alkaline addition increased the amount of short chain carboxylic acids

- Different feedstocks produce a different array of carboxylic acids and at different concentrations. Formic acid, acetic acid, succinic acid, levulinic acid, and malonic acid are the majority of the polar components generated by HTL
- Aqueous phase from HTL has the potential to contribute to the economics of the process as valuable products can be obtained out of this phase. Apart from carboxylic acids and furan compounds, nitrogen and phosphorous can be obtained and used as fertilizers. In addition, water can be recovered out of this phase using membrane technology, and being energy valorized using anaerobic digestion.

9.2 Recommendations

Recommendations were suggested in each chapter. They present the next steps that, in my opinion, are necessary to advance research covered in every chapter of this dissertation. The recommendations presented here are more general, and focused on advancing thermo-chemical biomass valorization technology towards further steps in scaling-up to a commercial facility.

9.2.1 Blending of substrates to exploit synergetic effects already observed for the HTL of mixtures of model substrates

The research presented in this dissertation was focused in the study of individual substrates. However, it has been reported that the quality and yield of bio-crude oil, and other phases produced in the HTL process, depends on the ratio of lipids, protein, and carbohydrates in the biomass.

Therefore, research should move from the study of individual feedstocks towards blends of substrates, that can potentially achieve a more uniform feedstock, with optminized production and quality of the desired HTL phase.

9.2.2 Expand experimental conditions for selected feedstocks

With respect to the study of the effect of reaction conditions on the yield and quality of HTL products, I would recommend to focus on food waste and dairy manure and perform comprehensive design of experiments and sensitivity analysis of the variables. In this study, only two conditions of temperature and reaction time were explored. These conditions are not enough to disclose non-linear relationship between variables and responses, and support response surface methodology. Expanding conditions to evaluate experimental results at central points, and what are called α points, would have the potential to find optimal conditions to achieve the best yield and/or quality of HTL phase of interest. Overlapping these response surfaces for optimum yield and quality with economic response surfaces (generated from expenses related with experimental conditions used and potential value of the products obtained) we would be able to find optimum areas of operation. Dairy manure and food waste are suggested for expanded experimental studies because generation is not seasonal (unlike pomaces), and because of the promising yields and bio-crude qualities shown in this work.

9.2.3 Moving into continuous process: Heat integration and pumping requirements

The medium-long term recommendation for hydrothermal liquefaction technology of organic waste is to move towards continuous processes suitable for industrial implementation. Two issues

(among others) have to be improved for this technology to be an industrial reality. Pumping of material at the desired rate, and, most importantly, heat integration. The energy requirements for HTL are high, even though no heat is "wasted" in water vaporization. The heat contained in the exit stream needs to be re-utilized for the process to be energetically favorable. Different potential options are available as pre-heating the input stream of biomass or use this heat for other applications (electricity generation, cooling systems for animals if the HTL unit is close to a group of farms, etc.).

For the experimental set-up used in this research, biomass was located inside the reactor while bringing the system to reaction conditions. The reason for this way of operation was constraints in our pumping capabilities, which has an effect in the results obtained, and makes them difficult to extrapolate to a real industrial operation, where pumping capabilities allow for pumping biomass slurries at higher solid content to the reactor when reaction conditions are reached. Therefore, to get closer to an industrial operation protocol, this research tried (and my recommendation is to continue this path in future studies) to pump preheated biomass inside the reactor at the conditions of the reaction using a piston. This operational design will set-up a real initial time of reaction, without any heating-up ramping.

By shifting the technology from a batch process to a continuous operation, we would be able to increase throughput, product uniformity and reliability, and decrease the high load of labor associated with operation of batch systems.

9.2.4 Separation of phases obtained from HTL processes

In shifting the process to an industrially feasible system, the use of organic solvents dichloromethane (DCM) and ethyl acetate to separate aqueous and bio-crude oil phases is certainly undesired for several reasons. First, the economics of the process will not justify the use of large volumes of these solvents. More importantly, the use of these solvents hinders the sustainability of the process, because of their petrochemical origin and toxicity. Therefore, my recommendation is to use life cycle analysis to find suitable solvents to substitute for DCM and ethyl acetate for the liquid phases separation of HTL. Derived esters from levulinic acid are being investigated for this purpose, because of similar polarity to DCM. Levulinic acid is a short-chain carboxylic acid that can be obtained through sustainable practices from renewable sources (it has been observed in the aqueous phase of the HTL media generated in this research). Furthermore, the whole idea of liquid-liquid separation can be substituted by other means of separation, such as centrifugation or some sort of chromatographic techniques that could sort molecules based on different functionalities, instead of entire phases (mixtures of molecules). These two alternative separation techniques would have an implicit energy requirement. That is why a life cycle analysis about HTL phases separation is crucial to optimize this important step of the technology.

The goal of this research was to contribute to shift the perception of organic waste from a material that is considered an environmental and economic liability, to a valuable asset that will add value to a company portfolio. By adopting thermochemical valorization technologies, companies will have the potential not only save money currently spent in waste disposal, but also they will be able to extract its inherent value. Furthermore, these actions would potentially attract a growing number

of environmentally responsible investors, and their image on a more sustainable-committed society will set them apart from their competitors. Therefore, additional investigation that link the science and engineering knowledge with a business model is necessary. Economic analysis of the technology is required to identify the scale of the system that constitute a threshold for profitability. These recommendations are suggested from my strong belief that hydrothermal liquefaction technology for biomass valorization will contribute, sooner than later, to change the way we consider and treat organic waste.

APPENDIX I

CHARACTERIZATION OF THE SOLID PRODUCTS FROM HYDROTHERMAL LIQUEFACTION OF WASTE FEEDSTOCKS FROM FOOD AND AGRICULTURAL INDUSTRIES.

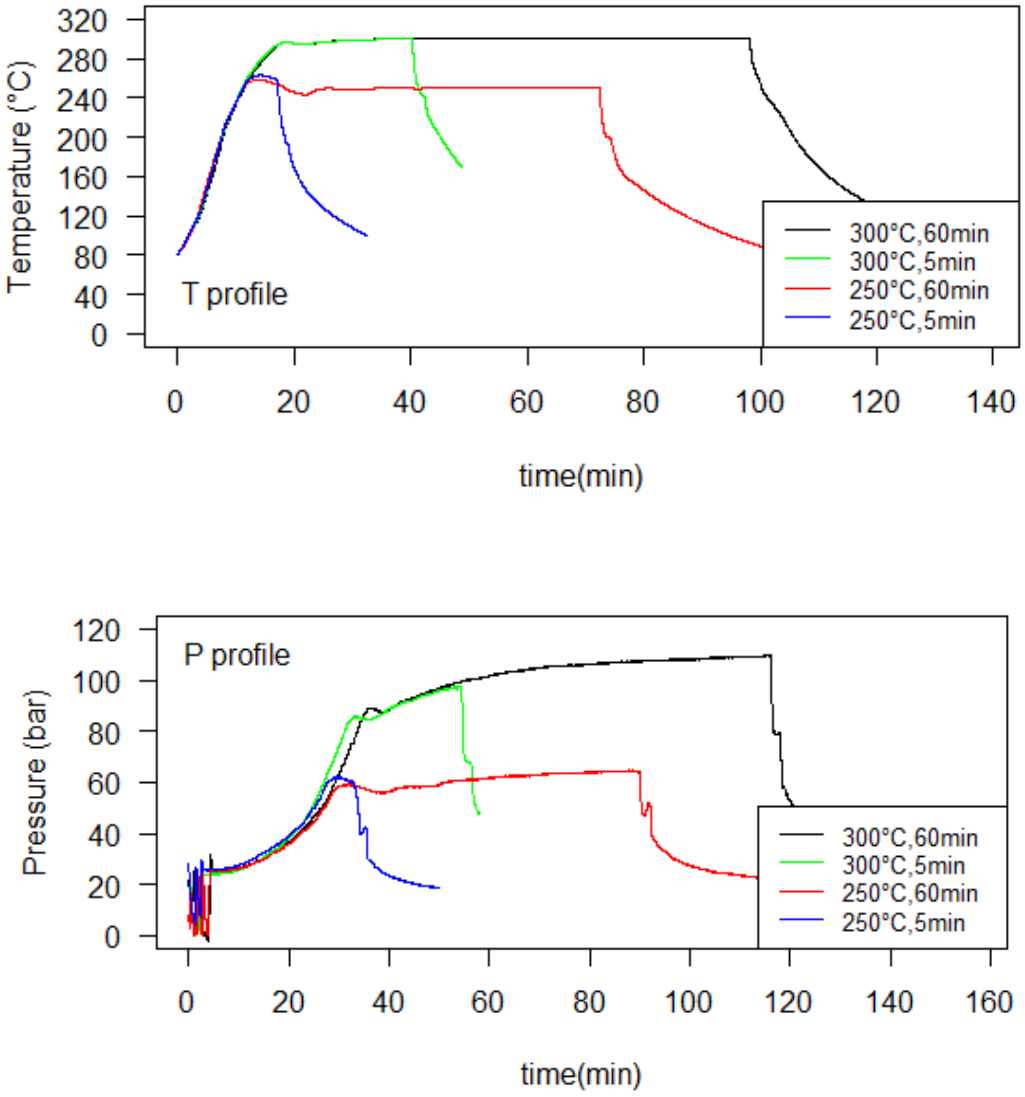

Figure AI-1. Temperature and pressure profiles for apple pomace as representative example. Time 0 in T profile chart corresponds to the moment when the system reaches 80˚C. Time 0 in the P profile chart corresponds to when logging-in starts to show the reactor purge with N_2

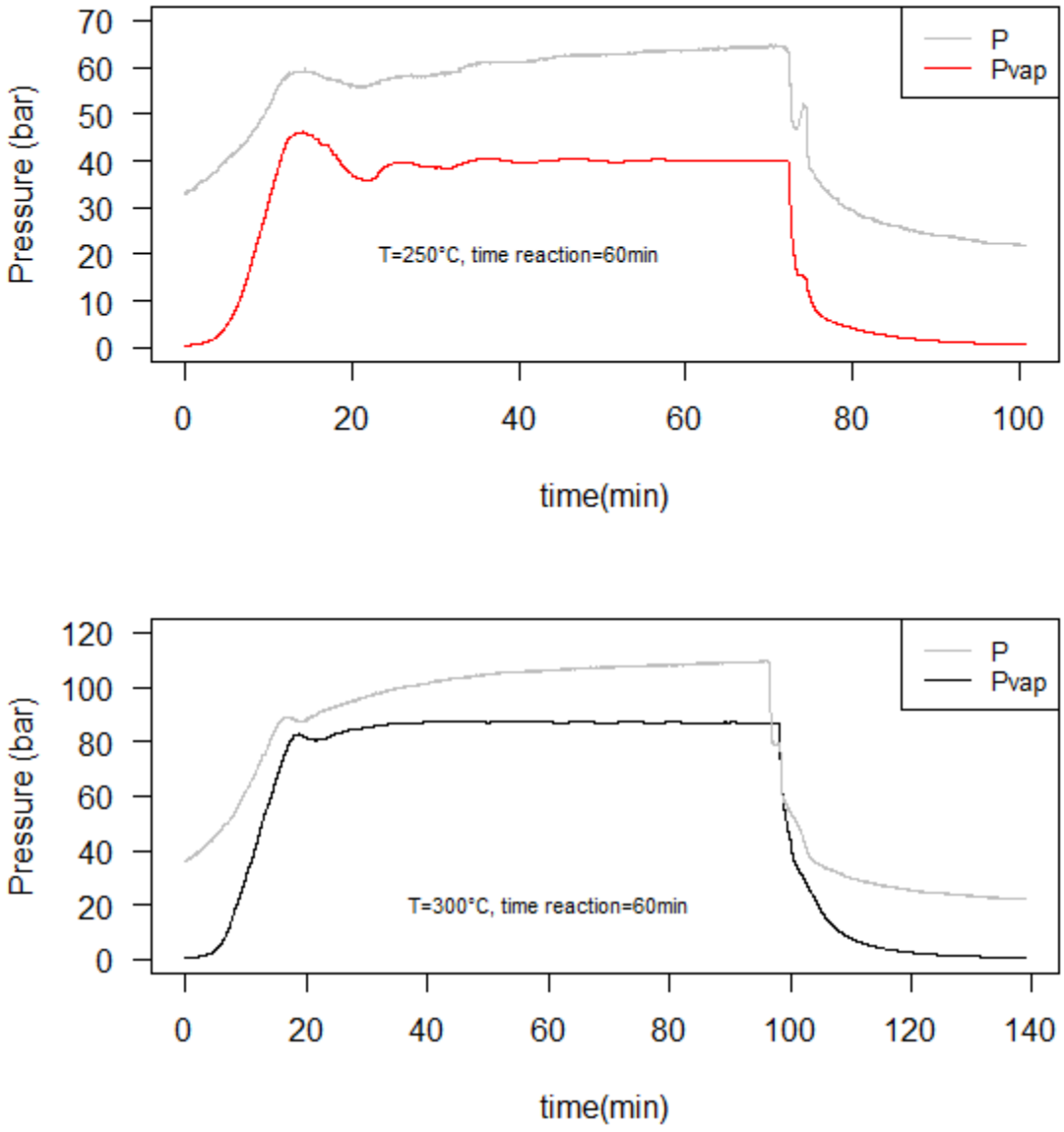

Figure AI-2. Confirmation of HTL operational conditions (Pressure of system is always above the saturation pressure of water at every temperature). Time 0 in this chart corresponds to the time when the system reaches 80˚C

Table AI-1. Average pH of HTL medium after reaction. Values represent the mean of three replicate experiments ± standard deviation.

Temperature (˚C)	Time (min)	Manure	Waste activated sludge	Food waste	Apple pomace	Red wine pomace	Whiskey stillage	Yogurt Whey	Olive oil pomace
250	5	8.2±0.1	8.4±0.0	3.9±0.0	3.7±0.0	4.2±0.0	4.0±0.1	3.8±0.0	4.2±0.1
250	60	8.6±0.1	8.7±0.1	4.0±0.1	4.0±0.0	4.8±0.1	4.3±0.1	3.9±0.0	4.2±0.0
300	5	7.4±0.0	8.7±0.1	4.1±0.0	3.9±0.0	5.0±0.0	4.5±0.1	4.0±0.0	4.1±0.0
300	60	7.5±0.1	8.4±0.1	4.4±0.1	4.0±0.1	4.9±0.0	4.8±0.1	4.2±0.0	4.1±0.1

Table AI-2. Coefficient values for a linear regression model of hydro-char yield (y) as a function of the ash content (x_1) and pH (x_2) of the raw feedstock. The ANOVA test showed statistical significance ($p<0.001$) for the presented coefficients.

Variable	Coefficient value
x_1-Ash	-0.1484
x_2-pH	7.1251

Table AI-3. Elemental analysis and ash content of hydro-char generated from all feedstock at each reaction conditions. Values are in wt% of dry hydro-char and represent the mean of three replicate experiments ± standard deviation.

Temperature (˚C)	Time (min)	C	N	H	Ash	O	Atomic C/H
Manure		35.6±0.2	2.4±0.0	3.9±0.1	33.8±0.3	24.2±0.1	0.75±0.04
250	5	36.1±3.6	1.1±0.1	3.7±0.6	46.6±1.4	10.6±3.0	0.82±0.05
250	60	32.7±0.6	1.3±0.1	2.8±0.1	52.3±0.7	10.9±0.1	0.99±0.01
300	5	30.1±1.2	1.4±0.1	2.4±0.1	58.7±3.1	7.4±2.6	1.04±0.02
300	60	30.3±1.5	1.6±0.3	2.5±0.2	59.6±3.0	6.0±1.3	1.01±0.02
Waste activated sludge		30.9±0.3	3.9±0.2	4.2±0.2	38.8±0.3	22.2±0.4	0.62±0.03
250	5	20.1±0.7	1.1±0.2	2.3±0.2	69.5±1.1	7.0±0.3	0.73±0.04
250	60	18.3±0.4	1.1±0.1	2.0±0.0	74.9±0.3	3.7±0.5	0.75±0.01
300	5	17.4±1.2	1.7±0.7	1.8±0.1	76.0±2.1	3.1±0.3	0.80±0.02
300	60	27.4±2.0	0.9±0.2	3.1±0.2	53.1±1.6	15.4±0.9	0.73±0.03
Food waste		47.9±0.5	2.7±0.1	7.0±0.2	5.6±0.0	36.6±0.5	0.57±0.05
250	5	59.2±2.6	3.9±0.2	5.5±0.9	6.2±2.0	25.1±3.0	0.91±0.09
250	60	63.2±2.2	4.7±0.0	4.9±0.2	7.7±0.6	19.5±2.0	1.08±0.03
300	5	64.0±1.4	5.0±0.2	4.2±0.1	13.0±2.5	13.8±0.8	1.28±0.02
300	60	67.4±2.4	5.0±0.3	4.5±0.4	10.1±2.4	12.9±1.5	1.25±0.06
Red wine pomace		50.5±0.4	2.7±0.2	5.7±0.2	9.6±0.3	31.6±0.7	0.74±0.06
250	5	63.9±0.6	3.1±0.1	5.3±0.1	0.9±0.4	26.8±0.8	1.00±0.01
250	60	68.8±0.6	3.3±0.1	5.0±0.0	1.1±0.5	21.7±0.2	1.14±0.01
300	5	69.1±0.5	3.5±0.0	4.7±0.0	4.1±0.3	18.6±0.4	1.24±0.01
300	60	68.6±1.0	3.4±0.1	4.3±0.3	4.7±2.1	19.0±2.6	1.32±0.04

Temperature (˚C)	Time (min)	C	N	H	ash	O	Atomic C/H
Whiskey stillage		46.9±0.1	4.1±0.2	6.5±0.0	3.7± 0.2	38.8± 0.1	0.59±0.02
250	5	62.8±1.5	5.0±0.4	5.5±0.1	0.4±0.2	26.3±1.6	0.95±0.02
250	60	66.4±1.8	5.2±0.9	5.6±0.2	0.9±0.1	21.8±1.5	0.98±0.02
300	5	71.5±0.6	5.3±0.1	4.8±0.1	2.3±0.4	16.1±1.0	1.26±0.01
300	60	73.7±0.3	4.9±0.3	5.8±0.5	2.9±0.3	12.8±0.5	1.07±0.09
Yogurt whey		19.8±0.1	0.7±0.0	2.6±0.1	54.1±0.4	22.7±0.0	0.64±0.03
250	5	37.9±2.2	3.9±0.7	3.3±0.6	N/A	N/A	0.99±0.15
250	60	57.3±1.2	3.9±0.6	3.7±0.7	N/A	N/A	1.35±0.30
300	5	54.3±2.2	3.9±0.7	3.3±0.2	N/A	N/A	1.38±0.12
300	60	42.3±1.6	2.9±0.2	2.8±0.2	N/A	N/A	1.25±0.04
Olive oil pomace		56.1±0.3	2.5±0.0	7.1±0.1	3.9±0.7	31.5±0.2	0.65±0.02
250	5	58.3±0.8	1.4±0.2	5.6±0.1	5.5±0.8	29.6±1.0	0.86±0.00
250	60	63.3±0.3	1.7±0.0	4.5±0.1	8.1±1.5	22.3±1.7	1.16±0.02
300	5	67.2±2.1	2.1±0.2	4.0±0.4	8.1±2.3	17.6±0.2	1.43±0.19
300	60	67.8±1.3	2.7±0.1	4.8±0.3	8.1±2.0	16.7±1.0	1.19±0.06

Table AI-4. Higher heating values (HHV) of generated hydro-char and percentage of change with respect to HHV of raw feedstock given in parenthesis. Values represent the mean of three replicate experiments ± standard deviation.

Temperature (°C)	Time (min)	Manure	Waste activated sludge	Food waste	Apple pomace	Red wine pomace	Whiskey stillage	Olive oil pomace
250	5	15.6±2.0 (+17.4)	8.9±0.5 (-28.8)	23.4±3.1 (+72.4)	25.7±0.9 (+42.2)	24.4±0.6 (+24.8)	24.5±1.0 (+34.0)	22.4±0.6 (-4.7)
250	60	13.1±0.3 (-1.7)	8.4±0.3 (-32.5)	24.9±1.6 (+83.1)	29.0±0.2 (+61.0)	26.6±0.3 (+35.8)	26.6±1.3 (+45.6)	23.9±0.4 (+0.8)
300	5	12.3±0.8 (-7.4)	7.9±0.6 (-36.8)	25.2±0.7 (+85.1)	30.6±0.3 (+69.4)	26.7±0.2 (+36.6)	28.1±0.6 (+53.8)	25.3±0.3 (+6.5)
300	60	12.8±0.7 (-3.6)	11.0±1.2 (-11.9)	26.9±1.9 (+98.2)	31.3±0.2 (+73.7)	26.7±0.4 (+32.8)	30.9±1.1 (+69.2)	26.7±1.1 (+12.7)

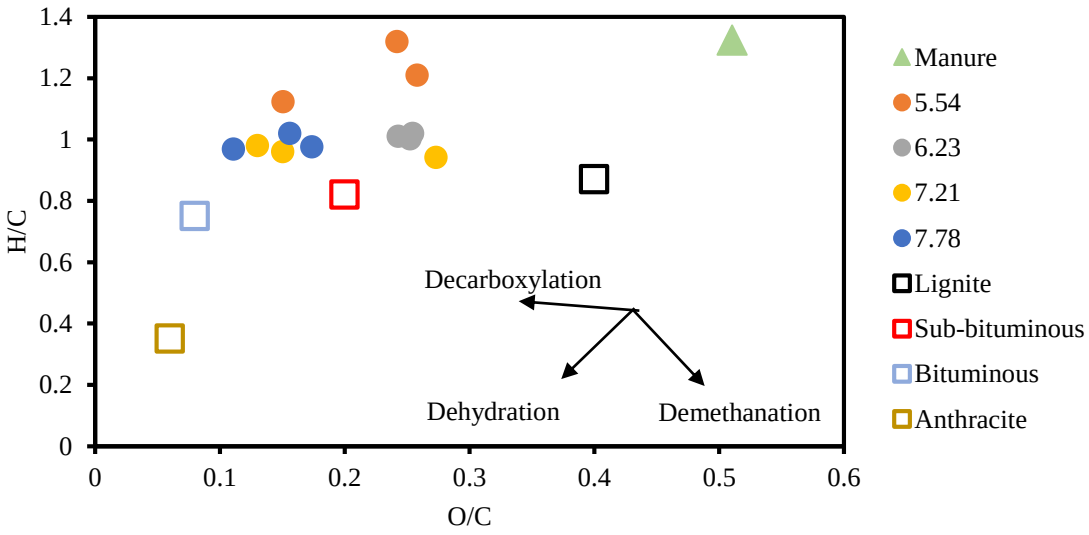

Figure AI-3. Van Krevelen diagram for manure, and comparison with forms of coal

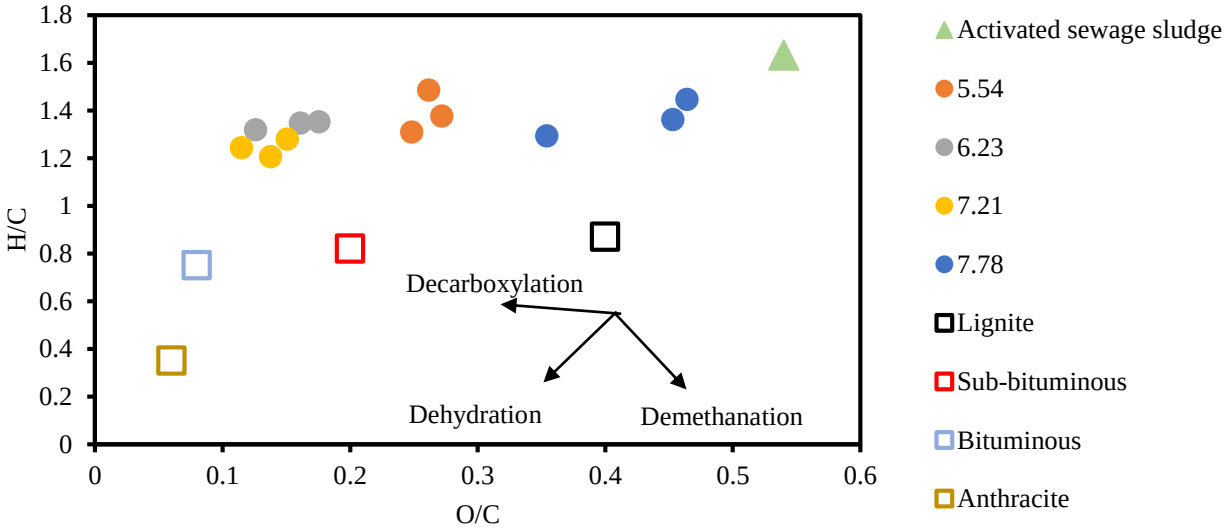

Figure AI-4. Van Krevelen diagram for activated sewage sludge, and comparison with forms of coal

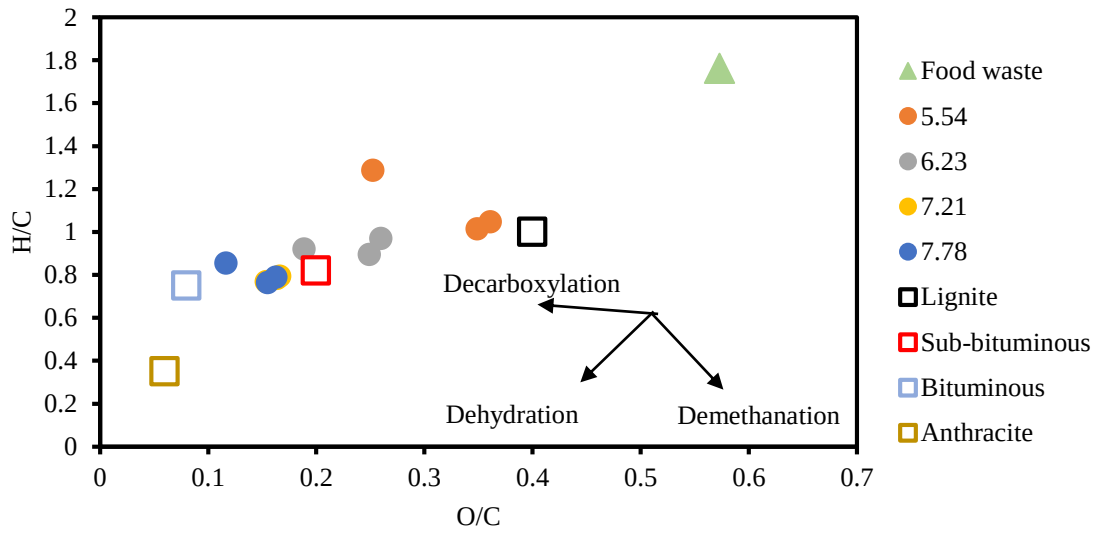

Figure AI-5. Van Krevelen diagram for food waste, and comparison with forms of coal

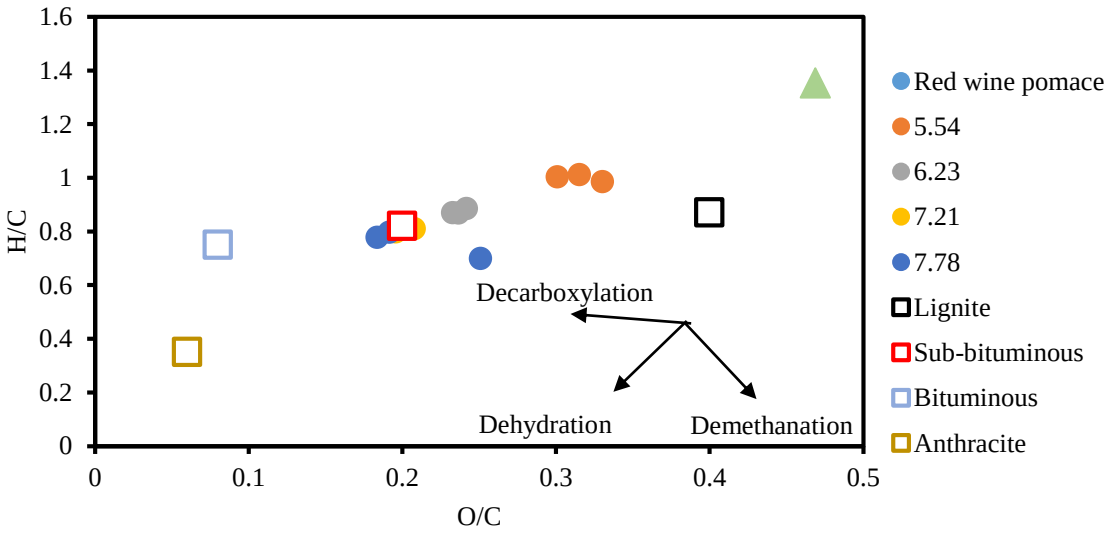

Figure AI-6. Van Krevelen diagram for red wine pomace, and comparison with forms of coal

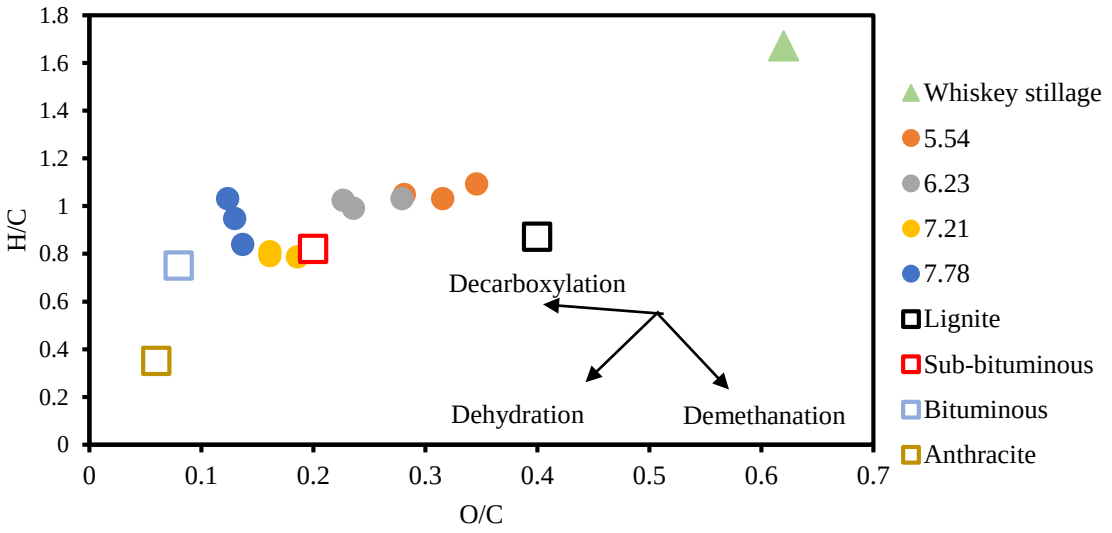

Figure AI-7. Van Krevelen diagram for whiskey stillage, and comparison with forms of coal

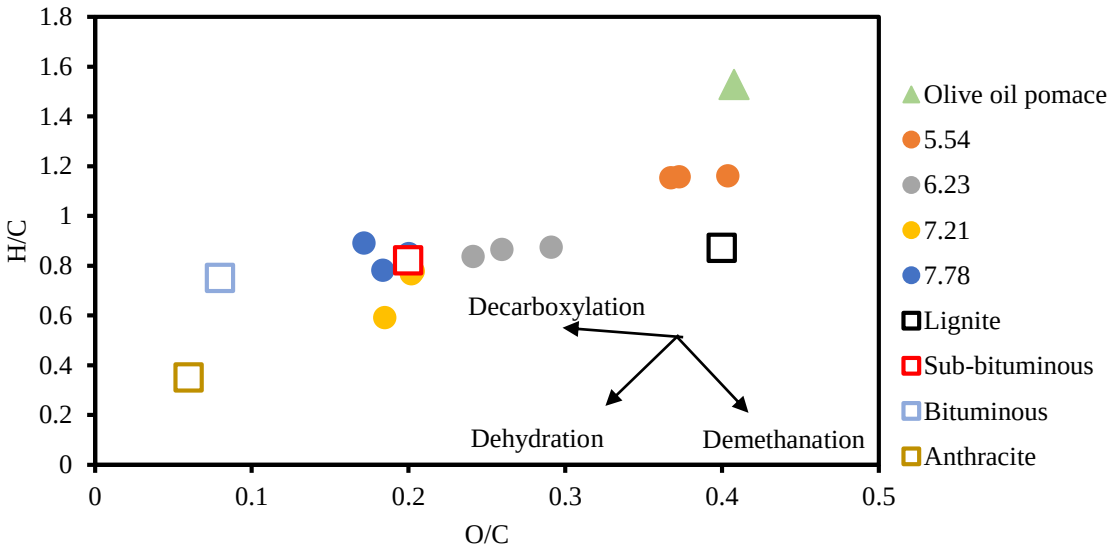

Figure AI-8. Van Krevelen diagram for olive oil pomace, and comparison with forms of coal

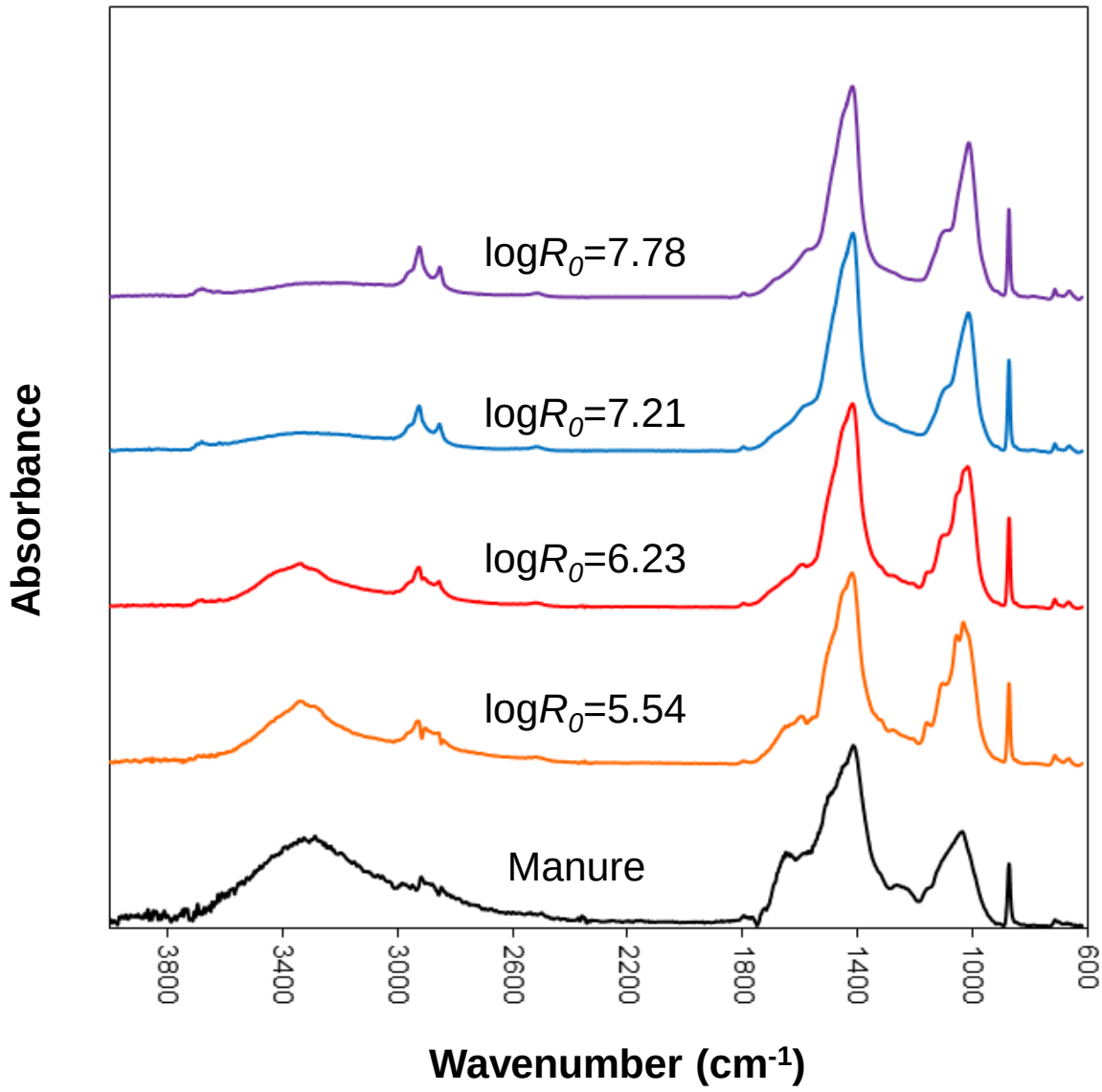

Figure AI-9. FTIR spectra of hydro-char from manure at different severity factors (log R_0). Every spectra is the average of three replicates for the three samples obtained at every severity factor (triplicate measurements of triplicate experiments, average of nine spectra total). Spectra was ATR corrected, cut between 4000–620 cm^{-1}, base-line corrected, and vector normalized. They were place in a waterfall layout for comparison purposes.

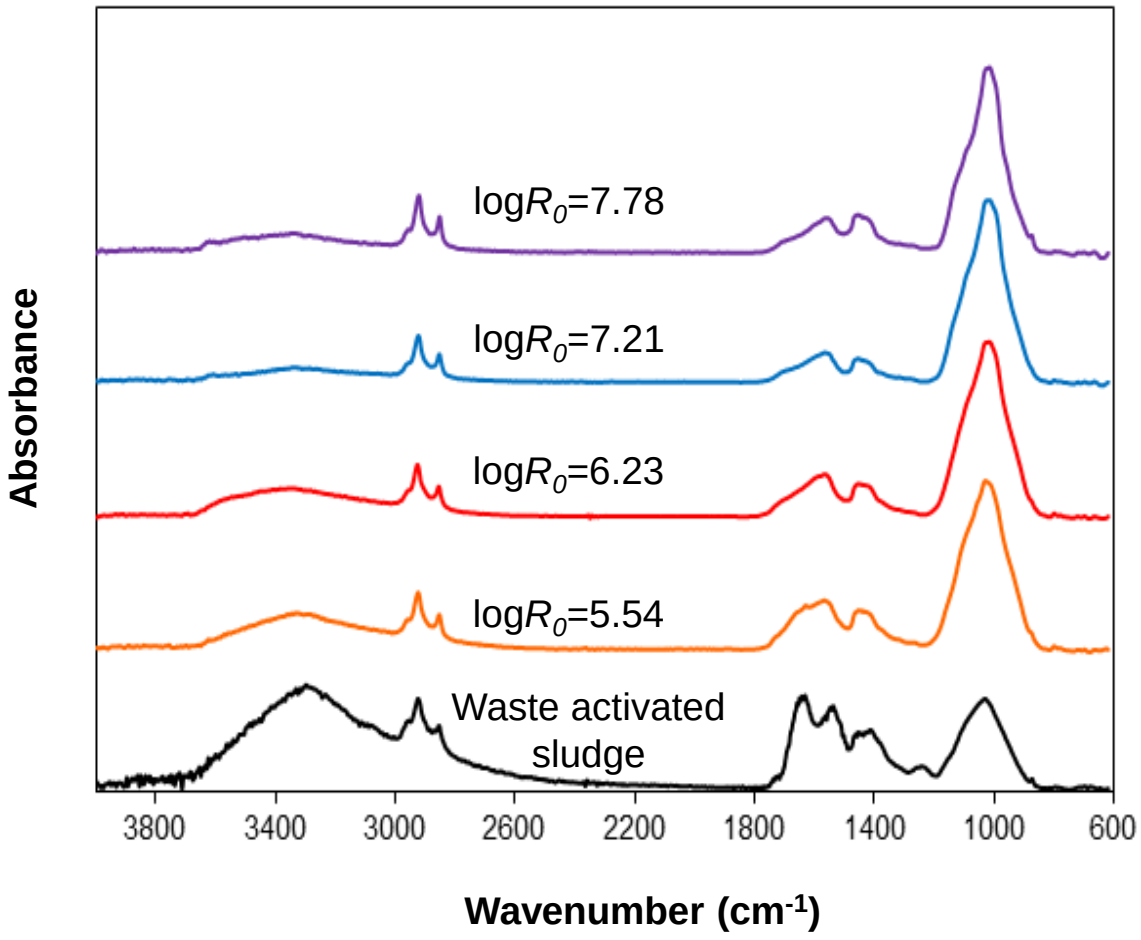

Figure AI-10. FTIR spectra of hydro-char from waste activated sludge at different severity factors (log R_0). Every spectra is the average of three replicates for the three samples obtained at every severity factor (triplicate measurements of triplicate experiments, average of nine spectra total). Spectra was ATR corrected, cut between 4000–620 cm^{-1}, base-line corrected, and vector normalized. They were place in a waterfall layout for comparison purposes.

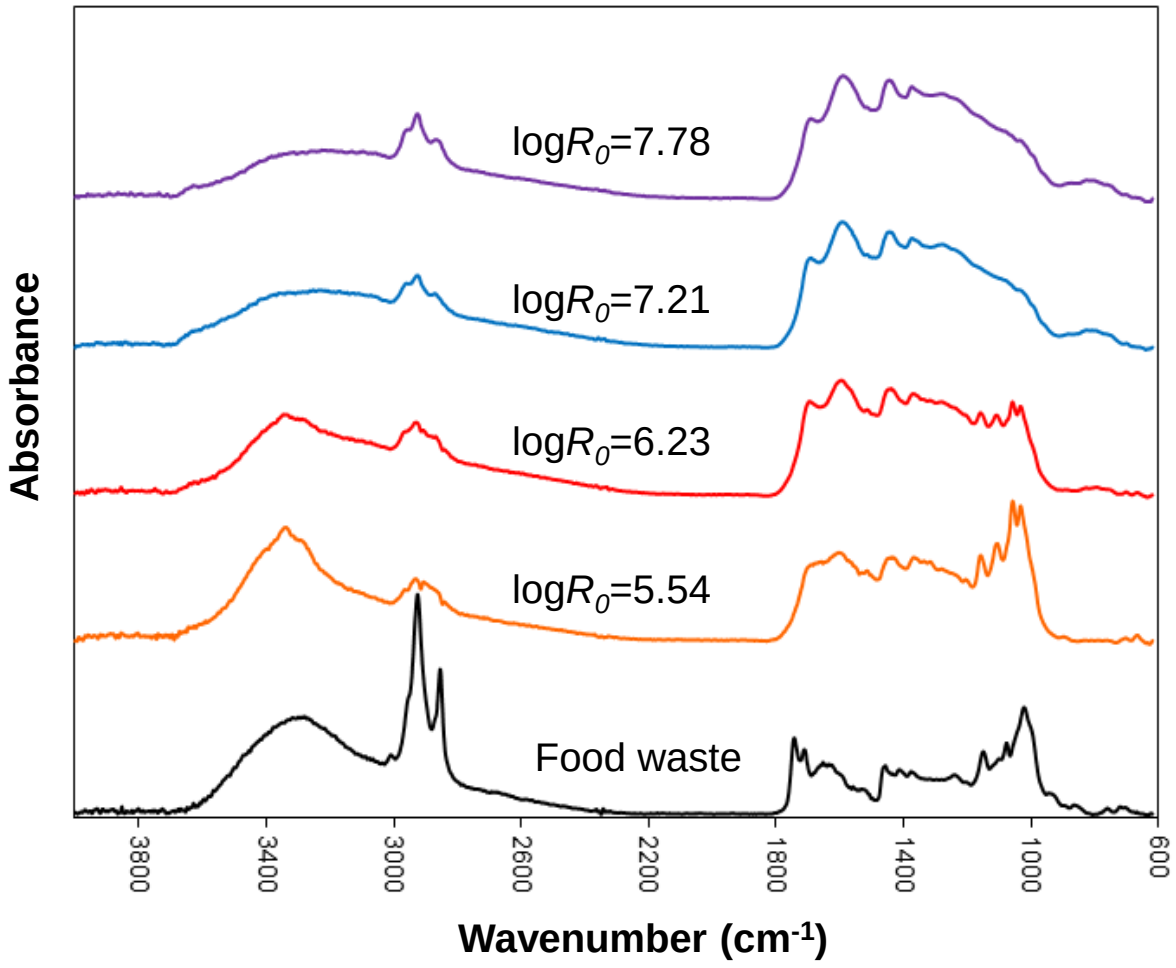

Figure AI-11. FTIR spectra of hydro-char from food waste at different severity factors (log R_0). Every spectra is the average of three replicates for the three samples obtained at every severity factor (triplicate measurements of triplicate experiments, average of nine spectra total). Spectra was ATR corrected, cut between 4000–620 cm^{-1}, base-line corrected, and vector normalized. They were place in a waterfall layout for comparison purposes.

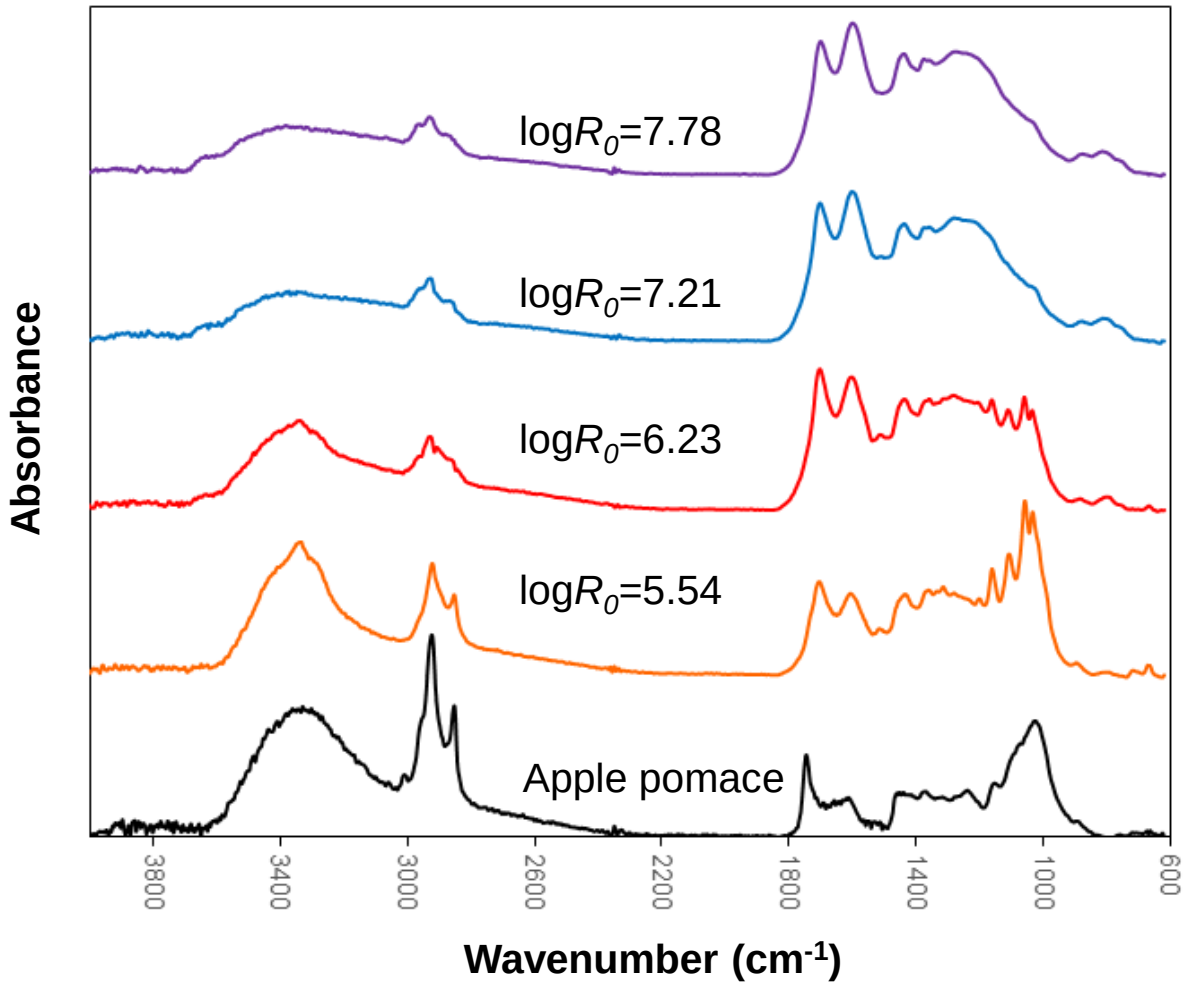

Figure AI-12. FTIR spectra of hydro-char from apple pomace at different severity factors (log R_0). Every spectra is the average of three replicates for the three samples obtained at every severity factor (triplicate measurements of triplicate experiments, average of nine spectra total). Spectra was ATR corrected, cut between 4000–620 cm^{-1}, base-line corrected, and vector normalized. They were place in a waterfall layout for comparison purposes.

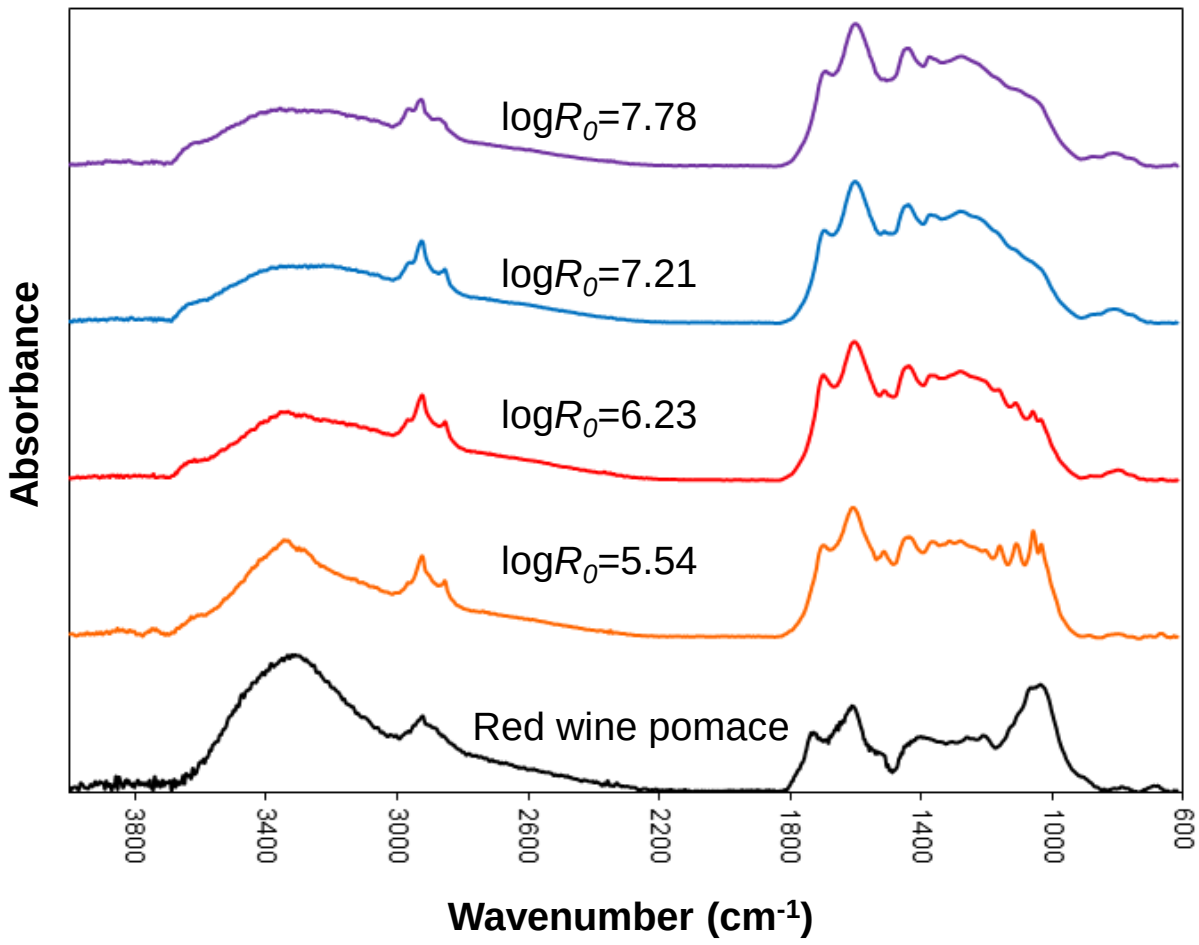

Figure AI-13. FTIR spectra of hydro-char from red wine pomace at different severity factors (log R_0). Every spectra is the average of three replicates for the three samples obtained at every severity factor (triplicate measurements of triplicate experiments, average of nine spectra total). Spectra was ATR corrected, cut between 4000–620 cm^{-1}, base-line corrected, and vector normalized. They were place in a waterfall layout for comparison purposes.

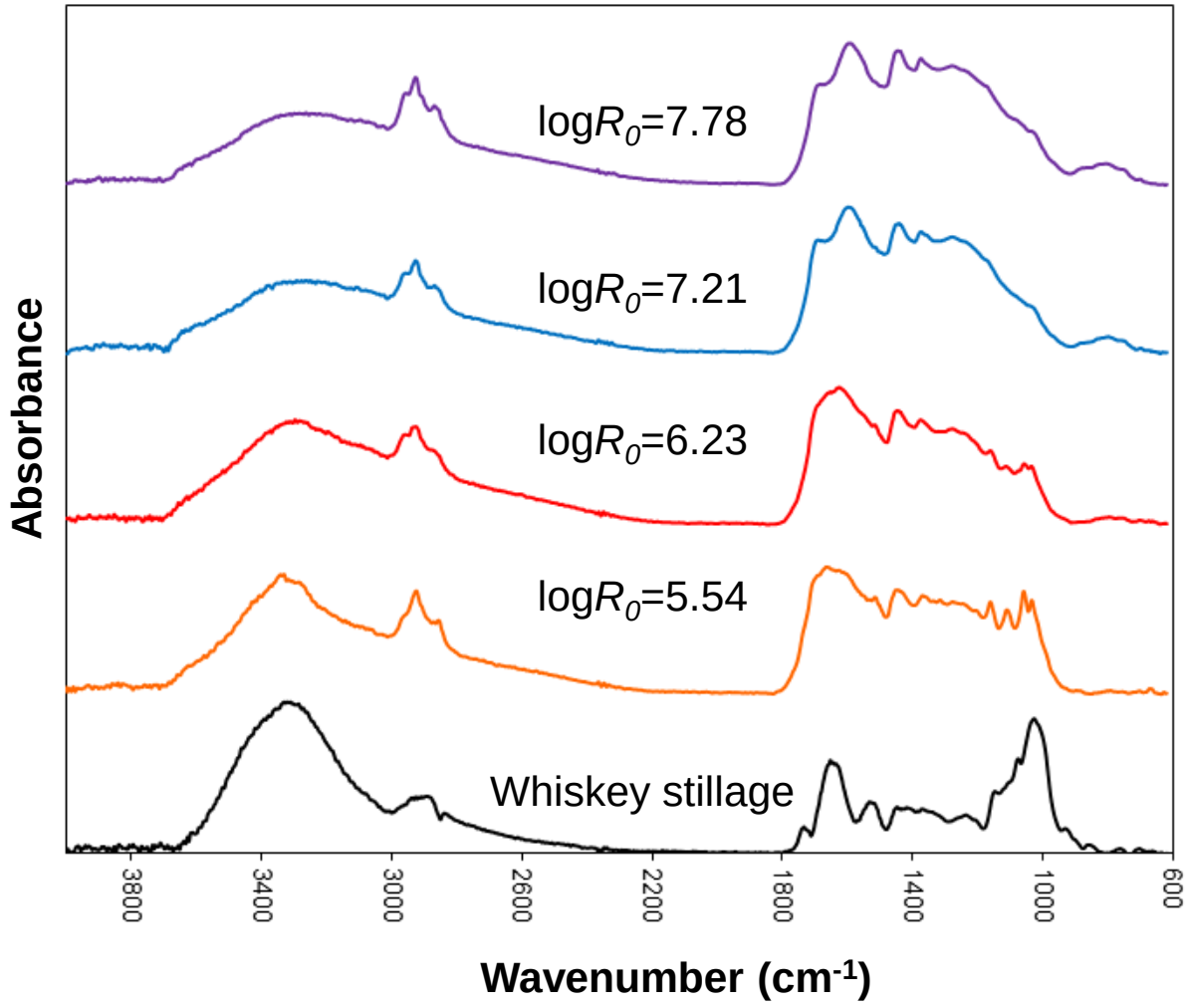

Figure AI-14. FTIR spectra of hydro-char from whiskey stillage at different severity factors (log R_0). Every spectra is the average of three replicates for the three samples obtained at every severity factor (triplicate measurements of triplicate experiments, average of nine spectra total). Spectra was ATR corrected, cut between 4000–620 cm^{-1}, base-line corrected, and vector normalized. They were place in a waterfall layout for comparison purposes.

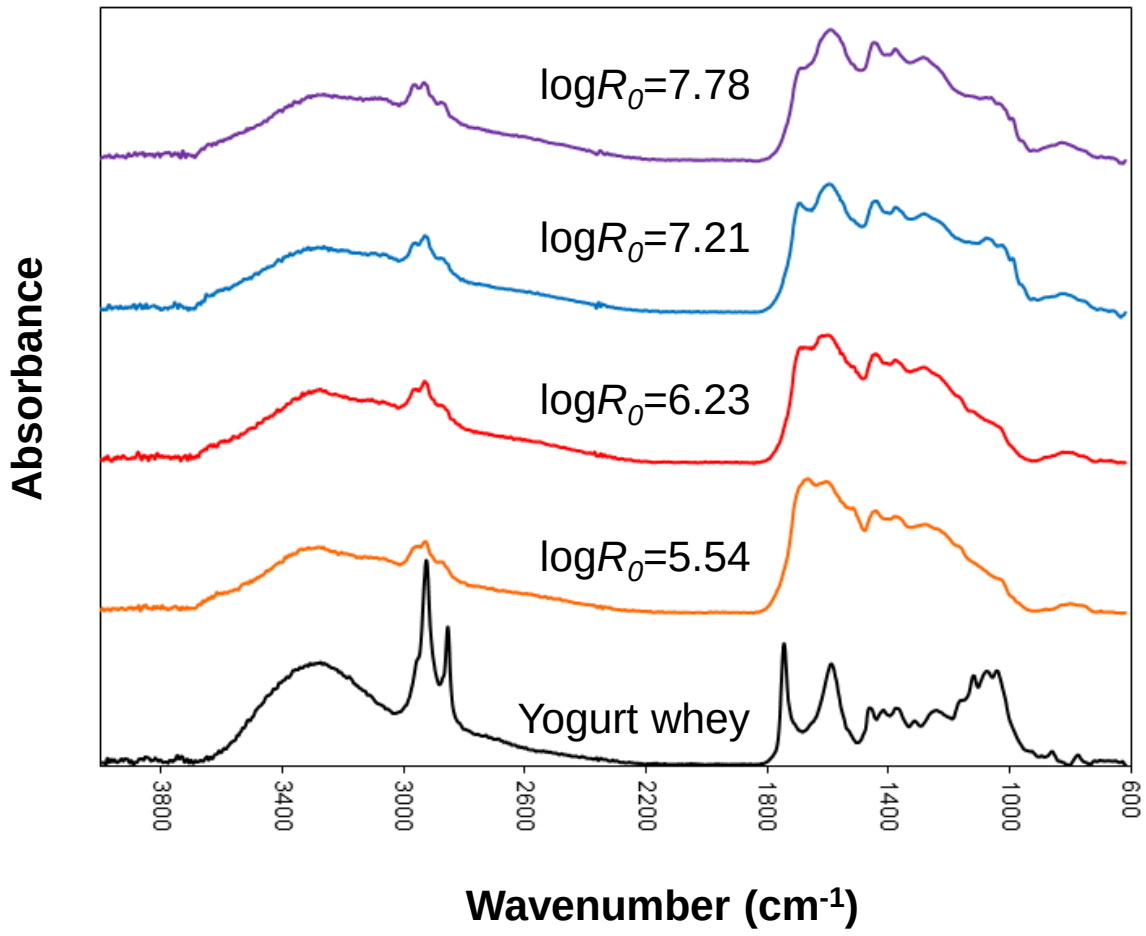

Figure AI-15. FTIR spectra of hydro-char from yogurt whey at different severity factors (log R_0). Every spectra is the average of three replicates for the three samples obtained at every severity factor (triplicate measurements of triplicate experiments, average of nine spectra total). Spectra was ATR corrected, cut between 4000–620 cm^{-1}, base-line corrected, and vector normalized. They were place in a waterfall layout for comparison purposes.

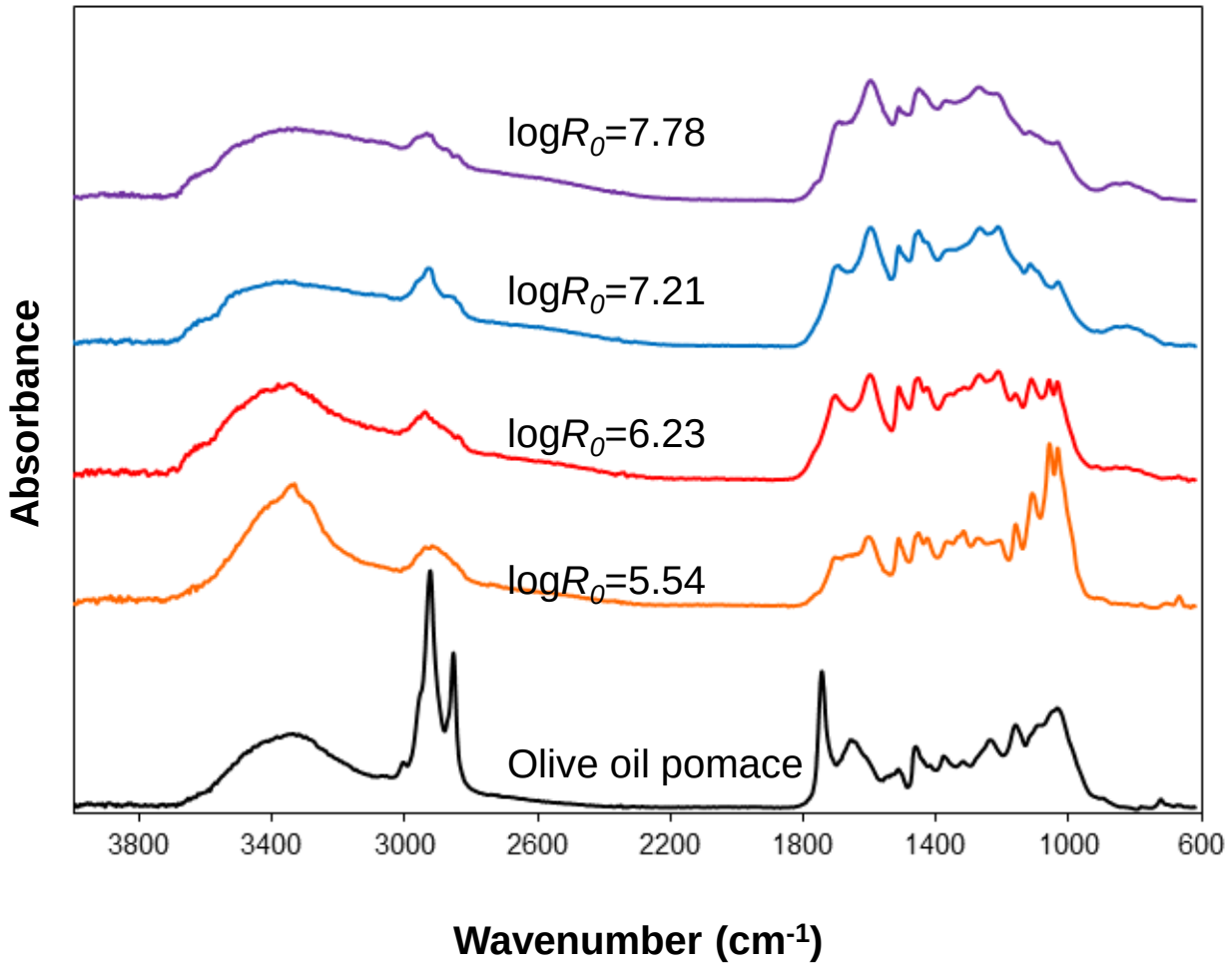

Figure AI-16. FTIR spectra of hydro-char from olive oil pomace at different severity factors (log R_0). Every spectra is the average of three replicates for the three samples obtained at every severity factor (triplicate measurements of triplicate experiments, average of nine spectra total). Spectra was ATR corrected, cut between 4000–620 cm^{-1}, base-line corrected, and vector normalized. They were place in a waterfall layout for comparison purposes.

Table AI-5. Assignment of wavenumbers typically found in biomass with the corresponding chemical structure according to literature.

Wavenumber (cm^{-1})	Chemical structure	References
3700–3000	Intra- and intermolecular hydrogen bonding	(Abidi, Cabrales, and Haigler 2014)
2920–2850	CH_2 (asymmetrical and symmetrical stretching)	(Abidi, Cabrales, and Haigler 2014)
1799 and 1652	Water in sample	(Saika et al. 2005), (Li, Wang, and Wu 2016)
1793	Carbonyl functionalities	(Cornelissen et al. 2008)
1770–1780	C=O stretch	(Illinois State University 2015)
1760–1766	Carbonyl in a 5 membered-ring (hemicellulose)	(Mossoba 1998)
1734 and 1726	C=O stretching vibrations in the ester groups	(Shi and Yang 2012), (Bodirlau, Teaca, and Spiridon 2009) (Heredia-Guerrero et al. 2014)
1716	C=O carboxyl group	(Syngellakis 2014)
1691	C=O conjugated with aromatic ring	(Liu et al. 2017)
1630	Extractable carbonyl compounds formed from lignin or possibly hemicelluloses	(Nuopponen and Vourinen 2005)
1620–1680	C=C aliphatic stretch	(Du, Valla, and Bollas 2013)
1600	Aromatic ring vibration and C=O stretch (lignin)	(Painter et al. 1983), (Xu et al. 2013)
1583–1593	C=C aromatic 6 members ring	(Foo et al. 2016)
1540–1560	C=C ring polynuclear aromatic	(Foo et al. 2016)
1500–1510	Aromatic skeletal vibrations (lignin)	(Stewart et al. 1995), (Haykir and Bahcegul 2013)
1468	CH_2 stretch	(Heredia-Guerrero et al. 2014)

1406	Carboxylate group stretching	(Magalhaes et al. 2012)
1370–1390	Aromatic methyl group	(Foo et al. 2016)
1386	C-O stretching alcohols	(Srinivasan et al. 2005)
1353	Weak C-H bend	(Lobo and Bonilla 2003)
1317	CH_2 rocking cellulose	(Szymanska-Chargot and Zdunek 2013), (Abidi, Cabrales, and Haigler 2014)
1292	C-O phenolic group	(Siontorou et al. 2015)
1167	C-O stretching of ester group	(Kline et al. 2010)
1160	C-O-C asymmetrical stretching (hemicellulose and cellulose)	(Xu et al. 2013) (Sim et al. 201AD)
1130–1140	Aromatic C-H in-plane deformation	(Galletti et al. 2015)
1124	C-H in plane deformation aromatics (lignin)	(Gunasekaran and Ponnusamy 2005)
1083	C-O stretching secondary alcohol	(Bouchard et al. 1990)
1055	C-O stretch cellulose	(Abidi, Cabrales, and Haigler 2014)
1015–1031	C-O stretching primary alcohols	(Kline et al. 2010)
1003 and 986	C-O valence vibration and ring stretch (cellulose)	(Xu et al. 2013) (Abidi, Cabrales, and Haigler 2014)
977	Rocking C-H	(Arivazhagan, Sambathkumar, and Jeyavijayan 2010)
972	Methine group	(Setiawan and Aulia 2017)
928	Glycosidic linkage (cellulose)	(Xu et al. 2013)
912–910	C-H out of plane in positions 2,5, and 6 (Guaiacyl, lignin)	(Poletto and Zattera 2013), (Yue and Li 2016)
904	Antysymmetric out of phase ring stretch of amorphous cellulose	(Stewart et al. 1995)
891	CH_3 rock cellulose	(Yao, Xu, and Feng 2003)
874	Glycosidic linkage (cellulose and hemicellulose)	(Xu et al. 2013)

775 and 734	C-H bending (aromatics)	(Castle 2009) (Strezov 2012)
723	CH_2 aliphatic (alkanes)	(Hagemann et al. 1989) (Heredia-Guerrero et al. 2014)

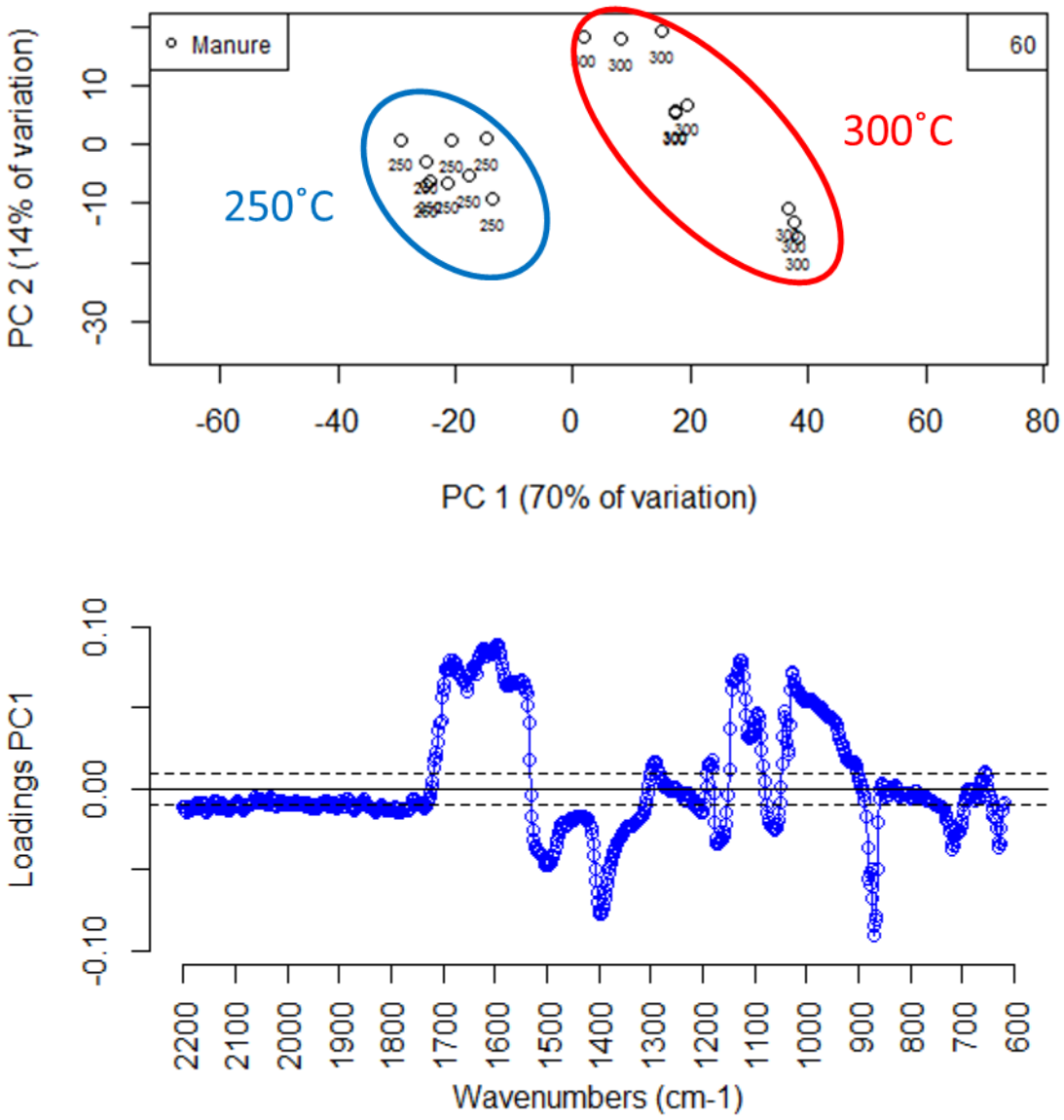

Figure AI-17. PCA for FTIR spectra of hydro-char generated from manure: (a) bi-plot for all FTIR spectra of hydro-char generated at 60 minutes, showing the effect of the temperature; and (b) loading plot of PC1 vs. FTIR wavenumber showing the specific wavenumbers that contributed to the scattering, provided in Table 4.

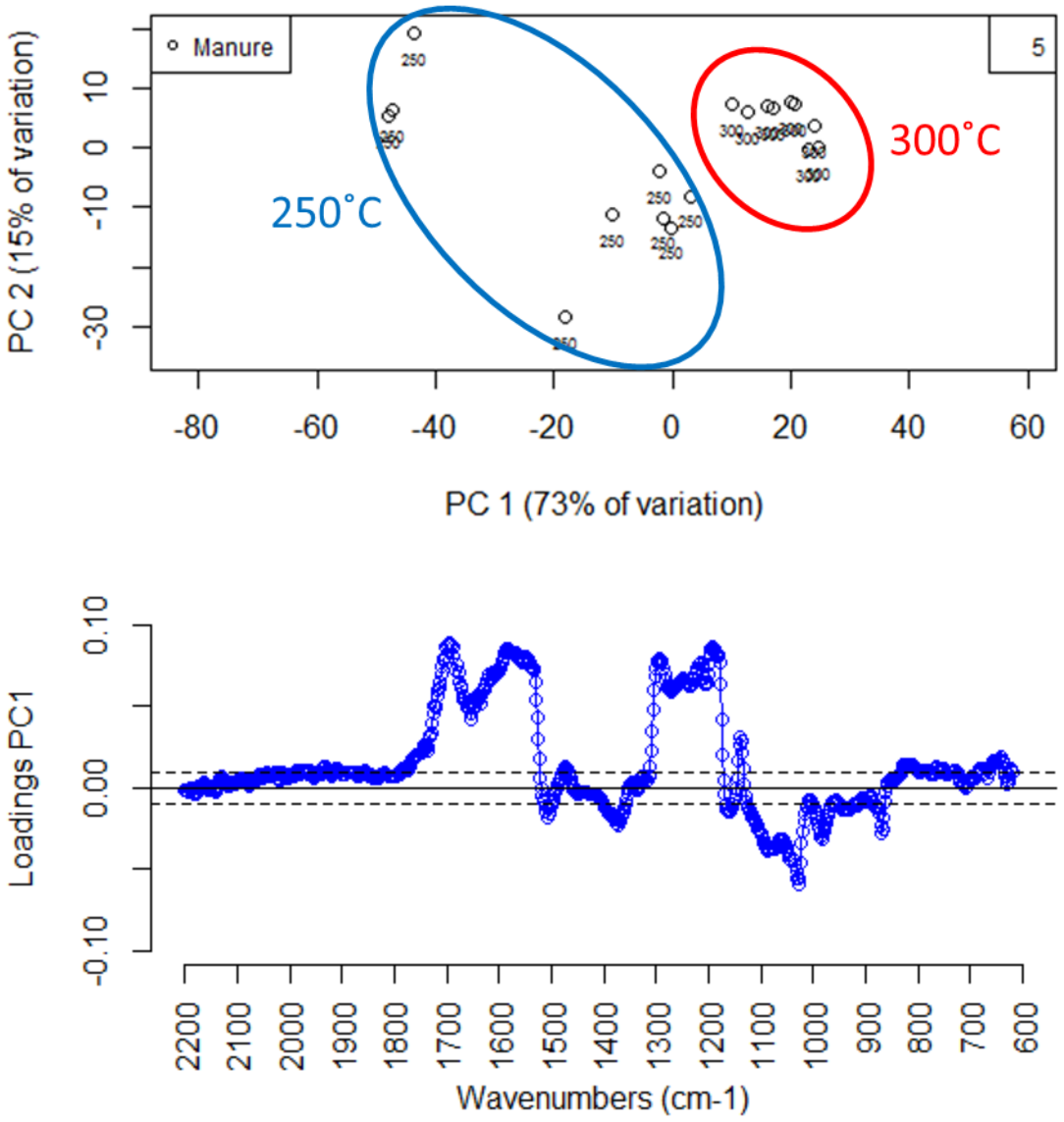

Figure AI-18. PCA for FTIR spectra of hydro-char generated from manure: (a) bi-plot for all FTIR spectra of hydro-char generated at 5 minutes, showing the effect of the temperature; and (b) loading plot of PC1 vs. FTIR wavenumber showing the specific wavenumbers that contributed to the scattering, provided in Table 4.

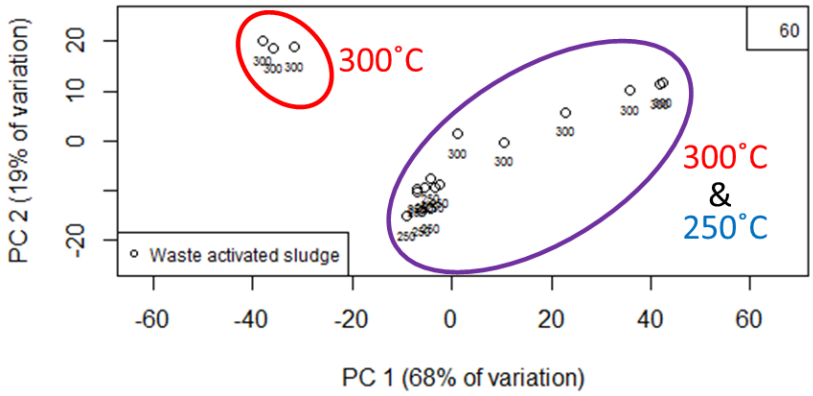

Figure AI-19. PCA for FTIR spectra of hydro-char generated from waste activated sludge: (a) bi-plot for all FTIR spectra of hydro-char generated at 60 minutes, showing the inconclusive effect of the temperature, as it was not possible to define two clusters of data corresponding to different temperatures (No loading plot shown)

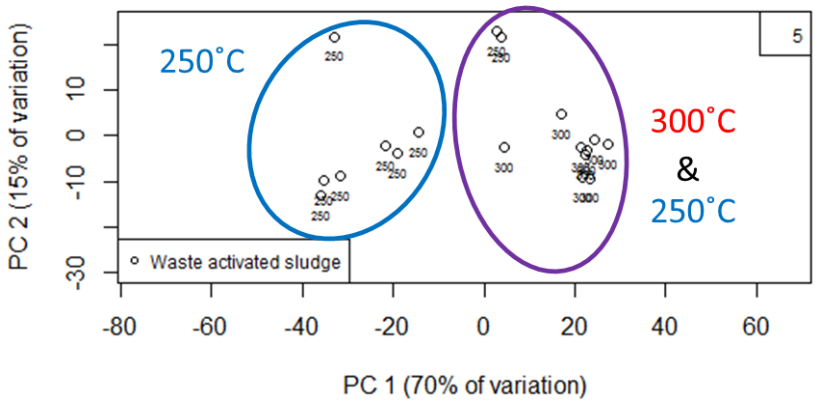

Figure AI-20. PCA for FTIR spectra of hydro-char generated from waste activated sludge: (a) bi-plot for all FTIR spectra of hydro-char generated at 5 minutes, showing the inconclusive effect of the temperature as it was not possible to define two clusters of data corresponding to different temperatures (No loading plot shown)

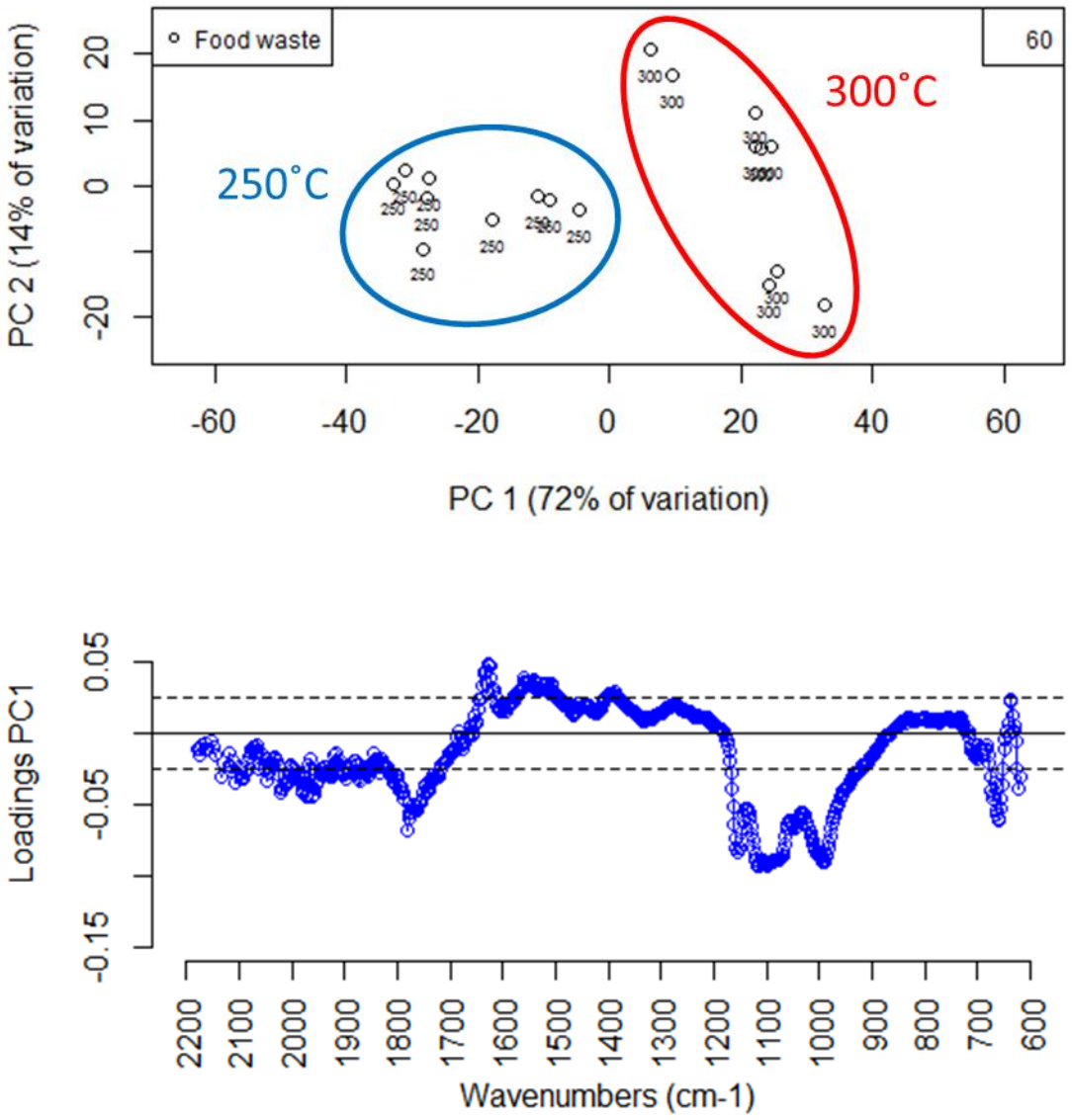

Figure AI-21. PCA for FTIR spectra of hydro-char generated from food waste: (a) bi-plot for all FTIR spectra of hydro-char generated at 60 minutes, showing the effect of the temperature; and (b) loading plot of PC1 vs. FTIR wavenumber showing the specific wavenumbers that contributed to the scattering, provided in Table 4.

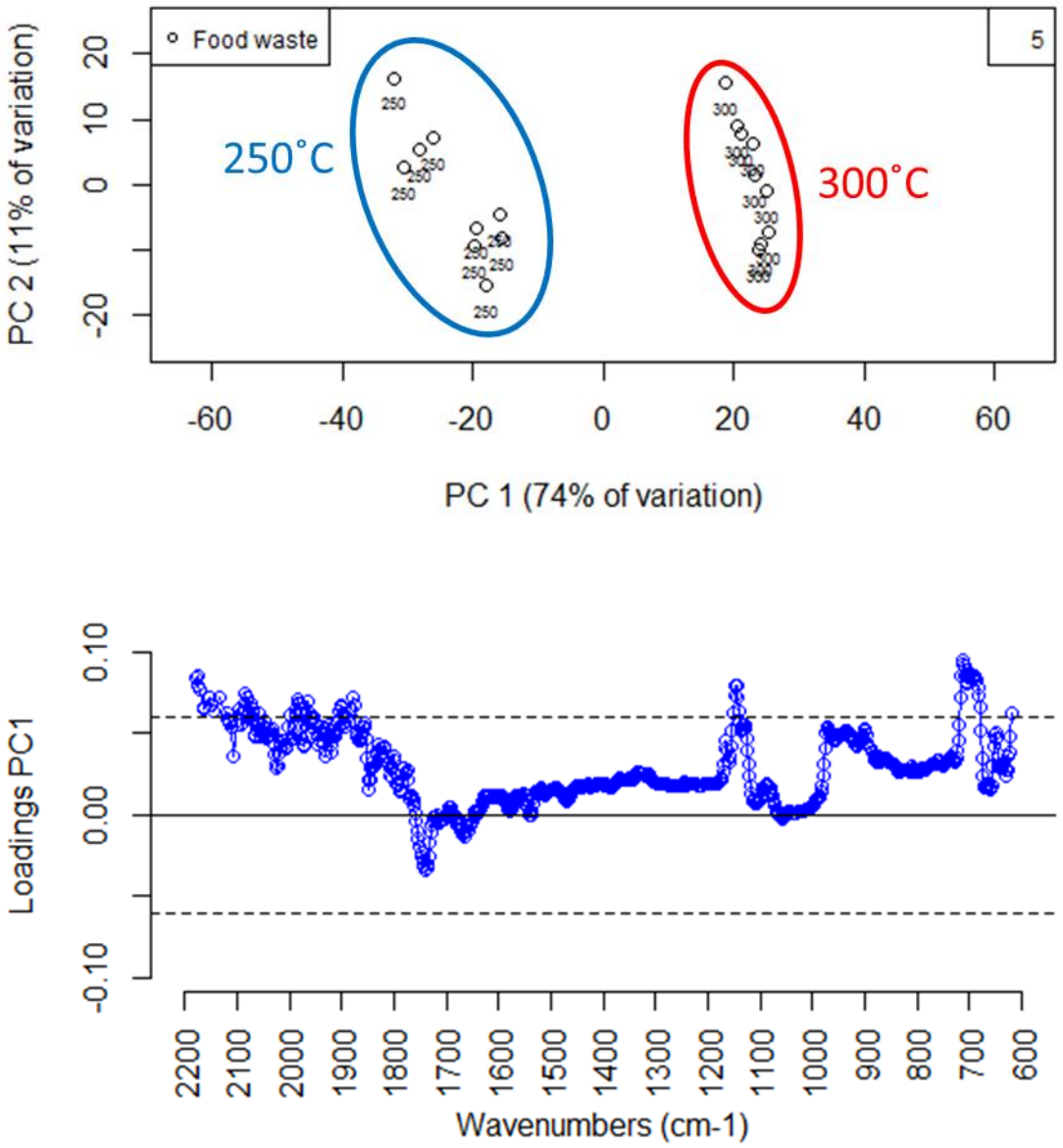

Figure AI-22. PCA for FTIR spectra of hydro-char generated from food waste: (a) bi-plot for all FTIR spectra of hydro-char generated at 5 minutes, showing the effect of the temperature; and (b) loading plot of PC1 vs. FTIR wavenumber showing the specific wavenumbers that contributed to the scattering, provided in Table 4.

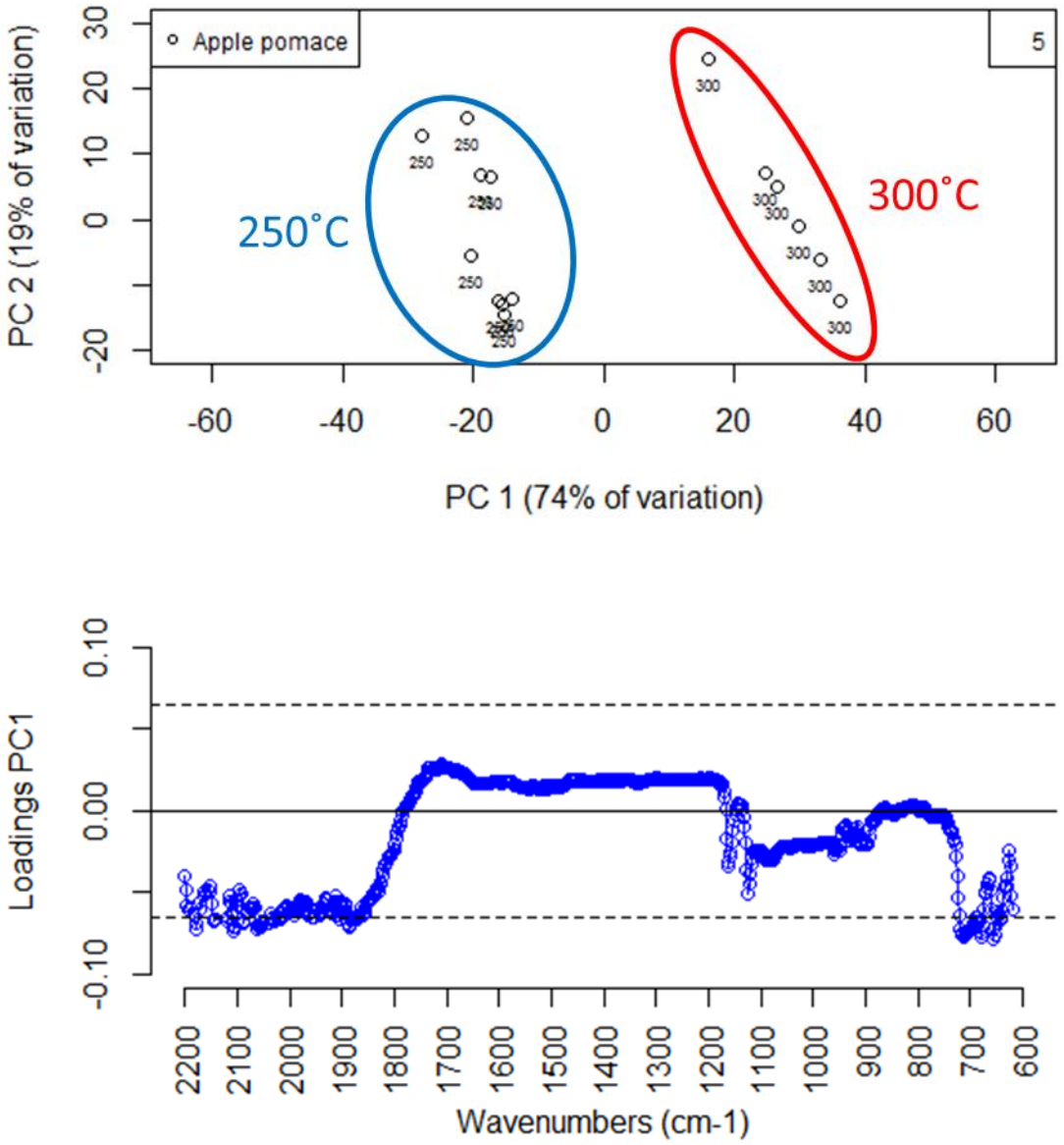

Figure AI-23. PCA for FTIR spectra of hydro-char generated from apple pomace: (a) bi-plot for all FTIR spectra of hydro-char generated at 5 minutes, showing the effect of the temperature; and (b) loading plot of PC1 vs. FTIR wavenumber. The loadings for all the wavenumbers in the loading plot are smaller than the threshold defined between 2200-1800 cm^{-1}. Hence, no conclusive information about what wavenumbers have the highest weight in the definition of PC1.

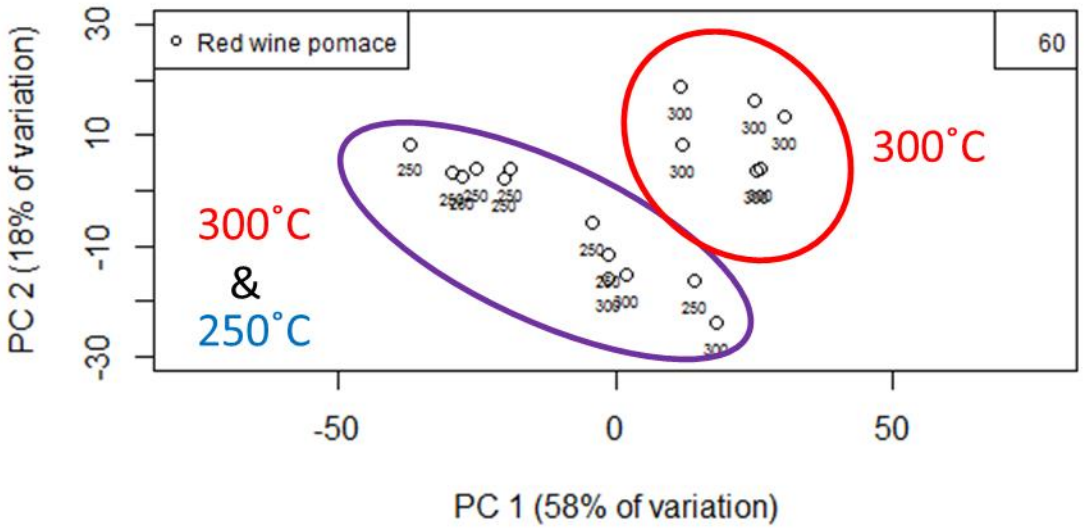

Figure AI-24. PCA for FTIR spectra of hydro-char generated from red wine pomace: bi-plot for all FTIR spectra of hydro-char generated at 60 minutes, showing the inconclusive effect of the temperature, as it was not possible to define two clusters of data corresponding to different temperatures (No loading plot shown)

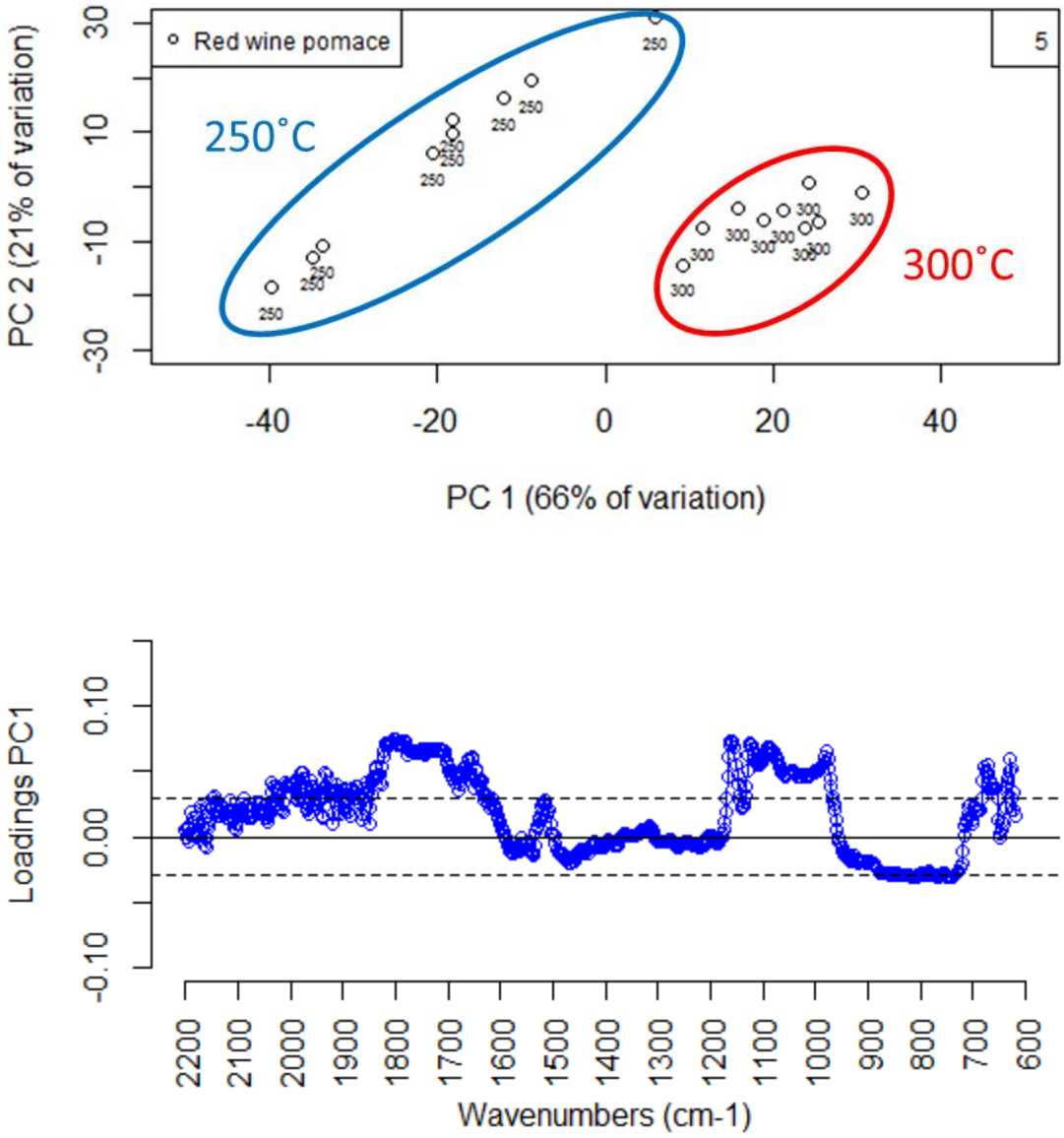

Figure AI-25. PCA for FTIR spectra of hydro-char generated from red wine pomace: (a) bi-plot for all FTIR spectra of hydro-char generated at 5 minutes, showing the effect of the temperature; and (b) loading plot of PC1 vs. FTIR wavenumber showing the specific wavenumbers that contributed to the scattering provided in Table 4.

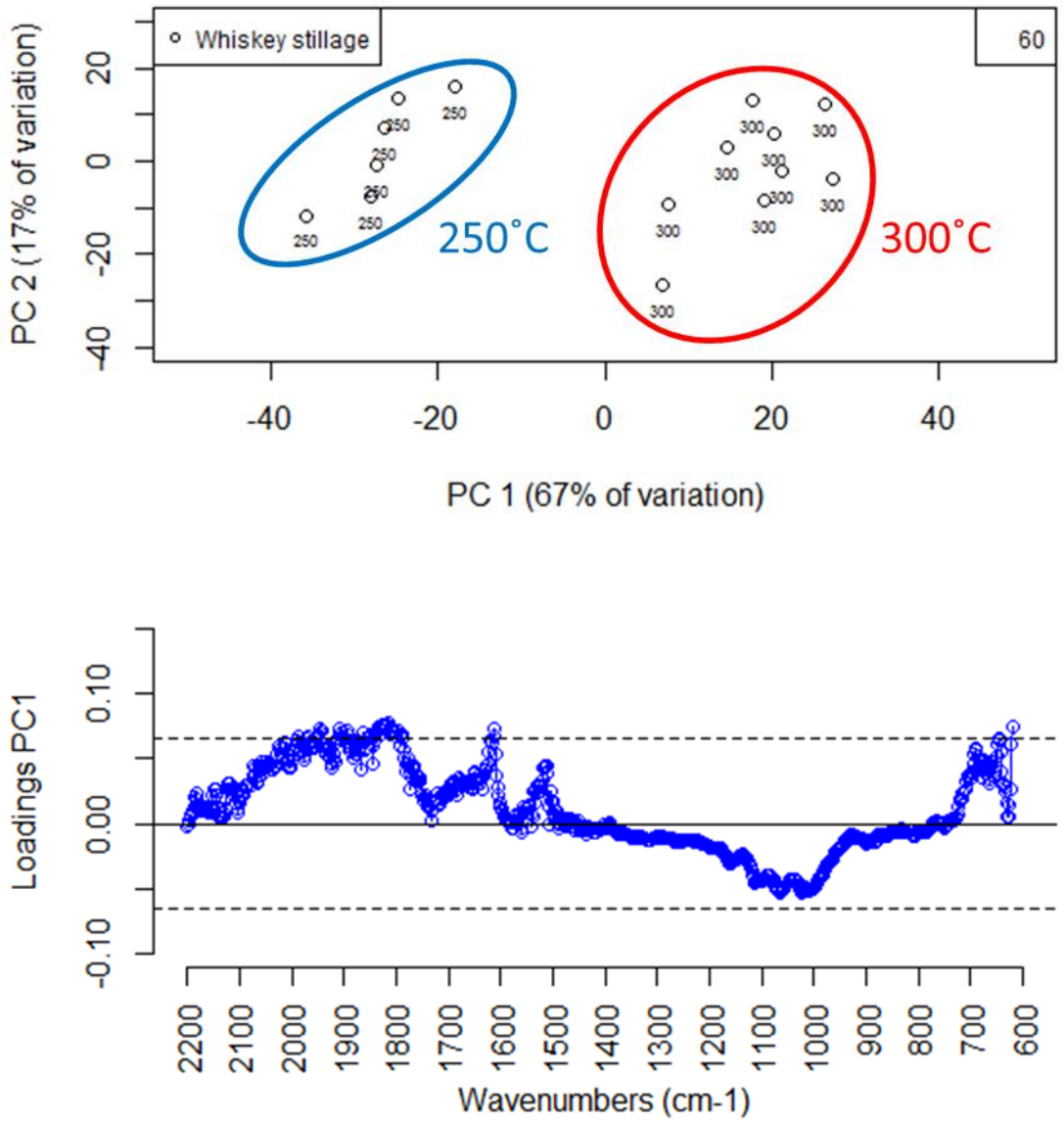

Figure AI-26. PCA for FTIR spectra of hydro-char generated from whiskey stillage: (a) bi-plot for all FTIR spectra of hydro-char generated at 60 minutes, showing the effect of the temperature; and (b) loading plot of PC1 vs. FTIR wavenumber. The loadings for all the wavenumbers in the loading plot are smaller than the threshold defined between 2200-1800 cm^{-1}. Hence, no conclusive information about what wavenumbers have the highest weight in the definition of PC1.

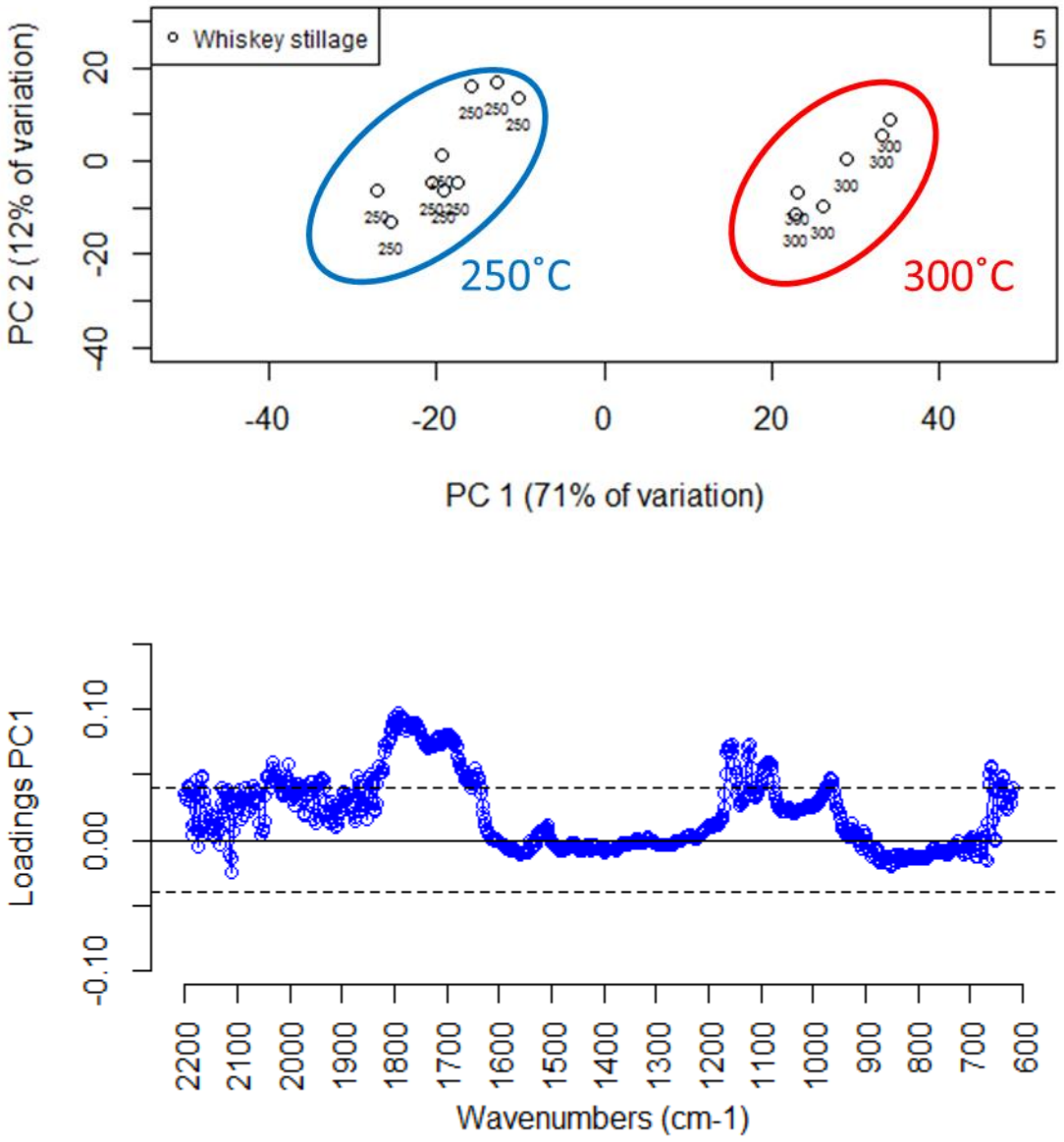

Figure AI-27. PCA for FTIR spectra of hydro-char generated from whiskey stillage: (a) bi-plot for all FTIR spectra of hydro-char generated at 5 minutes, showing the effect of the temperature; and (b) loading plot of PC1 vs. FTIR wavenumber showing the specific wavenumbers that contributed to the scattering provided in Table 4.

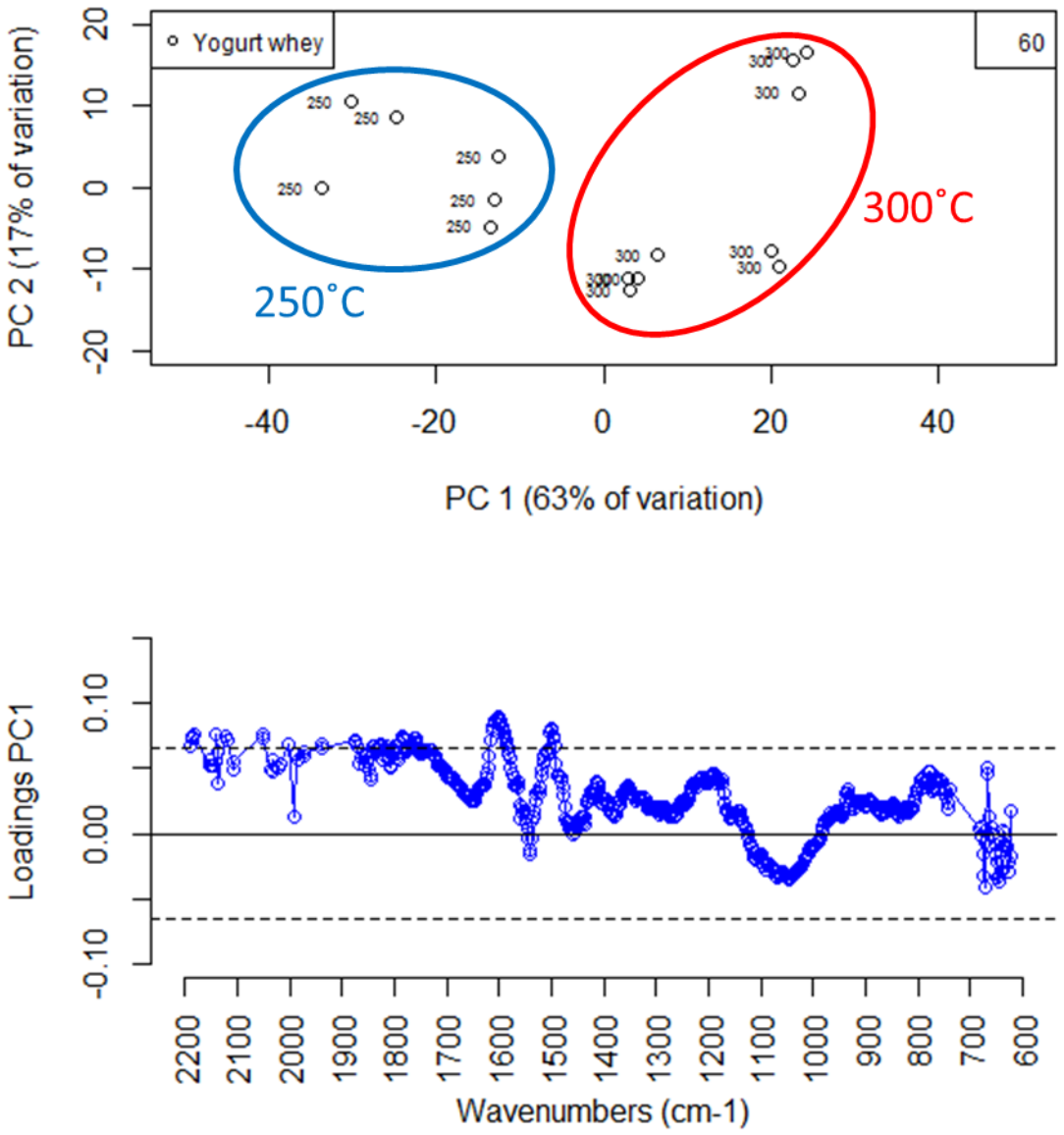

Figure AI-28. PCA for FTIR spectra of hydro-char generated from yogurt whey: (a) bi-plot for all FTIR spectra of hydro-char generated at 60 minutes, showing the effect of the temperature; and (b) loading plot of PC1 vs. FTIR wavenumber showing the specific wavenumbers that contributed to the scattering provided in Table 4.

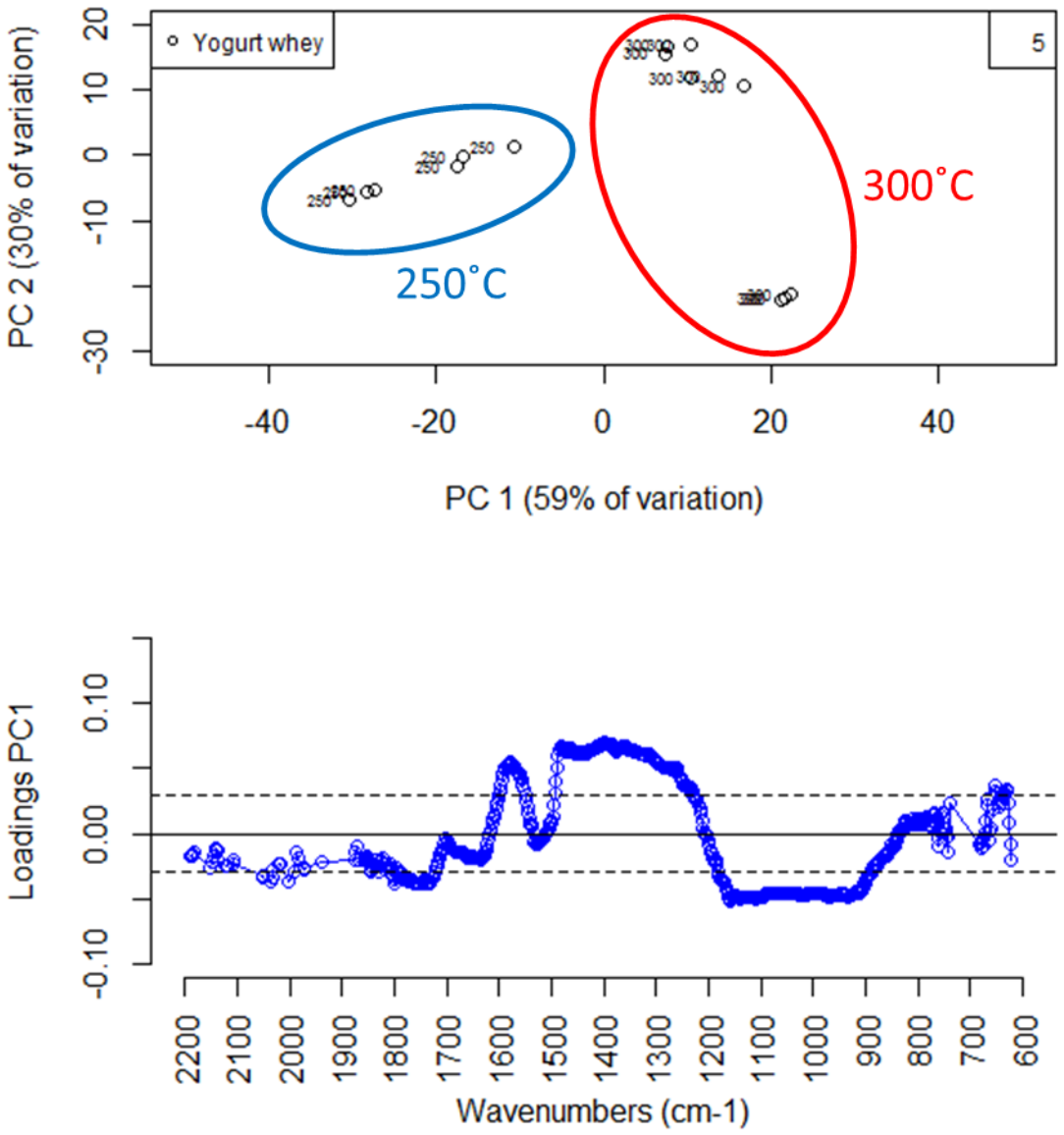

Figure AI-29. PCA for FTIR spectra of hydro-char generated from yogurt whey: (a) bi-plot for all FTIR spectra of hydro-char generated at 5 minutes, showing the effect of the temperature; and (b) loading plot of PC1 vs. FTIR wavenumber showing the specific wavenumbers that contributed to the scattering provided in Table 4.

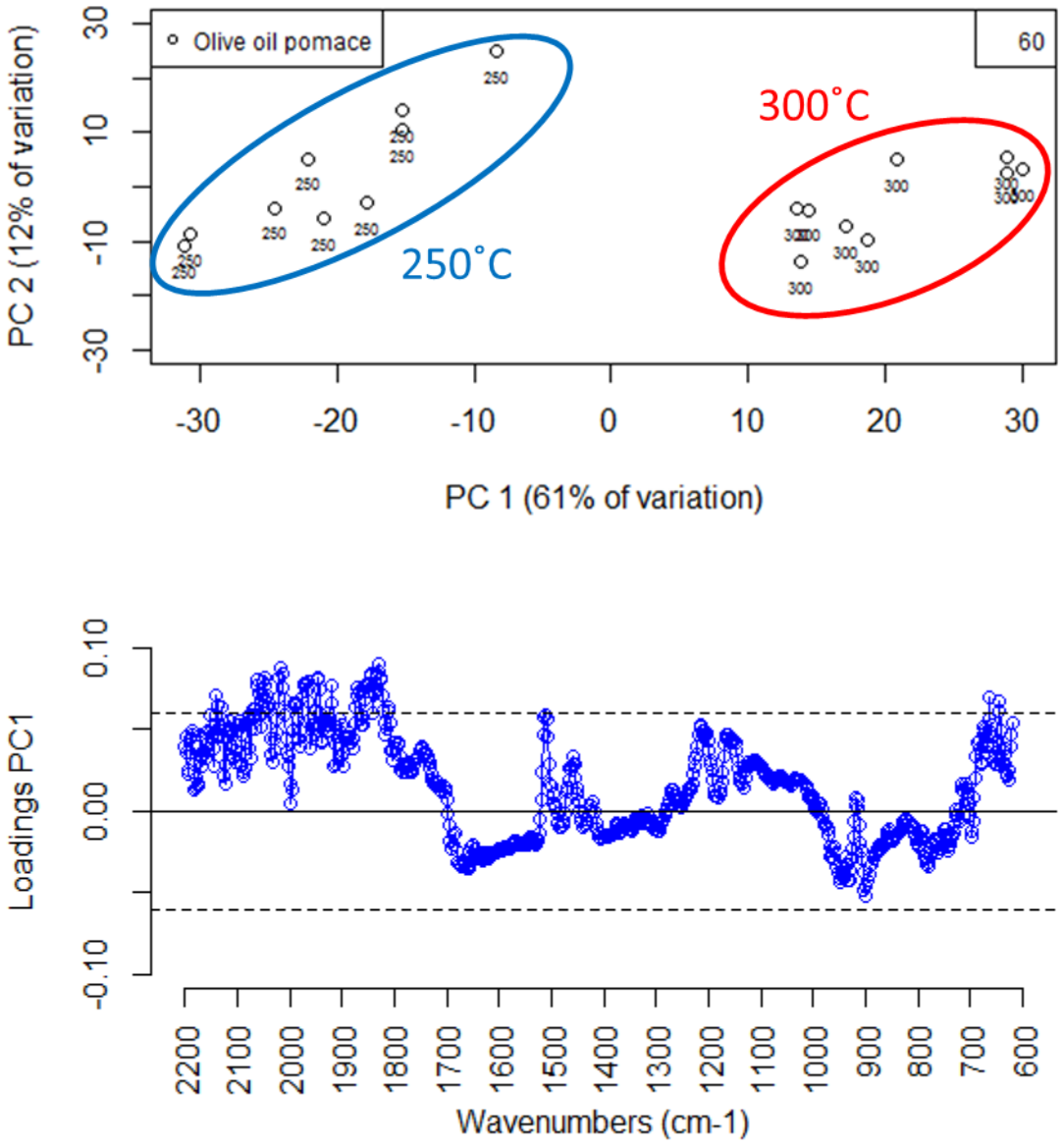

Figure AI-30. PCA for FTIR spectra of hydro-char generated from olive oil pomace: (a) bi-plot for all FTIR spectra of hydro-char generated at 60 minutes, showing the effect of the temperature; and (b) loading plot of PC1 vs. FTIR wavenumber. The loadings for all the wavenumbers in the loading plot are smaller than the threshold defined between 2200-1800 cm^{-1}. Hence, no conclusive information about what wavenumbers have the highest weight in the definition of PC1.

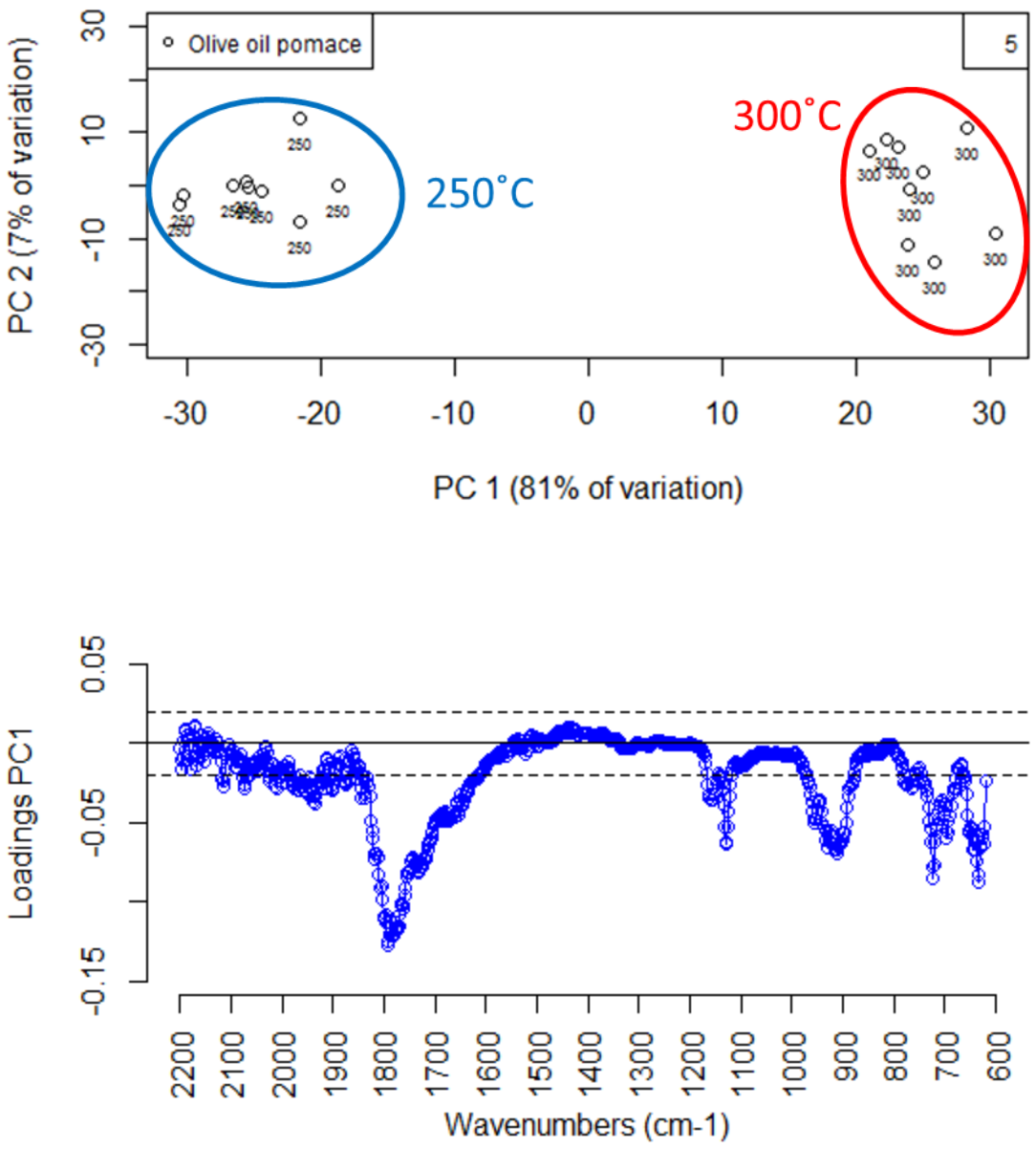

Figure AI-31. PCA for FTIR spectra of hydro-char generated from olive oil pomace: (a) bi-plot for all FTIR spectra of hydro-char generated at 5 minutes, showing the effect of the temperature; and (b) loading plot of PC1 vs. FTIR wavenumber showing the specific wavenumbers that contributed to the scattering, provided in Table 4.

References

Abidi, N, L Cabrales, and C Haigler. 2014. "Changes in the Cell Wall and Cellulose Content of Developing Cotton Fibers Investigated by FTIR Spectroscopy." *Carbohydrate Polymers* 100: 9–16.

Arivazhagan, M, K Sambathkumar, and S Jeyavijayan. 2010. "Density Functional Theory Study of FTIR and FT-Raman Spectra of 7-Acetoxy-4-Methyl Coumarin." *Indian Journal of Pure & Applied Physics* 48 (716–722).

Bodirlau, R, C Teaca, and I Spiridon. 2009. "Preparation and Characterization of Composites Comprising Modified Hardwood and Wood Polmers/poy(vinyl Chloride)." *BioResources* 4 (4): 1285–1304.

Bouchard, J, T Nguyen, E Chornet, and R Overend. 1990. "Analytical Methodology for Biomass Pretreatment — Part 1: Solid Residues." *Biomass* 23 (4): 243–61.

Castle, R. 2009. *The Chemistry of Heterocyclic Compounds, Condensed Pyridazines Including Cinnolines and Phthalazines*. Edited by Science.

Cornelissen, T, J Yperman, G Reggers, S Schreurs, and R Carleer. 2008. "Flash Co-Pyrolysis of Biomass with Polylactic Acid Part 1. Influence on Bio-Oil Yield and Heating Value." *Fuel* 87 (7): 1031–41.

Du, S, J Valla, and G Bollas. 2013. "Characteristics and Origin of Char and Coke from Fast and Slow, Catalytic and Thermal Pyrolysis of Biomass and Relevant Model Compounds." *Green Chemistry* 15: 3214–29.

Foo, G, A Rogers, M Yung, and C Sievers. 2016. "Steric Effect and Evolution of Surface Species in the Hydrodeoxygenation of Bio-Oil Model Compounds over Pt/HBEA." *ACS*

Catal. 6 (2): 1297–1307.

Galletti, A, A D'Alessio, D Licursi, C Antonetti, G Valentini, A Galia, and N Nassi. 2015. "Midinfrared FT-IR as a Tool for Monitoring Herbaceous Biomass Composition and Its Conversion to Furfural." *Journal of Spectroscopy* 2015: 12.

Gunasekaran, S, and S Ponnusamy. 2005. "Qualitative and Quantitative Analysis of Lignocellulosic Biomass Using Infrared Techniques: A Mini-Review." *Indian Journal of Pure & Applied Physics* 43: 838–43.

Hagemann, H, R Snyder, A Peacock, and L Madelkern. 1989. "Quantitative Infrared Methods for the Measurement of Crystallinity and Its Temperature Dependence: Polyethylene." *Macromolecules* 22: 3300–3606.

Haykir, N, and E Bahcegul. 2013. "Pretreatment of Cotton Stalk with Ionic Liquids Including 2-Hydroxy Ethyl Ammonium Formate to Enhance Biomass Digestibility." *Industrial Crops and Products* 41 (0): 430–36.

Heredia-Guerrero, J, J Benitez, E Dominguez, I Bayer, R Cingolani, A Athanassiou, and A Heredia. 2014. "Infrared and Raman Spectroscopic Features of Plant Cuticles: A Review." *Frontiers in Plant Science* 5 (305).

Illinois State University. 2015. "An Introduction to Laboratory Practices in Organic Chemistry."

Kline, L, D Hayes, A Womac, and N Labbe. 2010. "Simplified Determination of Lignin Content in Hard and Soft Woods via UV-Spectrophotometric Analysis of Biomass Disolved in Ionic Liquids." *BioResources* 5 (3): 1366–83.

Li, L, X Wang, and F Wu. 2016. "Chemical Analysis of Densification, Drying, and Heat Treatment of Scots Pine (Pinus Sylvestris L.) through a Hot-Pressing Process."

BioResources 11 (2): 3856–74.

Liu, Y, M Chen, Q Guo, Y Li, J Jiang, and J Shi. 2017. “Aromatic Compounds from an Aqueous Extract of ‘ban Lan Gen’ and Their Antiviral Activities.” *Acta Pharmaceutica Sinica B* 7 (2): 179–84.

Lobo, H, and J Bonilla. 2003. *Handbook of Plastic Analysis*. CRC Press.

Magalhaes, A, M Almeida, M Bezerra, N Ricardo, and J Feitosa. 2012. “Application of FTIR in the Determination of Acrylate Content in Poly(sodium Acrylateco-Acrylamide) Superabsorbent Hydrogels.” *Quim. Nova* 35 (7): 1464–67.

Mossoba, M. 1998. *Spectral Methods in Food Analysis: Instrumentation and Applications*. Edited by CRC Press.

Nuopponen, M, and T Vourinen. 2005. “Thermal Modifications in Softwood Studied by FT-IR and UV Resonance Raman Spectroscopies.” *Journal of Wood Chemistry and Technology* 24 (1): 13–26.

Painter, P, M Starsinic, E Squires, and A Davis. 1983. “Concerning the 1600 Cm-1 Region in the IR Spectrum of Coal.” *Fuel* 62.

Poletto, M, and A.J Zattera. 2013. “Materials Produced from Plant Biomass. Part III: Degradation Kinetics and Hydrogen Bonding in Lignin.” *Materials Research* 16 (5): 1065–70.

Saika, P, B Sarmah, S Mahiuddin, P Sengupta, P Saikia, D Bordoloi, and P Borthakur. 2005. “Limestone from New Umrangshu, Assam, India: Characterisation and Utilisation Properties.” *International Conference Mineral Processing Technology*, 187–93.

Setiawan, A, and F Aulia. 2017. “Development of More Friendly Food Packaging Materials

Base on Polypropylene through Blending with Polylacticacid." *AIP Conference Proceedings* 1803.

Shi, J, and Q Yang. 2012. "The Structural Changes of the Bagasses Hemicellulose during the Cooking Proces Involving Active Oxygen and Solid Alkali." *Carbohydrate Research* 359 (0): 65–69.

Sim, S, M Mohamed, N Lu, M Sarman, and S Samsudin. 201AD. "Computer-Assisted Analysis of Fourier Transform Infrared (FTIR) Spectra for Characterization of Various Treated and Untreated Agriculture Biomass." *BioResources* 7 (4): 5367–80.

Siontorou, C, M Bidikoudi, C Chandrinou, N Boukos, P Falaras, M Fardis, G Apostolopoulos, F Batzias, and D Sidiras. 2015. "Spectroscopic Assessment of Biomass Derived Adsorbents for Oil Spill Cleaning." *Journal of Research in Metalurgical and Civil Eng* 2 (1): 49–54.

Srinivasan, S, S Gunasekaran, U Ponnambalam, A Savarianandam, S Gnanaprakasam, and S Natarajan. 2005. "Spectroscopy and Thermodynamic Analysis of Enolic Form or 3-Oxo-L-Gulofuranolactone." *Indian Journal of Pure & Applied Physics* 43: 459–62.

Stewart, D, H. M Wilson, P. J Hendra, and I. M. Morrison. 1995. "Fourier-Transform Infrared and Raman Spectroscopic Study of Biochemical and Chemical Treatments of Oak Wood (Quercus Rubra) and Barley (Hordeum Vulgare) Straw." *Journal of Agricultural and Food Chemistry* 43.

Strezov, V. 2012. "System Approach to Biomass Pyrolysis: Product Characterisation." In *The Third International Conference on Bioenvironment, Biodiversity, and Renewable Energies*.

Syngellakis, S. 2014. *Biomass to Biofuels*. Wessex, UK: WIT Press.

Szymanska-Chargot, M, and A Zdunek. 2013. "Use of FT-IR Spectra and PCA to the Bulk

Characterization of Cell Wall Residues of Fruits and Vegetables Along a Fraction Process." *Food Biophys* 8 (1): 29–42.

Xu, F, J Yu, T Tesso, F Dowell, and D Wang. 2013. "Qualitative and Quantitative Analysis of Lignocellulosic Biomass Using Infrared Techniques: A Mini-Review." *Applied Energy* 104: 801–9.

Yao, J, XW Xu, and YY Feng. 2003. "FTIR Studies on the Chemical Composition of Wheat Straw in Different Layers." *Spectroscopy and Spectral Analysis* 23 (1): 58–60.

Yue, G, and S Li. 2016. *Clean Coal Technology and Sustainable Development*. *Proceedings of the 8th International Symposium on Coal Combustion*.

APPENDIX II

A COMPREHENSIVE STUDY ON THE EFFECT OF HYDROTHERMAL LIQUEFACTION (HTL) REACTION CONDITIONS AND FEEDSTOCKS CHARACTERISTICS ON THE MASS AND ENERGY DISTRIBUTION TOWARDS HTL PHASES, AND PHYSICO-CHEMICAL CHARACTERIZATION OF BIO-CRUDE OIL

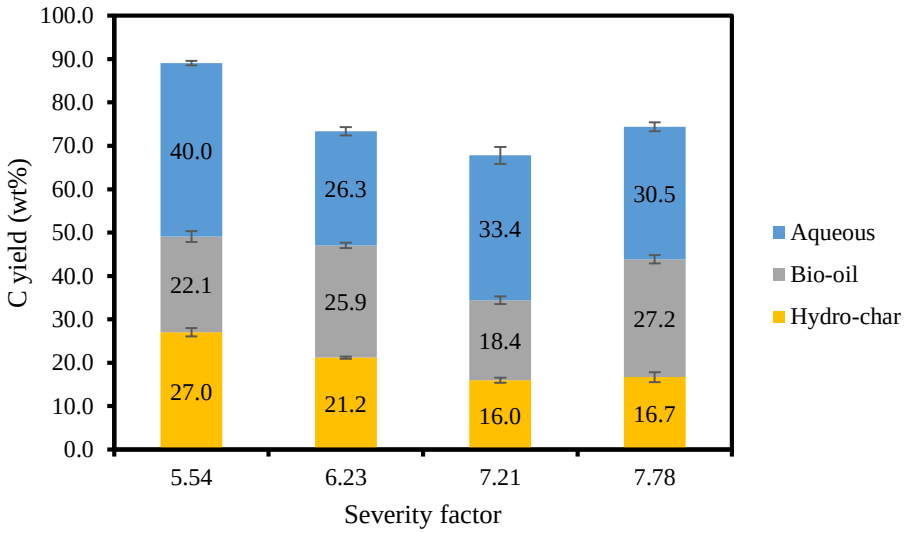

Figure AII-1. Carbon yield (wt%) towards the different phased of hydrothermal liquefaction of activated waste sludge. The values reported are the average of triplicate experiment and the error bars are the standard deviation.

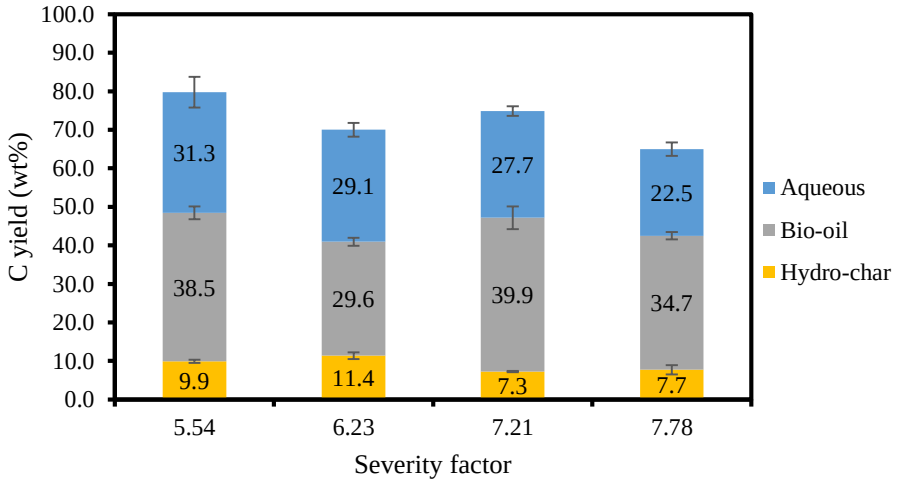

Figure AII-2. Carbon yield (wt%) towards the different phased of hydrothermal liquefaction of food waste. The values reported are the average of triplicate experiment and the error bars are the standard deviation.

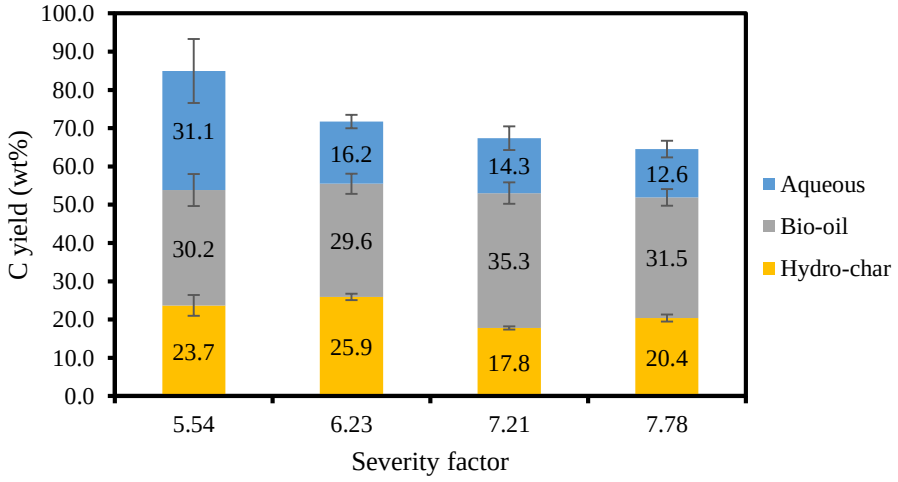

Figure AII-3. Carbon yield (wt%) towards the different phased of hydrothermal liquefaction of apple pomace. The values reported are the average of triplicate experiment and the error bars are the standard deviation.

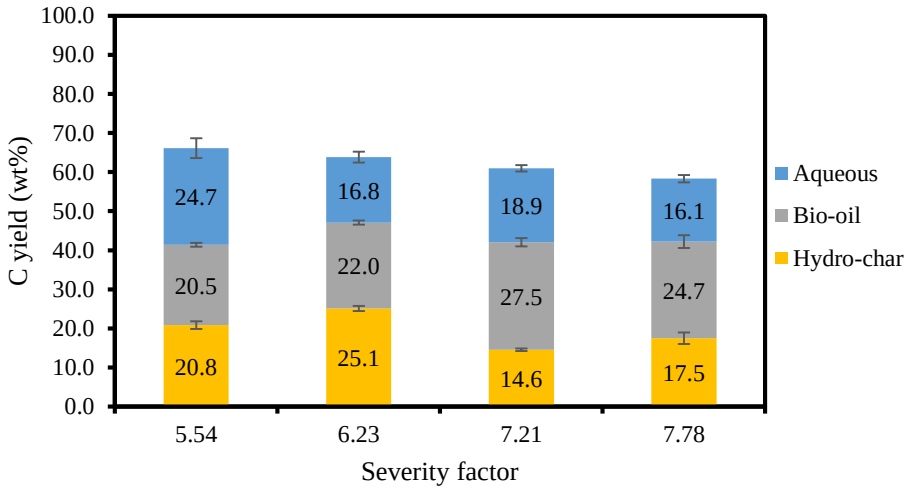

Figure AII-4. Carbon yield (wt%) towards the different phased of hydrothermal liquefaction of red wine pomace. The values reported are the average of triplicate experiment and the error bars are the standard deviation.

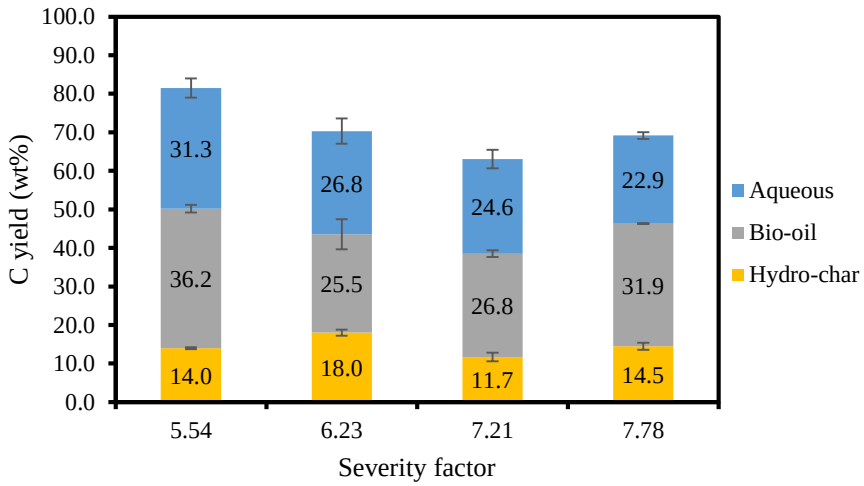

Figure AII-5. Carbon yield (wt%) towards the different phased of hydrothermal liquefaction of whiskey stillage. The values reported are the average of triplicate experiment and the error bars are the standard deviation.

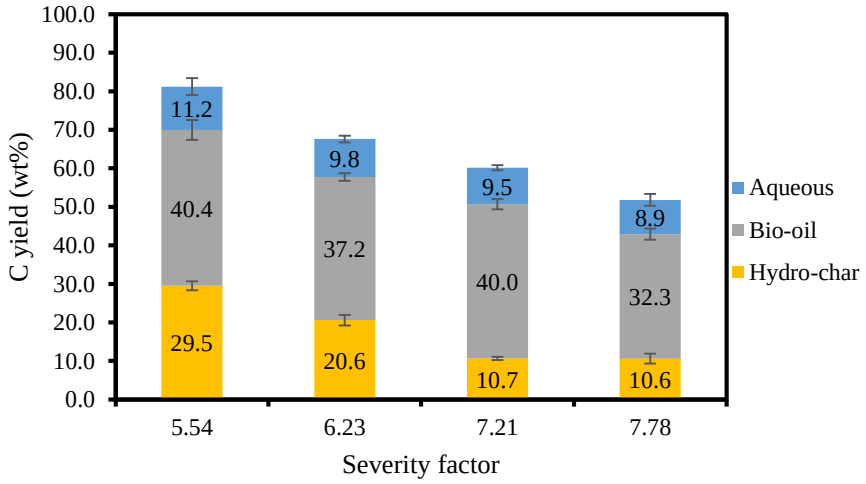

Figure AII-6. Carbon yield (wt%) towards the different phased of hydrothermal liquefaction of olive oil pomace. The values reported are the average of triplicate experiment and the error bars are the standard deviation.

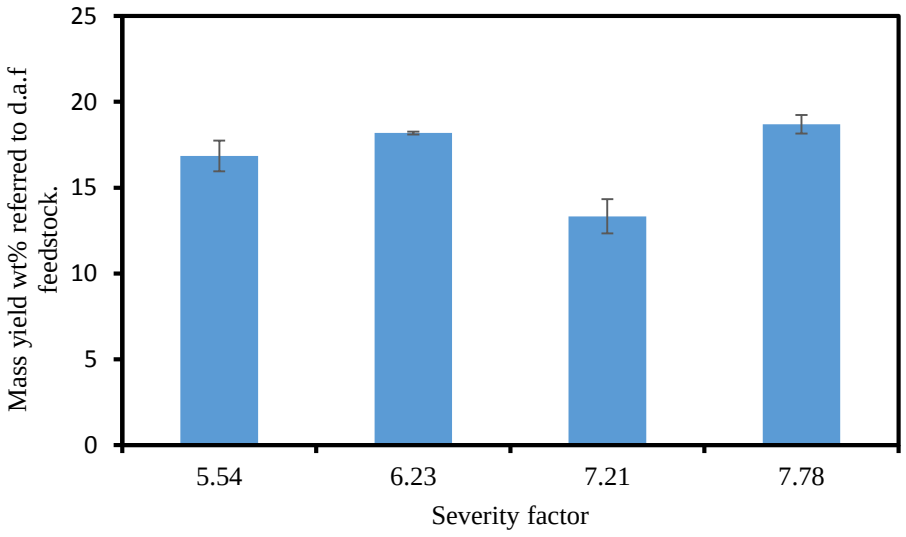

Figure AII-7. Mass yield (wt%) of bio-crude oil from the hydrothermal liquefaction of activated waste sludge. The values reported are the average of triplicate experiment and the error bars are the standard deviation.

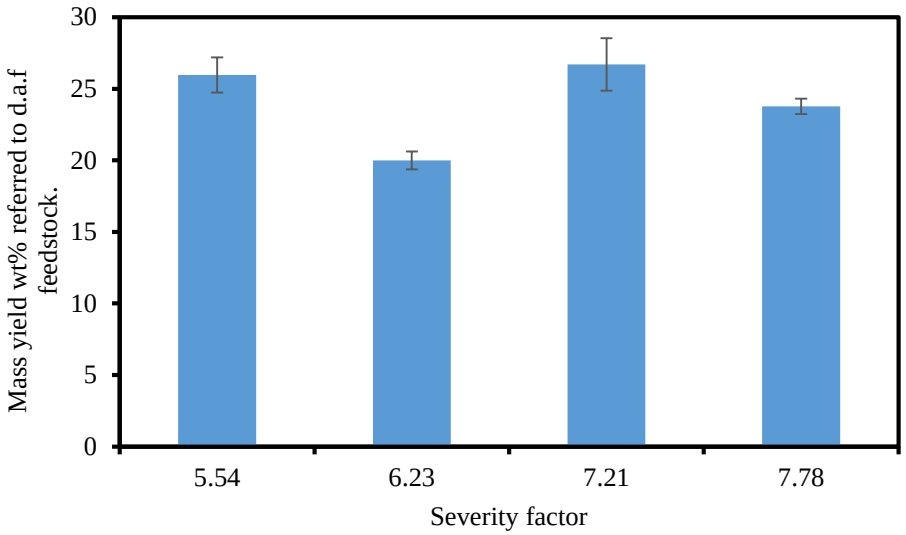

Figure AII-8. Mass yield (wt%) of bio-crude oil from the hydrothermal liquefaction of food waste. The values reported are the average of triplicate experiment and the error bars are the standard deviation.

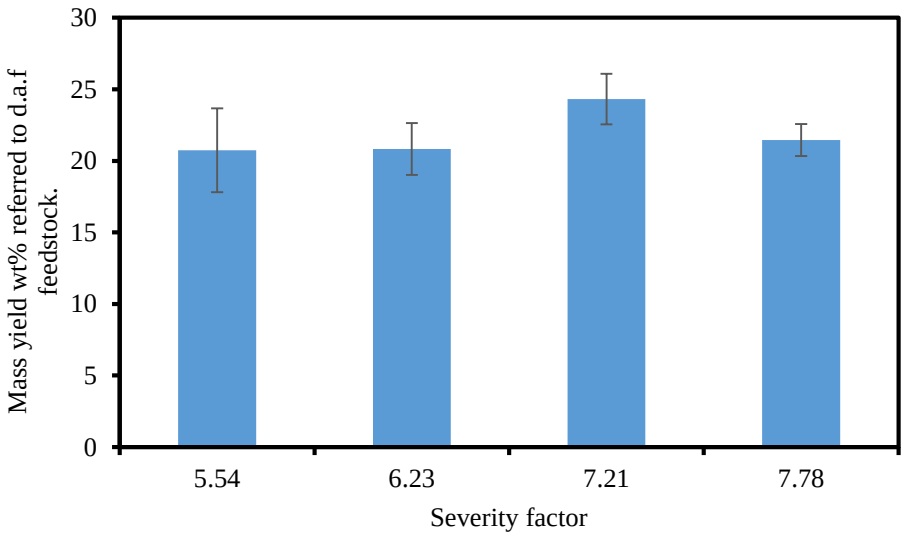

Figure AII-9. Mass yield (wt%) of bio-crude oil from the hydrothermal liquefaction of apple pomace. The values reported are the average of triplicate experiment and the error bars are the standard deviation.

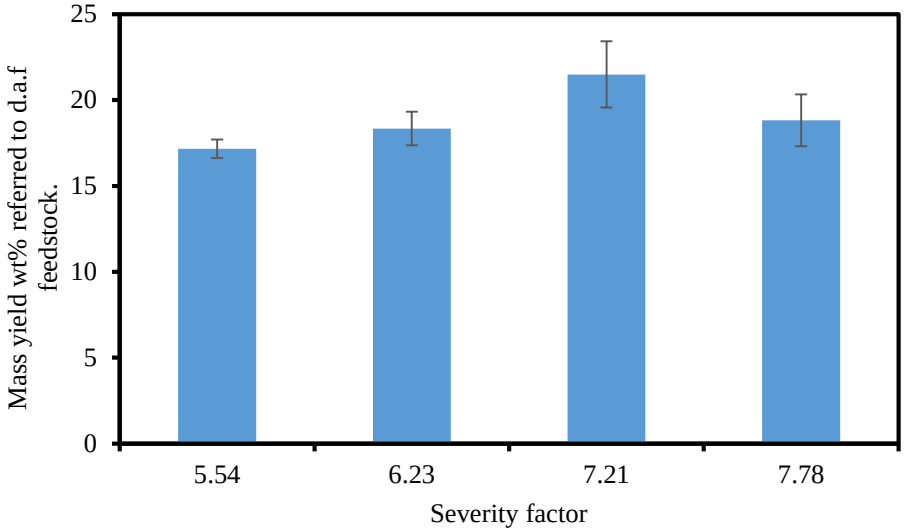

Figure AII-10. Mass yield (wt%) of bio-crude oil from the hydrothermal liquefaction of red wine pomace. The values reported are the average of triplicate experiment and the error bars are the standard deviation.

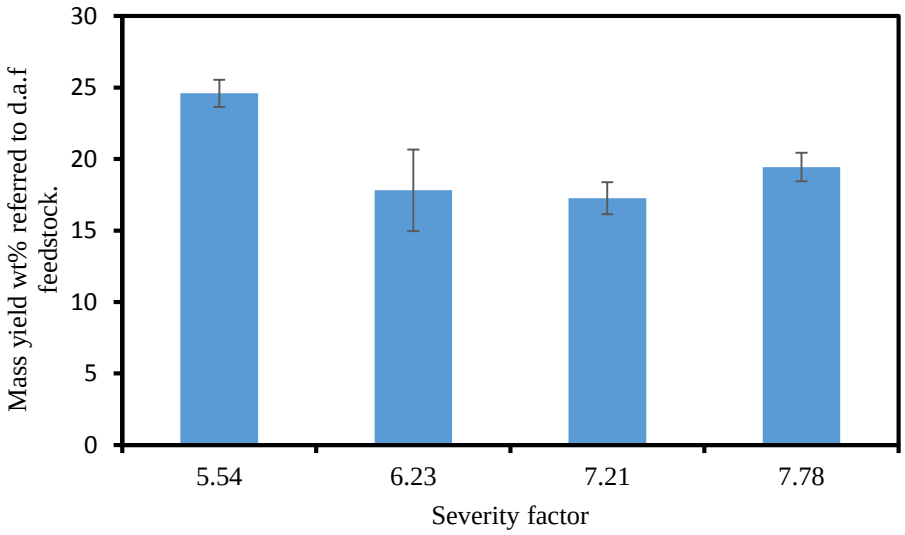

Figure AII-11. Mass yield (wt%) of bio-crude oil from the hydrothermal liquefaction of whiskey stillage. The values reported are the average of triplicate experiment and the error bars are the standard deviation.

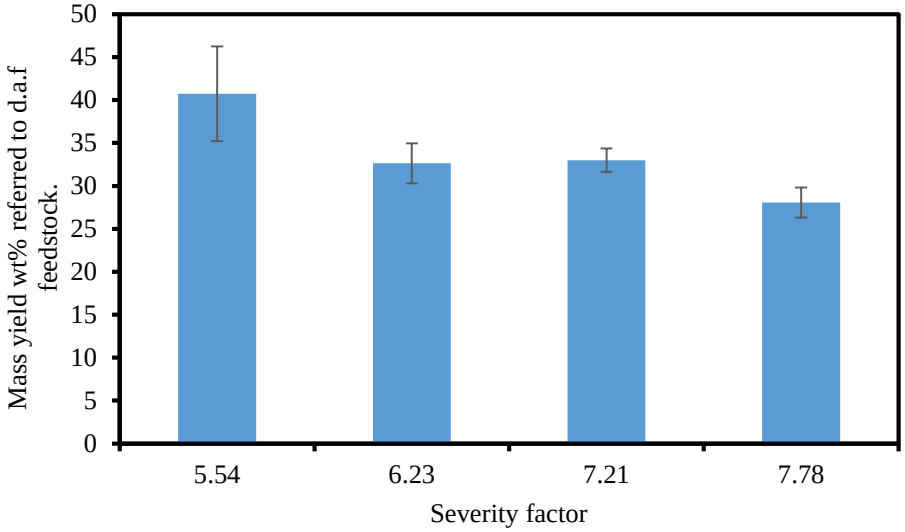

Figure AII-13. Mass yield (wt%) of bio-crude oil from the hydrothermal liquefaction of yogurt whey. The values reported are the average of triplicate experiment and the error bars are the standard deviation.

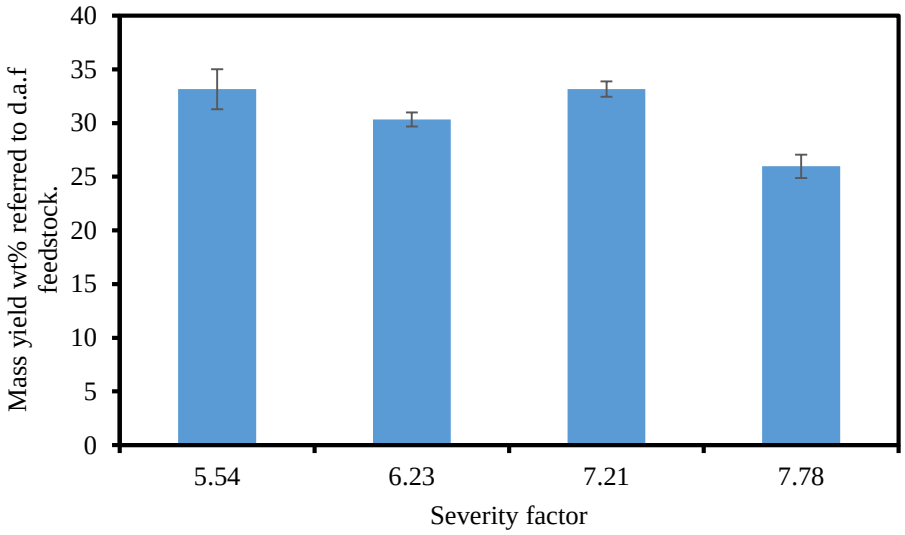

Figure AII-14. Mass yield (wt%) of bio-crude oil from the hydrothermal liquefaction of olive oil pomace. The values reported are the average of triplicate experiment and the error bars are the standard deviation.

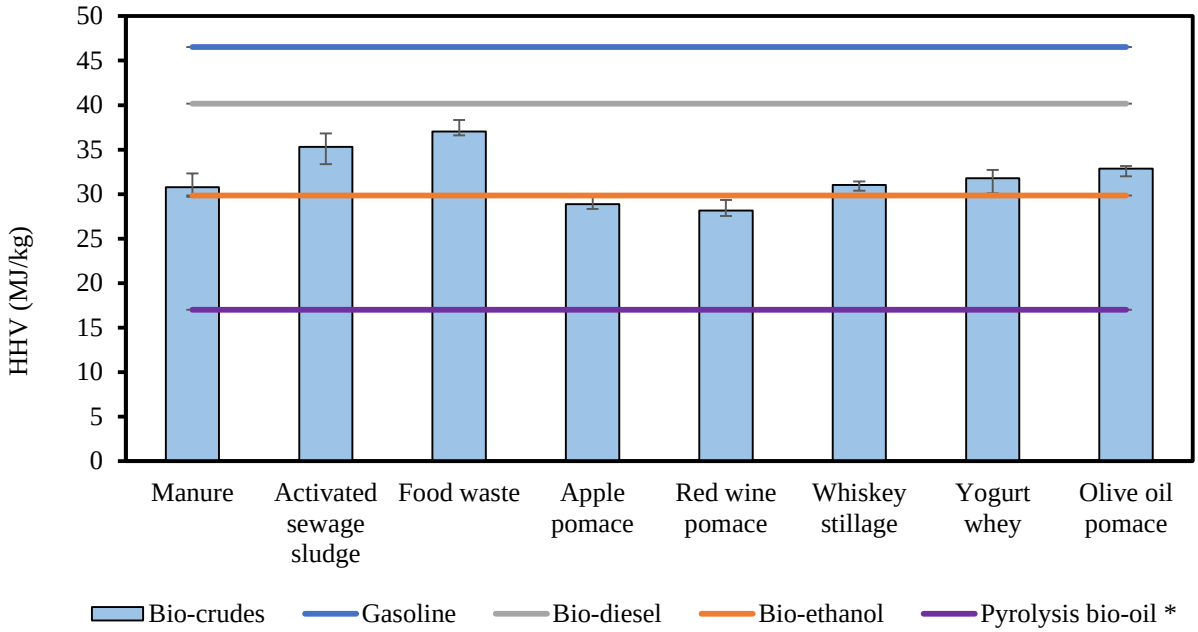

Figure AII-15. HHV (MJ/kg) for the bio-crude oils obtained from feedstocks HTL at severity factor 6.23 (250˚C and 60 minutes). The values are the average of three experiments, with error bars representing standard deviation. Also presenting the HHV of gasoline, bio-diesel, bio-ethanol and pyrolysis bio-oils* (before upgrading) for comparison purposes (Yin et al. 2010).

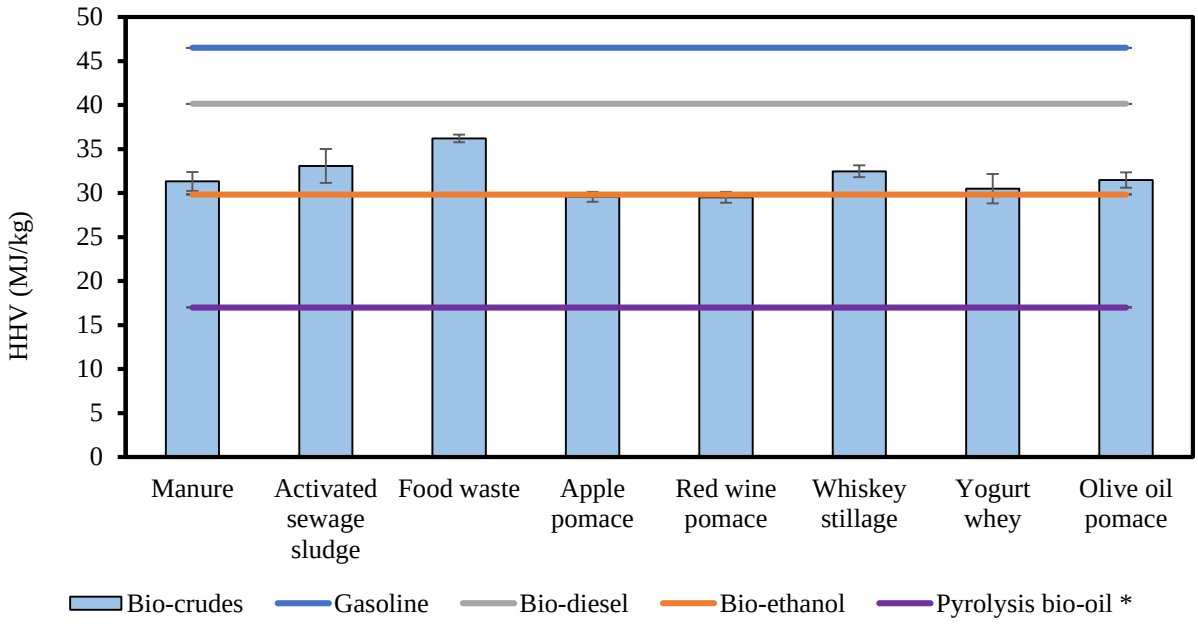

Figure AII-16. HHV (MJ/kg) for the bio-crude oils obtained from feedstocks HTL at severity factor 7.21 (300˚C and 5 minutes). The values are the average of three experiments, with error bars representing standard deviation. Also presenting the HHV of gasoline, bio-diesel, bio-ethanol and pyrolysis bio-oils* (before upgrading) for comparison purposes (Yin et al. 2010).

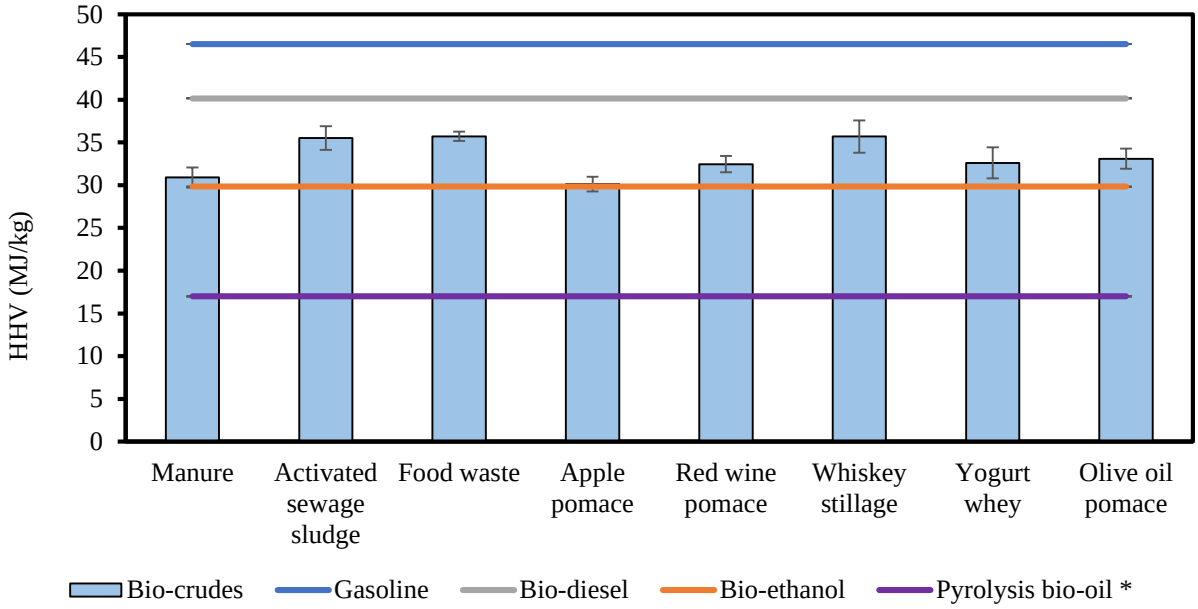

Figure AII-17. HHV (MJ/kg) for the bio-crude oils obtained from feedstocks HTL at severity factor 7.78 (300˚C and 60 minutes). The values are the average of three experiments, with error bars representing standard deviation. Also presenting the HHV of gasoline, bio-diesel, bio-ethanol and pyrolysis bio-oils* (before upgrading) for comparison purposes (Yin et al. 2010).

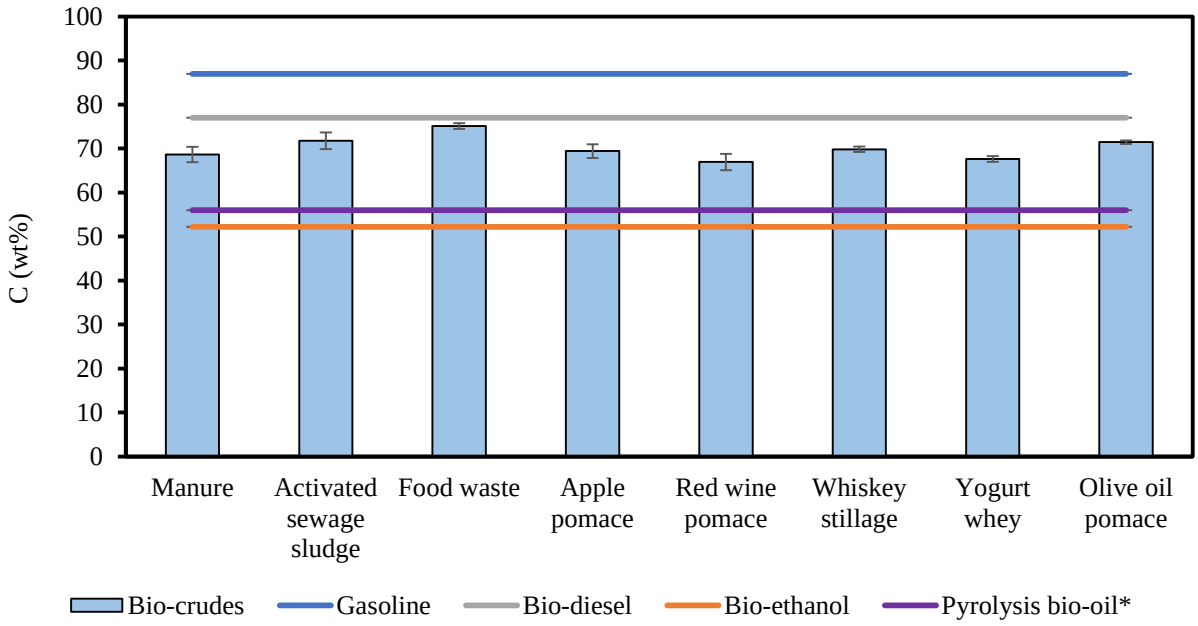

Figure AII-18. C content (wt%) for the bio-crude oils obtained from feedstocks HTL at severity factor 6.23 (250˚C and 60 minutes). The values are the average of three experiments, with error bars representing standard deviation. Also presenting the C content of gasoline, bio-diesel, bio-ethanol and pyrolysis bio-oils* (before upgrading) for comparison purposes (Yin et al. 2010).

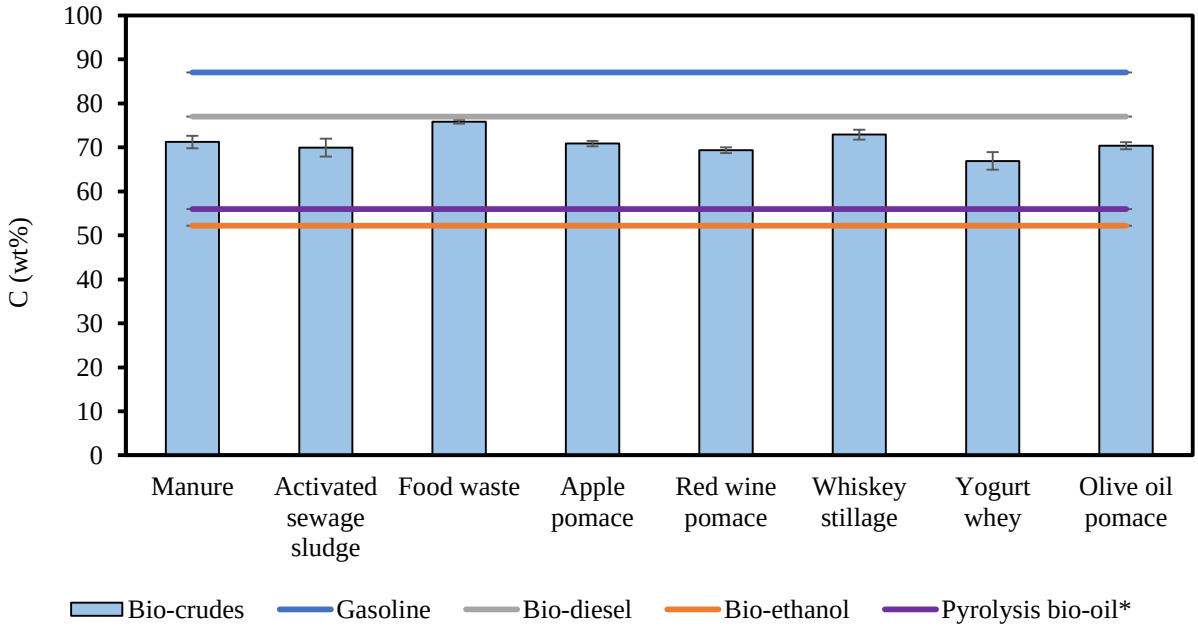

Figure AII-19. C content (wt%) for the bio-crude oils obtained from feedstocks HTL at severity factor 7.21 (300˚C and 5 minutes). The values are the average of three experiments, with error bars representing standard deviation. Also presenting the C content of gasoline, bio-diesel, bio-ethanol and pyrolysis bio-oils* (before upgrading) for comparison purposes (Yin et al. 2010).

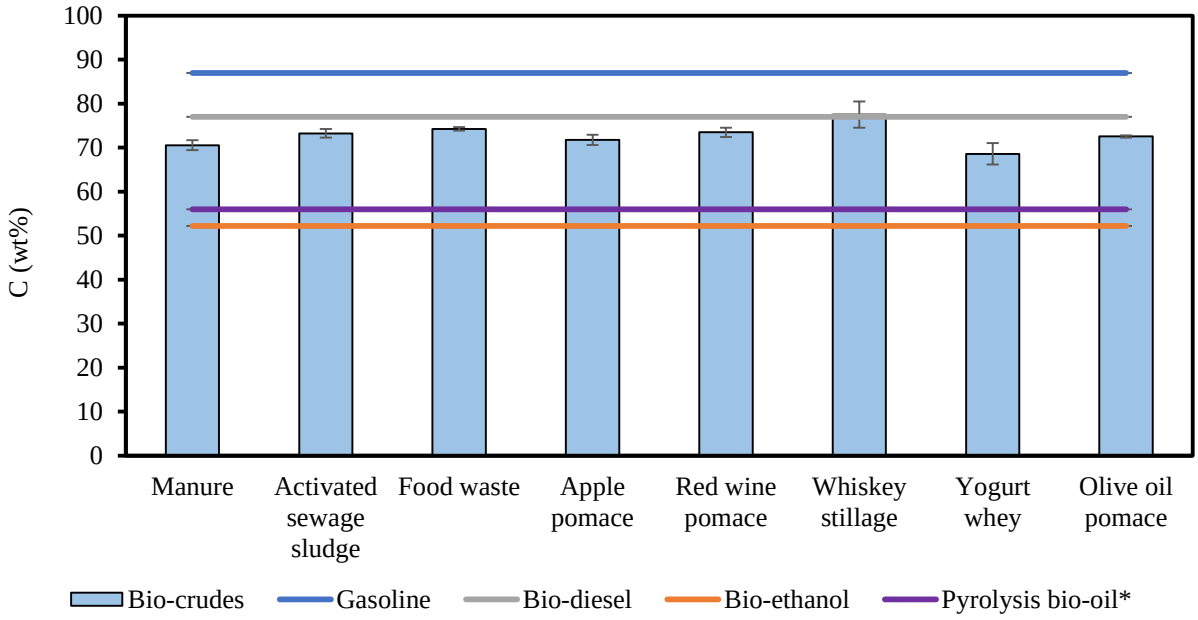

Figure AII-20. C content (wt%) for the bio-crude oils obtained from feedstocks HTL at severity factor 7.78 (300˚C and 60 minutes). The values are the average of three experiments, with error bars representing standard deviation. Also presenting the C content of gasoline, bio-diesel, bio-ethanol and pyrolysis bio-oils* (before upgrading) for comparison purposes (Yin et al. 2010).

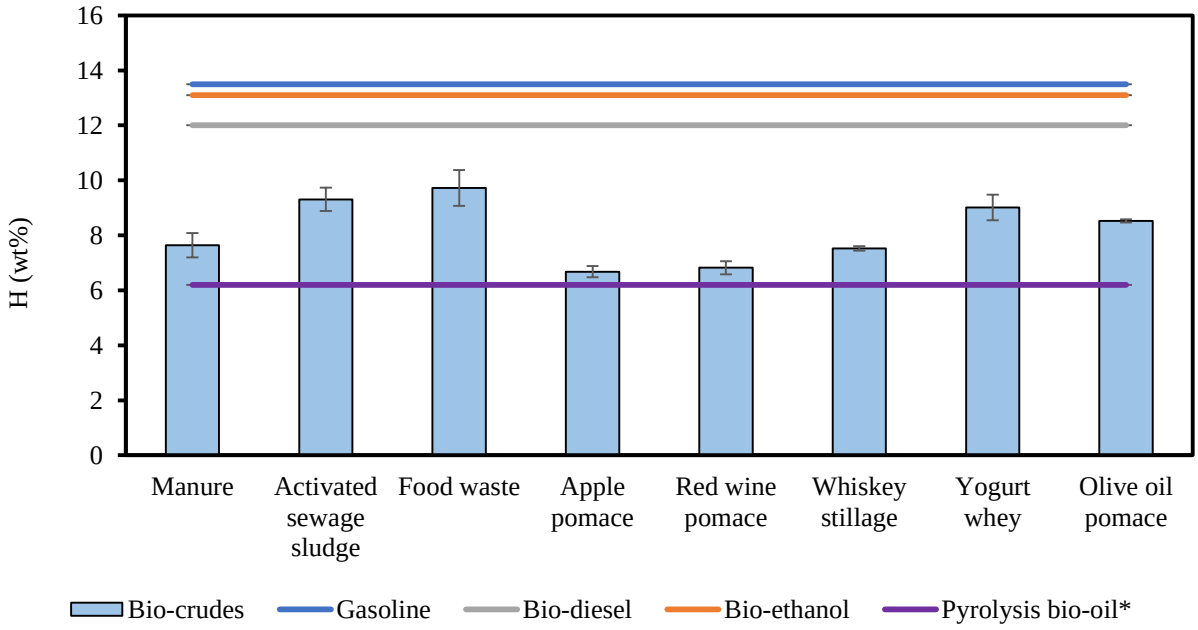

Figure AII-21. H content (wt%) for the bio-crude oils obtained from feedstocks HTL at severity factor 6.23 (250˚C and 60 minutes). The values are the average of three experiments, with error bars representing standard deviation. Also presenting the H content of gasoline, bio-diesel, bio-ethanol and pyrolysis bio-oils* (before upgrading) for comparison purposes (Yin et al. 2010).

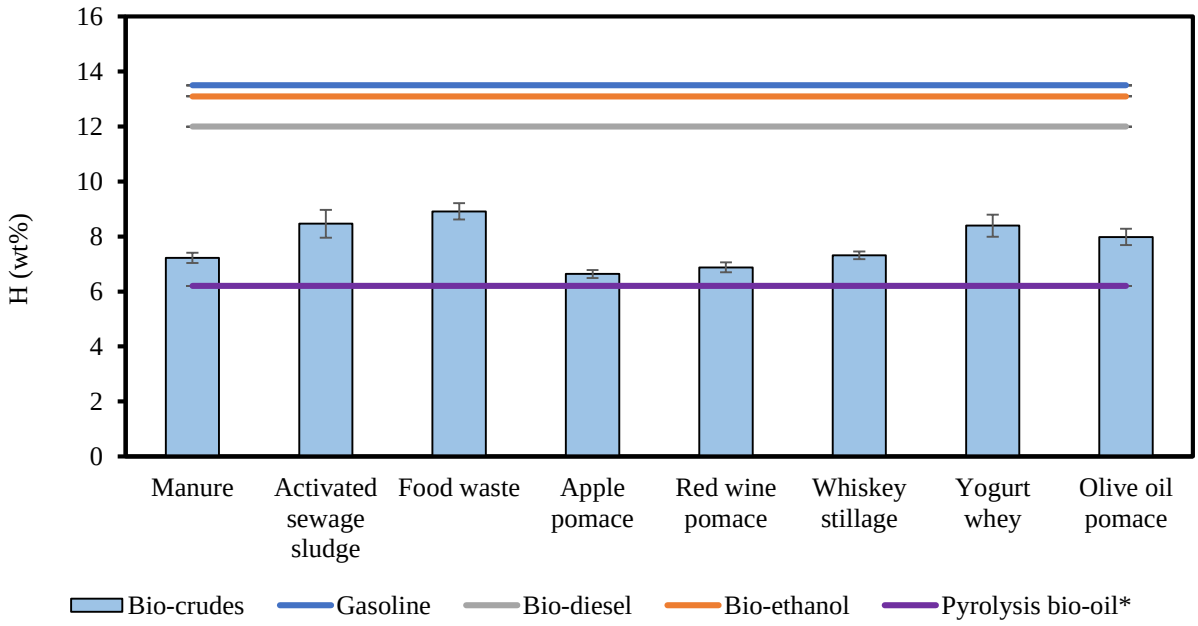

Figure AII-22. H content (wt%) for the bio-crude oils obtained from feedstocks HTL at severity factor 7.21 (300˚C and 5 minutes). The values are the average of three experiments, with error bars representing standard deviation. Also presenting the H content of gasoline, bio-diesel, bio-ethanol and pyrolysis bio-oils* (before upgrading) for comparison purposes (Yin et al. 2010).

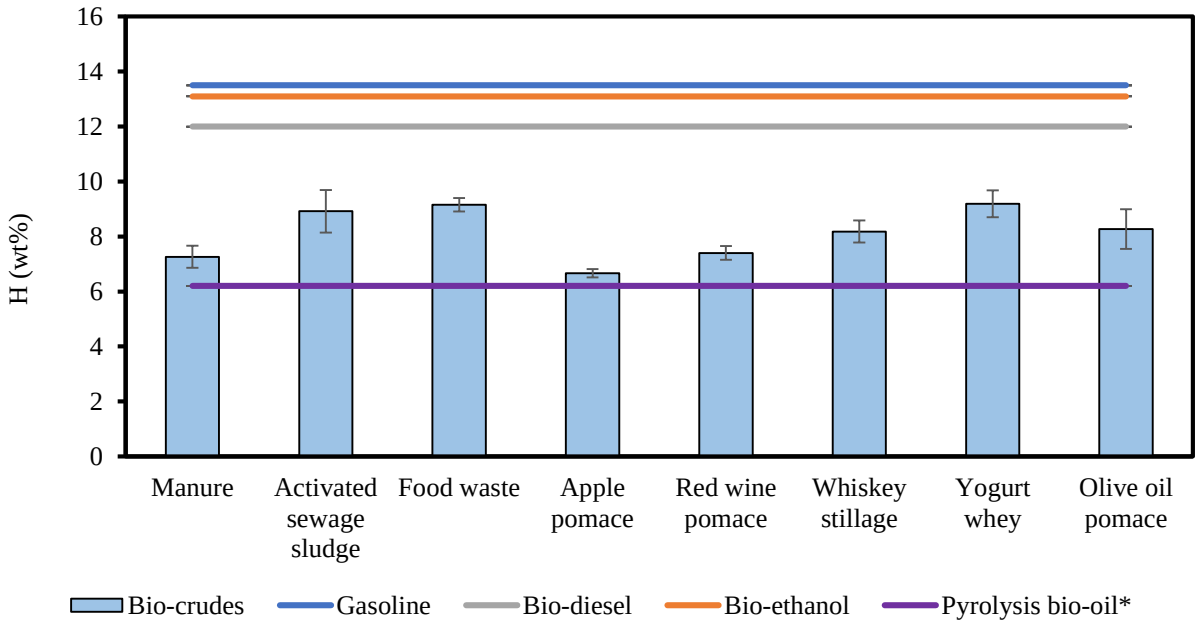

Figure AII-23. H content (wt%) for the bio-crude oils obtained from feedstocks HTL at severity factor 7.78 (300˚C and 60 minutes). The values are the average of three experiments, with error bars representing standard deviation. Also presenting the H content of gasoline, bio-diesel, bio-ethanol and pyrolysis bio-oils* (before upgrading) for comparison purposes (Yin et al. 2010).

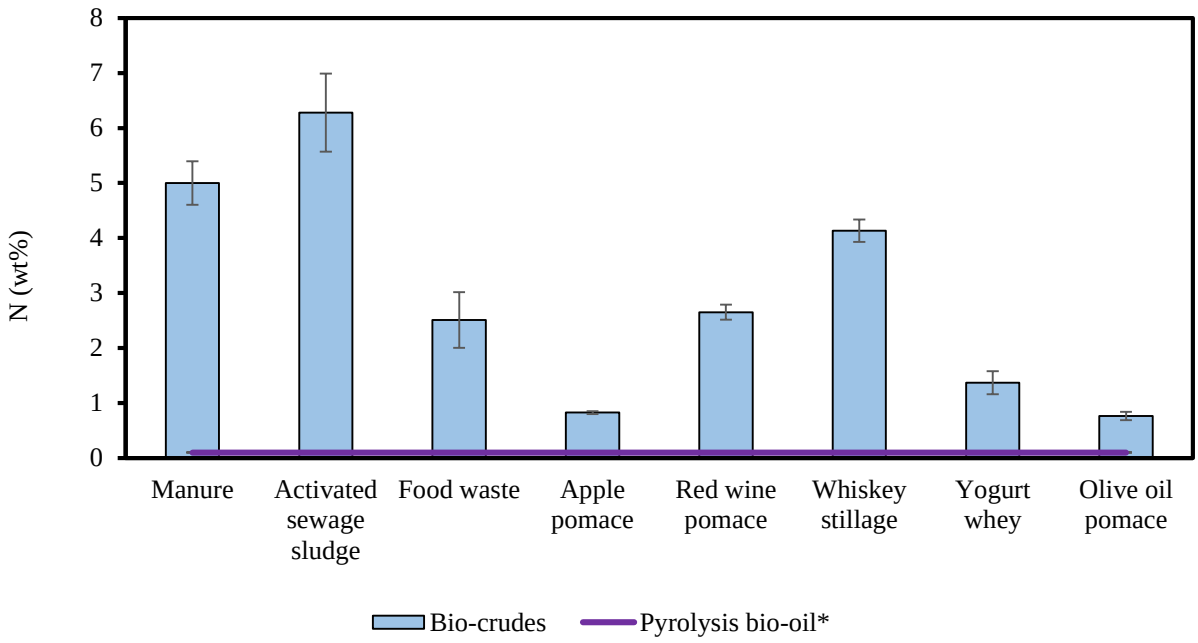

Figure AII-24. N content (wt%) for the bio-crude oils obtained from feedstocks HTL at severity factor 6.23 (250˚C and 60 minutes). The values are the average of three experiments, with error bars representing standard deviation. Also presenting the H content of gasoline, bio-diesel, bio-ethanol and pyrolysis bio-oils* (before upgrading) for comparison purposes (Yin et al. 2010). Gasoline, bio-diesel, and bio-ethanol contain 0 wt% N.

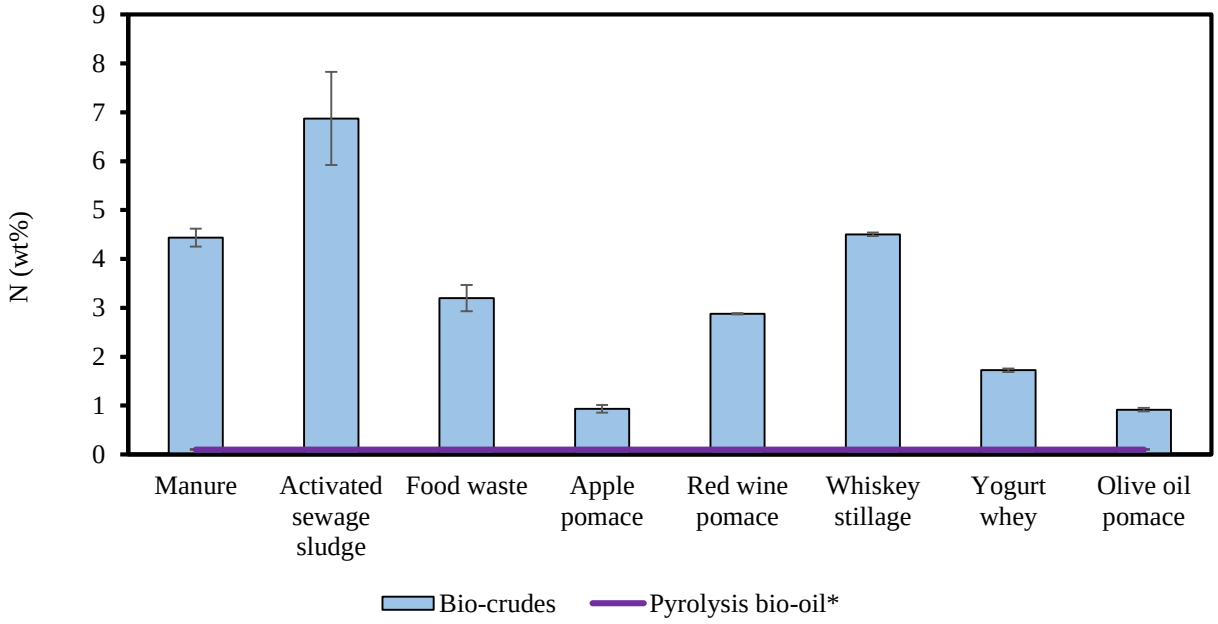

Figure AII-25. N content (wt%) for the bio-crude oils obtained from feedstocks HTL at severity factor 7.21 (300˚C and 5 minutes). The values are the average of three experiments, with error bars representing standard deviation. Also presenting the H content of gasoline, bio-diesel, bio-ethanol and pyrolysis bio-oils* (before upgrading) for comparison purposes (Yin et al. 2010). Gasoline, bio-diesel, and bio-ethanol contain 0 wt% N.

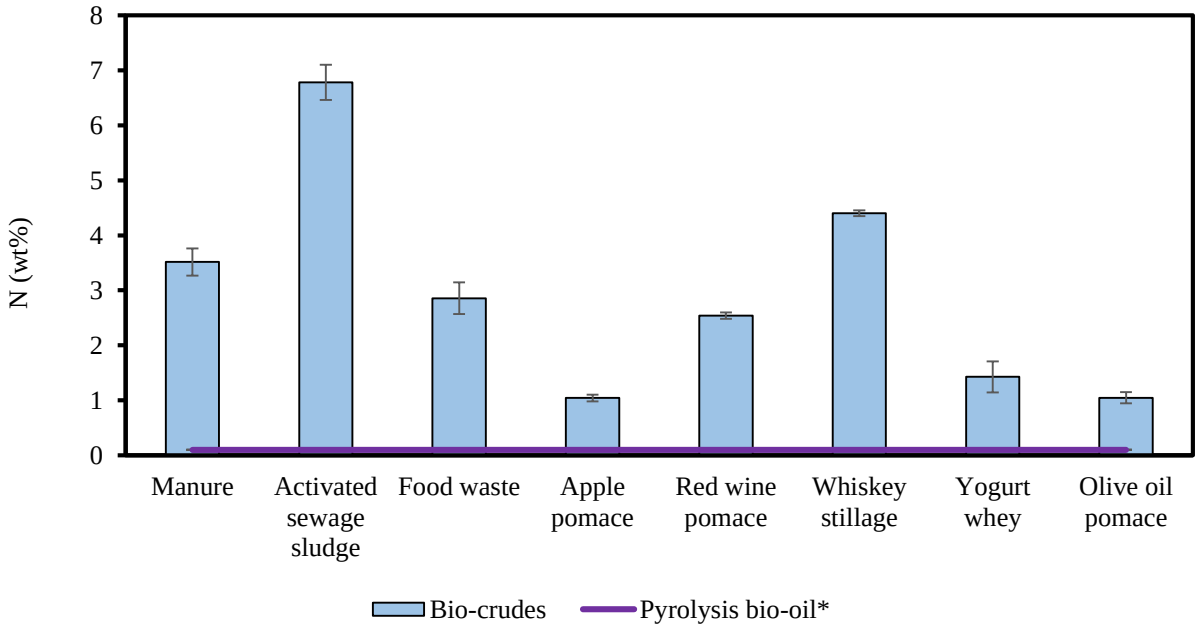

Figure AII-26. N content (wt%) for the bio-crude oils obtained from feedstocks HTL at severity factor 7.78 (300˚C and 60 minutes). The values are the average of three experiments, with error bars representing standard deviation. Also presenting the H content of gasoline, bio-diesel, bio-ethanol and pyrolysis bio-oils* (before upgrading) for comparison purposes (Yin et al. 2010). Gasoline, bio-diesel, and bio-ethanol contain 0 wt% N.

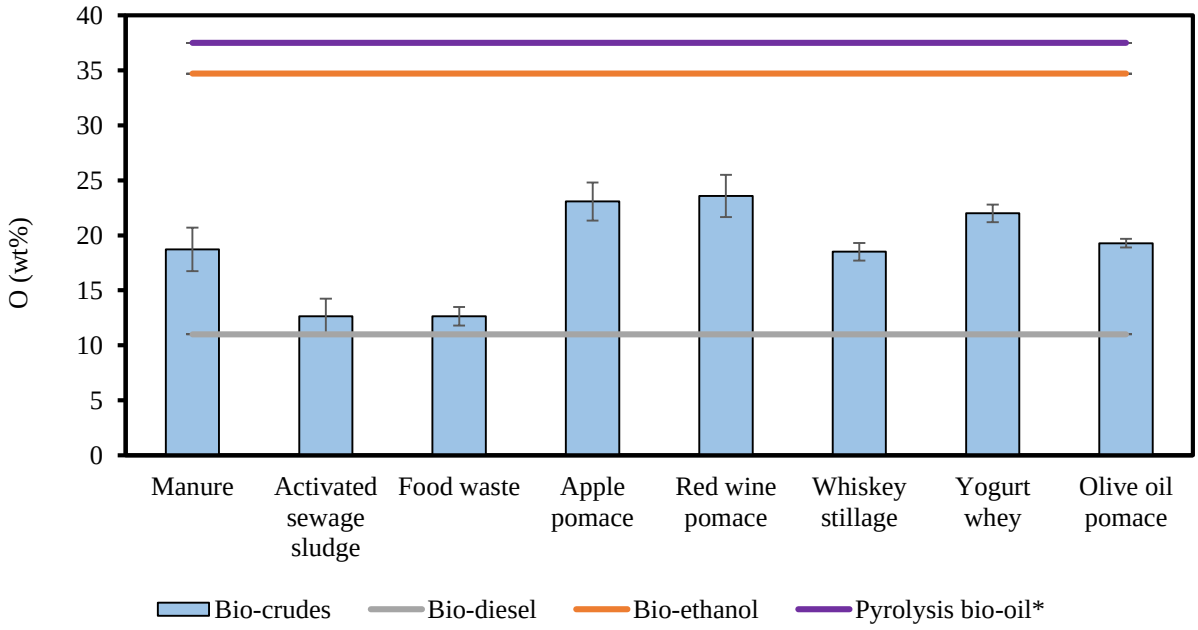

Figure AII-27. O content (wt%) for the bio-crude oils obtained from feedstocks HTL at severity factor 6.23 (250˚C and 60 minutes). The values are the average of three experiments, with error bars representing standard deviation. Also presenting the N content of gasoline, bio-diesel, bio-ethanol and pyrolysis bio-oils* (before upgrading) for comparison purposes (Yin et al. 2010). Gasoline contains 0 wt% O.

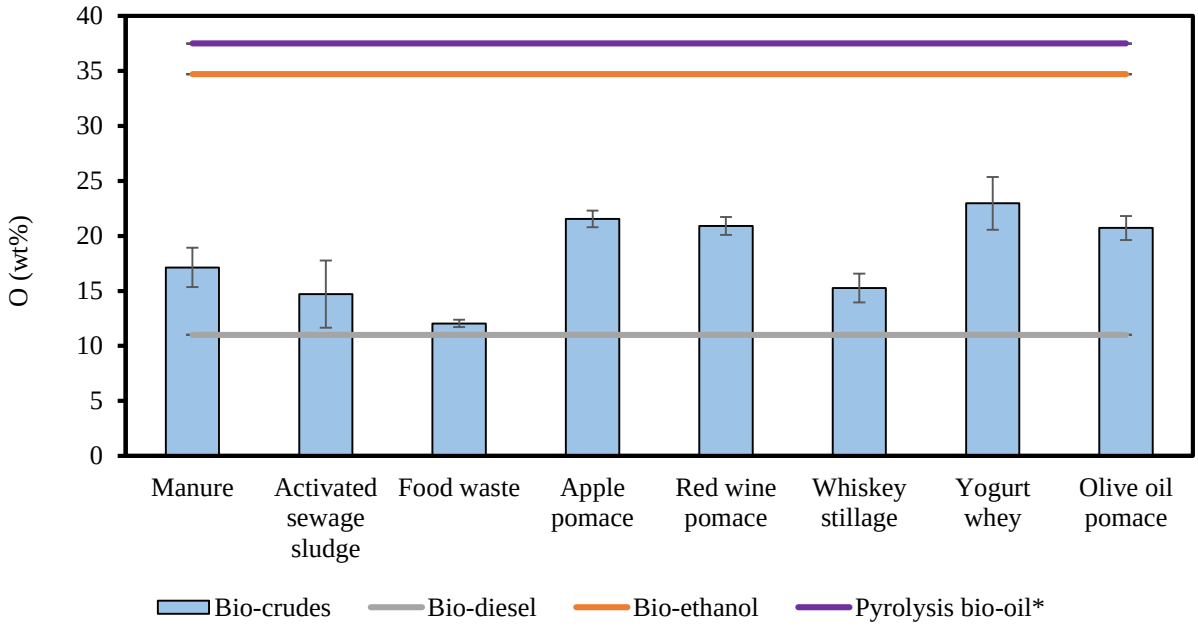

Figure AII-28. N content (wt%) for the bio-crude oils obtained from feedstocks HTL at severity factor 7.21 (300˚C and 5 minutes). The values are the average of three experiments, with error bars representing standard deviation. Also presenting the N content of gasoline, bio-diesel, bio-ethanol and pyrolysis bio-oils* (before upgrading) for comparison purposes (Yin et al. 2010). Gasoline contain 0 wt% O.

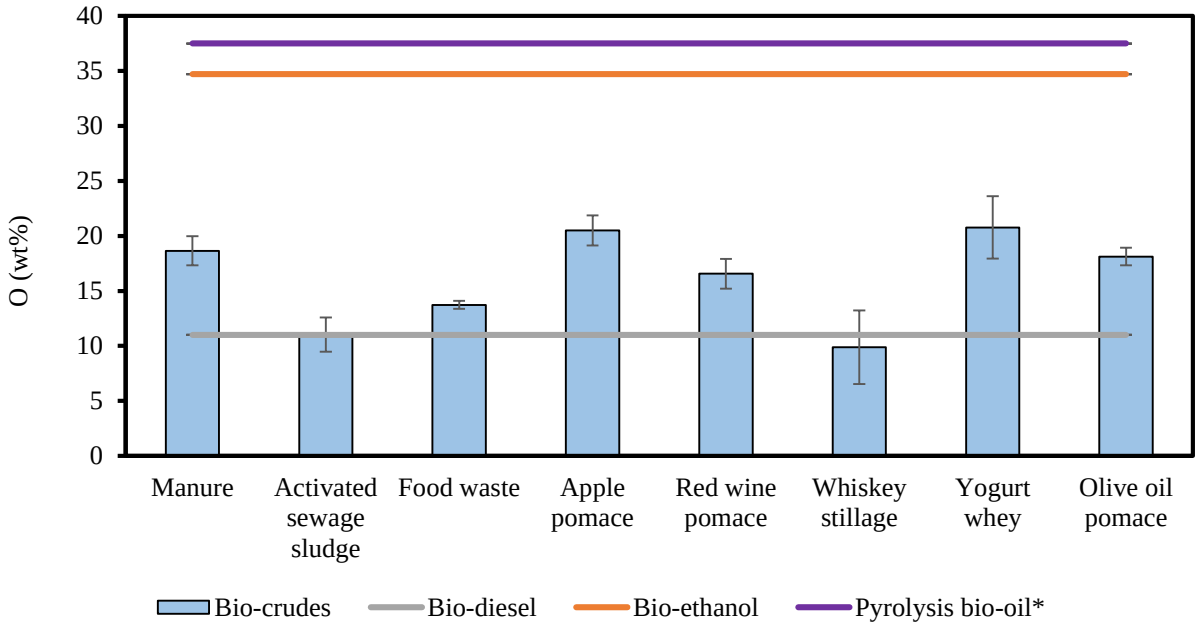

Figure AII-29. O content (wt%) for the bio-crude oils obtained from feedstocks HTL at severity factor 7.78 (300˚C and 60 minutes). The values are the average of three experiments, with error bars representing standard deviation. Also presenting the N content of gasoline, bio-diesel, bio-ethanol and pyrolysis bio-oils* (before upgrading) for comparison purposes (Yin et al. 2010). Gasoline contain 0 wt% O.

Table AII-1. HHV (MJ/kg) for bio-crude oils produced at all the severity factors for every feedstock. Magnitude of HHV upgrade (%) referred to the initial feedstock. The values presented are the average of three experiments and the error is the standard deviation.

Temperature (°C)	Time (min)	Manure	Waste activated sludge	Food waste	Apple pomace	Red wine pomace	Whiskey stillage	Yogurt whey	Olive oil pomace
Feedstocks		13.3±0.5	12.5±0.6	19.7±1.0	18.0±0.9	19.6±0.9	18.3±0.7	6.3±0.2	23.2±1.1
250	5	27.6±2.6	31.2±2.4	38.8±0.7	29.7±0.1	28.6±0.7	35.2±0.7	29.2±4.3	33.2±0.8
Change (%)		107.6±19.9	150.5±19.2	96.7±4.9	64.5±0.7	46.2±3.7	93.0±4.1	363.5±117.8	43.2±3.3
250	60	30.8±1.54	35.3±1.5	37.0±1.3	28.9±1.1	28.2±1.2	31.04±0.4	31.8±0.91	32.1±0.3
Change (%)		131.4±11.6	183.3±12.3	87.9±9.7	63.1±6.2	44.0±6.1	70.0±2.1	404.7±24.8	41.8±1.2
300	5	31.3±1.1	33.1±1.9	36.2±0.4	29.6±0.6	29.5±0.6	32.4±0.8	30.5±1.7	31.5±0.9
Change (%)		135.6±8.1	165.7±15.4	83.84±3.1	58.9±3.1	51.0±3.2	77.3±4.4	384.1±45.9	35.8±3.8
300	60	30.9±1.2	35.1±1.4	35.7±0.5	30.1±0.8	32.4±1.0	36.1±2.2	32.6±1.8	33.1±1.2
Change (%)		132.3±8.8	185.1±11.2	81.34±4.0	60.0±4.7	65.6±4.9	97.8±12.0	417.4±49.3	42.7±5.1

Table AII-2. Elemental composition (wt%) of the bio-crude oils obtained from HTL.

Temperature (˚C)	Time (min)	C	N	H	O	Atomic H/C	Atomic O/C
Manure		35.6±0.2	2.4±0.0	3.9±0.1	24.2±0.1	1.32±0.04	0.51±0.05
250	5	66.09±3.46	5.12±0.36	6.56±0.88	22.91±3.49	1.19±0.14	0.26±0.05
250	60	68.64±1.76	5.00±0.40	7.64±0.44	18.72±1.99	1.34±0.05	0.21±0.03
300	5	71.22±1.44	4.43±0.18	7.23±0.19	17.13±1.80	1.22±0.01	0.18±0.02
300	60	70.57±1.14	3.52±0.25	7.26±0.40	18.64±1.33	1.23±0.05	0.20±0.02
Waste activated sludge		30.9±0.3	3.9±0.2	4.2±0.2	22.2±0.4	1.63±0.09	0.54±0.04
250	5	66.19±2.54	8.64±0.67	8.30±0.78	16.87±2.66	1.50±0.09	0.19±0.04
250	60	71.78±1.88	6.28±0.71	9.31±0.43	12.63±1.61	1.56±0.03	0.13±0.02
300	5	69.94±2.01	6.87±0.95	8.46±0.50	14.71±3.05	1.45±0.04	0.16±0.04
300	60	73.27±0.95	6.78±0.32	8.92±0.77	11.03±1.56	1.46±0.13	0.11±0.02
Food waste		47.9±0.5	2.7±0.1	7.0±0.2	36.6±0.5	1.76±0.08	0.57±0.04
250	5	75.48±0.78	1.52±0.33	10.80±0.21	12.19±0.65	1.72±0.02	0.12±0.01
250	60	75.13±0.68	2.51±0.51	9.72±0.66	12.64±0.83	1.55±0.09	0.13±0.01
300	5	75.84±0.43	3.20±0.27	8.92±0.30	12.04±0.33	1.41±0.05	0.12±0.00
300	60	74.26±0.40	2.86±0.29	9.16±0.25	13.73±0.36	1.48±0.03	0.14±0.00
Apple pomace		48.1±0.5	1.1±0.0	6.6±0.2	42.6±0.3	1.64±0.05	0.66±0.03
250	5	71.17±0.21	0.92±0.06	6.60±0.11	21.31±0.61	1.11±0.02	0.22±0.00
250	60	69.42±1.54	0.83±0.03	6.68±0.20	23.08±1.73	1.15±0.01	0.25±0.02
300	5	70.87±0.62	0.93±0.08	6.64±0.15	21.56±0.76	1.12±0.02	0.23±0.01
300	60	71.80±1.15	1.04±0.06	6.66±0.15	20.50±1.36	1.11±0.01	0.21±0.02
Red wine pomace		50.5±0.4	2.7±0.2	5.7±0.2	31.6±0.7	1.35±0.06	0.47±0.05
250	5	66.83±0.43	2.84±0.17	7.12±0.32	23.22±0.67	1.28±0.05	0.26±0.01
250	60	66.95±1.86	2.65±0.14	6.82±0.24	23.57±1.92	1.22±0.04	0.26±0.03
300	5	69.33±0.65	2.88±0.01	6.88±0.18	20.91±0.82	1.19±0.02	0.23±0.01
300	60	73.49±1.07	2.54±0.06	7.40±0.25	16.56±1.36	1.21±0.02	0.17±0.02

Temperature (˚C)	Time (min)	C	N	H	O	Atomic H/C	Atomic O/C
Whiskey stillage		46.9±0.1	4.1±0.2	6.5±0.0	38.8± 0.1	1.67±0.12	0.62±0.03
250	5	72.75±0.59	2.37±0.23	9.39±0.30	15.48±0.66	1.55±0.04	0.16±0.01
250	60	69.84±0.65	4.13±0.20	7.52±0.09	18.51±0.79	1.29±0.02	0.20±0.01
300	5	72.92±1.13	4.50±0.03	7.32±0.14	15.27±1.30	1.20±0.00	0.16±0.02
300	60	77.53±3.01	4.40±0.05	8.18±0.40	9.89±3.35	1.27±0.01	0.10±0.04
Yogurt whey		19.8±0.1	0.7±0.0	2.6±0.1	22.7±0.0	1.57±0.04	0.86±0.04
250	5	63.65±5.49	1.24±0.10	8.69±0.94	26.42±6.38	1.65±0.06	0.32±0.11
250	60	67.62±0.64	1.37±0.21	9.01±0.47	22.00±0.80	1.60±0.08	0.24±0.01
300	5	66.91±2.02	1.72±0.04	8.40±0.40	22.97±2.40	1.50±0.03	0.26±0.04
300	60	68.61±2.45	1.43±0.28	9.19±0.49	20.77±2.83	1.65±0.06	0.23±0.04
Olive oil pomace		56.1±0.3	2.5±0.0	7.1±0.1	31.5±0.2	1.56±0.05	0.42±0.03
250	5	71.11±0.76	0.63±0.03	8.85±0.24	19.40±0.96	1.63±0.05	0.20±0.01
250	60	71.45±0.38	0.76±0.07	8.52±0.05	19.29±0.40	1.60±0.08	0.20±0.01
300	5	70.37±0.82	0.92±0.04	7.98±0.30	20.73±1.09	1.51±0.03	0.22±0.01
300	60	72.56±0.25	1.05±0.10	8.27±0.72	18.13±0.79	1.61±0.07	0.19±0.01
Bio-ethanol (Yin et al. 2010)		52.2	0	13.1	34.7	3.0	0.50
Bio-diesel (Yin et al. 2010)		77	0	12	11	1.9	0.11
Pyrolysis bio-oil (before upgrade) (Yin et al. 2010)		54-58	0-0.2	5.5-7.0	35-40	1.3	0.50
Gasoline (Yin et al. 2010)		85-88	N/A	12-15	0	1.87	0.0

Yin, S, R Dolan, M Harris, and Z Tan. 2010. “Subcritical Hydrothermal Liquefaction of Cattle Manure to Bio-Oil: Effects of Conversion Parameters on Bio-Oil Yield and Characterization of Bio-Oil.” *Bioresource Technology* 101 (10): 3657–64.

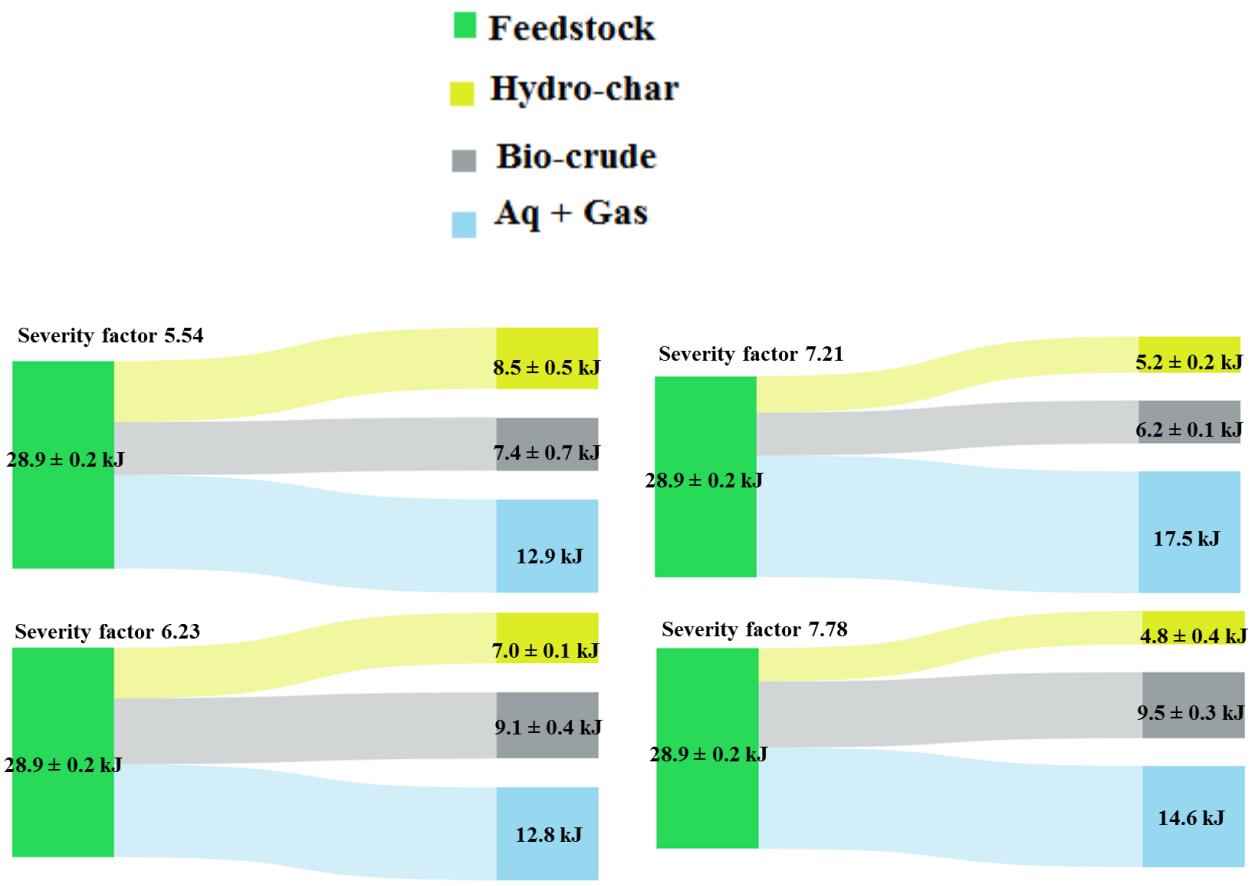

Figure AII-30. Sankey diagram representing the distribution of the energy content in activated waste sludge feedstock towards HTL phases upon reaction at different severity factors. Values presented are the average of 3 experiments, and the errors are the standard deviation. Aq + gas phase energy content was calculated by difference.

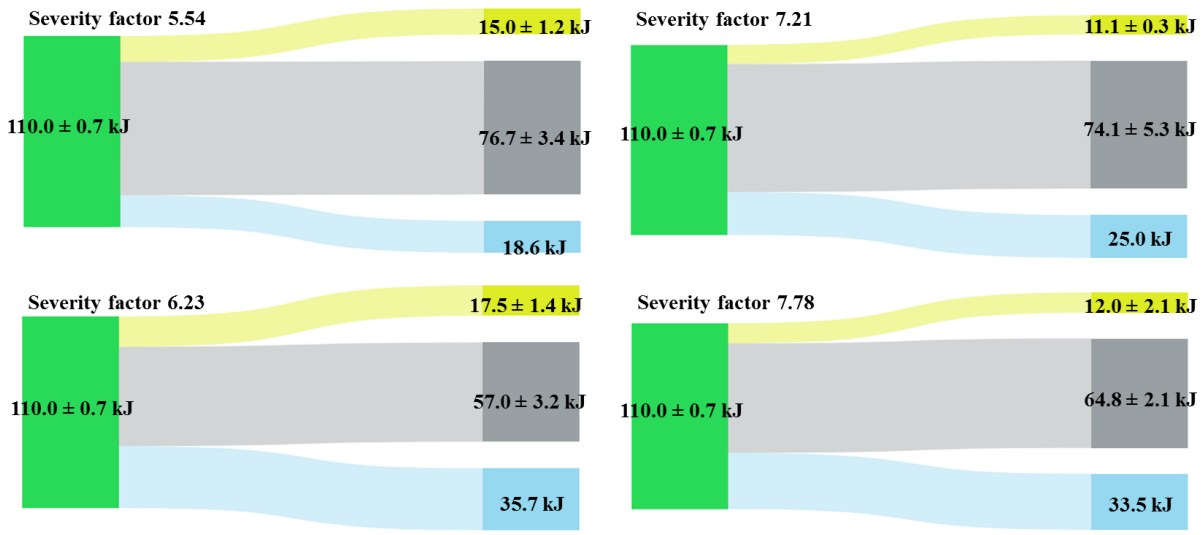

Figure AII-31. Sankey diagram representing the distribution of the energy content in food waste feedstock towards HTL phases upon reaction at different severity factors. Values presented are the average of 3 experiments, and the errors are the standard deviation. Aq + gas phase energy content was calculated by difference.

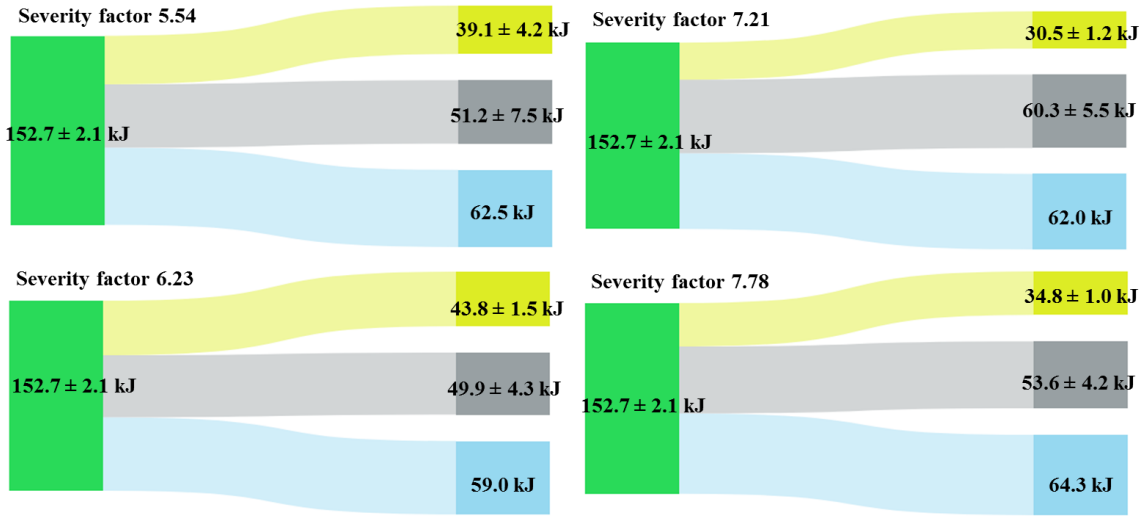

Figure AII-32. Sankey diagram representing the distribution of the energy content in apple pomace feedstock towards HTL phases upon reaction at different severity factors. Values presented are the average of 3 experiments, and the errors are the standard deviation. Aq + gas phase energy content was calculated by difference.

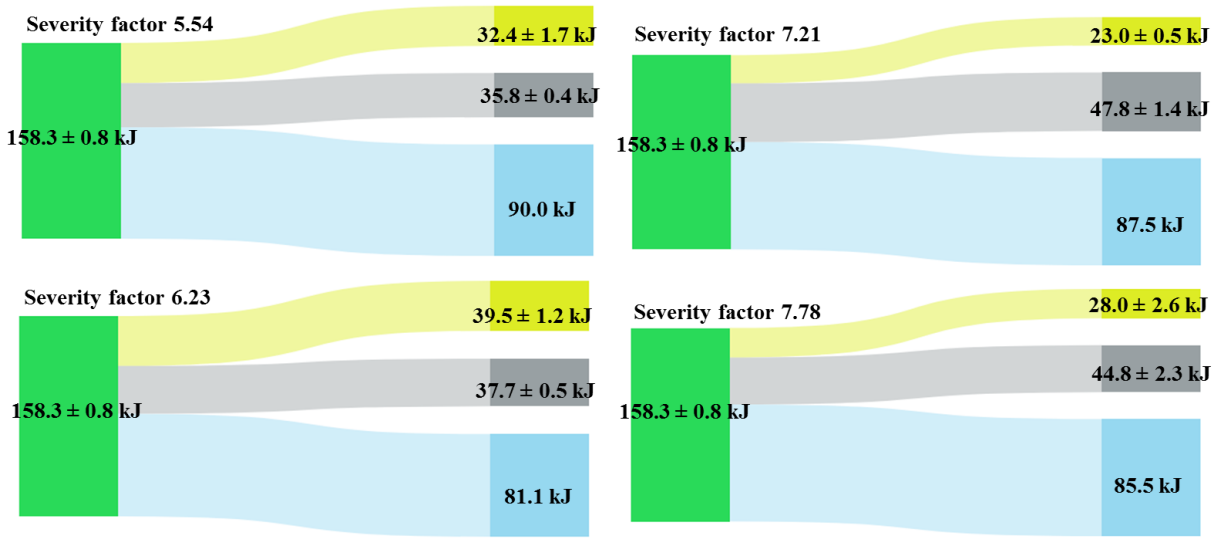

Figure AII-33. Sankey diagram representing the distribution of the energy content in red wine pomace feedstock towards HTL phases upon reaction at different severity factors. Values presented are the average of 3 experiments, and the errors are the standard deviation. Aq + gas phase energy content was calculated by difference.

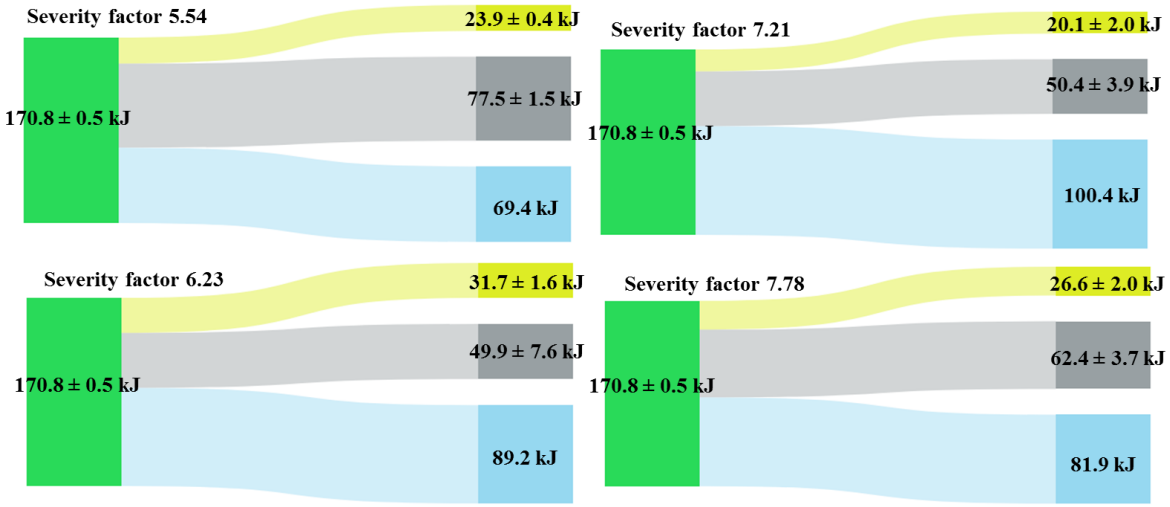

Figure AII-34. Sankey diagram representing the distribution of the energy content in whiskey stillage feedstock towards HTL phases upon reaction at different severity factors. Values presented are the average of 3 experiments, and the errors are the standard deviation. Aq + gas phase energy content was calculated by difference.

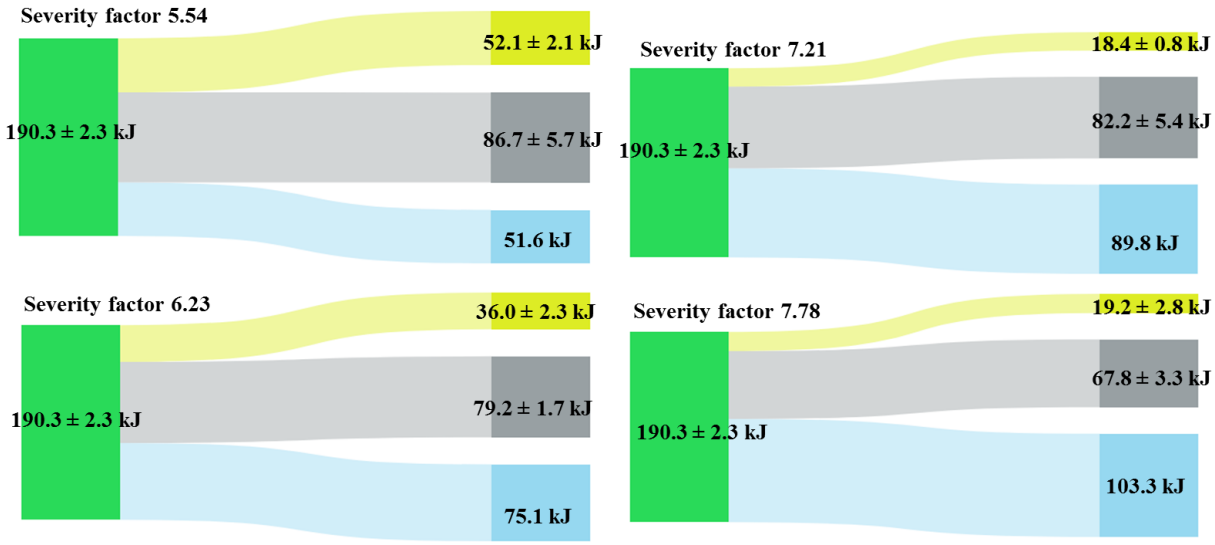

Figure AII-35. Sankey diagram representing the distribution of the energy content in olive oil pomace feedstock towards HTL phases upon reaction at different severity factors. Values presented are the average of 3 experiments, and the errors are the standard deviation. Aq + gas phase energy content was calculated by difference.

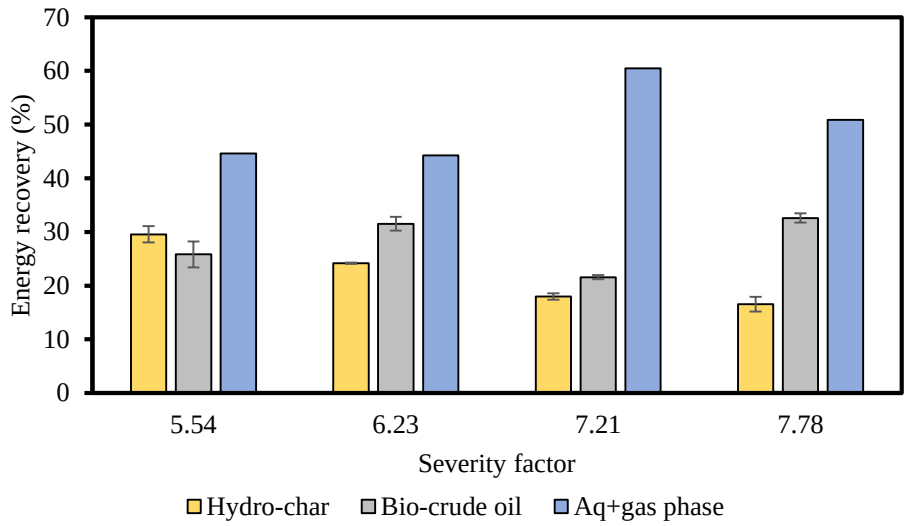

Figure AII-36. Energy recovery (%) from feedstock within the phases obtained from HTL process for activated waste sludge. Values presented are average of 3 experiments, and the error bars represent the standard deviation. Aq + gas phase energy recovery was calculated by difference to 100%

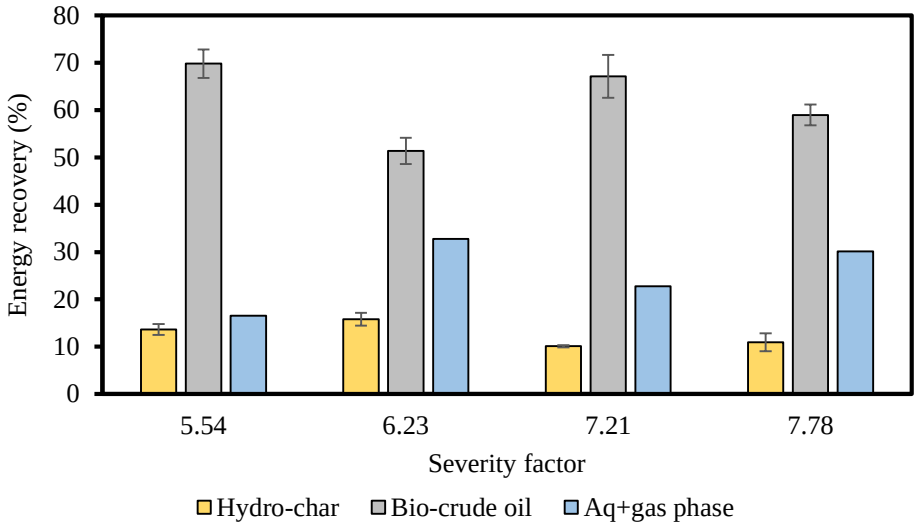

Figure AII-37. Energy recovery (%) from feedstock within the phases obtained from HTL process for food waste. The values presented are average of 3 experiments, and the error bars represent the standard deviation. Aq + gas phase energy recovery was calculated by difference to 100%

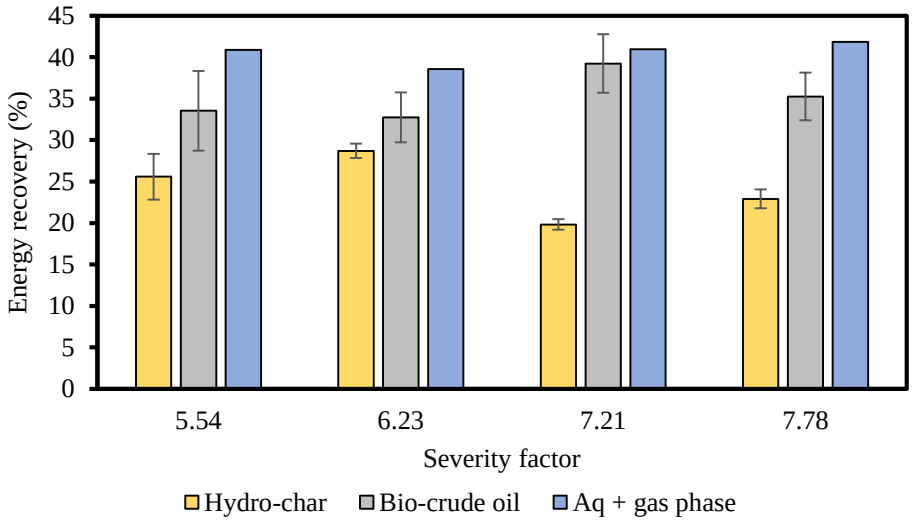

Figure AII-38. Energy recovery (%) from feedstock within the phases obtained from HTL process for apple pomace. The values presented are average of 3 experiments, and the error bars represent the standard deviation. Aq + gas phase energy recovery was calculated by difference to 100%

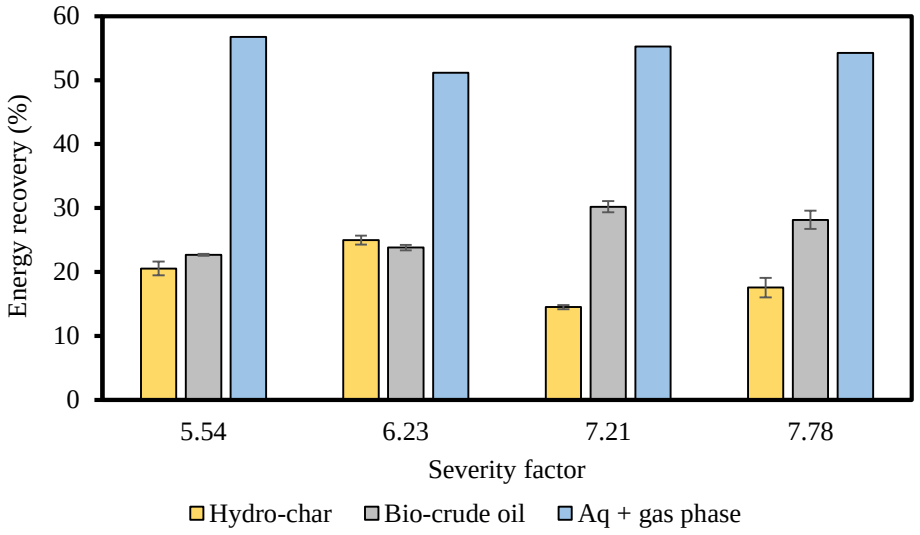

Figure AII-39. Energy recovery (%) from feedstock within the phases obtained from HTL process for red wine pomace. The values presented are average of 3 experiments, and the error bars represent the standard deviation. Aq + gas phase energy recovery was calculated by difference to 100%

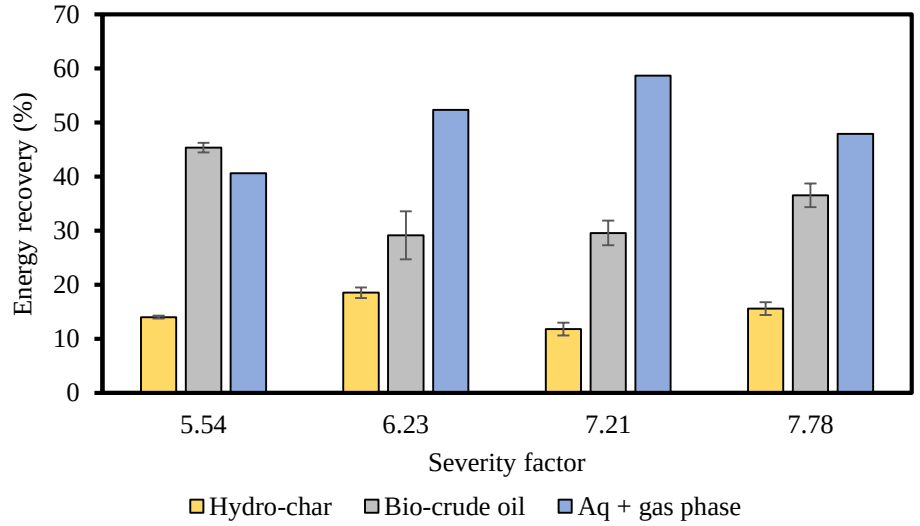

Figure AII-40. Energy recovery (%) from feedstock within the phases obtained from HTL process for whiskey stillage. The values presented are average of 3 experiments, and the error bars represent the standard deviation. Aq + gas phase energy recovery was calculated by difference to 100%

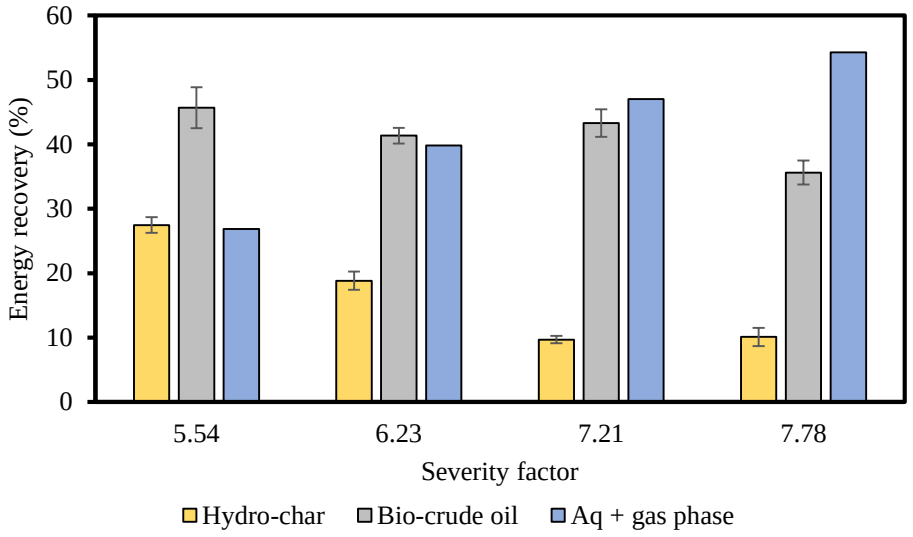

Figure AII-41. Energy recovery (%) from feedstock within the phases obtained from HTL process for olive oil pomace. The values presented are average of 3 experiments, and the error bars represent the standard deviation. Aq + gas phase energy recovery was calculated by difference to 100%

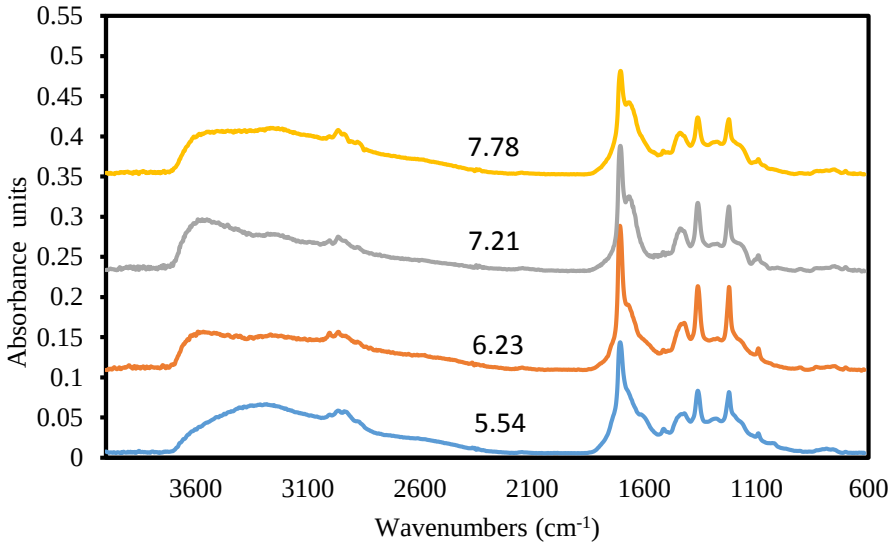

Figure AII-42. FTIR spectra for the bio-crude oils obtained from food waste for all the severity factors studied. Every spectra is the average of 3 experiments and 32 scans per experiment.

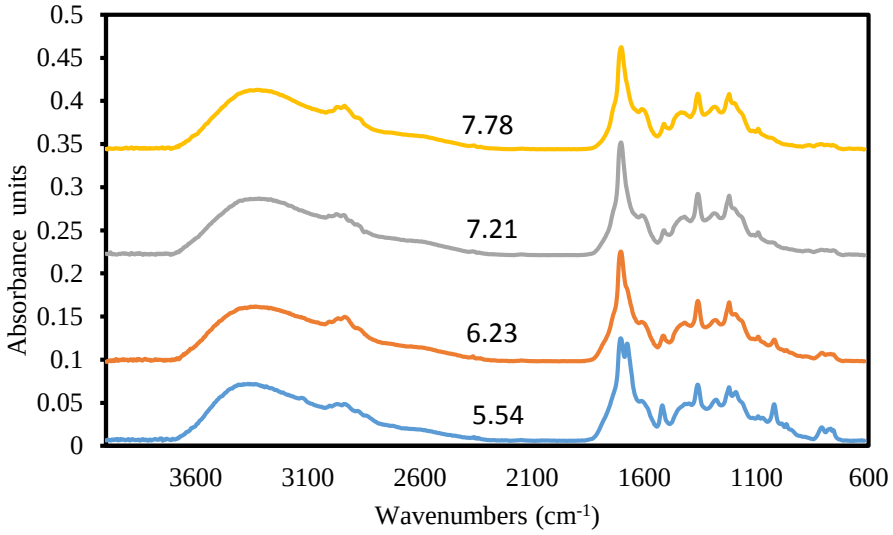

Figure AII-43. FTIR spectra for the bio-crude oils obtained from apple pomace for all the severity factors studied. Every spectra is the average of 3 experiments and 32 scans per experiment.

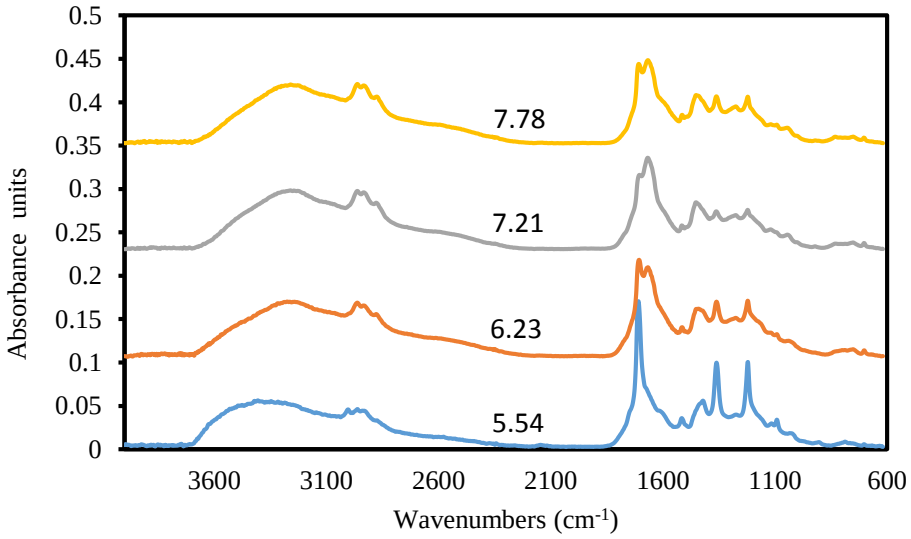

Figure AII-44. FTIR spectra for the bio-crude oils obtained from whiskey stillage for all the severity factors studied. Every spectra is the average of 3 experiments and 32 scans per experiment.

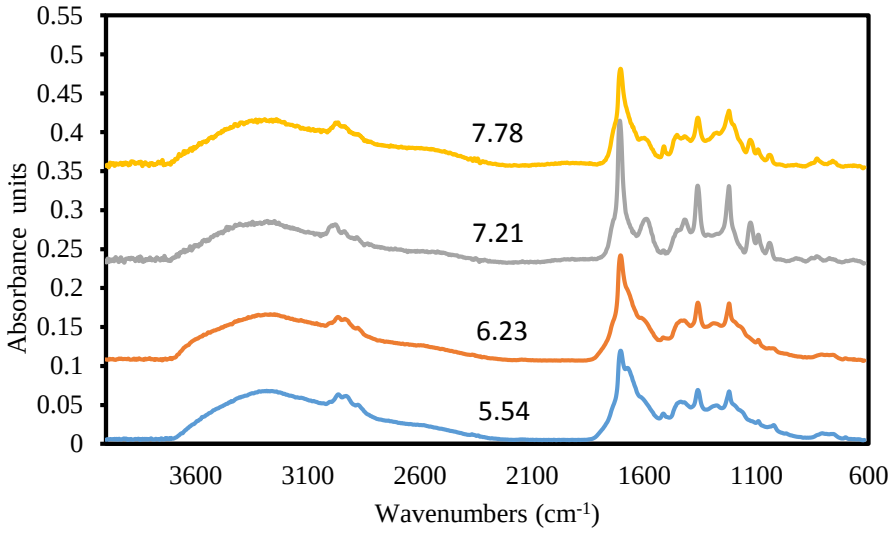

Figure AII-45. FTIR spectra for the bio-crude oils obtained from yogurt whey for all the severity factors studied. Every spectra is the average of 3 experiments and 32 scans per experiment.

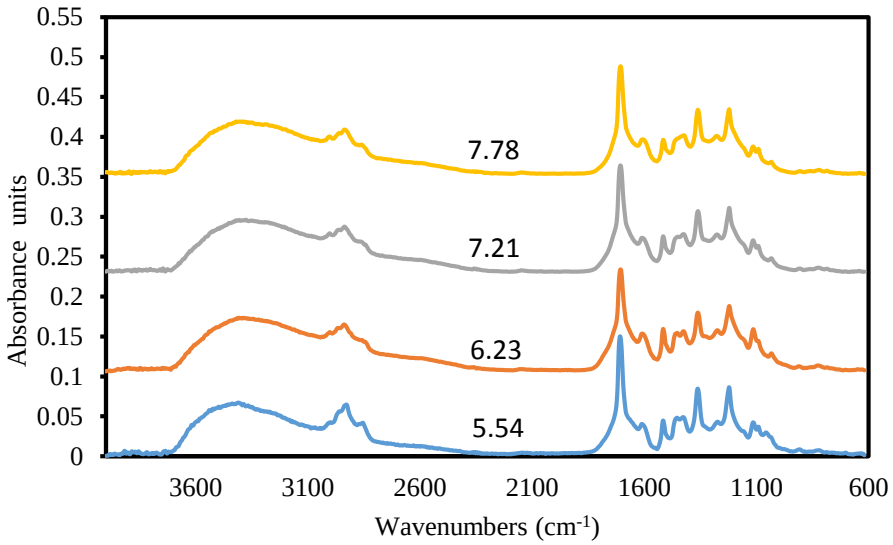

Figure AII-46. FTIR spectra for the bio-crude oils obtained from olive oil pomace for all the severity factors studied. Every spectra is the average of 3 experiments and 32 scans per experiment.

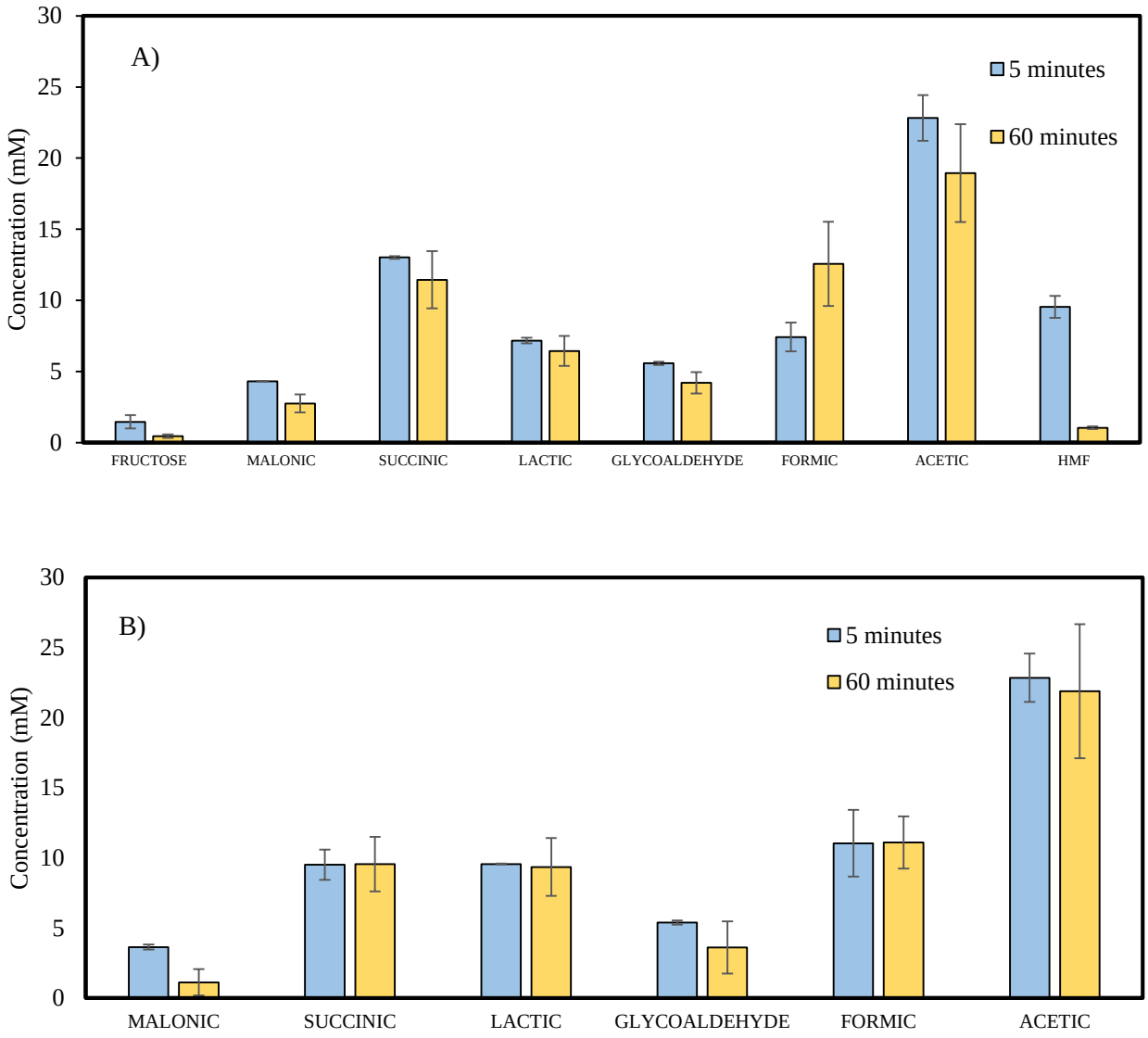

Figure AII-47. HPLC for aqueous phase of apple pomace at A) 250 and B) 300˚C. The values presented are the average for three experiments, and the error bars represent the standard deviation.

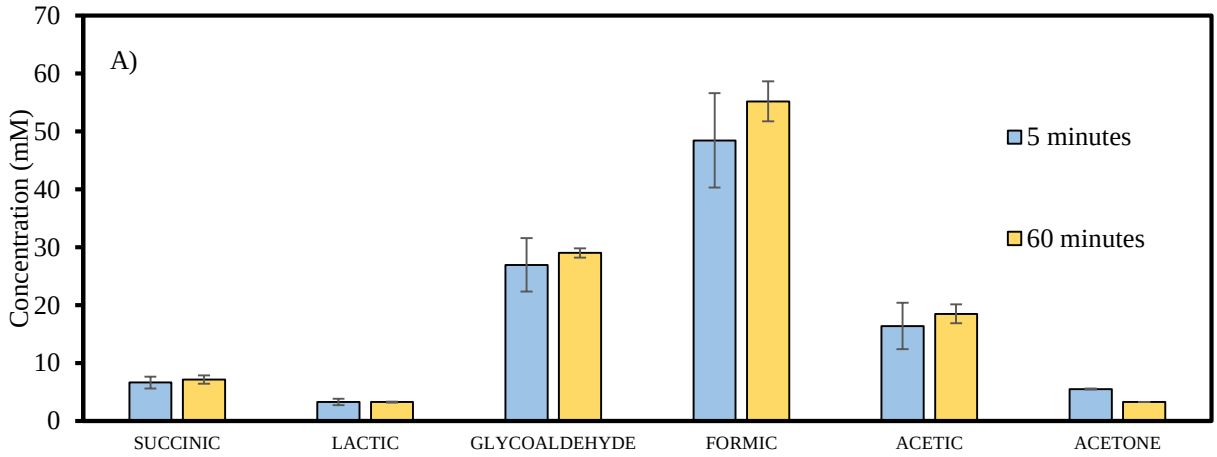

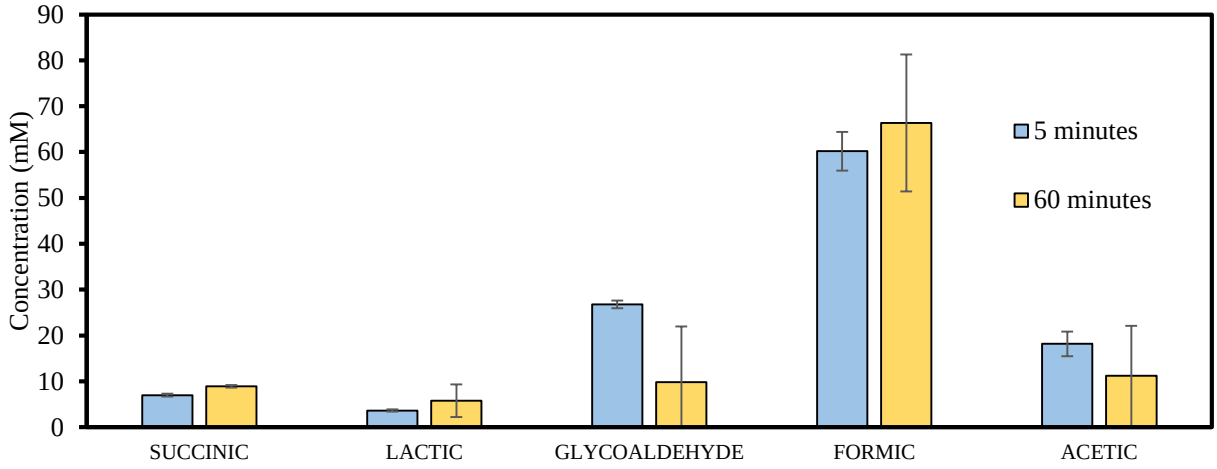

Figure AII-48. HPLC for aqueous phase of food waste at A) 250 and B) 300˚C. The values presented are the average for three experiments, and the error bars represent the standard deviation